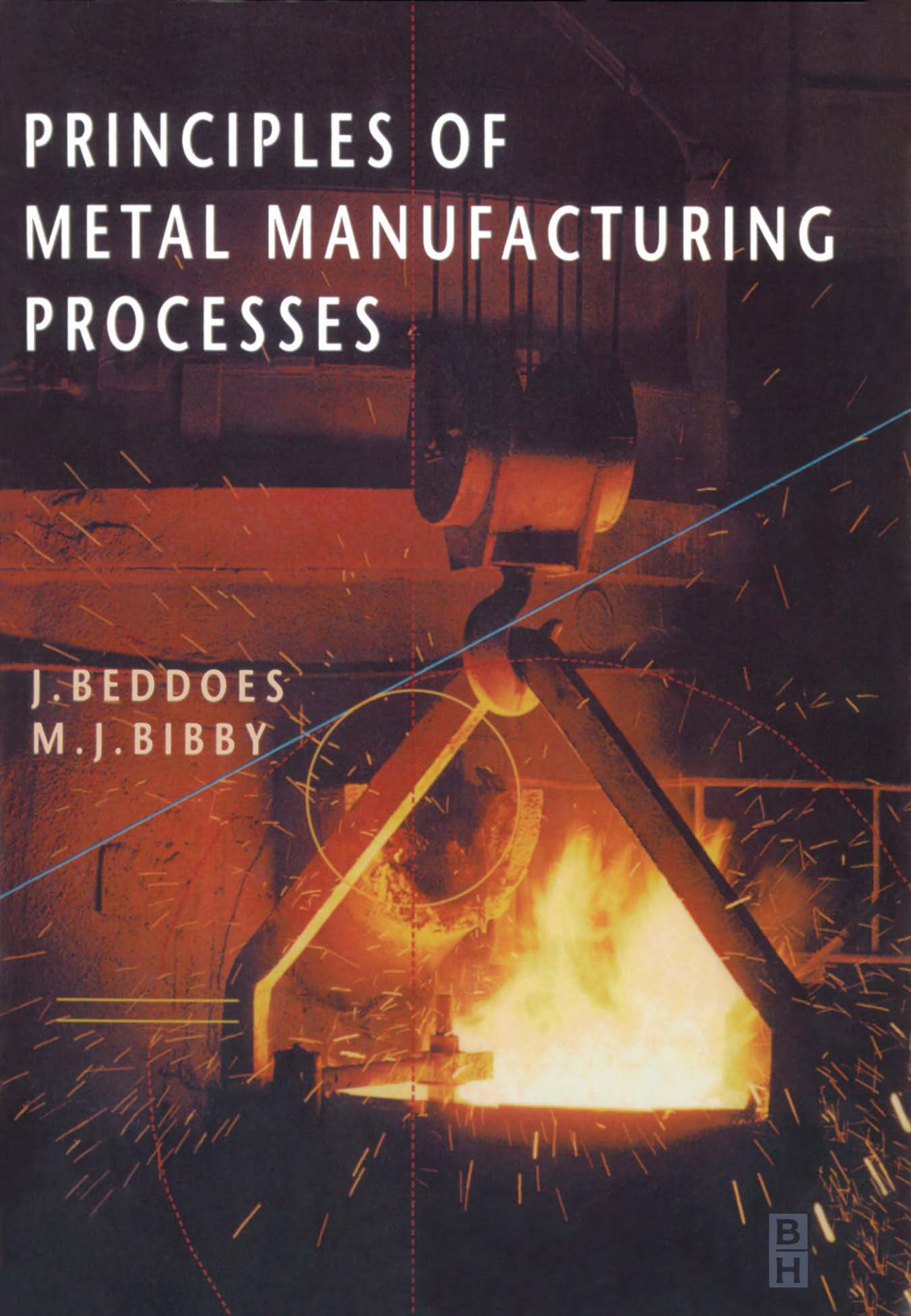


PRINCIPLES OF METAL MANUFACTURING PROCESSES

The background of the cover is a photograph of a metal manufacturing process. A large, glowing orange molten metal ladle is being poured into a mold. A crane hook is visible above the ladle. The scene is filled with bright orange sparks and a blue line of light, suggesting a high-temperature industrial environment.

J. BEDDOES
M. J. BIBBY

Principles of Metal Manufacturing Processes

This Page Intentionally Left Blank

Principles of Metal Manufacturing Processes

J. Beddoes & M. J. Bibby
Carleton University, Canada



ELSEVIER
BUTTERWORTH
HEINEMANN

AMSTERDAM • BOSTON • HEIDELBERG • LONDON • NEW YORK • OXFORD
PARIS • SAN DIEGO • SAN FRANCISCO • SINGAPORE • SYDNEY • TOKYO

Elsevier Butterworth-Heinemann
Linacre House, Jordan Hill, Oxford OX2 8DP
200 Wheelers Road, Burlington, MA 01803

First published 1999
Reprinted 2003

Copyright ©1999, 2003, J. Beddoes and M. J. Bibby. All rights reserved

The right of J. Beddoes and M. J. Bibby to be identified as the authors of this work has been asserted in accordance with the Copyright, Designs and Patents Act 1988

No part of this publication may be reproduced in any material form (including photocopying or storing in any medium by electronic means and whether or not transiently or incidentally to some other use of this publication) without the written permission of the copyright holder except in accordance with the provisions of the Copyright, Designs and Patents Act 1988 or under the terms of a licence issued by the Copyright Licensing Agency Ltd, 90 Tottenham Court Road, London, England W1T 4LP. Applications for the copyright holder's written permission to reproduce any part of this publication should be addressed to the publisher

Permissions may be sought directly from Elsevier's Science & Technology Rights Department in Oxford, UK: phone: (+44) 1865 843830, fax: (+44) 1865 853333, e-mail: permissions@elsevier.co.uk. You may also complete your request on-line via the Elsevier homepage (<http://www.elsevier.com>), by selecting 'Customer Support' and then 'Obtaining Permissions'

British Library Cataloguing in Publication Data

A catalogue record for this book is available from the British Library

Library of Congress Cataloguing in Publication Data

A catalogue record for this book is available from the Library of Congress

ISBN 0 340 73162 1

For information on all Elsevier Butterworth-Heinemann publications visit our website at www.bh.com
--

Transferred to digital printing 2006
Printed and bound by Antony Rowe Ltd, Eastbourne

Contents

<i>Preface</i>	viii
1. Metal processing and manufacturing	1
1.1 Introduction	1
1.2 The manufacturing engineering discipline	1
1.3 Materials used in manufacturing	3
1.4 Raw materials to finished product	4
1.5 Primary manufacturing processes – steelmaking	4
1.6 Primary manufacturing processes – aluminium production	12
1.7 Secondary manufacturing	15
1.8 Problems	16
2. Solidification and casting processes	18
2.1 Introduction	18
2.2 Major casting techniques	18
2.3 Solidification mechanism	30
2.4 Solidification volume shrinkage	36
2.5 Heat transfer during solidification	40
2.6 Defects produced during casting	49
2.7 Shape casting materials	57
2.8 Design of shape castings for manufacturing	61
2.9 Problems	63
Case study 1: Manufacture of can body stock – 1. Casting	67
Case study 2: Cosworth–Ford casting process	72
3. Stress and strain during deformation	76
3.1 Introduction	76
3.2 Engineering stress–strain	76
3.3 True stress and true strain	80
3.4 Relationship between engineering and true stress–strain	86
3.5 Deformation work	88
3.6 Physical significance of the strain hardening exponent	91

3.7 Hot deformation	91
3.8 Superplasticity	95
3.9 Problems	96
4. Bulk deformation processes	99
4.1 Introduction	99
4.2 Friction during bulk deformation	100
4.3 Forging	103
4.4 Extrusion	115
4.5 Drawing	121
4.6 Rolling	122
4.7 Analytical methods for bulk deformation processes	132
4.8 Problems	135
Case study 3: Manufacture of can body stock – 2. Rolling	138
5. Sheet forming processes	142
5.1 Introduction	142
5.2 Formability	142
5.3 Shearing	144
5.4 Bending	146
5.5 Stretch forming	150
5.6 Deep drawing	152
5.7 Effect of anisotropic sheet properties on formability	158
5.8 Pressworking of metals	162
5.9 Problems	162
Case study 4: Manufacture of can body stock – 3. Sheet forming	166
6. Powder metallurgy	173
6.1 Introduction	173
6.2 Powder production	175
6.3 Powder characteristics	180
6.4 Powder compaction	181
6.5 Metal injection moulding	187
6.6 Problems	188
7. Machining processes	190
7.1 Introduction	190
7.2 Mechanical machining methods	191
7.3 Nontraditional machining processes	223
7.4 Comparison of methods	228
7.5 Problems	229
8. Joining processes	232
8.1 Introduction	232
8.2 Welding	232
8.3 Brazing	263

8.4 Soldering	267
8.5 Problems	267
Case study 5: Processing to produce automobile radiators	270
Case study 6: Manufacture of stainless steel automotive exhaust systems	275
9. Surface modification for wear resistance	279
9.1 Introduction	279
9.2 Types of wear	280
9.3 Diffusional processes	286
9.4 Flame and induction hardening	297
9.5 Plating processes	300
9.6 Thin film coatings	303
9.7 Problems	306
Appendix A: Useful constants	309
Appendix B: Useful conversion factors	310
Appendix C: Hardness conversion	312
Index	313

Preface

This book is primarily intended for undergraduate students enrolled in mechanical, manufacturing, materials/metallurgy or industrial engineering programmes. Several books dealing with the subject of metal manufacturing processes are already available – so why this book? The justification is the absence of an introductory quantitative, rather than a primarily descriptive, book on this topic, suitable for undergraduate students. A predominantly descriptive treatment of metal manufacturing processes tends to diminish the importance and development of the engineering associated with the technology of these processes and fails to provide the student with the analytical tools required to develop sound judgement. This book addresses these shortcomings and will hopefully stimulate interest in the challenges inherent to industrial metal manufacturing processes.

It follows from the foregoing that the presentation of metal manufacturing processes in this book contains considerable quantitative or semiquantitative analysis. For students to appreciate this it is necessary to have some prerequisite knowledge. Therefore, this book may not be suitable for an entry level course in most undergraduate engineering programmes. In particular, it is assumed that students will have completed an introductory engineering materials course that includes topics such as crystallographic structures and deformation, phase diagrams, major engineering materials systems etc. Also, a reasonable level of mathematical ability, some mechanics of materials and a rudimentary knowledge of heat transfer principles are useful, but not absolutely required.

A deliberate effort has been made to keep this book concise rather than encyclopaedic. It is anticipated that the contents of this book can be rigorously presented in a single-term course, with the expectation that students will read, and hopefully understood, the entire book. The disadvantage of conciseness is that most readers will be able to rightly identify important metal manufacturing processes not included. In this regard individual lecturers may want to supplement the book as they see fit.

In keeping with the more quantitative nature of this book, many of the end-of-chapter problems require numerical calculations. However, it is emphasized that the calculations are by and large approximate, because of the many simplifying assumptions necessary to model various processes. Nevertheless, these problems help to reinforce an understanding of the major factors controlling the various processes presented. Furthermore, it is rarely necessary, and often not possible, for

engineers to generate exact solutions. Rather, timely approximate solutions are often more useful. Consequently, it is hoped that the end-of-chapter problems are helpful for students to develop an understanding and appreciation of metal manufacturing processes. A solution set to these problems is available.

A unique aspect of this book is the series of metal processing case studies included at appropriate places. These provide an appreciation of the technology and multi-disciplinary nature inherent to metal manufacturing processes. The products described will be familiar to most but, probably, few will have considered the implications of manufacturing, even if they have considered the design. Case studies also emphasize that manufacturing steps, even at the early stages of processing, have a definite influence on the final product properties. This illustrates that only through a knowledge of a material's response to manufacturing processes can the final product properties be predicted and understood. Historically, understanding the interrelationship between processing and product properties has led to improvements or new product forms.

This book should also prove useful to practising engineers in the metal processing industries. It is the authors' experience that industry often requires rapid answers to engineering questions, but does not have resources or time for thorough analyses. The information contained in this book should help practising manufacturing engineers with sound first-order judgement.

The authors would like to express their appreciation to the many individuals and organizations that have assisted with the preparation of this book. In particular, thanks are due to P. Ramsahoye for his help with preparation of the manuscript. Also, the generosity of many organizations and companies who have given permission for use of copyrighted information is acknowledged, with recognition as appropriate throughout the book.

J. Beddoes and M.J. Bibby
Carleton University
October 1998

This Page Intentionally Left Blank

Metal processing and manufacturing

1.1 Introduction

It is generally understood that engineers design products. However, an element of this activity that is often underestimated is the necessity for engineers to design processes capable of making products. *Manufacturing* is the term used to describe the making of products. The product design and manufacturing disciplines are closely related because consideration of how a component is to be manufactured is often a defining criterion for successful design.

The manufacturing discipline has existed in various forms since the *tool age*. Until the nineteenth century it was largely an activity reserved for craftsmen. The *industrial revolution* during the second half of the nineteenth century introduced manufacturing mechanization. The use of machines for spinning and weaving in the textile industry is generally acknowledged to be the beginning of modern manufacturing. During this same time, Bessemer (1855) in England and William Kelly (1857) in the United States proposed methods for the mass production of steel. This was followed by the Hall–Héroult process (1885) for smelting aluminium. These processes provided relatively cheap sources of the materials required to drive the industrial revolution. To a large extent, many technological advancements were the result of the availability of new engineering materials. By the end of the nineteenth century basic machines were available for many rudimentary metal-forming operations. Furthermore, the introduction of interchangeable parts allowed machines to be assembled and repaired without the necessity of hand fitting. The development of the manufacturing activity has progressed rapidly during the last 100 years and is now a multidisciplinary process involving design, processing, quality control, planning, marketing and cost accounting. This book considers only those aspects of manufacturing processes directly related to metal processing.

1.2 The manufacturing engineering discipline

Manufacturing has developed into an enormously diverse and complex field. Consequently, the presentation of a generalized body of knowledge on the subject is not an easy task. However, as manufacturing activities employ many engineers, it is

2 Metal processing and manufacturing

important to understand the basic principles on which, through experience, a practising engineer can build more specialized knowledge.

It is widely recognized that a continuing supply of engineers well versed in the manufacturing discipline is an essential element of a well developed industrial economy. The importance of manufacturing has led to the introduction of undergraduate engineering courses dealing with this subject. To limit the scope of the subject and to provide a coherent basis for introductory study, this book deals only with metal processing operations emphasizing metalshaping procedures. Metalshaping operations are of particular importance because metallic materials are most often the load-bearing components of many engineered products and structures. Therefore, an understanding of the processing of these materials is basic to design and structural engineering. Although many of the fundamental concepts presented deal with metals, they can be applied to many other material systems.

The presentation and analysis of manufacturing processes differs from that of most other engineering disciplines. The analyses of some metal processes are dealt with by theories based on the physical sciences in the usual way. Such analyses follow the traditional scientific or engineering approach of developing theories and models to understand physical phenomena. Somewhat unique to the metal processing discipline is the use of empirical or semiempirical relationships for the analyses of many processes that are less well understood. As such empirical 'laws' would seem to be less rigorous than those based on physical laws, it is worth commenting on why these relationships were developed and why they are still useful.

As the industrial revolution progressed, many metal processes came into widespread use simply because they worked. Due to the rudimentary nature of metallurgical knowledge and mechanical engineering available at the time, and the complexity of the processes, a detailed understanding of many operations was impossible. Of course, this problem did not deter plant operators from using processes that worked and provided good financial returns. Over time, experience allowed the development of empirical relationships to help predict the response of a system to various changes. The continuing widespread use of some of these relationships is a testament of their value to the manufacturing discipline. It is clear, then, that the development of many metalshaping processes preceded theories or models to explain why they work.

Throughout the twentieth century engineering knowledge has progressed sufficiently that many of the empirical secrets of various processes have been understood. Furthermore, the speed with which numerical techniques can be carried out by modern computers permits the analysis of many operations that, previously, were nearly impossible. A thorough understanding is still not always possible because of the complexity and interdisciplinary nature of the many processes of interest. Consequently, many operator-derived rules, combined with some fundamentals, have evolved into semiempirical engineering relationships that are still used. It may be asked: if semiempirical relationships have served successfully for so long, why bother to develop a fundamental understanding? The answer is that, through an enhanced understanding of the fundamental physical laws controlling metalshaping, these processes can be significantly improved in terms of throughput, efficiency, quality, environmental impact etc. Also, the additional knowledge often permits the extension of some

operations to include new product forms. As useful as semiempirical relationships are, the knowledge developed must include the fundamentals as much as possible. This is emphasized at various points throughout the text.

1.3 Materials used in manufacturing

One definition of manufacturing is the conversion of either raw or semifinished materials into finished parts. Such a definition serves to emphasize the importance of materials in manufacturing operations. In fact, the choice of material for a given manufacturing situation may be the limiting consideration. In general, a material must satisfy two criteria. First, the relevant mechanical, corrosive, electrical or physical properties of the material must be sufficient to ensure failure-free performance of the final product. Second, the material should be easy and inexpensive to fabricate. Inexperienced engineers tend to underestimate the importance of this latter requirement, often leading to frustration and redesign.

An enormous number of engineering materials are available to the contemporary designer, including a wide range of metals and alloys, plastics, ceramics and composite materials. It has been estimated that there are over 100 000 choices. Therefore, it is often a difficult decision for the designer to select the best material for a given manufacturing situation. Many handbooks detail material properties, or otherwise provide information regarding the properties that may be required for various applications. The wealth of information available in this regard should not be either underestimated or hopefully underutilized. It is not the aim of this book to provide material selection guidelines, but rather to focus on processing principles and semiempirical models where appropriate.

Metals are often selected for engineered parts because of a combination of properties and cost factors. Indeed, many engineers may not appreciate the fortuitous circumstances that led to the widespread use of steel. Not only is steel a low cost choice for many applications, it also has a desirable combination of the mechanical properties that are often critical. In many components the presence of highly stressed regions, due for example to stress concentrations, local wear, corrosion etc., is almost unavoidable. As a consequence, local stresses often exceed the yield strength or *elastic limit*, causing local plastic deformation. If the component was to be made of a brittle metal with little plastic capacity, cracks would develop, which could lead to sudden catastrophic failure in practice. As many steel grades possess high plastic capacity, local deformation in highly stressed areas effectively transfers loads to other less critical areas of a product or structure without initiating fracture. Furthermore, the strength and toughness properties of steels can be altered by appropriate heat treatment cycles and compositional modification. As a consequence many steel alloys have been developed for various applications, and the total tonnage of steel produced is about 50 times that of the next most widely used engineering metal, aluminium (Table 1.1). It is clear then, that for many applications, the selection of a steel grade is not only the sensible choice but also the most economical. In view of the desirable attributes of steel for engineering applications, this book focuses primarily on steel processes. Nonetheless, the principles developed are reasonably general and can be applied to other materials.

4 Metal processing and manufacturing

Table 1.1 Materials used in manufacturing

Material	Approximate world production (tonnes $\times 10^6$)	Approximate relative cost	Density (kg/m ³)	Approximate volume produced (m ³ $\times 10^6$)
Iron (steel)	768	1	7 900	97
Aluminium	18	3	2 700	6.7
Copper	11	5	8 900	1.2
Zinc	7	4	7 100	1
Lead	5	3	11 300	0.41
Nickel	0.7	10	8 900	0.08
Magnesium	0.4	8	1 700	0.23
Tin	0.3	20	5 800	0.05
Titanium	0.1	26	4 500	0.02
Polymers	85		900–2200	56

Despite the comments of the previous paragraph, many other metals have important engineering applications that cannot be effectively served by steel. Often these applications require a specific combination of mechanical properties. An example is the high strength to weight ratio required in many aerospace applications that favour the use of aluminium or titanium alloys. Note, however, that there is generally a cost penalty associated with attaining these specialized properties (Table 1.1).

Since the late 1950s the use of polymers has grown tremendously and the volume of polymers produced is second only to that of steel. Many products have been reengineered to exploit the specific advantages offered by polymers. Many of the manufacturing processes used for metals have somewhat analogous counterparts for plastics, although accommodation for the pronounced viscoelastic nature of plastics is required.

1.4 Raw materials to finished product

Manufacturing operations can be generally classified into *primary* and *secondary* processes. For metals, primary manufacturing usually refers to the conversion of ores into metallic materials. Secondary manufacturing is generally understood to mean the conversion of the products from the primary operation into semifinished or finished parts. For example, the fabrication of automobile engine blocks from a primary melt of iron or aluminium is said to be secondary manufacturing. It is often difficult to classify a particular metalshaping operation as either a primary or secondary process in an absolute sense, as it can be difficult to delineate between the various steps within an integrated manufacturing process. In this book the emphasis is placed on typical secondary manufacturing operations. Nonetheless, to appreciate the complexity of the processing required to produce a finished part, the primary operations of refining steel from iron ore and aluminium from bauxite are described in the following two sections.

1.5 Primary manufacturing processes – steelmaking

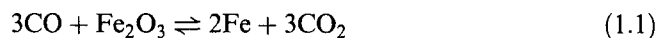
The vast majority of *pig iron* produced from iron ores is processed by *blast furnaces*. The evolution of the modern blast furnace can be traced back to the twelfth century

and the high carbon product of these early furnaces became known as *cast iron*. Despite these early beginnings, the details of the internal operation of blast furnaces are still not completely understood, partly due to the problem of simulating on a small scale the appropriate operating conditions. Blast furnaces are typically more than 30 m high and about 10 m in diameter. The structure is roughly cylindrical and lined with refractory firebrick, supported by a water-cooled outer steel shell.

A modern blast furnace is shown schematically in Fig. 1.1. Four main ingredients are charged into the blast furnace to produce pig iron.

1. *Iron Ore* The two ores most commonly used in North America are *haematite* (Fe_2O_3) and *magnetite* (Fe_3O_4). Major deposits of these ores occur in areas surrounding Lake Superior, Eastern USA and in the Labrador Trough along the border of Quebec and Labrador. The Scandinavian countries, France and Spain, together with Russia, account for most of the iron ore mined in Europe. In addition to haematite and magnetite, *siderite* (FeCO_3) is a commercially important ore mined in Europe. Several other ores are used in smaller amounts for commercial steelmaking. These ores have lower iron contents and contain *gangue*, which is mostly silica and alumina. Interestingly, one of the most common iron ores, *iron pyrite* (FeS_2 – fool's gold), is mined to yield the more valuable elements of copper, nickel, zinc, gold and silver often found in association with iron pyrite. Iron is sometimes recovered as a byproduct after separation of the more valuable metals and sulphur.
2. *Coke* Coke is the residual solid product obtained by heating coal at $>550^\circ\text{C}$ in the absence of air, driving off all the volatile constituents of the coal. It acts as the fuel, burning to produce carbon monoxide and to reduce the iron oxide to iron. Coking coal is found in many parts of the world.
3. *Limestone* Limestone is a rock consisting predominantly of calcium carbonate (CaCO_3). Within the blast furnace it combines with impurities in the ore to form a *slag* which floats on molten pig iron and is separately tapped into a ladle. Slags consist mostly of the oxides of silicon, aluminium, calcium and magnesium, and can be used in making concrete or as railroad ballast.
4. *Hot Air* Hot air or the *blast* is provided to burn the coke.

As seen in Fig. 1.1, pulverized iron ore, coke and limestone are admitted to the top of the blast furnace via the *skip incline*. A preheated air blast is provided to the furnace through a series of nozzles located toward the bottom of the furnace. The furnace operates continuously, with a series of complex chemical reactions occurring as the material moves down the shaft of the furnace. The principal reactions are the burning of the coke to produce carbon monoxide and the subsequent reduction of the ore into pig iron according to the reaction



Typically about 800 t of pig iron are tapped from the blast furnace about five times a day, with the blast furnace operated continuously 7 days a week. About 1400 t of ore, 500 t of coke, 320 t of limestone and 3200 t of air are used to produce the 800 t of pig iron. About 90% of the iron contained in the ore is converted to pig iron. The remaining product is removed primarily as slag or as a gaseous *top gas*, which is combustible and is used for heating the incoming blast. The pig iron produced contains 2.5–5%

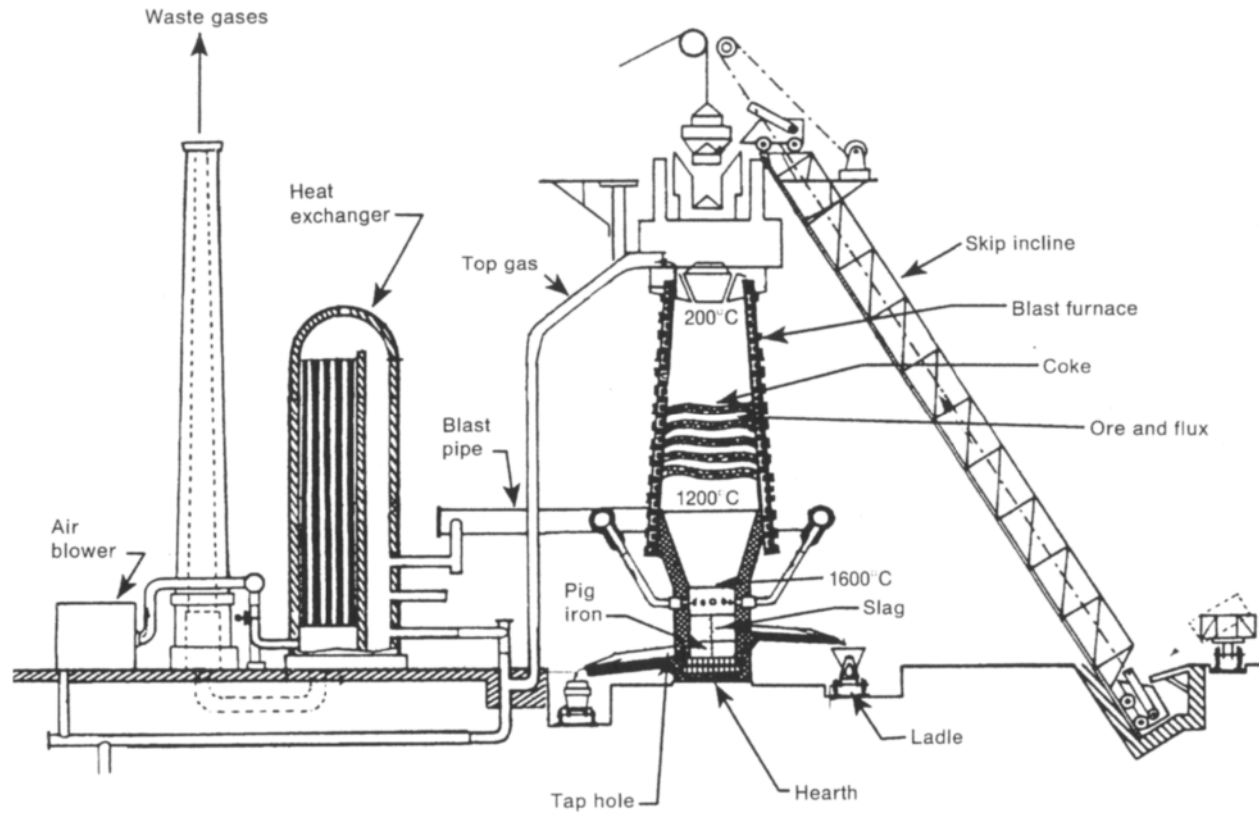


Fig. 1.1 Diagram of a blast furnace for the production of pig iron.

carbon, 1–3% silicon and various amounts of manganese, sulphur and phosphorus originally from the ore, or picked up from the coke.

Due to the high capital and operating cost of blast furnaces, considerable effort has been devoted to producing metallic iron directly from the ore. Such *direct reduction* processes differ from blast furnace operations since oxygen is removed from the ores (e.g. $2\text{Fe}_2\text{O}_3 \rightarrow 4\text{Fe} + 3\text{O}_2 \uparrow$) at temperatures below the melting points of the materials in the process. The various processes examined include almost every known technique for bringing the reactants into contact, but only a few are commercially viable, with direct production processes accounting for only a small percentage of the world's pig iron production.

Steel is produced from molten blast furnace pig iron in a *converter* furnace by oxidizing the carbon, sulphur, phosphorus and other impurities in the pig iron. To achieve the refining action the molten pig iron is brought into contact with air, or more recently oxygen, so that impurities are burned by transforming them into oxides. The oxides are less dense than the molten steel and float on the surface as a liquid slag, which can be separated. In addition to pig iron, some converter furnaces can process recycled scrap steel. Due to the ability to process scrap, such converter furnaces are often the initial processing step at many steel mills.

The *Bessemer* converter was developed in the 1850s and provided much of the steel required to drive the industrial revolution during the late 1800s. The process consisted of pouring pig iron into a converter mounted horizontally to allow tilting (Fig. 1.2). A blast of air was introduced through *tuyères* in the bottom of the converter and

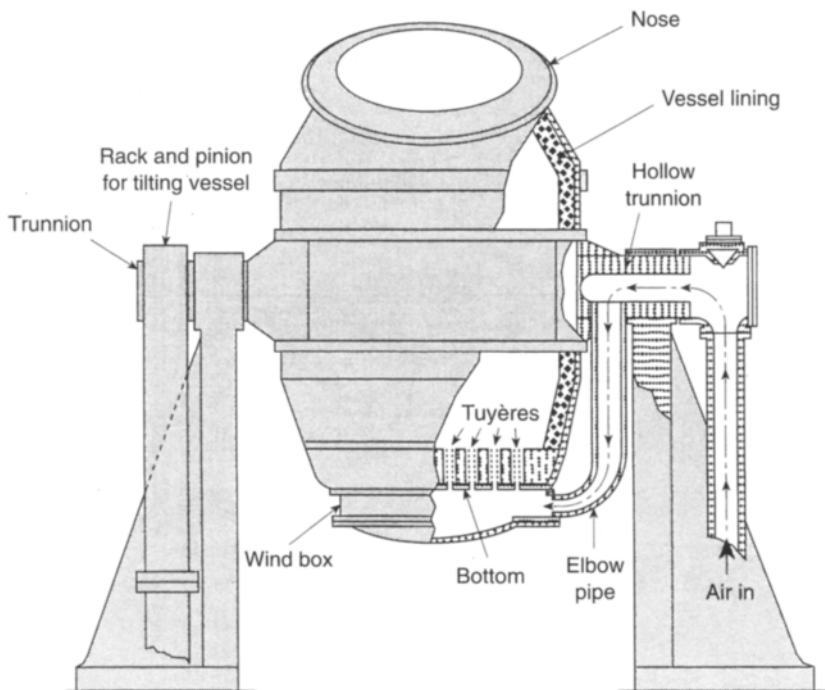


Fig. 1.2 Schematic of a Bessemer steel converter. (Reproduced courtesy of The AISE Steel Foundation.)

8 Metal processing and manufacturing

oxidized carbon in the pig iron to carbon monoxide, which burns further at the mouth of the converter to produce carbon dioxide. The air blast also oxidizes the other impurities, which end up in the floating slag. The separation of the slag from the molten steel may be promoted by the addition of lime. The combustion of the impurities into oxides is an exothermic reaction and the heat released raises the temperature of the molten metal. The principle application for the steel product of the Bessemer process in the late 1800s were the rails for railways, which were far more durable than the cast iron rails they replaced. A drawback of the Bessemer process was nitrogen, picked up by the molten metal from the air blast, which can embrittle the steel.

Shortly after the Bessemer process the *open hearth* process was developed. An open hearth furnace consists of a shallow refractory lined basin equipped with doors through which the raw materials or *charge* can be added (Fig. 1.3). A charge consists of measured quantities of pig iron, limestone, iron ore and scrap metal. Heat is supplied by fossil fuel burners with large *regenerators* or *checkers* that reclaim some waste heat for preheating the combustion air. During the 4–10 h cycle at the operating

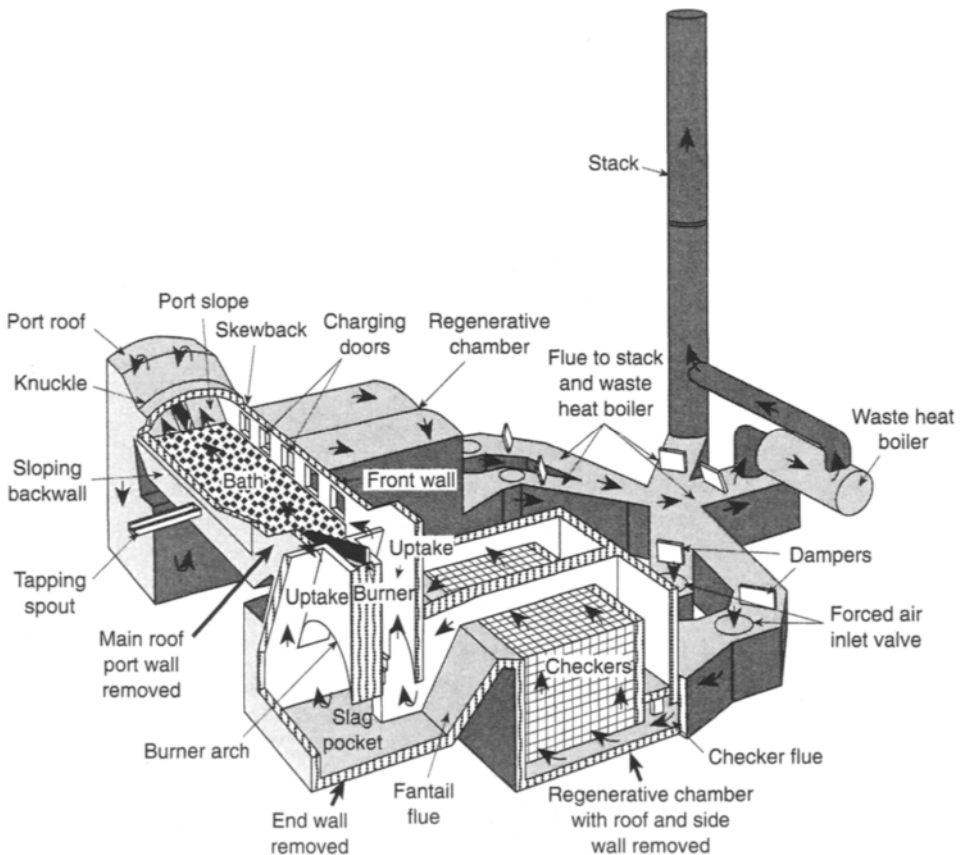


Fig. 1.3 Open hearth steel converter (reproduced courtesy of The AISE Steel Foundation).

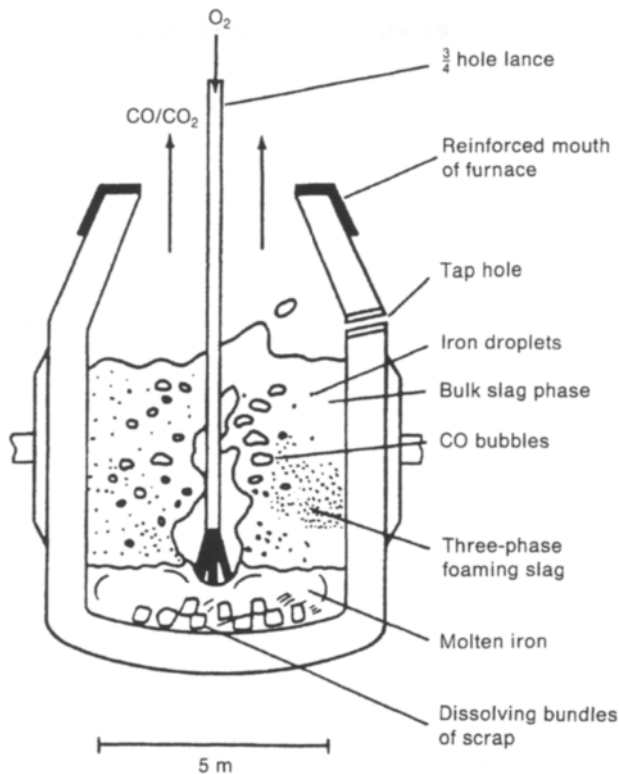


Fig. 1.4 Cross-section through a basic oxygen steel converter. (Reprinted with permission from *ASM Materials Engineering Dictionary*, edited by J.R. Davis (1992) ASM International, Materials Park, OH 44073-0002, Fig. 30, p. 33.)

temperature, the charge is refined through the reduction of the carbon, silicon and manganese by oxygen contained within the combustion air or additions of iron oxide. Impurities such as sulphur and phosphorus are collected in a slag by reacting with a *flux*, typically lime. Good-quality grades of carbon or low alloy steel, with low nitrogen content (which reduces brittleness) can be produced in an open hearth furnace. For this reason, the open hearth furnace accounted for 90% of the steel produced by the middle of the twentieth century. However, the size, expense and long operating cycles of these furnaces have virtually eliminated this process from commercial operation in the Western world, where almost all steel is now produced using basic oxygen and electric arc furnaces.

The *basic oxygen* furnace (Fig. 1.4) was introduced into commercial operation in the 1950s and now accounts for more than half of total steel production in the Western world. The process consists of blowing oxygen through a molten charge, by way of a water cooled steel lance. The charge is contained in a vessel, with a capacity of up to 300 t, capable of tilting, not unlike that used in the Bessemer process. During the oxygen blast the temperature rises rapidly, because of the oxidation of carbon to CO, which boils through the melt producing a long blue flame exiting the vessel. The oxygen converts some iron back into iron oxide which immediately

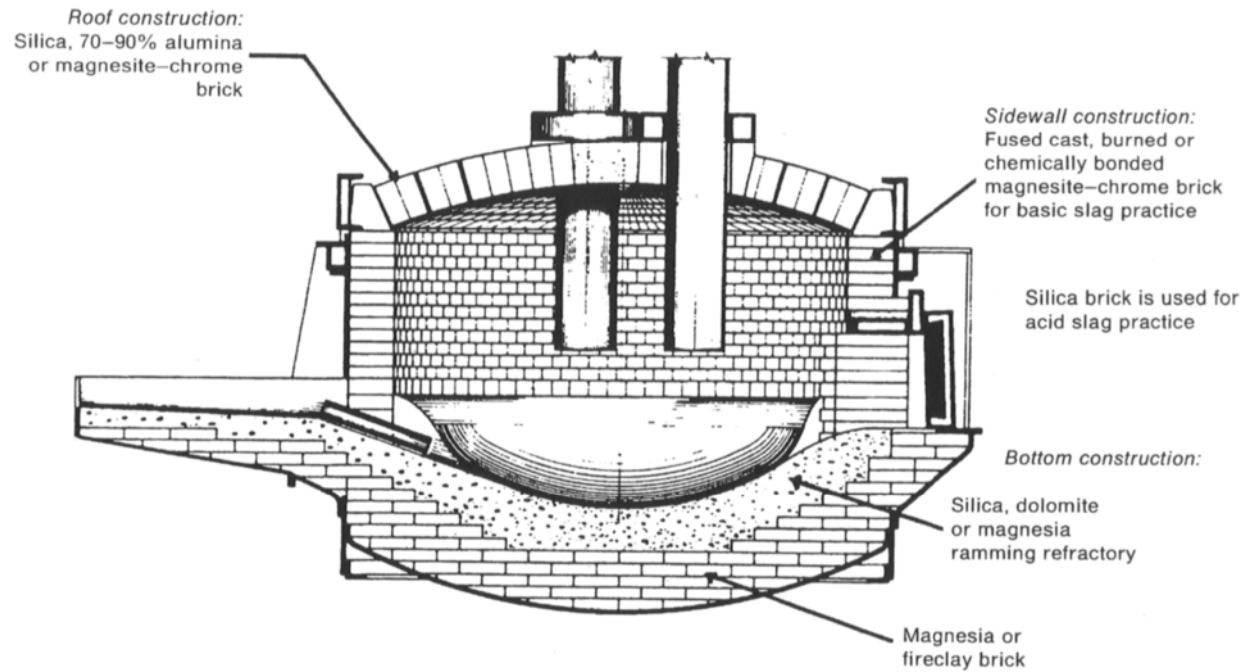


Fig. 1.5 (a) Typical electric arc furnace for steel production. (Reprinted with permission from *ASM Specialty Handbook Stainless Steel*, edited by J.R. Davies (1994) ASM International, Materials Park, OH 44073-0002, Fig. 1, p. 120.)

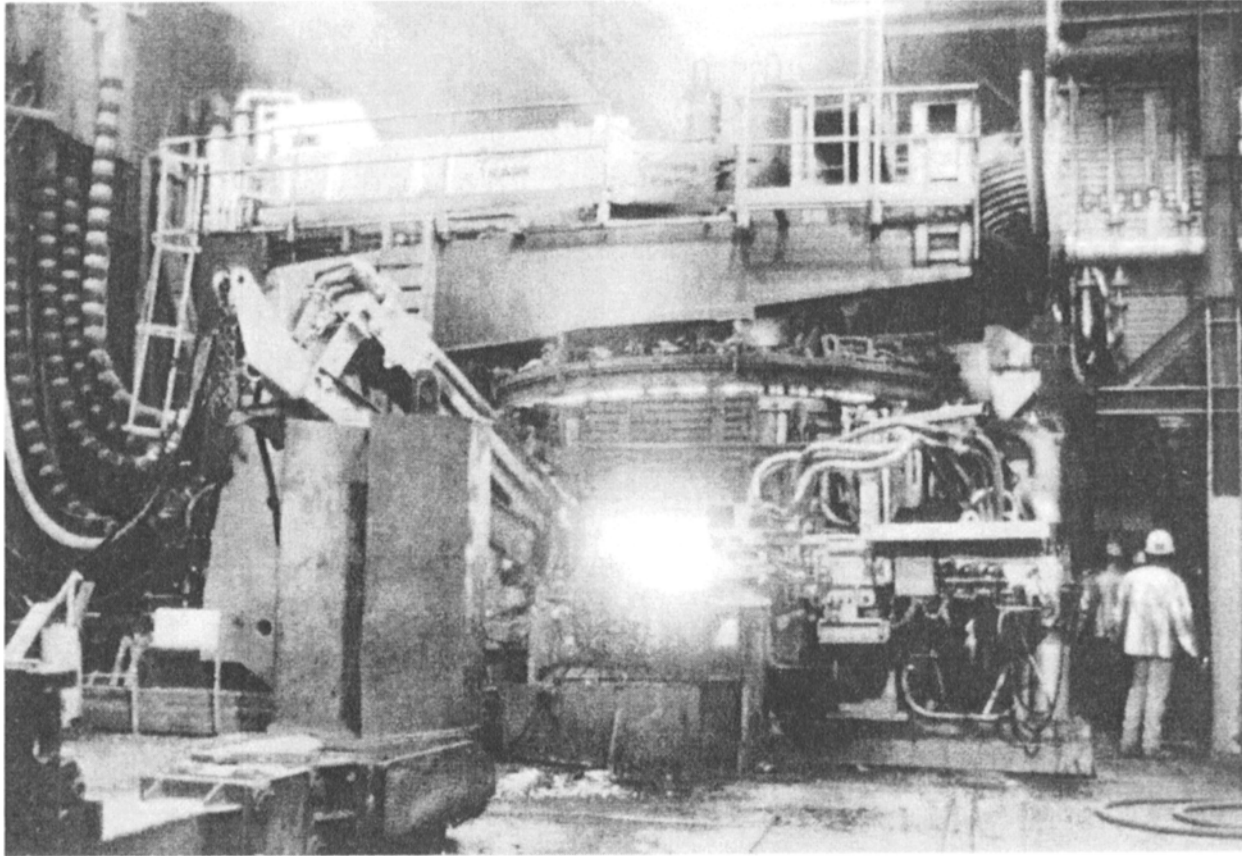


Fig. 1.5 (b) 80 t electric arc furnace capable of pouring about 70 t of steel every 75 min. The cantilevered steel structure above the furnace removes the roof for charging; the open facing door is for oxygen, carbon and lime injection during the conversion process.

reacts with the lime flux and removes sulphur, phosphorus and other impurities which end up in the slag. The advantage of this process is that no external fuel is directly used and the conversion process is relatively rapid. Also, the use of oxygen, rather than air as in the Bessemer process, prevents the introduction of nitrogen, ensuring that a relatively ductile steel is produced. In about 20 min, a composition of <0.1% C, 0.25% Mn, 0.02% S and 0.015% P can be achieved, with the whole process of charging, refining and pouring completed in about 45 min. To meet the composition specifications for a plain carbon steel requires about 70% molten pig iron from a blast furnace, with the remainder of the charge being scrap. Therefore, basic oxygen furnaces are usually operated at integrated steel mills consisting of a blast furnace, basic oxygen converters and associated scrap recycling operations.

In an *electric arc* furnace, electric arcs are used to provide heat. This furnace has carbon electrodes that extend through the roof (Fig. 1.5). A three-phase potential of about 40 V is applied at a high current of about 12 000 A. The charge of up to about 200 t usually contains a high portion of steel scrap. To add the charge, the furnace roof is removed and the charge dropped from large overhead clam-shell scrap buckets. During melting, carbon is oxidized into CO by injecting oxygen into the molten bath. The addition of fluxes removes other impurities into the slag that floats on the molten steel. A major advantage of the electric arc furnace is the ability to control the chemistry of the slag so that a wide variety of steels can be produced. A large percentage of the steel processed through electric arc furnaces starts out as scrap and, therefore, does not require pig iron, or the associated blast furnace, for the charge. This reduces the capital cost of producing molten steel considerably and has led to an increase in the number of so called *mini-mills*. These operations typically consist of: one or more electric arc furnaces that predominantly melt charges of nearly 100% scrap; a continuous casting machine for the production of plate, bar or rod (see Chapter 2); and downstream bulk deformation processes (see Chapter 4). Mini-mills are not usually associated directly with a blast furnace operation.

1.6 Primary manufacturing processes – aluminium production

Of the metallic engineering materials aluminium is second only to steel in tonnage (Table 1.1). It is the most abundant metallic element in the earth's crust, with sufficient proven reserves to satisfy demand for the foreseeable future. Despite the abundance of aluminium, it does not occur naturally in metallic form and commercial processes only exist for the refinement of a few aluminium ores. The most important ore is *bauxite*, which contains about 75% hydrated alumina ($\text{Al}_2\text{O}_3 \cdot 3\text{H}_2\text{O}$ and $\text{Al}_2\text{O}_3 \cdot \text{H}_2\text{O}$). Bauxite is found in southern France and in subtropical regions, the Caribbean, Australia and Africa, and is usually recovered by open pit mining. The vast majority of bauxite tonnage is converted into aluminium using a combination of two processes, both developed towards the end of the 1800s, the *Bayer* process and the *Hall–Héroult* process.

The Bayer process is a series of complex chemical reactions, usually carried out on a large scale continuous basis (Fig. 1.6). To start, the bauxite is ground into powder and mixed with a solution of *caustic soda* (NaOH), the liquor in Fig. 1.6, and delivered to

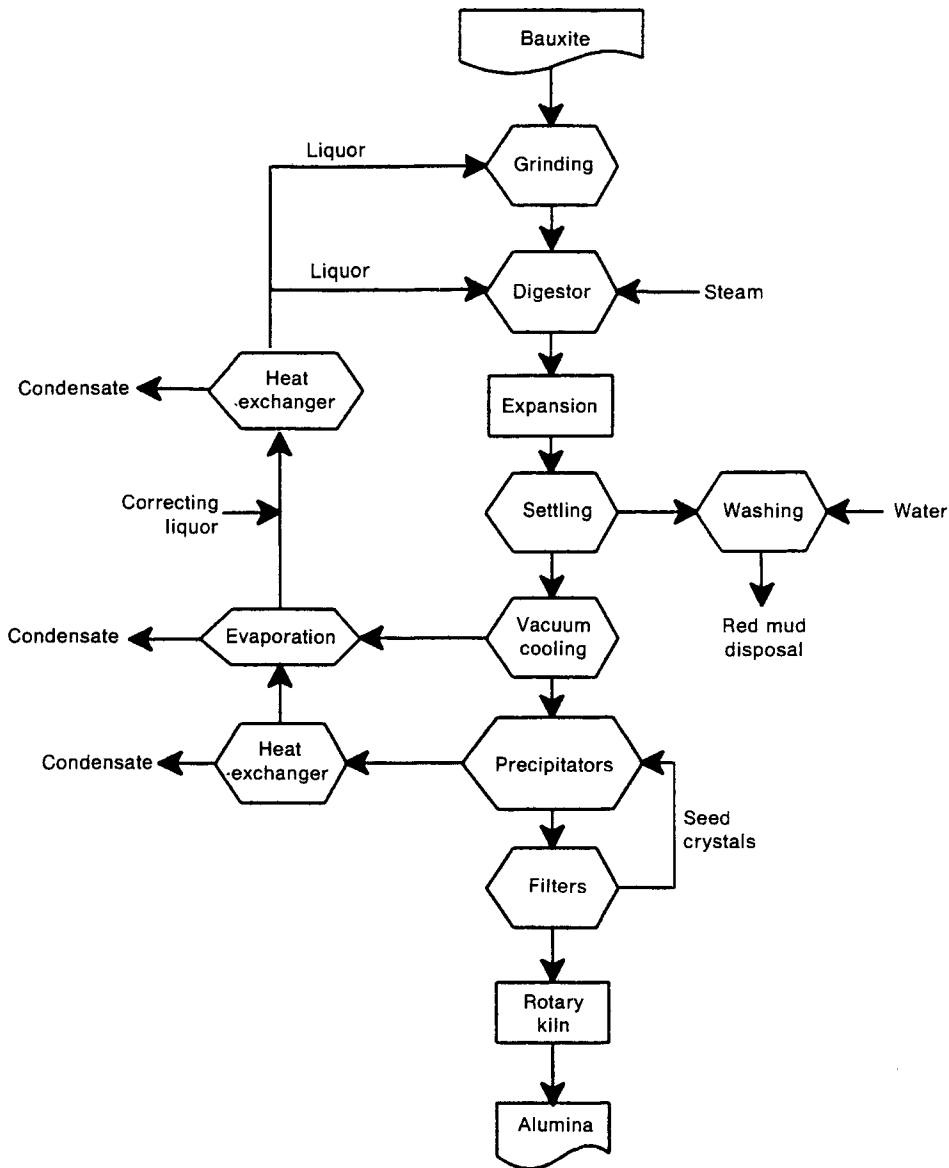
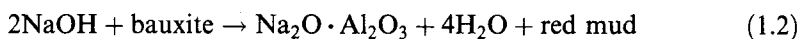


Fig. 1.6 Flow diagram of the Bayer process for the conversion of bauxite into alumina.

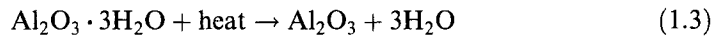
digesters in which, under pressure and temperatures up to 270°C , a solution of sodium aluminate, water and *red mud* develops according to the reaction



The red mud consists mostly of oxides of iron and titanium and other impurities from the bauxite, which settle out of the sodium aluminate solution and are removed. Red mud is a major byproduct of the process, with about as much red mud produced as alumina. Despite intensive efforts, no application for red mud has been developed

that comes close to consuming the amount produced. Consequently red mud is disposed of under the sea or in secured landfills that can eventually revert to agricultural use.

After removal of the red mud, the sodium aluminate is pumped to *precipitators*, in which alumina is precipitated by agitation, after the addition of seed crystals. The alumina precipitate is filtered and about half returned to the precipitators as seeds, to continue the process. The remainder is transferred to rotary kilns or *calciners*. Calciners operate at temperatures of about 1200°C and the combined water is removed according to the reaction



The resulting alumina (Al_2O_3) is a white powder similar in appearance to table salt and is the starting product for the Hall–Héroult process. Alumina also has important

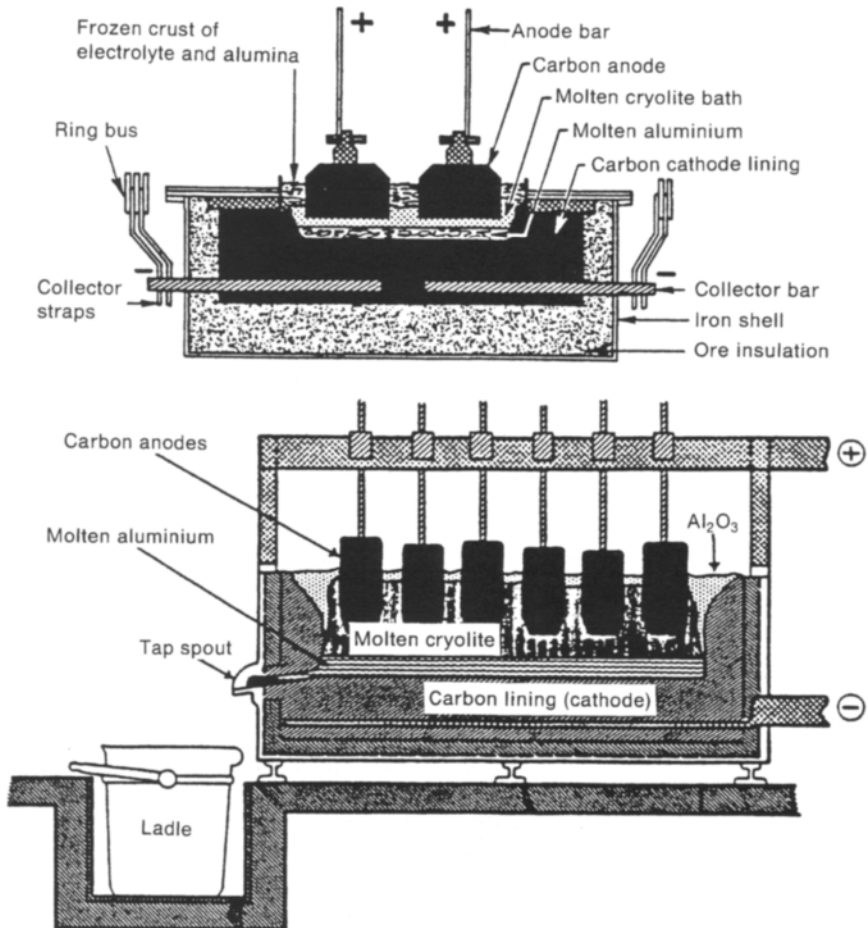


Fig. 1.7 Diagrams of (a) end view and (b) side view of electrolytic cell for the reduction of alumina to aluminium. (Reprinted with the permission of ASM International, Materials Engineering Institute.)

applications for several chemical processes and products, as well as being used for polishing compounds (i.e. toothpaste and metal polishing).

Alumina is converted into metallic aluminium in electrolytic cells referred to as *pots*, many of which are connected in series to form a *potline*. Pots are constructed of steel with refractory lining and carbon blocks acting as the cathode (Fig. 1.7). Alumina is dissolved in an electrolyte of molten *cryolite* (Na_3AlF_6) at about 950°C , with the addition of AlF_3 , which lowers the melting point and vapour pressure. Carbon anodes suspended above the cell dip into the electrolyte bath. Large electrical currents are passed through the cell (typically about 230 000 A at 4–5 V d.c.), and aluminium metal is deposited at the cathode which is tapped or siphoned into ladles for delivery to the *casthouse* and pouring into ingots. One pot produces about 900 kg of 99.5% purity aluminium each day. The remaining 0.5% consists mostly of impurities of iron and silicon. Oxygen is released at the anodes and reacts with the carbon to form CO and CO_2 , consuming the carbon anodes, which must be replaced about every 2 or 3 weeks. Electricity is a major requirement of the process – about 13 500 kWh is consumed to produce 1 t of aluminium. Furthermore, the development of high currents at low potentials requires large rectifying stations. The large electrical consumption required is the major reason that aluminium smelters are usually located close to sources of inexpensive electrical power.

A major effort in recent years has been directed at controlling the effluent from potlines, which contains sulfur dioxide (from the anode material), CO, CO_2 and fluorides, which are particularly damaging to plants and farm animals. All new aluminium smelters are equipped with extensive dry scrubber systems, and some older smelters have been shut down or retrofitted with effluent-control systems.

The production of steel and aluminium have been described to give examples of important primary manufacturing processes. Analogous reduction processes exist for other nonferrous metals, many of which are also based on *electrolytic reduction*. Although the focus of this text is secondary manufacturing, many integrated manufacturing operations involve both primary and secondary manufacturing. It is important to appreciate the complexity, diversity and technology utilized in the primary manufacturing field to, among other things, fully appreciate the integrated manufacturing processes.

1.7 Secondary manufacturing

The conversion of primary products into secondary finished or semifinished components can take place by one of several alternative routes. Many machine parts and metal products can be traced through Fig. 1.8. For example, an automotive crankshaft can start out as a primary steel melt and then take shape as a secondary casting. Alternatively, it may be *forged* (bulk deformation) from a primary billet, bar, or metal powder preform. Regardless of the technique used to obtain the secondary shape, it is almost always heat treated and finish machined. The major secondary metalshaping processes are shown in Fig. 1.8. Each of these major operations is the subject of one of the chapters that follow.

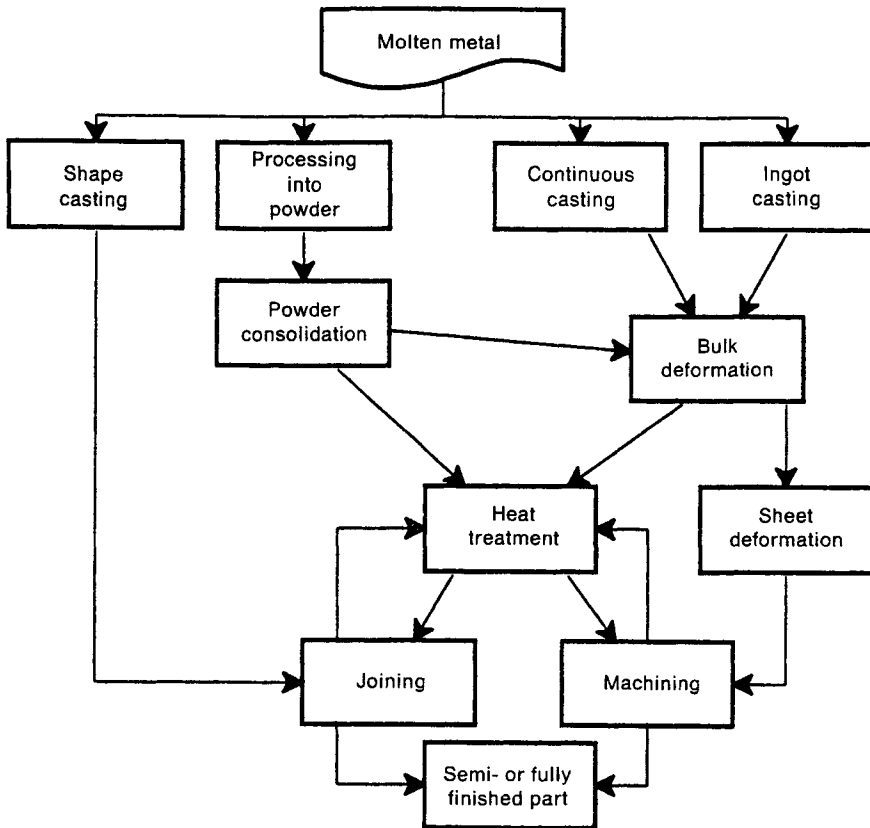


Fig. 1.8 Major secondary metalshaping processing routes.

1.8 Problems

- 1.1 List the four basic raw materials used in making pig iron and explain their functions.
- 1.2 Describe the operation of an electric arc converter and list the advantages or disadvantages of this type of steel converter compared to other types of steel converters.
- 1.3 List the types of steel converters and give the primary advantage for each of the steel conversion processes.
- 1.4 Identify the similarities and differences between the Bessemer steel converter process and the basic oxygen converter process.
- 1.5 Explain why steels produced in open hearth or basic oxygen furnaces can have a lower nitrogen content than steel produced in a Bessemer converter. Why is a low nitrogen content desirable?
- 1.6 Identify the major products of the Bayer and Hall–Héroult processes.

- 1.7 Identify three primary manufacturing processes not discussed in this chapter.
- 1.8 Discuss the difference between primary and secondary manufacturing.
- 1.9 Why is steel one of the most important materials used in engineering design?
- 1.10 What is pig iron? How is it produced?
- 1.11 Why is external fuel not needed in the basic oxygen steelmaking process?

Solidification and casting processes

2.1 Introduction

Perhaps the most basic method of metal shaping is to pour a melt of liquid metal into a formed mould to cool into a solid part, namely casting. Casting processes must be well controlled to ensure sound products. This requires appropriate preparation of the liquid and solidification in a quiescent manner. The casting and solidification processes involve pouring and cooling the liquid metal. Therefore, in addition to the metallurgical knowledge required to understand the evolution of the microstructure and mechanical properties during casting, a knowledge of the heat transfer and fluid mechanics occurring during pouring and cooling is also necessary. In this chapter the most common casting processes are described and the basic metallurgy, heat transfer and fluid mechanics principles are introduced to provide a basic understanding of casting processes and the mechanism of solidification.

2.2 Major casting techniques

There are many casting methods in commercial operation. Consistent with the presentation in Chapter 1, and the fact that steel and aluminium alloys are the two most common engineering metals, the following discussion focuses on these two metal systems. However, many of the processes presented can be applied to other metals and alloys. To simplify the presentation, the various methods are grouped into three generic classifications as follows.

2.2.1 Ingot casting

The ingot casting of steel and aluminium consists of producing relatively simple cross-sectional shapes, such as 15 cm diameter circles or rectangles up to 60 cm by 150 cm, in various lengths. Typically ingots are less than 10 m long, weighing from several hundred to several thousands of kilograms.

Steel ingots are poured in large moulds, which are usually tapered to facilitate removal. The moulds are commonly made from graphite or blast furnace pig iron.

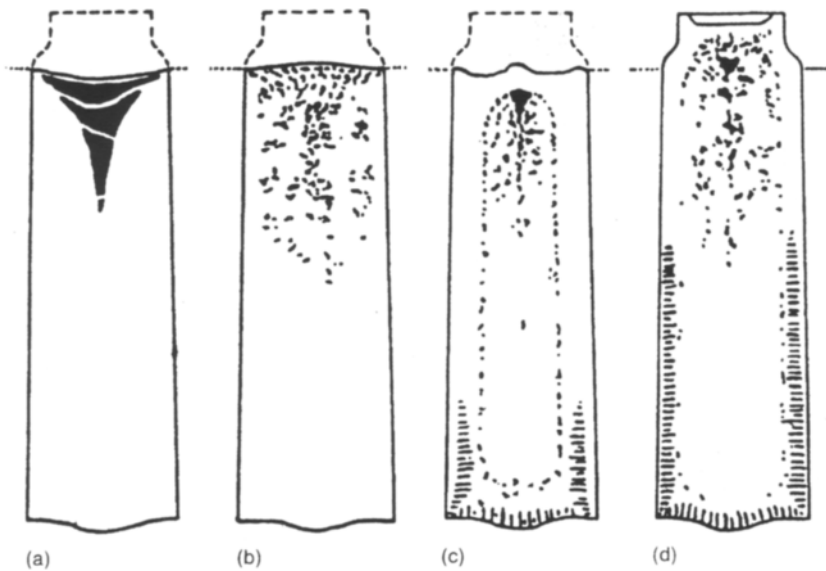


Fig. 2.1 Steel ingot structures: (a) killed steel ingot; (b) semikilled steel ingot; (c) rimmed ingot; and (d) capped ingot. (Reproduced courtesy of The AISE Steel Foundation.)

Although the fundamental process of steel casting is relatively straightforward, several issues require special attention. One of these is the control of imperfections and porosity, which may occur during solidification due to the evolution of gases (primarily oxygen, but also hydrogen, carbon dioxide etc.) dissolved within the liquid steel. The degree of gas that evolves results in four generic types of steel ingots.

Killed steel is fully deoxidized prior to pouring into the casting mould. The dissolved gases in the liquid steel react with the deoxidizing agents that are added to the melt before pouring. Deoxidizing agents are typically aluminium, silicon, ferro-silicon or ferromanganese. Deoxidizers have a higher affinity for oxygen and form metallic oxides, which float to the top of the molten bath to form a *slag* layer. In this manner, when the steel is poured into the mould and solidifies, the concentration of dissolved gases is sufficiently low that during solidification gas bubbles or *blowholes* do not form and an ingot free of porosity is produced. A *pipe* develops due to the liquid–solid shrinkage (Fig. 2.1(a)) which is usually removed and discarded prior to further processing. Pipe formation is discussed later in this chapter. Almost all steel grades containing $>0.3\%C$ are killed.

A *semikilled* steel is partially deoxidized and thus contains some blowholes, usually concentrated near the top of the ingot. This is because the static pressure exerted by the liquid steel, due to gravity, prevents porosity formation in the lower half of the ingot (Fig. 2.1(b)). Typically, the volume of the blowholes resulting from gases trapped within the solidified ingot compensates for the shrinkage due to solidification, and consequently pipe formation is minimized. Therefore, compared to killed steels, the yield is larger, but the quality is lower. Most steels containing between 0.15 and 0.3% C are semikilled.

In a *rimmed* steel, sufficient deoxidizing agents are added prior to pouring to provide only minimal control over the gas level. Sufficient gas evolves from the liquid

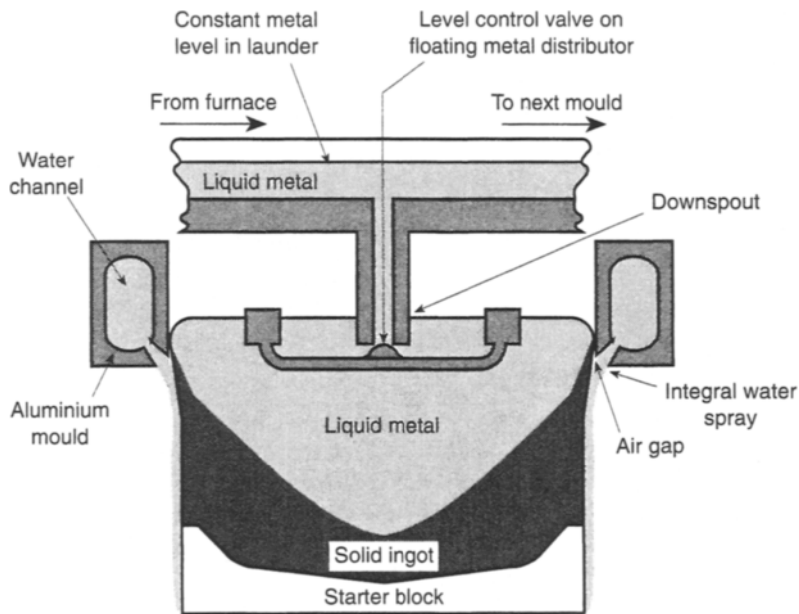


Fig. 2.2 Diagram of the direct chill casting process for aluminium ingots.

steel after pouring that a strong boiling action or *rimming* occurs. The gases evolved form blowholes even in the bottom half of the ingot (Fig. 2.1(c)). Most steels containing between 0.06 and 0.15% C are rimmed steels. Rimmed steels have the desirable characteristic of an outer ingot skin of relatively clean metal. However, this depends on the skill of the steelmaker.

Capped steels are variants of rimmed steels. After pouring the metal into the mould, the rimming action is allowed to proceed for about 1 min, at which time a cap is placed over the open end of the ingot mould, essentially stopping the rimming action. In this manner, an outer surface relatively free of blowholes is produced (Fig. 2.1(d)), and compositional segregation that occurs in the ingot centre is reduced compared to a rimmed ingot. The phenomenon of compositional segregation is discussed later in this chapter. This process is particularly advantageous for steel with $>0.15\%C$.

Aluminium ingots are cast using the *direct chill* (DC) process, shown schematically in Fig. 2.2. In DC casting the aluminium is poured into a shallow water-cooled mould. When the metal begins to solidify, the starter block is lowered at a controlled rate (typically about 9 cm/min) and water is sprayed onto the surface of the freshly solidified metal as it exits the mould. In this manner, the outer periphery of the ingot is solidified by heat transfer through the mould, while the bulk of the ingot is solidified by the water spraying on the outer ingot surface. Typically, several ingots will be cast simultaneously from one stream of molten aluminium. A disadvantage of DC casting is that the outer layer has a different metallurgical structure than the inner regions because of the difference in solidification rate caused by the two-step cooling. Consequently, the surface layers of the ingot must be *scalped* or machined away prior to further processing. This disadvantage can be eliminated if the water-cooled mould is

replaced by an electromagnetic field that produces horizontal forces which hold the liquid aluminium in place. This eliminates the mould, and the formation of an outer layer with a different metallurgical structure, resulting in improved quality and efficiency. Excellent control of all pouring and casting parameters are necessary with electromagnetic casting, but the improved quality of the ingot produced has made it the favoured technique for the production of high quality aluminium products, such as ingots that eventually end up as beverage cans.

Cast ingots are almost always processed into semifabricated products such as coils, forging preforms, extrusions etc., using one of the bulk deformation processes outlined in Chapter 4.

2.2.2 Continuous casting

The casting of ingots is essentially a batch process, that produces large sections requiring substantial subsequent processing. Large mechanical equipment that has high construction and operational costs are necessary to break down most ingots. To reduce these costs, *continuous casting* procedures have been developed for both ferrous and nonferrous metals. Much smaller cross-sectional shapes can be produced directly from the liquid metal with the continuous casting process, thereby eliminating the handling and processing problems associated with large ingots. The benefits of continuous casting were identified by Sir Henry Bessemer, but it took nearly 100 years to overcome the various technical difficulties before there was any significant commercialization.

The equipment arrangement for the continuous casting of steel varies, depending on the product to be produced (slab, bar, rod etc.). Fig. 2.3 is the arrangement for the continuous casting of slab. Although an advantage of continuous casting is a reduction in the size of the equipment required, compared to ingot casting, steel continuous casting operations are still large in scale, with the total height of the equipment shown in Fig. 2.3 typically about 30 m. The continuous casting operation begins by hoisting a ladle of appropriately treated liquid steel to the top of the works. Through a stopper/nozzle arrangement in the bottom of the ladle, the steel is poured into a *tundish*. The tundish serves as a reservoir in which the steel resides for about 10 min. This allows empty ladles to be replaced without stopping the casting process and helps to improve the steel quality as impurities float to the top of the tundish, forming a slag. A steady stream of molten metal flows out of the bottom of the tundish into a water cooled copper mould, that has the cross-sectional shape of the *strand* to be cast. As the metal passes through the mould sufficient heat is removed so that the outer periphery of the strand is solidified. After exiting the mould, multiple water jets play onto the strand to solidify its core.

Once solidification is complete, various pinch rolls, straighteners and other such equipment are used to control the movement of the solid strand. It is then reheated and cut into manageable lengths of 6–12 m. The solid strand is usually curved from a vertical to horizontal orientation to save space in the works. Control of the process is essential: if the primary cooling of the strand by the mould is inadequate or if metal is passed through the mould too quickly, the outer periphery will not solidify enough to retain the still liquid core. In such a circumstance, the liquid

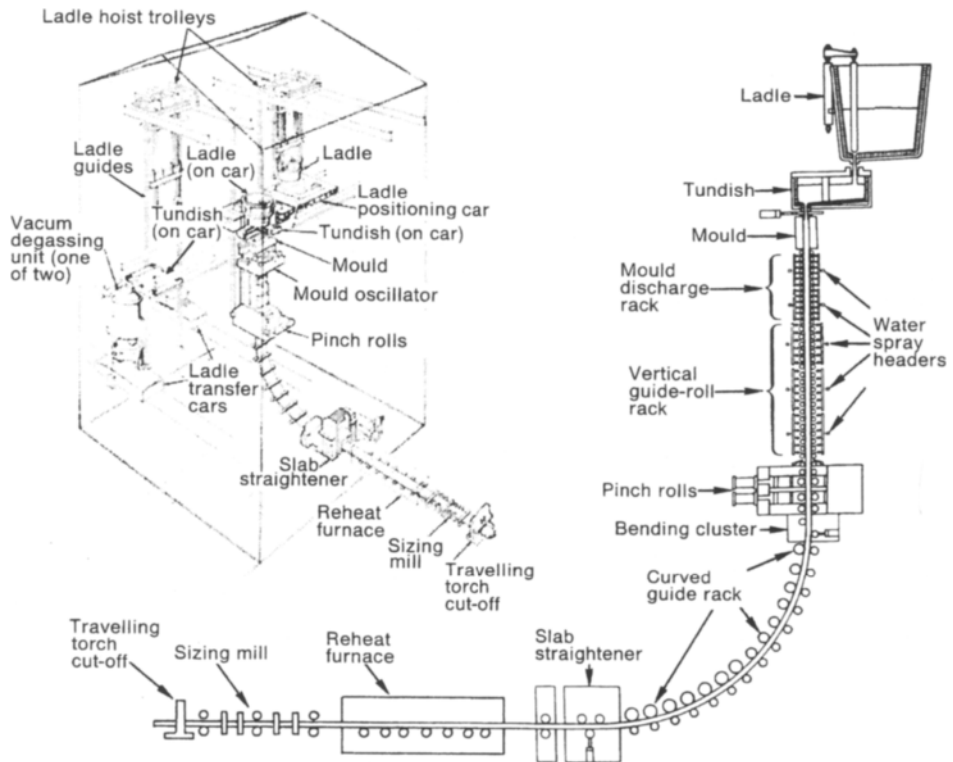


Fig. 2.3 Schematic cross-section of a continuous slab caster for the production of a single slab strand. The inset shows the general arrangement of equipment in the works. (Reproduced courtesy of The AISE Steel Foundation.)

core can break out, due to a substantial pressure head, and spill over the adjacent equipment causing expensive damage and safety hazards. The continuous casting machine shown in Fig. 2.3 is capable of producing a slab shaped strand up to 25 cm thick and nearly 200 cm wide. Nearly 3000 t can be cast continually without stopping.

Despite the technical challenges of continuous casting steel, the advantages of the technique have made it a popular process. Approximately three-quarters of the steel produced world-wide is now continuously cast. In countries where there is a modern well-developed steel industry the percentage is much higher. For example, in Canada more than 30 continuous casting machines account for more than 96% of steel production. Often continuous casting machines are operated in conjunction with an electric arc furnace to recycle scrap steel into useable products. This combination is usually referred to as a *mini-mill*.

The commercialization of nonferrous metal continuous casting preceded the continuous casting of steels, as the lower melting temperature of many nonferrous metals (e.g. aluminium, copper, lead, zinc) reduced the technical challenges. There are several continuous casting methods for nonferrous metals, some of which produce a thin strip (<3 mm) in widths up to 180 cm. One of the more common nonferrous

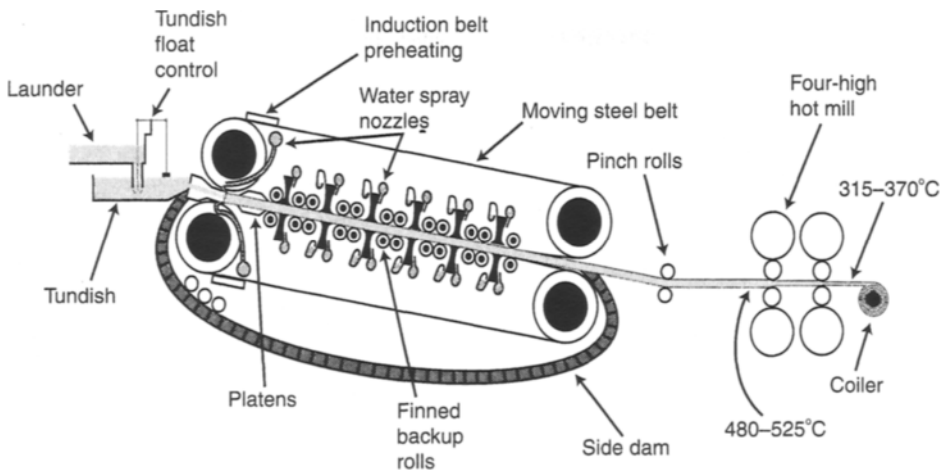


Fig. 2.4 Diagram of Hazlett strip casting machine for nonferrous metals. (Reproduced courtesy of Hazlett Strip-Casting Corp.)

techniques is the Hazlett caster shown in Fig. 2.4. In this process, molten metal is introduced between two mild steel endless belts. The belts move parallel to each other, forming conveyor-like walls. The molten metal is rapidly solidified by water, which is circulated at high velocity on the opposite side of the steel belts. The strip produced is usually delivered to rolling mills that are operated in conjunction with the caster. Hazlett casters are used for producing aluminium, copper, zinc and lead strip, in thicknesses of about 18–50 mm and up to 130 cm in width.

Although the economics of producing metal slabs, bar or strip via continuous casting are favourable, it has not entirely displaced ingot casting. The metallurgy of many alloys is not suitable for continuous casting, and poor mechanical properties can result. In particular, for alloys with a large temperature range in which both liquid and solid phases exist, control of the solidification process is difficult during continuous casting. This problem can be appreciated by examining Fig. 2.5, where it is clear that solidification is not complete until a location well beyond the mould. Furthermore, when the molten metal first contacts the mould, a thin solid skin forms. However, thermal contraction causes the skin to separate from the mould almost immediately after solidification and the rate of heat withdrawal by the mould quickly drops to near zero. This phenomenon can cause major metallurgical and process control problems, which limit the range of alloys that can be continuously cast. For example, despite intensive efforts, the aluminium alloy widely used for beverage cans cannot be successfully continuously cast to meet the demands of beverage can production.

2.2.3 Shape casting

Many complex shapes cannot be produced by ingot or continuous casting because of geometrical or economical constraints. Shape casting is often the method of choice for

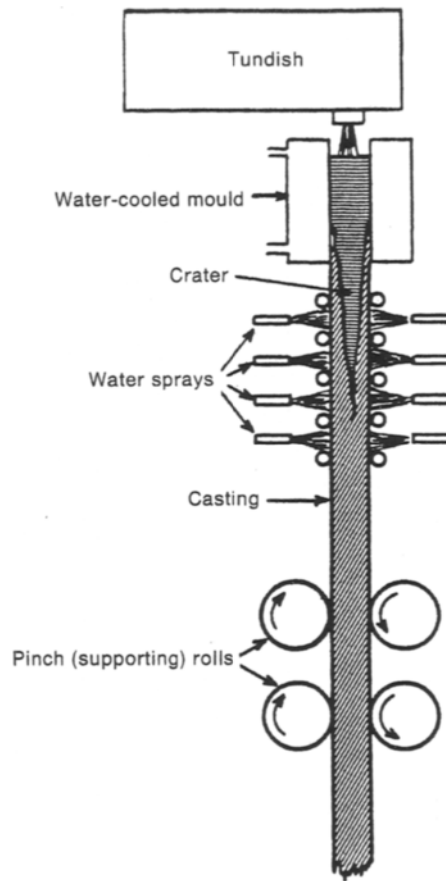


Fig. 2.5 Diagram showing detail of liquid–solid transformation during continuous casting. (Reproduced courtesy of The AISE Steel Foundation.)

the manufacture of complex items, such as automotive engine blocks, wheels and pistons such as the one shown in Fig. 2.6. Essentially, in shape casting, molten metal is poured into a mould that has been formed into the shape of the part required. Shape casting differs from ingot or continuous casting in that bulk deformation processes are rarely used to achieve the desired geometry. Most shape-cast parts require some subsequent finishing, usually removal of the molten metal feeding system, cleaning and finish machining of some surfaces.

A myriad of shape casting techniques are used to produce a large variety of parts, and such facilities are much more common than ingot or continuous casting operations. In part this is because of the relatively low capital cost required for some shape casting techniques and the fact that lower tonnages can be cast economically. The following sections provide a brief description of the major shape casting techniques, but it should be mentioned that this is far from a complete description of the techniques available.

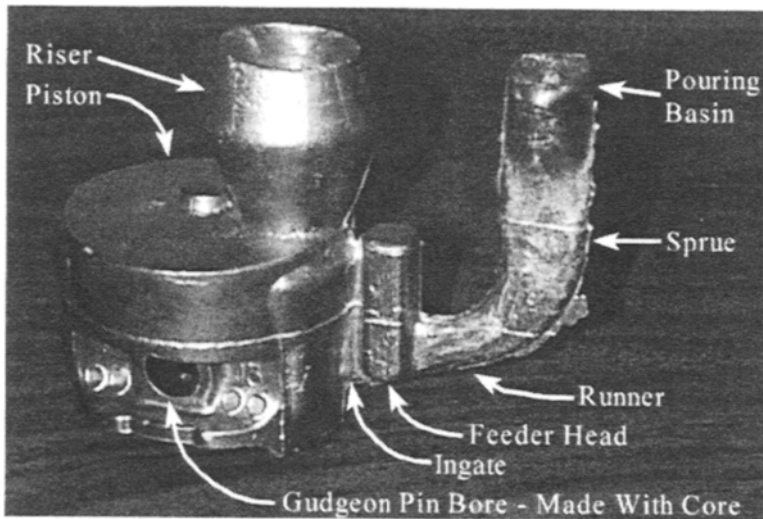


Fig. 2.6 Casting of a piston for an internal combustion engine with feeding system and riser still attached.

Sand casting

Sand casting, the most basic and widely used method of shape casting, has a history dating back to pre-biblical times. As the name implies sand is used as the mould material. The process has the advantages of low capital investment, design flexibility and large alloy selection. The major steps involved when sand casting a pipe with an integral flange are illustrated in Fig. 2.7. A split wooden or metal master *pattern* is made of the shape to be cast. One half of the pattern is positioned on a bottom board and surrounded by the *drag* (bottom) half of the moulding *flask* (step 1). A parting compound (step 2), such as talc, is sprinkled over the pattern to facilitate separation of the pattern from the mould prior to pouring the liquid metal. Often a fine sand is placed against the pattern and then a coarser sand mixture is used to fill the rest of the drag. A fine sand provides a relatively good surface finish on the cast part. The sand is packed tightly to ensure that the shape of the pattern is retained and excess sand removed. The drag is inverted and the top half, or *cope*, of the mould prepared in the same manner as the drag (step 3).

A feeding system for delivery of the molten metal is formed in the cope. This typically consists of a *pouring basin*, a *sprue* (vertical metal transfer channel), *runners* (horizontal transfer channels) and *ingates* connecting the runners to the mould cavity. The feeding system can be made part of the pattern or can be carved into the split mould after the pattern has been removed. In addition to the feeding system, *riser* cavities are designed into strategic positions, as shown in Fig. 2.7. These serve as reservoirs of molten metal which are fed into the casting as it cools to compensate for solidification shrinkage.

The cope and drag are separated and the pattern removed (step 4). A *core* of sand mixed with resin or ceramic is placed in the mould to form the hollow of the pipe. The strength of the core must be higher than the rest of the mould to prevent damage from the inrush of molten metal. The cope and drag are reassembled (step 5) and clamped together, ready for receipt of the metal. The metal is poured from a small ladle into

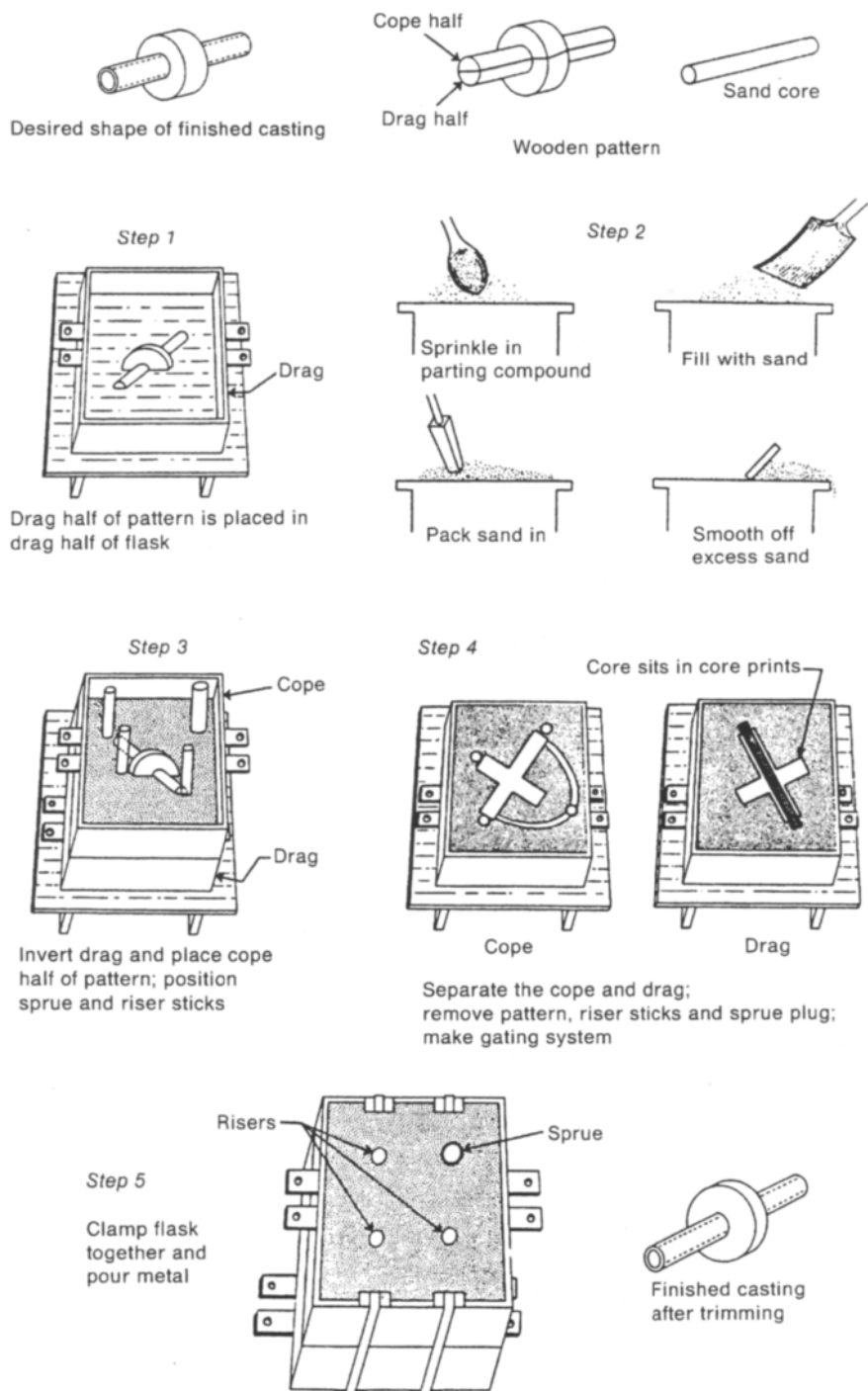


Fig. 2.7 Steps involved in processing a sand casting. (Reprinted with the permission of ASM International, Materials Engineering Institute.)

the sprue, flows into the mould cavity and solidifies. Once solidification is complete the mould is broken and the cast part removed, all sand cleaned off and the riser and feeding system are cut away.

To sand cast complex shapes, the sand must be sufficiently strong to hold the mould shape. One technique to achieve this is the so-called *CO₂ technique*, in which *water glass* ($\text{Na}_2\text{SiO}_2 \cdot n\text{H}_2\text{O}$) is added to the sand. After making the mould, CO_2 is forced to permeate the sand, causing a reaction which forms Na_2CO_3 and a gel of $x\text{SiC}_2 \cdot n\text{H}_2\text{O}$. The gel serves as a bonding agent and provides a firmer sand mould. This offers the advantage of better dimensional tolerances and improved surface finish.

Although the sand casting of simple shapes, such as that of Fig. 2.7, is easily visualized, the process is also used for complex-shaped parts where the mould design is a good deal more intricate. Automobile engine parts, such as crankcases and cylinder heads, have been sand cast since the beginning of the automobile industry. Initially these parts were sand castings of *cast iron*, but are now mostly aluminium silicon alloys. The sand casting process for automotive components continues to be refined, as exemplified by the recently introduced *Cosworth process*, outlined at the end of this chapter.

Permanent mould casting

A disadvantage of sand casting is that a new mould is required for every part cast. Although this may be acceptable where production quantities are small, it is often unacceptable for large-scale production, for which a permanent mould is more suitable. In its simplest form permanent mould casting involves pouring the metal into a mould that is usually metallic and can be reused many times. This can complicate the mould design considerably and increase the mould cost, because provision must be made to remove the casting without breaking the mould. The metallic mould must be made of a metal with a higher melting temperature than that of the metal being cast. This limits the use of the permanent mould casting process for steels.

A major advantage of permanent mould casting is the high thermal conductivity of metallic moulds compared to sand moulds. This causes rapid solidification and cooling, which in turn results in a smaller grain size and refined microstructures. These features contribute to improved strength for permanent mould cast parts. In addition, the metallic mould offers better dimensional tolerances and an improved surface finish compared to sand castings. These advantages must be balanced against the increased cost of permanent mould casting.

There are several methods of permanent mould casting, the simplest of which is *gravity casting*. This process is ostensibly the same as sand casting except that the metallic mould is not broken after each part is made. The metal is poured into the top of a mould and fills it with the assistance of gravity only. The major technical challenge compared to sand casting is designing a reusable mould that permits easy removal of the part.

A permanent mould process widely used for rapid, high volume production is *die casting*. Instead of metal being fed into the mould by gravity, the metal is forced into the mould by external pressure. In *low pressure die casting*, a pneumatic pressure of around 0.5–1 atm against the surface of the molten metal forces the metal up a feeding system into the mould cavity, as shown in Fig. 2.8. Note the inherent

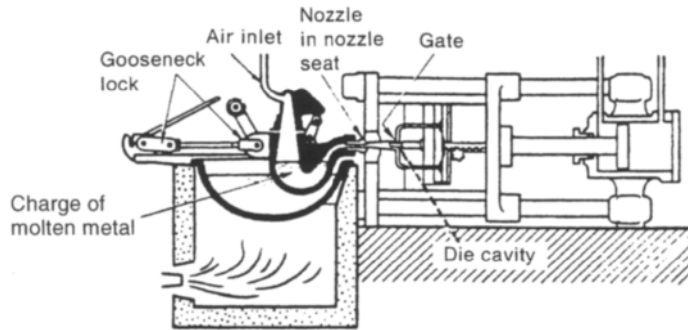


Fig. 2.8 Schematic of a low pressure or gooseneck die casting machine. (Reproduced from *Casting Aluminum*, with permission of Alcan Aluminium Limited.)

complexity of the mould, which must be rigidly clamped during metal filling and subsequently opened for part removal. The low injection pressure requires the use of very fluid alloys which makes the casting more prone to internal porosity than the *high pressure die casting* process of Fig. 2.9. High pressure die casting makes use of a pneumatically or hydraulically actuated plunger to force the molten metal into the die cavity with much higher pressure than possible during low pressure die

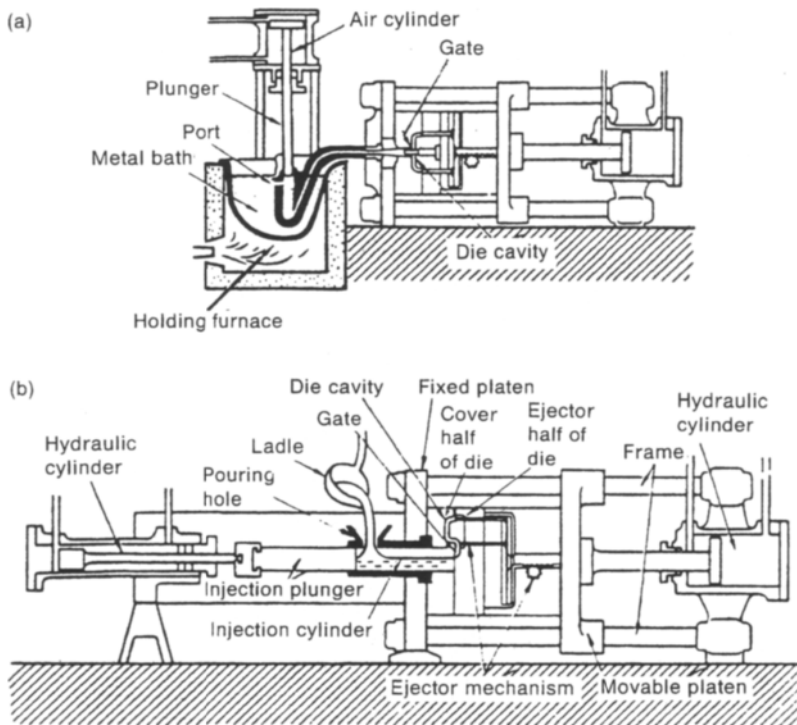


Fig. 2.9 High pressure die casting machines utilizing (a) a holding furnace or (b) a ladle and plunger for filling the die cavity. (Reproduced from *Casting Aluminum*, with permission of Alcan Aluminium Limited.)

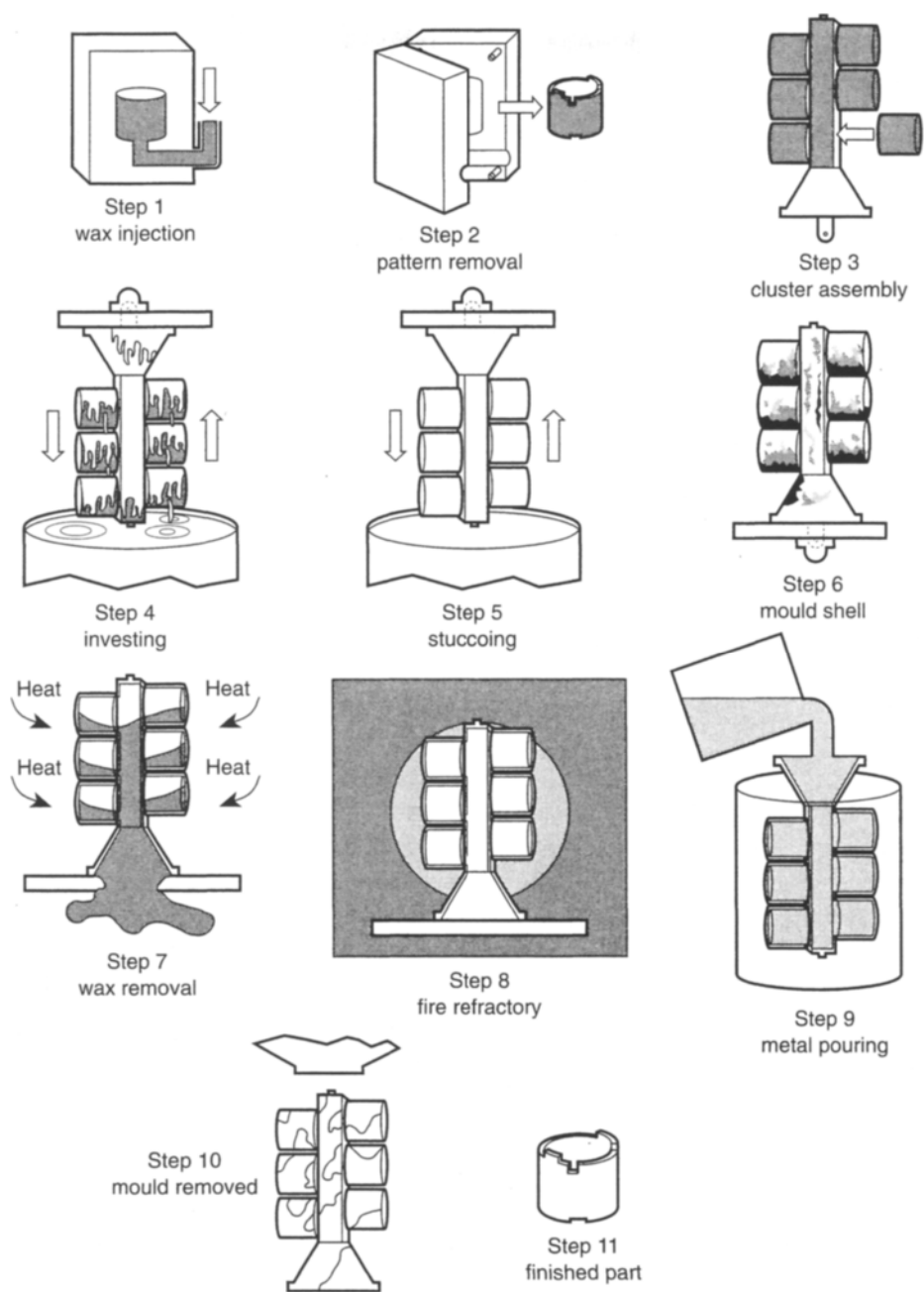


Fig. 2.10 The steps involved in investment casting. (Reproduced by permission of the Investment Casting Institute.)

casting. High pressure die casting is therefore more suitable for complex shapes and internal porosity is reduced. For the die casting of aluminium alloys the holding furnace of Fig. 2.9(a) is often eliminated because of reactions between the molten aluminium and the injection plunger and cylinder. Instead of the holding furnace, sufficient liquid aluminium for one casting is fed into the feeder tube using a ladle. This type of die casting process is used for the manufacture of many aluminium automotive components, such as the piston illustrated in Fig. 2.6. The use of a ladle, rather than metal injection, can increase the cycle time, making the process less productive. Sometimes, to avoid reduced productivity, a different feed metal is substituted for aluminium, as is sometimes the case for automobile carburettors or throttle body fuel injectors which are often die cast from zinc-based alloys.

Investment casting

The investment or lost wax casting process produces parts with dimensional tolerances and surface finishes unmatched by other casting processes. This casting technique dates back to Egyptian times (1500 bc) when it was used to make ornate bronze bowls and vases. Today, complex shapes, such as internally cooled gas turbine blades, are manufactured using investment casting without the requirement for extensive final machining or finishing operations. Indeed, the alloys used for manufacturing gas turbine blades are extremely difficult to machine, which makes investment casting particularly useful for these parts.

The complex process of investment casting is illustrated in Fig. 2.10. Initially a mould is used to prepare a wax pattern of the part to be made (step 1). The wax pattern is made using a process similar to that of gravity or die casting. Individual patterns are assembled, using wax, into a cluster of several patterns (step 3). The cluster is dipped or invested (step 4) in a refractory slurry (one definition of the word 'invest' is 'to cover') and then the refractory strengthened by stuccoing (step 5). This yields a refractory mould containing the wax patterns (step 6), which are subsequently melted and the wax collected for reuse (step 7). The refractory mould is strengthened by *firing* at high temperature (step 8) and then finally molten metal is poured into the mould (step 9). Once the metal has solidified, the refractory mould is broken revealing the cluster of cast parts (step 10), and each part is then removed from the cluster (step 11). Although this process may seem overly tedious, no other technique exists for manufacturing the intricate shapes of many gas turbine components.

Sand, permanent mould and investment casting are only three of a myriad of casting processes. However, these three processes exemplify the vast array of casting techniques and products that can be produced this way. Several casting processes are unique to particular industries or products, and the number, diversity and efficiency of casting processes are continually evolving.

2.3 Solidification mechanism

It is clear from the preceding section that many casting techniques are available for metal solidification. However, the fundamental solidification mechanism for all casting processes is similar. In the relatively short time required for a casting to solidify,

the initial micro- and macrostructure of the cast part is formed. As alluded to in previous sections, these structural elements control many of the properties of the casting and the response to subsequent forming operations. Therefore, it is important to understand the metallurgical mechanisms that occur during solidification and cooling.

2.3.1 Solidification of pure metals

The solidification of a solid phase from a liquid invariably requires the creation of new surfaces that separate the liquid and solid phases. Energy is required to produce these new surfaces. Therefore, *surface energy* is associated with the liquid–solid interface. This is analogous to the energy associated with a grain boundary surface in a solid. The energy to create new surfaces requires that liquids cool below their equilibrium freezing temperature or that they are *undercooled*, before solidification begins, as illustrated in Fig. 2.11. Solidification will occur more spontaneously if there is a high degree of undercooling. The degree of undercooling necessary for solidification is minimized if existing surfaces are present, which act as nuclei for solid crystals. As such, when a metal is poured into a cooler mould, the mould walls act as the initial nuclei for solidification. In this manner, many small *chill crystals* with random crystallographic orientations nucleate along the mould walls, as shown in Fig. 2.12.

The conduction of heat from the liquid through the chill crystals to the cooler mould creates a temperature gradient within the newly formed solid phase. Additionally, the *latent heat of solidification* is released at the solid–liquid interface, creating the temperature profile shown in Fig. 2.13, with an interface temperature above that of both the liquid and solid phases. Consequently, heat is conducted away from the interface to the solid, as well as to the undercooled liquid.

The steep temperature gradient, ahead of the advancing solid phase, causes the solid–liquid interface to become unstable and protrusions to grow into the liquid

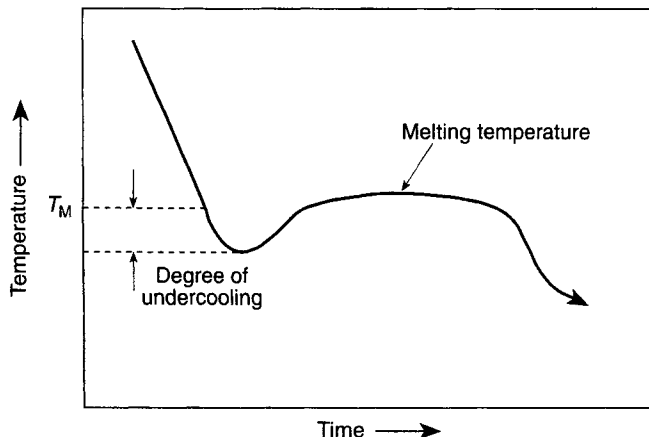


Fig. 2.11 Cooling curve for a pure metal illustrating the degree of undercooling required to initiate solidification.

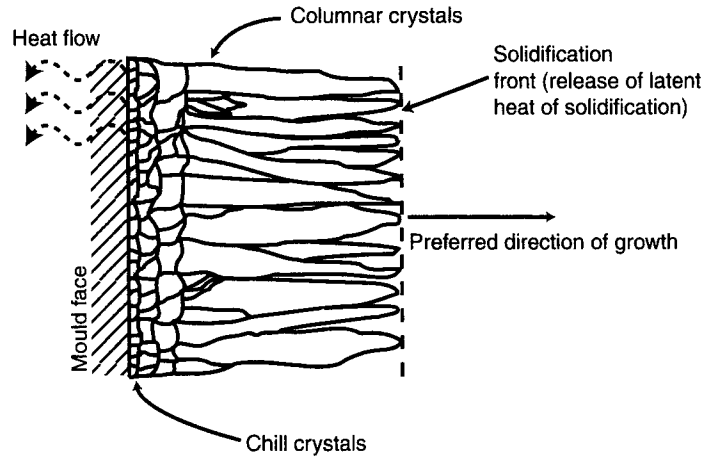


Fig. 2.12 Initial solidification of chill crystals and columnar crystals in a casting.

at a faster rate than would otherwise evolve from a stable interface. The faster growth rate of the protrusions occurs because they are surrounded by more highly under-cooled liquid metal as they grow further from the stable liquid–solid interface. The rapid growth of protrusions from the liquid–solid interface leads to a transition from a flat interface to a *dendritic* structure (Fig. 2.14). The dendrites grow in preferred crystallographic directions, $\langle 100 \rangle$ for cubic and $\langle 10\bar{1}0 \rangle$ for hexagonal metals, and consequently secondary or tertiary dendrite arms often form. In the casting of Fig. 2.12 dendrites grow perpendicularly away from the mould wall, developing into columnar grains. A consequence of the formation of columnar grains is that pure metals often have a cast structure similar to that shown in Fig. 2.15.

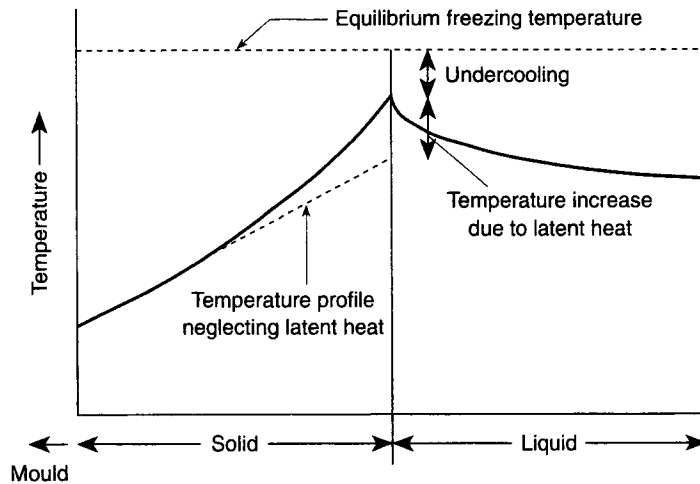


Fig. 2.13 Temperature profile from the mould, through solid chill crystals to the liquid.

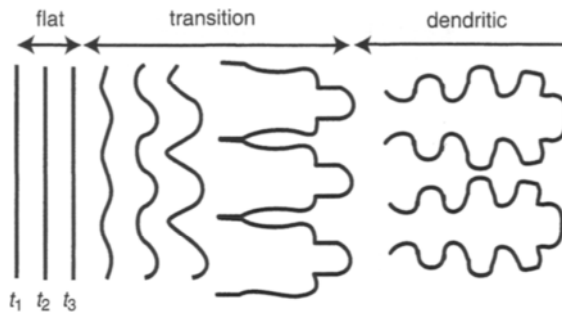


Fig. 2.14 Illustration of transition from flat to a dendritic liquid–solid interface. The mould surface is to the left.

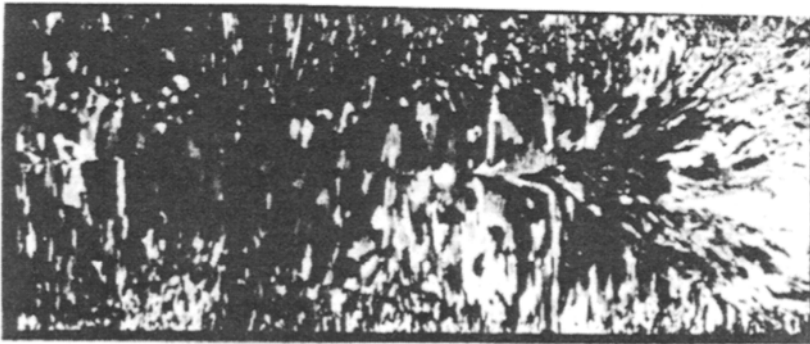


Fig. 2.15 Cast grain structure of a bar displaying chill crystals adjacent to the mould walls, some of which grow into columnar grains. (Reprinted with permission from *Continuous Casting of Non-Ferrous Metals and Alloys*, H.D. Merchant, D.E. Tyler, and E.H. Chia, Fig. 3, page 287, © The Minerals, Metals & Materials Society (TMS), Warrendale, PA, 1988.)

2.3.2 Solidification of alloys

Pure metals solidify at a unique temperature. Alloys, however, solidify over a range of temperatures. For example, the 50 wt% Cu–50 wt% Ni alloy of Fig. 2.16 begins to solidify at 1310°C, the *liquidus* temperature, but does not become fully solid until 1260°C, the *solidus* temperature. During solidification, the temperature range between the liquidus and solidus is referred to as the *mushy zone*, as the metal is in a liquid–solid state. Proper control of the heat transfer from the liquid–solid mushy zone to the casting mould can be difficult, and this can give rise to a number of defects as well as difficulty in controlling the entire solidification process. Difficulties associated with solidification control in the mushy zone regions is the problem that makes continuous casting of alloys with a large mushy zone difficult or impossible with current technology.

The undercooling that occurs during the solidification of pure metals (Fig. 2.11), technically called *thermal* undercooling, also occurs during the solidification of alloys. Additionally, a second type of undercooling – *constitutional* undercooling – occurs in many alloys, compounding the effects of thermal undercooling. Combined,

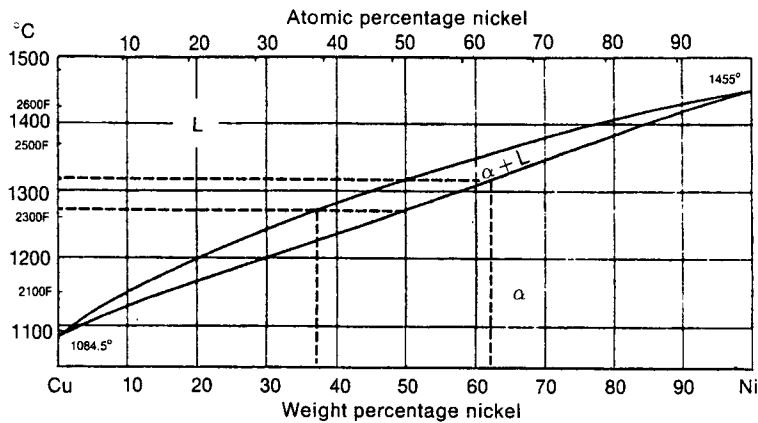


Fig. 2.16 Cu-Ni phase diagram.

these two types of undercooling give rise to a well developed dendrite structure in many alloys. Constitutional undercooling results when the freezing metal has a composition different from that of the liquid from which it is solidifying. To understand this phenomenon, consider the solidification of a 50:50 wt% Cu-Ni alloy (Fig. 2.16). When the temperature of the casting falls to the liquidus line (1310°C) the first solid to appear has a composition of 62 wt% Ni, but the liquid has a composition of 50 wt% Cu. At a temperature just above the solidus (1260°C) the solidifying product has a composition of about 50 wt% Cu, while the liquid remaining has a composition around 37 wt% Ni. In other words, the first solid is Ni rich, whereas the liquid is enriched in the low-melting-point component, in this case Cu. As a consequence of compositional differences between the solidified and liquid phases during solidification, the dendrite arms can have substantially different compositions from the metal that solidifies in the *interdendritic regions*. Local compositional differences resulting from cooling through two phase regions is termed *microsegregation* or *coring*. The Cu-Ni alloys are part of a family of corrosion-resistant alloys known as *monels*. When they are cast, coring causes a considerable decrease in the corrosion resistance. In many alloys the mechanical properties can also be seriously degraded by coring.

Like the solidified structure of pure metals, chill crystals and columnar grains also develop during alloy casting. As a consequence of the combined effects of thermal and constitutional undercooling, solidification nuclei can form in the central regions of an alloy casting. Thus, solidification in this central region can occur by the formation and growth of new grains, rather than continued growth of columnar grains from the mould wall. This mechanism leads to randomly oriented, equiaxed grains in the central region shown in Fig. 2.17. The grain structure here is generally coarser than the chill crystals that form at the mould wall.

Columnar grain boundaries are favourable sites for embrittling impurities and porosity, which gives rise to poor mechanical properties and formability. Often casting is only the beginning of the fabrication process and the subsequent plastic forming operations, such as forging, may eliminate the columnar structure through deformation and recrystallization. Nevertheless, in most castings a *grain refiner* is added

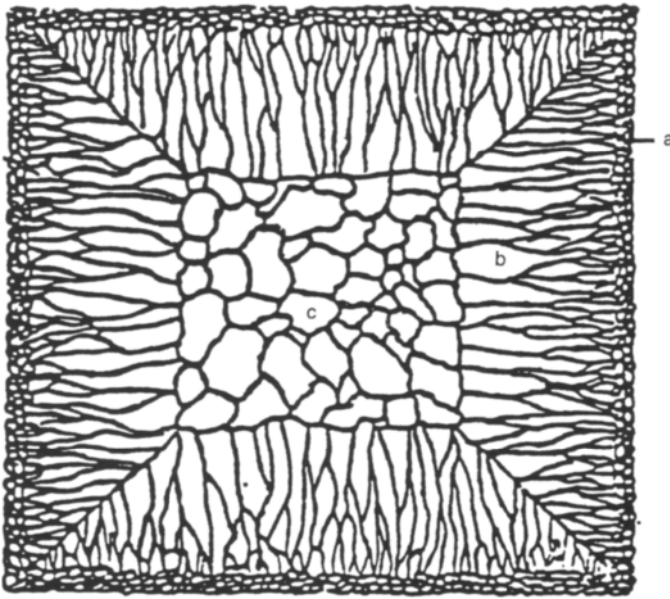


Fig. 2.17 Sketch of solidified grain structure of an alloy: (a) chill crystals; (b) columnar grains; and (c) region of coarse equiaxed grains in centre.

during solidification to provide uniform nucleation of grains throughout the casting. Vanadium is an effective grain refiner for steel, whereas titanium and niobium can be used for light metals such as aluminium and magnesium as well as steel. Most direct chill or continuously cast aluminium is grain refined by the addition of titanium diboride. Appropriate additions of grain refiners during casting can completely eliminate the formation of columnar grains and produce a uniform equiaxed grain structure throughout the cast thickness, such as that illustrated in Fig. 2.18.

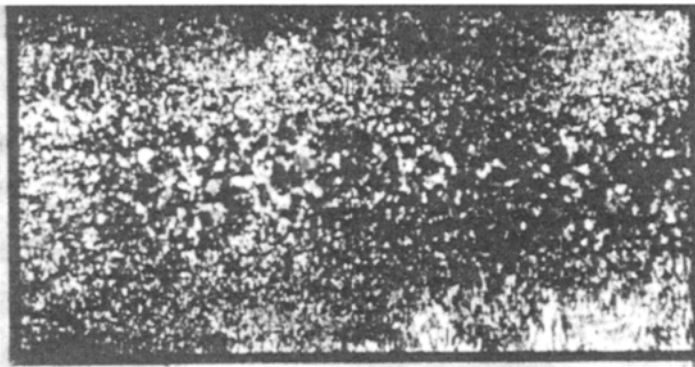


Fig. 2.18 Cast structure of the same alloy as Fig. 2.15, but with a fine grained equiaxed structure throughout. (Reprinted with permission from *Continuous Casting of Non-Ferrous Metals and Alloys*, H.D. Merchant, D.E. Tyler, and E.H. Chia, Fig. 3, page 287, © The Minerals, Metals & Materials Society (TMS), Warrendale, PA, 1988.)

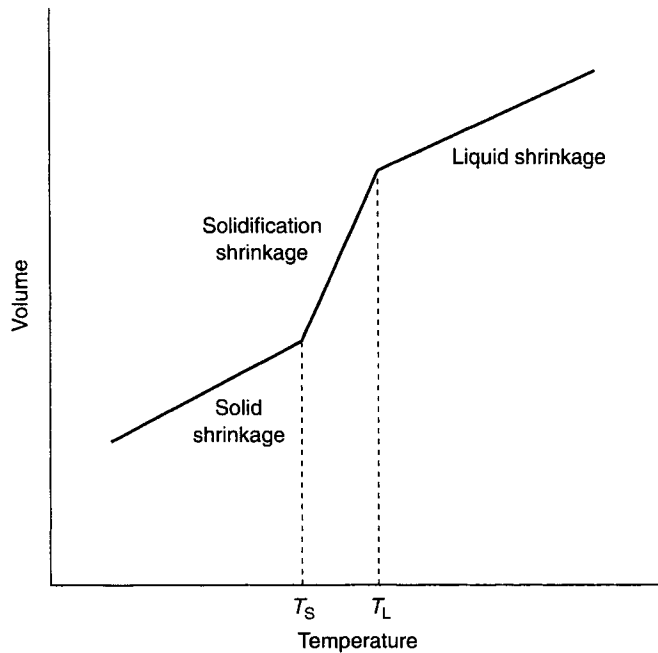


Fig. 2.19 Changes in volume as a metal alloy solidifies.

2.4 Solidification volume shrinkage

As a metal casting solidifies and cools, the volume decreases, as shown in Fig. 2.19. The reader may wish to consider why the volume of most metals decreases on solidification, whereas the volume of water increases when it changes to ice. There are three major contributions to volume shrinkage: liquid shrinkage, solidification shrinkage and solid shrinkage. The amount of shrinkage occurring for a few common metals is listed in Table 2.1. Liquid shrinkage does not cause casting problems, as long as sufficient metal is available to fill the shrinkage cavity. To account for solidification shrinkage the casting pattern must be oversized appropriately and risers added to prevent the formation of shrinkage cavities during solidification.

The effect of solidification and solid shrinkage is illustrated by sand casting a cube, as shown in Fig. 2.20. The casting first forms a solid skin at the mould–liquid interface as it begins to solidify (Fig. 2.20(b)). This effectively isolates the liquid remaining in the central region of the cube. As this material solidifies, it shrinks and a void forms

Table 2.1 Solidification and solid shrinkage for casting metals

Metal	Solidification shrinkage (%)	Coefficient of thermal expansion (α)	Solid shrinkage (%)
Aluminium alloys	7	25×10^{-6}	6.7
Cast iron	1.8	13×10^{-6}	4
Steel	3	14×10^{-6}	7.2
Copper alloys	5.5	17×10^{-6}	6

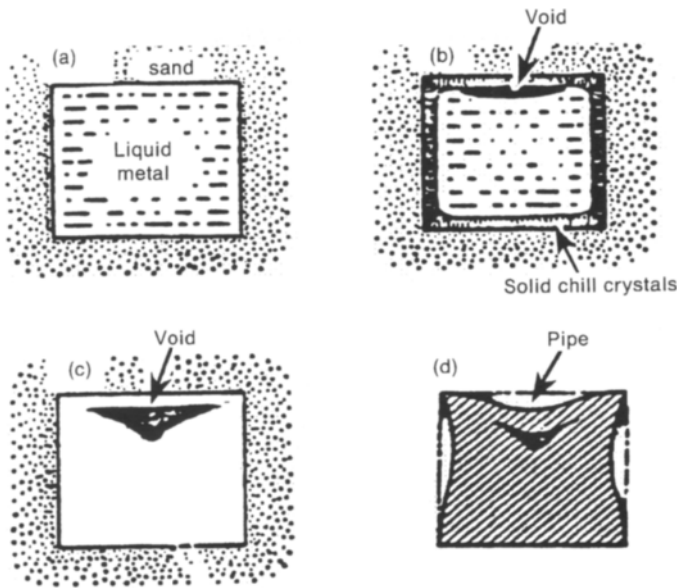


Fig. 2.20 Shrinkage occurring during sand casting of a cube (see text for explanation).

(Fig. 2.20(c)). Void formation in this manner is termed *macroporosity*. Further solidification and solid shrinkage causes distortion and produces a solidification *pipe* at the top of the cube (Fig. 2.20(d)).

To prevent macroporosity and pipe formation, risers are used which act as a source of liquid metal to compensate for the solidification shrinkage that would otherwise form. A cube casting incorporating a riser is shown in Fig. 2.21. As the casting

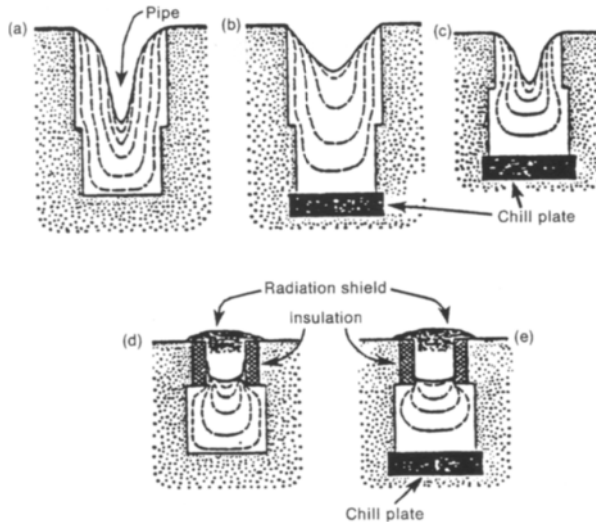


Fig. 2.21 Sand casting the same cube as Fig. 2.20, but with a riser (a), chill plate (b) and (c), insulation and radiation shield (d), and all three (e).

solidifies and shrinks, liquid metal from the riser is drawn into the casting. In this manner, the voids and solidification pipe form in the riser rather than in the casting. This requires that the riser does not solidify prior to the casting. In effect, risers represent excess metal to the casting which must be removed. Therefore, it is necessary to minimize their size and number. Metal chills, insulation and radiation shields can be used to modify the heat transfer, thereby minimizing the riser size required (as shown in Fig. 2.21).

Example 2.1 Solidification shrinkage and safety of ingots for remelting

During processing some products may undergo more than one melting and casting operation. Sometimes this is done to improve the metallurgical structure of the product, but more often so that large quantities of metal can move through industrial processes in an efficient manner. For example, it is not practical to produce a large number of finished products at a large primary smelter. Instead, a number of ingot sizes are produced from primary operations that can then be transported to other facilities for remelting and casting into semifinished or fully finished forms. One of the common ingot forms produced at aluminium smelters is the *sow*. It is produced by pouring aluminium, taken directly from the pots in a ladle, into an open steel mould, such as that shown in Fig. E2.1. Each sow weighs about 700 kg, and is approximately 1 m square and 0.5 m high. Sows of this size are easily moved by forklifts and trucks. The casting of sows is not unlike the casting of the cube shown in Fig. 2.20, except that instead of a sand mould, a steel mould is used for durability

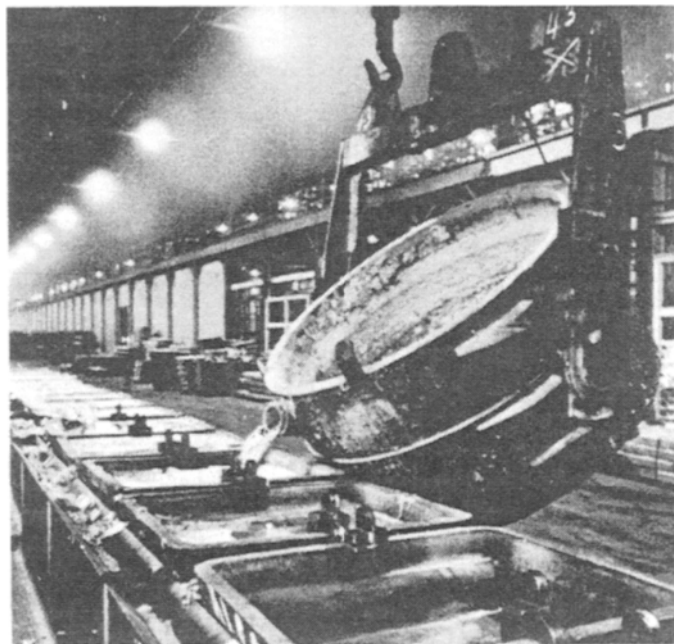


Fig. E2.1 Pouring of sows at an aluminium smelter. (Reproduced courtesy of the Aluminum Association, from *Guidelines for Handling Molten Aluminum*, 1990.)

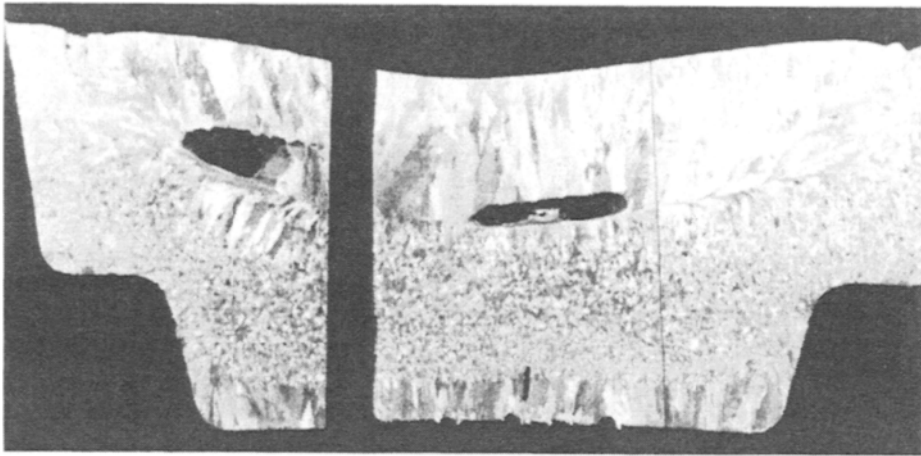


Fig. E2.2 Internal structure of an aluminium sow, revealed by cutting and grinding the sow, followed by etching. (Reproduced courtesy of the Aluminum Association, from *Guidelines for Handling Molten Aluminum*, 1990.)

and reusability. Consequently, the sow exhibits many undesirable features. As seen in Fig. E2.2, the sow has columnar grains around the periphery of the ingot, which are larger at the top surface due to a lower heat extraction rate from this region (heat is absorbed by the steel mould much faster than by the air above the sow). Columnar grains generally have poor mechanical properties but, as the sow is remelted as part of further processing this is of little consequence. Additionally, as in Fig. 2.20, the top of the sow is depressed due to thermal shrinkage. Again, this is of little consequence (sows are sold by weight, not volume).

Most importantly, however, is the occurrence of quite large shrinkage voids or macroporosity inside the sow, as seen in Fig. E2.2. Often cracks that occur along the boundaries of weak columnar grains connect the shrinkage voids to the top surface. Consequently, if the sow is left unprotected in rain or snow, it is possible for water to enter and possibly fill the shrinkage voids. Water inside the shrinkage voids can lead to disastrous results when the sow is remelted. As the sow is heated for melting, the water vaporizes and expands. The expanding vapour cannot escape, because melting of the outer surface of the sow seals the cracks that allowed water to enter. This causes high internal pressures which can cause the sow to break open, potentially exposing water vapour to molten aluminium. Violent explosions of the molten aluminium can occur in these circumstances: first, the rapidly expanding water vapour can eject molten aluminium from the melting furnace; second, the water vapour can react with the aluminium, releasing large amounts of chemical energy. Although this sequence of events may seem unlikely, it does happen, with the typical result shown in Fig. E2.3. These events often lead to needless injury or loss of life.

To avoid such explosions, it is imperative that sows are protected from rain or snow and are stored in dry locations. Additionally, many facilities have drying ovens, in which sows are heated to a temperature below the melting temperature, but high enough to vaporize and drive off any water in the shrinkage voids. This operation

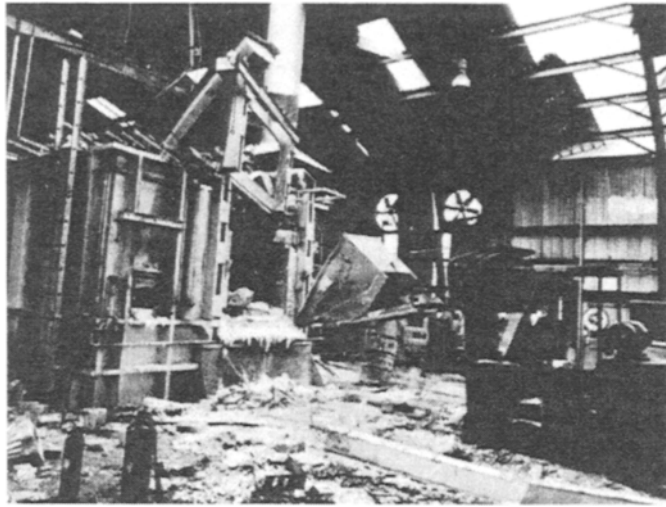


Fig. E2.3 Result of molten aluminium explosion. Note part of casting house roof blown off. (Reproduced courtesy of the Aluminum Association, from *Guidelines for Handling Molten Aluminum*, 1990.)

requires an extended time, which reduces its economic viability, thus making it more important that sows are kept dry. In general terms it is important to avoid any moisture in contact with molten metals for the safety reasons demonstrated by this example.

2.5 Heat transfer during solidification

While a casting is solidifying and cooling, heat is transferred from the metal to the mould. Control of this heat transfer is critical for the production of sound, porous-free castings. In addition, the cooling characteristics have a considerable influence on the grain size and microstructure of the cast part, thereby determining the mechanical properties. As well as these metallurgical factors, the high heat transfer rates inherent in some casting processes can cause large thermal gradients and stresses. Such thermal stresses may cause unacceptable distortion of the mould during solidification, leading to a poor cast shape.

To develop an appreciation of the importance of heat transfer in the casting process, it is advantageous to examine a few basic principles of conductive heat flow. These principles can be demonstrated by considering a simple shape or continuous casting model.

2.5.1 Conductive heat flow during shape casting

To demonstrate the heat transfer during solidification, a simplified one-dimensional model is used (Fig. 2.22). It is assumed that a metal is solidified against a flat mould surface, and that a uniform thickness of solid metal forms at all locations.

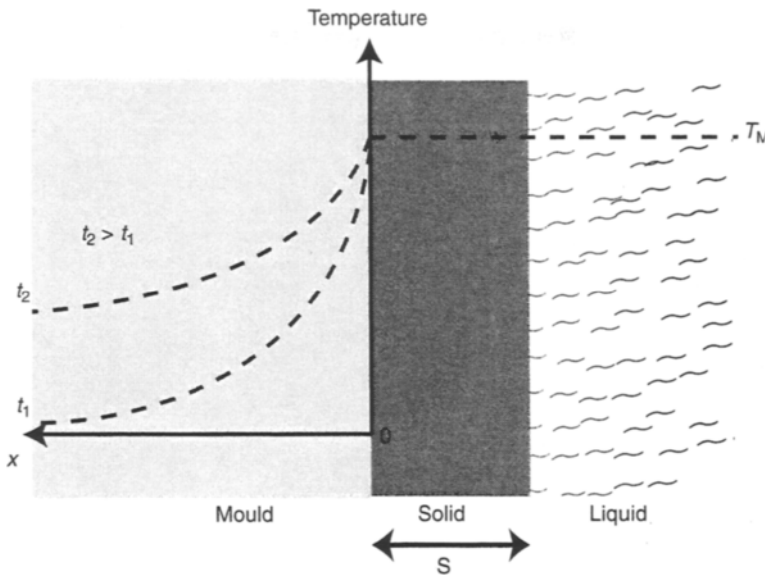


Fig. 2.22 One-dimensional heat transfer model for high conductivity metal and low conductivity mould.

To further simplify the analysis three more assumptions are made:

1. There is no thermal resistance at the casting–mould interface. This assumption is not strictly true for many casting processes, as solidification shrinkage often causes the solidifying metal to pull away from the mould, as shown for the direct cast aluminium ingot shown in Fig. 2.2.
2. No temperature gradient exists within the solid or liquid metal. Again, this assumption simplifies the real physical situation, as there must be a temperature gradient in both the liquid and solid metal or heat would not transfer. However, as the thermal conductivity of the metal is high compared to the thermal conductivity of the mould, temperature differences in the metal are small compared to those in the mould.
3. The mould is semi-infinite in size and the mould thermal properties are uniform.

Also note that the assumption of a planar liquid–solid interface means that dendritic formation has been suppressed. Although these assumptions obviously simplify the real physical situation, they permit a solution to the model of Fig. 2.22 that provides useful information about the solidification process.

It is evident that the heat flux at any distance x in the mould is proportional to the temperature gradient, which may be expressed mathematically as

$$\vec{J} = -k_m \frac{\partial T}{\partial x} \quad (2.1)$$

where: \vec{J} is the heat flux
 k_m is the thermal conductivity of the mould
 T, x are as defined in Fig. 2.22.

42 Solidification and casting processes

The minus sign indicates that heat flows down the temperature gradient (from hot to cold). Partial derivatives are used in equation 2.1 as the temperature gradient is also time dependent. The Fourier relationship for the temperature distribution as a function of time and location is given by

$$\frac{\partial^2 T}{\partial x^2} = \frac{1}{\alpha_{th}} \frac{\partial T}{\partial t} \quad (2.2)$$

where α_{th} is the thermal diffusivity, defined as

$$\alpha_{th} = \frac{k_m}{C_m \rho_m} \quad (2.3)$$

where: C_m is the heat capacity of the mould material
 ρ_m is the density of the mould material.

Thus, the amount of heat that transfers (or diffuses) from one position in a solid to another position is proportional to the thermal conductivity and inversely proportional to the capacity of the material to absorb heat (i.e. acts as a heat sink).

The differential equation 2.2 is common to problems involving transport phenomena in solids, such as heat transfer or atomic diffusion in solids. Although not easily solved, the solution to equation 2.2 has the general form

$$T(x) = A \int \exp\left(\frac{-\lambda^2}{4\alpha_{th}}\right) d\lambda + B \quad (2.4)$$

where

$$\lambda = \frac{x}{\sqrt{t}}$$

The integral of equation 2.4 cannot be evaluated directly, but may be re-expressed using the *Gaussian error function*. This function is useful for solving transport problems in semi-infinite solids. It represents the convergence of the series

$$\text{erf}(z) = \frac{2}{\sqrt{\pi}} \left(z - \frac{z^3}{3 \times 1!} + \frac{z^5}{5 \times 2!} - \frac{z^7}{7 \times 3!} + \dots \right) \quad (2.5)$$

or the integral

$$\text{erf}(z) = \frac{2}{\sqrt{\pi}} \int_0^z \exp(-x^2) dx$$

Values for $\text{erf}(z)$ are listed in Table 2.2. The constants A and B in equation 2.4 are evaluated using the boundary conditions for the model of Fig. 2.22, which are

$$\begin{aligned} T(x) &= T_M \quad \text{at } x = 0 \\ T(x) &= T_0 \quad \text{at } x = \infty \end{aligned} \quad (2.6)$$

Using these boundary conditions, the solution to equation 2.2 is

$$T(x, t) = T_M + (T_0 - T_M) \text{erf}\left(\frac{x}{2\sqrt{\alpha_{th}t}}\right) \quad (2.7)$$

Table 2.2 Gaussian error function

z	$\text{erf}(z)$	z	$\text{erf}(z)$
0	0	1.0	0.843
0.025	0.028	1.1	0.880
0.05	0.056	1.2	0.910
0.1	0.113	1.3	0.934
0.15	0.168	1.4	0.952
0.2	0.223	1.5	0.966
0.3	0.329	1.6	0.976
0.4	0.428	1.8	0.989
0.5	0.521	2.0	0.995
0.6	0.604	2.2	0.998
0.7	0.678	2.4	0.999
0.8	0.742	∞	1.0
0.9	0.797		

where: T_0 is the initial mould temperature
 T_M is the metal melting temperature.

The temperature at any location within the mould as a function of time following the pouring of the metal can be calculated using equation 2.7. This by itself is useful, but the real value comes from the other parameters that can be derived from this relationship.

In many casting operations, rather than the mould temperature, it is the temperature gradient within the mould that is important. As liquid metal may be poured in a short time period into a cold mould, the temperature gradient can be large and the induced thermal shock may lead to the cracking of some mould materials. Without presenting the details, the temperature gradient in the mould is obtained by differentiating equation 2.7, to obtain

$$\frac{\partial T}{\partial x} = \frac{T_M - T_0}{\sqrt{\pi\alpha_{th}t}} \exp\left(-\frac{x^2}{4\alpha_{th}t}\right) \quad (2.8)$$

A useful quantity derived from equation 2.7 is the time required for solidification. This can be obtained by a heat flux balance at the mould–metal interface. The heat flux away from the interface into the mould is given by equation 2.1, evaluated at $x = 0$, or

$$\bar{J}_{m_{x=0}} = -k_m \left. \frac{\partial T}{\partial x} \right|_{x=0} \quad (2.9)$$

Substituting equations 2.8 and 2.3 into 2.9 gives the heat flux across the mould–metal interface as

$$\bar{J}_{m_{x=0}} = -\sqrt{\frac{k_m \rho_m C_m}{\pi t}} (T_M - T_0) \quad (2.10)$$

where: ρ_m is the density of the mould material
 C_m is the heat capacity of the mould material.

If the metal is cast at the melting temperature, then the heat entering the mould can

only come from the latent heat of solidification of the metal, or

$$\begin{aligned}\frac{dQ}{dt} &= \rho_C \Delta H_f \frac{dV}{dt} \\ &= \rho_C \Delta H_f A \frac{dS}{dt}\end{aligned}\quad (2.11)$$

where: dQ/dt is the heat transfer rate from the metal to the mould

ρ_C is the density of the casting

ΔH_f is the latent heat of solidification

V is the volume of solidified metal

A is the area of the mould–metal interface

S is the thickness of solidified metal; see Fig. 2.22.

The heat flux corresponding to this equation is

$$\vec{J}_C = \rho_C \Delta H_f \frac{dS}{dt} \quad (2.12)$$

where J_C is the heat flux across the mould–metal interface.

As the heat flux away from the mould–metal interface must be equal to the heat flux to the mould–metal interface, equations 2.10 and 2.12 can be equated and integrated to provide the solidification distance in terms of the elapsed time since the metal was poured into the mould

$$S = \frac{2}{\sqrt{\pi}} \frac{T_M - T_0}{\rho_C \Delta H_f} \sqrt{k_m \rho_m C_m t} \quad (2.13)$$

From Fig. 2.22 it is evident that

$$S = \frac{V}{A} \quad (2.14)$$

and combining this equation with equation 2.13 and rearranging gives the solidification time as

$$t = \left[\frac{\pi}{4} \left(\frac{\rho_C \Delta H_f}{T_M - T_0} \right)^2 \frac{1}{k_m \rho_m C_m} \right] \left(\frac{V}{A} \right)^2 \quad (2.15)$$

Values for the various constants of equation 2.15 are listed in Table 2.3.

Example 2.2 Dimensions of a semi-infinite mould!

One of the assumptions in the derivation of equations 2.1 to 2.15 was that the mould is of semi-infinite dimensions. To check the error introduced by this assumption, consider the following.

A metal with a melting temperature of 700°C is poured into a sand mould that is initially at 30°C. How thick must a mould be to be considered semi-infinite for times of 1 min, 5 min and 15 min after pouring the metal?

Solution In agreement with Fig. 2.22, assume that the mould surface is $x = 0$; let L be the thickness of the mould.

Table 2.3 Thermal properties for casting materials

(a) Mould and metal constants			
Material	Specific heat C_p (J/g°C)	Density ρ (g/cm ³)	Thermal conductivity k (W/m · °C)
Sand	1.16	1.5	0.60
Plaster	0.90	1.1	0.34
Mullite	0.77	1.6	0.37
Iron	0.70	7.9	73
Aluminium	0.90	2.7	202
Copper	0.39	9.0	385
Magnesium	1.07	1.7	156
(b) Liquid metal constants			
Metal	Melting point T_m (°C)	Latent heat of solidification H_f (J/g)	Specific heat C_p (J/g°C)
Iron	1540	280	0.77
Aluminium	660	396	1.05
Copper	1083	220	0.52
Magnesium	650	384	1.38

The semi-infinite mould condition means that the temperature at $x = L$ does not increase substantially above T_0 , which in this case is 30°C.

Therefore, in equation 2.7, $T(L, t) \approx 30^\circ\text{C}$.

To determine the value of L find the maximum value of equation 2.7 for $t = 1$ min, 5 min and 15 min.

For this problem the values of T_M and T_0 are fixed, so $T(L, t)$ is maximized when

$$\operatorname{erf}\left(\frac{x}{2\sqrt{\alpha_{\text{th}}t}}\right) \text{ is maximum (see equation 2.7)}$$

For a sand mould, from Table 2.3, $C_m = 1.16 \text{ J/g}^\circ\text{C}$, $\rho_m = 1500 \text{ kg/m}^3$, $k_m = 0.6 \text{ W/m}^\circ\text{C}$:

$$\alpha_{\text{th}} = \frac{k_m}{C_m \rho_m} = \frac{0.6 \text{ J/s} \cdot ^\circ\text{C}}{1160 \text{ J/kg}^\circ\text{C} \times 1500 \text{ kg/m}^3} = 3.4 \times 10^{-7} \text{ m}^2/\text{s}$$

From Table 2.2, the error function is practically at its maximum value when $z = 2$. Therefore, for this example, assume

$$\frac{x}{2\sqrt{\alpha_{\text{th}}t}} = 2$$

and setting $x = L$ and solve for L , with $t = 1$ min, 5 min and 15 min.

For $t = 1$ min,

$$L = 2 \times 2\sqrt{3.4 \times 10^{-7} \text{ m}^2/\text{s} \times 60 \text{ s}} = 18 \text{ mm}$$

Repeating the calculation for $t = 5$ min and 15 min gives $L = 40 \text{ mm}$ and $L = 70 \text{ mm}$, respectively. If the mould has a thickness of less than these values, then it cannot be considered semi-infinite and equation 2.7 will be invalid.

To check, calculate $T(L, t)$ using equation 2.7 for one of the times, say $t = 1 \text{ min}$:

$$\begin{aligned} T(18 \text{ mm}, 1 \text{ min}) &= 700^\circ\text{C} + (30^\circ\text{C} - 700^\circ\text{C})\text{erf}\left(\frac{18 \text{ mm}}{2\sqrt{3.4 \times 10^{-7} \text{ m}^2/\text{s} \times 60 \text{ s}}}\right) \\ &= 33.4^\circ\text{C} \end{aligned}$$

close to the initial temperature of 30°C , verifying the infinite mould assumption.

The terms within the square brackets [] of equation 2.15 are all constants and so it can be simplified to

$$t = C \left(\frac{V}{A} \right)^2 \quad (2.16)$$

This relationship is known as *Chvorinov's rule*. Although it has been derived in terms of one-dimensional solidification, this rule can be applied to more complex shapes to provide a first approximation of the solidification behaviour.

Chvorinov's rule applied to riser design

It is clear from Fig. 2.20 that, unless properly designed, undesirable shrinkage voids or *macroporosity* can develop within the cast shape. Therefore, *risers* must be located and sized appropriately so that solidification begins in the central regions of the cast part and proceeds outwards, ending in the risers. In this manner, the last metal to solidify is in the risers, which will contain the macroporosity, and eventually be removed from the final cast shape. This means the time for the riser to solidify, calculated from equation 2.16, must be more than the solidification time for the casting. For this purpose, equation 2.16 can be expressed as the following inequality:

$$\left(\frac{V}{A} \right)_{\text{riser}} > \left(\frac{V}{A} \right)_{\text{casting}} \quad (2.17)$$

Riser designs that satisfy this inequality ensure that shrinkage porosity in the cast part is avoided. Riser size may be calculated according to equation 2.17. On the other hand, riser size may be minimized, over and above that calculated, by utilizing insulators, chills or radiation shields as shown in Fig. 2.21. These devices alter the time for solidification by changing the constant C in equation 2.16.

Example 2.3 Riser design

A spherical casting of diameter 10 cm has a cylindrical riser 5 cm in diameter and 10 cm high. Will the riser prevent macroporosity in the casting?

Solution

$$\begin{aligned} \left(\frac{V}{A} \right)_{\text{riser}} &= \frac{\pi 5^2 \times 10/4}{\pi 5 \times 10 + \pi 5^2/4} = 1.11 \text{ cm} \\ \left(\frac{V}{A} \right)_{\text{casting}} &= \frac{4/3\pi(10/2)^3}{4\pi(10/2)^2 - \pi 5^2/4} = 1.78 \text{ cm} \end{aligned}$$

As

$$\left(\frac{V}{A}\right)_{\text{riser}} \neq \left(\frac{V}{A}\right)_{\text{casting}}$$

the casting will solidify last and contain solidification shrinkage or macroporosity.

Note: The calculation of the riser area includes the cylindrical surface of the riser plus one circular end – the other end of the riser is in contact with the casting and, therefore, no heat transfer occurs across this area. Likewise, the same area is subtracted from the area of the casting.

2.5.2 Heat transfer during continuous casting

The development of heat transfer theory for a continuous casting process is beyond the necessary scope of this book. However, an example to illustrate how the results of heat transfer theory can be applied is instructive, because successful continuous casting depends on correct mould design and heat transfer control. Referring to Fig. 2.5, it is easy to envisage that, if the mould design and heat transfer are not correct, then liquid metal will issue from the bottom of the mould, causing equipment damage and safety hazards. It is evident that the mould length, metal flow rate and heat transfer system are all related. Similar to many other heat transfer problems, these factors may be related by nondimensional parameters. Three such parameters that have been developed for the continuous casting process are

$$\begin{aligned} \text{dimensionless mould length } Y^* &= \frac{h_f^2 y}{u k_s \rho C_s} \\ \text{dimensionless latent heat } H^* &= \frac{H_f}{C_s (T_M - T_o)} \\ \text{dimensionless solidified thickness } S^* &= \frac{h_f \delta}{k_s} \end{aligned} \quad (2.18)$$

where: h_f is the film heat transfer coefficient between the metal and the mould
 k_s is the thermal conductivity of the solid metal
 δ is the thickness of the solidified skin of metal adjacent to the mould
 y is the distance from the top of the mould
 C_s is the specific heat of the solidified metal
 u is the speed of withdrawal of the solid strand
 ρ is the density of the metal
 T_M is the metal melting temperature
 T_o is the ambient temperature
 H_f is the latent heat of solidification.

With the aid of Fig. 2.23, these parameters can be used to calculate several process variables, such as mould length, skin thickness at the mould exit, casting speed or mould cooling requirements – as demonstrated in the following example.

Example 2.4 Mould length for continuous casting

Steel is continuously cast in a manner similar to that of Fig. 2.5. The steel is poured at the melting temperature of 1500°C and solidifies into a strand of $50\text{ cm} \times 8\text{ cm}$ which is withdrawn from the mould at 280 cm/min . The solid skin at the mould exit is to be 1.5 cm thick and the film heat transfer coefficient between the metal and the mould is $1500\text{ W/m}^2 \cdot ^\circ\text{C}$. The mould is maintained at 20°C . Calculate the mould length required.

Solution From Table 2.3, assuming steel constants are the same as for iron,

$$H_f = 280\text{ kJ/kg}, \quad k_s = 73\text{ W/m}^\circ\text{C}, \quad \rho = 7900\text{ kg/m}^3, \quad C_s = 0.70\text{ kJ/kg}^\circ\text{C}$$

From the question it is known that when $y = L$ (the mould length), then $\delta = 0.015\text{ m}$

$$S^* = \frac{h_f \delta}{k_s} = \frac{1500 \times 0.015}{73} = 0.31$$

also

$$H^* = \frac{H_f}{C_s(T_M - T_o)} = \frac{280}{0.70 \times 1480} = 0.27$$

With $y = L$, $u = 0.047\text{ m/s}$ and, using Fig. 2.23,

$$Y^* = \frac{h_f^2 L}{u k_s \rho_m C_s} = 0.12$$

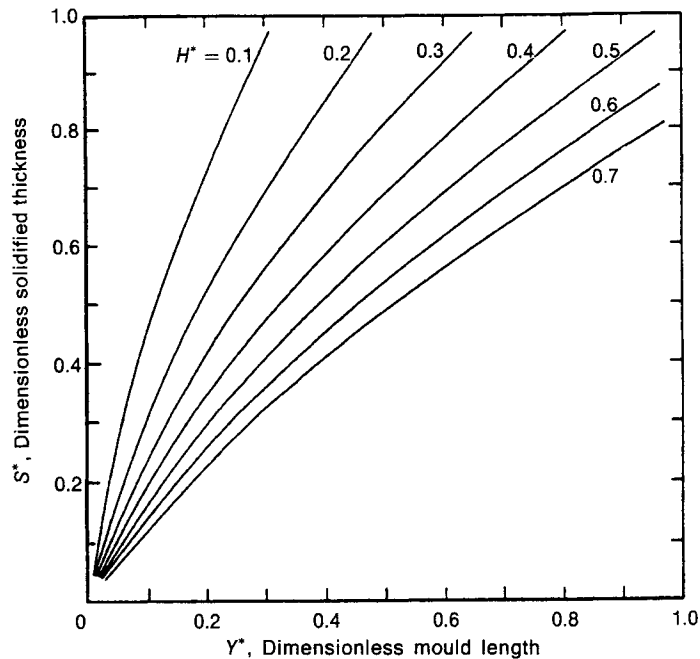


Fig. 2.23 Relationship between nondimensional parameters of equation 2.18 for continuous casting. (Reproduced courtesy of the Institution of Mining and Metallurgy.)

Hence

$$L = \frac{0.12 \times 0.047 \times 73 \times 7900 \times 700}{1500^2} = 1.0 \text{ m}$$

The mould length required is about 1 m.

2.6 Defects produced during casting

The formation of macroporosity resulting from shrinkage during solidification and cooling has already been identified as a potential problem. Through judicious sizing and placement of risers macroporosity is avoidable in well engineered shape castings. However, several other characteristics of metal solidification can also lead to a number of different types of defects. This section identifies the causes and preventative measures required to avoid such defects.

2.6.1 Microporosity

A ramification of a dendritic interface is that feeding liquid metal to areas between dendrites is difficult. Fig. 2.24(a) illustrates the solidification of a well developed dendritic interface. As the metal between each solid dendrite solidifies and cools, it shrinks and unless additional liquid metal can be fed into this region *microporosity* forms between the dendrites, or in the *interdendritic* regions. At temperatures corresponding to the mushy zone most liquid metals are very viscous, therefore it is often difficult for liquid metal to penetrate the complex-shaped dendrites, giving rise to microporosity. In contrast to macroporosity, microporosity occurs on a much finer scale and usually has an irregular shape, as seen in Fig. 2.25. This is one of the major factors limiting the length of channels through which liquid metal can be

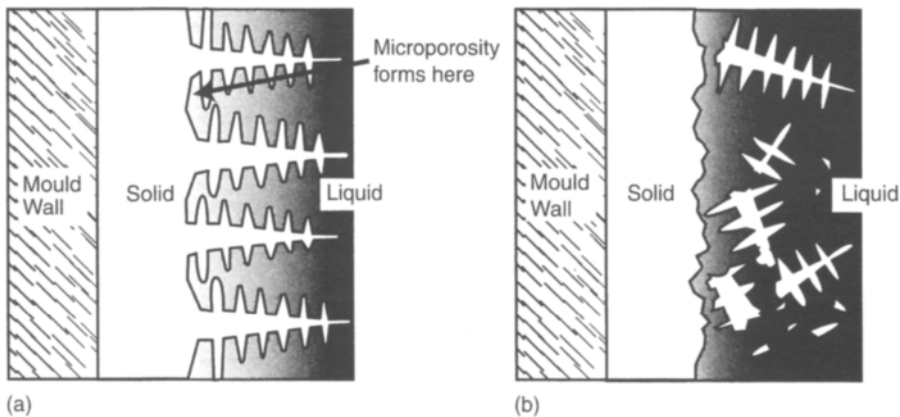


Fig. 2.24 Diagram of solidifying dendritic structure: (a) dendrite growth leading to microporosity in interdendritic regions; (b) equiaxed dendritic solidification.

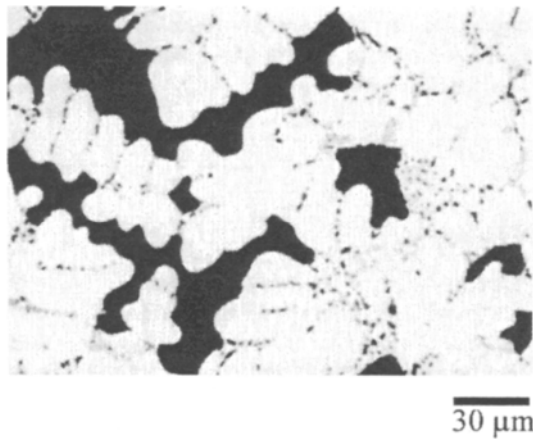


Fig. 2.25 Microporosity (black regions) in Al-9wt% Si alloy. (Reproduced courtesy of Aluminium-Verlag Marketing & Kommunikation GmbH, Düsseldorf.)

fed. Microporosity can be avoided by ensuring that the liquid metal velocity in the mould is high. In this manner, the force of the liquid metal flowing against the growing dendrites actually fractures them and they become oriented randomly within the casting, as illustrated in Fig. 2.24(b). This technique results in an *equiaxed dendritic* cast microstructure, such as that shown in Fig. 2.26. Although this reduces the occurrence of microporosity, the dendritic structure and microsegregation (coring) still remain.

Microporosity can also be reduced by changing the alloy composition, i.e. by casting *eutectic* compositions. Microporosity is most serious when the dendritic arms are long, effectively hindering liquid metal flow. Long dendrites occur when the alloy being cast has a large mushy zone. Since eutectic alloys solidify at one temperature, no mushy

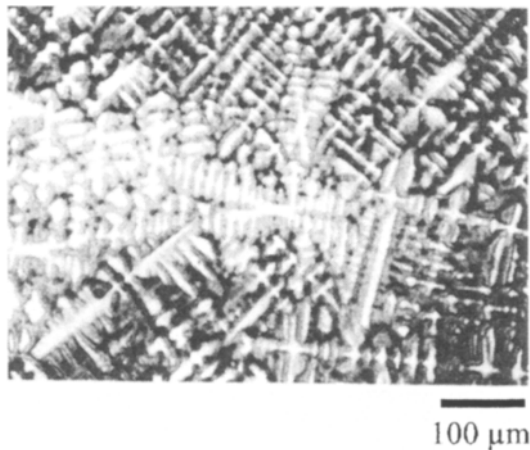


Fig. 2.26 Equiaxed dendritic structure in 70 wt% Cu-30 wt% Zn. Regions of different contrast are the result of coring.

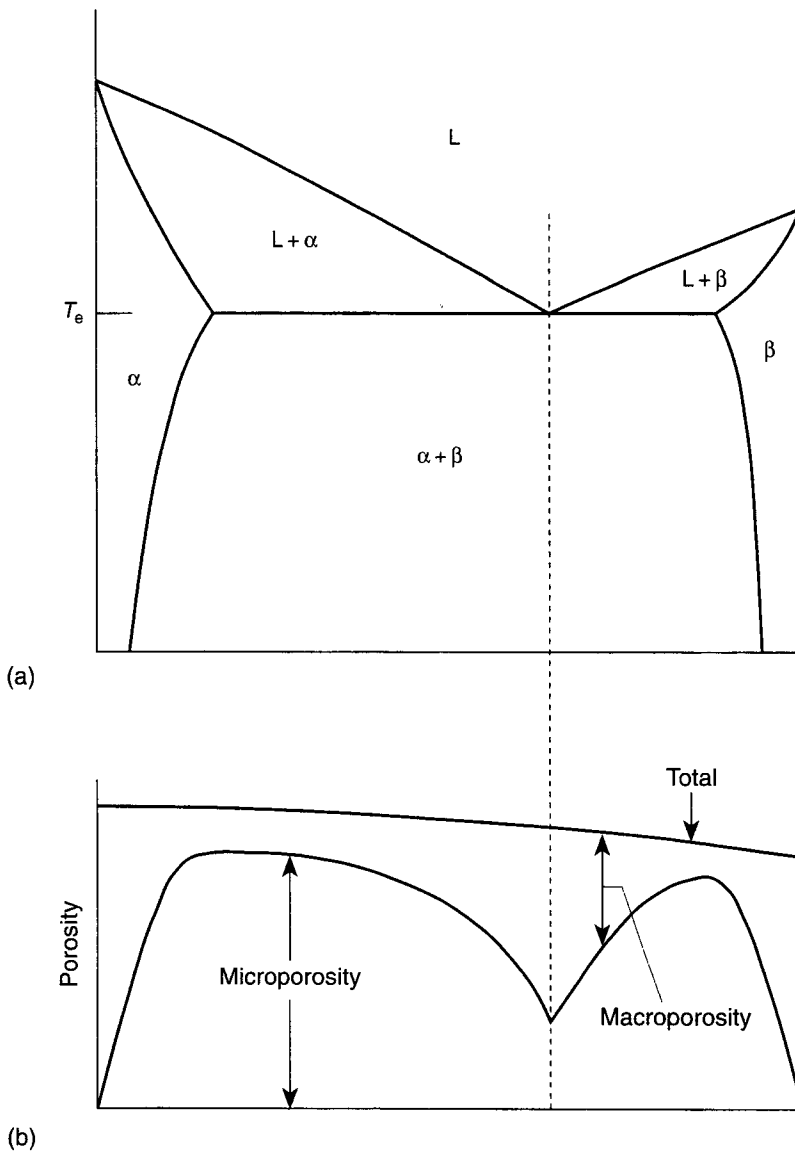
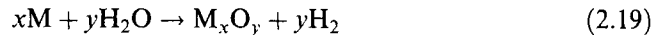


Fig. 2.27 (a) Phase diagram for a binary system with a eutectic transformation. (b) Graph of relative amounts of micro- or macroporosity as a function of composition.

zone exists and microporosity is reduced. Note that, as shown in Fig. 2.27, eutectic alloys and alloys with a large mushy zone develop equivalent amounts of porosity. However, for the eutectic alloy, most of the porosity will occur as macroporosity, which is more easily handled by the appropriate use of risers. This characteristic makes the manufacture of sound castings from eutectic alloys easier. Unfortunately, the mechanical properties of most eutectic compositions are not suitable for many applications.

2.6.2 Gas porosity

Both micro- and macroporosity are caused by shrinkage during solidification and cooling. In contrast, *gas porosity* is caused by the absorption of gases into the liquid metal prior to solidification. The most troublesome gas is hydrogen which usually comes from moisture in the atmosphere, either naturally or as a result of burning fossil fuels for heating and melting. Hydrogen and liquid metal can react according to the relationship



where: M is the metal being melted
 x, y balance the chemical reaction.

At the high temperatures adjacent to the liquid metal surface, the molecular hydrogen produced by this reaction decomposes into atomic hydrogen and may be absorbed into solution in the liquid metal. The solubility of hydrogen in metals increases with temperature and increases sharply at the melting temperature, as shown for aluminium in Fig. 2.28. The decrease in hydrogen solubility during solidification for common metals is listed in Table 2.4. During solidification and cooling most of the hydrogen absorbed by the metal in the liquid state is unable to escape. Therefore, if preventative measures are not taken, the large decrease in hydrogen solubility on solidification and cooling causes the formation of hydrogen bubbles within the solidifying casting.

Gas porosity degrades the quality of castings. One problem associated with gas porosity is the formation of *blisters* during subsequent processing, often due to expansion of the trapped gas during annealing or other heat treatments. In contrast

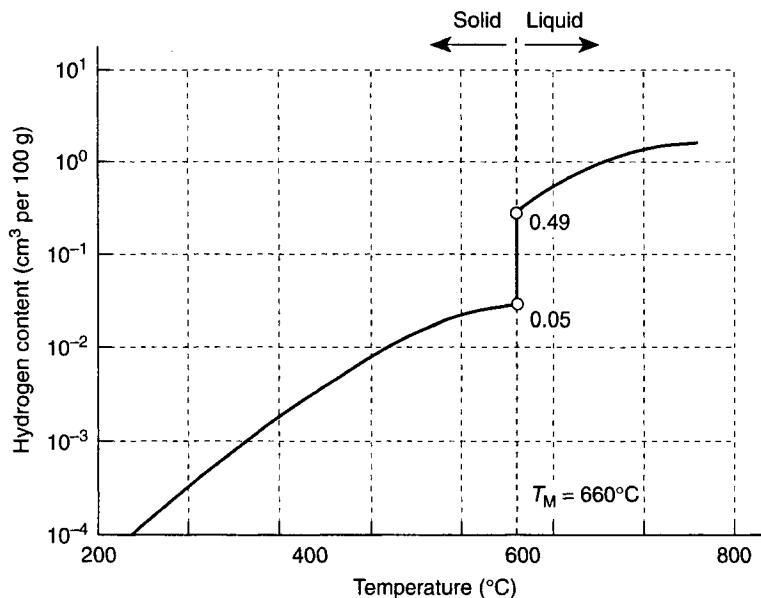


Fig. 2.28 Hydrogen solubility in aluminium as a function of temperature at one atmosphere.

Table 2.4 Solubility of hydrogen in metals

Metal	[H] _L in liquid at T_M and 1 atm of H_2 (cm ³ per 100 g)	[H] _S in solid at T_M and 1 atm of H_2 (cm ³ per 100 g)
Al	0.49	0.05
Cu	5.17	3.1
Fe	27	7
Ni	39	18

to solidification shrinkage, which is vacuous and usually irregularly shaped, gas porosity contains hydrogen and is usually spherical.

Hydrogen, and other gases, such as oxygen, enter the liquid metal by diffusion from the atmosphere. The equilibrium concentration of the gas in the liquid metal can be determined from *Sievert's law* according to

$$[G] = k\sqrt{p_g} \quad (2.20)$$

where: $[G]$ is the equilibrium solubility of the gas

k is an equilibrium constant

p_g is the partial pressure of the gas at the metal surface.

Using this expression the volume of gas porosity in a casting can be calculated, as in the following example.

Example 2.5 Hydrogen porosity in iron

Calculate the percentage of gas porosity in an iron casting if the partial pressure of hydrogen in contact with the molten iron is 0.1 atm. What hydrogen partial pressure is required to eliminate the gas porosity?

Solution From Table 2.4 at 1 atm, $[H]_L = 27 \text{ cm}^3 \text{ per } 100 \text{ g}$ and $[H]_S = 7 \text{ cm}^3 \text{ per } 100 \text{ g}$.

From Table 2.3, $\rho = 7.9 \text{ g/cm}^3$. Therefore, at 1 atm,

$$k = \frac{[H]_{L1}}{\sqrt{p_g}} = \frac{27}{\sqrt{1}} = 27$$

so, at 0.1 atm, $[H]_{L0.1} = 27\sqrt{0.1} = 8.54 \text{ cm}^3 \text{ per } 100 \text{ g}$.

As $[H]_S = 7 \text{ cm}^3 \text{ per } 100 \text{ g}$, then $8.54 - 7 = 1.54 \text{ cm}^3 \text{ per } 100 \text{ g}$ of hydrogen will form gas porosity.

Volume of 100 g of iron $= 100 \text{ g} / 7.9 \text{ g/cm}^3 = 12.7 \text{ cm}^3$.

Total volume of metal and gas porosity $= 12.7 + 1.54 = 14.2 \text{ cm}^3$.

Gas porosity $= 1.54 / 14.2 \times 100 \approx 11\%$. This is clearly an unacceptable level of porosity.

Partial pressure required to eliminate porosity There cannot be more than $[H]_S$ in liquid metal, so

$$7 \text{ cm}^3 \text{ per } 100 \text{ g} = 27\sqrt{p_g}$$

which gives $p_g = 0.067 \text{ atm}$.

Note that a low atmosphere pressure of hydrogen is required to avoid gas porosity.

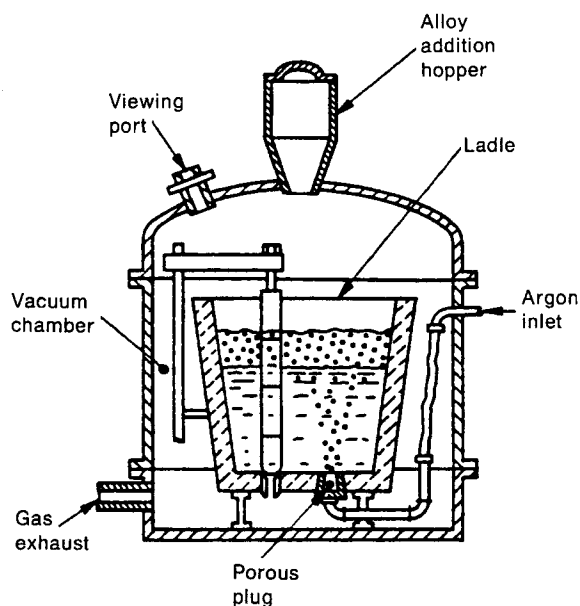


Fig. 2.29 Arrangement of ladle vacuum degassing of steel. (Reproduced courtesy of The AISE Steel Foundation.)

It is apparent from the example that avoidance of hydrogen porosity requires low pressure above the surface of the liquid metal. To achieve this, steel is often *vacuum degassed* while in the ladle immediately prior to casting. Several arrangements are in use for vacuum degassing, but all involve exposing the liquid steel to a vacuum and allowing the dissolved hydrogen within the metal to diffuse into the vacuum, and subsequently be drawn away with pumping equipment. As the rate of hydrogen removal depends on the surface area of the molten steel, argon can be used to stir the steel which aids the removal of hydrogen (Fig. 2.29). Alternatively, the steel can be poured into a vacuum chamber in a stream with a high surface area. Notice that the equipment arrangement for continuous casting, shown in Fig. 2.3, includes a ladle degassing station.

Aluminium is usually degassed with a mixture of chlorine, nitrogen and argon. Small batches of aluminium can be degassed using a solid that contains chlorine compounds – usually in the form of hexachloroethane – that vaporize or decompose at the temperature of molten aluminium. These solids are most often plunged to the bottom of the liquid and stirred vigorously to achieve the maximum reaction with the melt. They also contain *fluxes*, usually other chlorides and fluorides, that help separate nonmetallic impurities into a floating slag layer that is easily skimmed from the aluminium below. A drawback of this process is that the effluent produced contains toxic fluorides and chlorides that must be treated before release.

Larger melts of aluminium can be degassed by bubbling a mixture of chlorine and argon gas through the melt. Although many operations utilize high proportions of chlorine, less than 5% chlorine is sufficient to achieve good degassing action. Low chlorine levels minimize the hazards (both safety and environmental) associated with the degassing operation. Larger continuous casting or ingot casting operations

often use in-line degassing equipment that treats the metal as it passes through the *launder* (see Fig. 2.2) immediately prior to casting.

2.6.3 Aspiration

It should be apparent from the preceding section that prior to pouring a casting, considerable effort is directed towards ensuring that the liquid melt is clean and degassed. Therefore, during the pouring operation it is important that the quality of the metal is not compromised. For example, molten metals react quickly with the surrounding atmosphere to produce a surface oxide. This oxide layer often adheres well to the molten metal surface (e.g. aluminium) and serves to protect the underlying metal from further oxide contamination. However, if the metal is not poured in a quiescent manner the protective oxide can be ingested into the metal and solidified into the casting as nonmetallic *inclusions*. Such inclusions degrade the properties of the casting. Often great effort is made to carefully handle the liquid metal for this reason.

For instances in which metal is poured into permeable moulds, as in sand casting, atmospheric gases can be introduced to the metal through *aspiration*. Aspiration occurs when the pressure anywhere in the liquid metal falls below atmospheric pressure, which most often happens in the vertical sprue (see Figs 2.6 and 2.7). For a sprue with vertical walls, air enters the metal flow as shown in Fig. 2.30. Consequently, the

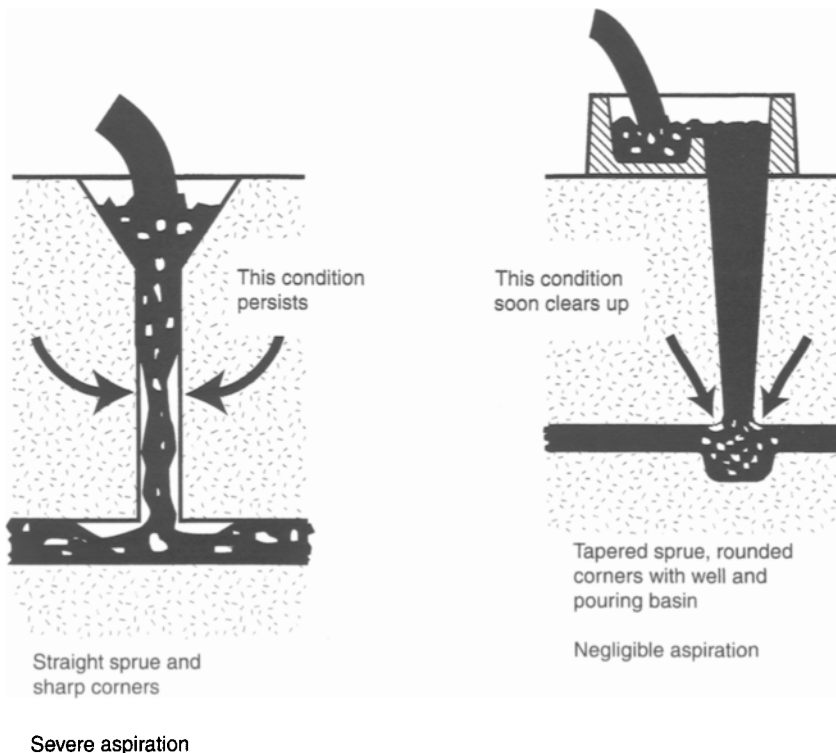


Fig. 2.30 Aspiration in a sprue during sand casting.

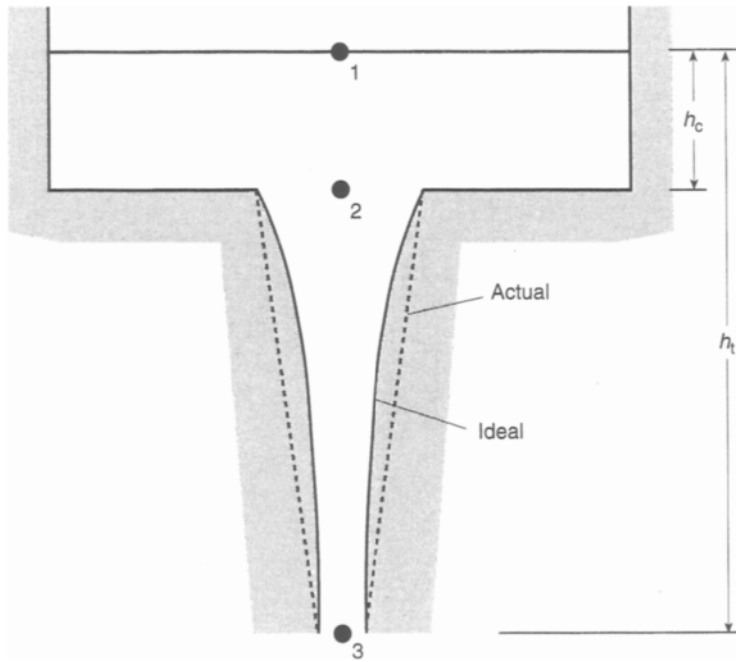


Fig. 2.31 Geometry of sprue for sand casting.

sprue must be tapered. The taper required to avoid aspiration can be calculated using *Bernoulli's* equation. Referring to Fig. 2.31, and applying Bernoulli's equation between points 1 and 2, gives

$$h_1 + \frac{v_1^2}{2g} + \frac{p_1}{\rho g} = h_2 + \frac{v_2^2}{2g} + \frac{p_2}{\rho g} \quad (2.21)$$

where: h_1, h_2 are the elevations of points 1 and 2

v_1, v_2 are the velocities at points 1 and 2

p_1, p_2 are the pressures at points 1 and 2

ρ is the metal density.

Since liquid metals are incompressible liquids, $p_1 = p_2 = p_3 = p_{\text{surface}} = 1 \text{ atm}$ and, assuming that $v_1 \approx 0$, then solving equation 2.21 between points 1 and 2 gives

$$v_2 = \sqrt{2gh_c} \quad (2.22)$$

where h_c is as defined in Fig. 2.31. Similarly, solving equation 2.21 between points 1 and 3 gives

$$v_3 = \sqrt{2gh_t} \quad (2.23)$$

where h_t is as defined in Fig. 2.31.

From the principle of flow continuity

$$A_2 v_2 = A_3 v_3 \quad (2.24)$$

where A_2 and A_3 are the areas at points 2 and 3. Combining equations 2.22 through 2.24 yields

$$\frac{A_2}{A_3} = \sqrt{\frac{h_c}{h_t}} \quad (2.25)$$

This equation provides an estimate of the maximum taper ratio required to prevent aspiration. If Bernoulli's equation is applied along the whole length of the sprue, a parabolic shaped riser is generated, as shown in Fig. 2.31. However, a straight taper is more practical and will suffice to prevent aspiration in most cases.

The sprue generally gives way to horizontal elements in the feeding system – runners and ingates (see Fig. 2.7). The impact of molten metal on the relatively weak sand mould can lead to mould damage and misshapen castings. Therefore, the runners and ingates must be designed to withstand the metal impact and reduce the metal velocity sufficiently so that the shape of the mould cavity is not compromised.

2.7 Shape casting materials

It is clear that virtually all metals must be cast at some point in their processing history (although a relatively small tonnage is directly solidified to powder – see Chapter 6). However, several alloy systems have been specifically designed to give good castability and useful mechanical properties. These alloy systems are described in this section.

Some of the advantages of eutectic alloys as casting materials have already been highlighted. The fluidity of these materials is high and the risk of microsegregation and microporosity is lower than for other alloys. In addition, eutectics are low-melting-point metals requiring less energy for melting. However, alloys that are entirely eutectic often lack toughness. Consequently, many commercial casting materials have near-eutectic compositions. These compositions are close enough to the eutectic composition to take advantage of the good casting characteristics, but far enough away to provide sufficient ductile primary phase material for service reasons.

2.7.1 Cast iron

Cast iron deserves special attention since it is used more than any other material for shape castings. In fact the tonnage of cast iron used for shape casting is greater than all other metals combined for this purpose. Cast irons have significantly higher carbon content than steels, ranging between 1.7 and 3.5%. Cast irons are produced with four characteristic microstructures. The development of each of these microstructures is explained in the following, with the aid of the iron–carbon phase diagram (Fig. 2.32).

White cast iron

White cast iron typically contains about 3–3.5% C. The microstructure of this material develops during cooling from the liquid phase. A 3% C white cast iron begins to

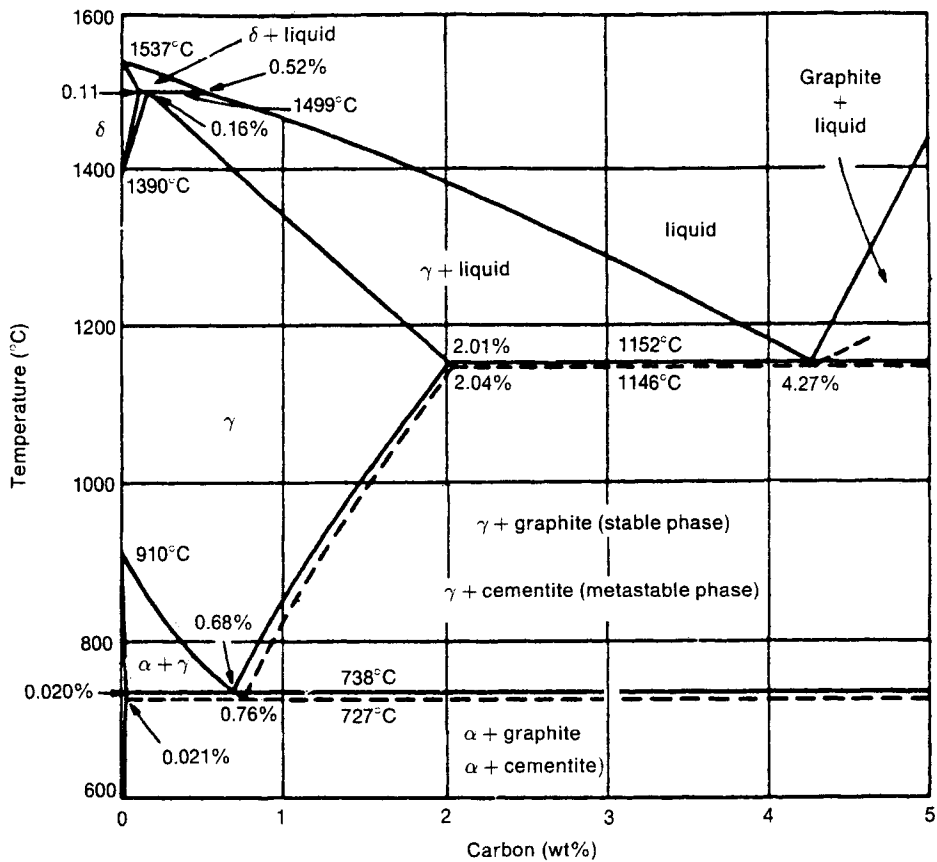


Fig. 2.32 Fe-C phase diagram.

solidify to austenite at about 1300°C (Fig. 2.32). On reaching 1146°C the eutectic reaction of $L \rightarrow \gamma + \text{Fe}_3\text{C}$ occurs and *cementite* (Fe_3C) forms. At the eutectoid temperature of 727°C the austenite transforms to $\alpha + \text{Fe}_3\text{C}$ with a pearlite morphology. Consequently, the final microstructure contains pearlite and cementite. As cementite has a complex crystal structure, plastic deformation via dislocation slip processes is very difficult, rendering white cast iron very brittle. However, white cast iron has good abrasion resistance and is used in grinding mills, mining equipment and rolls for finishing steel, among many other applications.

Gray cast iron

Gray cast iron has ostensibly the same composition as white cast iron, but is slowly cooled during casting. Slow cooling has an important influence on the microstructure and, thus, on the mechanical properties. To understand the properties of gray cast iron, it must be realized that cementite is not truly an equilibrium phase. Given sufficient time cementite will decompose to iron and graphite. This decomposition is of virtually no importance when considering the metallurgy of steels, which is why the iron carbon phase diagram is usually presented to show cementite rather than

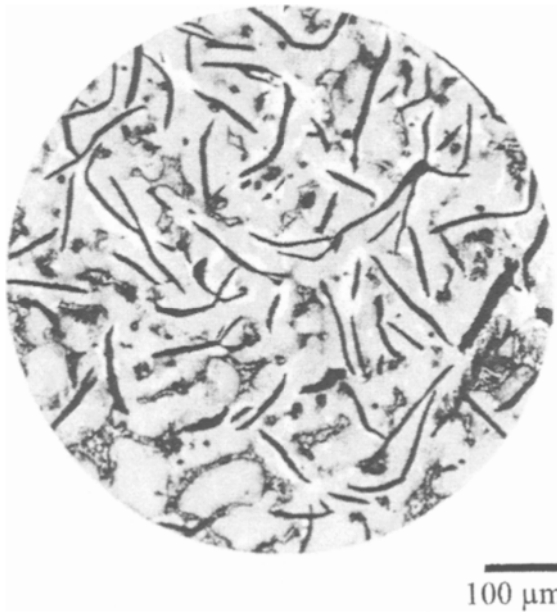


Fig. 2.33 Microstructure of gray cast iron; black phase is graphite. (Reproduced courtesy of The AISE Steel Foundation.)

graphite. The phase boundaries for graphite are superimposed on the phase diagram of Fig. 2.32 for comparison purposes. The important difference is that during slow cooling, carbon forms graphite in the form of flakes instead of cementite. Similar to white cast iron formation, the austenite that solidifies at $>1152^{\circ}\text{C}$ (the iron–graphite eutectic; see Fig. 2.32) usually transforms to pearlite on cooling below 738°C (the iron–graphite eutectoid; see Fig. 2.32). Some gray cast iron also contains a phase referred to as *steadite*, which forms as a result of phosphorus retained from blast furnace materials. Depending on the composition and cooling rate, some gray cast iron may also contain ferrite (α), with the microstructure, in this case, shown in Fig. 2.33. However, regardless of the phase mixture in gray cast iron, the most notable structural feature is the presence of the graphite flakes.

An important characteristic of gray cast iron is that the graphite flakes increase in volume during solidification. This volume expansion counterbalances most of the solidification shrinkage that would otherwise occur, making the production of sound castings with minimal use of risers much easier. This is the primary reason for the widespread use of gray cast iron in the production of many complex shaped castings. Unfortunately, the morphology of the graphite flakes cause stress concentrations, leading to very low ductility and brittle behaviour. In addition to good castability, the graphite flakes give rise to good vibration damping capacity and good tribological properties. These attributes make gray cast iron ideally suited for machine housings, pipe fittings and automotive engine blocks, although in this last application aluminium is replacing it for weight reduction reasons. Fire hydrants are usually cast from gray cast iron because it is inexpensive, easy

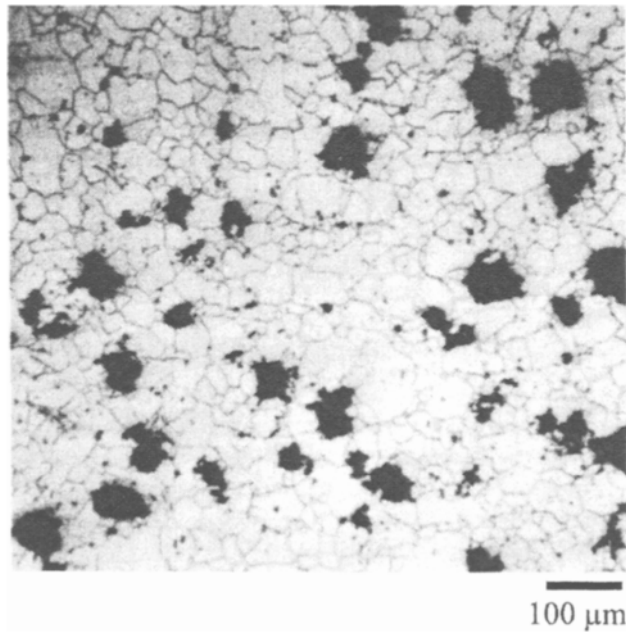


Fig. 2.34 Microstructure of malleable cast iron; black phase is graphite. (Reprinted with permission from *ASM Materials Engineering Dictionary*, edited by J.R. Davis (1992) ASM International, Materials Park, OH 44073-0002, Fig. 316, p. 266.)

to cast, and shears easily when struck by a car, thus avoiding undue injury to occupants.

Malleable cast iron

Malleable cast iron is made by heating white cast iron to temperatures in the range of 820–1000°C for several days. During this time the cementite separates into graphite nodules in a matrix of relatively pure ferrite (α), as shown in Fig. 2.34. Malleable cast iron has good shock resistance and machinability, with much improved strength and ductility compared to white cast iron.

Nodular or ductile cast iron

Nodular or ductile cast iron is a compositional modification of gray cast iron. By adding a small amount of magnesium the graphite flakes that would normally form develop as graphite nodules, resulting in the structure of Fig. 2.35. This microstructure offers much better mechanical properties, notably about 15% ductility, which makes this a competitive material with steel for casting crankshafts or other machinery parts.

2.7.2 Aluminium casting alloys

The castability of aluminium is greatly influenced by alloying elements that modify the oxide that forms on the surface of the molten aluminium, altering its fluidity.

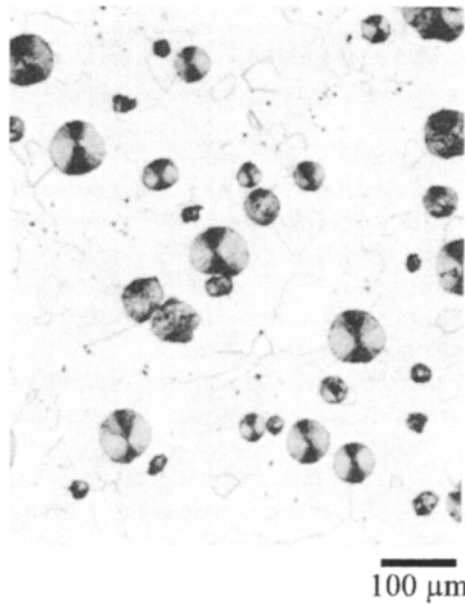


Fig. 2.35 Microstructure of nodular or ductile cast iron. (Reprinted with permission from *ASM Materials Engineering Dictionary*, edited by J.R. Davis (1992) ASM International, Materials Park, OH 44073-0002, Fig. 139, p. 130.)

Silicon is the most important addition in this regard. It improves the fluidity of aluminium, making the casting of intricate shapes more practical. Furthermore, the Al–Si system exhibits a eutectic reaction at 11.7% Si and 577°C, a lower melting temperature than either pure aluminium or silicon. Eutectic Al–Si alloys are used for thin-walled intricately shaped castings. However, the largest volume of Al–Si alloys contain <11.7% Si, to encourage the formation of a primary aluminium-rich phase and thereby improve the mechanical properties. These alloys have found widespread use for various shapes, particularly automotive applications. In fact, they are displacing cast iron as the favoured material for automotive crankcases and housings for transmission cases, oil pans, cylinder heads etc., primarily because of the weight savings possible. The Cosworth process for sand casting Al–Si alloys is described in greater detail at the end of this chapter. Table 2.5 summarizes the composition, properties and typical applications of some Al–Si casting alloys.

2.8 Design of shape castings for manufacturing

It should be evident that shape cast parts must meet all the design criteria required of the finished component. However, as mentioned in Chapter 1, it is also important to design components for efficient manufacturing. For shape castings several design attributes are necessary to ensure that acceptable parts are made. A few of these are highlighted below.

- **Draft:** Sand castings must be designed so that the pattern can be easily removed from the cope and drag during the moulding of the sand (see Fig. 2.6).

Table 2.5 Properties and applications of Al–Si casting alloys

Alloy	Composition (wt%)				Tensile properties ^a			Applications
	Si	Mg	Cu	Fe	Ultimate tensile strength (MPa)	Yield strength (MPa)	Elongation (%)	
319.2	6	0.1	3.5	0.6	250	165	2.0	Engine crankcases, cylinder heads
C355.2	5	0.55	1.2	0.13	270	200	3.0	Highly stressed parts, aircraft castings, pistons
A356.2	7	0.37	0.1	0.12	275	205	6.0	Wheels, truck chassis parts
G6290	12	0.1	0.1	0.5	175	65	7.5	Thin walled housings

^a Properties are given for sand castings in the T6 or peak strength temper, except that G6290 properties are for sand casting in the F or fabricated temper.

To demonstrate the requirement for a draft, imagine a sand castle made by using a bucket with tapered sides, and then with a bucket having straight sides – the necessity for a draft should be evident. Usually, 1–3° is sufficient.

- **Pattern allowance:** As metals shrink during solidification and cooling, the pattern must be oversized slightly. Typical shrinkage factors are given in Table 2.1.
- **Section thickness:** It is difficult to force viscous molten metals into long thin sections. Because of this there is a minimum section thickness that can be shape cast. This minimum varies depending on the casting technique and alloy. For example, moderate sized sand castings should have a section thickness of >3 mm, whereas 1 mm can be achieved with pressure die casting. In addition to these minimums, sharp changes in section thickness should be avoided. These contribute to feeding problems and lead to localized solidification shrinkage due to different cooling rates. To avoid section changes, generous radii or cores should be used.
- **Residual stresses:** Different cooling rates within a casting can cause thermal stresses during cooling and residual stresses in the final cast part. Stresses during cooling can sometimes cause cracking of the cast part, a phenomenon referred to as *hot cracking*. During service, residual stresses may combine with externally applied stresses to increase the effective stress level, possibly leading to premature failure.

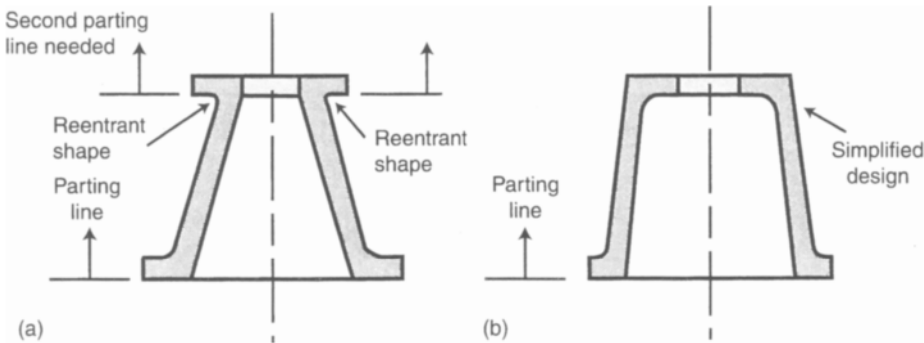


Fig. 2.36 A shape casting with (a) reentrant shape and (b) a possible solution.

Some shape cast parts undergo a *stress relieving* heat treatment prior to service to avoid this problem.

- **Reentrant shapes:** Reentrant shapes, such as that shown in Fig. 2.36, should be avoided as a mould split at more than one *parting line* is required. This causes undue complication in the mould design, and is easily avoided by altering the shape of the cast part.

2.9 Problems

- 2.1 Identify two products that you think were made using (a) ingot casting, (b) continuous casting and (c) shape casting. Discuss the reasons for your selections.
- 2.2 State one advantage and one disadvantage of each of the shape casting techniques described in this chapter.
- 2.3 Identify the causes of porosity in metal castings. Explain briefly how each type can be minimized.
- 2.4 Briefly outline the mechanism responsible for the formation of dendrites in casting a pure metal. Why is a dendritic structure disadvantageous?
- 2.5 If you sectioned a cast part, you are likely to observe voids within the casting. Explain how you would distinguish between solidification porosity and gas porosity in terms of the void shape and location.
- 2.6 The tapered plate shown in Fig. P2.6 is to be cast in sand using the horizontal riser/sprue shown. The cast part contains centreline shrinkage at the location shown. Explain the cause of the centreline shrinkage. Sketch an improved riser/sprue arrangement so that shrinkage in the tapered plate is avoided.

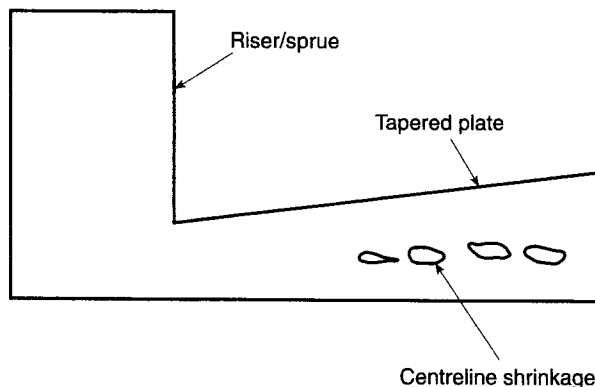


Fig. P2.6 Problem 2.6.

- 2.7 (a) Using data from Table 2.3, plot the temperature profile in a large sand mould containing an aluminium casting 5 min after pouring. (Assume a 1-D conduction heat flow model and a pouring temperature equal to the melting temperature.)

- (b) Calculate the heat flux flowing from this casting 5 min after pouring.
(c) Calculate the growth rate of the solid–liquid interface 5 min after pouring.
(d) Calculate the total thickness solidified after 5 min.
(Answers: (b) $\approx 2.1 \text{ J/cm}^2 \cdot \text{s}$, (c) $\approx 0.002 \text{ cm/s}$, (d) 1.18 cm)
- 2.8 (a) A very large iron plate of thickness 100 mm is cast by pouring iron at its melting temperature into a sand mould, such that heat is withdrawn from both faces of the solidifying plate. Estimate by calculation the time for the plate to solidify if the initial mould temperature is 25°C.
(b) Because in part (a) the iron is cast at its melting point, the liquid iron sometimes begins to solidify prior to filling the entire mould. To solve this problem the iron is heated to 60°C above its melting temperature prior to pouring. Calculate the new solidification time if the initial mould temperature is 25°C.
Hint: An approximate method of calculating the effect of the additional 60°C on the cooling time is to add the heat content of the liquid iron – the $C_{pl} \cdot \Delta T$ – to the latent heat of solidification.
(Answers: (a) about 1.1 h, (b) about 1.5 h)
- 2.9 A 10 cm high cylindrical riser is positioned on top of a 10 cm \times 10 cm \times 10 cm cube casting, as shown in Fig. P2.9. The riser extends from the top face of the cube through to the surface of the mould, as illustrated. Assume no heat is lost through the top of the riser to the atmosphere. An insulator is placed

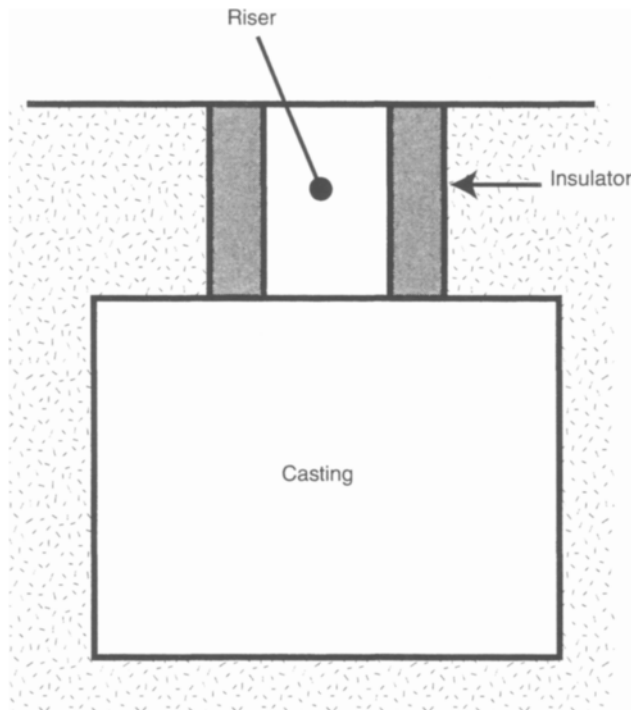


Fig. P2.9 Problem 2.9.

around the riser which effectively doubles the cooling time. Estimate (by calculation) the diameter of the cylindrical riser required to prevent macroporosity. (Answer: ≈ 5 cm)

- 2.10 A cylindrical casting is 0.1 m in diameter and 0.5 m in length. Another casting of the same material is elliptical in cross-section, with the major axis twice the length of the minor axis, and has the same cross-sectional area and length as the cylindrical casting. Both pieces are cast using the same conditions. What is the ratio of the solidification time of the elliptical casting to the solidification time of the circular casting? The perimeter P and area K of an ellipse are

$$P = 2\pi\sqrt{\frac{a^2 + b^2}{2}}; \quad K = \pi ab$$

where the major and minor axes of the ellipse are $2a$ and $2b$, respectively.

(Answer: elliptical section takes ≈ 0.83 of the time required for solidification of the cylinder)

- 2.11 What are the advantages and disadvantages of using eutectic alloys for shape casting?
- 2.12 Fig. P2.12 is the Al-Si phase diagram. You are considering making a shape casting from two alloys, one containing 2% Si, the other containing 12% Si.

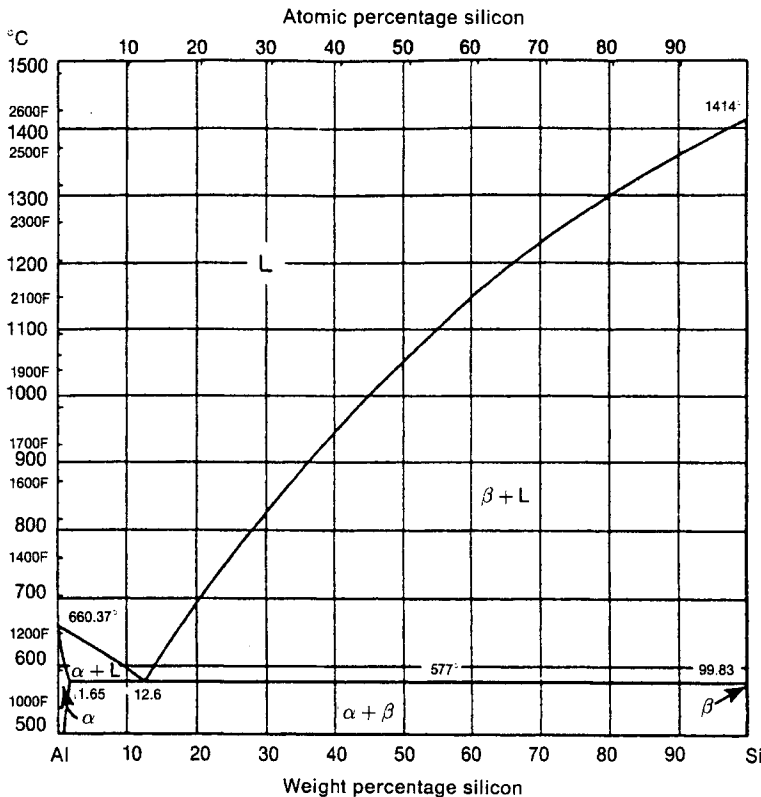


Fig. P2.12 Al-Si phase diagram.

Of these two alloys: (a) which will be more prone to coring, (b) which will be easier to feed, and (c) which will be more prone to microporosity? Explain your answers.

- 2.13 By examining Fig. 2.28, explain why metals should be cooled to a temperature as low as possible prior to casting.
- 2.14 Calculate the relative amount of hydrogen absorbed in molten aluminium cast in an atmosphere where the partial pressure of hydrogen is 10^{-3} atm, compared to the amount of hydrogen absorbed in molten aluminium in a vacuum where the partial pressure of hydrogen is 10^{-9} atm. Express your answer as the ratio $[H]_{\text{atmosphere}} : [H]_{\text{vacuum}}$.
(Answer: 1000)
- 2.15 The maximum equilibrium solubility of hydrogen at a partial pressure of 1 atm in liquid magnesium is 26 cm^3 per 100 g. This drops to 18 cm^3 per 100 g upon solidification. The density of Mg (liquid and solid) is 1.74 g/cm^3 .
- (a) What would be the gas porosity (volume of H_2 /total volume) of the Mg casting if liquid saturated with hydrogen at 1 atm were allowed to solidify?
- (b) What partial pressure of hydrogen should be maintained over the melt if a pore free casting is required?
- (Answers: (a) 12.2% porosity, (b) 0.48 atm)
- 2.16 How does the form of carbon in cast iron influence the brittleness of cast iron parts? How is the form of carbon in cast iron parts altered to control these properties?

Case study 1: Manufacture of can body stock – 1. Casting

The aluminium beverage can is familiar to almost everyone. In North America, the production of aluminium cans outstrips that of both nails and paper clips and consumes about one-fifth of all aluminium produced. The aluminium beverage can was first introduced in 1964 and since then has become the dominant package for carbonated and noncarbonated refreshments, and beer. What is less familiar is the enormous engineering effort required to achieve this dominant position and the impressive technology associated with the manufacture of beverage cans. Although the term 'hi-tech' is most often used to refer to computer and electronic technologies, there is little doubt that the aluminium beverage can represents a hi-tech product.

It must be emphasized that a successful product is only possible if there is a well engineered manufacturing process, but in addition various product attributes must be satisfied. Some of the more obvious major product attributes for beverage cans include: (a) attractive appearance; (b) easy to open; (c) easily cooled; (d) environmentally innocuous; and (e) inexpensive. A few of the less obvious product attributes are: (a) good corrosion resistance, as some beverages are acidic and others are very reactive with many metals; and (b) high strength, as most beer is thermally pasteurized after canning, developing internal pressures in excess of 620 kPa (90 psi). It is the last of each of these product attributes that are at the heart of the engineering challenge associated with beverage can manufacture.

The major steps in the manufacture of beverage cans are illustrated in Fig. C1.1. It should be clear that the manufacture of aluminium beverage cans is a multistep process that exemplifies several of the metal processing techniques discussed in this book. Therefore, the various steps in Fig. C1.1 are discussed at the end of the appropriate chapters as indicated.

Casting of beverage can stock

The casting of high quality beverage can stock involves more than just a well controlled solidification process. Beverage can manufacture demands metal of the highest

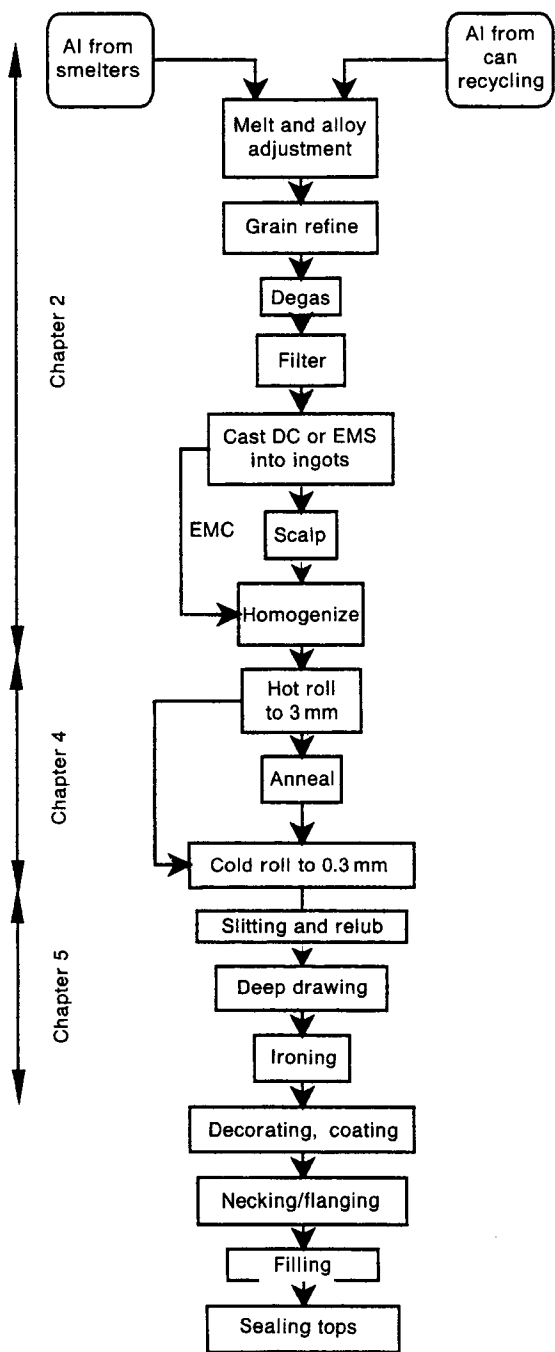


Fig. C1.1 Flow diagram of processing of can body stock.

quality in terms of composition, gas content, inclusion density and ingot microstructure. Therefore, prior to casting, treatment of the liquid aluminium is necessary.

The aluminium for beverage can manufacture comes primarily from two sources: metal delivered to the casting facility directly from aluminium smelters, and aluminium processed from recycled beverage cans. Can stock casting facilities may be directly adjacent to the smelter or remotely located. In the former case, aluminium is usually taken from the potlines in ladles directly to holding furnaces in the casting facility. In the latter case, metal will be solidified into an easily transportable form (possibly the sows of Fig. E2.2) and remelted at the can stock casting facility. Metal may also be available from recycling operations. In North America over 60% of used beverage cans are collected for recycling. The recycling operation is technically demanding, in that environmental emissions must be minimized without compromising process efficiency or the quality of the final product. The recycling of beverage cans is successful because of the economic and environmental benefits. Economically, there is a large demand for cans, making the expense of collecting them worthwhile. Environmentally, the processing of a used can into a new can uses only 5% of the energy necessary to manufacture a can from virgin aluminium (recall from Chapter 1 the substantial electrical energy required for aluminium reduction).

The aluminium is melted in *reverberatory* furnaces similar to that of Fig. C1.2. The furnaces are usually fired by a fossil fuel, have a capacity of 30–100 t of liquid aluminium, with a liquid metal depth usually not more than 90 cm. As the latent heat of aluminium is relatively high (see Table 2.3) a large amount of heat input is necessary for melting. Therefore, considerable attention is given to maximizing the fuel efficiency, including: control of the furnace atmosphere pressure, preheating of combustion air, and sophisticated control of the air/fuel ratio.

As beverage cans are drawn to very thin gauges, excellent formability is necessary, demanding metal of the highest quality. Therefore, once completely melted, a series of operations to improve the liquid metal quality are initiated. Often the metal is transferred via troughs (referred to as *launders*) from the melting furnace to a *holding* furnace. While in the holding furnace the composition of the melt is analysed and alloying elements added as necessary. Virtually all cans are made from two alloys, AA-3004 (1.25 wt% Mn, 1 wt% Mg) for the body and AA-5182 (4.5 wt% Mg, 0.4 wt% Mn) for the lids. The holding furnace is designed to maintain the aluminium at the correct temperature in a quiescent manner. The temperature is held as low as

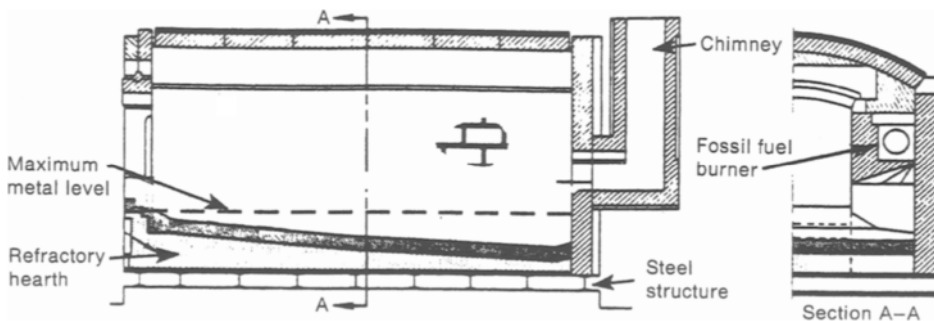


Fig. C1.2 Profile of a typical reverberatory furnace for melting aluminium.

possible above the melting temperature, consistent with maintaining a completely liquid melt, to prevent excessive absorption of hydrogen (see Fig. 2.28). While in the holding furnace, the metal is usually treated with various *fluxing* agents that help separate nonmetallic inclusions into a slag layer that floats on the aluminium surface and can be easily removed. Any heavy inclusions will sink to the bottom of the furnace and become trapped. The metal is poured from the holding furnace by tilting the whole furnace using hydraulic jacks. In this manner, metal is always poured from the surface of the melt in a quiescent fashion, thereby avoiding ingestion of air and oxides, and trapping heavy inclusions in the holding furnace.

On leaving the holding furnace the metal undergoes three important processes prior to entering the casting moulds for solidification. First, a grain refiner is added directly to the flowing metal in the launder. The most common grain refiner for aluminium is a mixture of submicron sized TiB_2 and Ti_3Al intermetallic particles. These particles are suspended in an aluminium rod of about 12 mm diameter which is fed into the launder and melted by the flowing aluminium. Since the intermetallic particles have high melting temperatures, they remain solid throughout the process and act as nuclei for solidification, giving a fine-grained ingot structure. Second, the liquid aluminium passes through an *in-line degasser*. The degasser introduces fine bubbles of an N–Cl–Ar mixture into the aluminium to react with dissolved hydrogen, removing it to the atmosphere. Many casting centres avoid the use of Cl because of environmental and safety considerations. Furthermore, a mixture of N–Ar is effective for degassing. Finally, the metal is filtered through a bed of alumina balls that remove any remaining inclusions. These liquid metal treatments should produce aluminium containing a desirable suspension of grain refining particles, $<0.10 \text{ cm}^3$ per 100 g of dissolved hydrogen and no second phase particles larger than $20 \mu\text{m}$.

Almost all can body stock is cast using the direct chill (see Fig. 2.2) or electromagnetic (EM) casting procedures. Usually several ingots of about 60 cm in thickness and up to 230 cm in width can be cast simultaneously to lengths between 4 and 7.5 m.

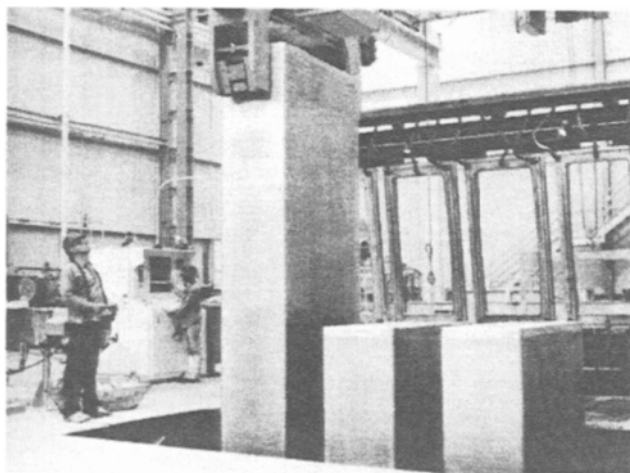


Fig. C1.3 Removal of a direct chill cast ingot of can body stock from casting machine. Five ingots cast at once (two not shown) of $66 \text{ cm} \times 228 \text{ cm} \times 7.5 \text{ m}$ ($\approx 68\,000 \text{ kg}$ each). Note casting moulds tilted upwards for removal. (Reproduced courtesy of Alcan Aluminum Corp., Cleveland.)

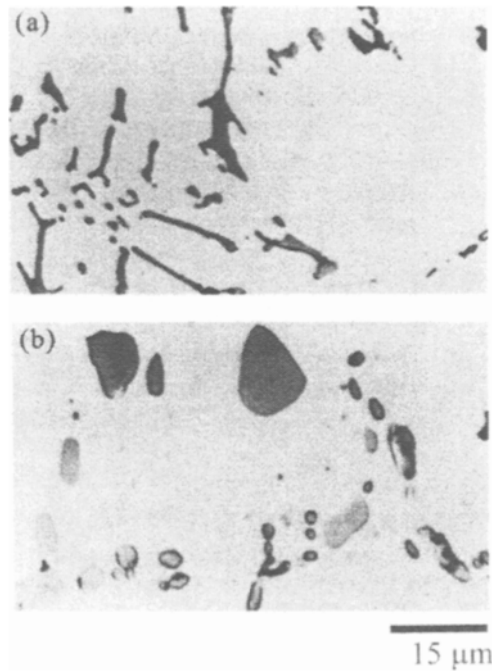


Fig. C1.4 Structure of a DC ingot of Al–Mn alloy: (a) as cast structure; (b) after homogenization. (Reproduced courtesy of Aluminium-Verlag Marketing & Kommunikation GmbH, Düsseldorf.)

The ingots are removed from the casting pits by overhead cranes, as seen in Fig. C1.3. Direct chill casting produces ingots containing an undesirable surface microstructure that results from the initial solidification occurring due to cooling through the aluminium mould (see Fig. 2.2). Consequently, about 12 mm of the ingot surface must be removed by large milling machines (*scalpers*). During EM casting no contact between the liquid aluminium and mould occurs and, therefore, the necessity for scalping is removed. Thus, EM casting improves the process efficiency and is becoming more widely used for casting can stock. Several attempts to produce can body stock by continuous casting have been made. However, the radically different solidification rate of the continuous casting process does not lead to a microstructure suitable for the ironing process (discussed at the end of Chapter 5).

The last step in preparing ingots for hot rolling (discussed at the end of Chapter 4) is *homogenization*. Iron and silicon are found in almost all aluminium alloys, because they occur within the bauxite from which aluminium is refined and their removal during the Bayer and Hall–Héroult processes is difficult. During solidification Fe and Si combine with the Al and other alloying additions to form *constituent* particles of $(\text{FeMn})\text{Al}_6$ and $\alpha\text{-Al}(\text{Fe}, \text{MnSi})$. These particles usually solidify with a *script* morphology similar to that of Fig. C1.4(a), which if not modified will degrade formability. Therefore, the ingots must be homogenized by heating to about 570°C for an extended time. This allows diffusional processes to alter the composition and shape of the constituent particles, which become more spherical (Fig. C1.4(b)). Following homogenization the ingot is cooled to the hot rolling temperature and delivered straight to the hot mill.

Case study 2: Cosworth– Ford casting process

When the internal combustion engine was introduced in the late nineteenth and early twentieth centuries, cast iron was almost universally used for cylinder heads and engine crankcases. A notable exception is the crankcase used on the Wright Flyer of 1903 which was made from an Al–Cu alloy. Cast iron has many desirable attributes for the manufacture of heads and crankcases. The oxides that form during pouring do not degrade the properties of the casting substantially and the iron expands during solidification due to the formation of graphite. These characteristics make the production of sound castings from cast iron relatively easy. Furthermore, cast iron is cheap, widely available and has good vibration damping properties. All of these factors made cast iron the material of choice for automobile engine castings for many decades. In contrast, aluminium easily ingests oxides during pouring, causing deleterious inclusions. It suffers from relatively large shrinkage on solidification and, during the period that automobiles were first introduced, it was expensive and not widely available. Nevertheless, the low density of aluminium was sufficiently advantageous that by the 1960s, it was being widely used for the heads and crankcases of high performance engines. A leading supplier of such engines was Cosworth Engineering, whose V-8 engine developed into the most successful Formula-1 powerplant by the early 1970s. However, the continuing demand for increased power led to several major engine failures caused by entrapment of oxide inclusions where two streams of metal flow together during mould filling, such as between valve seats. These failures highlighted the requirement for a new aluminium shapecasting technology.

A major cause of oxide inclusions in aluminium castings is the multiple turbulent transfers between the furnace, ladle and mould. To eliminate these transfers, in the Cosworth process the aluminium is transferred from a holding furnace to the sand mould by electromagnetically pumping the liquid aluminium up a feeding system that is external to the mould, as shown schematically in Fig. C2.1. This upfiling of the mould ensures a tranquil flow of metal, with minimal ingestion of oxides. Furthermore, electric furnaces are used extensively for melting and maintaining the liquid aluminium temperature, thereby avoiding absorption of hydrogen from fossil fuel combustion. To ensure that hydrogen from the surrounding air is not absorbed by the liquid aluminium, a nitrogen atmosphere is maintained within the holding

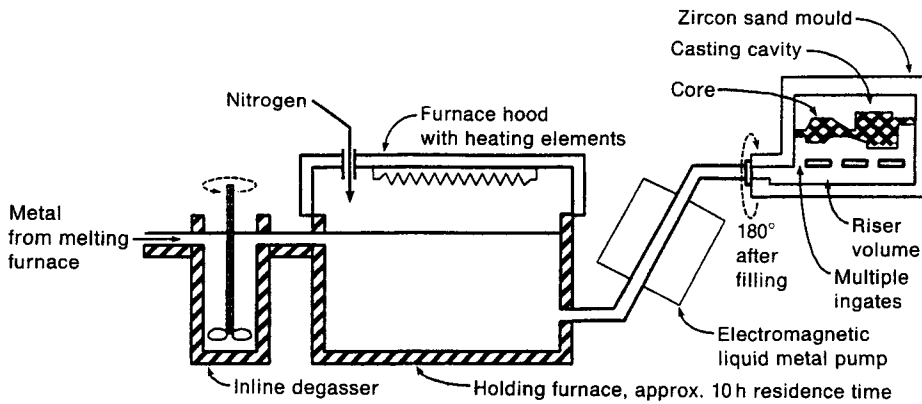


Fig. C2.1 Diagram of Cosworth-Ford casting process.

furnace. The liquid aluminium is held in a holding furnace sufficiently long that any impurities sink to the bottom or float to the surface and are not trapped in the metal flow to the casting mould which is taken from mid-depth of the holding furnace. After filling, the mould is rotated 180° to ensure that any regions of the casting cavity not completely filled during pumping are filled by gravity from metal within the risers. Rotation also allows the mould to be detached from the feeding system for cooling, thereby freeing the filling system for the next mould. These techniques have successfully produced castings with less than 0.001% porosity.

The casting of engine components clearly demands good dimensional control. As sand castings typically have insufficient dimensional control, extensive machining of critical surfaces of the castings is required. To obtain improved dimensional control, the Cosworth process uses zircon sand rather than the more common silica sand. Fig. C2.2 illustrates the major advantage of zircon, which is primarily its very low

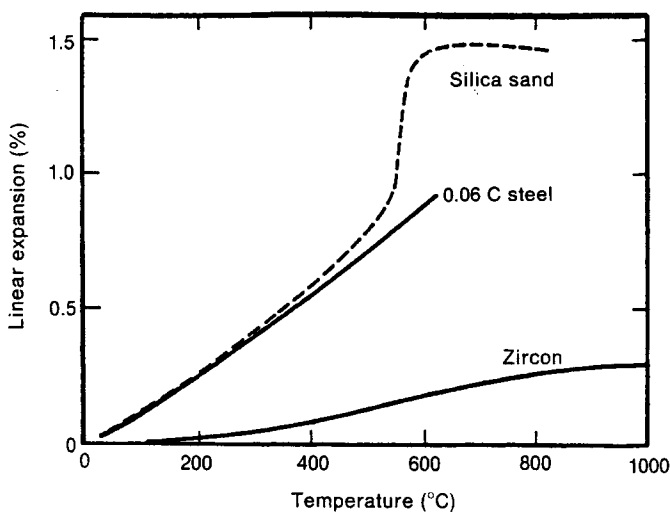


Fig. C2.2 Comparison of thermal expansion of silica sand versus zircon sand used for the Cosworth-Ford casting process.

coefficient of thermal expansion. As such, the change in mould dimensions when the metal is poured, solidified and cooled is greatly reduced, thereby maintaining much better dimensional accuracy and reducing the need for finish machining. Another advantage of zircon is higher thermal conductivity, which causes faster solidification, producing a more refined microstructure. An additional advantage is that the density of zircon sand is close to that of aluminium, thus minimizing buoyant forces on cores during filling. The major disadvantage of zircon sand is that it costs about ten times as much as silica sand. Thus, to make the Cosworth process economically viable, the zircon must be recycled. Hence, in conjunction with the casting developments a recycling process was also developed that successfully reclaims and recycles more than 99% of the zircon sand.

This process has helped Cosworth maintain a leading position as an engine supplier to automobile racing teams. Moreover, the Cosworth process was selected by Ford for the production of passenger car engine blocks. Ford further developed this casting

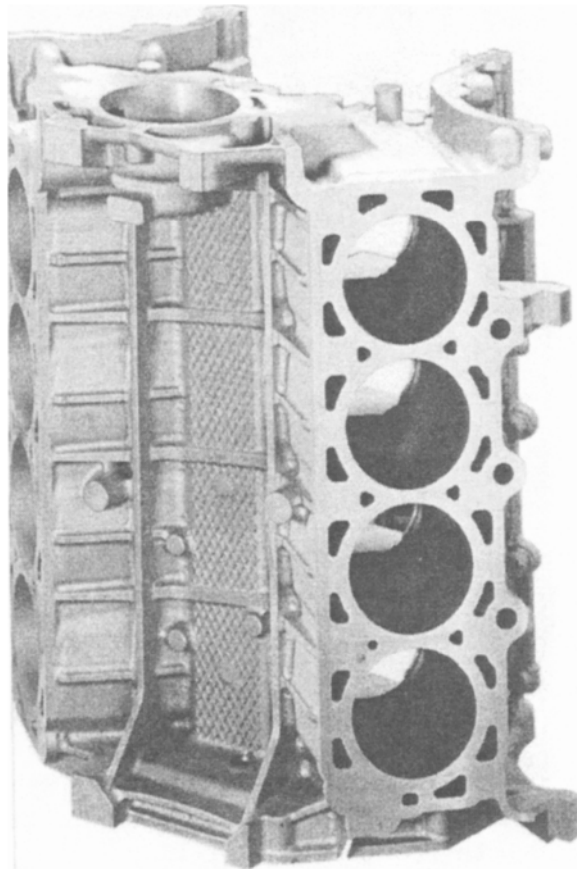


Fig. C2.3 V-8 engine block cast using the Cosworth–Ford process. (Photograph courtesy of Ford Motor Company, Windsor Aluminium Plant, Windsor, Ontario, Canada.)

technology to make it more suitable for high volume production rates. This casting technology is sufficiently important to Ford that a new casting plant utilizing an improved form of the Cosworth process is now in operation in Windsor, Ontario. This facility has the capability of casting more than one million V-6 and V-8 engine blocks per year, such as that shown in Fig. C2.3, used by both Ford and Jaguar.

Stress and strain during deformation

3.1 Introduction

The ingot and continuous casting operations, outlined in the previous chapter, rarely yield a finished product that does not need further processing. Typically, ingots or strands are further processed by one of several *bulk deformation* operations, often followed by additional shaping via *sheet deformation*, *machining* or *joining*. The principles that underlie all of these processes are presented in Chapters 4–8. However, to analyse deformation processes, an understanding of the relationships between stress, strain and deformation is necessary. These relationships are presented in this chapter.

During metal deformation, large changes in part geometry may occur. It is often important to understand the consequences of the geometrical shape change on the internal structure of the metal. Externally, force and power are applied to deform the part. Internally, the part reacts based on its microstructure and properties. These internal and external effects can usually be quantified to some degree by calculations involving the stress–strain relationships of the workpiece. In this chapter basic stress–strain concepts are briefly introduced to illustrate their usefulness for metal deformation problems.

3.2 Engineering stress–strain

The response of a material to mechanical loads is often measured by a uniaxial tension test. A tensile specimen, such as shown in Fig. 3.1, is loaded with a force, F . The extension of the sample, typically measured by a change in gauge length, is recorded and the results displayed as a load–extension curve. Load–extension curves characteristic of low carbon steel and many nonferrous metals are shown in Fig. 3.1. Since both load and extension are clearly dependent on specimen size, they are not unique material properties. Consequently, tensile test results are almost always expressed as stress and strain. *Engineering stress* is defined as

$$\sigma_a = \frac{F}{A_o} \quad (3.1)$$

where: σ_a is the engineering stress

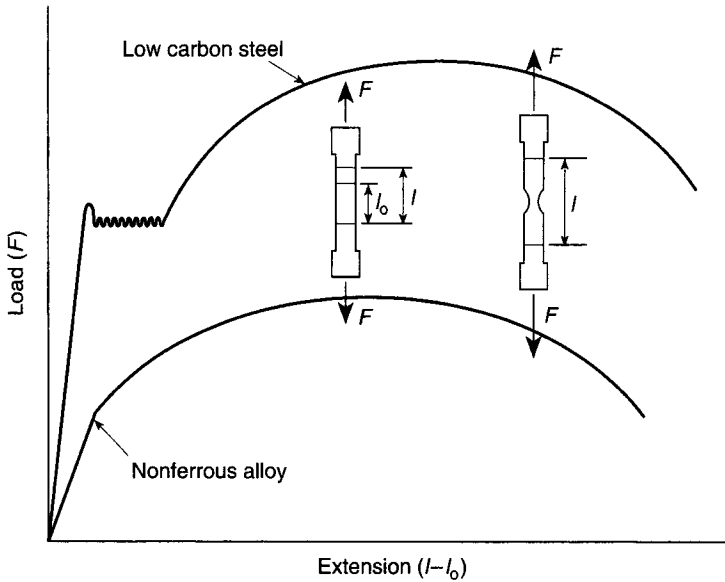


Fig. 3.1 Schematic load–extension curves for a low carbon annealed steel (note pronounced yield point) and a nonferrous alloy.

F is the applied load

A_0 is the original cross sectional area of the tensile sample.

Engineering strain is used to normalize the dependence of the load–extension results on the specimen gauge length, and is defined as

$$e = \frac{l - l_0}{l_0} \quad (3.2)$$

where: e is the engineering strain

l is the gauge length at load F

l_0 is the original gauge length of the tensile sample.

Engineering strain is often expressed as a percentage or 100 times the value of equation 3.2. The quantities expressed in equations 3.1 and 3.2 are referred to as engineering stress and strain, respectively. However, as will become evident, this does not imply that engineers should only be interested in stress and strain calculated according to these expressions.

Engineering stress–strain curves for low carbon annealed steel and nonferrous alloys are shown in Fig. 3.2. Initially, at low strain, a material deforms *elastically* and there is a linear dependence of stress on strain. At these low strains, *Hooke's law* applies:

$$\sigma_a = Ee \quad (3.3)$$

where E is Young's or the elastic modulus.

Eventually a point is reached where the engineering stress–strain relationship is no longer linear. This represents the limit of proportionality, beyond which equation 3.3 no longer applies and the material undergoes permanent *plastic deformation*. In some

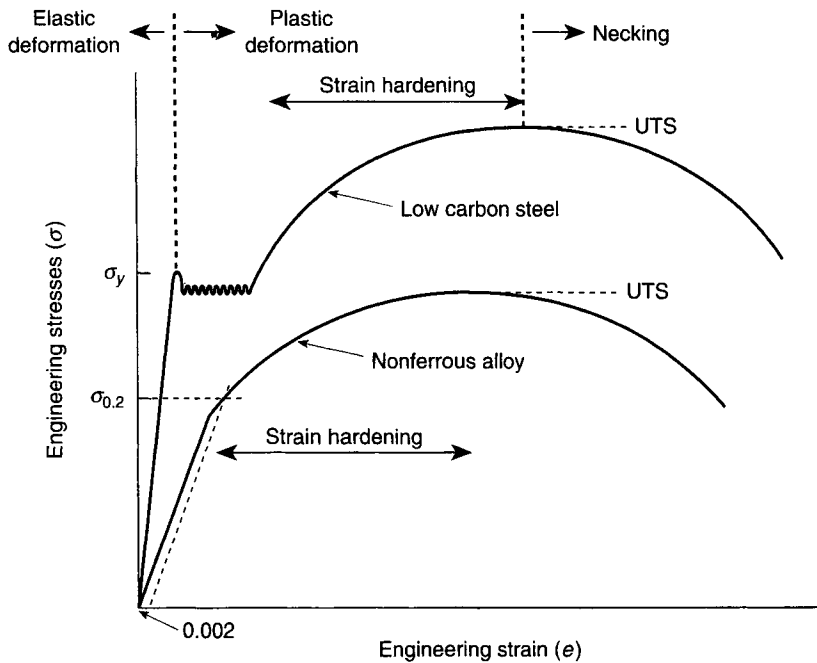


Fig. 3.2 Engineering stress–strain curves corresponding to the load extension curves of Fig. 3.1.

metals, notably low carbon annealed steels, there is an abrupt change between the elastic and plastic strain regions. In such cases the proportional limit is relatively easily measured and the *yield stress*, σ_y in Fig. 3.2, is relatively easily defined. For other materials the proportional limit is less well defined, because the transition from elastic to plastic strain occurs gradually. In these cases the *0.2% offset yield stress* is used to approximate the onset of plastic strain. To calculate the 0.2% offset yield stress, a line intersecting the engineering strain axis at 0.002 strain (0.2% strain) is drawn parallel to the elastic part of the engineering stress–strain curve, as shown in Fig. 3.2. The engineering stress at which this line crosses the engineering stress–strain curve is referred to as the 0.2% offset yield stress, $\sigma_{0.2}$. The yield stresses for several steels and aluminium alloys are listed in Table 3.1.

At strains beyond the yield point, plastic deformation occurs. The engineering stress required to continue extending the specimen increases due to *strain hardening*, which results primarily from an increasing dislocation density. Strain hardening continues until a maximum is reached and the engineering stress required to increase the engineering strain decreases. The maximum engineering stress represents the highest load-carrying capacity of the cross-sectional area and is called the *ultimate tensile strength* (UTS; see Fig. 3.2). Both the 0.2% yield strength and UTS are widely used for engineering design purposes. A summary of the yield strength and UTS values for some common engineering materials is contained in Table 3.1.

Up to the point at which the load begins to decrease (the UTS), the plastic deformation is relatively uniform along the whole length of the sample gauge section. This is referred to as *homogeneous deformation*. Beyond the UTS, as the load decreases,

Table 3.1 Properties of steel and aluminium alloys (annealed condition)

Material composition ^a	Hot worked			Cold worked					
	Temp (°C)	Strain rate strength constant, C (MPa) $\epsilon = 0.5$	Strain rate sensitivity exponent, m $\epsilon = 0.5$	Strength constant, K (MPa)	Strain hardening exponent, n	Yield strength $\sigma_{0.2}$ or σ_y (MPa)	Ultimate tensile strength (MPa)	Elongation (%)	RA (%)
<i>Steels</i>									
1008 sheet (0.08C)	1000	100	0.1	600	0.25	180	320	40	70
1015 bar (0.15C)	800	150	0.1	620	0.18	300	450	35	70
	1000	120	0.1						
	1200	50	0.17						
1045 (0.45C)	800	180	0.07	950	0.12	410	700	22	45
	1000	120	0.13						
	1000	190	0.13						
8620 (0.2C, 1Mn, 0.4Ni, 0.5Cr, 0.4Mo)	1000	170	0.1	1300	0.3	250	600	55	65
302 stainless steel (18Cr, 9Ni)	1000	140	0.08	960	0.1	280	520	30	65
410 stainless steel (13Cr)	1000	140	0.08	960	0.1	280	520	30	65
<i>Al alloys</i>									
AA-1100 (99Al)	300	60	0.08	140	0.25	35	90	35	
	500	14	0.22						
AA-2017 (3.5Cu, 0.5Mg, 0.5Mn)	400	90	0.12	380	0.15	100	180	20	
	500	36	0.12						
AA-3004 (1.1Mn, 1Mg)						59	200	10	
AA-7075 (6Zn, 2.5Mg, 1Cu)	450	40	0.13	210	0.13	100	230	16	

localized deformation occurs as shown in Fig. 3.1. Such localized deformation is called *necking*, and the UTS may be viewed as the onset of *plastic instability*. Necking causes a local decrease in the cross-sectional area of the test sample, reducing its load-carrying capacity. Eventually necking exhausts the plasticity in this region, causing the specimen to rupture. *Ductility* is the ability of a material to accommodate plastic deformation without fracturing and is often measured by the elongation to final fracture, or engineering strain to fracture. Elongation to failure is thus calculated as

$$e_f = \frac{l_f - l_o}{l_o} \quad (3.4)$$

where l_f is the final gauge length at fracture. Note that e_f depends on the initial gauge length and can only be used to compare the ductility of different materials if they are tested with the same gauge length. Table 3.1 lists the elongation based on a 50 mm (2 in) gauge length.

A quantity for measuring ductility that in principle is not dependent on gauge length is the *reduction in area*, given as

$$RA = \frac{A_o - A_f}{A_o} \quad (3.5)$$

where: RA is the reduction in area

A_o is the original cross-sectional area

A_f is the cross-sectional area at the fracture location.

This quantity is independent of the sample gauge length. Moreover, it reflects the local deformation in the necked region, in contrast to the elongation to failure (equation 3.4) which assumes deformation is uniform along the entire gauge length. Therefore, the reduction in area is considered to be a better measure of ductility. Unfortunately, it is also somewhat more difficult to measure. Reductions in area for some common engineering materials are listed in Table 3.1.

Engineering stress and strain are useful for many engineering design applications. However, it must be recognized that engineering stress and strain are based on the initial area or gauge length. Hence, once the material plastically deforms, the engineering stress and strain represent only approximations of the real stress and strain. For many engineering design problems, this approximation does not cause a problem, because permanent or plastic deformation of most structures cannot be tolerated. However, for metalshaping situations large plastic deformations often occur and are necessary. In such instances, the approximations inherent in engineering stress and strain values are unacceptable. For this reason the *true stress* and *true strain*, as defined in the next section, are utilized.

3.3 True stress and true strain

To account for the changing dimensions of the tensile test specimen with load, the true stress is defined as

$$\sigma_t = \frac{F}{A} \quad (3.6)$$

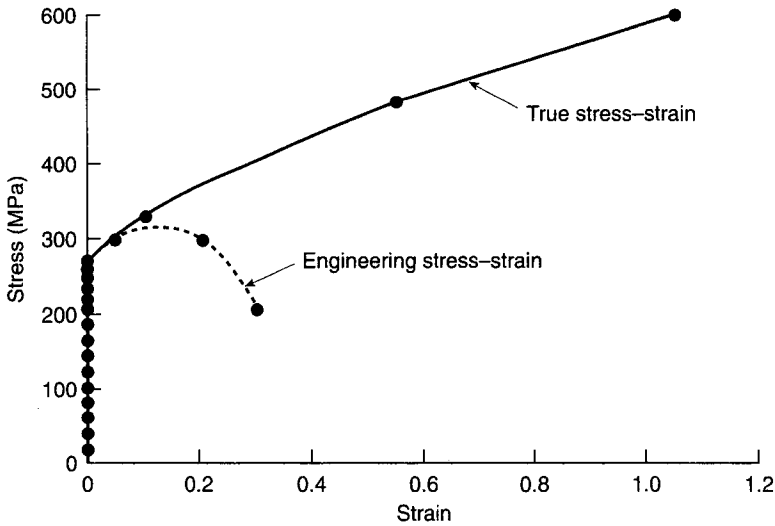


Fig. 3.3 Comparison between true and engineering stress-strain curves for a low carbon annealed steel.

where: σ_t is the true stress

A is the cross-sectional area at load F .

Note that the only difference between equation 3.6 and the definition of engineering stress, equation 3.1, is the use of the instantaneous area (true stress) or initial area (engineering stress), respectively. It should be evident that the latter is considerably easier to measure. Furthermore, for the elastic deformation region (where dimensional changes are small), the initial and instantaneous areas are approximately the same, so $\sigma_a \approx \sigma_t$. Therefore, for many design purposes, where large dimensional changes do not occur, the use of the engineering stress is sufficient and much easier to measure. Although the difference between engineering stress and true stress is negligible during elastic deformation, once the yield point is reached, and plastic deformation occurs, the difference becomes considerable, as illustrated in Fig. 3.3.

In a similar fashion, true strain is based on the instantaneous specimen length, rather than the original length. As such, the true strain (or incremental strain) is defined as

$$d\varepsilon = \frac{dl}{l} \quad (3.7)$$

where: l is the length at load F

ε is the true strain.

The true strain at load F is then obtained by summing all the increments of equation 3.7, as shown in Fig. 3.4. Arithmetically, this can be written as

$$\varepsilon = \sum_n d\varepsilon = \frac{dl_0}{l_0} + \frac{dl_1}{l_1} + \frac{dl_2}{l_2} + \frac{dl_3}{l_3} + \dots + \frac{dl_n}{l_n} \quad (3.8)$$

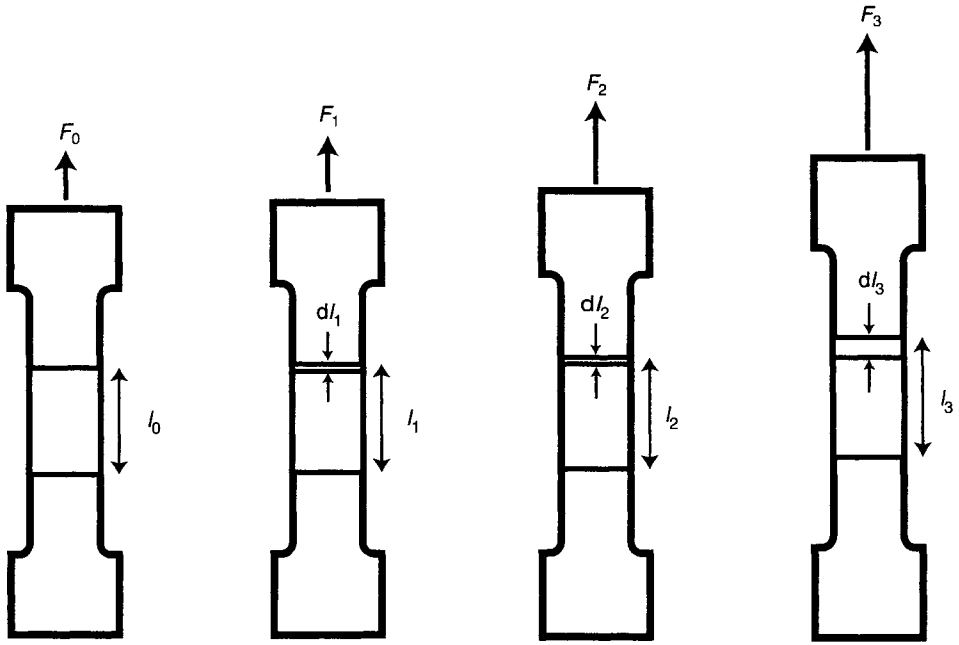


Fig. 3.4 Summation of incremental strains to give true strain: $F_0 < F_1 < F_2 < F_3$.

Taken to the limit, equation 3.8 can be rewritten to give a simple definition for true strain

$$\varepsilon = \int_{l_0}^l \frac{dl}{l} = \ln \frac{l}{l_0} \quad (3.9)$$

It should be noted that both the definition of true strain (equation 3.9) and engineering strain (equation 3.2) are only dependent on the specimen dimensions. Therefore, strain is not a material property, but rather a function of the shape or geometrical change that occurs. This is an important point, that proves useful for the analysis of deformation processes, where dimensional changes necessary are often known, but the corresponding component stresses are required. This situation is dealt with more extensively in Chapters 4 and 5. A characteristic of each material is an ability to accommodate a certain amount of strain (or shape change) before failure, which is the definition of ductility.

Referring again to Fig. 3.3, it is clear that beyond the region of elastic deformation the difference between true strain and engineering strain can be substantial. Therefore, it is absolutely essential that true stress and true strain concepts be used whenever there are large plastic deformations, such as during forging, rolling, extrusion, sheet metal forming etc. These processes are discussed in Chapters 4 and 5.

Equation 3.9 uses length increments to calculate true strain. Therefore, it can only be applied when the strain along the gauge length is uniform. As explained in the previous section, this limits its applicability to strains less than that required for the onset of necking. Once necking begins, the local strain at the necked cross-section

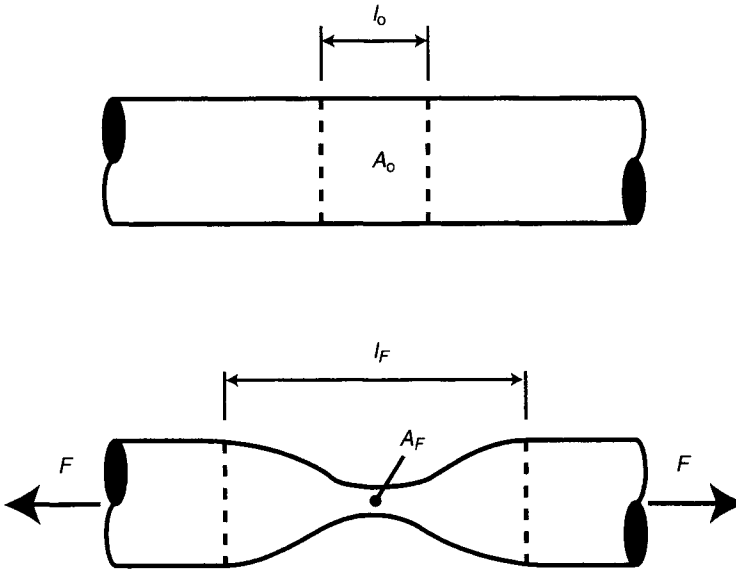


Fig. 3.5 Dimensional changes occurring during necking of a tensile sample.

is higher than elsewhere along the gauge length, and it is necessary to modify equation 3.9 to reflect this situation in the following manner.

Consider the small volume of the gauge length where necking occurs, the length l_0 shown in Fig. 3.5. The volume of material in the necked region before deformation is equal to the volume after deformation, or

$$A_0 l_0 = A_F l_F; \quad \text{or} \quad \frac{l_0}{l_F} = \frac{A_F}{A_0} \quad (3.10)$$

where: A_0 is the cross-sectional area prior to necking
 A_F is the mean cross-sectional area after necking.

Note that *volume constancy* is assumed during deformation. Volume constancy is an important characteristic of metal deformation – in essence it is the continuity equation for metal deformation problems and will prove useful in the solution of several problems in Chapters 4 and 5. Combining equations 3.9 and 3.10, the definition of true strain can be rewritten as

$$\varepsilon = \ln \frac{A_0}{A_F} \quad (3.11)$$

The use of equation 3.11 allows calculation of true strain beyond the onset of necking. Indeed, it is often used right up to the point of fracture, as implied by Fig. 3.3. However, this is not strictly correct, as equation 3.11 only applies when the deformation across the necked cross-section is uniform. When failure is imminent *ductile tears* open in the interior of the specimen creating inhomogeneous strain. Moreover, the presence of the neck causes lateral stress in addition to the applied longitudinal stress. The stress state is therefore no longer uniaxial, but triaxial in the necked region. Despite this situation the true stress–true strain curve is still a useful approximation and is

sufficient for many engineering purposes. In view of this, the true strain in the necked region at fracture is often used as a fundamental measure of the plastic capacity of a material. Combining equations 3.5 and 3.11 provides the following

$$\varepsilon_f = \ln \left(\frac{1}{1 - RA} \right) \quad (3.12)$$

Equation 3.12 shows that there is a unique relationship between the reduction in area (RA) and the true strain to fracture. By virtue of this observation it is apparent that the reduction in area is also a fundamental measure of the plastic capacity of a material.

Example 3.1 Usefulness of true strain – 1

- (a) A bar of length l_0 is uniformly extended until its length $l = 2l_0$. Compute the values of engineering and true strain for this extension.
- (b) To what final length, l , must a bar of initial length, l_0 , be compressed if the strains are to be the same (except for sign) as those in part (a)?

Solutions

(a)

$$e = \frac{\Delta l}{l_0} = \frac{2l_0 - l_0}{l_0} = 1.0$$

$$\varepsilon = \ln \left(\frac{l}{l_0} \right) = \ln(2) = 0.693$$

(b)

$$e = -1 = \frac{l - l_0}{l_0}$$

Therefore, $l = 0$. This means the bar must be compressed to zero thickness! (Clearly an engineering strain of -1 is impossible to achieve.)

$$\varepsilon = -0.693 = \ln \left(\frac{l}{l_0} \right), \quad \text{so } l = l_0 \exp(-0.693) = \frac{l_0}{2}$$

With this definition, the bar need only be compressed to half its initial length to induce the same true strain as in part (a). This is physically more reasonable compared with the requirements when engineering strain is used.

Note: True strains for equivalent deformation in tension and compression are identical except for the sign.

Example 3.2 Usefulness of true strain – 2

A bar of 10 cm initial length is elongated to 20 cm in three stages as follows:

stage 1: 10 cm increased to 12 cm

stage 2: 12 cm increased to 15 cm

stage 3: 15 cm increased to 20 cm.

Assuming homogeneous strain in each stage calculate:

- the engineering strain for each stage and compare the sum of the three engineering strains with the overall value of engineering strain;
- repeat part (a) for true strains.

Solutions

- $e_1 = \frac{2}{10} = 0.2$; $e_2 = \frac{3}{12} = 0.25$; $e_3 = \frac{5}{15} = 0.33$; so $e_1 + e_2 + e_3 = 0.78$, but $e_{\text{overall}} = \frac{10}{10} = 1.0$;
- $\varepsilon_1 = \ln(\frac{12}{10}) = 0.18$; $\varepsilon_2 = \ln(\frac{15}{12}) = 0.22$; $\varepsilon_3 = \ln(\frac{20}{15}) = 0.29$; so $\varepsilon_1 + \varepsilon_2 + \varepsilon_3 = 0.69$; also $\varepsilon_{\text{overall}} = \ln(\frac{20}{10}) = 0.69$.

Note: Using true strains, the sum of the increments equal the overall strain. Thus true strains are additive. This is not true of engineering strains.

Example 3.3 Implication of volume constancy – 1

Show that the law of incompressibility or volume constancy requires that $\varepsilon_x + \varepsilon_y + \varepsilon_z = 0$, where the subscripts x , y and z indicate the principal axis of an orthogonal coordinate system.

Solution Consider a rectangular volume of sides x_0 , y_0 and z_0 and let it deform slightly to another rectangular prism with sides x , y and z . By definition,

$$\varepsilon_x = \ln \frac{x}{x_0}, \quad \varepsilon_y = \ln \frac{y}{y_0}, \quad \varepsilon_z = \ln \frac{z}{z_0}$$

Therefore

$$\begin{aligned} \varepsilon_x + \varepsilon_y + \varepsilon_z &= \ln \frac{x}{x_0} + \ln \frac{y}{y_0} + \ln \frac{z}{z_0} \\ &= \ln \frac{xyz}{x_0 y_0 z_0} = \ln \frac{V}{V_0} \end{aligned}$$

Assuming volume constancy, $V = V_0$, so that

$$\varepsilon_x + \varepsilon_y + \varepsilon_z = \ln 1 = 0$$

The plastic region of a true stress–true strain curve for many materials has the general form of the *Hollomon equation*, which is

$$\sigma_t = K \varepsilon^n \quad (3.13)$$

where: n is the *strain hardening exponent*

K is the *strength constant*.

Both n and K are material properties and are listed in Table 3.1 for some common engineering materials. The strain hardening exponent physically reflects the rate at which the material strain hardens. To clarify the meaning of this, consider the logarithmic equivalent of equation 3.13

$$\ln \sigma_t = \ln K + n \ln \varepsilon \quad (3.14)$$

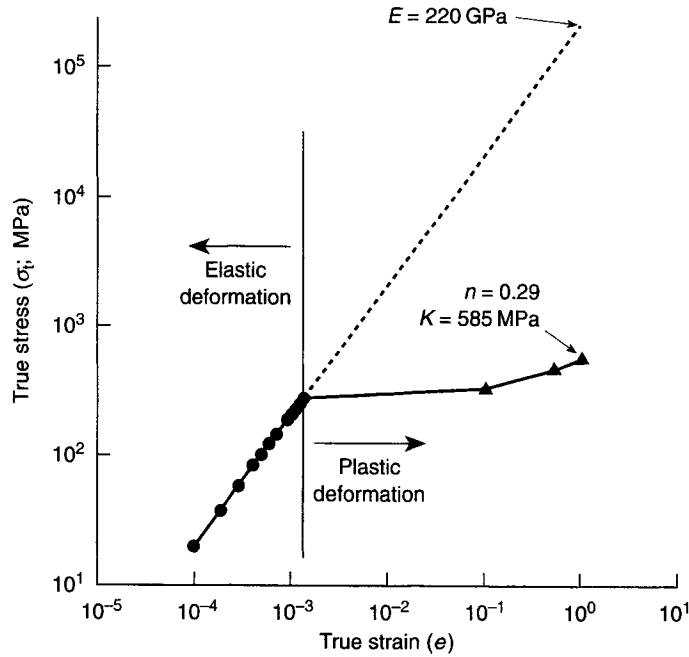


Fig. 3.6 Logarithmic representation of true stress–true strain data of Fig. 3.3.

The derivative of this equation has the form

$$\frac{d\sigma_t}{\sigma_t} = n \left(\frac{d\epsilon}{\epsilon} \right) \quad (3.15)$$

that is, the fractional change in true stress caused by a fractional change in true strain is determined by the strain hardening exponent, n . Therefore, the stress increases rapidly with strain for a material that has a large strain hardening exponent, such as 302 stainless steel (see Table 3.1), compared to a material where n is low, such as 410 stainless steel.

There is a similarity between Hooke's law, used to describe the elastic response of a material to mechanical load ($\sigma_t = E\epsilon$), and equation 3.13 ($\sigma_t = K\epsilon^n$), used to describe the response of a material to mechanical loads in the plastic region. The constants n and K are often found by plotting the true stress–true strain data in logarithmic form (Fig. 3.6). Experimental data usually conforms reasonably well to a straight line in both the elastic and plastic regions. The constants n and K are extracted according to equation 3.14, where n is the slope of the line and K is the intercept at $\epsilon = 1.0$. Elastic stress data plotted on the same diagram provides a value of Young's modulus when extrapolated to $\epsilon = 1.0$.

3.4 Relationship between engineering and true stress–strain

Engineering and true stress–strain are related mathematically in the region up to the UTS where deformation is homogenous. There is, then, a relationship between true

strain and engineering strain in this region. From equation 3.2 the engineering strain can be expressed as

$$e = \left(\frac{l}{l_0} \right) - 1 \quad (3.16)$$

Substituting equation 3.9 into equation 3.16 and rearranging gives

$$\varepsilon = \ln(e + 1) \quad (3.17)$$

At the same time, the true strain at the UTS is numerically equal to n . This is shown as follows. At the UTS, the force that the specimen can withstand is a maximum. Therefore, in terms of the force-extension diagram (Fig. 3.1) the derivative dF/dl is zero. This derivative can be expressed in terms of stress and area:

$$F = \sigma_t A \quad (3.18)$$

Differentiated with respect to length at the maximum load, this yields

$$\frac{dF}{dl} = \sigma_t \left(\frac{dA}{dl} \right) + A \left(\frac{d\sigma_t}{dl} \right) = 0 \quad (3.19)$$

Equation 3.19 can be rearranged as

$$\sigma_t dA = -A d\sigma_t \quad (3.20)$$

Substituting the Hollomon equation (equation 3.13) and its derivative into equation 3.20 provides

$$K\varepsilon^n \frac{dA}{A} = -Kne^{n-1} d\varepsilon \quad (3.21)$$

Note that the derivative of equation 3.11 is

$$d\varepsilon = -\frac{dA}{A} \quad (3.22)$$

or that the incremental strain is equivalent to the rate of change of the area. Substituting this into equation 3.21 and reducing the result gives

$$\varepsilon = n \quad (3.23)$$

Hence, n represents the limiting strain for homogeneous deformation. This relationship, combined with equation 3.17, provides a way of calculating the engineering strain at the UTS; that is,

$$e_{UTS} = \exp(n) - 1 \quad (3.24)$$

where e_{UTS} is the engineering strain at the UTS.

Relationships also exist for converting between engineering stress and true stress for the region of homogeneous strain – strains up to the UTS. By combining equations 3.1 and 3.6,

$$\frac{\sigma_t}{\sigma_a} = \frac{A_0}{A} \quad (3.25)$$

The logarithmic form of this equation is equivalent to true strain; therefore,

$$\ln \frac{\sigma_t}{\sigma_a} = \varepsilon \quad (3.26)$$

Combining this equation with equation 3.17 gives

$$\sigma_t = \sigma_a(e + 1) \quad (3.27)$$

Thus, for the region of homogeneous deformation (up to the UTS), it is possible to obtain the true stress from the engineering stress and strain by using equations 3.17 and 3.27. Likewise, the true stress corresponding to the UTS can be calculated by combining equations 3.24 and 3.27, to generate

$$\sigma_{t_{\text{UTS}}} = \text{UTS} \exp(n) \quad (3.28)$$

This allows the calculation of the true stress at maximum load from the tabulated values for UTS and n in Table 3.1. In fact, it is important to realize that from the equations given in this section it is possible to calculate the true stress and true strain corresponding to the engineering stress and strain for all strains up to the UTS. Therefore, data from a simple engineering stress–strain tensile test is sufficient to generate the true stress–true strain curve, for strains up to the UTS.

Example 3.4 Hollomon equation

A metal obeys the Hollomon relationship and has a UTS of 300 MPa. To reach maximum load requires an elongation of 35%. Find K and n .

Solution

UTS = 300 MPa at $\varepsilon = n$; $e_{\text{UTS}} = 0.35$ using $e_{\text{UTS}} = \exp(n) - 1$

$$n = \ln(e_{\text{UTS}} + 1) = \ln(1.35) = 0.3$$

From $\sigma_t = \sigma_a(e + 1)$

$$\sigma_{t_{\text{UTS}}} = 300(1.35) = 405 \text{ MPa}$$

From the Hollomon equation, $\sigma_t = K\varepsilon^n$

$$405 = K(0.3)^{0.3}; \quad K = 581 \text{ MPa}$$

Therefore, $\sigma_t = 581\varepsilon^{0.3}$

Note: The Hollomon relationship was determined from knowledge easily obtained from the engineering stress–strain test.

3.5 Deformation work

Work is defined as the product of force and distance. A quantity equivalent to work per unit volume is the product of stress and strain. Since the relationship between stress and strain in the plastic range depends on the particular stress–strain curve, the work per unit volume can be calculated by referring to Fig. 3.7. Note that the area under the true stress–strain curve for any strain ε_1 is the *energy per unit volume*, u , or *specific energy*, of the deformed material. This is expressed as

$$u = \int_0^{\varepsilon_1} \sigma \, d\varepsilon \quad (3.29)$$

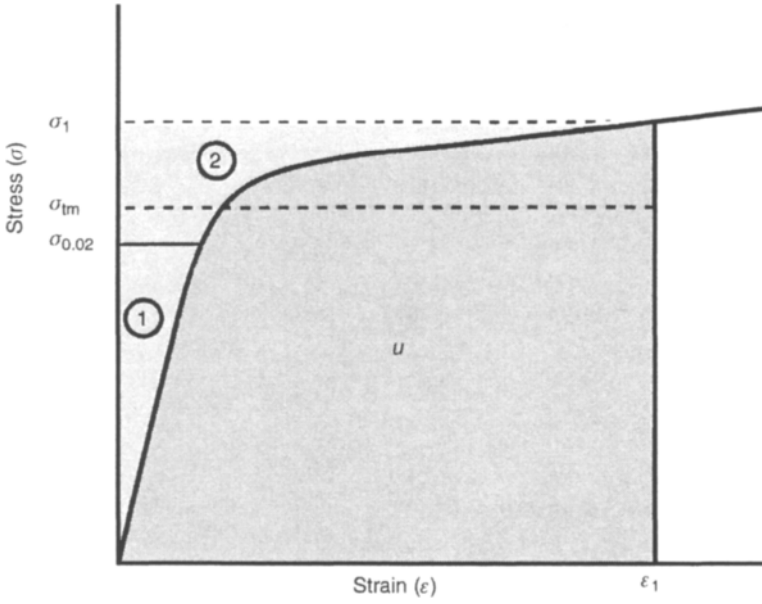


Fig. 3.7 True stress–true strain curve, illustrating energy per unit volume, u , as area below $\sigma - \epsilon$ curve. σ_{tm} is the mean true stress for deformation to ϵ_1 , determined by equating areas ① and ②.

As seen by equation 3.13, the true stress–strain curves can be represented by the Hollomon equation, hence equation 3.29 may be rewritten as

$$u = K \int_0^{\epsilon_1} \epsilon^n d\epsilon \quad (3.30)$$

Integrating equation 3.30 gives

$$u = \frac{K\epsilon_1^{n+1}}{n+1} = \sigma_{tm}\epsilon_1 \quad (3.31)$$

where σ_{tm} is the *mean true flow stress* of the material defined graphically in Fig. 3.7. The energy per unit volume in terms of the mean flow stress is $\sigma_{tm}\epsilon_1$ and equation 3.31 can be rewritten as

$$\sigma_{tm} = \frac{K\epsilon_1^n}{n+1} \quad (3.32)$$

This equation now gives the mean true flow stress as a function of the total strain, ϵ_1 . Equation 3.31, when combined with the volume of the workpiece V , gives the total work required for metal deformation as

$$W_t = \frac{KV\epsilon_1^{n+1}}{n+1} \quad (3.33)$$

The work calculated according to equation 3.33 assumes that the deformation is homogeneous throughout the deforming part. As this is often not the case, the quantity calculated from equation 3.33 is referred to as the *ideal deformation work*, W_i .

Example 3.5 Ideal work of deformation

Deformation of fully annealed AA-1100 aluminium is governed by the Hollomon equation. If a 10 cm long bar of this material is pulled in tension from a diameter of 12.7 mm to a diameter of 11.5 mm, calculate the following:

- (a) the ideal work per unit volume of aluminium required;
- (b) the mean stress in the aluminium during deformation;
- (c) the peak stress applied to the aluminium.

Solutions

- (a) Calculate total strain during deformation

$$\begin{aligned}\varepsilon &= \ln \frac{A_o}{A} = 2 \ln \frac{d_o}{d} \\ &= 2 \ln \frac{12.7}{11.5} = 0.199\end{aligned}$$

Calculate the total volume of bar

$$V = \frac{\pi d^2}{4} \times l = \frac{\pi (0.0127 \text{ m})^2}{4} \times 0.1 \text{ m} = 1.26 \times 10^{-5} \text{ m}^3$$

From Table 3.1 for AA-1100, $K = 140 \text{ MPa}$ and $n = 0.25$. Note that, as $\varepsilon < n$, the deformation is homogeneous

$$\begin{aligned}W_i &= K \times \frac{\varepsilon_1^{n+1}}{n+1} \times V \\ &= 140 \times 10^6 \frac{\text{N}}{\text{m}^2} \times \frac{0.199^{1.25}}{1.25} \times 1.26 \times 10^{-5} \text{ m}^3 = 187.5 \text{ N m (J)}\end{aligned}$$

- (b) Mean stress during deformation

$$\begin{aligned}\sigma_{\text{tm}} &= K \times \frac{\varepsilon_1^n}{n+1} \\ &= 140 \text{ MPa} \times \frac{0.199^{0.25}}{1.25} = 74.8 \text{ MPa}\end{aligned}$$

- (c) Peak (maximum) stress applied, from Hollomon equation

$$\sigma_t = K \varepsilon_1^n = 140 \text{ MPa} \times 0.199^{0.25} = 93.5 \text{ MPa}$$

The ideal work of deformation always underestimates the actual work of deformation, because no account is made for the work required to overcome frictional forces or *redundant work* required for localized internal shearing of the workpiece.

The redundant work occurs because during many deformation processes, planar surfaces in the starting material do not remain planar as a result of the deformation. To understand this, consider the reduction in thickness of a bar through stationary dies as illustrated in Fig. 3.8. The ideal work of deformation only accounts for the work due to the strain necessary to reduce the workpiece thickness from t_0 to t_1 . However, it is clear that as a result of the bending and unbending of individual elemental volumes of the workpiece, internal shear has occurred. The plane AB

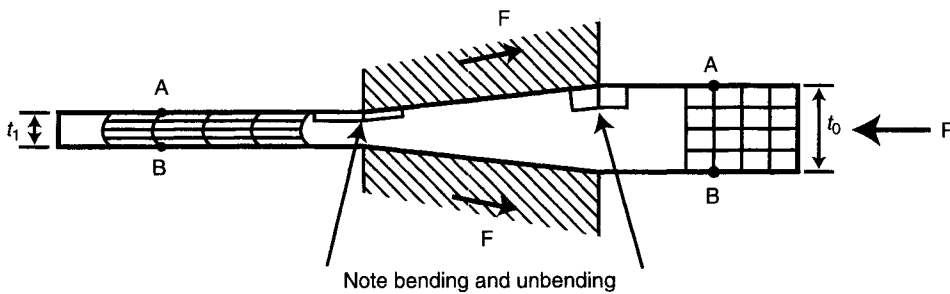


Fig. 3.8 Illustration of deformation of a bar through stationary dies. Redundant work is due to internal shear, causing planar surfaces to become nonplanar.

before deformation is no longer planar after deformation. Clearly, work will be required for the associated internal shearing, which is not included in the calculation of equation 3.33. Despite not accounting for redundant work, equation 3.20 is useful for providing a minimum estimate of the work required for deformation processes. Various methods of estimating the contribution of friction and redundant work to the deformation process are presented in Chapter 4.

3.6 Physical significance of the strain hardening exponent

The strain hardening exponent n is useful in determining the behaviour of materials during many working operations. For example, the high n value of austenitic stainless steels (e.g. 302 SS of Table 3.1) is an indication of poor machinability. This is because the cutting action of the tool causes strain hardening ahead of the tool. Due to the high n value, this causes a large increase in strength and hardness. Thus the cutting tool is always working against higher-strength material, requiring larger cutting forces. The mechanics of machining are presented in Chapter 7.

In contrast, a high n value is desirable for sheet formability, in which resistance to local necking, or reduction in sheet thickness, is necessary. When a high n value material begins to neck, the deforming region rapidly strain hardens, causing subsequent plastic deformation to occur in the surrounding softer metal. This produces a long diffuse neck, as seen in Fig. 3.9. In contrast, necking in a material with a low n value occurs more locally, causing failure at a lower strain. It is noteworthy that many plastics strain harden rapidly, providing them with good sheet forming characteristics, but often causing poor cutting properties.

3.7 Hot deformation

By definition, *hot working* is deformation at temperatures above one-half the absolute melting temperature (the melting temperature in Kelvin). By contrast, cold working usually occurs at below 0.3 of the absolute melting temperature. During hot working several metallurgical mechanisms operate concurrently. Strain hardening (or *work*

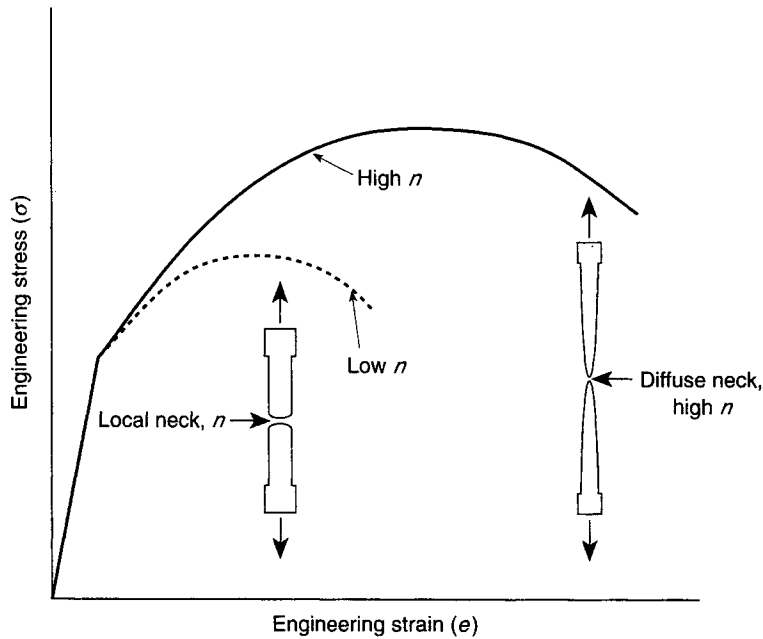


Fig. 3.9 Schematic engineering stress–strain curve for a low n and a high n material, to illustrate the effect of strain hardening on necking.

hardening) can occur as a result of an increase in dislocation density. However, because of the elevated temperature, sufficient internal energy may be available to initiate *dynamic recovery* or *dynamic recrystallization*. These two processes are said to be dynamic, because they occur while the deformation is being applied. Both dynamic recovery and recrystallization serve to annihilate dislocations, causing softening. The combined effect of dynamic recovery/recrystallization is to lower the stress required for deformation. Therefore, the stress required for hot deformation represents a dynamic equilibrium between the hardening processes (dislocation generation) and the softening processes (dislocation annihilation). As a result of the competing hardening/softening processes there is often little difference between the initial and final strength or hardness. Moreover, full recrystallization often occurs while the part cools to ambient temperature. An important consequence of softening occurring during hot working is a reduction of the stress required for deformation, an important ramification of which is that less powerful metal working equipment may be used.

Both dynamic recovery and dynamic recrystallization require significant atomic motion to occur via *diffusion*. As a finite time is necessary for diffusional processes, the high temperature deformation properties of metals are dependent on the rate or time during which strain is applied. To account for time dependency, *strain rate* is defined as

$$\dot{\epsilon} = \frac{d\epsilon}{dt} \quad (3.34)$$

where: $\dot{\epsilon}$ is the strain rate
 t is the deformation time.

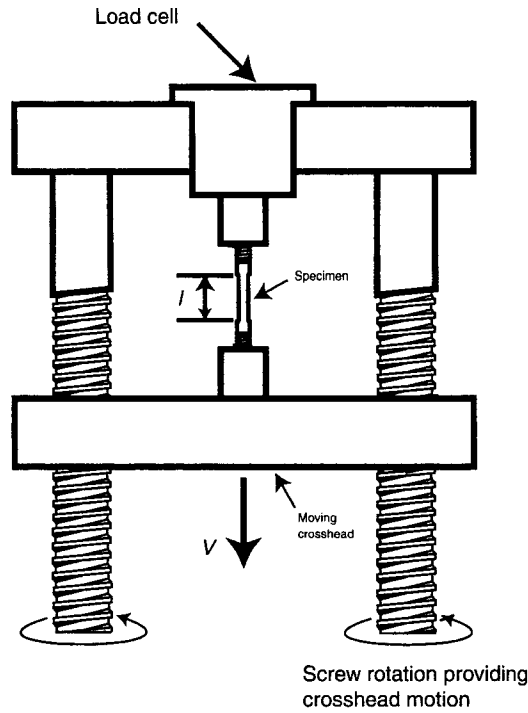


Fig. 3.10 Schematic of tensile testing machine, showing crosshead velocity and specimen length for calculation of strain rate.

For the simple case of uniaxial tension shown in Fig. 3.10, the strain rate is easily calculated as

$$\dot{\epsilon} = \frac{v}{l} \quad (3.35)$$

where: v is the cross-head velocity
 l is the instantaneous deformed length.

As with the definition of true strain, equations 3.34 and 3.35 only apply when deformation is homogeneous. For inhomogeneous deformation (i.e. once necking begins) the strain rate must be redefined as

$$\begin{aligned} \dot{\epsilon} &= \frac{d}{dt} \left(\ln \frac{A_0}{A} \right) \\ &= - \frac{1}{A} \frac{dA}{dt} \end{aligned} \quad (3.36)$$

To characterize the hot deformation behaviour of materials, true stress–true strain data is generated for a range of strain rates, which results in curves such as those shown in Fig. 3.11, typical for many metallic materials. When plotted as true stress versus strain rate (for a constant value of true strain) a linear relationship is often

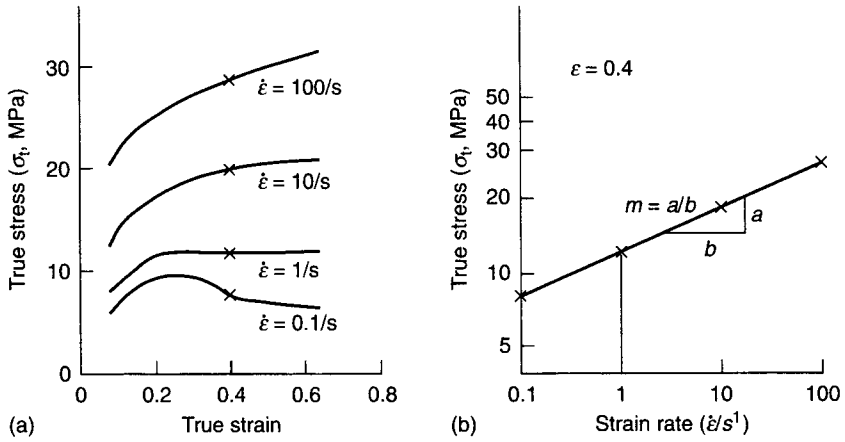


Fig. 3.11 (a) Typical true stress–true strain curves for hot working at various strain rates. (b) True stress versus strain rate at a constant value of strain.

found. The equation of such a plot (Fig. 3.11(b)) is

$$\ln \sigma_t = m \ln \dot{\epsilon} + \ln C$$

$$\sigma_t = C \dot{\epsilon}^m \quad (3.37)$$

where: m is the *strain rate sensitivity exponent*
 C is the *strain rate strength constant*.

Note that in principle this equation only applies to one value of true strain, although for many engineering materials m is not strongly dependent on true strain. Hence in practice, the m value can be used over some range of true strains. C and m are listed in Table 3.1 for several engineering materials.

Example 3.6 Implication of volume constancy – 2

Show that the law of incompressibility or volume constancy also requires that:
 $\dot{\epsilon}_x + \dot{\epsilon}_y + \dot{\epsilon}_z = 0$.

Solution Consider a cube with sides parallel to the axes of the x , y , z coordinate system and let the lengths of the sides be dx_0 , dy_0 , dz_0 . The volume within this cube is $V_0 = dx_0 dy_0 dz_0$. Let an increment of time pass such that the strain rates can effect an incremental distortion. The new side lengths are

$$dx_1 = dx_0(1 + \dot{\epsilon}_x dt)$$

$$dy_1 = dy_0(1 + \dot{\epsilon}_y dt)$$

$$dz_1 = dz_0(1 + \dot{\epsilon}_z dt)$$

The new volume is $V = dx_1 dy_1 dz_1$, but volume constancy demands that $V = V_0$. Substituting,

$$V = V_0 = dx_0 dy_0 dz_0(1 + \dot{\epsilon}_x dt)(1 + \dot{\epsilon}_y dt)(1 + \dot{\epsilon}_z dt)$$

but $V_0 = dx_0 dy_0 dz_0$, so

$$V_0 = V_0[1 + (\dot{\epsilon}_x + \dot{\epsilon}_y + \dot{\epsilon}_z) dt + (\dot{\epsilon}_x \dot{\epsilon}_y + \dot{\epsilon}_y \dot{\epsilon}_z + \dot{\epsilon}_z \dot{\epsilon}_x) dt^2 + (\dot{\epsilon}_x \dot{\epsilon}_y \dot{\epsilon}_z) dt^3]$$

For small dt , $dt \gg dt^2 \gg dt^3$ so that, neglecting second-order effects,

$$\dot{\epsilon}_x + \dot{\epsilon}_y + \dot{\epsilon}_z = 0$$

3.8 Superplasticity

The effect of m on hot deformation behaviour is somewhat analogous to that of the strain hardening exponent n (equation 3.13) for cold deformation. A high m value causes a considerable increase in strength and hardness of the material at high strain rates, leading to a requirement for higher forming forces. Alternately, for high m materials a slow strain rate may be necessary. This can lead to unacceptably long, and often uneconomical, forming times. An important advantage of a high m value is that, like a high n value, improved formability results from the tendency to form a diffuse rather than a local neck, similar to that illustrated in Fig. 3.9. The effect of m on the tendency for necking or localization of deformation can be examined by combining equations 3.6, 3.36 and 3.37, to give

$$\frac{F}{A} = C \left(-\frac{1}{A} \times \frac{dA}{dt} \right)^m \quad (3.38)$$

Note that dA/dt represents that rate of shrinkage of the cross-section or the necking rate. Rearranging equation 3.38 to isolate the neck rate gives

$$\frac{dA}{dt} = \left(\frac{F}{C} \right)^{\frac{1}{m}} \times \frac{1}{A^{\frac{1-m}{m}}} \quad (3.39)$$

As $m \rightarrow 1$, the rate of reduction of area becomes independent of the cross-sectional area and the deformation only depends on the applied load and the constant C . This means that any irregularities in the cross-sectional area remain, but do not increase. That is, as soon as a local neck forms, it stays, but does not get bigger and necking deformation is displaced to other cross-sectional locations. An example of a material with $m \approx 1$ is hot glass.

For most metals, Table 3.1 gives typical m values between 0.1 and 0.3. However, in some circumstances, metals can attain m values as high as about 0.8, giving rise to very diffuse necks. The benefit of such behaviour, termed *superplasticity*, is very high elongations often exceeding several hundreds or thousands of percent. A common criterion for superplastic deformation is that $m > 0.5$. To attain such deformations, several conditions are necessary, including: (a) a small grain size, typically smaller than $10 \mu\text{m}$; (b) a high deformation temperature, above 0.4 of the absolute melting temperature; (c) a well-controlled slow strain rate, typically below $3 \times 10^{-4}/\text{s}$; and (d) a stable grain size at the deformation temperature. Achieving these conditions has been accomplished for several ferrous and nonferrous alloys. Superplastic forming has found application for forming complicated architectural shapes, as well as structural airframe and aeroengine components of complex shapes.

The metallurgical mechanisms occurring during superplastic flow differ from the strain hardening and dynamic recovery/recrystallization processes discussed previously for most hot working operations. Instead, superplastic deformation occurs predominantly by *grain boundary sliding* and *grain rearrangement*. Both of these mechanisms require a large grain boundary area, hence the need for a small grain size. They are accommodated by grain boundary diffusion, which is a temperature-activated process, hence the requirement for elevated temperature.

3.9 Problems

- 3.1 During stress-strain tension tests many engineering materials exhibit a decrease in engineering stress prior to final fracture. However, the true stress increases continuously until final fracture occurs. Explain this apparent anomaly.
- 3.2 A metal has an elongation to failure of 25% and a reduction of area of 50%. Did this metal neck when tested in uniaxial tension? Support your answer by calculation and explain.
(Answer: necking occurs)
- 3.3 During a tensile test of a round metal specimen with an initial diameter of 12.8 mm, a maximum load of 53.4 kN is reached. At this load the cross-sectional area is 60% of the starting initial area. Calculate the mean true flow stress of the metal during this deformation.
(Answer: 457 MPa)
- 3.4 (a) A metal specimen with a cross-sectional area of 5 cm^2 is pulled in tension. The UTS is 250 MPa and the cross-sectional area corresponding to the UTS is 4 cm^2 . Find K and n . (Answer: $K = 437\text{ MPa}$, $n = 0.22$)
 (b) If a piece of this metal that is 5 cm wide and 20 cm long is deformed, in a similar fashion to that illustrated in Fig. 3.8, from a thickness of 2 cm to 1.8 cm, what is the ideal work of deformation? (Answer: 4.8 kJ)
 (c) Does the calculation of part (b) under- or overestimate the work required for deformation.
 (d) After the deformation of part (b), estimate the yield strength of the metal.
(Answer: 267 MPa)
- 3.5 A cylinder of material is compressed at a constant strain rate of $10^{-2}/\text{s}$ from a starting height of 1 cm to a height of 0.3 cm. What is the time required for the compression?
(Answer: 120 s)
- 3.6 A uniaxial tensile test is performed and the UTS is measured to be 28 ksi. When true stress is plotted against true strain on logarithmic scales, the experimenter calculates that the strength constant is 50 ksi and the strain hardening exponent is 0.25. Determine the accuracy of the calculated values.
(Answer: error is 1.8%)

- 3.7 True strain can be defined as either

$$\varepsilon = \ln \frac{l}{l_0} \quad \text{or} \quad \varepsilon = \ln \frac{A_0}{A}$$

With the aid of a typical engineering stress–engineering strain curve, illustrate the domain for which each of the true strain definitions is *not* applicable. Give reasons for your answer.

- 3.8 A fully annealed bar is deformed from a diameter of 5 mm to a diameter of 4 mm, causing work hardening so that the yield strength of the bar after deformation is 490 MPa. The bar is then further deformed to a diameter of 3 mm and more work hardening occurs, increasing the yield strength to 603 MPa. The bar is then fully annealed at the 3 mm diameter and then deformed to a diameter of 2 mm. Calculate the yield strength of the bar at the 2 mm diameter. Assume (a) that the strain during deformation does not exceed the true strain to fracture, and (b) that plastic deformation of the bar obeys the Hollomon equation.
(Answer: 569 MPa)
- 3.9 The initial diameter of a tensile test specimen is 10 mm. After a certain load is applied the diameter is reduced to 8 mm. Calculate the engineering strain and true strain when the diameter is 8 mm. State any assumptions.
(Answer: engineering strain = 0.56, true strain = 0.44)
- 3.10 A metal bar has initial dimensions of 76 mm length, 12.7 mm width and 7.6 mm thickness. After a load is applied a student measures the new dimensions as 89 mm length, 11.9 mm width and 7.1 mm thickness. Comment on the accuracy of the measurements of the deformed bar.
- 3.11 A specimen of 10 mm diameter is tensile tested and a maximum load of 5 kN recorded with a corresponding 20% reduction in the cross-sectional area. A second specimen of the same material is loaded to a true strain of $n/2$ (where n is the stress exponent). What load is applied to the second specimen?
(Answer: 4774 N)
- 3.12 A cylinder is compressed at a constant strain rate of $10^{-3}/\text{s}$. What is the time required to compress the cylinder to two-thirds of its original height? What will be the time required to compress the cylinder to one-third of the original height?
(Answer: for two-thirds height the time is 410 s, for one-third height the time is 1100 s)
- 3.13 During a high temperature tensile test of a material, it is noted that changing the strain rate by a factor of 10 increases the true stress by a factor of 3. Is this material superplastic? Support your answer by calculation.
(Answer: not superplastic)
- 3.14 A cylinder of 10 cm height and 5 cm^2 initial cross-sectional area is hot compressed with a force of 5 kN. The die–workpiece interface is lubricated with boron nitride, which is very effective at reducing friction, and therefore friction effects can be ignored. The hot deformation equation for the metal of the

cylinder is

$$\sigma_t = 20\dot{\epsilon}^{0.5} \text{ MPa}$$

Calculate the cylinder height 20 s after the force is applied.

Hint: use the differential form for strain rate, i.e.

$$\dot{\epsilon} = \frac{d\epsilon}{dt}$$

(Answer: 3.02 cm)

- 3.15 (a) A metal conforms to the hot deformation relationship

$$\sigma_t = 200 \left(\frac{d\epsilon}{dt} \right)^{0.5} \text{ MPa}$$

where $d\epsilon/dt$ is expressed in s^{-1} . A rod of this material 30 cm long and 1 cm^2 cross-sectional area is oriented vertically, fixed at its upper end and a mass of 10 kg attached to the lower end. Assuming homogeneous deformation (and negligible changes in cross-sectional area), calculate the length of the rod 1 h after loading.

(Answer: $\approx 32.7 \text{ cm}$)

- (b) From the information provided in part (a) is the deformation behaviour of this material superplastic? State a reason for your answer.
- (c) List the four conditions usually necessary for superplastic deformation to occur.
- 3.16 A 5 cm long, 1.28 cm diameter rod of high strength aluminium is tested in tension to failure. The yield strength and UTS were found to be 345 MPa and 485 MPa, respectively, and the total elongation to failure is 18%.
- (a) Calculate the load at yielding and the load at the ultimate tensile strength.
- (b) Assuming that necking occurs when the specimen has elongated uniformly by 15%, what is the instantaneous diameter at the onset of necking?
- (c) What is the true stress at the onset of necking?
- (d) What are the values of n and K for the Hollomon equation.
- (Answer: (a) $\text{load}_{YS} = 44\,400 \text{ N}$, $\text{load}_{UTS} = 62\,400 \text{ N}$, (b) $D = 1.19 \text{ cm}$, (c) 562 MPa , (d) $K = 740 \text{ MPa}$, $n = 0.14$)

Bulk deformation processes

4.1 Introduction

Most metallic materials are subjected to plastic forming during some part of the manufacturing cycle. The stress–strain principles applicable to all deformation techniques were presented in the previous chapter. However, it is useful to divide the discussion of industrial deformation processes into two parts, the bulk forming processes and sheet metal processes. The fundamental difference between these two generic processes is that in bulk forming the whole volume of the workpiece is deformed, whereas in sheet metal forming there is only localized plastic deformation, typically involving a change in sheet thickness. The principles of bulk deformation are discussed in this chapter and sheet metal processes are dealt with in Chapter 5.

The major bulk deformation processes are illustrated in Fig. 4.1. They include *forging*, *extrusion*, *drawing* and *rolling*. The deformation may occur in all regions of the workpiece concurrently, as in forging, or sequentially, as in rolling, extrusion or drawing. All the bulk deformation processes require contact between the working surfaces (dies or rolls) and the workpiece. The size of the workpiece can vary from less than a few grams (e.g. individual thumbtacks) to ingots of many tonnes that may require motors of several thousand horsepower to drive the bulk deformation equipment.

Metals can be formed either hot (above the recrystallization temperature) or cold. Greater deformation is possible and lower forming energies are required during hot working. However, cold forming produces improved surface finish and increases the strength of the product due to strain hardening.

In this chapter, the four bulk deformation processes shown in Fig. 4.1 are described and techniques for estimating the forces, energy and power required for each process presented. It is emphasized that these techniques provide estimates only. The calculation of forming forces is a complex problem and a rigorous solution requires advanced biaxial and triaxial plasticity theory. Some of the advanced techniques for solving multidimensional deformation problems are briefly outlined at the end of this chapter. However, approximate solutions are possible by using uniaxial true stress and strain concepts and some engineering judgement. Such calculations are sufficient for many purposes and are useful in demonstrating the general principles and mechanisms of deformation processing.

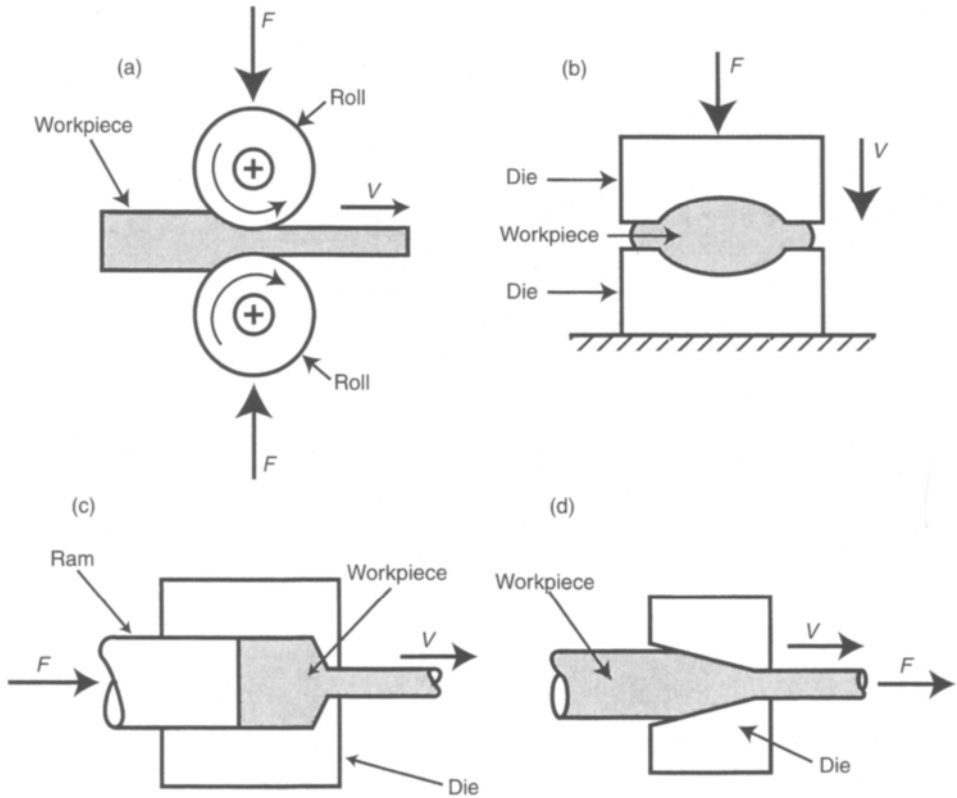


Fig. 4.1 Schematic representations of basic bulk deformation processes: (a) rolling, (b) forging, (c) extrusion, and (d) drawing.

4.2 Friction during bulk deformation

As the forces required for bulk deformation are often substantial, the die–workpiece friction forces can be significant. The forces at the die–workpiece interface are usually described by the nondimensional parameter, the *coefficient of friction*, defined as

$$\mu = \frac{N}{F} \quad (4.1)$$

where: μ is the coefficient of friction

N is the force required to move the body or workpiece along the die

F is the normal force (Fig. 4.1(b)).

For metal forming problems, this mechanical definition of friction may be more usefully restated by normalizing the forces by the area of the die–workpiece interface, to give

$$\mu = \frac{\tau_i}{p} \quad (4.2)$$

where: τ_i is the average interface frictional shear stress
 p is the normal pressure, often the die pressure applied.

This definition of friction coefficient implies that the frictional force is proportional to the normal force and that there must be relative movement between the die and workpiece surfaces. Interfaces at which these conditions exist undergo *slipping friction*.

Slipping friction does not always occur during metalworking. Due to the large forces often required, the die pressure p may increase to such an extent that the frictional shear stress is greater than the shear stress required for deformation of the workpiece. If this occurs, less energy is required for the metal to shear within the body of the workpiece than for the workpiece to move relative to the die. Therefore, the surface of the workpiece remains stationary with respect to the die surface. This is referred to as *sticking friction*, although no actual sticking together of the die and workpiece necessarily occurs. Thus, from equation 4.2, sticking friction occurs when

$$\tau_i = \mu p > \tau_w \quad (4.3)$$

where τ_w is the shear strength of the workpiece.

If the inequality of equation 4.3 is satisfied, the coefficient of friction becomes meaningless. Hence, sticking friction represents an upper limit to the interface stresses that can exist. Deformation with sticking friction usually requires greater energy and, because localized internal shearing of the workpiece occurs, results in less deformation homogeneity compared to slipping friction. For these reasons it is usually desirable to avoid sticking friction during bulk deformation processes.

Example 4.1 Maximum friction coefficient

Show that the maximum meaningful friction coefficient is 0.5.

Solution The internal shear stress within the workpiece is $\tau_i = \mu p$. The interface pressure p is the same as the interface stress, σ . Therefore the internal shear stress is $\tau_i = \mu \sigma$.

From the 'Tresca' or 'maximum shear stress' yield criterion, $\tau_{i\max} \approx 0.5\sigma$. The internal shear stress τ_i cannot exceed $\tau_{i\max}$, because when $\tau_i = \tau_{i\max}$ yielding of the workpiece in shear will occur. Therefore, $\tau_i = \mu p = 0.5\sigma = \tau_{i\max}$ and, as $p = \sigma$, then the maximum $\mu = 0.5$. A friction coefficient above 0.5 is not achievable as shearing of the workpiece will have occurred.

4.2.1 Lubrication to reduce friction

The magnitude of the friction forces is influenced by many factors, not the least of which is the application of a suitable *lubricant* to the die–workpiece interface. Lubricants serve to separate the die and workpiece surfaces, thereby reducing friction. Other desirable attributes of suitable lubricants are: protection of surfaces from wear, stability during the metal processing operations, ability to remove heat from the die–workpiece interface, and minimal toxicity.

Several lubrication mechanisms are exploited during bulk deformation processes to reduce friction. Associated with each of these mechanisms are specifically formulated

Table 4.1 Typical lubricants and approximate friction coefficients for bulk deformation processes

Material	Temperature	Forging		Extrusion		Drawing		Rolling	
		Lubricant	μ	Lubricant	μ	Lubricant	μ	Lubricant	μ
Al alloys	hot	solids	0.15	none	st ^a			mineral oil ^b	0.2
	cold	fatty oils	0.05	soap	0.05	mineral oil	0.04	mineral oil	0.03
Steel	hot	graphite	0.2	glass	0.02			mineral oil ^b	0.2
	cold	soaps	0.05	solids + soap	0.05	soap ^b	0.07	fatty oils ^b	0.07
Stainless steel	hot	graphite	0.2	glass	0.02			mineral oil ^b	0.2
	cold	mineral oils	0.1	mineral oil	0.01	soap	0.05	fatty oils ^b	0.1

^a Sticking friction conditions usually exist.

^b Lubricants are often mixed in an emulsion of water.

lubricants, a few of which are listed in Table 4.1. For metal processing operations, four of the more important lubrication mechanisms are as follows.

1. *Hydrodynamic lubrication* This is effective when there is a large relative velocity between the two surfaces. In such instances a continuous film of lubricant can be maintained between the two surfaces, the friction coefficient is greatly reduced and wear is almost eliminated. A familiar example of a hydrodynamically lubricated assembly is the journal bearings associated with automotive crankshafts. It is the bulk properties of the lubricant, such as viscosity, that controls the friction and wear. Hydrodynamic lubrication can be achieved and is desirable during drawing (Fig. 4.1(d)) but, as will become clear later in this chapter, it can be undesirable during rolling operations (Fig. 4.1(a)). Hydrodynamic lubricants are most commonly formulated from a base of predominantly mineral oils.
2. *Boundary lubrication* Boundary lubrication relies on a thin film of lubricant only a few molecules thick, so that the two surfaces are in contact at asperities only. Boundary lubricants are formulated from organic substances, such as fatty acids and soaps, that consist of long polar molecules that attach to, and sometimes chemically react with, the die or workpiece surface. The thin boundary films are effective at separating surfaces even under large normal forces. Boundary lubricants are most effective at low temperatures, as the long molecules break down with increasing temperature. They can be used separately or can be formulated into mineral oil-based lubricants.
3. *Mixed film lubrication* A combination of hydrodynamic and boundary lubrication, mixed film lubrication is of particular significance for metal processing lubricants. They are often mineral oil-based with additives designed to provide boundary lubrication. Such lubricants are useful to reduce friction between irregular surfaces, as illustrated in Fig. 4.2. Near asperities, where die–workpiece contact may occur, boundary lubrication predominates, but in other regions a hydrodynamic layer is created. This hydrodynamic layer can support large loads, as the incompressible lubricant is trapped in local pockets between asperities. The relative proportion of hydrodynamic to boundary lubrication that occurs depends on the lubricant viscosity and relative velocity between the die and workpiece.
4. *Solid film lubrication* This relies on low shear strength solids to separate the die and workpiece. Unlike hydrodynamic lubricants, solid films are effective when the

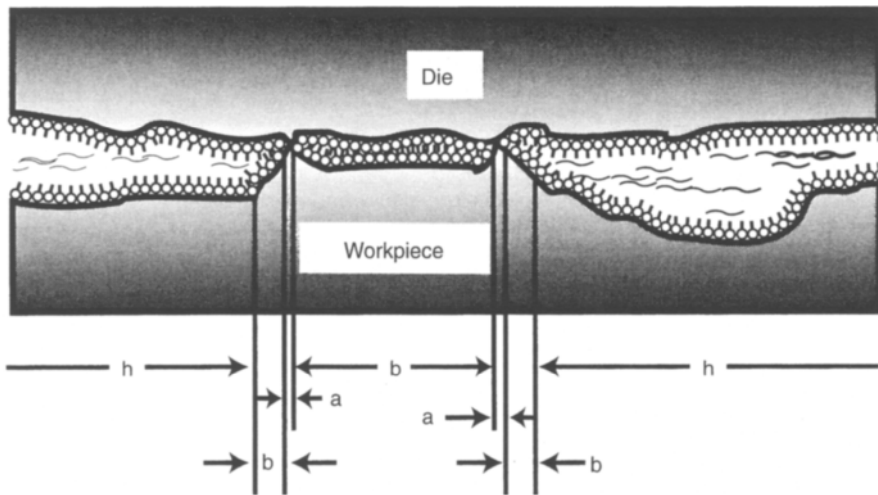


Fig. 4.2 Mixed film lubrication between die and workpiece: 'a' identifies regions of asperity contact, 'b' identifies boundary lubricated regions and 'h' identifies hydrodynamically lubricated regions.

relative velocity between the die and workpiece is low and, unlike boundary lubricants, solids remain effective to high temperatures. Several solids have been used as metalworking lubricants, including graphite, molybdenum disulfide and a variety of glasses. Solids are particularly useful for lubrication during hot forging.

4.3 Forging

Conceptually, forging is an inherently simple process. As shown in Fig. 4.3, the three basic types of forging are *open die*, *closed die* and *impression* forging. It is apparent that open die forging is less suitable for the production of complex finished shapes than closed die or impression forging; however, the tooling required is considerably less complicated and expensive. Closed die forging is appropriate for manufacturing complex shapes. It does demand close attention to die design and workpiece volume, as it is necessary to achieve complete filling of the forging cavity without generating excessive pressures against the die that may cause it to fracture. Impression forging alleviates this disadvantage by incorporating flash gutters into the die design to accommodate extra metal, or *flash*, not required for the forged part.

Each of the operations illustrated in Fig. 4.3 can be applied to small parts, such as the cold heading of nails or mechanical fasteners, or applied to workpieces the size of a cast ingot. The mechanical design of large forging presses can become quite complex. Among other things it can include provision for rapid loading/unloading of workpieces and fast replacement of die sets. A typical mechanical forging press is shown in Fig. 4.4.

Often it is not possible to form round or square ingots into complex shapes in one operation. In such cases, a *die set* is used, which consists of *blocker dies*, used to forge a rough shape into a semifinished part, and *finishing dies*, used to finish the process. An automotive connecting rod processed through a series of blocking and finishing

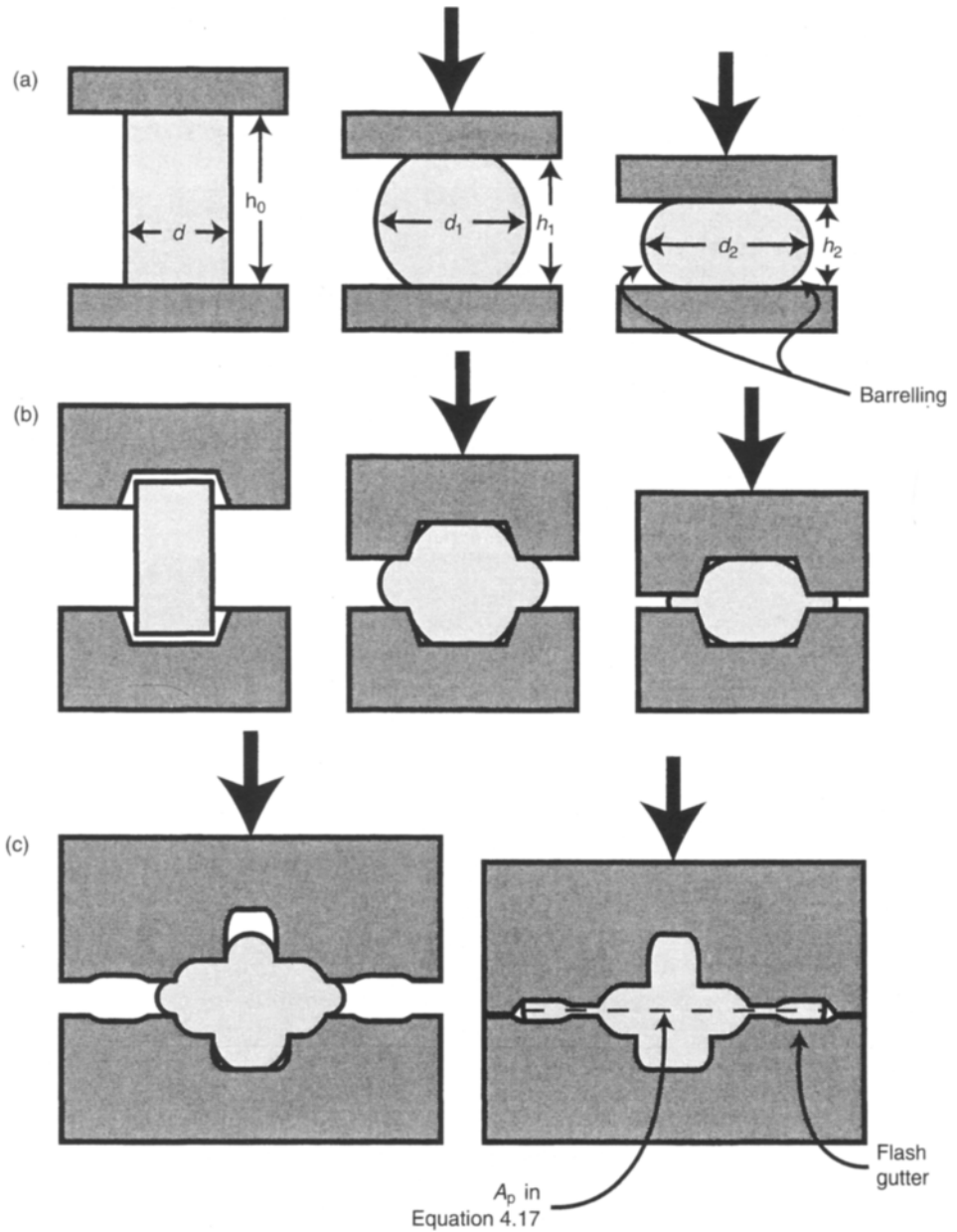


Fig. 4.3 The processes of (a) open die forging, (b) closed die forging, and (c) impression die forging.

dies is illustrated in Fig. 4.5. A round piece is preformed in an open die arrangement. It is then transferred to the blocker die where the part takes on the rough shape of the final part. The finishing die is used to bring the part to final tolerances and surface finish. A flash of excess metal develops during both the blocker and finishing operations, which is removed as a final operation.

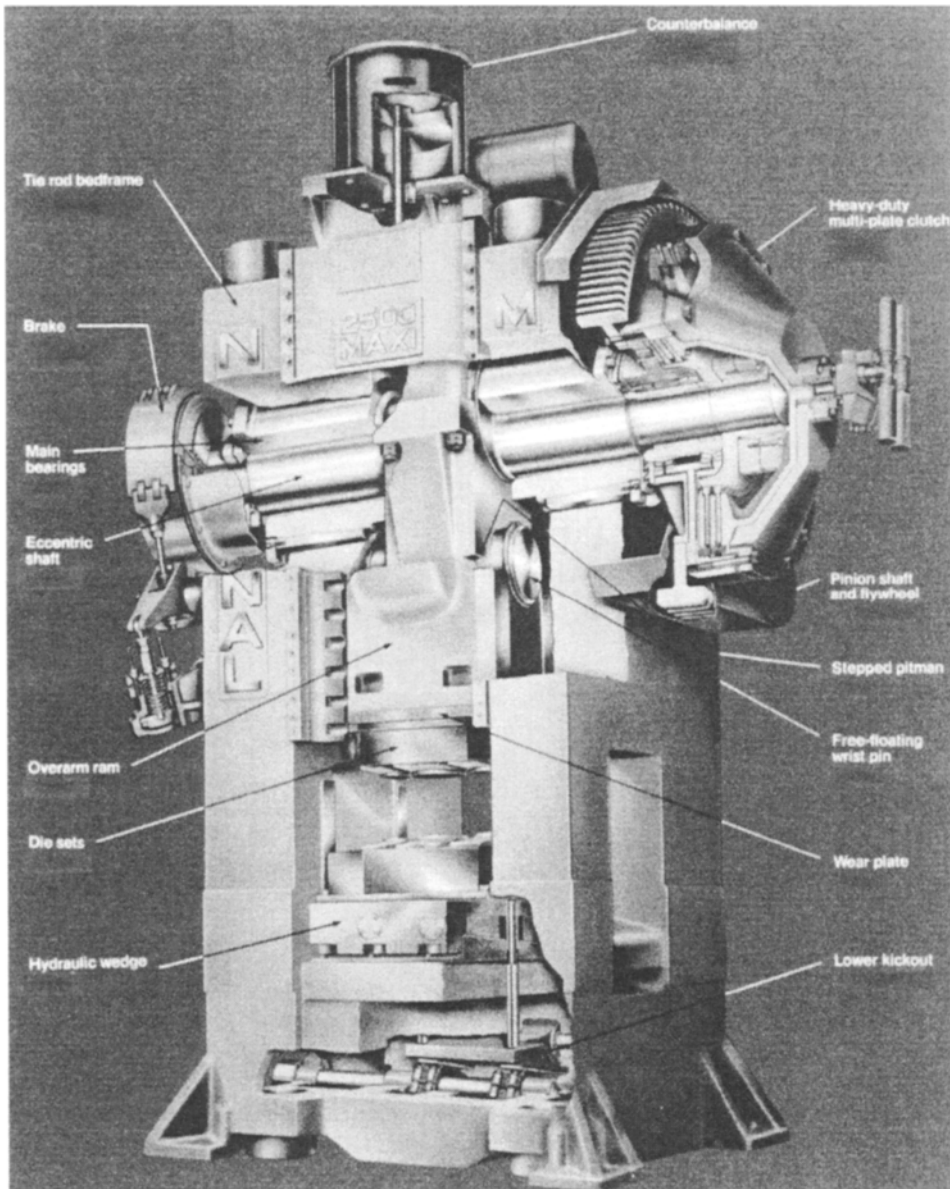


Fig. 4.4 A mechanical forging press, capable of applying a force of 22 700 kN (2500 t) with major components identified, about 8 m total height. (Photograph courtesy of National Machinery Company.)

Wherever possible the forging and die set should be designed for smooth metal flow. Sharp changes in section are to be avoided and generous fillet dimensions should be allowed. To facilitate removal from the die an outside draft of $3\text{--}5^\circ$ should be included, with an inside draft of $7\text{--}10^\circ$. The inside draft is larger to allow for thermal shrinkage as the part cools.

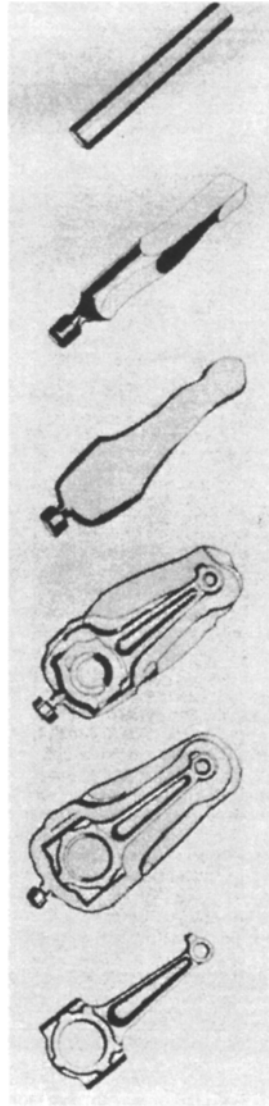


Fig. 4.5 Die set and forging steps for the manufacture of an automobile engine connecting rod. (Reproduced courtesy of Forging Industry Association.)

Typically, the mechanical properties of forged parts are better than those of cast or machined parts. To a large degree this is due to the formation of a grain structure which is elongated in the direction of deformation, causing the macrostructure shown in Fig. 4.6. The metal flow during forging can be visualized by the fibrous morphology of the microstructure. Thus, forging builds in a natural advantageous anisotropy with high mechanical properties in the plane of maximum strain, but perhaps inferior properties across the thickness. Therefore, the anisotropic properties of a forging are coordinated with the service load requirements. Furthermore, during the

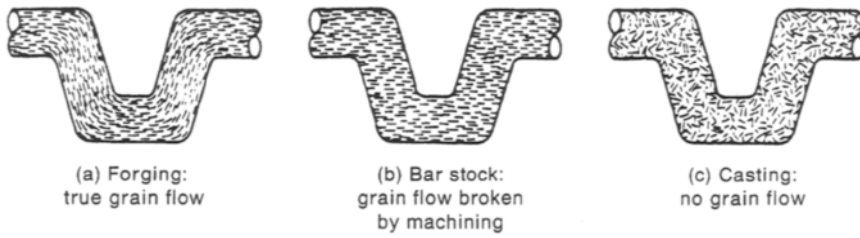


Fig. 4.6 Comparison of grain structure resulting from (a) forging, (b) machining, and (c) casting. (Reproduced courtesy of Forging Industry Association.)

forging deformation, the workpiece will often undergo *recrystallization*, thus developing a fine-grained microstructure and eliminating the cast dendritic structure that has inherently poor properties. If the workpiece is hot forged, then some of the segregation resulting from solidification will be eliminated. All of these factors often result in improved mechanical properties for forged parts compared to castings or machined components.

4.3.1 Cold upsetting a cylinder

The most basic forging process is the *upsetting* of a cylinder (Fig. 4.3(a)). Assume, for the moment, that the metal is cold formed (therefore is strain rate insensitive) and that the platen workpiece interface is frictionless. As the deformation proceeds the cylinder becomes shorter and the diameter increases. As the volume is constant,

$$A_0 h_0 = A_1 h_1 \quad (4.4)$$

where: A_0 is the initial cross-sectional area

h_0 is the original cylinder height

A_1 is the deformed area

h_1 is the deformed height.

The true strain associated with the upsetting operation is

$$\varepsilon = \ln \left(\frac{A_0}{A_1} \right) \quad (4.5)$$

From this the true stress required for upsetting (often called the *flow stress* in forming situations) can be calculated using the Hollomon equation as

$$\begin{aligned} \sigma_t &= K \varepsilon^n \\ &= K \left[\ln \left(\frac{A_0}{A_1} \right) \right]^n \end{aligned} \quad (4.6)$$

Consequently, the forming force is given by

$$F = K \left[\ln \left(\frac{A_0}{A_1} \right) \right]^n A \quad (4.7)$$

The material strength constant, K , and strain hardening exponent, n , are listed for some common engineering materials in Table 3.1.

Recall that the ideal work for deformation is given by equation 3.33, which is

$$W_i = \frac{KV\varepsilon_1^{n+1}}{n+1}$$

where V is the volume of the cylinder, and ε_1 is the total true strain due to upsetting.

Power is the time rate of doing work, and therefore equation 3.33 can be used to calculate the average power consumed per cycle as

$$p_{av} = \frac{1}{t_{av}} \left(\frac{KV\varepsilon_1^{n+1}}{n+1} \right) \quad (4.8)$$

where: p_{av} is the average power per cycle
 t_{av} is the average time per cycle.

These calculations are useful for many operations for which an estimate of the deforming force and power are necessary to size the mechanical equipment required for a particular forging operation.

4.3.2 Hot upsetting a cylinder

In contrast to cold upsetting, if the cylinder of Fig. 4.3(a) is hot upset, then strain hardening effects are minimal, but strain rate effects become important. Again assuming the deformation to be homogeneous, uniaxial and frictionless, the following simple analysis is possible.

When the deformation is homogeneous, the strain rate is defined as

$$\begin{aligned} \dot{\varepsilon} &= \frac{1}{h} \times \frac{dh}{dt} \\ &= \frac{v}{h} \end{aligned} \quad (4.9)$$

where: $\dot{\varepsilon}$ is the strain rate
 v is the platen velocity
 h is the instantaneous height of the cylinder.

In Chapter 3 the true stress during hot working as a function of strain rate was given (equation 3.37) as

$$\sigma_t = C\dot{\varepsilon}^m$$

where C is the strain rate strength constant, and m is the strain rate sensitivity exponent.

The deformation force is obtained by combining equations 4.9 and 3.37 to give

$$F = C \left(\frac{v}{h_1} \right)^m A_1 \quad (4.10)$$

The work done can be defined as

$$W = \int_{h_0}^h F dh \quad (4.11)$$

To obtain an estimate of the magnitude of the work and power, most hot forging operations can be approximated as constant strain rate processes. Thus, combining equations 4.10 and 4.11 gives

$$\begin{aligned} W &= CV\dot{\epsilon}^m \int_{h_0}^{h_1} \frac{dh}{h} \\ &= CV\dot{\epsilon}^m \epsilon_1 \end{aligned} \quad (4.12)$$

and, once again, the average power necessary to upset a cylinder is the time rate of doing work, or

$$p_{av} = \frac{1}{t_{av}} \times CV\dot{\epsilon}^m \epsilon_1 \quad (4.13)$$

4.3.3 Upsetting a cylinder with friction

Although friction-free upsetting is useful for demonstrating the principles of forging, it is unrealistic in practice, as friction is almost certain to develop between the die and workpiece. Horizontal platen friction causes the cylinder to assume the barrelling shape shown in Fig. 4.3(a). As discussed earlier in this chapter, in the extreme the friction forces will be so high that the material adjacent to the platen cannot slide along the platen–workpiece interface – sticking friction. The barrelling causes secondary horizontal stresses, and the associated redundant work increases the vertical stress required for deformation. The amount of barrelling, and the consequent redundant work, depends upon the friction coefficient, which can be estimated from the data of Table 4.1. Using the friction coefficient, the average vertical flow stress is estimated with the aid of Fig. 4.7, which gives a friction multiplying factor Q_a . This factor is

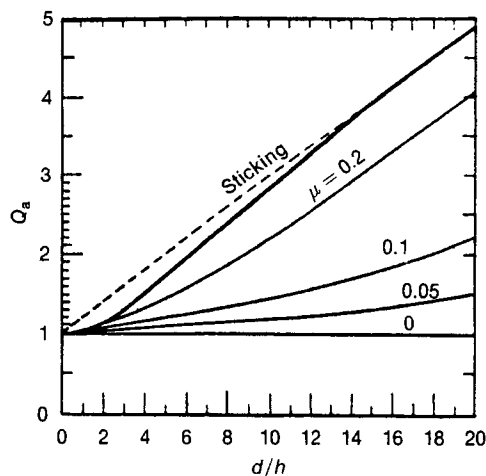


Fig. 4.7 Plot giving multiplying factors for forging as a function of friction coefficient and geometry. (Reprinted from *Journal of Mechanical Working Technology*, 6, J.A. Schey, T.R. Verner, S.L. Takomana, "The Effect of Friction on Pressure in Upsetting at Low Diameter-To-Height Ratios", 23–33 (1982), with permission from Elsevier Science.)

combined with the true stress for deformation (the flow stress) to give an estimate for the actual stress required for deformation according to

$$\sigma_a = Q_a \sigma_t \quad (4.14)$$

where: σ_a is the stress required for deformation including friction

σ_t is the uniaxial flow stress in the absence of friction

Q_a is the multiplying factor (Fig. 4.7).

The deforming force in this case is then

$$F = Q_a \sigma_t A_m \quad (4.15)$$

where A_m is the mean cross-sectional area of the workpiece.

Example 4.2 Cold upsetting

A 302 stainless steel cylinder of height 12 cm and diameter 7 cm at room temperature is compressed to a height of 2 cm between large platens. Mineral oil is used as a lubricant between the cylinder and platens. Calculate the force necessary and stress on the platens.

Solution $F = Q_a \sigma_t A_m$; for 302 stainless steel: $\sigma_t = 1300 \epsilon^{0.3}$ MPa (Table 3.1); coefficient of friction with mineral oil, $\mu = 0.1$ (Table 4.1); to find Q_a using Fig. 4.7, calculate d/h .

From volume constancy, $A_o h_o = A_m h$ so that

$$A_m = \frac{A_o h_o}{h}$$

where the subscript m denotes the mean area or diameter. Therefore,

$$d_m^2 = d_o^2 \frac{h_o}{h} = 7^2 \frac{12}{2}; \quad d_m = 17.2 \text{ cm}$$

and

$$\frac{d_m}{h} = \frac{17.2}{2} = 8.57$$

From Fig. 4.7, $Q_a \approx 1.3$, so $\sigma_a = Q_a \sigma_t$, or

$$\begin{aligned} \sigma_a &= Q_a K \left[\ln \frac{A_o}{A} \right]^n \\ &= 1.3 (1300 \times 10^6) \left(\ln \left[\frac{7^2}{17.2^2} \right] \right)^{0.3} \\ &= 2015 \text{ MPa} \end{aligned}$$

The force required is

$$\begin{aligned} F &= \sigma_a A_m = 2015 \text{ MPa} \times \frac{\pi (0.172 \text{ m})^2}{4} \\ &\approx 46\,500 \text{ kN} \quad (\approx 4740 \text{ t}) \end{aligned}$$

Note: From this calculation, the relatively large forging press of Fig. 4.4 is not capable of cold upsetting the relatively small cylinder of this example.

Example 4.3 Hot upsetting

The 302 stainless steel cylinder of the previous example is hot upset at 1000°C to a height of 2 cm by a platen moving at 2 cm/s. Graphite is used as the lubricant between platen and workpiece. Calculate the forging force necessary.

Solution $F = \sigma_t Q_a A_m$; for 302 stainless steel at 1000°C: $\sigma_t = 170\epsilon^{0.1}$ MPa from Table 3.1; coefficient of friction $\mu = 0.2$ from Table 4.1; $d_m = 17.2$ cm, $d_m/h = 8.57$ from Example 4.2; $Q_a \approx 1.9$ from Fig. 4.7.

$$\begin{aligned} F &= Q_a \sigma_t A_m \\ &= 1.9 \left[170 \times 10^6 \left(\frac{2}{2} \right)^{0.1} \right] \pi \frac{(0.172^2)}{4} \quad \left(\text{recall } \dot{\epsilon} = \frac{v}{h} \right) \\ &= 7500 \text{ kN} \quad (\approx 765 \text{ t}) \end{aligned}$$

Note: For the same deformation operation, increasing the forging temperature reduces the power required by about a factor of nearly 3. This is despite the higher friction coefficient associated with hot deformation.

4.3.4 Forging of rectangular workpieces

The estimation of the forces necessary for the forging of rectangular parts is similar to that for upsetting, but with one important difference related to the stress state of the workpiece. If the width of the workpiece is considerably greater than the length ($w > 10L$ in Fig. 4.8), frictional resistance along the width prevents deformation from taking place in this direction. Hence, deformation occurs in two dimensions only. A *plane strain* stress state exists. A detailed analysis would demonstrate that the forces required for plane strain deformation are considerably greater than those for upsetting cylinders. This can be understood by realizing that plane strain deformation is more constrained than plane stress deformation. An interface multiplying factor can be obtained for this situation in much the same way as for cylinder upsetting. Estimating the interface friction coefficient from the data of Table 4.1, the multiplying factor is then drawn from Fig. 4.9, and the average interface stress calculated according to

$$\sigma_p = Q_p \sigma_t \quad (4.16)$$

where: σ_p is the interface pressure in plane strain
 Q_p is the multiplying factor from Fig. 4.9.

Although the forging of a rectangular shape may seem like a special case, there are many examples of plane strain deformation. An important plane strain deformation process is flat rolling, which is discussed later in this chapter.

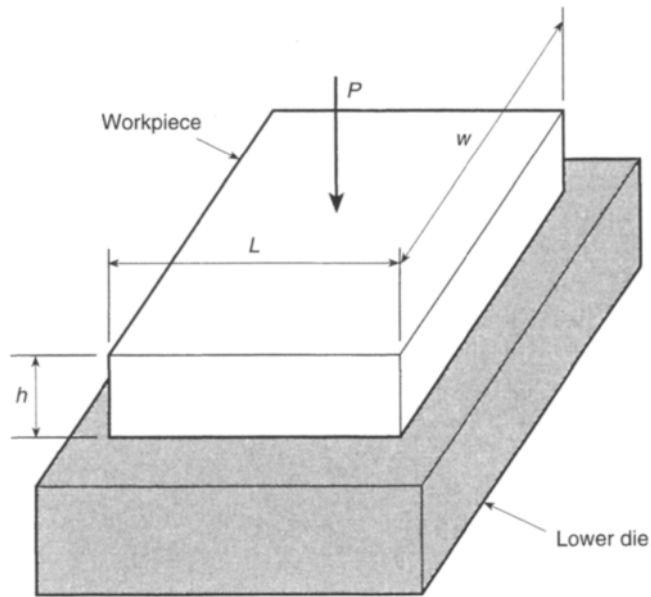


Fig. 4.8 Dimensional system for forging of rectangular workpieces.

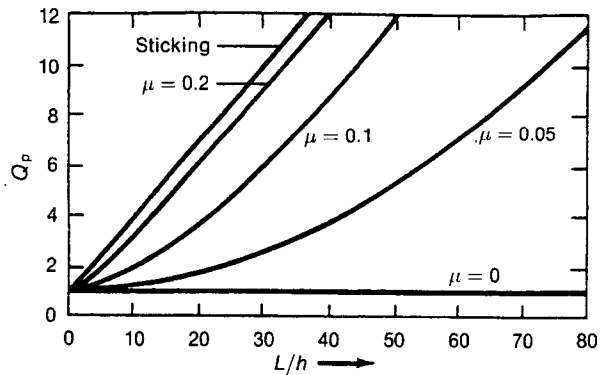


Fig. 4.9 Multiplying factor for plane strain compression.

4.3.5 Closed die and impression forging

The complexity of the deformation occurring during closed die and impression forging makes reliable estimation of the forces required quite difficult. However, approximate values may be obtained by using an analysis technique similar to that presented for open die forging.

The most difficult part of the analysis is often the calculation of the strain. Although the equations for uniaxial strain are straightforward, closed die and impression forging are clearly not uniaxial deformation problems, with different strains

Table 4.2 Multiplying factors for closed die and impression forging

Forging shape	Q_c	Q_h
Simple shape, no flash	3–5	2.0–2.5
Simple shape, with flash	5–8	3
Complex shape	8–12	4

applied to different parts of the workpiece. However, the approximate average strain can be estimated according to

$$\varepsilon_{av} = \ln \frac{h_o}{h_m} = \ln \frac{h_o A_p}{V} \quad (4.17)$$

where: h_o is the average initial height

h_m is the average final height

V is the workpiece volume

A_p is the projected area of the deformed workpiece.

The projected area is the planar area between the die and the deformed workpiece, including flash. The planar area through the deformed workpiece of a typical closed die forging is shown in Fig. 4.3(c). Using the average strain of equation 4.17, the true stress can be calculated using the Hollomon equation, and the actual stress estimated according to

$$\sigma_d = Q_c \sigma_t \quad (4.18)$$

where: σ_d is the estimate of the stress for closed die forging

σ_t is the true stress according to the Hollomon equation

Q_c is determined from Table 4.2.

Equations 4.17 and 4.18 are useful for closed die and impression forging operations at temperatures below the recrystallization temperature. However, most operations such as this are performed hot, so that strain rate effects become important. The average strain rate can be estimated from

$$\dot{\varepsilon} = \frac{v}{h} = \frac{v A_p}{V} \quad (4.19)$$

where: v is the die velocity

V is the workpiece volume

A_p is the projected area.

The average flow stress is calculated using the strain rate of equation 4.19 from equation 3.37, and the actual stress estimated, utilizing Q_h from Table 4.2, according to

$$\sigma_h = \sigma_t Q_h \quad (4.20)$$

From the estimated stress of equation 4.20 or 4.18 (for hot or cold forging, respectively) the forging force can be estimated by multiplying σ_h or σ_d , as appropriate, by the projected area.

4.3.6 Forging and friction

Although the foregoing analysis may seem straightforward, it may not be always immediately obvious how a workpiece will deform. For example, consider the case of open die forging of the circular ring of Fig. 4.10. With the knowledge that during deformation the workpiece volume will remain constant, at least four possibilities for the deformation of this ring can be easily identified:

1. r_o increases, r_i remains the same
2. r_o increases, r_i decreases
3. r_o remains the same, r_i decreases
4. r_o increases, r_i increases.

The factors controlling the deformation are the ratio of the inner and outer radius, and the friction between the workpiece and dies. Clearly the deformation that occurs will be that requiring the least energy. For a given geometry this problem can be solved using the *upper bound* technique described briefly later in this chapter. With the availability of an accurate analytical solution for this geometry, the *ring compression test* is often used to determine the workpiece–die friction coefficient.

Another special deformation situation, where the mode requiring the least energy is an important consideration, is buckling during the open die forging of tall cylinders. If the cylinder of Fig. 4.11 is to be compressed, rather than flattening in a fashion

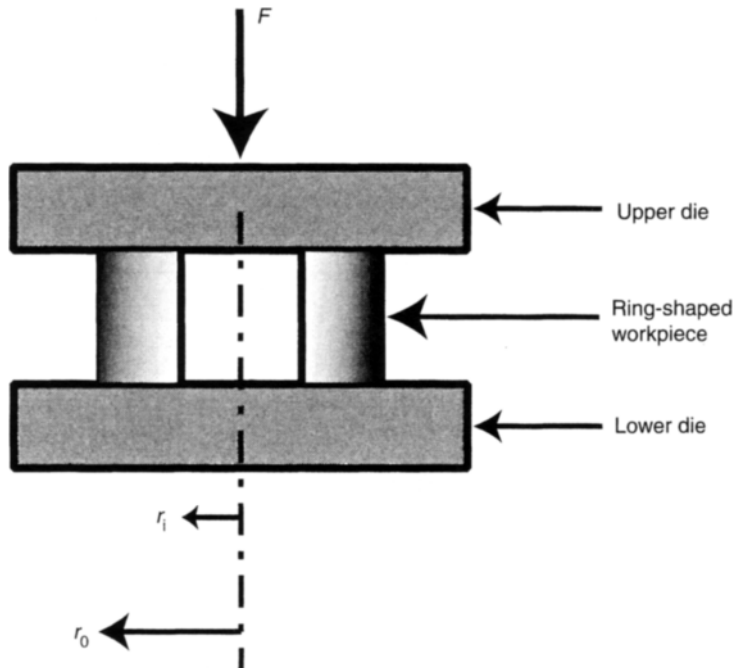


Fig. 4.10 Illustration of the open die compression forging of an axisymmetric shaped ring.

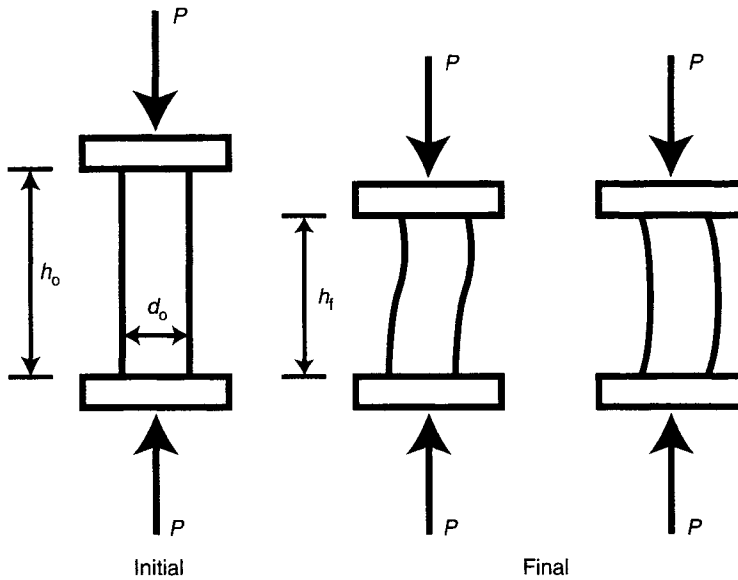


Fig. 4.11 Buckling of a tall cylinder during open die forging.

similar to that shown in Fig. 4.3(a), it may instead buckle, as illustrated. Buckling is likely to be a lower energy deformation mode if $h_o/d_o > 2$.

4.4 Extrusion

The major extrusion processes are shown in Fig. 4.12. *Forward extrusion* (Fig. 4.12(a)) is the most common process and is used for the hot extrusion of both ferrous and non-ferrous metals. In *backward extrusion* (Fig. 4.12(b)) the movement of the ram is in the opposite direction to that of the emerging extrusion. In both forward and backward extrusion, the billet material adjacent to the die opening may not be extruded due to friction between the workpiece and the chamber. This results in a *dead metal zone* which cannot be extruded. The *impact extrusion* method of Fig. 4.12(c) is often used for the production of collapsible tubes or containers such as spray cans. A punch impacts a metal *slug* at a relatively high velocity and forces the slug material to flow at a high strain rate upwards around the punch.

Extrusion presses must be of rugged design to be able to withstand the large forces necessary for metal deformation. A typical forward extrusion press is shown schematically in Fig. 4.13. Such presses are typically hydraulically actuated, in the force range between 15 000 kN and 45 000 kN (≈ 1500 and 4600 t). The *billet* is usually produced using one of the ingot casting processes outlined in Chapter 2. The press is designed to allow fast die changes so that different cross-sectional shapes may be produced. A large array of extruded shapes can be manufactured, as demonstrated by Fig. 4.14.

Like forging, extrusion can be performed hot (above the recrystallization temperature) or cold. Lower ram forces and a fine grained recrystallized structure are possible

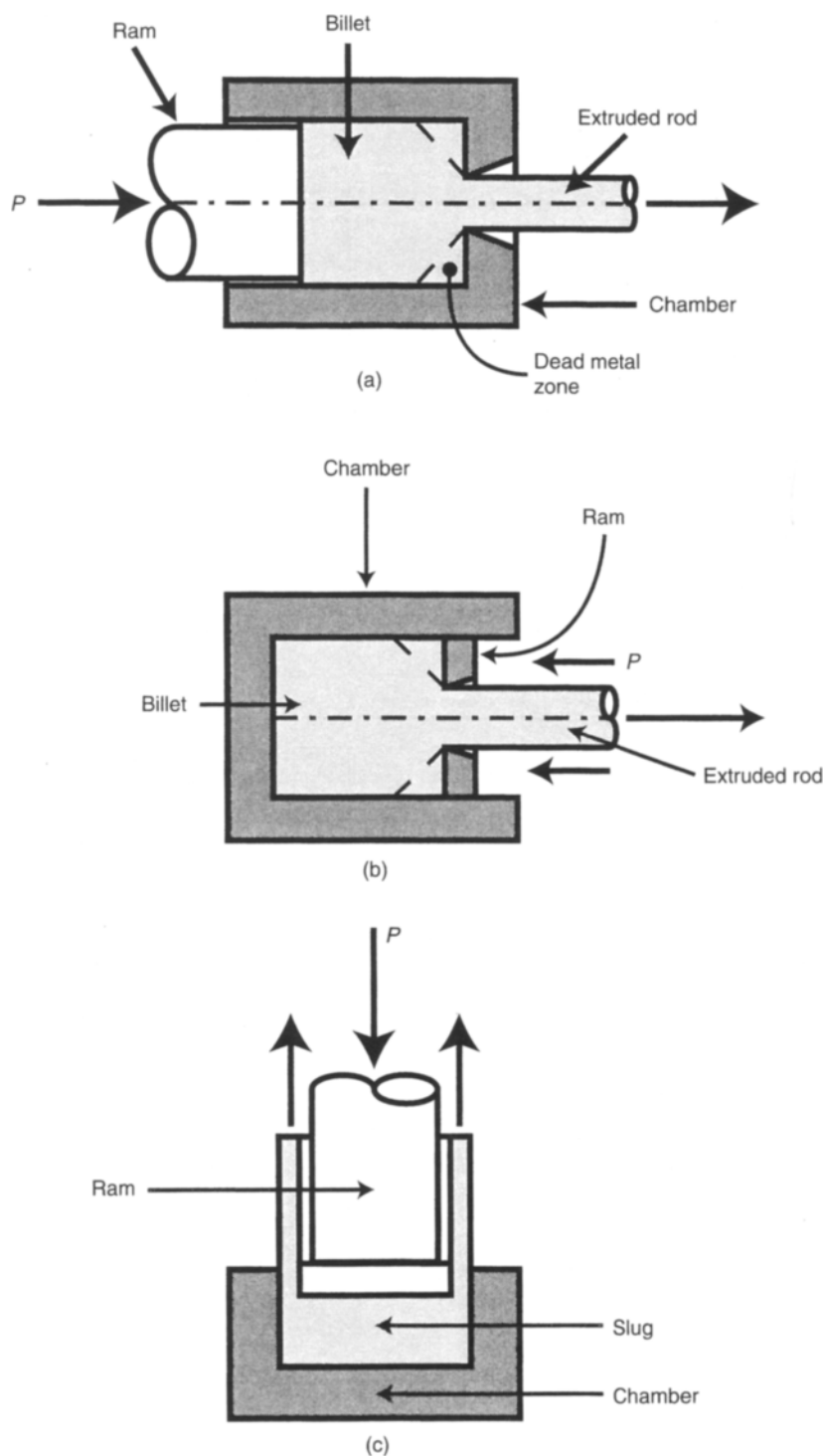


Fig. 4.12 (a) Direct extrusion, (b) backward extrusion, and (c) impact extrusion.

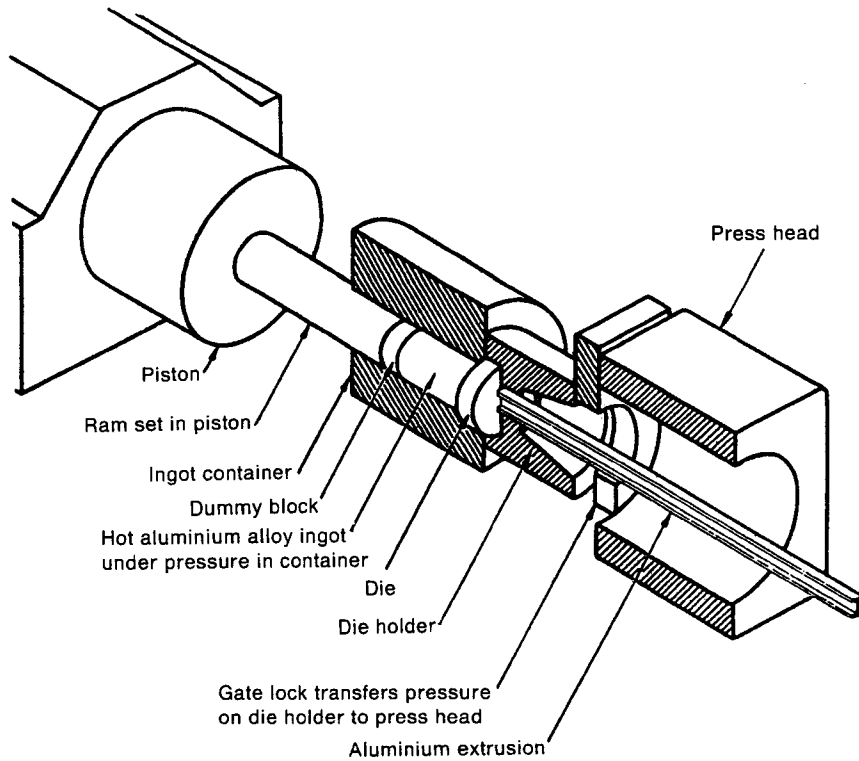


Fig. 4.13 Schematic of a forward extrusion press. (Reproduced from *Handbook of Aluminum*, with permission of Alcan Aluminium Limited.)

when hot extrusion is used. However, a better surface finish and higher strengths (strain hardened metal) are provided by cold extrusion.

4.4.1 Cold extrusion

The same general approach used for forging calculations is applied for estimating extrusion loads. However, when the process is continuous and steady state, as are extrusion, wire drawing, and rolling, the *mean flow stress* during the deformation process must be used rather than the final flow stress, because at any time during the process some material will not yet be deformed, whereas other material will be completely deformed. Thus, for continuous or steady state processes, the mean flow stress calculated from equation 3.32 is used, which is

$$\sigma_{tm} = \frac{K\varepsilon_1^n}{n+1}$$

Once the mean flow stress is obtained, the extrusion pressure can be calculated from

$$p_e = Q_e \sigma_{tm} \quad (4.21)$$

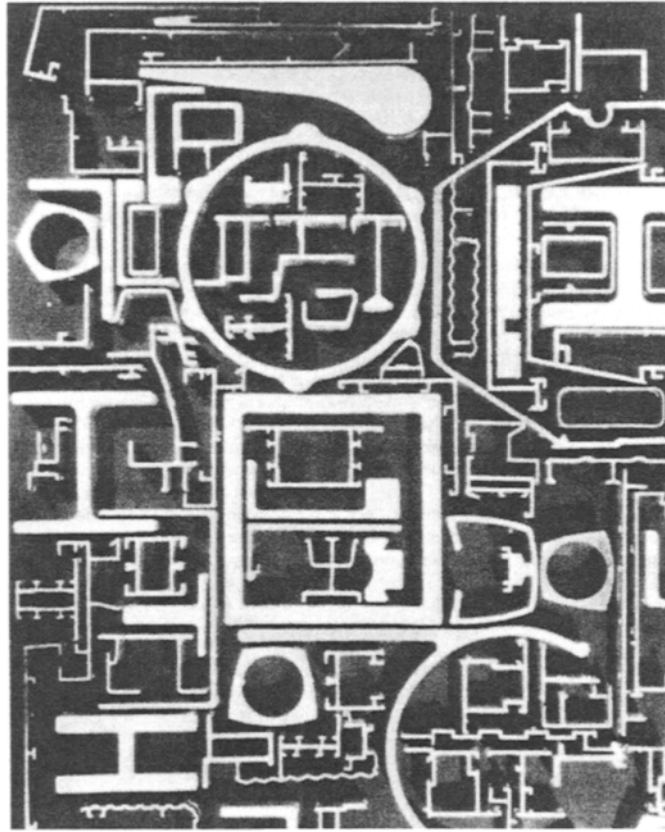


Fig. 4.14 Cross-sectional shapes produced by extrusion. (Reproduced courtesy of Aluminium-Verlag Marketing & Kommunikation GmbH, Düsseldorf.)

where: p_e is the extrusion pressure

Q_e is the multiplying factor for extrusion.

Experience has shown that Q_e depends heavily on the extrusion ratio

$$R_e = \frac{A_o}{A_f} \quad (4.22)$$

where: R_e is the extrusion ratio

A_o is the initial cross-sectional area of the billet

A_f is the final product area.

The multiplying factor for extrusion, Q_e , is related to the extrusion ratio according to

$$Q_e = 0.8 + 1.2(\ln R_e) \quad (4.23)$$

Substituting this into equation 4.21 provides an expression for the extrusion pressure, p_e

$$p_e = \sigma_{tm}[0.8 + 1.2(\ln R_e)] \quad (4.24)$$

In extrusion processes where no lubricant is used, the frictional resistance can be high and extrusion equipment must be able to handle not only the deformation resistance, but the frictional resistance as well. Meaningful coefficients of friction for extrusion are difficult to obtain and it is generally considered better to estimate an extreme value based on sticking friction conditions. Thus, it is assumed that the metal deforms by shearing next to the chamber wall and a shearing resistance must be added to the deformation pressure. The frictional contribution to the punch pressure required can be calculated using the area over which this friction acts. In this manner the frictional resistance force will be

$$F_f = \tau_t \pi D l \quad (4.25)$$

where: F_f is the frictional resistance force

τ_t is the shear flow strength of the material

D is the diameter of the deforming billet

l is the length of the frictional resistance (taking into account any dead metal zone).

The total pressure at the punch is comprised of both the extrusion and frictional pressures, or

$$p_p = p_e + p_f \quad (4.26)$$

where: p_p is the punch pressure required for extrusion

p_f is the frictional pressure required to overcome friction.

Combining equations 4.24 and 4.25, and substituting into 4.26, yields the punch pressure required:

$$p_p = \sigma_{tm} [0.8 + 1.2 \ln R_e] + \frac{\tau_t 4l}{D} \quad (4.27)$$

The true shear stress of the material can be estimated from the flow stress, by making use of Tresca's failure criterion as

$$\tau_t = 0.5 \sigma_t \quad (4.28)$$

The punch or ram must be able to apply the punch pressure, p_p , calculated according to equation 4.27. Therefore, the yield strength of the punch material must exceed the punch pressure.

The total force on the punch is obtained from

$$F_p = p_p A_p \quad (4.29)$$

where: F_p is the punch force

A_p is the punch area.

It is important to ensure that the mechanical design of the extrusion press is capable of reacting to this force.

The punch force multiplied by the punch velocity provides a power requirement for the extrusion press as

$$P = F_p v \quad (4.30)$$

where: P is the extrusion power requirement

v is the velocity of the extrusion ram or punch.

As pointed out at the beginning of this chapter, these calculations provide approximate values only, but they serve as guidelines that are useful in practice, as well as providing insight into the parameters controlling the extrusion process.

4.4.2 Hot extrusion

As might be expected, strain rate effects become important during hot extrusion. A detailed analysis of the extrusion processes of Fig. 4.12 gives the mean strain rate during extrusion as

$$\dot{\epsilon}_m = \frac{6vD_o^2 \ln R_e}{D_o^3 - D^3} \quad (4.31)$$

where: $\dot{\epsilon}_m$ is the mean strain rate

v is the punch velocity

D_o is the billet diameter

D is the extruded product diameter.

From this mean strain rate, a mean flow stress can be calculated using equation 3.37, and equations 4.27 to 4.30 can then be used to calculate punch pressure.

Example 4.4 Impact extrusion of fire extinguishers

Your company makes 4 lb fire extinguishers by impact extruding AA-1100 aluminium. The slugs for impacting have a diameter of $4\frac{1}{2}$ in and are $\frac{1}{2}$ in thick. The punch used for impacting is $4\frac{1}{8}$ in diameter, as is the fire extinguisher inside diameter. It is required that 100 fire extinguishers be extruded per minute. Calculate the punch force and average power required.

Solution

$$A_o = \pi \frac{d_o^2}{4} = \pi \frac{4.5^2}{4} = 15.9 \text{ in}^2$$

$$A_f = \pi \frac{(d_o^2 - d_f^2)}{4} = \pi \frac{(4.5^2 - 4.125^2)}{4} = 2.54 \text{ in}^2$$

$$A_{\text{punch}} = \pi \frac{d_{\text{punch}}^2}{4} = \pi \frac{4.125^2}{4} = 13.4 \text{ in}^2$$

$$R_e = \frac{A_o}{A_f} = 6.25; \quad \epsilon = \ln R_e = 1.83$$

For AA-1100 from Table 3.1, $K = 140 \text{ MPa}$ or $20\,304 \text{ psi}$ and $n = 0.25$. The average mean true stress for the process is calculated as follows

$$\sigma_{tm} = K \left[\frac{\epsilon^n}{n+1} \right] = 20\,394 \left[\frac{1.83^{0.25}}{1.25} \right] = 18\,976 \text{ psi}$$

$$Q_e = 0.8 + 1.2 \ln R_e = 2.99$$

$$p_e = 18\,976 \times 2.99 = 56\,738 \text{ psi}$$

$$F_p = p_e \times A_p = 56\,738 \times 13.4 = 760\,293 \text{ lb}_f \approx 380 \text{ t}$$

Work for extrusion

$$W = K \frac{\epsilon^{n+1}}{n+1} \times V$$

$$V \text{ (volume)} = \pi \frac{4.5^2}{4} \times 0.5 = 8 \text{ in}^3$$

$$W = 20\,304 \frac{(1.83)^{1.25}}{1.25} \times 8 = 23\,000 \text{ ft lb}_f$$

The average time for extrusion of one fire extinguisher is $60/100 = 0.6 \text{ s}$ per unit.

The average power (time rate of doing work) is

$$p_{av} = 23\,000 \text{ ft lb}_f \text{ per } 0.6 \text{ s} = 38\,300 \text{ ft lb}_f \text{ per s or } \approx 70 \text{ horsepower}$$

Note: During impact extrusion no account is made for frictional effects, because the metal is extruded up around the punch (Fig. 4.12(c)) and it therefore is not in contact with the chamber during deformation.

4.5 Drawing

Long products of small cross-sectional area are usually pulled through a die, rather than pushed as in extrusion. Such a *drawing* process is shown in Fig. 4.15. Drawing is particularly suitable for the fabrication of long lengths of small diameter wire (down to 0.01 mm) with good dimensional accuracy.

During drawing, indirect compression causes deformation of the workpiece. That is, the tension applied to the emerging product (σ_d in Fig. 4.15) causes compression against the die face and deforms the material. To avoid deformation after the wire has emerged from the die, the maximum drawing force that can be applied is limited by the yield strength of the emerging product. In practice, the drawing stress is limited to about 60% of the flow stress of the emerging product, which limits reductions to about 35% in most cases. The rate at which small wire-type products can be drawn is very high – up to 50 m/s. Heavier sections that cannot be wound into a roll must be drawn straight and line speeds are usually slower – about 1 m/s.

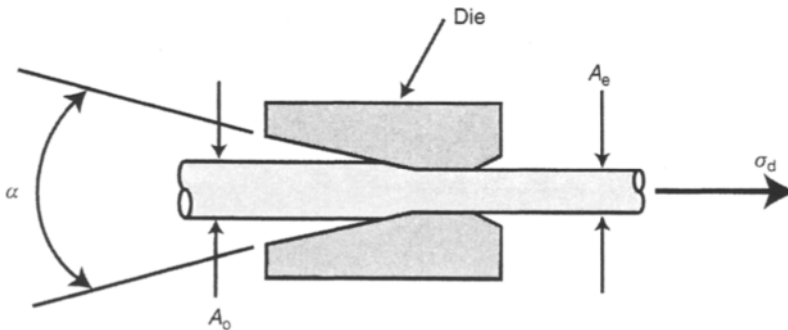


Fig. 4.15 Basic mechanism of drawing, showing the approach angle, α .

The most important parameters determining the drawing stress, σ_d , required are: the friction coefficient (which may be estimated from Table 4.1); the approach angle, α in Fig. 4.15, which is typically between 6° and 10° ; and the reduction ratio. Using these parameters σ_d can be estimated from

$$\begin{aligned}\sigma_d &= \sigma_{tm} \left(\frac{3.2}{\Delta + 0.9} \right) [\alpha + \mu] \\ \Delta &= \frac{\alpha}{r} [1 + (1 - r)^{1/2}]^2 \\ r &= 1 - \frac{A_e}{A_o}\end{aligned}\tag{4.32}$$

where σ_{tm} is calculated according to equation 3.32, the terms α , A_e and A_o are defined in Fig. 4.15, and μ is obtained from Table 4.1.

From σ_d the drawing force required can be obtained knowing the cross-sectional area of the emerging product. If σ_d is greater than about 60% of the yield strength of the drawn product then the drawing force will cause necking or breakage, necessitating a lower reduction ratio.

4.6 Rolling

Rolling is one of the most important bulk deformation techniques. For example, it is used to reduce the cross-section of large ingots or plate, which emerge from the ingot or continuous casting techniques described at the beginning of Chapter 2 for producing a wide variety of finished and semifinished components. These include structural steel sections, automotive body sheet, food/beverage container sheet, building siding etc. Rolling mills vary in size from hand operated units for light gauges of soft metals, to units requiring thousands of horsepower.

Several rolling mill configurations are in common usage, two of which are illustrated in Fig. 4.16. The simplest arrangement is the *two-high* mill, consisting of upper and lower driven rolls between which the workpiece passes (Fig. 4.16(a)). This mill has the advantage of relatively low momentum and, therefore, can easily reverse direction so that the workpiece can pass back and forth through the mill stand. *Reversing two-high breakdown* mills are often used for reducing large ingots into long slender plates. The construction of a typical two-high reversing breakdown mill is illustrated in Fig. 4.17. In the configuration shown the upper and lower rolls are driven by separate motors, to provide faster reversing action and smaller individual motor sizes. However, it is also common to drive both rolls from a single motor via a gearbox.

The *four-high* mill consists of two driven work rolls, with large back-up rolls that provide increased stiffness (Fig. 4.16(b)). The back-up rolls prevent the work rolls from bowing due to the rolling pressure which, if not controlled, results in rolled products, thicker at the centre than at the edges. For this reason four-high mills are used when the sheet thickness must be controlled accurately. A typical four-high mill for the production of plate is illustrated in Fig. 4.18.

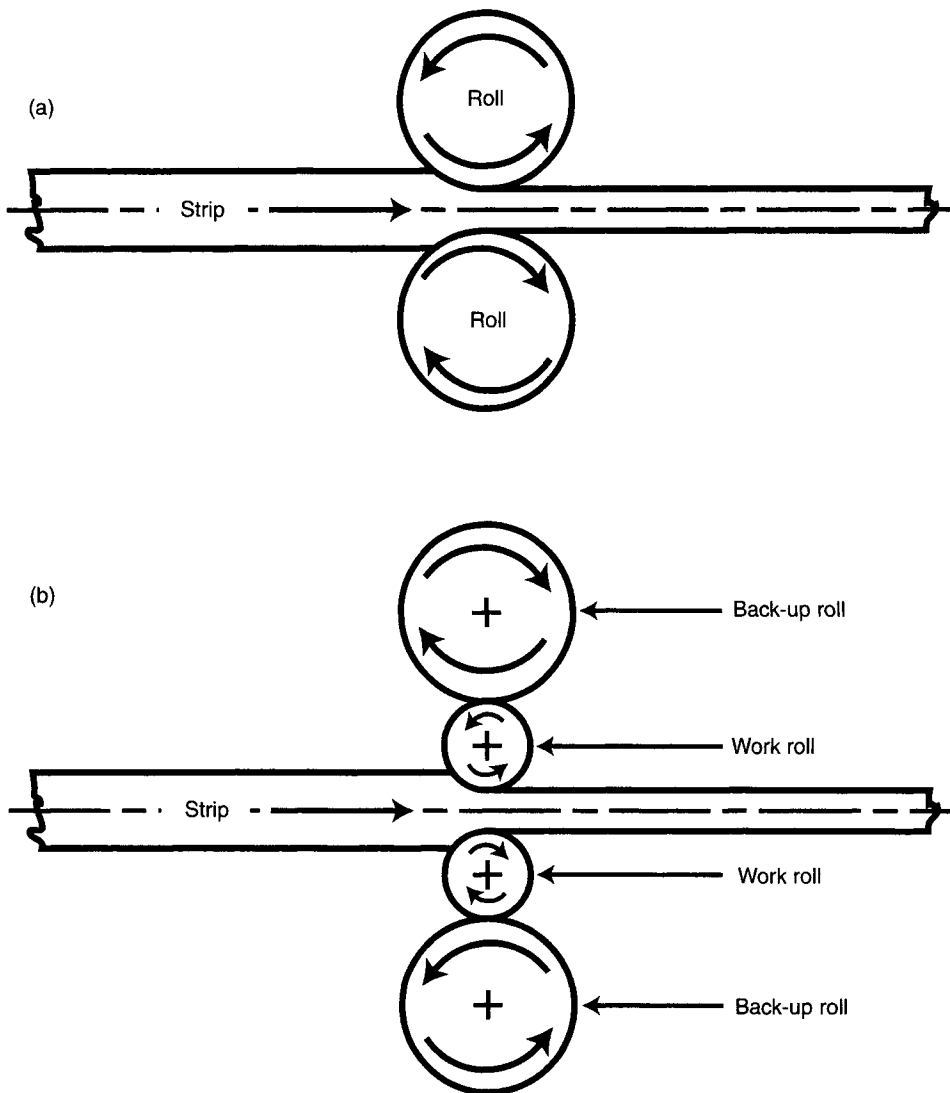


Fig. 4.16 Diagrams of (a) two-high rolling mill and (b) four-high rolling mill.

It is common to position several four-high mill stands in a *tandem* arrangement such as the three-stand four-high tandem mill for cold rolling shown in Fig. 4.19. This not only reduces the handling of coils between multiple passes, but can also reduce the coil storage space required in rolling works. Furthermore, additional flexibility in the control of the sheet metallurgy is obtained. As will become clear later in this section, friction between the workpiece and roll surface is a key element of the rolling process and this friction leads to heat generation in the rolls and workpiece. In the latter, this heat may be used to advantage to control the strain hardening that occurs but, in the former, heat generation causes thermal expansion of the rolls which leads to changes in the sheet thickness. Therefore, to produce flat sheet

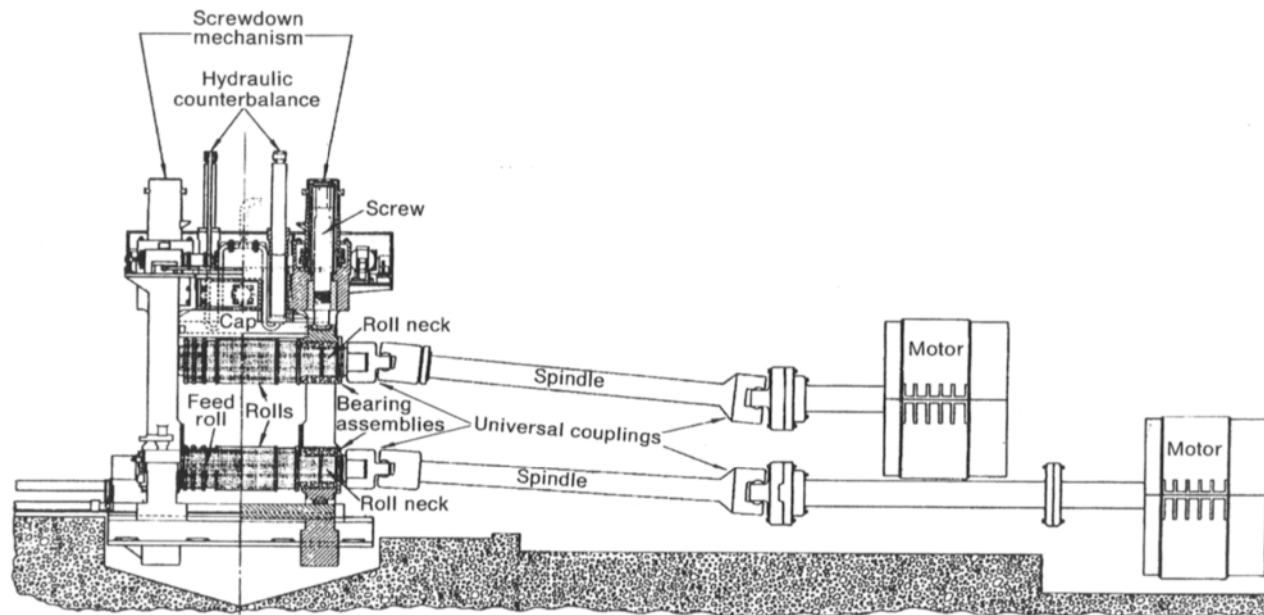


Fig. 4.17 General arrangement of typical reversing two-high breakdown mill. (Reproduced courtesy of The AISE Steel Foundation.)

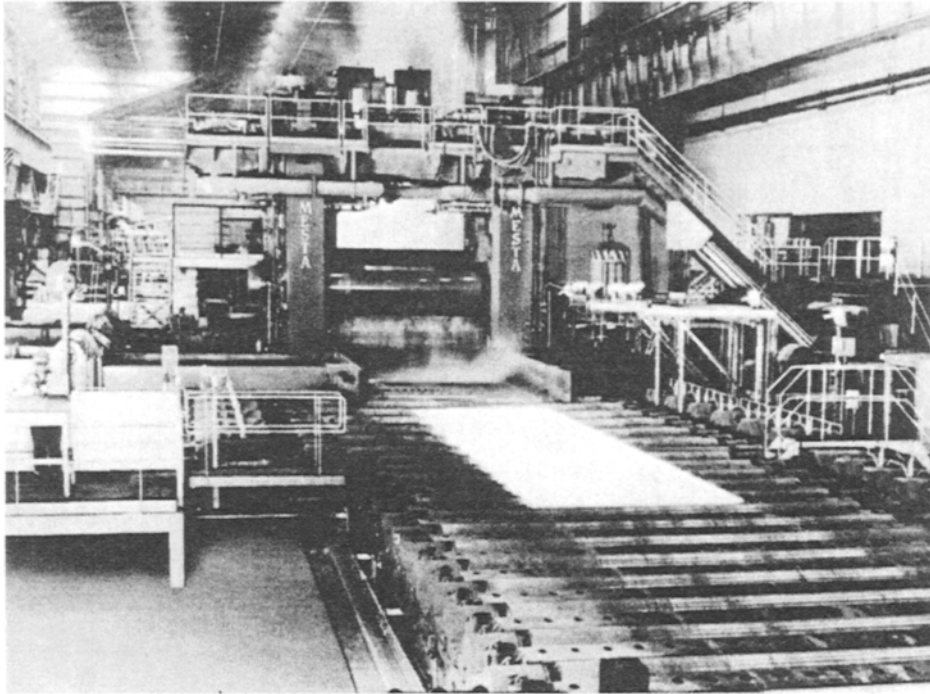


Fig. 4.18 Entry side of a four-high mill for the production of plate. Each work roll is driven by a 6000 horsepower (4470 kW) direct current motor. (Reproduced courtesy of The AISE Steel Foundation.)

on tandem mills real-time control of *bending jacks* between the work roll and back-up roll, and lubricant/coolant sprays are required. Additionally, as each stand of the tandem mill is rolling sheet of different thickness, motor speeds for each stand must be carefully coordinated. If one stand runs at an incorrect speed the sheet will either break or accumulate between the mill stands.

An interesting mill configuration is the *Sendzimir* mill of Fig. 4.20. In a Sendzimir mill each work roll is supported along its entire length by two back-up rolls, which in turn are supported by successive layers of larger intermediate rolls. The advantage of this arrangement is that the mill is very stiff and resists deflection, allowing very

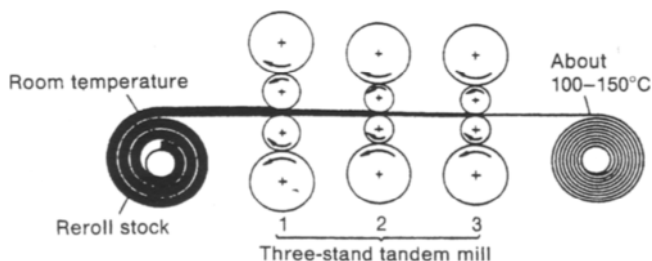


Fig. 4.19 A three-stand four-high tandem mill for cold rolling. Note temperature increase due to heat generation during rolling. (Reproduced courtesy of Aluminium-Verlag Marketing & Kommunikation GmbH, Düsseldorf.)

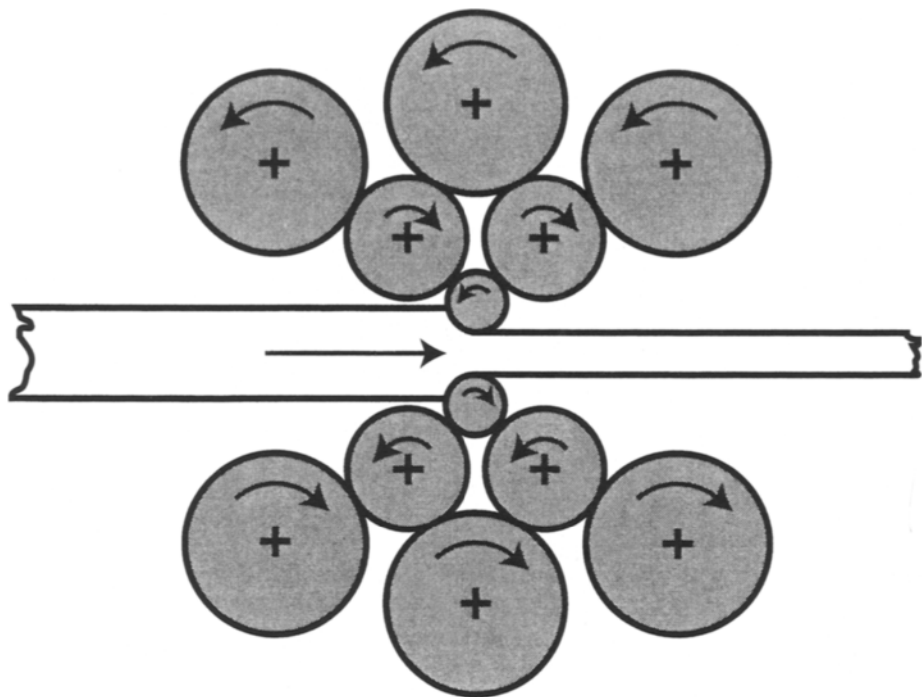


Fig. 4.20 Arrangement of rolls in a Sendzimir mill.

flat sheet to be produced. Also, as will become clear later in this section, reducing the roll diameter lowers the power requirement for a given reduction and allows lighter gauges to be produced. Therefore, a Sendzimir mill can produce very flat, thin sheet in a single pass, with minimal power requirements. A variation on the Sendzimir mill is the *planetary mill* of Fig. 4.21. This arrangement also incorporates

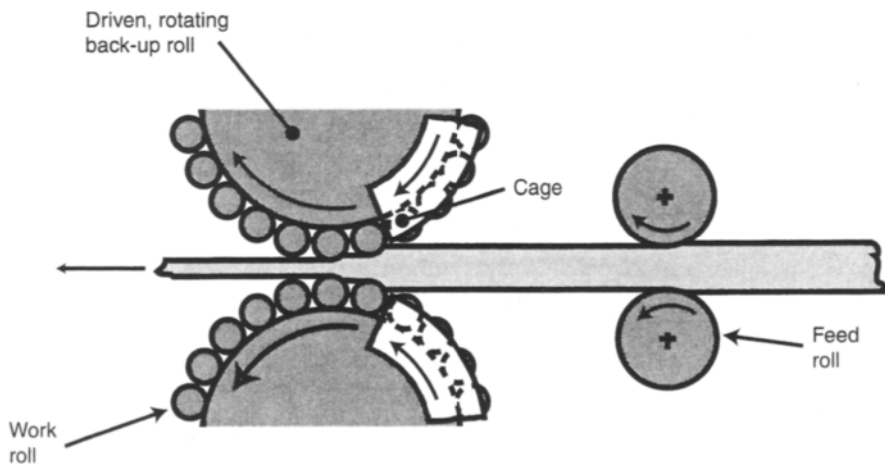


Fig. 4.21 Arrangement of rolls in a planetary mill.

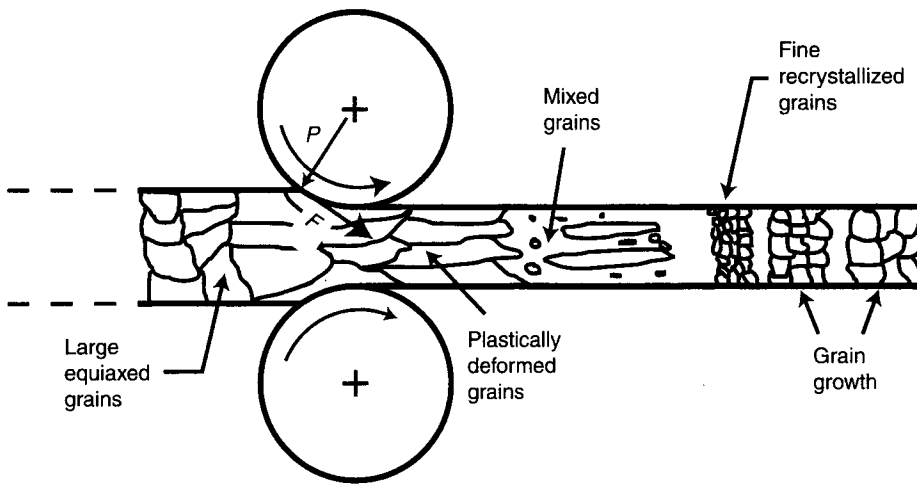


Fig. 4.22 Schematic representation of grain structure produced during hot rolling.

small-diameter work rolls, supported by stiff back-up rolls which provides many of the advantages of the Sendzimir mill. The main drawback of both mill arrangements is their mechanical complexity, particularly the problem of supporting the roll bearings in the mill stand.

Thick gauges, greater than about 6 mm, are almost always *hot rolled*, which is defined as rolling at a temperature greater than the recrystallization temperature – roughly half of the absolute melting temperature. A recrystallized microstructure results from hot rolling (Fig. 4.22). This is due to *dynamic recrystallization* (recrystallization that occurs during the simultaneous application of elevated temperature and deformation). As metals soften with increasing temperature, hot rolling has the advantage of requiring less power than comparable *cold rolling*, but also requires lubricants that do not break down under the combined action of the heat and rolling pressure. Cold rolling is usually defined as processing at less than 0.3 of the absolute melting temperature. Much better surface finish and dimensional control are achieved by cold rolling. Consequently, the final rolling pass for most quality critical applications is cold. Since recrystallization does not occur during cold rolling, a strain hardened microstructure consisting of plastically deformed grains elongated in the rolling direction is produced. Even during cold rolling the friction inherent in the process can cause substantial heating of the sheet, especially in tandem mill arrangements. This heating may cause some *dynamic recovery*, thereby reducing the amount of strain hardening retained in the sheet. Consequently, proper selection of cold rolling reductions is essential to optimize the mechanical properties of the finished product.

Shapes other than flat sheet can be formed by using contoured rolls. Basic structural sections such as tees, channels and angles are routinely formed in this manner. Often these shapes are hot rolled in multiple passes through a reversing mill that has the geometry corresponding to each pass at a different width location across the roll face, similar to the rolls shown in Fig. 4.17.

4.6.1 Rolling forces and power

The simplified geometry of flat rolling is shown in Fig. 4.23. It should be clear that the exit strip velocity, v_1 , is greater than the entry velocity. However, as the rolls rotate at a constant speed, it follows that there is only one point along the angle of contact α , where the roll and workpiece both move at the same speed. This point is referred to as the *neutral point*. On the entry side of the neutral point, the roll face speed is greater than the speed of the strip and, similarly, on the exit side of the neutral point, the roll face speed is slower than the strip speed. At all points, other than the neutral point, this difference in speed causes frictional forces that act in the direction of the neutral point. In forging, extrusion and drawing the existence of friction during deformation

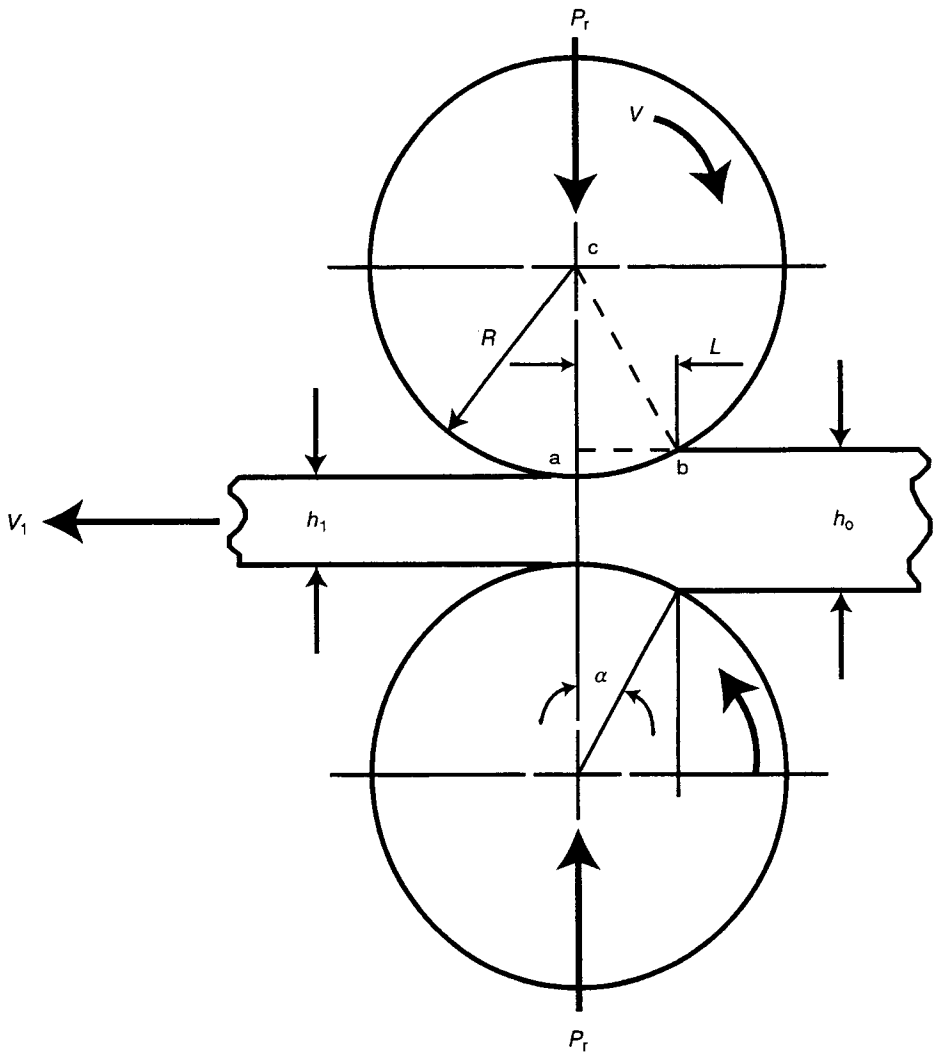


Fig. 4.23 Geometry of flat rolling.

is detrimental, causing deformation inhomogeneity and increased power requirements. However, friction is essential to the rolling process. It is the frictional forces that transmit the power from the rolls to the workpiece which causes the deformation. If the friction coefficient during rolling were to go to zero, the rolls would simply skid on stationary strip, with no work done. Because of this, lubrication during rolling must be well controlled so that skidding is avoided.

The forces during flat rolling can be calculated by estimating the *contact length*, L , shown in Fig. 4.23. By applying Pythagoras's theorem to the triangle abc of Fig. 4.23 and neglecting second-order terms, the contact length between the roll face and the workpiece can be estimated as

$$L = \sqrt{R(h_o - h_1)} \quad (4.33)$$

where: L is the roll contact length

R is the roll radius

h_o is the entry thickness of the sheet

h_1 is the exit thickness of the sheet.

When $h/L < 1$ (i.e. the rolls are large compared to the sheet thickness) deformation will be nearly plane strain and relatively homogeneous, and the roll pressure can be estimated in a fashion similar to that for forging rectangular parts (equation 4.16) or

$$p_r = \sigma_{tm} Q_p \quad (4.34)$$

where: p_r is the roll pressure

σ_{tm} is the mean flow stress

Q_p is the multiplying factor (Fig. 4.9).

Note that for the forging process, deformation occurs in all regions of the workpiece concurrently, and in equation 4.16 the stress value used corresponds to the stress existing at the end of the press stroke. However, for rolling, where deformation occurs sequentially, the mean true flow stress is applied in equation 4.34. The roll force can be calculated from

$$F_r = LwQ_p\sigma_{tm} \quad (4.35)$$

where w is the width of the rolled strip.

Note that although the length of the rolled strip increases, the width remains essentially constant if $w/h_1 > 10$, which is the case for most commercial rolling operations. From equation 4.35 it can be seen that reducing the contact length, L , by reducing the roll radius (equation 4.33) will lower the roll force, even for the same entry and exit thicknesses. This illustrates the advantage of four-high or Sendzimir mills, in which the work roll diameter is reduced, thus lowering the rolling forces without compromising the mill stiffness and hence the ability to produce flat sheet.

If $h/L > 1$ (i.e. the workpiece is thick compared to roll radius) then inhomogeneous deformation predominates. This often corresponds to sticking friction conditions which is not usually a desirable situation, but can occur during the breakdown rolling of large ingots. The roll pressure is obtained from a relationship similar to equation 4.34, except that a different multiplying factor is used, so that

$$p_r = \sigma_{tm} Q_i \quad (4.36)$$

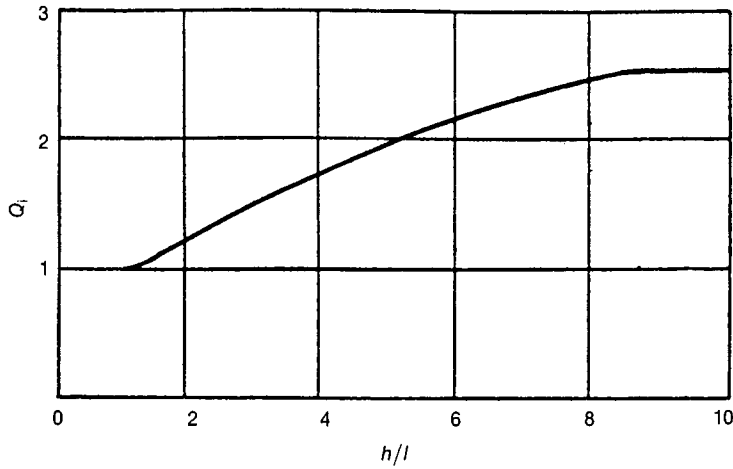


Fig. 4.24 Multiplying factor for inhomogeneous rolling. (Reproduced from R. Hill, *The Mathematical Theory of Plasticity*, 1950, by permission of Oxford University Press.)

where \bar{Q}_i is the multiplying factor for inhomogeneous deformation obtained from Fig. 4.24.

For cold rolling, σ_{tm} in equations 4.34 to 4.36 is calculated according to equation 3.32. However, for hot rolling, the mean flow stress must correspond to the average strain rate, which is

$$\dot{\epsilon} = \frac{v}{L} \ln \left(\frac{h_o}{h_1} \right) \quad (4.37)$$

where v is the roll face velocity. This mean strain rate for rolling can be substituted into equation 3.37, to yield the mean true flow stress for hot rolling.

Inhomogeneous deformation during rolling can lead to the *alligatoring* defect, sometimes referred to as *split ends*, shown in Fig. 4.25. Such defects must be avoided, as the thick sections involved can cause substantial damage to the ancillary equipment of the mill stand. Analysis of the rolling process using the *upper bound* technique (briefly described later in this chapter) indicates that alligatoring occurs if the rolling geometry satisfies the inequality

$$\frac{h_o}{R} > \left(\frac{h_o}{h_1} - 1 \right) \times 1.81 \quad (4.38)$$

with the parameters defined as in Fig. 4.23.

By assuming that the rolling force acts roughly in the centre of the contact length (L) and that both the upper and lower rolls are driven (which is the usual practice), the rolling torque can be estimated as

$$T = F_r L \quad (4.39)$$

where T is the rolling torque. The power requirement can be calculated from the torque as

$$\text{Power} = \omega T \quad (4.40)$$

where ω is the angular velocity of the rolls.

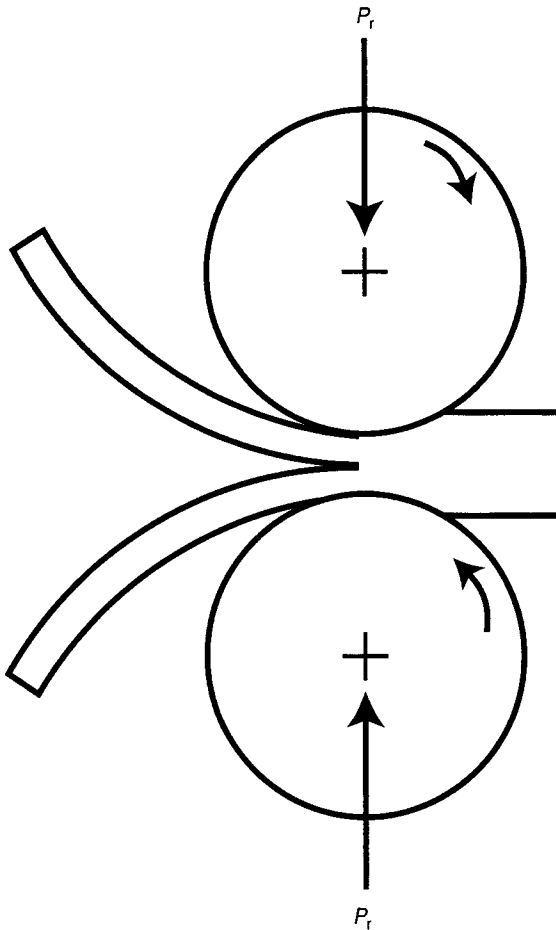


Fig. 4.25 Illustration of alligatoring that can form during rolling due to inhomogeneous deformation.

Example 4.5 Cold rolling of bronze

A part is cold rolled from 5 wt% Sn bronze ($K = 720 \text{ MPa}$, $n = 0.46$). The rectangular shape is 10 cm wide and has an initial thickness of 1 mm. A 30% reduction in height is taken in a single pass on a mill with 150 mm diameter rolls, at an entry velocity of 0.8 m/s. A mineral oil lubricant ($\mu \approx 0.1$) is applied. Calculate: (a) the roll force, and (b) the mill power required. Repeat for 75 mm diameter rolls.

Solution $h_0 = 1.0 \text{ mm}$; reduction = 30%; $h_1 = 1(1 - 0.3) = 0.7 \text{ mm}$; $\varepsilon = \ln(1/0.7) = 0.357$.

(a) Calculate the mean true stress during rolling

$$\sigma_{\text{tm}} = \frac{K\varepsilon^n}{n+1} = \frac{720 \times 0.357^{0.46}}{1.46} = 307 \text{ MPa}$$

Calculate h/L (use average h)

$$h = \frac{1 + 0.7}{2} = 0.85 \text{ mm}$$

$$L = \sqrt{R(h_0 - h_1)} = 4.7 \text{ mm}$$

$$\frac{h}{L} = 0.18 < 1$$

With $h/L < 1$, i.e. plane strain, use Q_p from Fig. 4.9 for $\mu = 0.1$ to obtain $Q_p \approx 1.2$. Calculate rolling force

$$F_r = LwQ_p\sigma_{tm} = 4.7 \times 10 \times 1.2 \times 307 = 173 \text{ kN}$$

Torque and power:

$$T = F_r L = 173 \times 4.7 = 813 \text{ N m}$$

$$P = \omega T; \quad \omega = \frac{v}{R} = \frac{0.8}{0.075} = 10.6 \text{ rad/s}$$

$$P = 10.6 \times 813 = 8.6 \text{ kW}$$

(b) Repeat for rolls of 75 mm diameter

$$L = \sqrt{R(h_0 - h_1)} = 3.4 \text{ mm}$$

so

$$\frac{h}{L} = \frac{0.85}{3.4} = 0.25$$

h/L is still less than 1 so, again from Fig. 4.9, $Q_p \approx 1.1$ (use $\mu = 0.1$ as before). Force, torque and power become

$$\text{Force: } F_r = 3.4 \times 10 \times 1.1 \times 307 = 115 \text{ kN}$$

$$\text{Torque: } T = 115 \times 3.4 = 391 \text{ N m}$$

$$\text{Power: } P = \frac{0.8}{0.0375} \times 391 = 8.3 \text{ kW}$$

Note: For smaller diameter rolls, the force torque and power required are reduced. This is a major advantage to the use of small diameter rolls. However, the disadvantage is that smaller rolls will deflect more due to the roll separating force, making the production of flat sheet more difficult.

4.7 Analytical methods for bulk deformation processes

The problems presented in this chapter apply to simple idealized situations where the stress state can be readily determined. In actual metalworking processes, the workpiece is often subjected to a complex stress state that may vary in all three dimensions and may also vary with time. Compounding this complexity are the die-workpiece friction interactions. Exact analytical solutions for metal-forming processes are difficult to obtain and so simplifying assumptions are inevitable. However, analytical techniques have been developed that can predict the loads associated with more

complex metal deformation geometries with reasonable accuracy. Each of these techniques is briefly described in this section.

4.7.1 Limit analysis – bounding techniques

As exact solutions to metal deformation problems are often not possible, it can be useful to calculate an *upper bound* and *lower bound* to the force/power requirements, that overestimate and underestimate the actual force/power requirements, respectively. The actual power necessary is bracketed between these two estimates, leading to the identification of these techniques as limit analysis.

To calculate the upper bound a velocity field corresponding to the deformation within the workpiece is assumed. This velocity field must be consistent with the shape change that is occurring and must, for all deformed geometries, satisfy volume constancy, i.e. the sum of orthogonal strains and strain rates must always equal zero (see Examples 3.3 and 3.6). As the strain rate is defined as the velocity over a length, the velocity field assumed determines the strain rate throughout the volume of the workpiece during deformation. The energy consumed by the deforming workpiece is calculated using the assumed velocity field and the appropriate material properties. From the conservation of energy, the internal energy consumed is equal to the energy delivered by external forces or stresses.

A major factor influencing the accuracy of the solution is the suitability of the velocity distribution used to model the deformation processes. The determination of the velocity distribution is not a trivial task. Often techniques similar to those of inviscid or incompressible fluid mechanics are used, in particular the concepts of *stream* and *potential* functions. Of all the various valid velocity fields available, the one that minimizes the total energy (power) input required will be closest to reality. An advantage of the upper bound technique is that it will always overestimate the power required for any deformation geometry and so is inherently conservative. Rolling, forging, drawing and extrusion processes have been analysed quite successfully utilizing this technique. Associated with the upper bound technique is the lower bound method, which always underestimates the deformation loads required. Thus, used together, these two techniques provide bounds for the actual deformation conditions.

4.7.2 Slip-line analysis

In this procedure a network of *slip-lines* are constructed that intersect each other orthogonally (Fig. 4.26). The slip-lines correspond to the directions in which the metal yields in shear and must satisfy the conditions of static equilibrium of forces, mass continuity and boundary conditions. In this technique the metal is assumed to deform only by shear along the slip-lines, i.e. the metal between slip-lines is rigid. It is also assumed that no strain hardening occurs along the slip lines. Thus, the blocks of Fig. 4.26 can slide along each other, but cannot deform or separate. As such, the metal velocity in the direction normal to a slip-line must be the same for points across the slip-line from one another. The work done by the indenter of

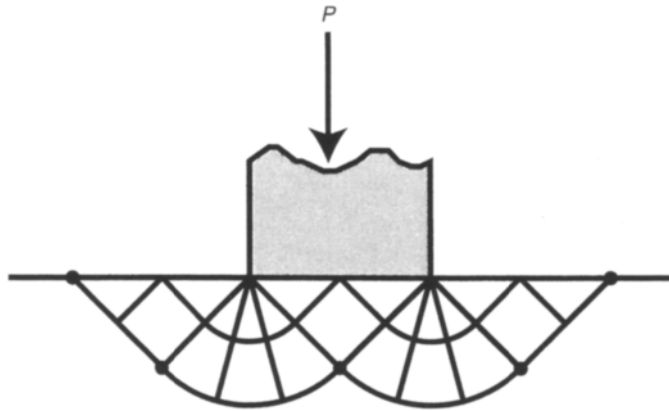


Fig. 4.26 A slip-line field for plane strain indentation of a semi-infinite slab.

Fig. 4.26 can be estimated by realizing that it must be equal to the internal work done by shearing the blocks against one another.

The slip-line method has been successfully applied to forging, rolling and extrusion problems to predict stresses, material flow and temperature variations within a workpiece.

4.7.3 Visioplasticity

This technique consists of placing a grid pattern on a surface or within the volume of a workpiece and measuring the distortion of the grid after some incremental deformation. In this manner the displacements, strains and strain rates may be determined, and then through plasticity equations the stresses calculated. Often the workpiece surface is printed with an array of circles, which on deformation transform to ellipses. By measuring the major and minor elliptical axes, orthogonal strains can be calculated. Alternatively, the workpiece can be modelled using different coloured layers of wax or plasticine. The wax/plasticine model is then deformed, cut along any plane of interest and the interior displacements determined from the deformation of the coloured layers. The wax or plasticine can be deformed using dies made of wood, with quick and easy changes possible to the die geometry. This provides an economical technique to quickly determine the local strains associated with a deformation operation and relies on the fact that strain is a geometrical property only, not a material property. Having determined the strain associated with a deformation process, this can be compared to the material properties of the intended workpiece to judge the suitability of a particular deformation procedure.

4.7.4 Finite element method

In the finite element method (FEM) the deformation zone is divided into multiple elements, interconnected at nodal points. The velocity distribution for each element

is approximated in a manner similar to the slip-line technique. This generates a set of simultaneous equations representing unknown velocity vectors. Solving these equations gives the actual velocity distributions and, combined with knowledge of the deformed geometry and strain rates, stresses can be calculated. The technique can incorporate friction conditions and relatively complex problems can be solved numerically. The accuracy depends on the shape and number of elements utilized. Extensive FEM numerical solutions inevitably require considerable computer processing.

The two major types of FEM analyses are the *elastic-plastic method* and the *rigid-viscoplastic method*. The former method assumes that the deformation consists of a recoverable elastic component and a nonrecoverable plastic component. The method has been applied to many of the processes described in this chapter. Due to the large difference in the elastic and plastic behaviour of materials the deformation steps applied must be small. This requirement tends to make the technique time consuming and less economical.

In the rigid-viscoplastic method, the deformation stresses are primarily dependent on the strain rate. Larger deformation steps can be applied and the method is particularly useful for hot deformation during which most materials are strain-rate sensitive. Several rigid-viscoplastic commercial FEM programs are available.

4.8 Problems

- 4.1 Identify two advantages and two disadvantages of hot working versus the cold working of metals.
- 4.2 A cylinder ($h_o = 4$ cm, $d_o = 2$ cm) is compressed by an open die forging process. The true strain to fracture for the cylinder is $\epsilon_f = 1.5$ and the governing deformation relationship is

$$\sigma_t = 400\epsilon^{(0.5)} \text{ MPa}$$

The lubricant used provides a friction coefficient of 0.1. The process is limited by either platen yielding or fracture. If the yield stress of the platens is 800 MPa, do the platens yield or does the specimen fracture?

(Answer: specimen cylinder fractures)

- 4.3 (a) AA-1100 aluminium 10 cm billets are cold extruded to a round bar of 5 cm diameter. Calculate the extrusion force necessary. The original length of the billet is 500 mm.
 (b) If the extrusion ram of the press of part (a) is made of a high strength tool steel with a yield strength of $\sigma_{0.2} = 1000$ MPa, would it be possible to extrude the 10 cm billet to a 5 cm diameter bar without deforming the ram? Justify your answer.
 (Answers: (a) $F \approx 5$ MN; (b) yes, it is possible to extrude billet without deforming the ram)
- 4.4 A square bar is reduced in cross-section by extruding it seven times through dies of decreasing size. During each of the seven extrusion operations the reduction in the cross-sectional area is 35%. Calculate:

- (a) the total true strain applied
- (b) the final length of the bar, in terms of the initial length of the bar
- (c) the total engineering strain applied.

(Answers: (a) 3.01, (b) $20.3l_0$, (c) 19.3)

- 4.5 You are involved in the design of a large cold rolling mill. The intended mill application is flat rolling of a 1045 steel strip of 1.5 m width, from 3 mm to 2.2 mm thickness in one pass. The roll diameter is fixed at 0.25 m and the envisaged lubrication system should result in a friction coefficient of 0.05.

- (a) Calculate the roll separating force.
- (b) If the intended strip exit speed is 4 m/s, what is the mill motor power required for the 3 mm to 2.2 mm thickness reduction? (Both top and bottom rolls will be driven.)
- (c) For this application do you recommend a two-high or four-high mill configuration? State reasons for your answer.

(Answers: (a) 10.3 MN, (b) about 3.6 MW, (c) use four-high)

- 4.6 (a) The motors of a rolling mill are capable of producing 1000 horsepower (746 kW) when the work rolls are rotating at 100 rpm. The mill is to be used for cold rolling AA-1100 aluminium plate from 25 mm to 20 mm thickness. The mill has an efficient lubrication system that effectively reduces the roll workpiece interface friction to low values (therefore assume frictional effects are negligible). If the work roll diameter is 60 cm, what is the maximum width that can be rolled at full power?

- (b) Is the rolling deformation of the strip in part (a) homogeneous? Briefly explain your answer.

(Answers: (a) 64 cm, (b) homogeneous)

- 4.7 Explain the advantages and limitations of using small diameter rolls in a metal rolling mill.

- 4.8 (a) A tensile sample cut from a piece of sheet metal has an original cross-sectional area of 20 mm^2 . During a tensile test the maximum load is measured as 3.5 kN at which point the cross-sectional area is 12 mm^2 . A piece of sheet 10 cm long and 2 cm wide, of the same material from which the tensile sample was cut, is cold rolled from a thickness of 1 mm to 0.8 mm.

- (i) Calculate the ideal work of deformation for the rolling operation.
- (ii) Does this calculation underestimate or overestimate the work required?
- (b) If a different piece of the cold rolled sheet of part (a) is 0.5 m wide and rolled at 50 m/min on work rolls of 500 mm diameter, estimate the rolling mill power required for the thickness reduction from 1 mm to 0.8 mm. Assume mineral oil is used as a lubricant, giving a friction coefficient of 0.1.
- (c) If it is desired to reduce the power required for the rolling operation of part (b), what modifications to the process can be made? (The dimensions of the initial and final rolled sheet cannot be altered.)

(Answers: (a) ideal work of deformation is 55 N m, underestimates, (b) 18.8 kW)

- 4.9 The motors on a rolling mill are rated at 100 kW maximum power and a maximum speed of 60 rpm. The maximum force that the rolling mill can apply is

1000 kN. The roll–workpiece interface is lubricated with mineral oil, giving a coefficient of friction of 0.1. The mill is to be used to roll aluminium sheet with an initial thickness of 4 mm, a strength constant of 200 MPa and a strain hardening coefficient of 0.18.

- (a) From a simple geometrical analysis of the rolling geometry it can be shown that

$$(h_o - h_1)_{\max} = \mu^2 R$$

where: R is the roll radius

μ is the friction coefficient

h_o is the initial sheet thickness

h_1 is the rolled thickness.

With this information, calculate the minimum thickness to which the sheet can be rolled.

- (b) For the reduction calculated in part (a), if the motors are run at 100% power and speed, what is the maximum width of sheet that can be rolled?

(Answers: (a) 2.4 mm, (b) ≈ 0.34 m)

Case study 3: Manufacture of can body stock – 2. Rolling

As outlined in Fig. C1.1, the manufacture of can body stock includes both hot and cold rolling. Hot rolling usually utilizes an integrated *hot line* of the type illustrated in Fig. C3.1, with a total length of several hundred metres. The hot line consists of a roller table connecting a *breakdown* mill with a tandem mill and associated ancillary equipment. Ingots at about 550°C are delivered to the hot line directly from homogenization by an overhead crane or rail equipment and placed on the powered roller table for delivery to the breakdown mill.

The breakdown mill is usually a four-high mill capable of reversing direction. The ingot is passed back and forth through the mill about 15 times, causing a reduction in thickness from about 60 cm to about 4 cm. The breakdown mill requires d.c. motors of several thousand kilowatts, capable of applying the large reductions necessary and quickly reversing direction. Since during breakdown rolling the ingot (now being rolled into *plate*) thickness is relatively large, inhomogeneous deformation occurs through the plate thickness. Consequently, unless the thickness of the ingot/plate during each pass through the breakdown mill is controlled appropriately, the end of the ingot may alligator, potentially preventing the ingot/plate from entering the mill for successive passes. To ensure the ends of the plate remain square and true, they may be cropped during breakdown rolling in a plate shear.

On completion of breakdown rolling, the ingot that has been rolled into plate to about 4 cm thick (but possibly 75 m long and now about 300°C) is delivered to the tandem mill for further rolling to a coilable thickness, usually about 3 mm. The tandem mill contains multiple stands (six in Fig. C3.1), with the plate being rolled simultaneously in all stands. As the thickness of the plate is reduced in each rolling stand, the plate speed is always increasing and the mill speeds must be carefully controlled to guard against pulling the plate apart or allowing the plate to bunch up between stands. Each of the tandem mill stands consist of a four-high roll arrangement so that the sheet thickness across the width of the plate can be well controlled. At the exit of the tandem mill is an X-ray gauge that continually monitors the *sheet* thickness and adjusts the final stand rolling pressure accordingly. On leaving the last of the tandem mill stands, the 3 mm thick sheet may be moving at upwards of 60 km/h. Prior to coiling, the sheet edges may be trimmed in a *slitter* to remove

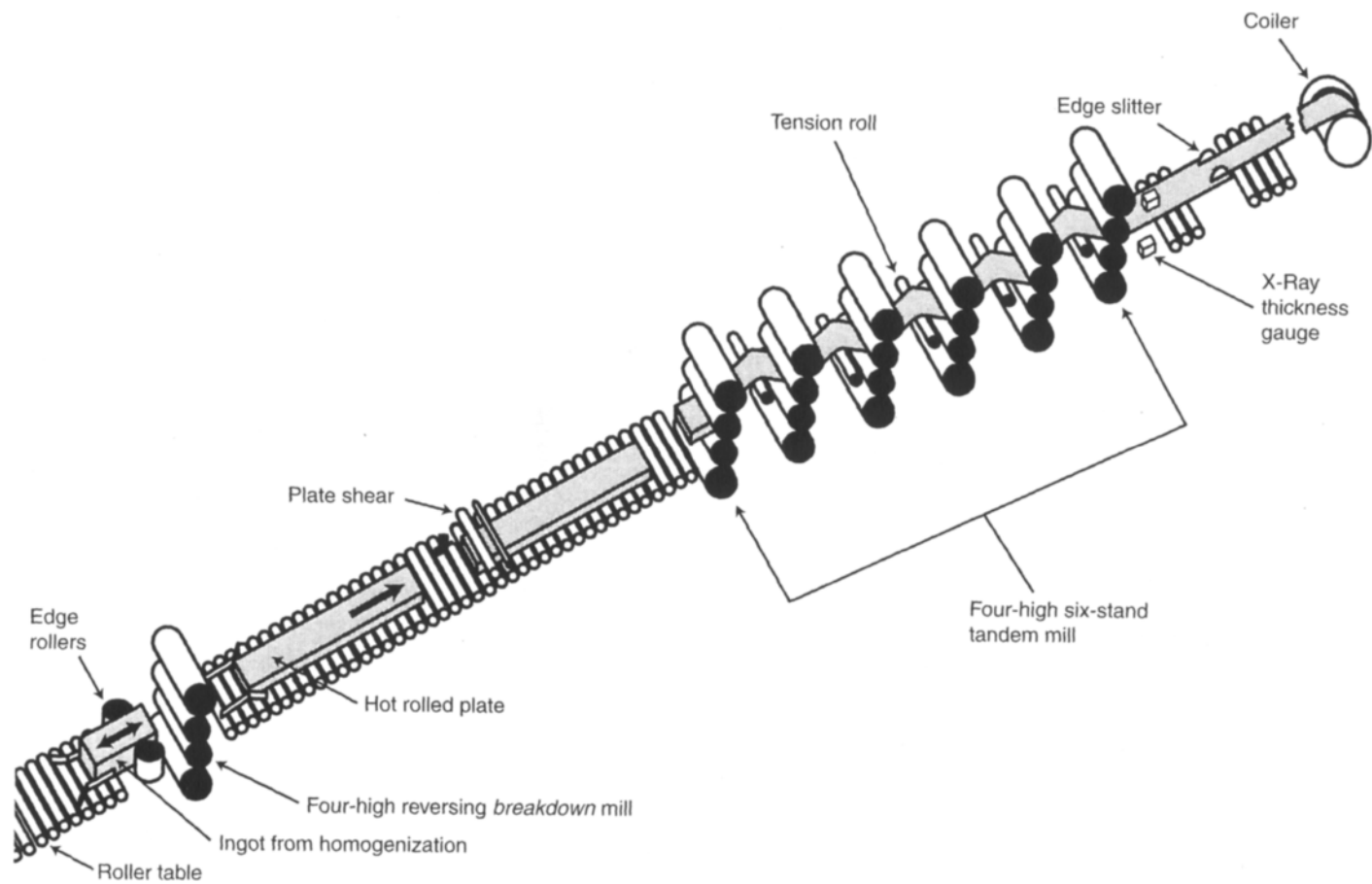


Fig. C3.1 Diagram of an aluminium hot line for rolling direct cast ingots.

edge cracks. An advantage of the electromagnetic casting procedure, discussed in Chapter 2, is a decreased requirement for edge trimming and therefore greater recovery of the rolled width.

An integrated hot line for rolling can body stock represents a major investment for even the largest of aluminium companies. Therefore, it is imperative that the hot line is operated at maximum efficiency at all times. Typically, an ingot will be delivered to the breakdown mill at a rate of about one every 5 min (that is, more than 3 000 000 kg of can stock rolled per day). To achieve such production rates requires well engineered equipment operated by skilled operators with the aid of advanced automation and monitoring techniques. It is not uncommon for the control system for each mill stand to have several linked computers together with an operator.

During hot rolling a grain structure with a preferred orientation develops (the reasons for this are discussed in the next chapter). A ramification of the oriented or *textured* structure is nonuniform deformation in the plane of the sheet, which causes considerable problems during can making (see Case Study C4 at the end of Chapter 5). To control the grain orientation or texture, the coils of hot rolled sheet are annealed to a fully recrystallized state prior to cold rolling. The annealing is most often done in batch type furnaces that hold between 10 and 20 coils. To fully anneal can stock requires 2 h at 370°C, plus heat-up and cool-down time. To protect the sheet surfaces, annealing must be done in an inert atmosphere. If the furnaces are fired by a fossil fuel, the combustion products can be used as an inert atmosphere. This requires sophisticated furnace combustion and atmosphere control to ensure that no unburnt fuel enters the furnace, which may subsequently combust, potentially with explosive force. The occasional annealing furnace explosion is evidence that sufficient care is not always exercised.

Finally, the annealed sheet is cold rolled to a final gauge of about 0.3 mm. This reduction may be achieved by multiple passes through a single-stand cold mill or tandem cold mills (see Fig. 4.19). Regardless, to ensure adequate gauge control, the cold mills are invariably four high. To achieve the high production tonnages, sheet speeds in the mill may approach 100 km/h on the finishing pass. Typically, the thickness tolerance is about ± 0.0125 mm and no waviness of the sheet is allowable. To

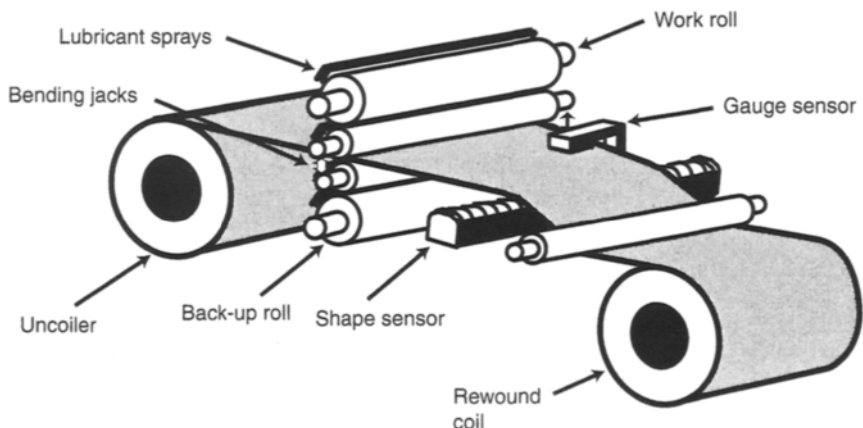


Fig. C3.2 General arrangement of equipment on a four-high cold mill for rolling can body stock.

achieve these gauge and flatness requirements most mills utilize *shape sensor rolls*, *work roll bending jacks*, *lubricant coolant sprays* and *gauge sensors* (Fig. C3.2) across the width of the sheet to control the profile of the work rolls. Given the high sheet speeds, the analysis of the data gathered and appropriate control of the mill system requires extensive computerization of the rolling process and powerful control actuators to impart the necessary roll deflections. Clearly, for such operations it is essential that the mill design and control, as well as the sheet metallurgy, is properly understood and coordinated for the process to succeed. The 0.3 mm cold rolled sheet of can body stock has a yield strength of about 280 MPa and an ultimate tensile strength of 310 MPa.

Sheet forming processes

5.1 Introduction

In large measure the importance of sheet forming is due to the availability of high quality and relatively low cost flat-rolled metal strip. Conversely, the importance of sheet forming underlines the importance of the rolling process discussed in the previous chapter. Typically, sheet metal is produced by high speed cold rolling of coils, which may weigh from several kilograms to several thousand tonnes. The subsequent localized deformation of the cold rolled strip by *sheet metal working* techniques produces many useful shapes, such as car body parts, food or beverage containers, window screen frames and countless other products. This chapter introduces the most common sheet forming operations.

As discussed in Chapter 1, many metalworking operations have been developed with virtually no rudimentary knowledge of the mechanics involved. This was the case for most sheet forming practices, which have been developed by trial and error, and depended on the skill of the artisan. To some degree, the success of sheet forming is based on the skills developed by these early artisans and many modern sheet forming techniques still rely on skilled operators. However, the increasing demand for rapid and successful product and process development requires analytical techniques to predict anticipated performance. Therefore, in this chapter, the basic mechanics and metallurgy of sheet forming operations are presented. Although this should provide a fundamental understanding of the factors influencing sheet forming performance, exact solutions only exist for the simplest of sheet forming operations. Nevertheless, an understanding of the basics can be used to provide guidance during the development and operation of more complex sheet forming processes.

5.2 Formability

Formability is a measure of the relative ease with which a metal can be plastically deformed. It is a key attribute for metals intended for sheet forming. The measurement of formability is, unfortunately, considerably more difficult than the definition. Several formability tests exist and yet there are relatively few standards, with the most

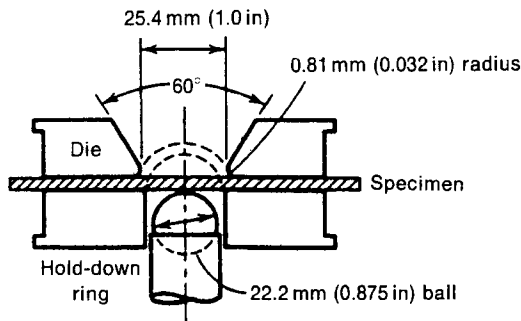


Fig. 5.1 Tooling for Olsen cupping test. (Reprinted with permission from *ASM Materials Engineering Dictionary*, edited by J.R. Davis (1992) ASM International, Materials Park, OH 44073-0002, Fig. 352, p. 297.)

relevant test depending on the process and product of interest. A semiquantitative measure of formability can be obtained from *cupping tests* of which the most common is the *Olsen* cupping test. The general set-up for this test is shown in Fig. 5.1 and involves deforming the sheet into a cup by a ball shaped tool. The height of the cup at the instant that the punch force starts to decrease is an indication of the formability. The decreasing punch force corresponds to the onset of localized necking. As failure is associated with local necking, metals with a high strain hardening exponent, n , usually exhibit better formability. (Recall from Chapter 3 that necking begins when the applied strain is equal to the strain hardening constant n ; see equation 3.23.)

In addition to localized necking, poor formability may cause several undesirable surface features. These include *orange peel* and *stretcher strain* marks. Orange peel refers to a grainy surface appearance. Such a surface arises due to the different orientations of individual grains within a polycrystalline metal. As the deformation of each grain is limited by a finite number of slip systems, the magnitude of the deformation for individual grains may differ, causing surface roughening. The tendency for orange peeling can be reduced by decreasing the grain size.

Stretcher strains or *Lüders lines* are caused by localized plastic deformation due to inhomogeneous yielding. These lines can criss-cross the surface of the workpiece and may be visibly objectionable. Avoiding visible stretcher strains is key to several sheet formed components, such as automobile body sheet, which is usually formed from cold-rolled low-carbon steel. As was illustrated in Fig. 3.2, these steels exhibit a pronounced yield point and the initial plastic deformation can be discontinuous. This phenomenon is caused by interstitial carbon and nitrogen solute diffusing to dislocations. The interstitial atoms form *solute atmospheres* adjacent to dislocations and prevent homogeneous initiation of dislocation slip. The result is visible stretcher strains which are unacceptable for automotive body components. To prevent the formation of stretcher strains, most low carbon sheet is *temper rolled* prior to forming. Temper rolling involves cold rolling the sheet about 1–3% to introduce a small amount of plastic deformation, causing dislocations to break free from their carbon atmospheres, which allows subsequent homogeneous sheet metal forming. If the forming does not occur sufficiently soon after temper rolling, then diffusion will again cause the formation of carbon solute atmospheres. Therefore, temper rolling is usually

applied at the automobile sheet forming facility immediately prior to the forming of body parts. Alternately, Lüders lines can be avoided by using *low interstitial steels*. The composition and processing of these steel grades is modified to result in very low concentrations of interstitial atoms, thereby preventing the formation of solute atmospheres and removing the requirement for temper rolling prior to sheet forming.

5.3 Shearing

Typically the dimensions of cold rolled strip are quite large and, therefore, the first sheet metal process applied often involves *shearing*. The shearing process is a straight-forward cutting action between a punch and a die, as shown in Fig. 5.2. As the punch penetrates the workpiece plastic deformation occurs initially (Fig. 5.2(b)), followed by the shearing action (Fig. 5.2(c)) and, finally, the fracture strength of the remaining intact sheet is exceeded causing final fracture (Fig. 5.2(d)). The sheet thickness over

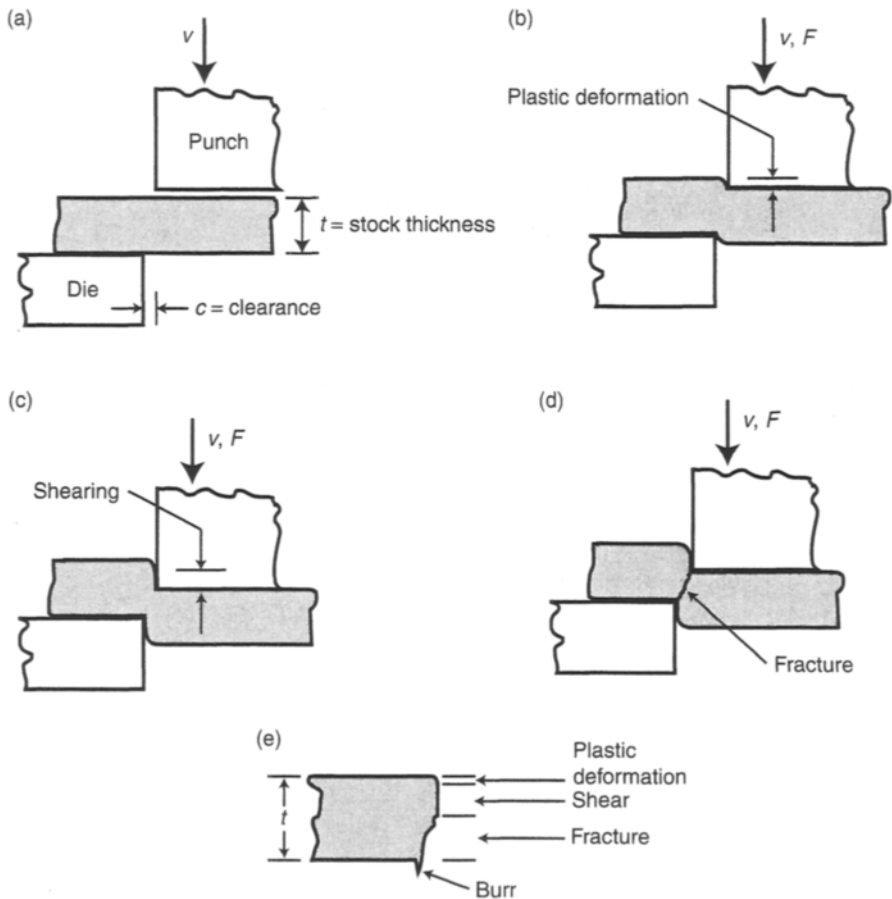


Fig. 5.2 (a) General arrangement of tooling for shearing, (b) initial cutting occurring by plastic deformation, (c) shearing during punch penetration, (d) fracture following shearing, and (e) morphology of sheared cut.

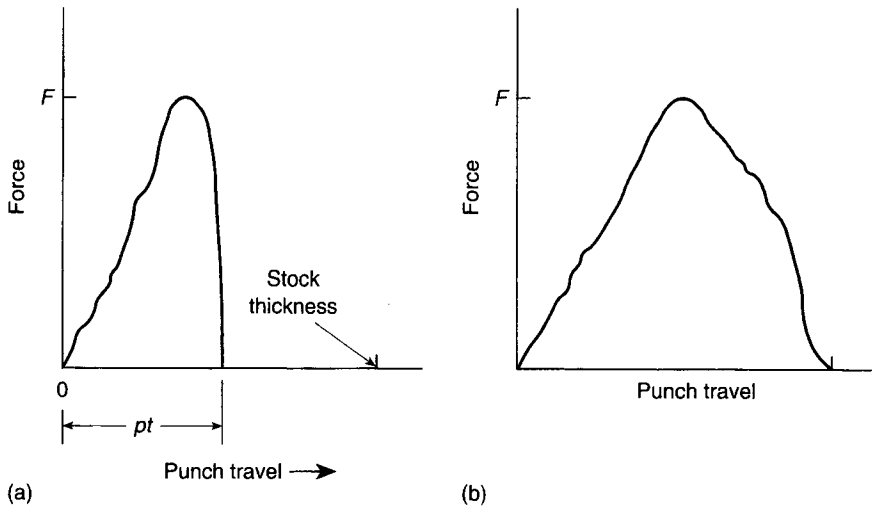


Fig. 5.3 Force required for shearing with (a) optimum clearance and (b) incorrect clearance. (p = fraction of the stock thickness (t) through which the punch has travelled.)

which each of these processes occurs is apparent from an examination of the sheared edges, as shown in Fig. 5.2(e). Once the shearing action causes fracture of the sheet (Fig. 5.2(d)) the punch force, F , quickly drops to zero. The thickness through which each of the shearing mechanisms occurs depends on the punch–die clearance, identified in Fig. 5.2(a). The optimum clearance will cause fracture when the punch has penetrated about halfway through the sheet. Therefore, the shearing force increases until fracture occurs and then rapidly drops to zero, as shown in Fig. 5.3. Improper clearance will require greater energy for shearing (energy is the area below the force–distance plots of Fig. 5.3) and will cause excessive burring on the cut edge. Usually the optimum clearance is between 4% and 8% of the sheet thickness.

If the cutting action during shearing involved shearing of the whole thickness, then the force required could be calculated according to

$$F_s = \tau_s \times A \quad (5.1)$$

where: F_s is the shearing force

τ_s is the shear strength of the workpiece

A is the area of the cut edge.

However, it is clear from Fig. 5.2 that the plastic deformation occurring results in a tensile component to the cutting action. Therefore, a more realistic value for the shearing force is obtained from the semi-empirical relationship

$$F_s = 0.7(UTS)A = 0.7(UTS)tl \quad (5.2)$$

where: t is the sheet thickness

l is the length of the cut.

It is apparent from this equation that to reduce the cutting force, the area being cut at any one time should be reduced. For this reason many shearing operations utilize angled cutting tools. This is analogous to the action of hand held scissors, the

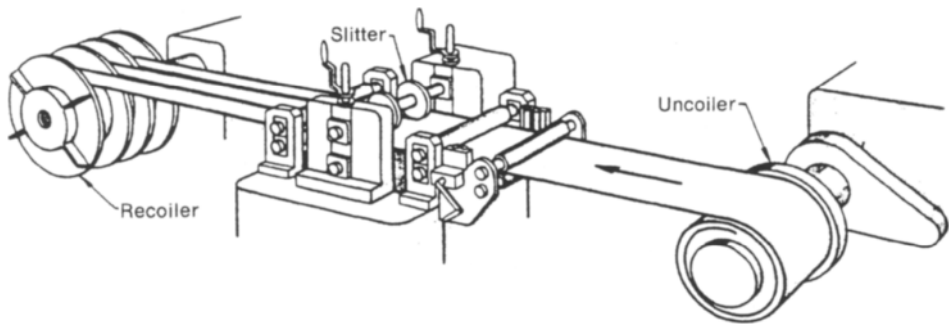


Fig. 5.4 Typical slitting line for edge trimming or cutting rolled sheet into multiple widths. (Reprint permission from *ASM Metals Handbook, Desk Edition*, edited by H.E. Boyer and T.L. Gall (1985 International, Materials Park, OH 44073-0002 (formerly American Society for Metals, Metals Park, OH 44073), p. 26.25, Fig. 4.)

blades of which close at an angle, rather than parallel to each other. The arrangement would increase the area cut at any one time, making the scissors difficult to operate.

An important shearing operation is the *slitting* of flat rolled sheet into narrower widths. Slitting machines, such as that shown in Fig. 5.4, utilize rotating slitting knives to shear the sheet, at sheet speeds sometimes exceeding 100 km/h. Often various final inspection and quality control functions are incorporated into a slitting line.

5.4 Bending

Sheet metal *bending* is conceptually a straightforward operation often carried out using a *press brake* similar to that shown in Fig. 5.5. Usually the press brake punch

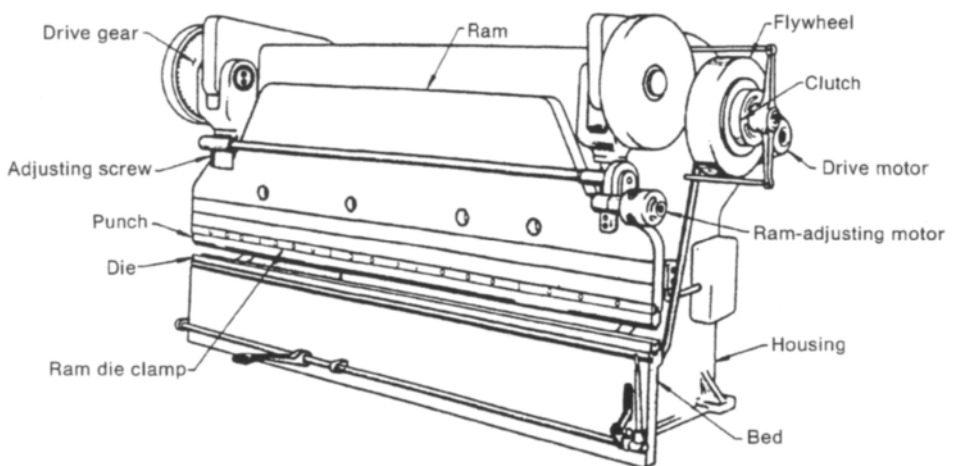


Fig. 5.5 Major components and layout of a press brake for bending. (Reprinted with permission from *ASM Metals Handbook, Desk Edition*, edited by H.E. Boyer and T.L. Gall (1985), ASM International, Materials Park, OH 44073-0002 (formerly American Society for Metals, Metals Park, OH 44073), p. 26.10, Fig. 21.)

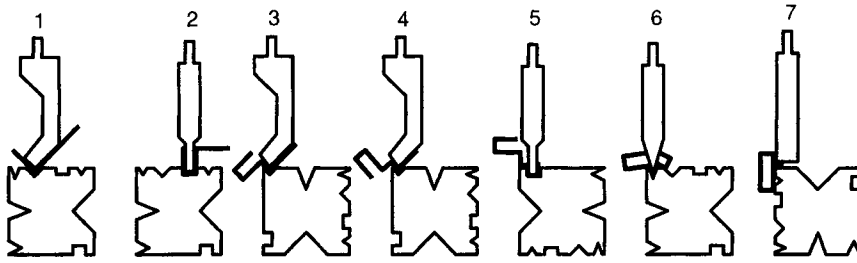


Fig. 5.6 Press brake bending of sheet to fabricate a closed rectangular section in seven steps.

and die are relatively simple shapes, but with intelligent design and multiple press strokes even complex shapes can be produced. Figure 5.6 illustrates the press brake steps necessary to fabricate a closed box section, by repositioning the die and changing the punch profile. Press brakes are available in a variety of sizes and may be capable of applying quite large bending forces. For example, to form a 90° bend in 19 mm thick steel plate, with a bend radius of 19 mm over a 3 m length, requires a press brake with a 530 tonne (600 ton) force capacity. Although 19 mm thick steel plate is hardly ‘sheet metal’, such bending still only causes localized deformation, as opposed to the bulk deformation processes presented in the previous chapter. It is therefore interesting and useful to consider this in the context of sheet forming.

To successfully design the tooling for operations such as that of Fig. 5.6 requires a knowledge of the major parameters associated with bending, which include: minimum bend radius, the springback angle and the press force.

During bending the sheet outer radius is in tension, while the inner radius is in compression. The absolute minimum radius that can be formed is limited by the true strain at the outer radius, which cannot exceed the fracture strain of the sheet. For bending according to the geometry of Fig. 5.7, the following relationship can be developed using similar triangles

$$\frac{l_f}{l_o} = \frac{R+t}{R+\frac{t}{2}} \quad (5.3)$$

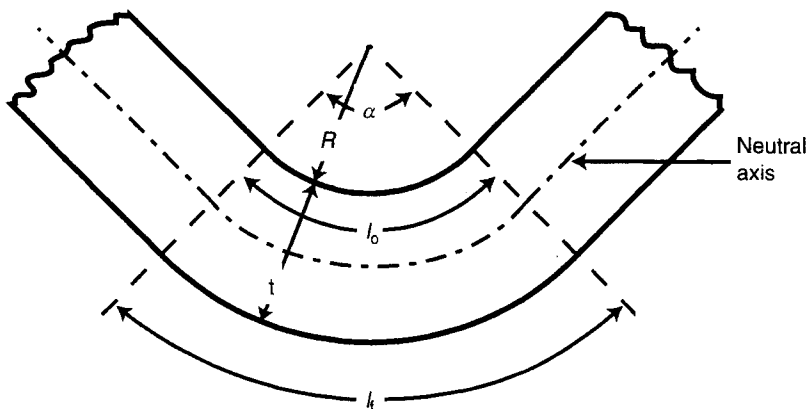


Fig. 5.7 Simplified bending geometry.

where: l_f is a length at the outer radius
 l_o is the neutral axis length
 R is the bend radius
 t is the sheet thickness.

Since failure occurs when $\varepsilon = \varepsilon_f$, equation 5.3 can be expressed as

$$\varepsilon_f = \ln \left[\frac{R_m + t}{R_m + \frac{t}{2}} \right] \quad (5.4)$$

where R_m is the minimum bend radius.

Often, it is more convenient to rearrange equation 5.4 to provide the minimum bend radius in terms of the reduction in area. This is achieved by utilizing the relationship between reduction in area and true strain to fracture (equation 3.12), to give

$$R_m = t \left[\frac{1}{2RA} - 1 \right] \quad (5.5)$$

The primary assumption behind equation 5.5 is that the neutral axis remains at the midthickness during bending, which is only justified for materials with a reduction of area at failure of <0.2 . For more ductile materials, the following is an improved relationship:

$$R_m = t \frac{(1 - RA)^2}{2RA - RA^2} \quad (5.6)$$

One of the difficulties that must be considered during bending operations is the *springback* that occurs when bending forces are released, due to the elastic recovery. Essentially when the bending forces are released the angle α in Fig. 5.7 increases slightly, potentially causing dimensional inaccuracies. A detailed analysis (beyond the scope necessary for this book) yields a relationship for the springback radius of curvature, as follows:

$$\frac{R_b}{R_f} = 4 \left[\frac{R_b \sigma_{0.2}}{tE} \right]^3 - 3 \left[\frac{R_b \sigma_{0.2}}{tE} \right] + 1 \quad (5.7)$$

where: R_b is the bend radius
 R_f is the springback radius
 E is the elastic modulus
 $\sigma_{0.2}$ is the 0.2% yield stress
 t is the sheet thickness.

Finally, by treating the sheet as a beam in bending, an approximation of the bending force can be calculated from simple beam theory as

$$F = K \frac{lt^2 UTS}{w} \quad (5.8)$$

where: l is the length of the bend
 t is the sheet thickness
 K is a die geometry factor (see Fig. 5.8)
 w is the die opening width in Fig. 5.8
 UTS is the ultimate tensile strength.

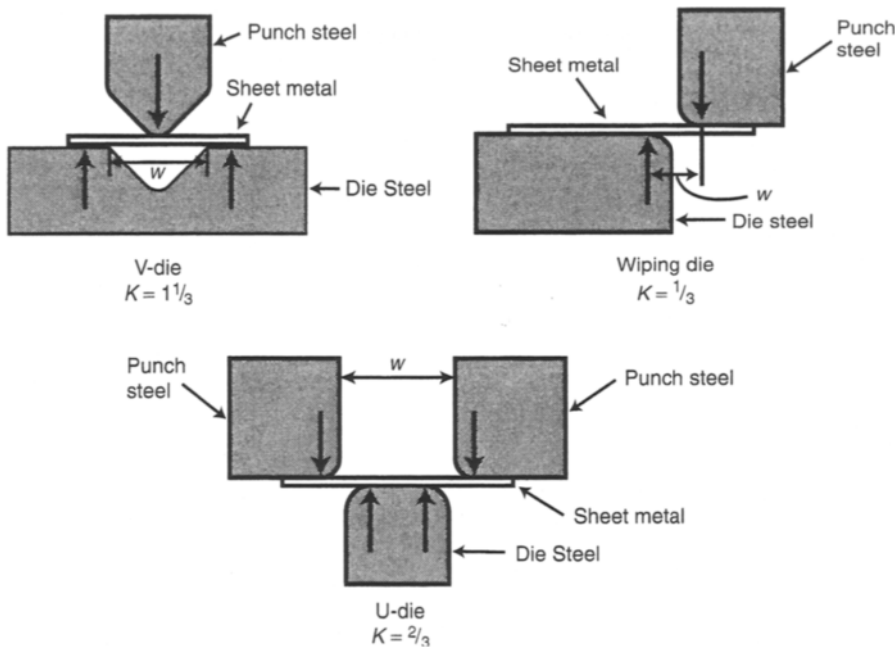


Fig. 5.8 Common types of punch and die arrangements for bending and the associated die geometry factor, K .

Example 5.1 Sheet bending

A piece of sheet metal is to be bent using a wiping die as shown in Fig. E5.1. The metal has a modulus of elasticity of 200 GPa, a yield strength of 350 MPa and a UTS of 500 MPa. What will be the springback radius of curvature and approximately what punch force will be required if the die radius is 10 mm?

Solution Using equation 5.7,

$$\frac{R_b}{R_f} = 4 \left[\frac{R_b \sigma_{0.2}}{tE} \right]^3 - 3 \left[\frac{R_b \sigma_{0.2}}{tE} \right] + 1$$

$$\frac{R_b}{R_f} = 4 \left[\frac{0.010 \times 350 \times 10^6}{0.003 \times 200 \times 10^9} \right]^3 - 3 \left[\frac{0.010 \times 350 \times 10^6}{0.003 \times 200 \times 10^9} \right] + 1 = 0.983$$

so $R_f = 10/0.983 = 10.17$ mm, as compared to the desired 5 mm.

Using equation 5.8 and $K = 1/3$, from Fig. 5.8, die opening

$$w = 10 + 10 + 3 = 23 \text{ mm}$$

$$F = K \frac{lt^2 \text{UTS}}{w}$$

$$= \frac{1}{3} \times \frac{0.045 \times 0.003^2 \times 500 \times 10^6}{0.023} = 2935 \text{ N } (\approx 650 \text{ lb}_f)$$

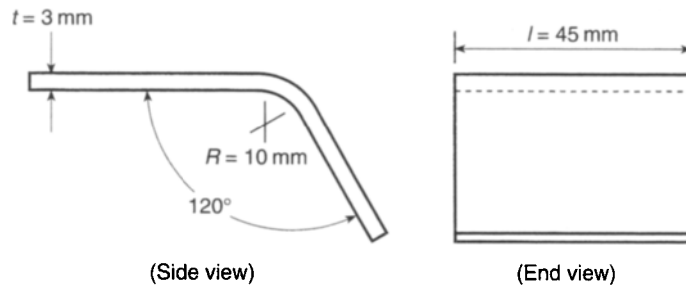


Fig. E5.1 Example 5.1.

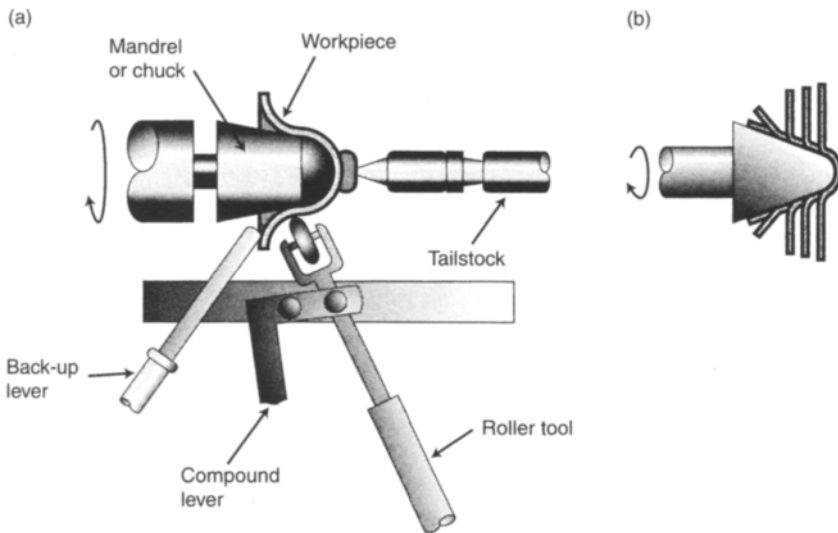


Fig. 5.9 Bending by spinning, showing (a) the tooling arrangement and (b) the progressive deformation of the workpiece.

5.4.1 Spinning

Spinning is a unique form of bending, shown schematically in Fig. 5.9, which shapes a blank with a tool that presses the blank around a preshaped form. The operation often proceeds at relatively high speeds and is most suitable for making simple axisymmetric shapes such as bowls and light reflectors, but it can be utilized to manufacture complex shapes. Although Fig. 5.9 only indicates that the metal is bent around the form, the sheet thickness is sometimes reduced, in which case the process is referred to as *shear spinning*. For softer metals and low production volumes the form is often constructed from wood.

5.5 Stretch forming

The process referred to as *stretch forming* is shown in Fig. 5.10. Essentially a die is forced against sheet metal that is firmly held by clamps. The shape desired is

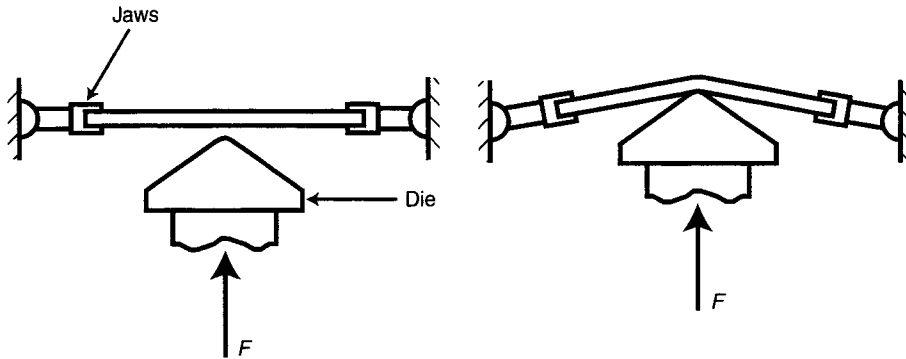


Fig. 5.10 Schematic representation of simple stretching.

formed entirely by tensile stretching and the limiting strain is that which causes local deformation due to necking. As mentioned in Section 5.2, it follows that materials with a high strain hardening exponent, n , or high strain rate exponent, m , would have the best stretch formability. Therefore, when the geometry of the forming operation is such that the stress state is uniaxial, the *forming limit* is reached when the local strain is equivalent to the strain at which necking begins, or

$$\epsilon_{\text{limit}} = \epsilon_{\text{UTS}} = n \quad (5.9)$$

More often, the geometry of the stretching operation causes biaxial strains. For such instances, the forming limit is often determined using the *punch-stretch* test which, as seen in Fig. 5.11, involves forming of a hemispherical dome in the test sheet. Prior to testing the sheet is imprinted with a grid of circles that deform into ellipses. By measuring the axes of the ellipse after deformation the local strain in two dimensions (ϵ_1 and ϵ_2 in Fig. 5.11) can be easily calculated. The results of such tests are usually

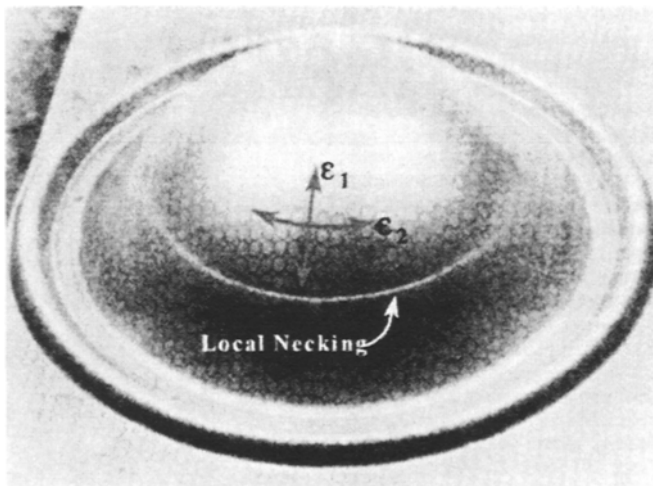


Fig. 5.11 Test sample after the punch-stretch test. (Reprinted with permission from *ASM Metals Handbook, Desk Edition*, edited by H.E. Boyer and T.L. Gall (1985), ASM International, Materials Park, OH 44073-0002 (formerly American Society for Metals, Metals Park, OH 44073), p. 34.41, Fig. 10.)

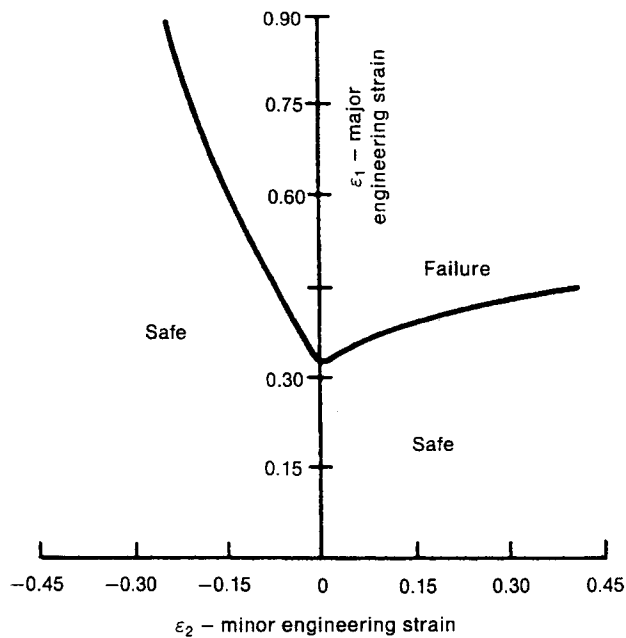


Fig. 5.12 Example of forming limit diagram for an aluminium killed steel. (Reprinted with permission from *ASM Materials Engineering Dictionary*, edited by J.R. Davis (1992), ASM International, Materials Park, OH 44073-0002, Fig. 196, p. 173.)

presented in the form of a *forming limit diagram*, an example of which is shown in Fig. 5.12. On this diagram the primary strain causing the shape change is the *major strain* (ϵ_1 in Fig. 5.11) and the transverse strain is referred to as the *minor strain* (ϵ_2 in Fig. 5.11). For each combination of major and minor strain the point at which necking begins is plotted, thus defining a region in which forming can be accomplished without necking (the safe region in Fig. 5.12) and a region in which necking will occur (the fail region). It is important to note that if a minor strain is applied, the strain to necking is increased, allowing greater shape change to occur. Figure 5.12 indicates that compressive minor strain is more effective than a tensile minor strain for increasing the major strain that can be safely applied. This effect is a useful observation with regard to the *deep drawing* process.

5.6 Deep drawing

The deep drawing operation is shown schematically in Fig. 5.13. Deep drawing was patented in 1857, using an arrangement similar to that of Fig. 5.13(a), utilizing only a punch and die. Deep drawing is now of enormous commercial importance, with many food containers and other similar packages deep drawn. For example, it is a preliminary step in the manufacture of aluminium beverage cans. More often, however, the arrangement shown in Figs 5.13(b) and 5.13(c) is used, utilizing a punch, die and blankholder. The workpiece to be formed is usually produced by shearing a circle from cold rolled sheet.

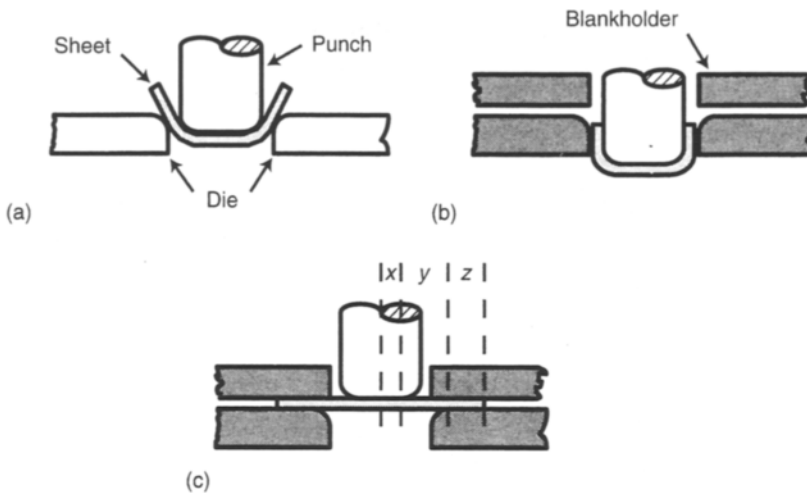


Fig. 5.13 (a) Original deep drawing concept, (b) deep drawing utilizing a blankholder, and (c) deformation zones during deep drawing (see text).

To help understand the forming process, the circular workpiece can be divided into the three zones shown in Fig. 5.13(c) (i.e. x , y and z). The material in zone x will form the bottom of the drawn cup. This material must slide freely along the surface of the punch and undergoes some stretching, but typically the change in thickness during the drawing of the material in zone x is minimal. The material in zone y forms the bottom corner radius of the cup. During drawing the material of zone y predominantly undergoes bending. Material in zone z is drawn radially inwards. The effect of this decrease in radius and circumference is to cause the sheet thickness to increase and induce compressive hoop stresses in the material of zone z . The role of the blankholder is to ensure that, as the material in zone z moves radially inward, the compressive hoop stresses do not cause wrinkling of the workpiece, as shown in Fig. 5.14.

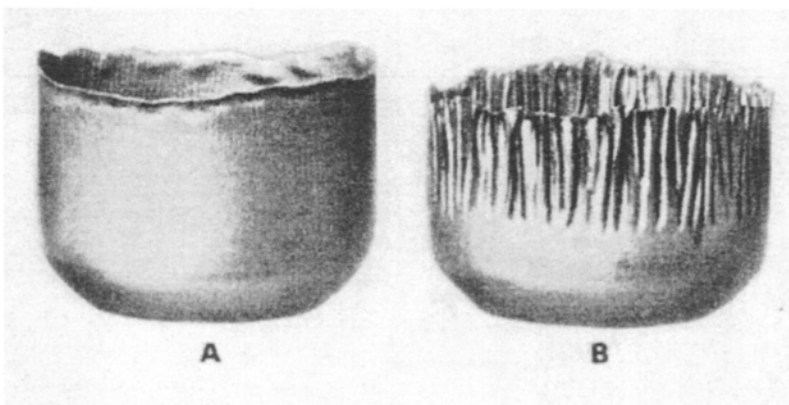


Fig. 5.14 Cups deep drawn with (a) correct blankholder pressure and (b) insufficient blankholder pressure causing sidewall wrinkling. (Reproduced from *Forming Aluminum*, with permission of Alcan Aluminium Limited.)

Thus, the selection of the correct blankholder force is critical to successful drawing. The blankholder pressure is typically about 1.5% of the workpiece yield stress. As the material of zone z passes over the die radius to form the walls of the deep drawn cup, it is bent and then unbent. Finally, to form the lower portion of the cup wall, some regions of zone z are stretched with significant thinning occurring. As a result of these complex operations it is not unusual for a deep drawn cup to have a thicker cup wall at the top than at the bottom.

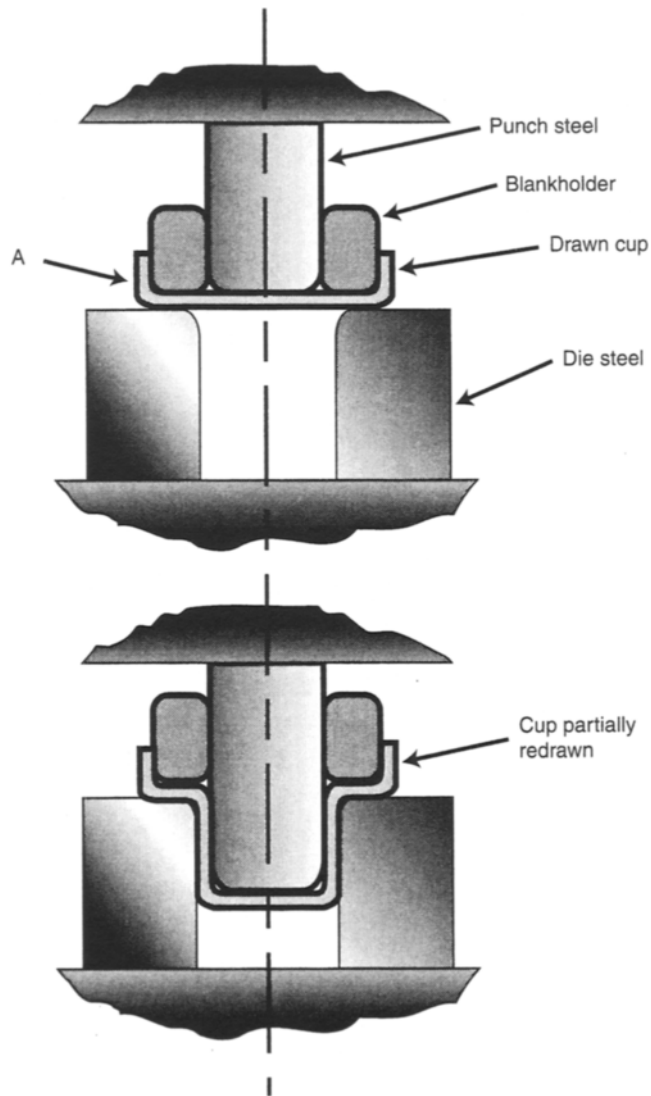


Fig. 5.15 General arrangement of redrawing. Metal identified at A is bent and unbent twice during redrawing.

5.6.1 Redrawing

If a very deep cup is desired, the original blank needs to have a large diameter, making prevention of wrinkling in zone z difficult. Therefore, for the forming of tall and narrow cups a *redrawing* operation, as shown in Fig. 5.15, is often utilized. The amount of drawing during the redraw is always less than the initial drawing stage. This is because, as indicated in Fig. 5.15, metal already stretched during the initial stage is forced to undergo two further bending and unbending processes. Metals that strain harden rapidly are often difficult to redraw without an anneal following the initial drawing operation.

Due to the complex nature of deformation during deep drawing, a rigorous analytical treatment is quite difficult. However, there is a limit to the depth of cup that can be produced. This limit, or the *limiting draw ratio* (LDR), is attributable to the build up of compressive stresses and the subsequent tensile stresses in zone z , as it forms the walls of the cup. The LDR is estimated from

$$\text{LDR} = \frac{d_{\text{oMAX}}}{d_{\text{p}}} \quad (5.10)$$

where: d_{oMAX} is the maximum blank diameter that can be drawn without wrinkling
 d_{p} is the cup diameter.

The severity of a deep drawing operation is expressed as the percentage reduction (%Red) according to

$$\% \text{Red} = 100 \left(1 - \frac{d_{\text{p}}}{d_{\text{o}}} \right) \quad (5.11)$$

For ductile steels the limiting %Red during the initial drawing is typically 40%, and 25%, 15% and 11% for the first, second and third redraws, respectively. In conjunction with the data of Fig. 5.16 the %Red is useful for determining the feasibility of drawing procedures, as illustrated in the following example.

Example 5.2 Drawing and redrawing of a cup

Use Fig. 5.16 to determine whether a cup of 190 mm diameter can be fabricated from an initial blank of 460 mm diameter in three stages, with successive reductions of 40%, 20% and 15%. What is the minimum LDR required for this procedure?

Solution For the initial drawing operation with a 40% reduction, using Fig. 5.16 gives a cup diameter of about 275 mm or, using equation 5.11,

$$\begin{aligned} d_{\text{p}} &= d_{\text{o}} \left(1 - \frac{\% \text{Red}}{100} \right) \\ &= 460(1 - 0.4) = 276 \text{ mm} \end{aligned}$$

Likewise, for the first redrawing operation with 20% reduction applied to the 276 mm cup, Fig. 5.16 gives a redrawn cup diameter of 220 mm; the second redrawing operation with a 15% reduction applied to a cup of 220 mm diameter yields a final cup of 185 mm. This is less than the desired cup diameter of 190 mm, so the proposed process is possible if the percentage reductions are reduced slightly.

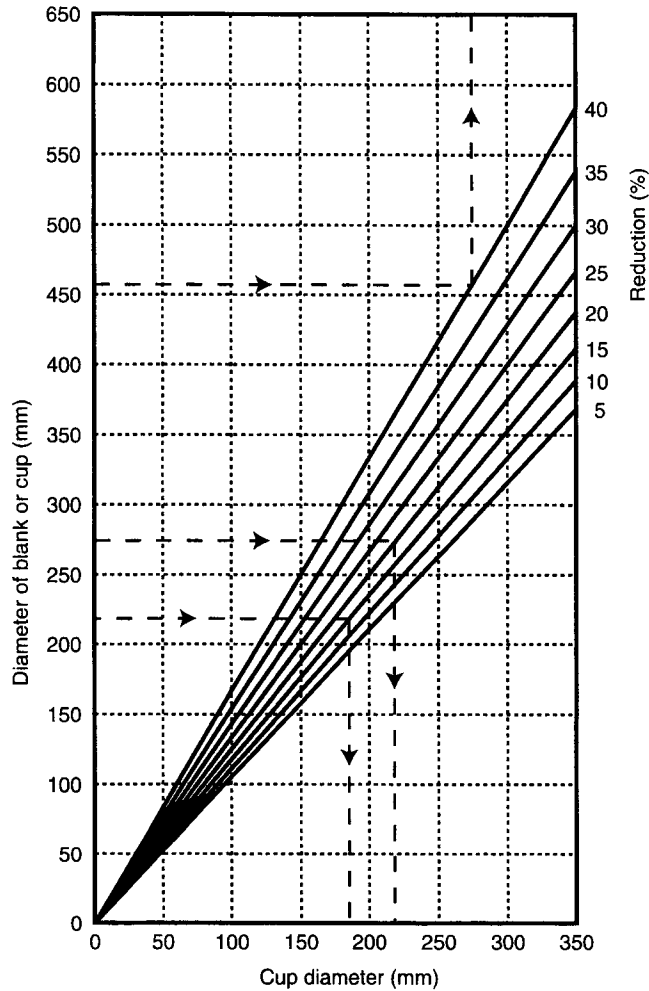


Fig. 5.16 Relationship between blank/cup size and percentage reduction. The dotted lines refer to Example 5.2.

The LDR required for these operations are

$$\begin{aligned} \text{Initial draw} \quad \text{LDR} &= 460/276 = 1.67 \\ \text{First redraw} \quad \text{LDR} &= 276/220 = 1.25 \\ \text{Second redraw} \quad \text{LDR} &= 220/185 = 1.19 \end{aligned}$$

Therefore, the sheet metal to be formed into the cup must have an LDR of at least 1.67.

Note: the percentage reduction decreases during each successive drawing/redrawing step.

The drawing or redrawing force required can be estimated from the following relationship

$$F_d = \pi d_p t_{\text{avg}} (\text{UTS}) \quad (5.12)$$

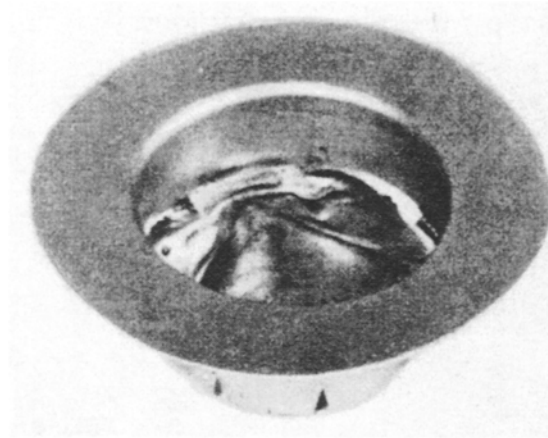


Fig. 5.17 Failure at bottom radius of a deep drawn cup. (Reproduced from *Forming Aluminum*, with permission of Alcan Aluminium Limited.)

where: F_d is the draw force
 d_p is the cup diameter
 t_{avg} is the wall thickness.

In this equation the UTS is used because this is the stress at which necking begins. Usually the average wall thickness is very close to the initial sheet thickness. If the drawing reduction is excessive then sheet failure will often occur near the bottom radius of the cup, as seen in Fig. 5.17. In this region a complex stress state exists and the wall thickness is unknown until after drawing. Therefore, the following empirical equation has been developed as an improved estimate of the drawing force

$$F_d = \pi d_p t_{avg} \times \text{UTS} \left[\frac{d_o}{d_p} - 0.7 \right] \quad (5.13)$$

5.6.2 Ironing

An alternative to redrawing for the forming of deep cups is the *ironing* process, illustrated in Fig. 5.18. An important difference between redrawing and ironing is that during ironing the inside diameter of the cup remains constant and the wall thickness is reduced markedly. In contrast, during redrawing the inside diameter is reduced. The force to cause the ironing deformation is transferred from the punch to the cup via the pressure exerted on the bottom and friction at the interface of the cup and the ironing die. Therefore, ironing operations require careful engineering to ensure that the punch force does not cause the bottom of the cup to tear-off, in a fashion similar to the failure shown in Fig. 5.17, and to ensure that appropriate lubrication is available at the cup–ironing die interface. This task is made more difficult by the fact that ironing is applied to cups that may have already been heavily worked during prior deep drawing. Often several ironing dies are stacked so that more than one ironing reduction can be applied to a single cup during each punch stroke.

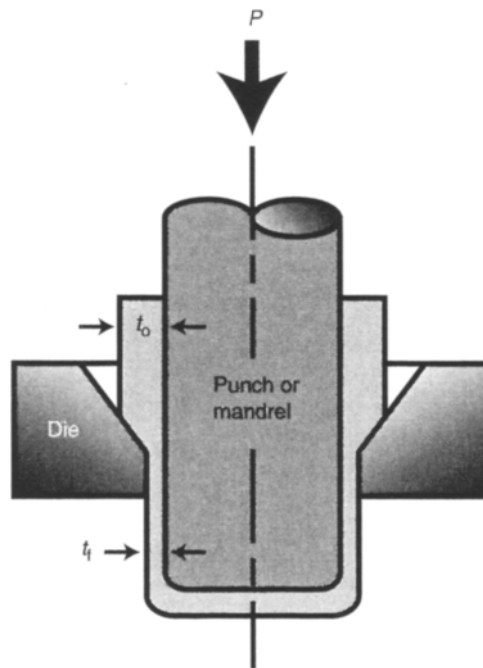


Fig. 5.18 Ironing press.

Successful ironing demands the best available press conditions to ensure proper alignment of the ironing dies with the punch. As mentioned previously, the tops of deep drawn cups usually have larger wall thicknesses and, due to the associated higher compressive hoop stress imposed during deep drawing, the tops of the cups usually strain harden to a greater extent than the bottoms. Consequently, the stroke force increases as ironing proceeds from the bottom to the top. Therefore, failure at the top of the cup may occur if the cup has insufficient ductility. The tendency for such failures to occur can be reduced by selecting alloys for ironing that do not strain harden rapidly (low n). For these alloys the difference between the strength of the bottom and top of deep drawn cups is minimized.

Deep drawing, redrawing and ironing are commercially important. For example, all of these processes are utilized during the manufacture of beverage cans (see the case study at the end of this chapter).

5.7 Effect of anisotropic sheet properties on formability

At the beginning of this chapter the importance of prior cold rolling, to produce a sheet suitable for forming processes, was emphasized. In most cold rolling operations the applied strain, and thus the level of strain hardening, in the direction of rolling, across the sheet width, and through the sheet thickness, is different. As a consequence, the sheet properties in the three directions are different. In addition to the difference in applied strain, the severe plastic deformation applied during rolling and similar

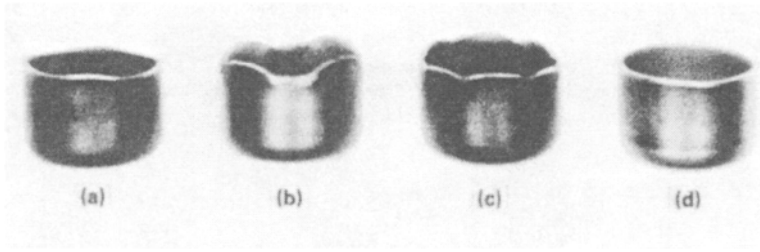


Fig. 5.19 Earing in deep drawn aluminium cups. Ears formed at (a) 90° to rolling direction, (b) 45° to rolling direction, (c) 90° and 45° to rolling direction, and (d) no ears. (Reprinted with permission from *ASM Aluminum Properties and Physical Metallurgy*, edited by J. Hatch (1984), ASM International, Materials Park, OH 44073-0002 (formerly American Society of Metals, Metals Park, Ohio, 44073), p. 127, Fig. 21.)

operations causes individual grains within the metal to assume a preferred crystallographic orientation or *texture*, with respect to the rolling direction.

The development of texture in sheet is a ramification of the fact that plastic deformation is limited to specific crystallographic slip systems. During deformation, individual grains tend to rotate such that deformation can occur on one, or possibly several, slip systems at a lower total energy level. The significance of the texture and directional sheet properties is *plastic anisotropy*, that causes the shape produced during forming to depend on the orientation of the forming forces with respect to the sheet rolling direction. A common defect resulting from plastic anisotropy is the formation of *ears* on deep drawn cups, as shown in Fig. 5.19. For most applications the ears must be trimmed, reducing metal recovery.

The magnitude of plastic anisotropy in sheet products is determined by measuring the strains of a tensile specimen strained to beyond its yield strength, but not beyond its UTS. For samples oriented longitudinally, transversely and at 45° to the rolling direction (Fig. 5.20), the width and thickness strains are calculated according to

$$\varepsilon_w = \ln \frac{w}{w_0}, \quad \varepsilon_t = \ln \frac{t}{t_0} \quad (5.14)$$

where: w_0 , w are the specimen width before and after straining
 t_0 , t are the specimen thickness before and after straining.

From these strains, the plastic anisotropy is defined as

$$r = \frac{\varepsilon_w}{\varepsilon_t} \quad (5.15)$$

The significance of the r value is that if $r > 1$ the material is more resistant to thinning than to deformation in the plane of the sheet, whereas if $r < 1$ the reverse is true. For many ductile metals, the r value varies with respect to the rolling direction and so it is useful to define the *mean anisotropy* as

$$r_m = \frac{r_0 + r_{90} + 2r_{45}}{4} \quad (5.16)$$

where the subscripts 0, 90 and 45 refer to the anisotropy of specimens with their lengths oriented at 0°, 90° and 45° to the sheet rolling direction, respectively, as illustrated in Fig. 5.20.

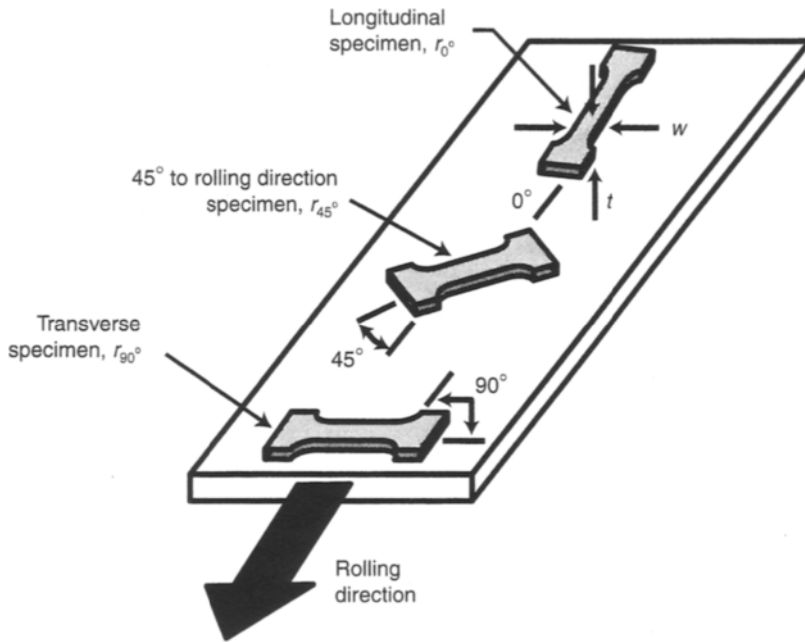


Fig. 5.20 Specimen orientation for determining plastic anisotropy.

For most sheet forming operations a high r value is desirable, as this causes planar strains that are large compared to through thickness strains. Consequently, there is less change in thickness for metals with a high r value. The retention of the sheet thickness provides more resistance to the punch pressure, providing higher LDR. This permits more severe forming operations before the onset of necking. The relationship between the r_m value and the LDR is shown in Fig. 5.21.

The tendency for metals to develop a texture, and associated plastic anisotropy, is related to the number of *slip systems* available for plastic deformation. Most metals of

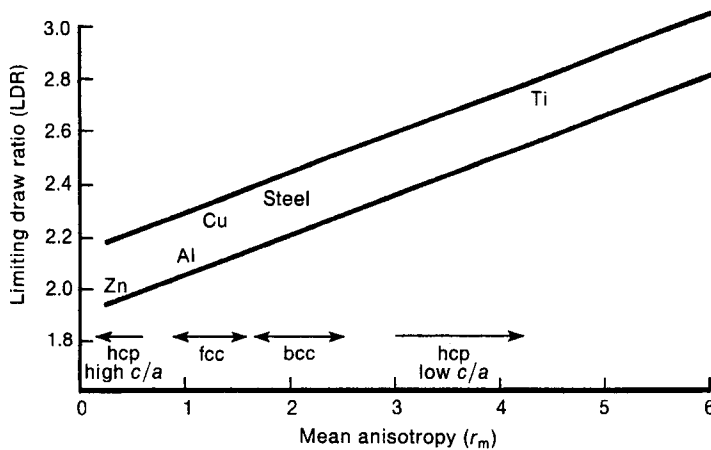


Fig. 5.21 Approximate relationship between the LDR and r , showing typical values for several metals.

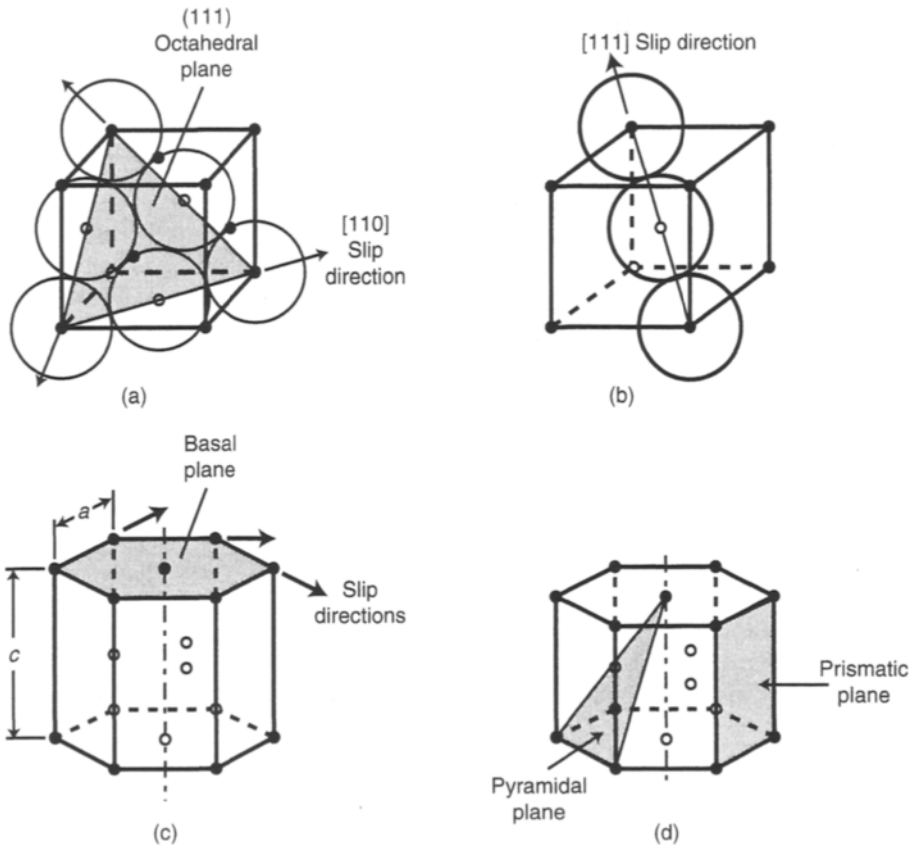


Fig. 5.22 Unit cells and slip systems for (a) fcc structures, (b) bcc structures, (c) high c/a ratio hcp structures, and (d) low c/a hcp structures.

engineering interest are face centred cubic (fcc), body centred cubic (bcc) or hexagonal close packed (hcp), as shown in Fig. 5.22. For hcp metals the plastic anisotropy depends on the c/a ratio (see Fig. 5.22). For materials with a high c/a ratio, such as zinc ($c/a = 1.856$), slip is limited to the *basal* or $\{0001\}$ plane. Thus, after even a modest rolling reduction of only 20–30% most of the grains will have rotated so that the basal plane is roughly parallel to the sheet surface. During subsequent sheet forming, slip occurs easily on the basal planes, causing a large change in thickness with a correspondingly small width strain. An analogy is a deck of cards – the plane between cards is equivalent to the basal plane, and sliding of one card over another, along ‘basal’ planes, reduces the height of the deck, but the width does not change. The low r values of hcp sheet, about 0.2 for zinc, leads to poor sheet forming characteristics. Conversely, if the c/a ratio is low, as for titanium ($c/a = 1.587$), then slip occurs on *pyramidal* $\{10\bar{1}1\}$ and/or *prismatic* $\{10\bar{1}0\}$ planes. This leads to deformation with minimal change in thickness, but large width strains. Hence, hcp metals with low c/a ratios have comparatively higher r values and are ideally suited to sheet forming. Unfortunately, the high cost of titanium (Table 1.1) limits its applicability in this respect.

Face centred cubic metals (Al, Cu, Ni) slip on *octahedral planes* (Fig. 5.22), creating 12 equivalent slip systems. This number of slip systems ensures isotropic properties if no texture is present, and an LDR of about 2.1 is typical. However, rolling reductions of more than 50% will cause texture development and subsequent formation of ears during deep drawing. With appropriate thermomechanical processing prior to sheet forming (e.g. rolling reductions and annealing treatments), the plastic anisotropy of fcc metals can be limited to manageable levels.

As shown in Fig. 5.22, bcc metals exhibit a unique slip direction, the $[111]$, but no dominant slip plane, with deformation occurring on the $\{110\}$, $\{112\}$ and $\{123\}$ planes, creating 48 slip systems. With such a large number of slip systems there is little tendency for texture development. Low carbon killed steels can exhibit r values approaching 2, corresponding to an LDR of about 2.4.

5.8 Pressworking of metals

Pressworking is a general term often used to describe sheet metal forming processes that utilize powered presses with permanent or semipermanent dies made of tool steels. A common example of pressworking is the *stamping* of automobile body components, which are usually made of steel, or less often aluminium. The complex shape of many pressworking operations means that the workpiece is subjected to a combination of shearing, bending, stretching and drawing, simultaneously. The analysis of such processes is quite difficult, due to the complex shapes and radically changing geometry with time. Although the preceding sections have highlighted the factors controlling these sheet forming processes, the techniques presented do not provide exact solutions for the complicated shapes often encountered in industry. Nevertheless, the principles presented are the same ones that apply to the pressing of complex shapes. These principles, combined with sound engineering judgement, can provide useful conclusions regarding the suitability of many processing parameters. The information presented in this chapter is intended to provide a foundation of knowledge on which sound engineering judgement required can be based.

Several advanced analysis techniques are applied to complex pressworking operations, including those presented at the end of Chapter 4. Another technique is *shape analysis*, which predicts the severity of sheet forming processes from the results of laboratory tests such as the Olsen cupping test (Fig. 5.1). Shape analysis combines the influence of the material, shape and die variables to predict the overall behaviour. The analysis involves: evaluating the formability of the workpiece under combined stretching and drawing conditions; identifying the critical location of the workpiece in terms of the forming severity; comparing the forming severity to the material properties; and if required, modification of the tooling to reduce the forming severity. The application of shape analysis frequently includes laboratory formability tests, and computer and/or experimental optimization to minimize the forming severity.

5.9 Problems

- 5.1 Is it desirable that metals used for stretch-forming operations have high or low strain hardening exponents? State reasons for your answer.

- 5.2 A piece of sheet metal has a true strain to fracture of 0.3. What is the minimum bend radius for a piece of this sheet metal if its thickness is 0.5 mm?
(Answer: about 0.60 mm)
- 5.3 A piece of sheet metal of length 500 mm and thickness 0.3 mm, with a UTS of 200 MPa, is to bend through 90° using either a v-die with a width of 50 mm or wiping die with die radii of 15 mm. Calculate the bending force for the two die arrangements.
(Answer: v-die ≈ 239 N; wiping die ≈ 100 N)
- 5.4 Sheet metal of two different alloys is produced by rolling to 0.100 in thickness. You must select one of these alloys for a sheet forming operation. To make the selection, tensile samples are cut from each alloy at 0° , 45° and 90° to the rolling direction. The gauge section of each tensile sample is 0.75 in wide. After subjecting all samples to the same tensile load, the samples plastically deform and the width and thickness for each alloy is measured, with the following results:

Cut	Alloy A	Alloy B
At 0°	$w = 0.65$ in, $t = 0.092$ in	$w = 0.70$ in, $t = 0.082$ in
At 45°	$w = 0.63$ in, $t = 0.093$ in	$w = 0.69$ in, $t = 0.083$ in
At 90°	$w = 0.67$ in, $t = 0.087$ in	$w = 0.71$ in, $t = 0.078$ in

Which of the two alloys would you select for sheet forming operations? Support your answer by calculation.

(Answer: alloy A)

- 5.5 You work for a new car manufacturer that has just introduced a low priced small car. It comes with plastic hubcaps as standard equipment! Unfortunately, the plastic is very brittle in subzero temperatures, and the hubcaps cannot be removed from the wheel without breaking. You are assigned the task of 'instantly' instituting a manufacturing change to solve the problem. One of your parts suppliers can stretch form the hubcaps starting immediately, from any one of the three alloys listed below. Which alloy is the most appropriate for a stretch forming operation and why?

Alloy	Yield stress (MPa)	Elongation (%)	Strain rate exponent (n)
1008 steel	180	40	0.24
5052 Al	90	25	0.13
1100 Al	35	35	0.25

(Answer: 1100 Al)

- 5.6 A 5 mm diameter circle is scribed onto a piece of sheet metal. After the sheet is deformed the circle has changed into an ellipse. The axis of the ellipse parallel to the sheet rolling direction is 7.5 mm, while perpendicular to the sheet rolling direction the ellipse axis is 3.8 mm. Calculate the plastic anisotropy in the direction perpendicular to the sheet rolling direction.
(Answer: ≈ 2.1)

- 5.7 A tensile specimen of cold rolled sheet has a rectangular cross-section with a width of 10 mm and a thickness of 1 mm. After loading, but before failure, the cross-section deforms to 9 mm width and 0.93 mm thickness. (a) Calculate the plastic anisotropy of this sheet. (b) What is the strain in the direction of the specimen gauge length?
(Answers: (a) 1.44, (b) 0.178)
- 5.8 Tensile type samples are machined from two alloys. The initial dimensions of the gauge section of the tensile samples is 50 mm in length and 6 mm in width. The tensile test of both samples is interrupted before the UTS and the dimensions of the samples measured as follows:
- Alloy A: length = 60 mm, width = 5.2 mm
Alloy B: length = 62 mm, width = 5.4 mm
- (a) Will necking have occurred in either alloy? Explain your answer.
(b) Which of the two alloys would you select for a deep drawing operation?
Support your answer by calculation.
(Answers: (a) no necking in either alloy; (b) choose alloy A, higher r value)
- 5.9 During the deep drawing of cold rolled sheet it is usual for *ears* to develop around the top of the cup shape produced. What is the fundamental cause of the formation of ears?
- 5.10 A certain material is known to have an r_0 of 1.5. The original dimensions of a tensile specimen oriented along the rolling direction are $w_0 = 10$ mm, $t_0 = 1$ mm and a gauge length of 20 cm (l_0). Calculate the change in these dimensions after an extension of 15% in gauge length. Assume uniform strain throughout.
(Answer: new length = 23 cm, new thickness = 0.95 mm, new width = 9.19 mm)
- 5.11 You work for a company that makes 1.5 V batteries. A new battery design to be put into production will require a zinc casing with an inside diameter of 40 mm and a height of 60 mm. You are to consider whether the battery casing should be made by deep drawing or impact (backward) extrusion. For zinc: ultimate tensile strength = 150 MPa, strength constant = 200 MPa, strain hardening exponent = 0.15.

For the deep drawing process:

- (a) The bottom and walls of the deep drawn battery casing are on average 0.5 mm thick. Estimate the diameter of the initial circular blank necessary.
(b) Calculate the drawing force required.
(c) Calculate the force required to shear the blank for deep drawing from a large sheet of zinc.
(d) Given that zinc has a hexagonal close packed structure, with a high c/a ratio, comment on whether the proposed deep drawing operation is a good idea. Briefly explain.
(Answers: (a) 106 mm, (b) 18.4 kN, (c) 17.5 kN)

For the impact extrusion process:

- (e) For a 0.5 mm wall thickness, calculate the punch force for impact extrusion.

- (f) If the bottom of the casing is still to be 0.5 mm thick, what is the required thickness of the initial blank?
 - (g) Calculate the force necessary to shear the blank for impacting from a large piece of zinc plate.
 - (h) Give a reason for the difference in force required to form the battery case by deep drawing (part (b)) and impact extrusion (part (e)).
- (Answers: (e) 1142 kN, (f) 3.3 mm, (g) 44.6 kN)

5.12 The company for which you work proposes to manufacture hair spray cans by shearing slugs from AA-1100 aluminium hot rolled strip and then impact (backward) extruding the slugs. Each slug is 50 mm diameter and 7 mm thick. With the tooling available six slugs can be sheared from the sheet with each press stroke. The cans are extruded one at a time with an inside diameter of 48 mm.

- (a) Your company owns only one press, but you believe that with good mechanical design of the tooling, both the shearing and impact extrusion operations can be done on this one press. The maximum force capacity of the press is 1500 kN. Does your press have sufficient capacity for both the shearing and impact extrusion operations? Support your answer by calculation.
- (b) To meet production requirements, the press must extrude 120 cans per minute. What is the power required for this operation?

(Answers: (a) press has capability for both operations, (b) about 10 kW)

Case study 4:

Manufacture of can body stock – 3. Sheet forming

From the can stock manufacturing case studies presented at the end of Chapters 2 and 4, the large capital investment inherent in the process is evident. This investment is justified by huge production numbers – more than 300 million cans produced per day in North America alone. To achieve these production numbers requires reliable production equipment and sheet of the highest quality. Typically, one plant will produce about 2 million cans per day with a reject rate not exceeding one can in 50 000. Defective cans may cause production line stoppages, reducing production output. In this section, the sheet forming mechanics of beverage can making are described, and then the interaction of some of the casting and rolling parameters with canmaking performance discussed.

The overall process of converting cold rolled sheet into finished cans is illustrated in Fig. C4.1. Of particular interest are the canmaking steps to transform coiled sheet into trimmed cans. This transformation consists primarily of deep drawing or *cupping*, redrawing, wall ironing, bottom forming and trimming. The formed shape after each of these operations is shown in Fig. C4.2. For the most part, all of these operations are performed on two major pieces of equipment: a *cupper* and a *bodymaker*.

The cupper shears circular discs from the incoming sheet and deep draws these into cups of about 9 cm diameter and 4 cm depth (Fig. C4.2(a)). As the sheet is uncoiled it is coated with an appropriate sheet forming lubricant, and inspected for thickness, flatness, width, pinholes etc. As the canmaking process proceeds at very fast speeds it is imperative to ensure that a defective sheet is not introduced that will reduce production and could damage expensive tooling.

To minimize the amount of skeleton scrap left after shearing the discs, most cuppers shear 12 or 14 discs at once across the sheet width, corresponding to sheet widths of about 170 cm. (The sheet of Fig. C4.1 produces six cups across the width.) Each sheared disc is just under 14 cm in diameter and is immediately drawn into a cup using the tool arrangement shown in Fig. C4.3. The major steps of the

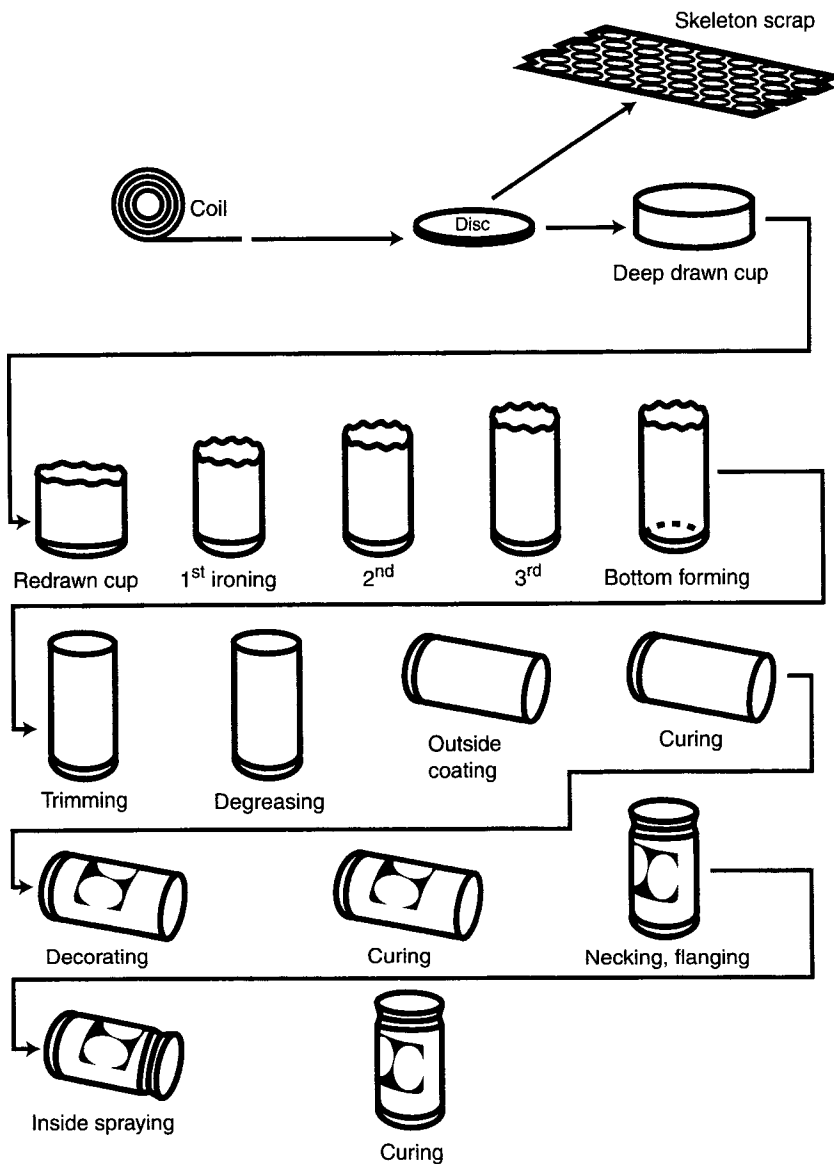


Fig. C4.1 Steps involved in canmaking by the draw, redraw and ironing process.

cupping operation (Fig. C4.3) are: (1) shearing of the disc between the knife edge and punch die; (2) drawing the disc around the die centre; (3) complete drawing of the flange into the cup wall; and (4) removal of the cup from the die centre using a stripper. After this operation the cups are collected by a conveyor for delivery to the bodymaker. Typically the cupper will run at about 180 strokes per minute, corresponding to more than 2000 cans per minute.

In the bodymaker the deep drawn cup is redrawn and ironed three times to form the cup bottom and walls. During redrawing the cup diameter is reduced and during

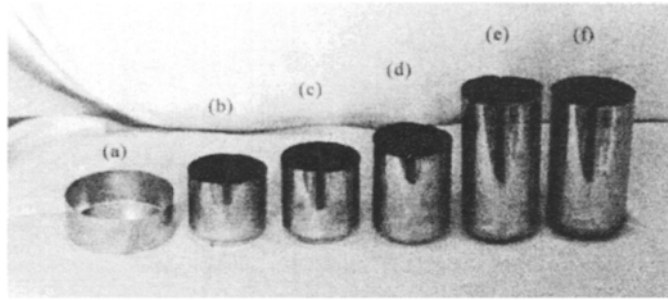


Fig. C4.2 Partially formed can body: (a) deep drawn cup, (b) redrawn cup, (c) first ironing stage, (d) second ironing stage, (e) third ironing stage, and (f) body after trimming.

ironing the cup wall thickness is reduced, as shown in Fig. C4.4. During ironing large reductions in wall thickness occur and, to maintain good can surface appearance and extend tool life, copious amounts of lubricant are required, with lubricant fed separately to each ironing ring. Notice in Fig. C4.4 that the punch bottom is profiled to

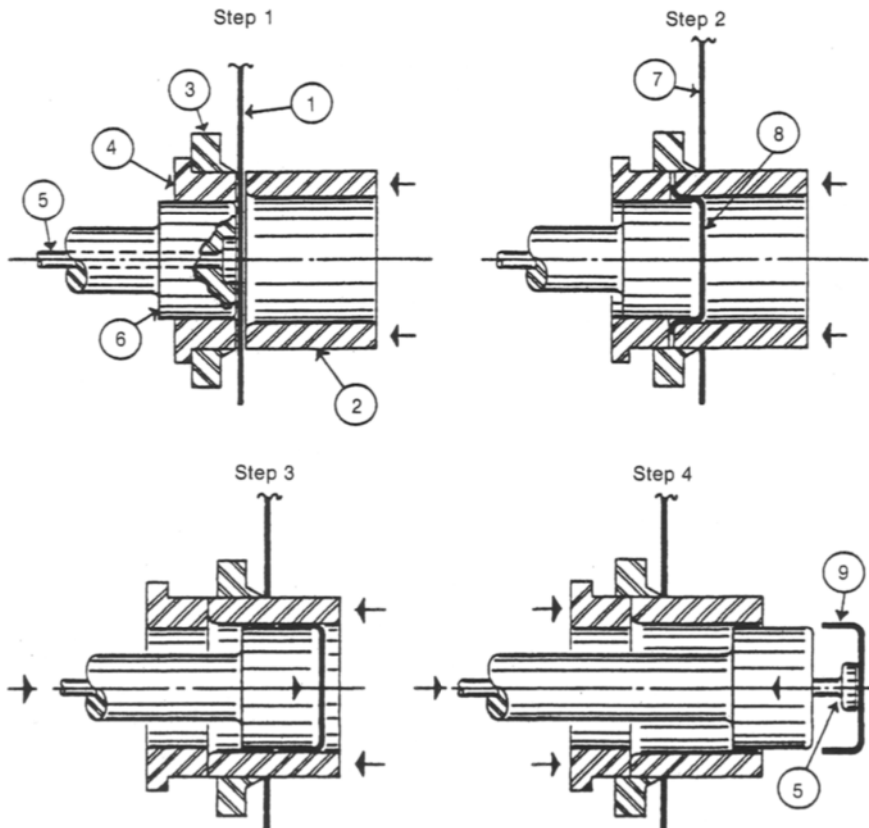


Fig. C4.3 General arrangement of tooling and steps of the cupping operation: 1 aluminium sheet, 2 punch die, 3 knife edge, 4 blankholder, 5 stripper, 6 die centre, 7 skeleton scrap, 8 partially formed cup, 9 deep drawn cup. (Reproduced courtesy of Texaco Inc.)

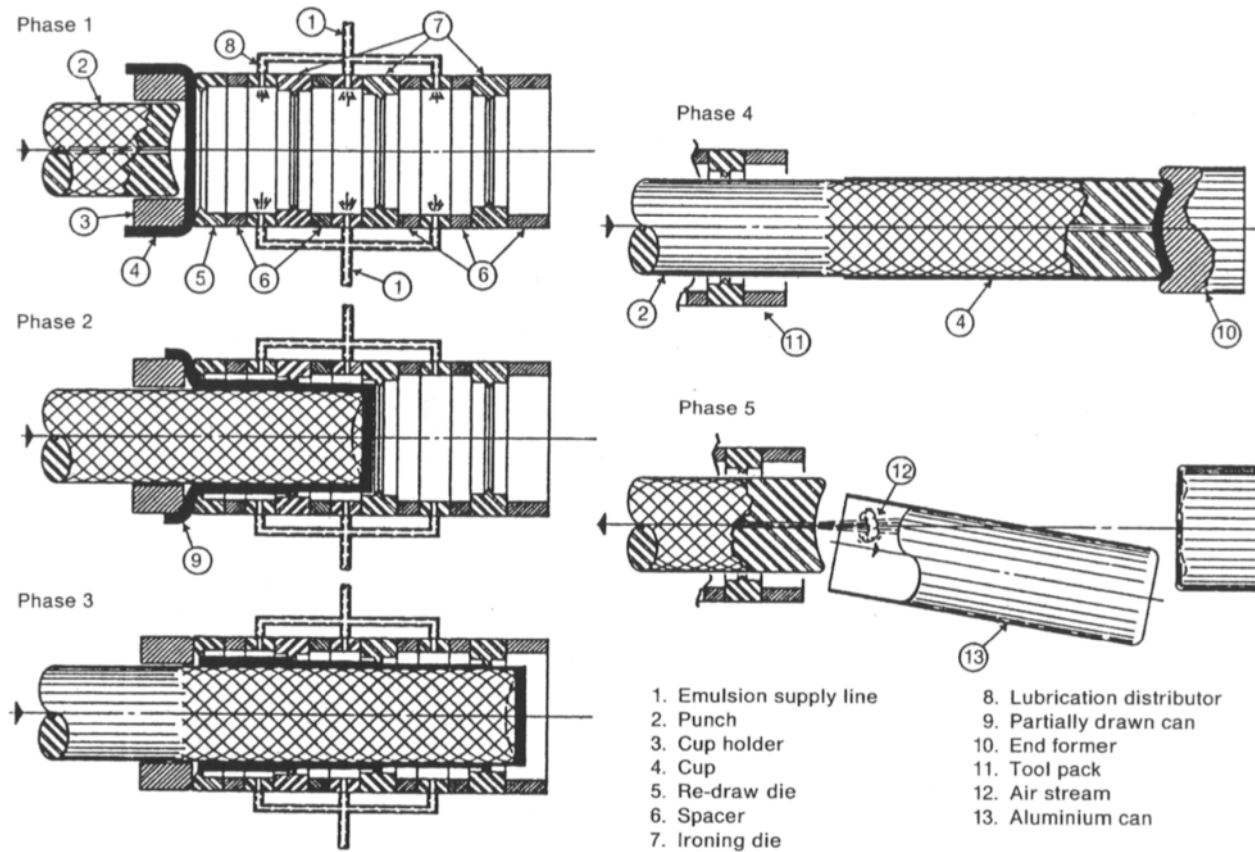


Fig. C4.4 General arrangement of tooling and forming of beverage can in the bodymaker. (Reproduced courtesy of Texaco Inc.)

match the end former, such that at the end of the bodymaker stroke a stretch-forming process occurs to form a dome on the bottom of the can.

During ironing the punch must move faster than the cup wall and the ensuing friction assists movement of metal into the ironing dies. Often the punch surface is knurled (as in Fig. C4.4), which increases the friction between the punch and the forming cup to aid metal motion into the ironing dies. Correct ironing die geometry is essential to ensure that plastic deformation of the cup wall occurs, rather than shearing. Most ironing dies have approach angles of $7\text{--}15^\circ$. Higher angles causes shearing, whereas lower angles are less effective at drawing the lubricant between the ironing die and cup wall. The total stroke of the bodymaker can be in excess of 50 cm. Such long strokes require presses of top mechanical design to ensure that the punch travel is aligned accurately during the entire length of the stroke. Any eccentricity between the punch and ironing rings is likely to cause tearing of the can during ironing, potentially jamming the bodymaker and damaging the tooling. One set of ironing dies should last 250 000 strokes at about 250 strokes per minute. Clearly at these press speeds, efficient delivery of cups to the bodymaker and removal of ironed cans is essential.

Following removal from the bodymaker, the top of the cup walls are trimmed, by a rotary shear, to remove any ears and provide a cup of the correct height for filling and fitting of the lid. A trimmed can body is illustrated in Fig. C4.2(f).

The sheet forming operations to make a can body occur at very high speeds and require tooling and sheet of the highest quality. Furthermore, the finished can must withstand internal pressures of 620 kPa, either during pasteurization of beer or as a result of carbonated beverages being left in a sunny location. Empty cans must have a column strength of at least 1100 N, which is the force applied during the filling process. These requirements, of high forming speeds and good mechanical strength, make several aspects of can stock processing the subject of extensive engineering.

Most drawn and ironed aluminium cans are made from AA-3004, an alloy of about 1.25 wt% Mn and 1 wt% Mg. This alloy develops strength both from Mn and Mg retained in solid solution and the presence of Fe- and Si-containing constituent particles (see Fig. C1.4), which are typically about $5\text{ }\mu\text{m}$ in size. In addition to contributing to strength development, the constituent particles have an important influence on bodymaker operations. During ironing, aluminium will tend to build up on the ironing tools, leading to premature die wear, and degradation of the can appearance from *scoring* of the can sidewalls. The presence of the constituent particles, which are harder than the aluminium matrix, serves to clean the dies of the metal build up. For this reason considerable work has been devoted to determining the influence of constituent particle type and morphology on the ironing behaviour of 3004. The only processing stages during which constituent particles can be modified is during casting and ingot homogenization (see Fig. C1.1). For cleaning of ironing rings it would be expected that large constituent particles may be beneficial. However, as the can wall is reduced to 0.075 mm thickness and is subjected to large stresses during ironing, large constituent particles (that are inherently not easily deformed) will cause excessive stress concentrations during ironing, leading to tearing of the can sidewall. Therefore, constituent particles must be carefully controlled, by casting at the correct speed, to ensure an appropriate solidification rate, and by careful ingot homogenization prior to hot rolling.

Any inclusions introduced during casting will act in a manner similar to overly large constituent particles. Inclusions usually originate from dirty scrap, entrapment of slag or oxides and furnace refractory particles that are not properly removed during filtering of the metal prior to casting and solidification. For sheet to survive the ironing process, the liquid metal from which it is produced must be filtered to remove all inclusions larger than about 10 μm . Given the volumes of metal required, this is not a trivial task!

The can body shown in Fig. C4.2(e) displays a low level of earing; however, the top of the can is visibly uneven. As the cost of the metal represents about half the cost of the can, it is imperative that earing be minimized, to reduce the amount of material to be trimmed. Acceptable ears are less than 1% of the wall height. Reducing the earing to these levels requires careful attention to the hot rolling, annealing and cold rolling schedule, and most aluminium suppliers will not divulge exact processing practices. Rolling tends to form a texture that gives rise to four ears at 45° to the rolling direction, whereas annealing produces four ears at 90° to the rolling direction. Therefore, appropriate rolling after annealing produces ears that tend to fill in the valleys that result from annealing. In this manner, a can with eight shallow ears can be produced that minimizes the trimming required.

As indicated in Case study 1, aluminium for beverage can bodies is produced via ingot casting. A considerable reduction in the processing cost would be possible if a continuous casting process were used, and several major aluminium companies have explored this possibility. However, solidification during continuous casting usually occurs more quickly than during ingot casting, primarily as a result of the smaller cross-sections being produced. This leads to a number of important metallurgical differences between continuously cast and ingot cast material, one of which is smaller constituent particles in continuously cast material. This reduces the ability of constituent particles to clean the ironing rings, shortening tool life and producing cans that have poor surface appearance. Also, a lower fraction of constituent particles increases the amount of the alloying elements that remain in solution. This alters the response of the sheet to the annealing and rolling processes. These two processes combine to control the level of earing that occurs during drawing. To date, continuously cast aluminium displays a higher level of earing than ingot cast material, causing the generation of more scrap during trimming. Efforts to produce acceptable can bodies from continuously cast aluminium are continuing.

A key factor contributing to the successful fabrication of can bodies is the use of AA3004 in the H19, or full hard, temper. This temper designation indicates that the sheet has been cold rolled to maximum hardness, which for 3004 corresponds to a rolling reduction of about 85%. Such high strength sheet is required so that the can body develops the mechanical strength necessary. AA3004-H19 has a yield strength of 275 MPa, a UTS of about 300 MPa and an elongation to failure of about 3%. Usually, alloys with such a low ductility would not be associated with good formability. However, during ironing the sheet is loaded in the ironing direction in tension and in the radial direction in compression. Biaxial tension–compression loading tends to create large shear stresses in the metal without the development of excessive tensile stresses that may cause necking and failure. This gives rise to the characteristic shape of the forming limit diagram of Fig. 5.12. (To illustrate this point, draw Mohr's circles for material loaded in uniaxial tension and biaxial tension–compression with the

same maximum tensile stress.) As metal deformation predominantly occurs via dislocation slip due to the action of shear stresses, the tension–compression stress state during ironing aids sheet deformation, without the onset of necking and failure. Moreover, as AA3004-H19 corresponds to the fully strain hardened temper, minimal further work hardening is possible during deformation of this temper which, therefore, exhibits a low n value (exemplified by the relatively similar values of yield and ultimate strengths). As explained in Section 5.6.2, alloys with a low n value are favoured for redrawing and ironing operations.

Powder metallurgy

6.1 Introduction

The casting processes of Chapter 2 convert liquid metal directly into desired solid shapes. Powder metallurgy processes offer a second option for producing specific solid shapes from an initial condition of no particular fixed shape. As the name implies, powder metallurgy (P/M) involves mixing metallic powders and compacting the mixture in a die. The compacted parts take the shape of the die and are then sintered or heated in a controlled atmosphere furnace to metallurgically bond the particles. The basic P/M processing steps are illustrated in Fig. 6.1. The two major steps unique to P/M processing are the manufacture of metal powders and the subsequent consolidation of the powder. This chapter describes these processes.

An important advantage of the P/M process is an ability to fabricate metals that are difficult to shape by other methods. An example of this is the forming of tungsten filaments for incandescent light bulbs. Tungsten melts at about 3400°C, above the temperature limit for most refractory materials, and therefore casting is not possible. Furthermore, the high hardness of tungsten makes it difficult to fabricate via deformation or machining processes. Therefore, the introduction of the incandescent light-bulb at the beginning of the 1900s necessitated the development of a P/M process for the manufacture of tungsten filaments that, with improvements, is still in use. Another early application of P/M was for the manufacture of *cemented carbide* machine tools of the type described in Section 7.2.6. Since these early applications, P/M processes have been applied to the manufacture of a wide variety of components and materials, some of which are listed in Table 6.1. Although P/M processes have found widespread use for small nonstructural components, applications also include highly stressed parts, such as the automotive connecting rod of Fig. 6.2.

Powder metallurgy processes derive their technological importance from several advantages including: an ability to produce parts directly to finished dimensions, or *near net shaping* with minimal material wastage; the potential for manufacturing parts with controlled levels of porosity, useful for producing filters and oil impregnated bearings; the possibility of producing alloys incompatible with other processing options; and rapid solidification during powder manufacture that produces a fine-scale dendritic structure, with minimal segregation, leading to improved mechanical properties. Despite these advantages, P/M processes are often less economical than

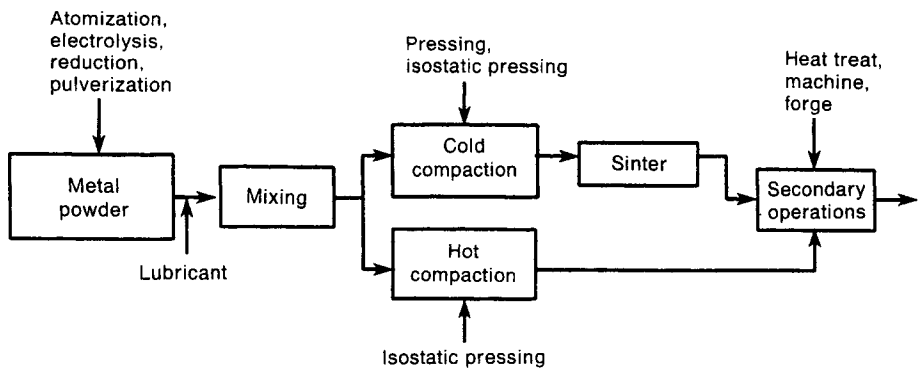


Fig. 6.1 Outline of major powder metallurgical processing steps.

Table 6.1 Selection of products manufactured by powder metallurgical processes

Application	Metals	Uses
Automotive	Cu, Fe, W	gears, bushings, valves, connecting rods, crankshaft bearing caps, belt pulleys
Gas turbines	Ni superalloys	turbine discs
Heat treating	Mo, W	furnace elements
Lubrication	Cu, Fe, Zn	abradable seals, self-lubricated bearings
Tooling	W, Mo, Mn	dies, punches, machining tools
Dental	Ag, Au	amalgams

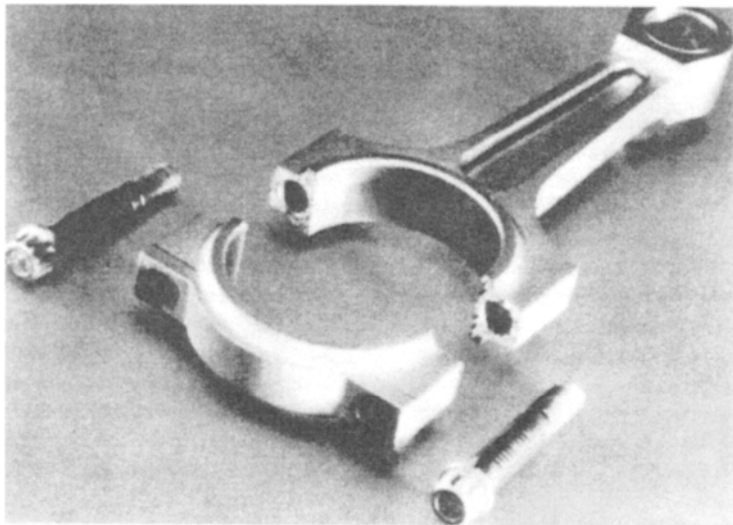


Fig. 6.2 Connecting rod for BMW V-8 automobile engine fabricated from steel powder, followed by forging. (Reproduced courtesy of GKN Sinter Metals, Germany.)

competitive manufacturing options, in part due to the expense of producing metallic powders. In addition, the high surface to volume ratio of powders makes some metals very reactive, introducing the possibility of excessive oxide/nitride levels in the finished component.

6.2 Powder production

A wide range of techniques are used for the manufacture of metallic powders utilizing a variety of processes, including reduction of metal oxides, electrolytic deposition, pulverization and atomization. Probably all metals can be made into powder using any of these processes; however, considerations of economics, purity, cleanliness and the requirement for particular physical or mechanical properties limits the applicability of each of the processes.

6.2.1 Atomization

Of the processes in use for the production of metallic powders those involving *atomization* account for the largest production volume. Powder manufacture by atomization consists of breaking up a liquid stream of molten metal into fine droplets by the impingement of water or gas jets or by centrifugal force.

Figure 6.3 illustrates the basic processes of *water atomization*. Molten metal, contained within a tundish, flows by gravity through a refractory nozzle into high pressure jets of water that break up the molten stream into fine droplets that rapidly

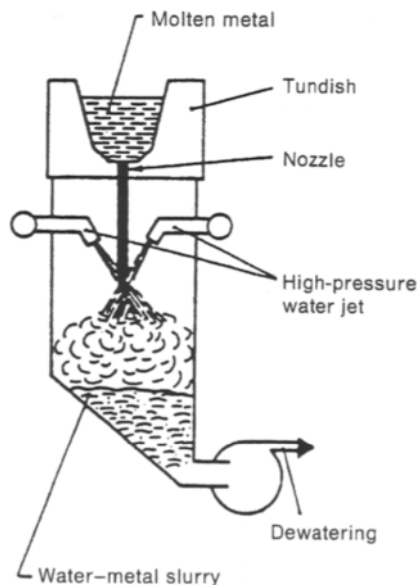


Fig. 6.3 Water atomization process for the production of metal powders. (Reproduced courtesy of European Powder Metallurgy Association.)

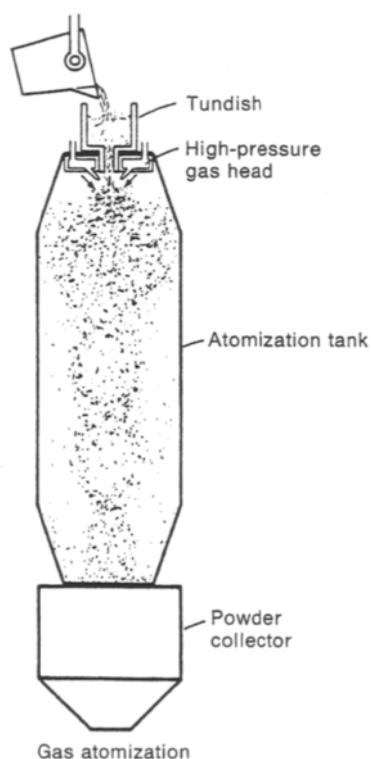


Fig. 6.4 Gas atomization process for the manufacture of metal powders. (Reprinted with permission from *ASM Metals Handbook, Ninth Edition*, Vol. 7, Powder Metallurgy (1984), ASM International, Materials Park, OH 44073-0002 (formerly American Society for Metals, Metals Park, Ohio 44073), p. 27, Fig. 3.)

solidify and cool within an atomization tank. Water pressure is typically between 5 and 20 MPa and the process produces powder with about 95% of the particles less than 150 μm in size. The powder is usually of a very irregular shape owing to the disintegration by the water jet and it may have a surface oxide film that is often removed by reduction processes.

Gas atomization is capable of producing powders that are more regularly shaped, and better cleanliness is possible compared to water atomization. The basic process is shown schematically in Fig. 6.4 and essentially consists of replacing the jet of water with a suitable gas, usually argon. As the cooling rate imparted by the gas jet is less than that of the water jet, the atomization tank must be larger to ensure droplet solidification prior to contact with the tank walls. The powder particle size is inversely proportional to the square of the gas jet velocity. Therefore, the production of fine powders requires high gas velocities, usually greater than 100 m/s. Figure 6.5 illustrates powder produced via gas atomization containing powder particles up to 500 μm in diameter. The use of an inert gas for solidification and cooling reduces undesirable surface oxide. Furthermore, the tundish of most gas atomization units is contained within a vacuum chamber, thereby avoiding undesirable reactions between the molten metal and surrounding atmosphere.

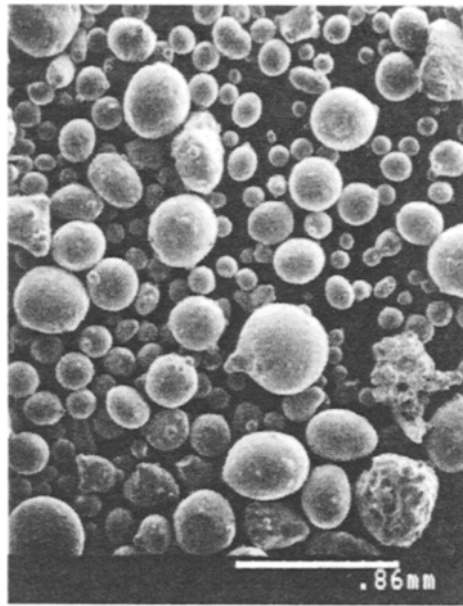


Fig. 6.5 Scanning electron micrograph of titanium powder produced by gas atomization.

A disadvantage of water and gas atomization is the necessity for a refractory nozzle through which the molten metal flows. This nozzle can introduce refractory particles into the molten metal stream. Despite efforts to separate refractory particles from the powder, some refractory particles may end up in the final consolidated component as nonmetallic inclusions. These inclusions reduce the resistance to fatigue failure, among other things. Another disadvantage of gas atomization is the possibility for the entrapment of argon within solidifying particles. Since the argon cannot diffuse from the powder particle, it can lead to gas porosity within the final consolidated part, again reducing the mechanical properties of the final product.

The problems outlined in the previous paragraph have led to the use of *centrifugal atomization* or the *rotating electrode process* to produce powder for highly stressed structural parts. In this process, illustrated in Fig. 6.6, a bar of the required composition is rotated at 10 000–20 000 revolutions per minute, while the end of the bar is melted by an arc struck between the bar and a tungsten cathode. As the bar rotates molten droplets fly off and are solidified in flight. As the molten metal never contacts any container material, the inclusion content of the powder produced is near zero. This is particularly beneficial for producing powders of titanium alloys, which are very reactive in the molten state.

6.2.2 Reduction of metal oxides

Several commercial processes exist for the production of metallic powders through the reduction of ores, with many of the processes unique to particular metals. One process used in Europe and North America for the manufacture of iron powders is

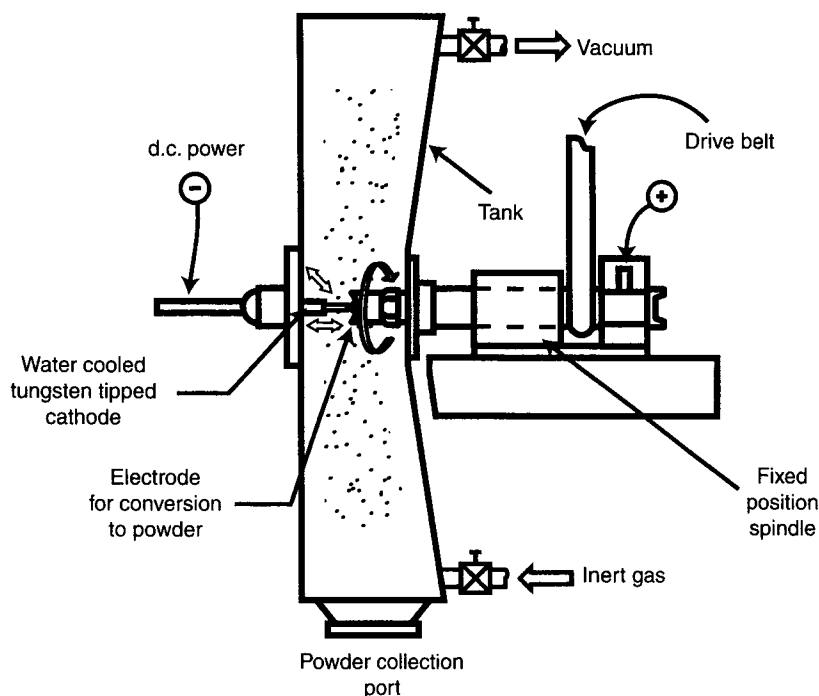
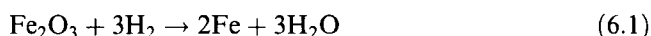


Fig. 6.6 Diagram of rotating electrode process for the manufacture of metallic powders.

the *Höganäs* process, in which pure magnetite is crushed, mixed with coke and limestone, and then heated to about 1260°C for several days to oxidize the carbon. The coke and limestone serve essentially the same purpose as they do in the steelmaking process described in Chapter 1 – the carbon in the coke reacts with the oxygen of the magnetite and the limestone reacts with sulphur and other impurities in the coke, forming a gangue and preventing contamination of the iron produced. After heating, about 96% of the magnetite is reduced to iron with about 0.3% carbon and 1% oxygen. The gangue and iron are magnetically separated and the iron particles annealed at 870°C in an atmosphere of dissociated ammonia, which serves to remove the carbon and reduce the oxygen level from 1% to about 0.3%. After light grinding the powder particle size is less than $180\text{ }\mu\text{m}$.

The *Pyron* process uses hydrogen as the reducing agent rather than the carbon of the *Höganäs* process. The starting material for the *Pyron* process is mill scale, which is crushed and then oxidized in air at 980°C to convert the various iron oxides within the mill scale into uniform ferric oxide (Fe_2O_3). The ferric oxide is then reduced at 980°C by exposure to hydrogen, the chemical reaction being



The resulting iron product is friable and easily crushed to a powder size of less than $180\text{ }\mu\text{m}$. This process is only commercially viable at locations where there is a reliable supply of mill scale, probably from a nearby steelworks, and a source of cheap hydrogen, probably from a nearby chemical manufacturer.

Hydrogen reduction is also used for the production of tungsten, nickel and molybdenum powders. It used to be common for the production of copper powders, but the introduction of continuous casting for copper production has reduced the available supply of copper scale.

6.2.3 Electrolysis

If appropriate conditions of composition, electrolyte chemistry, temperature, current density etc. are applied, a wide range of metallic powders can be produced via electrolysis. Manganese and chromium powders are produced in this way, but copper is the main metallic powder produced by electrolysis. Copper from an electrolyte of copper sulphate is plated onto lead cathodes. If the electrolyte cell conditions are controlled appropriately, then copper deposits as dendritic particles and can be easily removed or will simply fall off, collecting in the bottom of the electrolytic cell. The powder must be washed and filtered prior to furnace drying. Alteration of the furnace drying conditions can have a marked effect on the particle dimensional characteristics and apparent density. A particle size distribution with up to 95% of the particles below 45 μm in size can be produced with a copper content of greater than 99.5%.

6.2.4 Pulverization

Pulverization or *comminution* of solid metal into small pieces of powder can be achieved in a number of ways. However, these processes are most successfully applied to relatively hard and brittle metals, which fracture more readily as a result of the impact events causing pulverization. The simplest of the techniques is the use of a *tumbler ball mill*, as shown in Fig. 6.7. The mill contains hardened balls much larger than the powder particles. The metal to be pulverized is charged into the mill, usually in the form of coarse particles. During rotation of the tumbler, the pulverization occurs by the impact of the hardened balls against the charge, attrition due to the rubbing action between the charge and hardened balls, and shear or cleaving of the charge. Alternate milling processes also exist and include vibratory ball mills and attrition mills, both of which tend to be smaller in scale than the tumbler ball mill. An advantage of the pulverization processes is the ability to produce very fine powders, often with an average size of below 10 μm .

A potential disadvantage of these milling processes is the possible contamination of the powder. This can occur by two mechanisms, transfer of material from the hardened balls to the metallic powder and oxidation of the newly produced powder surfaces. The latter mechanism becomes more problematic as the powder particle size decreases, as the surface to volume ratio increases. This may lead to excessive oxygen contents in parts consolidated from such powder and a consequent deleterious influence on the mechanical properties.

The disadvantages of the previous paragraph are overcome by the *Coldstream* process. In this process granular metal is fed into a stream of gas at pressures up to 6.9 MPa, which is expanded adiabatically through a venturi. The supersonic stream of gas and granular metal impinges on a target, causing fragmentation of the metal

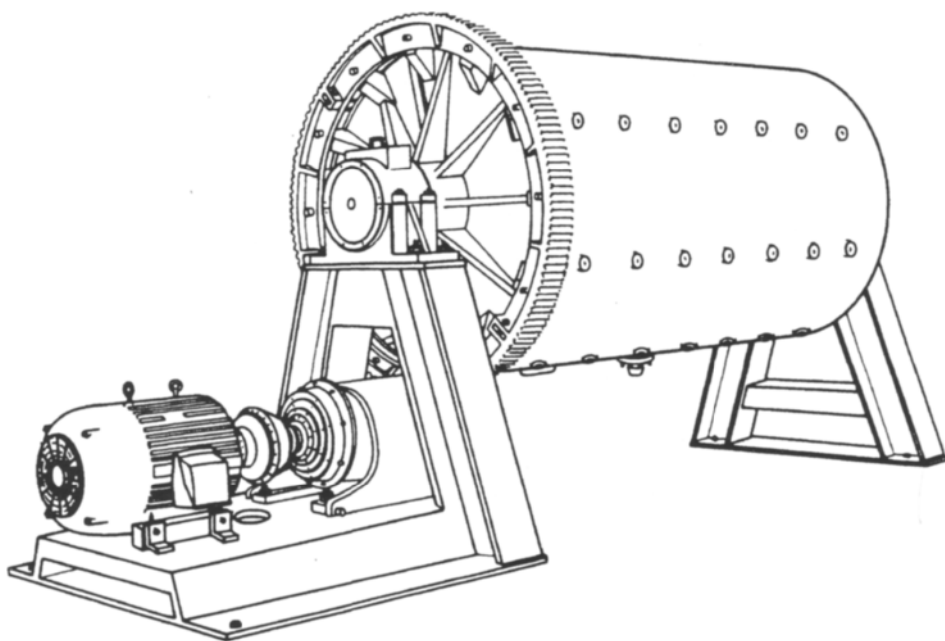


Fig. 6.7 Tumbler ball mill suitable for the production of metallic powders. (Reprinted with permis ASM Metals Handbook, Ninth Edition, Vol. 7, Powder Metallurgy (1984), ASM International, Materials Park, OH 44073-0002 (formerly American Society for Metals, Metals Park, Ohio 44073), p. 66, Fig. 18.)

into fine powder, typically less than $10\text{ }\mu\text{m}$ in size. The process operates at below room temperature, as the rapid expansion of the gas creates a strong cooling effect, which is greater than the heat generated by pulverization. This cooling is important because many metals become more brittle at low temperature, thereby aiding fragmentation. The low temperature also reduces the tendency for oxide formation on the powder surfaces. Oxidation reactions can be further reduced if an inert gas is used. To prevent contamination the target is often made from the same material being pulverized. The coldstream process is used to pulverize hard, brittle metals, such as tungsten carbide, tungsten, molybdenum and tool steels.

6.3 Powder characteristics

The characteristics of metal powders depend on the manufacturing processes used for their production, as well as their alloy chemistry. Powders can be characterized by several parameters, including: particle size and distribution; particle shape; surface area; and the ability of powder to flow, which influences the ease with which it fills a die cavity (discussed in the next section). A powder property which all of these parameters influence, and is important for the subsequent consolidation, is the powder density. The density can be expressed in terms of the *apparent density*, ρ_a , which refers to the weight of a unit volume of loose powder, or the *tap density*, ρ_t , which refers to the density when the receptacle is tapped or vibrated under specified

Table 6.2 Properties of metallic powders

Metal and powder condition	Apparent density, ρ_a (g/cm ³)	Tap density, ρ_t (g/cm ³)	Full density, ρ_s (g/cm ³)	Degree of densification, D_o
Copper			8.93	
Spherical	4.5	5.3		0.50
Irregular	2.3	3.14		0.26
Flake	0.4	0.7		0.04
Iron			7.85	
Electrolytic	3.31	3.75		0.42
Atomized	2.66	3.26		0.33
Aluminium			2.7	
Atomized	0.98	1.46		0.36

conditions during filling with powder. Typical values for these densities are listed in Table 6.2. The difference between the apparent and tap density provides an indication of the compressibility of the powder. A useful quantity for calculations dealing with the consolidation of powders is the *degree of densification*, D_o , defined as

$$D_o = \frac{\rho_a}{\rho_s} \times 100 \quad (6.2)$$

where ρ_s is the density of the fully consolidated metal. In this equation the apparent density is used, rather than the tap density, as vibrating the compaction tooling during filling is mechanically difficult. The degree of densification typical of several powders is listed in Table 6.2.

6.4 Powder compaction

As indicated in Fig. 6.1 powder compaction can occur via *cold compaction* and *sintering* or *hot compaction* processes. Cold compaction and sintering accounts for the larger volume of P/M parts produced. These processes are described in this section but, prior to compaction, the powder is mixed with a suitable lubricant to aid the flow of the powder along the tooling surfaces. Up to 1% by weight of an organic waxy lubricant is added, which must be evaporated during the sintering heating cycle to avoid contamination of the final product. Although adequate lubrication is required, too much lubricant or overmixing may completely coat the powder particles with lubricant, reducing the metal to metal contact and the subsequent strength of the compact.

6.4.1 Cold compaction

The purpose of cold compaction is to press the powder into a shape close to that of the final part and to impart to the powder compact sufficient *green strength* to maintain this shape. Most often cold compaction consists of pressing the powders in rigid steel dies at pressures between 150 and 900 MPa. A simple tooling arrangement for the cold compaction of a ring shape is illustrated in Fig. 6.8. The cold compacting

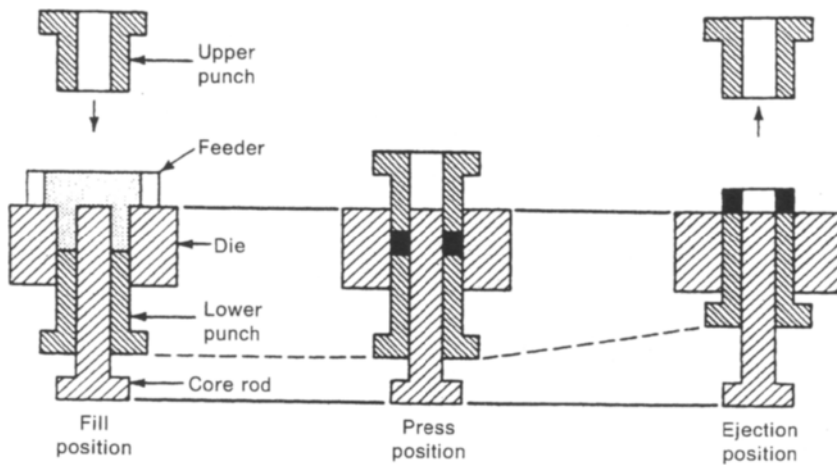


Fig. 6.8 Simple tooling arrangement for cold compacting a ring shaped part. (Reprinted with permission from *ASM Metals Handbook, Ninth Edition*, Vol. 7, Powder Metallurgy (1984), ASM International, Materials Park, OH 44073-0002 (formerly American Society for Metals, Metals Park, Ohio 44073), p. 333, Fig. 9.)

operation must ensure that the green density is as uniform as possible, as this is critical to attaining the maximum final product mechanical properties. A problem associated with achieving a uniform green density is that the powder does not behave as a liquid, and therefore the compacting pressure is not transmitted through the powder uniformly. As the compacting pressure is applied from one end only, the compact density varies along the compression axis. The uniformity of the green density can be improved if the pressure is applied from both ends, but the density is still lower in the middle of the compact. This limits the diameter to length ratio of compacts to a maximum of about three.

The nonuniformity of the compacting pressure through the compact also influences the green density that can be achieved. Compaction occurs in several stages, each with a different mechanism. The initial application of the compacting pressure causes two simultaneous processes: rearrangement of the powder particles, and cold welding of particles to their nearest neighbours. The rearrangement of particles causes cold welds to be fractured and reformed with new neighbours. Particle rearrangement combined with the applied pressure causes local plastic deformation of the powder at the contacting surfaces. The strain hardening associated with this plastic deformation is one of the factors limiting the final green density that can be obtained. The plastic deformation causes aggregates of powder to mechanically lock together, also limiting the green density achievable. The cold welding and mechanical locking that occurs in each location of the compact differs, because of the nonuniformity of the pressure distribution through the compact. This nonuniformity makes it easier to cold compact powders of irregular shape.

More uniform cold compacts are possible by utilizing hydrostatic pressure or *cold isostatic pressing*. In this process the powder is contained within a deformable mould, which is immersed in an oil filled cylinder (Fig. 6.9). When the cylinder is pressurized a green compact is formed that takes the shape of the flexible mould. As the hydrostatic pressure is more uniform and there are no frictional losses, the green density throughout the compact is more uniform.

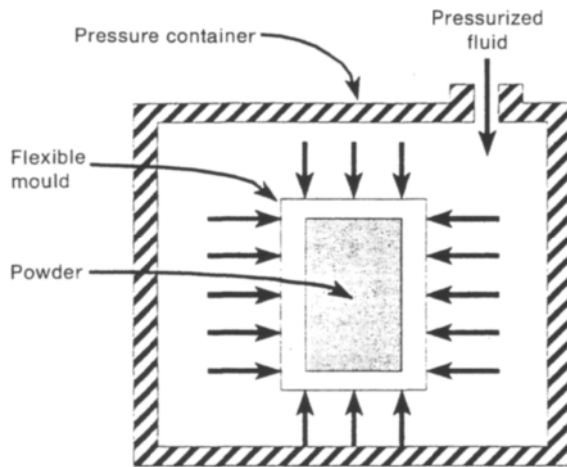


Fig. 6.9 Schematic cold isostatic pressing for cold compaction of powders.

6.4.2 Sintering

Sintering refers to the application of heat to the powder compact to increase its strength by bonding together the powder particles. The principal driving force for increasing the density and particle contact area during sintering is the lowering of the surface energy of the powder particles. The reduction of surface energy requires a decrease in the total surface area of the compact, primarily due to the closure of pores between powder particles. Although the lowering of the surface energy is the driving force, diffusion is the mechanism that leads to the increase in density. Surface tension drives atoms to regions where cold welding of adjacent particles has occurred. The atoms are transported by surface diffusion, volume diffusion and/or grain boundary diffusion. As atomic diffusion is a mass transport phenomenon, it is governed by equations of the form presented in Section 2.5.1 for the conductive heat flow during solidification. The primary difference between the mass transport phenomenon of atomic diffusion and that of heat conduction is that the thermal diffusivity, α_{th} , of equation 2.2 is replaced by the *diffusion constant*, which is determined by an equation of the form

$$D = D_0 \exp \left(\frac{-Q}{RT} \right) \quad (6.3)$$

where: D_0 is the frequency factor
 Q is an activation energy
 T is the absolute temperature
 R is the universal gas constant.

The frequency factor and activation energy are characteristic thermal constants for each material. The significance of this equation is discussed in greater detail in Chapter 9. The key point in terms of sintering is that equation 9.1 indicates that diffusion is a *thermally activated* process. Consequently, increasing the sintering temperature significantly increases the rate at which a powder compact densifies.

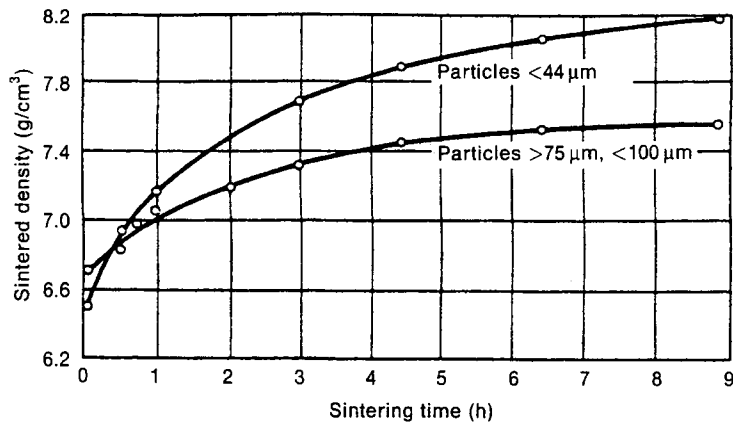


Fig. 6.10 Density as a function of sintering time for copper powder sintered at 865°C. (Reprinted with permission from *ASM Metals Handbook, Ninth Edition*, Vol. 7, Powder Metallurgy (1984), ASM International, Materials Park, OH 44073-0002 (formerly American Society for Metals, Metals Park, Ohio 44073), p. 310, Fig. 2.)

As sintering proceeds, the powder surface area decreases as the contact area increases. Since the powder surface energy is the driving force for the sintering process, as the surface area decreases, so does the driving force. Therefore, the rate of sintering decreases as the process continues. This is illustrated in Fig. 6.10 in terms of the sintered density as a function of the sintering time. The full density of copper is 8.9 g/cm³, which is not achieved even after long sintering times, as shown in Fig. 6.10. This highlights that sintered compacts will usually have some residual porosity.

The heating cycle during sintering comprises the three stages shown in Fig. 6.11. The initial heating rate must be chosen carefully to accomplish the removal of the wax lubricant added to the powder to aid the compaction process. All the lubricant must be evaporated from the entire thickness of the compact without decomposing into carbonaceous residues. If the heating rate is too rapid, the surface layers of the compact may begin to sinter before the heat penetrates sufficiently into the central regions of the compact to evaporate the lubricant. At the worst, this may cause blisters within the central regions and, at the least, will degrade the mechanical properties of the central regions. Additionally, a rapid heating rate may cause thermal

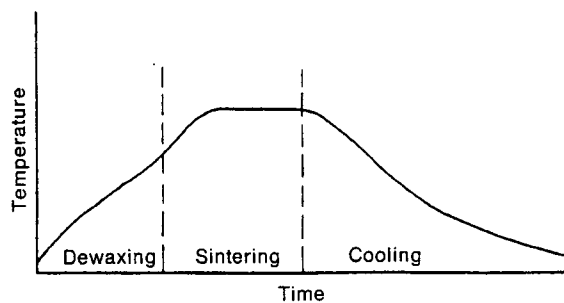


Fig. 6.11 Typical thermal cycle during sintering.

distortion between various sections of the compact, leading to poor dimensional control.

The sintering temperature is usually between 60% and 80% of the absolute melting temperature of the powder. To prevent excessive oxidation of the powder surfaces, sintering must be done in a protective atmosphere, usually a reducing atmosphere. Typically, the heat for sintering is produced by the combustion of fossil fuel, which if the fuel:air mixture is rich will produce combustion products containing up to 45% hydrogen, with some CO and CO₂, which is suitable to ensure protection of the powder surfaces during sintering. Alternatively, nitrogen-based atmospheres mixed with hydrocarbons can be used. These may be particularly economical at locations in proximity to oxygen steelmaking facilities, at which there are large amounts of nitrogen available.

Cooling from the sintering temperature must be sufficiently slow that thermal distortion is minimal. Components must be cooled sufficiently, such that excessive oxidation does not occur on removal from the furnace.

6.4.3 Hot compaction

The majority of P/M components are processed via cold compaction and sintering. However, hot compaction is used to a limited extent. The hot compaction process is similar to that shown in Fig. 6.8, except that the powder is heated and heat-resistant tooling is required. The advantage of hot pressing is that metals are softer at elevated temperatures, allowing a higher green density to be achieved without increasing the press capacity. In some cases it may be possible to avoid a subsequent sintering operation, but sintering will almost always further improve the density and, therefore, mechanical properties.

6.4.4 Hot isostatic pressing

An increasingly important hot compaction technique is *hot isostatic pressing* (HIP). This technique relies on the simultaneous application of hydrostatic pressure and temperature to the powder preform. As illustrated in Fig. 6.12, an HIP press consists of a thick walled pressure vessel that contains an electric heating furnace within a chamber into which is placed the powder preform. During pressing the chamber is pressurized with an inert gas, most commonly argon. Commercial HIP presses are capable of temperatures up to 2000°C and pressures up to 280 MPa. Typically, high pressure argon pumps are used to increase the HIP chamber pressure to about 70 MPa at ambient temperature, with the remaining pressure developed as the temperature is increased. Following the required time at maximum temperature and pressure, the temperature is lowered to ambient and the remaining pressure discharged.

A sample temperature–pressure cycle for HIP is illustrated in Fig. 6.13. In preparation, the powder is vacuum encapsulated within a can that will be flexible at the HIP pressures and temperatures. Most commonly, encapsulation cans are fabricated from

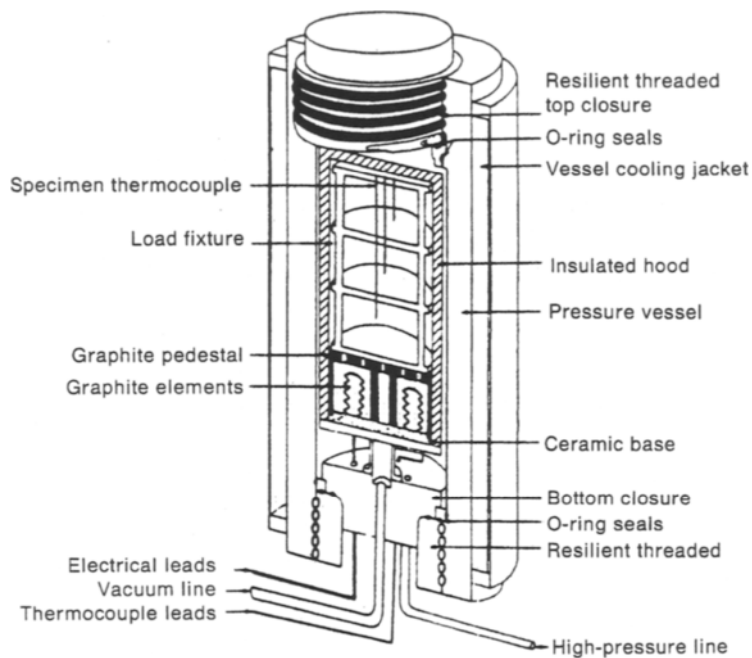


Fig. 6.12 Diagram of a hot isostatic pressing facility for hot compaction of powders.

stainless steel. The HIP process is capable of compacting and sintering powders in one step, whereas the vacuum encapsulation of powders ensures that powder contamination is avoided. However, the high capital and operating costs associated with HIP equipment limits the use of this process. It is used predominantly for producing near-net-shape parts of titanium or nickel alloys for gas turbine applications. Although not directly related to P/M processing, solidification shrinkage in castings

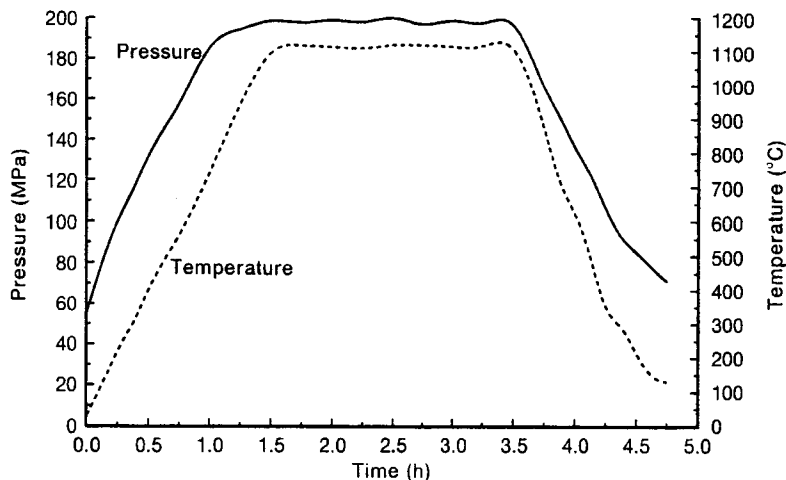


Fig. 6.13 Temperature and pressure profile for a nominal HIP cycle of 1100°C, 200 MPa for 2 h.

can be closed by the simultaneous application of temperature and pressure during HIP. Consequently, many investment castings for critical gas turbine engine components routinely undergo HIP following casting.

As pressure and temperature are applied simultaneously during HIP, the mechanisms controlling HIP consolidation differ from those for cold compaction or sintering. Initially, as the pressure increases, yielding occurs at the particle contact points. With increasing temperature and pressure this yielding increases as the metal softens. As yielding is virtually time independent, by the time the maximum temperature and pressure of Fig. 6.13 are reached considerable yielding and powder consolidation will have already occurred. By considering the hot deformation characteristics of metals an estimate for the density induced by powder yielding can be obtained from

$$D_y = \left[\frac{(1 - D_o)P}{1.3\sigma_f} + D_o^3 \right]^{1/3} \quad (6.4)$$

where: D_y is the density induced by yielding

P is the HIP pressure

σ_f is powder flow stress at the HIP temperature

D_o is the full density (Table 6.2).

Following yielding, diffusional mechanisms dominate the consolidation processes. Recall from equation 6.3 that diffusion is a thermally activated process requiring atomic motion which is time dependent. Therefore, to attain full density may require considerable time and is dependent on the powder apparent density, D_o , of Table 6.2.

6.5 Metal injection moulding

Many of the manufacturing processes applied to plastics can be traced to metal processing techniques. However, *metal injection moulding* (MIM) is an example where the reverse holds. Figure 6.14 illustrates a typical MIM process flowchart. The essential difference from more traditional P/M processing is that the metal powder is intimately mixed with organic thermoplastic binders to form a plastic jelly that is injected into moulds, as opposed to the gravity filling of powder into dies. Early applications of MIM utilized moulding equipment developed for plastic injection moulding. After removing the moulded 'green' part from the moulding machine, the binder is removed by evaporation or a solvent extraction technique, possibly followed by curing to burn off any remaining binder. Depending on the part geometry, binder removal may take a few hours to a few days to complete. Finally, the parts are sintered and, if necessary, secondary forming operations applied.

For the powder to be readily injectable requires fine powder, typically from 0.5–20 μm in diameter. Such fine powders, sometimes referred to as *metallic dust*, are relatively easily dispersed into the air, potentially causing a health hazard if inhaled or, as virgin metal dusts are pyrophoric, causing an explosion hazard. The explosive nature of metallic powders and dusts is associated with a high surface energy per unit mass and exothermic oxidation reactions. In some cases, metallic powders and dusts

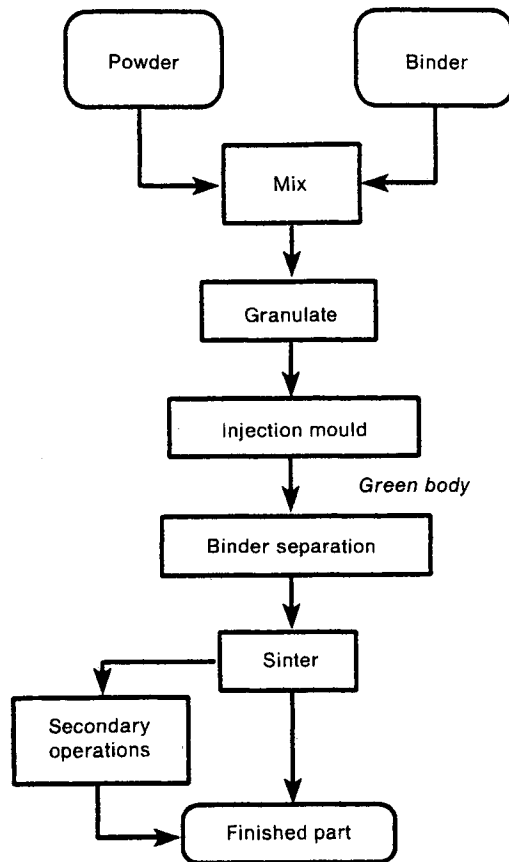


Fig. 6.14 Flowchart illustrating major processing steps for the metal injection moulding powder metallurgy process.

are slowly exposed to an oxidizing atmosphere to passivate the particle surfaces in a controlled manner. Metal powders and dusts are most suitably stored and shipped in containers pressurized with an inert gas.

The primary advantage of the MIM process is that complex shapes with excellent dimensional accuracy and greater than 99% density can be produced. The process tends to be more expensive than traditional P/M processes. However, for the complex shapes produced, other manufacturing options such as machining may be equally or more expensive than MIM. Since the late 1980s MIM has found increasing use for the manufacture of jewellery, computer hardware, and other relatively small but intricately shaped parts.

6.6 Problems

- 6.1 Explain why gas-atomized powders may be more difficult to cold compact than water-atomized powder.

- 6.2 Nitrogen-based atmospheres can be used for sintering. Explain why nitrogen is readily available as a byproduct of oxygen steelmaking.
- 6.3 Gas-atomized powder of type 410 stainless steel is to be hot isostatically pressed at 1000°C and 200 MPa. Estimate the density that might be achieved through plastic yielding of the powder.

Machining processes

7.1 Introduction

The casting and forming processes, presented in Chapters 2, 4 and 5, achieve metal shaping by either solidification or plastic deformation processes. These processes conserve the mass of the workpiece during processing, thereby making efficient use of material. However, there are also disadvantages. Dimensional tolerances may not be achievable with casting, or in many cases only with excessive cost. Many complex shapes are difficult to fabricate using various forming processes and large parts may require unreasonable forming forces. These disadvantages can be overcome if the desired shape is obtained by incrementally removing excess material by *machining*. The final machined geometry is circumscribed by the original workpiece and during machining the mass of the workpiece is reduced. Therefore, machining is often more costly in terms of raw materials, but can produce complex shapes that would be difficult or impossible to produce by casting or forming operations. Additionally, machining is often the most desirable process for low volume production quantities, because of its versatility combined with a relatively low incremental capital investment.

The number of machining operations available is unmatched except by the number of engineering materials! Given the variety and scope of machining methods, it is not the purpose of this chapter to give a comprehensive overview of all possible processes. Rather, consistent with previous chapters, a few of the important machining processes are briefly described and the principles controlling machining performance presented. This should provide a basic understanding which, combined with engineering judgement, can be applied more generally.

The most common machining operations rely on relative motion between the workpiece and a *cutting tool* that mechanically removes material in the form of *chips*. These include, among others, the processes of *turning*, *planing*, *shaping*, *drilling*, *milling* and *grinding*, which are discussed in this chapter. The performance of these processes is influenced by the cutting tool geometry, workpiece properties and cutting fluid. The interrelationships between these factors makes precise analysis of machining processes difficult. Nevertheless, the basic principles presented in this chapter are useful in predicting approximate machining performance. The repetitive nature of many of these operations makes automation desirable, and *numerically controlled*

machines are widely used. Other less traditional means of removing metal include *waterjet machining*, *electrochemical methods*, *electrical discharge machining*, *electron beam machining* and *laser processes*. These processes are described towards the end of this chapter.

7.2 Mechanical machining methods

Most mechanical machining operations are based on the generation of flat or cylindrical surfaces as these are the simplest to produce. The generation of new surfaces typically requires workpiece-tool relative motion in two directions, as illustrated in Fig. 7.1, for reducing the diameter of a bar by turning. The primary motion is the *cutting speed*, v , with secondary motion, the *cutting feed*, f . These two motions, together with the *cutting depth*, d_c , produce a *transient surface*. These three parameters influence many aspects of machining, including metal removal rate, machining time, tool wear, surface quality and power requirements. Notice, in Fig. 7.1, that the cutting speed is a result of workpiece motion and the cutting feed is the result of tool motion. Other machining operations utilize different combinations of relative motion, i.e. tool motion only, workpiece motion only or a combination. Also note in Fig. 7.1 that the cutting tool has only one cutting edge. This is referred to as a *single-point tool*. However, as will become clear in the following, many machining operations utilize *multiple point tools*, with more than one cutting surface.

7.2.1 Single-point machining methods

Single-point tools have a relatively simple geometry that contains one major cutting edge, as illustrated in Fig. 7.2. The major cutting edge is responsible for forming the chip, which flows past the tool *face*, and generating the transient surface, which passes

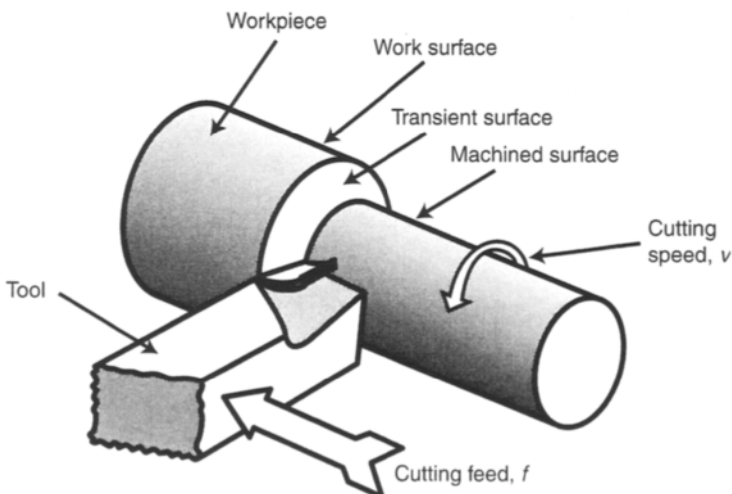


Fig. 7.1 Relative motions during turning.

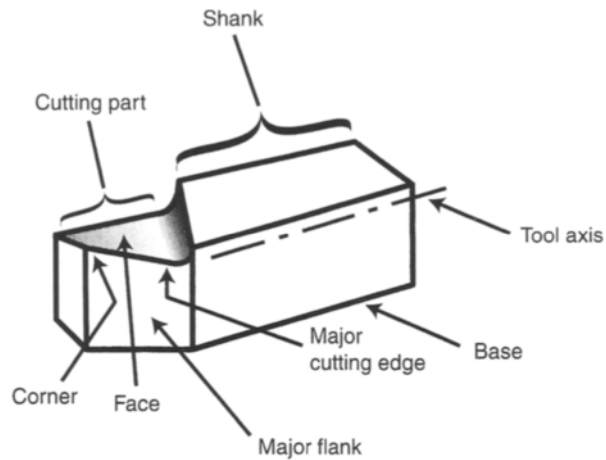


Fig. 7.2 Geometry of a single-point tool.

over the *flank*. Single-point tools are usually clamped into a *tool post* similar to that shown in Fig. 7.3, which contains provision for adjustment of the cutting edge position and angle with respect to the workpiece.

Turning operations

Most turning operations are carried out using a lathe, similar to that illustrated in Fig. 7.4. The primary cutting action, the cutting speed, derives from rotation of the workpiece which is clamped by the *chuck* and rotated by an electric motor via a gear-box located within the *headstock*. The secondary cutting motion, the cutting feed, is

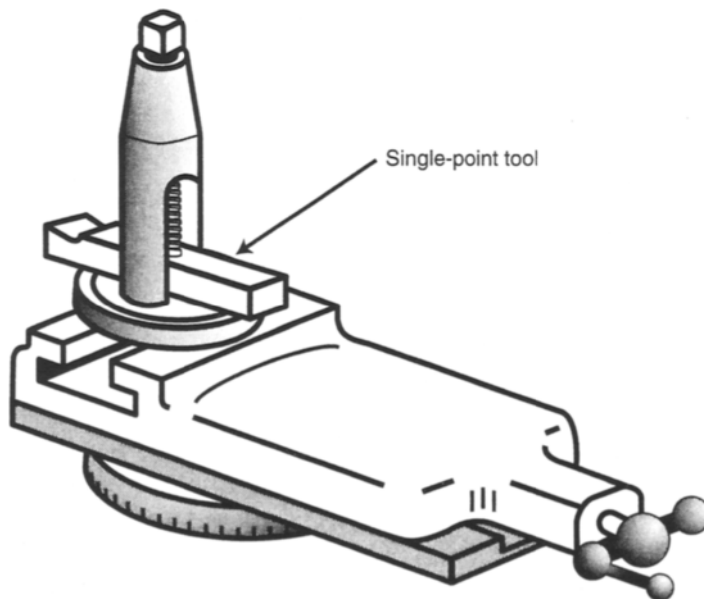


Fig. 7.3 Typical tool post for securing a single-point tool.

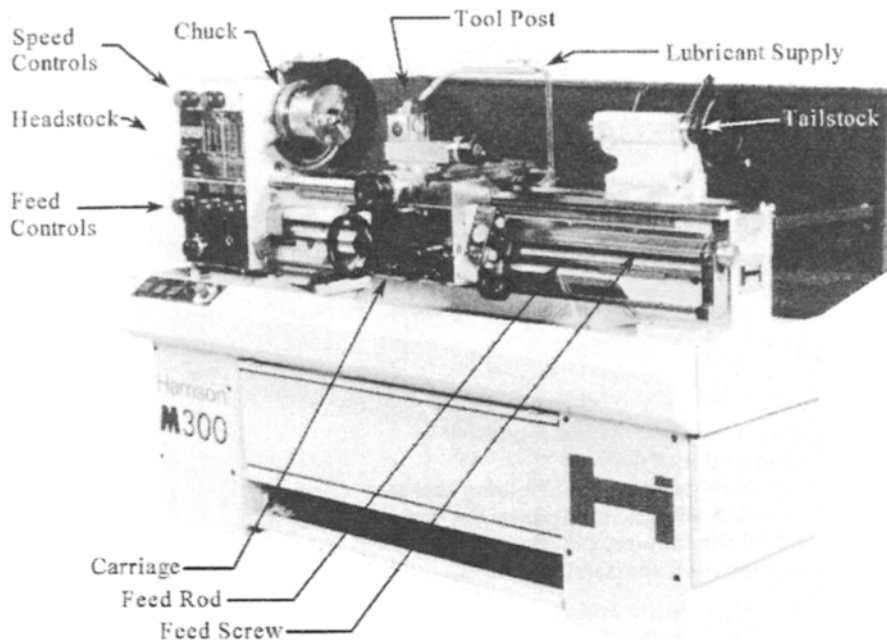


Fig. 7.4 A typical machine shop lathe with major components identified.

supplied by translation of the carriage and tool post assembly along *feed rods* and driven *feed screws*. Short workpieces are usually only supported by the chuck, whereas longer workpieces can also be supported by a *tailstock*.

Many machining operations are carried out on a lathe, including *cylindrical turning*, *facing*, *threading*, *boring* etc. Cylindrical turning and facing are shown in Fig. 7.5. The tool feed motion is in the axial direction for cylindrical turning and in the

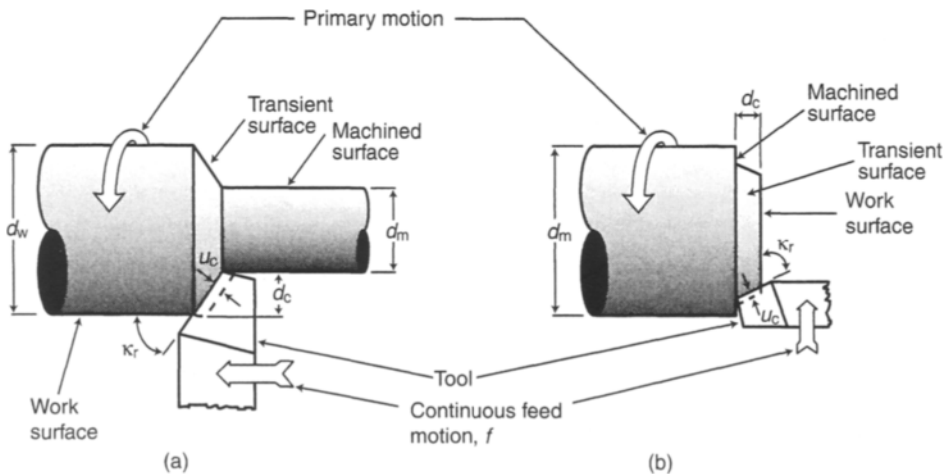


Fig. 7.5 Geometry of (a) cylindrical turning and (b) facing on a lathe.

radial direction during facing. Important parameters that influence these turning processes are the cutting speed, undeformed chip thickness, u_c , and metal removal rate (MRR). The geometry of cylindrical turning indicates that the average cutting speed is calculated according to

$$v_{av} = \frac{\pi N(d_w + d_m)}{2} \quad (7.1)$$

where: v_{av} is the average cutting speed
 N is the workpiece rotational frequency
 d_w, d_m are the dimensions shown in Fig. 7.5(a).

For the usual case when the depth of cut d_c is small compared to the diameter d_m , the metal removal rate is approximately

$$\text{MRR}_{\text{turning}} = \pi f d_c N d_m \quad (7.2)$$

where: MRR is the metal removal rate
 f is the feed distance per revolution
 d_c, d_m are the dimensions shown in Fig. 7.5(a).

For the facing operation of Fig. 7.5(b), the maximum cutting speed is

$$v_{\max} = \pi N d_m \quad (7.3)$$

where: v_{\max} is the maximum cutting speed
 d_m is the dimension shown in Fig. 7.5(b).

For the facing operation the maximum metal removal rate can be calculated according to equation 7.2. For both the turning and facing operations of Fig. 7.5, the undeformed chip thickness is

$$u_c = f \sin \kappa_r \quad (7.4)$$

where: f is the feed per revolution
 κ_r is the tool cutting edge angle; see Fig. 7.5.

Figure 7.6 illustrates two additional important operations performed using lathes. The thread cutting of Fig. 7.6(a) requires the tool path to follow a well coordinated motion, consisting of both axial and radial movement to generate a helix on the workpiece surface. This motion is controlled by the selection of appropriate gears in the headstock of the lathe so that the helix generated corresponds to a standard thread size. Typically, several passes of the tool along the workpiece are necessary to cut

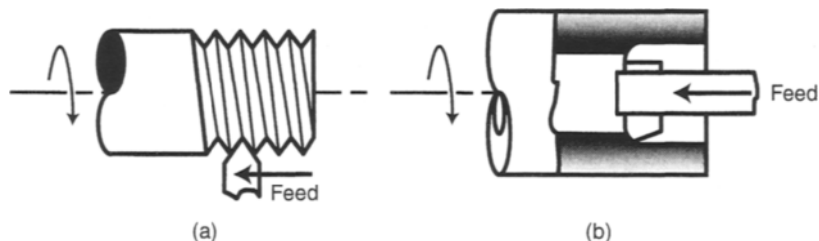


Fig. 7.6 Illustration of (a) thread cutting and (b) boring.

the full depth of the thread. Figure 7.6(b) shows the boring process, which can be used to increase the diameter of existing holes. When boring is done on a lathe the existing hole must be concentric with the workpiece rotation. A boring tool can also be used on machines other than a lathe, for example a drill press, allowing the enlargement of existing holes in a wider range of orientations.

Planing and shaping

Planing and *shaping* are single-point metal cutting operations with linear primary cutting motions. During shaping the primary motion is applied to the tool and the feed motion applied to the workpiece, as shown in Fig. 7.7. The tool geometry and the tool post are similar to that of Figs 7.2 and 7.3. As seen in Fig. 7.8, for shaping, the workpiece is typically clamped to a worktable and the tool clamped to a ram which moves in the primary cutting direction. An incremental feed motion is applied to the worktable between each stroke of the ram.

Shaping is useful for relatively small workpieces. However, larger components require an excessive ram stroke, reducing the accuracy with which the tool can be positioned. Therefore, for large workpieces, planing is preferred to shaping. During planing, the workpiece is clamped to a large worktable, arranged to provide the primary cutting motion, as shown in Fig. 7.9. The tool is mounted in a similar fashion to that shown in Fig. 7.8, with the intermittent feed motion applied to the tool. Accordingly, for planing, the primary cutting action is generated by workpiece motion, whereas for shaping the primary cutting action is generated by tool motion.

For the planing and shaping geometry of Fig. 7.10 the metal removal rate during cutting is

$$MRR_{\text{planing/shaping}} = vfd_c \quad (7.5)$$

where: f is the feed distance per stroke

d_c is the cutting depth

v is the tool velocity (shaping) or workpiece velocity (planing).

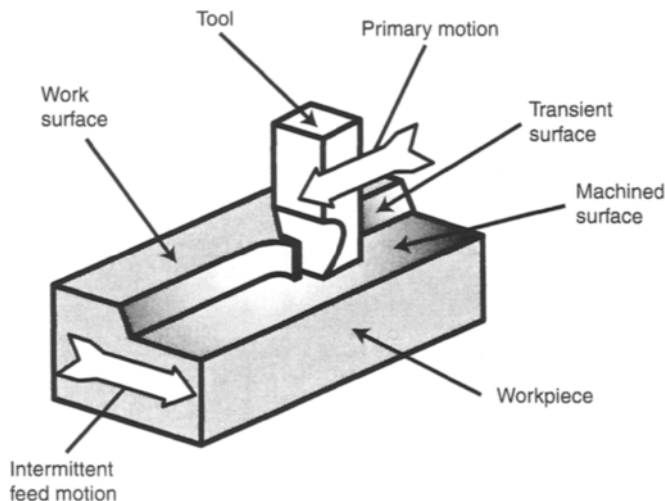


Fig. 7.7 Shaping process.

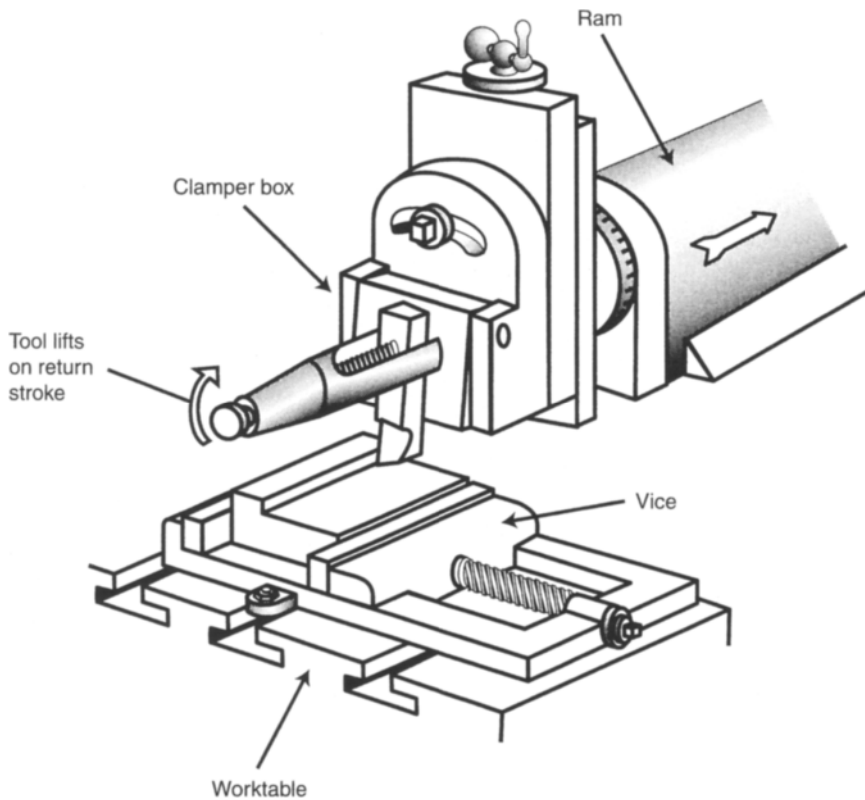


Fig. 7.8 Machine arrangement for shaping.

As the tool geometry is the same as for turning, the undeformed chip thickness can be calculated according to equation 7.4.

It is clear that planing and shaping can be used to prepare flat surfaces, but also, by rotating the clamber box and tool post in Fig. 7.8, a wide variety of notches, keys and inclined surfaces can be produced.

7.2.2 Multiple-point machining methods

A multiple-point tool has more than one cutting edge. To incorporate the multiple cutting edges, these tools typically have a more complex geometry than single-point tools and, therefore, are more expensive. However, the advantage is a higher metal removal rate, leading to improved productivity. A large variety of multiple point tools are available, many for specialized tasks. In this section, three of the most common multiple point machining methods, *drilling*, *milling* and *grinding*, are described.

Drilling

Drilling is used to create round holes in a workpiece. Further operations may be applied to drilled holes, for example the boring process described in Section 7.2.1. Most

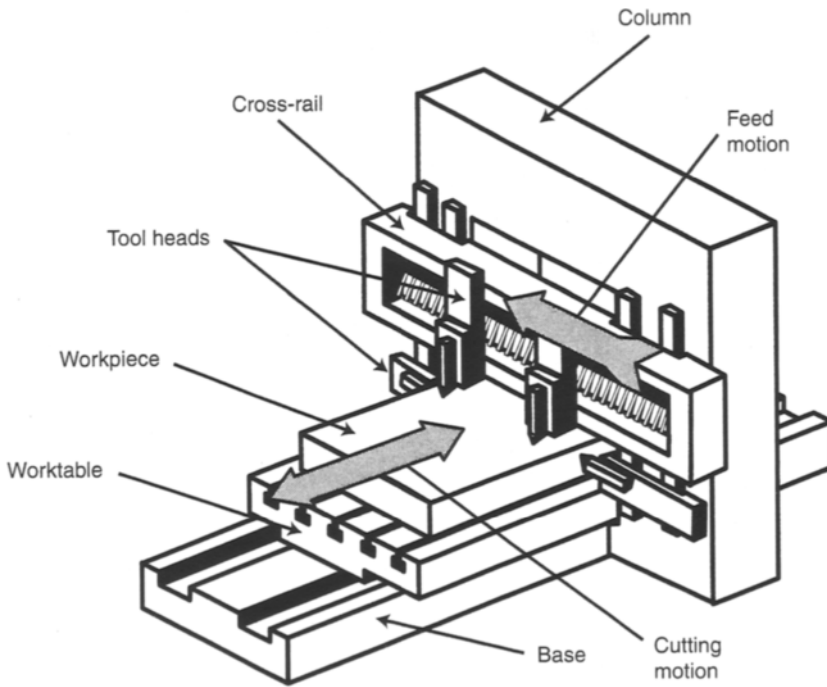


Fig. 7.9 Machine arrangement for planing.

commonly a tool referred to as a *drill bit* is mounted either in a hand-held drill or a *drill press*, such as that shown in Fig. 7.11. A typical twist drill bit geometry is shown in Fig. 7.12. The primary cutting motion is the drill bit rotation, while the feed motion is the movement of the drill bit along its axis of rotation into the workpiece. Note from Fig. 7.12 that the twist drill has two major cutting edges, one on each flank.

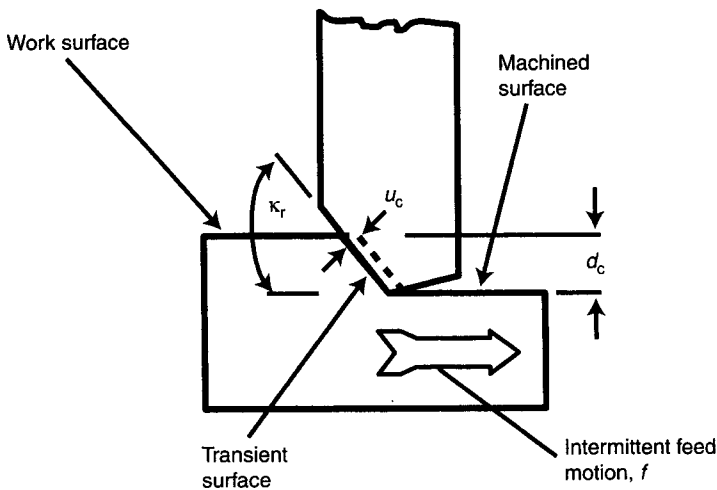


Fig. 7.10 Workpiece-tool geometry during planing and shaping.

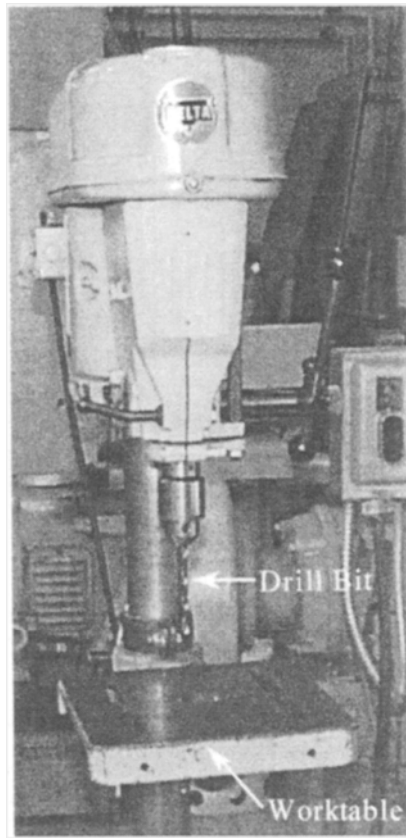


Fig. 7.11 Typical drill press, with drill bit clamped in chuck and workpiece clamped to worktable.

For the drilling process of Fig. 7.12 the metal removal rate is simply the product of the cross-sectional area of the drilled hole and the drill bit feed rate, or

$$\text{MRR}_{\text{drill}} = \frac{\pi D^2 N f}{4} \quad (7.6)$$

where: f is the drill bit feed per revolution (Fig. 7.12)

D is the hole diameter (Fig. 7.12)

N is the drill bit rotational speed.

As the twist drill has two cutting edges, it is apparent from Fig. 7.12 that the undeformed chip thickness is

$$u_{\text{cdrill}} = \frac{f}{2} \sin \kappa_r \quad (7.7)$$

Twist drills are usually suitable for holes with a length less than five times their diameter. Beyond this length the simultaneous removal of the chips up the *flutes* (see Fig. 7.12), and delivery of cutting lubricant/coolant down the flutes, becomes difficult. Drill bits specifically for drilling deep holes often have an internal hole centred along the bit axis so that lubricant/coolant can be pumped to the cutting edges.

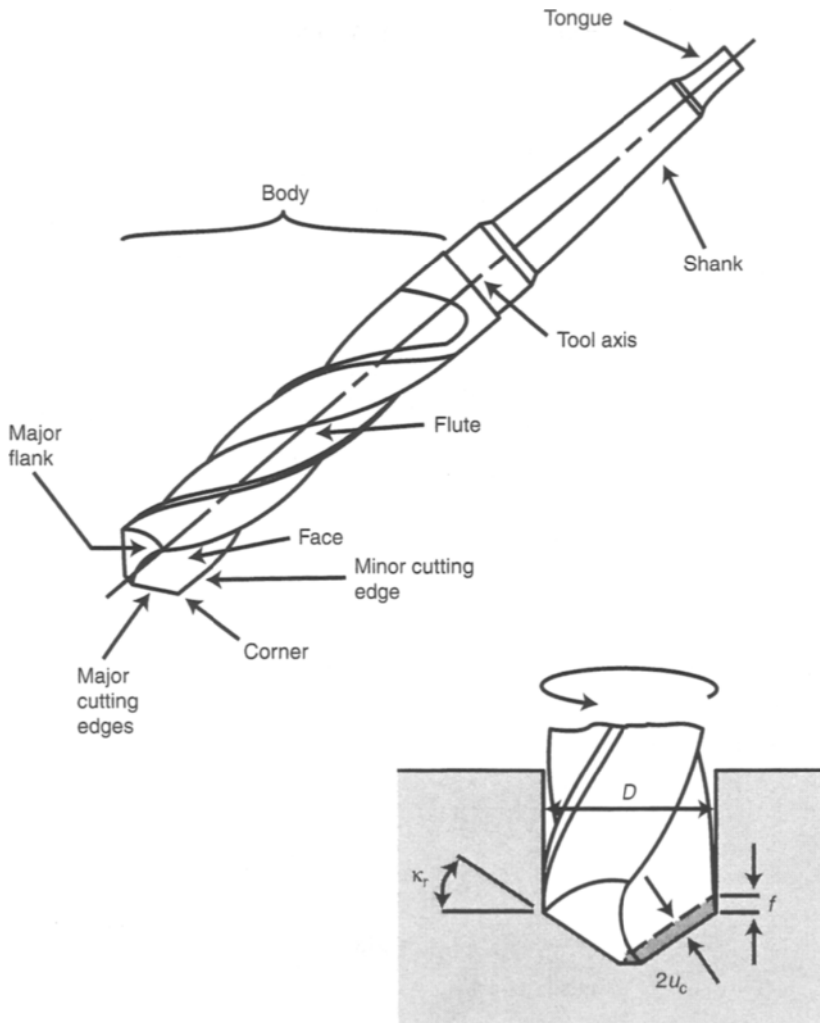


Fig. 7.12 Geometry of twist drill and detail of the drill-workpiece interface.

In addition to the twist drill bit, several other tools are often employed in drill presses for specialized operations, some of which are illustrated in Fig. 7.13. The purpose of the tools shown in Fig. 7.13 is self-explanatory. The major difference between *core drilling* and *reaming* is the improved surface finish and dimensional accuracy typically available from the latter.

Milling

Milling machines are capable of producing a wide range of cut geometries, including flat surfaces, angles, gear teeth and slotting. Each of the tools used for these operations is different and specialized. A typical tool-workpiece arrangement for milling a flat surface is shown in Fig. 7.14. The tool consists of multiple cutting edges arranged around an axis. The primary cutting action is produced by rotation of the

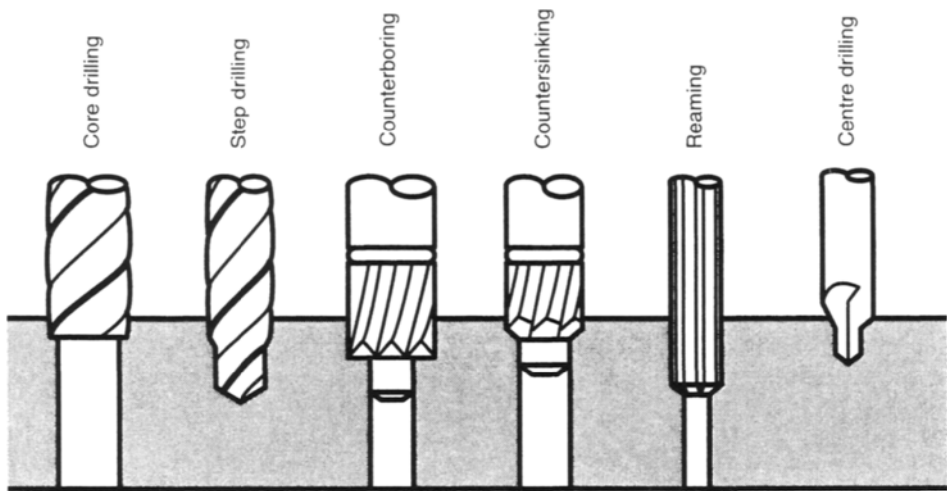


Fig. 7.13 Specialized tools for drill presses.

tool and the feed by motion of the workpiece. A wide variety of milling machines are available. A *column and knee type* milling machine, that may be found in many machine shops, is illustrated in Fig. 7.15. Milling machines with a vertical spindle are also available. Similar to previous operations, the workpiece is usually clamped to a worktable and the tool is held on an axis through the spindles.

Using the simplest of milling geometries involving a straight edged cutter and the tool axis orthogonal to the workpiece feed direction, as in Fig. 7.14, the effective

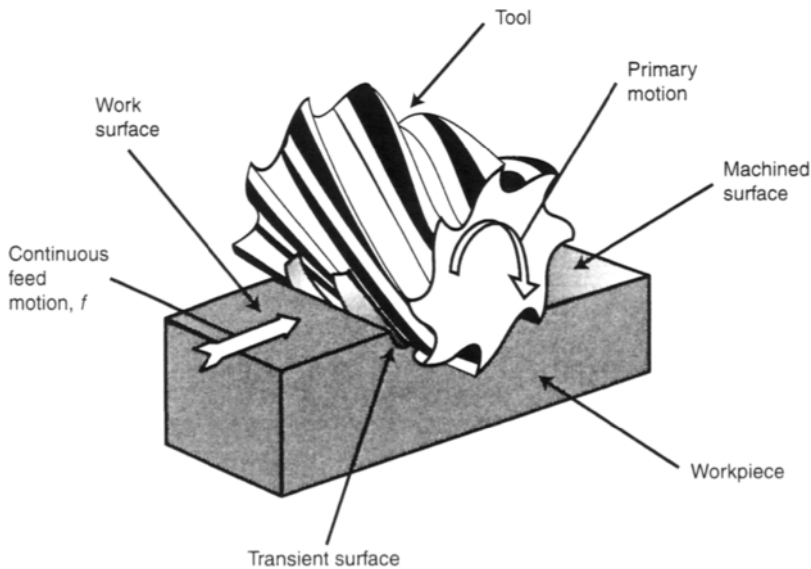


Fig. 7.14 Tool workpiece arrangement typical for milling.

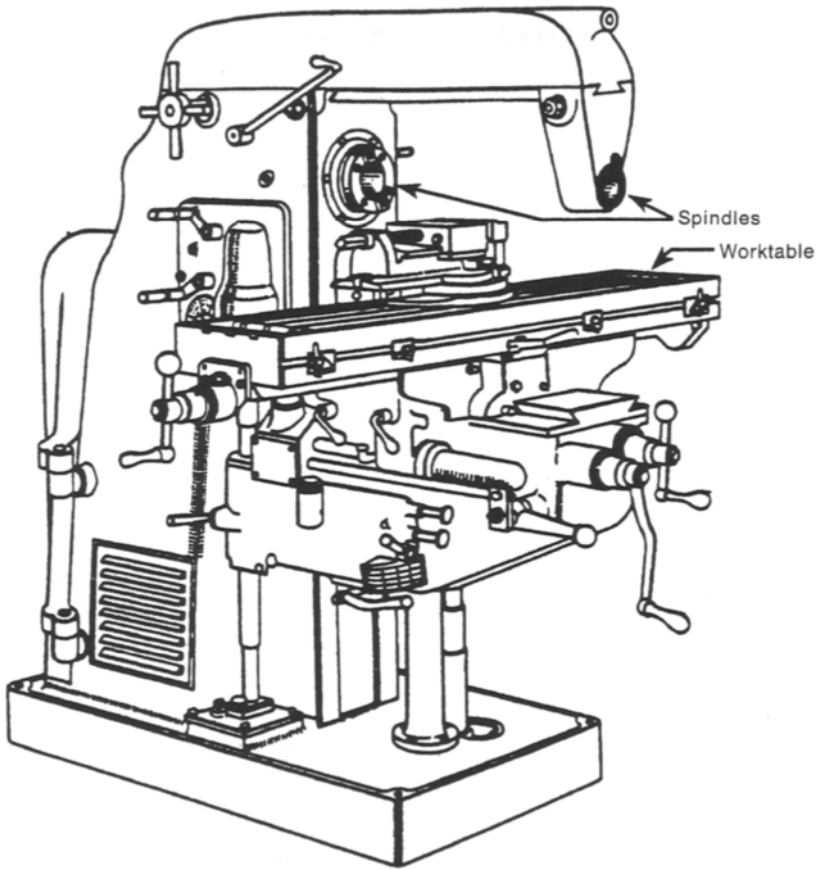


Fig. 7.15 Column and knee type milling machine.

feed per cutting edge will be

$$f = \frac{v_f}{Nn_t} \quad (7.8)$$

where v_f , N and n_t are defined in Fig. 7.16. The metal removal rate will be

$$\text{MRR}_{\text{milling}} = v_f d_c w \quad (7.9)$$

where: d_c is the cutting depth (Fig. 7.16)

w is the width of the tool-workpiece engagement.

As the feed of the milling tool is continuous, the undeformed chip thickness for each cutting edge varies as the cutting edge moves through the workpiece. An analysis of the milling geometry provides an estimate of the average undeformed chip thickness as

$$u_{\text{cavgmilling}} = \frac{v_f}{Nn_t} \sqrt{\frac{d_c}{D}} \quad (7.10)$$

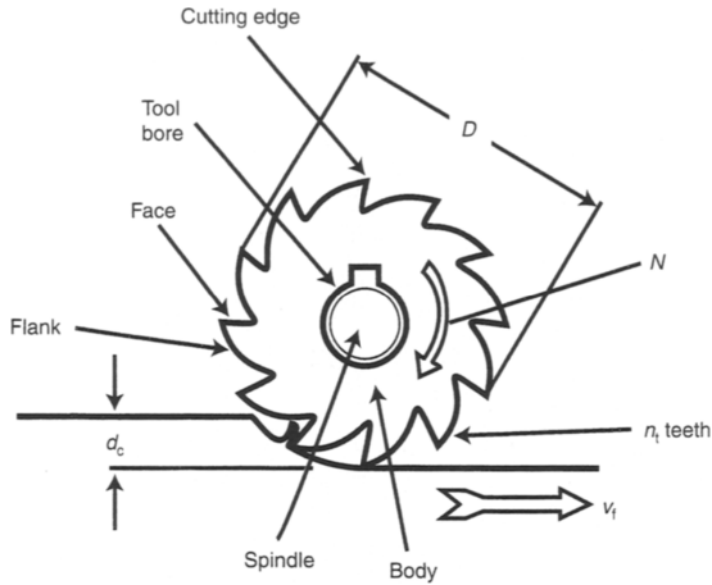


Fig. 7.16 Tool-workpiece details for orthogonal milling.

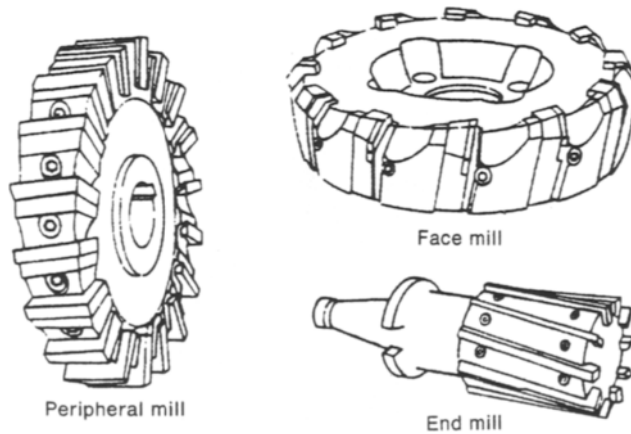


Fig. 7.17 Three common milling cutters. (Reprinted with permission from *ASM Materials Engineering Dictionary*, edited by J.R. Davis (1992), ASM International, Materials Park, OH 44073-0002, p. 278, Fig. 328.)

The variety of milling tools available cover a wide range of functions and shapes. Tools are usually classified according to their outside diameter, hole diameter and width, but may have an assortment of cutting profiles, some of which are illustrated in Fig. 7.17.

Grinding

Grinding is an abrasive process that removes material by causing accelerated wear of a surface. A huge range of grinding processes are available, including hand grinding operations, belt grinders and equipment employing rotating grinding wheels. A range

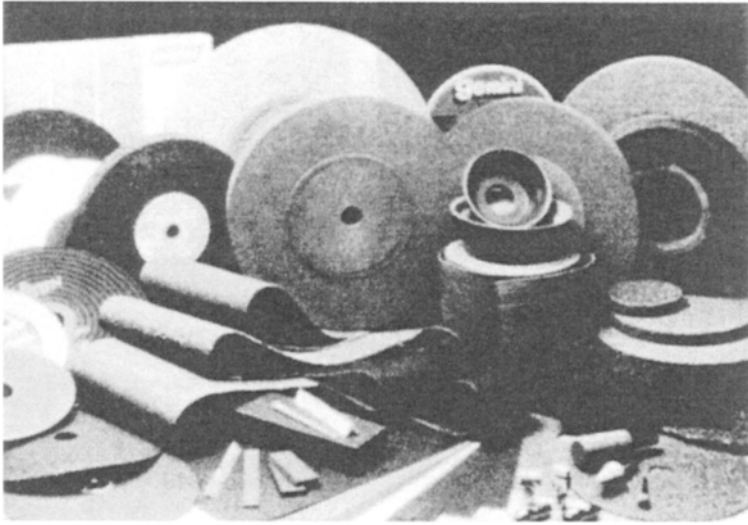


Fig. 7.18 An assortment of grinding wheels, belts and papers. (Reprinted with permission from *ASM Metals Handbook, Ninth Edition*, Vol. 16, Machining (1989), ASM International, Materials Park, OH 44073-0002, p. 435, Fig. 8.)

of grinding wheels, belts and papers are illustrated in Fig. 7.18. During grinding operations the primary cutting motion may be applied to either the workpiece or tool, depending on the geometry. The grinding medium consists of hard particles, usually silicon carbide or alumina, which provide the cutting action and are embedded in a matrix, formed into a useful shape. As the hard particles range in size and are usually randomly oriented within the matrix, it is often difficult to define an undeformed chip thickness, u_c , for each cutting edge, but this is typically in the range 0.000 25–0.025 mm. Grinding has several advantages, including the attainment of a good surface finish and dimensional accuracy with minimal applied pressure.

One of the most common grinding processes is that using a wheel for either surface or cylindrical grinding, as shown in Fig. 7.19. In both processes the primary cutting motion is due to rotation of the grinding wheel, while the feed motion is due to intermittent workpiece or wheel motion. Using the nomenclature of Fig. 7.19, the metal removal rate for these grinding processes can be estimated according to

$$\text{MRR}_{\text{surface grinding}} = f_s d_c v_{ts}; \quad \text{MRR}_{\text{cyl. grinding}} = \pi f_c D v_{tc} \quad (7.11)$$

The metal removal rate for many other grinding operations can often be determined from a simple consideration of the geometry and motions in a manner analogous to that in Fig. 7.19 and equation 7.11.

7.2.3 Machining methods – power

From the metal removal rate presented for each of the machining operations an estimate of the power required for each process is possible. Although the cost of

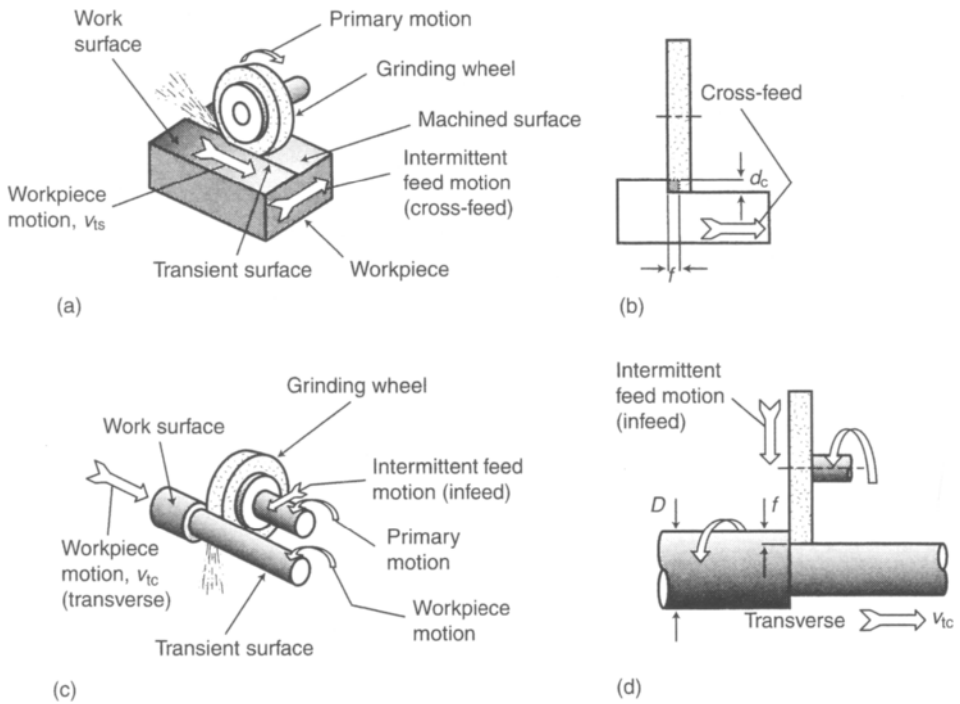


Fig. 7.19 Two common grinding operations: (a) and (b) surface grinding; (c) and (d) cylindrical grinding.

power may not represent an important operating cost, it is necessary to estimate because of machine limitations. Clearly, the power required will be proportional to the metal removal rate and also dependent on the cutting efficiency, η . The cutting efficiency is influenced by the mechanical drive system of the machine and the amount of energy converted to heat during machining. Typical cutting efficiencies are listed in Table 7.1 for each of the operations discussed, together with a summary of the other important attributes of these operations. Combining the efficiency, metal removal rate and *specific cutting energy* leads to an estimate of power, according to

$$P = \frac{p_s \times \text{MRR}}{\eta} \quad (7.12)$$

where: P is the power required
 η is the efficiency (Table 7.1)
 p_s is the specific cutting energy (Fig. 7.20)
MRR is the metal removal rate (equations summarized in Table 7.1).

The specific power, p_s , can be estimated from Fig. 7.20 and depends on the workpiece material, machining method, and the undeformed chip thickness, u_c , the equations for which are also summarized in Table 7.1.

Example 7.1 Facing on a lathe

A circular copper plate 300 mm in diameter is faced in a manner analogous to that of Fig. 7.5. The cutting tool has a major cutting edge angle of 60° , the depth of cut is

Table 7.1 Summary of machining characteristics

Machine type	Primary motion			Feed motion			Typical power (kW (hp))	Typical η	Typical maximum size of workpiece	Typical tolerance (mm)	Metal removal rate	Undeformed chip thickness, u_c
	Type ^a	Applied to	Speed range	Type ^b	Applied to	Range of feed, f (mm)						
Lathe Figs 7.4, 7.5	R	work	60–600 rpm	C	tool	0.15–0.65	3.7 (5)	0.70	$d_w < 360$ mm	0.013	$\pi f d_c N d_m$ eq 7.2	$f \sin \kappa_r$ eq 7.4
Shaper Figs 7.7, 7.10	L	tool	< 0.75 m/s	I	work	0.05–0.75	4 (5)	0.70	length up to 425 mm	0.075	$v f d_c$ eq 7.5	$f \sin \kappa_r$ eq 7.4
Planar Figs 7.9, 7.10	L	work	< 1.5 m/s	I	tool	0.5–2.5	30 (40)	0.80	length up to 8 m	0.064	$v f d_c$ eq 7.4	$f \sin \kappa_r$ eq 7.4
Drill press Figs 7.11, 7.12	R	tool	60–600 rpm	C	tool	up to 0.64	3.7 (5)	0.75	600×600 mm	0.013	$\pi D^2 N f / 4$ eq 7.6	$f / 2 \sin \kappa_r$ eq 7.7
Milling Figs 7.14, 7.16	R	tool	20–500 rpm	C	work	0.2–8.5 mm/s	up to 15 (20)	0.50	length up to ≈ 1 m	0.076	$v_t d_c w$ eq 7.9	$v_t / N n_t (d_c / D)^{1/2}$ eq 7.10
Grinding Fig. 7.19	R	wheel	2000 rpm	I	wheel or work	up to 6	up to 3.7 (5)	0.85	length < 0.6 m, dia. < 0.25 m	0.0025	$f_s d_c v_{ts}$ $\pi f_c D v_{tc}$ eq 7.8	0.000 25 to 0.025 mm

^a R = rotary, L = linear.

^b C = continuous feed, I = intermittent feed.

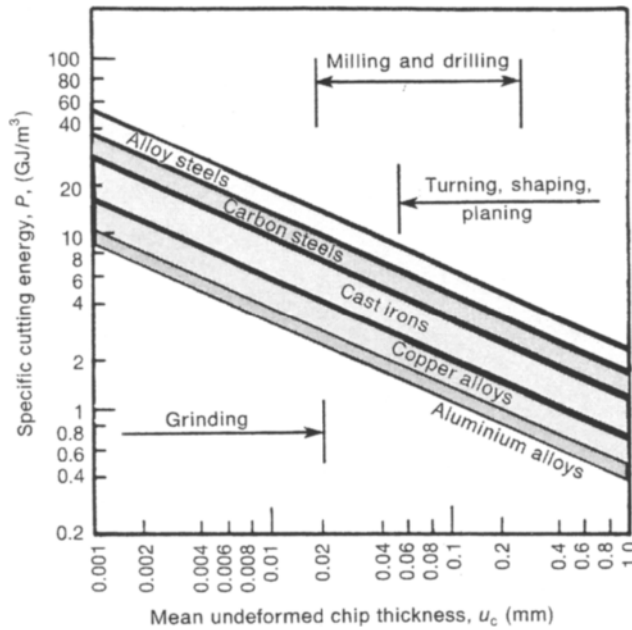


Fig. 7.20 Estimated values of specific cutting energy, p_s , for different materials and machining methods.

10 mm and the feed per revolution is 0.1 mm. If the lathe has a motor power of 4 kW, what is the maximum workpiece rpm (rotations per minute)? Recalculate the rpm for a feed of 0.4 mm.

Solution $\kappa_r = 60^\circ$ so, from equation 7.4, the undeformed chip thickness is

$$u_c = f \sin \kappa_r = 0.1 \sin 60^\circ = 0.0866 \text{ mm}$$

Using Fig. 7.20, the specific cutting energy, p_s , is estimated as 1.8 GJ/m^3 .

From Table 7.1 the efficiency, η , is taken as 0.7 and, from equation 7.12, the metal removal rate is calculated as

$$\text{MRR} = \frac{P\eta}{p_s} = \frac{4 \times 10^3 \text{ J/s} \times 0.7}{1.8 \times 10^9 \text{ J/m}^3} = 1555 \text{ mm}^3/\text{s}$$

Now, using equation 7.2 to calculate the rpm (N),

$$N = \frac{\text{MRR}}{\pi f d_c d_m} = \frac{1555 \text{ mm}^3/\text{s} \times 60}{\pi \times 0.1 \text{ mm} \times 10 \text{ mm} \times 300 \text{ mm}} = 100 \text{ rpm}$$

Repeating the calculations for $f = 0.4$ gives $p_s \approx 0.9 \text{ GJ/m}^3$, $\text{MRR} = 3111 \text{ mm}^3/\text{s}$, and therefore $N = 198 \text{ rpm}$.

Note: Increasing the feed reduces the specific cutting energy, as the lines of Fig. 7.20 have a negative slope. Although intuitively it would be expected that the larger feed would require a large cutting force, the rate at which material is removed is increased and therefore the amount of energy to remove one unit of material is reduced.

Example 7.2 Power for milling

A slab milling operation similar to that shown in Fig. 7.14 is performed on a medium carbon steel. The width of the steel is 50 mm and a 5 mm layer is to be removed in one pass of the tool. The steel is delivered to the tool at 2 mm/s and the tool is 40 mm in diameter, has 10 teeth and rotates at 150 rpm. Estimate the power required for this operation and the metal removal rate.

Solution

$$d_c = 5 \text{ mm}, \quad v_f = 2 \text{ mm/s}, \quad D = 40 \text{ mm}, \quad n_t = 10, \quad N = 150 \text{ rpm}.$$

Use equation 7.10 to calculate the undeformed chip thickness:

$$u_c = \frac{v_f}{N n_t} \sqrt{\frac{d_c}{D}} = \frac{2 \text{ mm/s}}{10 \times 2.5/\text{s}} \sqrt{\frac{5}{40}} = 0.028 \text{ mm}$$

Calculate the metal removal rate using equation 7.9:

$$\text{MRR} = v_f d_c w = 2 \text{ mm/s} \times 5 \text{ mm} \times 40 \text{ mm} = 400 \text{ mm}^3/\text{s}$$

From Fig. 7.20 estimate the specific cutting energy as $p_s = 8.5 \text{ GJ/m}^3$, and use $\eta = 0.5$ from Table 7.1. Then calculate power required from equation 7.12:

$$P = \frac{p_s \text{MRR}}{\eta} = \frac{8.5 \text{ GJ/m}^3 \times 400 \text{ mm}^3/\text{s}}{0.5} = 6.8 \text{ kW}$$

7.2.4 Machinability

It is desirable prior to machining a specific workpiece material to have an estimate of the ease with which the material can be machined, i.e. the *machinability*. Unfortunately, machinability is an ill-defined term. To a degree, the specific cutting energy presented in Fig. 7.20 could be used as an indication of machinability, as it is an indication of a material's resistance to cutting. However, resistance to cutting is only one factor influencing machinability. The ease of machining may also be rated in terms of: expected tool life; surface finish attainable; degree of dimensional control; sensitivity to changes in cutting conditions, such as speed, cutting depth, feed etc.; or force and energy required. Many rating systems have been developed in an attempt to rank materials, based on one or a combination of these factors. However, this proves to be a difficult task. Approximate machinability ratings are available based on comparing the machinability to AISI 1112 steel, which is assigned a machining rating of 1.0. More difficult-to-machine materials are given a lower rating, and easy-to-machine materials are assigned a higher rating. A few machinability ratings are listed in Table 7.2. If all other cutting conditions remain the same, these ratings can be used to compare the cutting speed required for a specific tool life for different materials. For example, for a tool to last as long machining a 1020 steel as it would to machine a 1112 steel would require reducing the cutting speed to 0.60 of that used for the 1112 steel. Also influencing the machinability are the deformation characteristics of the workpiece during machining. Notice that austenitic stainless steels (300 series

Table 7.2 Approximate machinability ratings for some metals

Material	Machinability rating	Material	Machinability rating
AISI 1112 steel	1.0	AISI 4140 leaded steel	0.70
AISI 1020 steel	0.60	304 stainless steel	0.25
AISI 1040 steel	0.61	Inconel Ni superalloys	0.1–0.2
AISI 3140 steel	0.55	AA-1100 aluminium	2.0
Mg alloys	5.0–10	AA-7075-T6 aluminium	1.0
		brass	2.0

stainless steels) are generally difficult to machine. This corresponds to their relatively high strain hardening exponent (see Table 3.1).

To improve machinability some alloys are compositionally adjusted. For example, lead has virtually no solubility in steel, aluminium or copper. Thus, lead forms globular particles in these alloys and, due to its low shear strength, becomes smeared at the tool–workpiece interface. In this form it acts as an effective solid lubricant. Recently, environmental concerns have caused the replacement of lead with bismuth in many alloys.

A problem with the machinability ratings of Table 7.2 is that the microstructural condition of the workpiece also alters machinability. This is shown clearly in Fig. 7.21 which relates the tool life and cutting speed for a low carbon steel. The information such as that shown in Fig. 7.21 can be important for process design. For example, if a heat treatment is to be applied to the workpiece, it may prove beneficial to machine either before or after the heat treatment step, depending on the relative machinability of the workpiece prior to and following the heat treatment. If the machining is carried out prior to heat treatment, the influence of the heat treatment on the dimensional control and surface finish should be considered, i.e. will the part

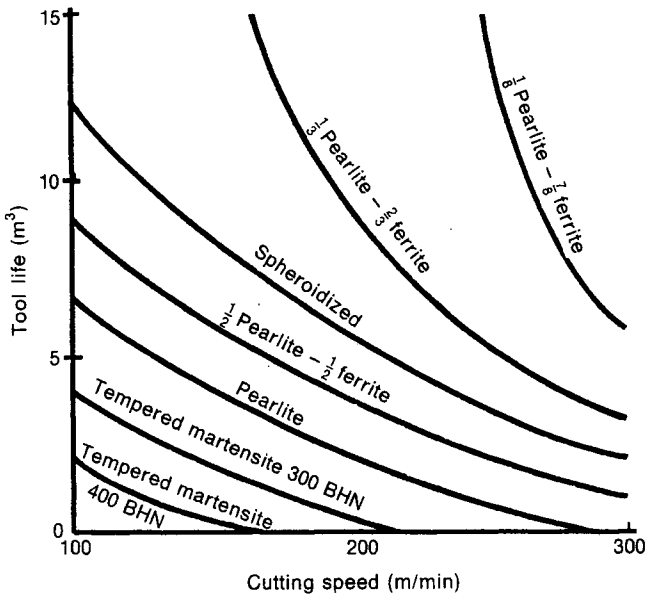


Fig. 7.21 Influence of microstructural condition on cutting speed and tool life for a low carbon steel.

distort during heat treatment or develop an unacceptable surface scale/oxide on the newly machined surfaces?

7.2.5 Mechanics of metal cutting

Previous sections have presented a description of the most common machining methods and a technique for estimating some of the associated major parameters. However, the complex nature of many machining processes can make these estimates quite approximate. To effectively diagnose machining problems an understanding of the basic mechanics of the process is required, such as that presented in this section.

A two-dimensional orthogonal cutting operation is shown schematically in Fig. 7.22, in which a sharpened tool removes a layer of material into a chip. Ideally, the metal deformation that occurs during formation of the chip occurs by shearing along the plane O–A of Fig. 7.22. Typically, the shearing occurs in successive steps, as shown in Fig. 7.23. An important parameter controlling the machining geometry is the angle of the planes of shear in Fig. 7.23, which is the *shear angle* ϕ in Fig. 7.22. It is desirable to express the shear angle in terms of the *tool rake angle* α , the cutting depth d_c and the chip thickness d'_c , because each of these quantities is readily measured. The geometry of Fig. 7.22 indicates that

$$\psi = \alpha + 90 - \phi; \quad \gamma = 90 - \psi \quad (7.13)$$

where each of the angles is defined in Fig. 7.22.

Combining these two equations gives

$$\gamma = \phi - \alpha \quad (7.14)$$

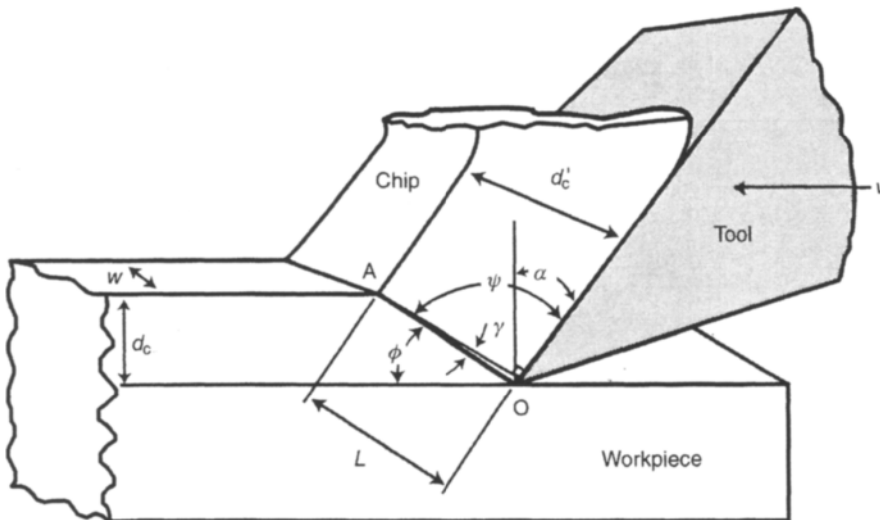


Fig. 7.22 Relevant geometry for orthogonal machining.

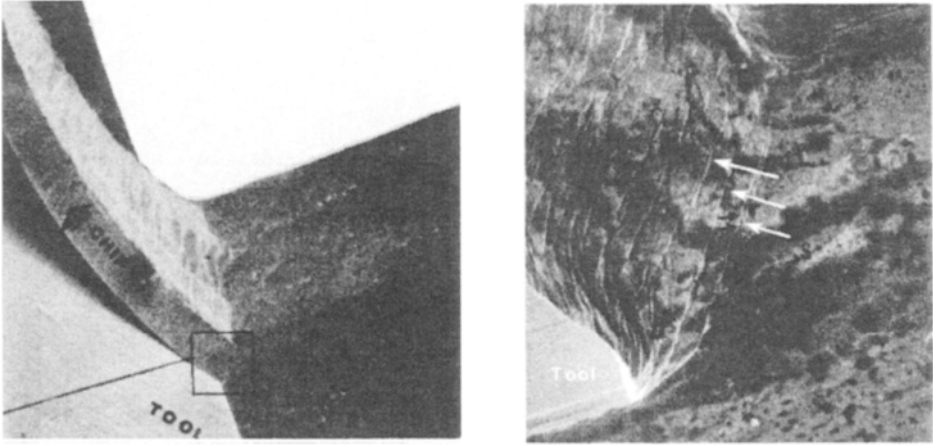


Fig. 7.23 Chip formation during the machining of polished gold, photographed in a scanning electron microscope. The photograph on the right is an enlargement of the boxed region in the left photograph. Arrows indicate several successive shear planes. (Reprinted with permission from *ASM Metals Handbook, Ninth Edition*, Vol. 16, Machining (1989), ASM International, Materials Park, OH 44073-0002, p. 9, Fig. 3.)

Using equation 7.14 the length of the shear plane, L , can be given in terms of the chip thickness as

$$L = \frac{d'_c}{\cos(\phi - \alpha)} \quad (7.15)$$

where d'_c is the chip thickness (Fig. 7.22).

Also, from the right-angle triangle of Fig. 7.22,

$$\begin{aligned} \sin \phi &= \frac{d_c}{L} \\ &= \frac{d_c}{d'_c} \cos(\phi - \alpha) \end{aligned} \quad (7.16)$$

Equation 7.16 can be simplified by expanding the cosine of the difference of two angles to

$$\sin \phi = \frac{d_c}{d'_c} (\cos \phi \cos \alpha + \sin \phi \sin \alpha) \quad (7.17)$$

Simplifying and rearranging equation 7.17 provides an expression for the shear angle in terms of the depth of cut, tool angle and chip dimensions:

$$\tan \phi = \frac{d_c}{d'_c} \times \frac{\cos \alpha}{1 - \frac{d_c}{d'_c} \sin \alpha} \quad (7.18)$$

The shear angle, equation 7.18, is an important machining parameter, which is expressed in terms of readily measurable quantities.

Cutting forces and Merchant's theorem

During orthogonal cutting, shown in Fig. 7.22, several forces act on the chip and workpiece, as defined in Fig. 7.24. The forces result from friction between the chip

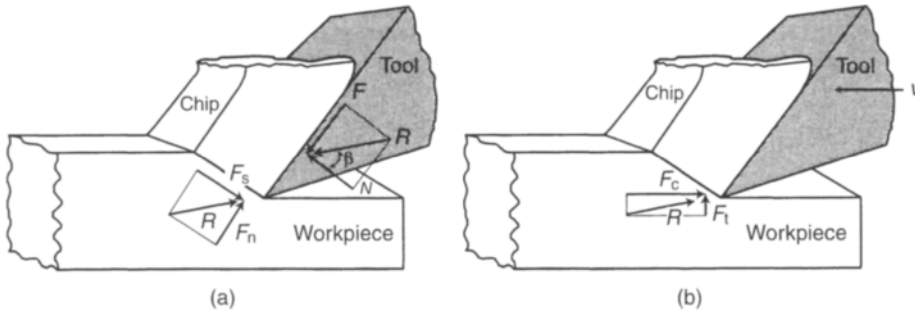


Fig. 7.24 Forces acting on chip and workpiece during orthogonal cutting.

and tool, causing the frictional force F and normal force N , and the force to cause internal shear deformation of the workpiece along the shear plane, F_s , and the associated normal force, F_n . The forces can be resolved into a resultant force, R , which in turn has components in the cutting direction, F_c , and thrust direction, F_t .

If the tool post, as shown in Fig. 7.3, is instrumented appropriately with force measuring devices (commonly referred to as a tool post dynamometer), then the forces F_c and F_t can be measured. Knowing these two forces and the geometry of Fig. 7.24, the other forces can be calculated according to

$$\begin{aligned} F &= F_c \sin \alpha + F_t \cos \alpha \\ N &= F_c \cos \alpha - F_t \sin \alpha \\ F_s &= F_c \cos \phi - F_t \sin \phi \\ F_n &= F_c \sin \phi + F_t \cos \phi \end{aligned} \quad (7.19)$$

The chip separates from the workpiece via shear deformation occurring along the shear plane. Recall from Chapter 3 that deformation requires work, which for the arrangement shown in Fig. 7.24 is supplied by the force and motion applied to the workpiece by the tool. As the cutting force F_c is in the direction of motion v , this force is responsible for the work done. From Fig. 7.24 it should be clear that

$$F_c = R \cos(\beta - \alpha) \quad (7.20)$$

where β is the friction angle shown in Fig. 7.24.

Merchant based his theorem on the assumption that the shear angle and chip dimensions, given in equation 7.18, will always correspond to the minimum value of the cutting force, F_c , of equation 7.20. This means that deformation during machining will occur according to the geometry that requires the least energy or work. This is analogous to the situation presented in Section 4.3.6 regarding deformation during forging. The shearing force F_s can be expressed in terms of the geometry and material shear strength as

$$F_s = R \cos(\phi + \beta - \alpha) \quad (7.21)$$

$$F_s = \tau_s w L \quad (7.22)$$

where: w , L are as defined in Fig. 7.22

τ_s is the shear strength of the workpiece.

The length of the shear plane is

$$L = \frac{d_c}{\sin \phi} \quad (7.23)$$

and, combining equations 7.20 through 7.23, provides

$$F_c = \frac{\tau_s d_c w \cos(\beta - \alpha)}{\cos(\phi + \beta - \alpha) \sin \phi} \quad (7.24)$$

As Merchant's theorem states that F_c is to be minimized, then the denominator of equation 7.24 must be maximized. Making the assumption that the friction angle β is independent of the shear angle α , then the maximum value of the denominator can be determined by differentiating the denominator with respect to ϕ and equating to zero:

$$\begin{aligned} y &= \cos(\phi + \beta - \alpha) \sin \phi \\ \frac{dy}{d\phi} &= -\sin(\phi + \beta - \alpha) \sin \phi + \cos(\phi + \beta - \alpha) \cos \phi = 0 \end{aligned} \quad (7.25)$$

Solving equation 7.25 gives

$$\begin{aligned} \tan(\phi + \beta - \alpha) &= \tan(90 - \phi) \\ 2\phi &= 90 - (\beta - \alpha) \end{aligned} \quad (7.26)$$

Figure 7.25 compares the result of Merchant's theorem, equation 7.26, to experimental measurements of the shear angle during machining of several metals. Given the rudimentary nature of the analysis and assumptions incorporated, correlation between theory and experiment is not exact. More importantly, however, the trends predicted by Merchant's theorem are correct. Essentially, Merchant's analysis suggests that to minimize the machining cutting force requires a large tool rake angle

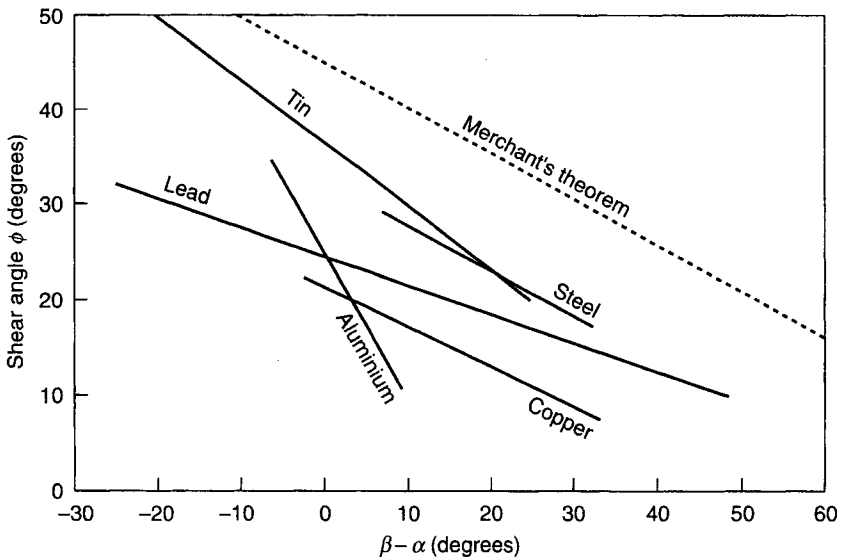


Fig. 7.25 Comparison of Merchant's theorem to experimental measurements.

α . However, from Fig. 7.22, it is seen that such a sharply raked tool would be fragile, leading to tool breakages. Furthermore, a sharply raked tool is less able to conduct heat away from the cutting edge, leading to high temperatures at the tool–workpiece interface. Excessive temperature at the interface is one of the leading causes of premature tool wear. Consequently, most machining operations utilize tools with rake angles of 20° or less.

Example 7.3 Orthogonal machining

A stainless steel bar of 5 mm width and a yield strength of 400 MPa is orthogonally machined in a fashion similar to that illustrated in Fig. 7.22. The tool rake angle is 15° and the depth of cut is set to 0.5 mm. These conditions produce a chip thickness of 0.7 mm. Calculate:

- the cutting force required;
- the coefficient of friction between the chip and tool.

Solution

- $\alpha = 15^\circ$, $\tau_s \approx \frac{1}{2} \text{YS} = 200 \text{ MPa}$, $d_c = 0.5 \text{ mm}$, $d'_c = 0.7 \text{ mm}$, $w = 5 \text{ mm}$.

Using equation 7.18:

$$\tan \phi = \frac{d_c}{d'_c} \times \frac{\cos \alpha}{1 - \frac{d_c}{d'_c} \sin \alpha} = \frac{0.5}{0.7} \times \frac{\cos 15^\circ}{1 - \frac{0.5}{0.7} \sin 15^\circ}$$

$$\phi = 40.2^\circ$$

From equation 7.26:

$$2\phi = 90 - \beta + \alpha$$

$$\beta = 90^\circ + 15^\circ - 2\phi = 24.5^\circ$$

And from equation 7.24:

$$\begin{aligned} F_c &= \frac{\tau_s d_c w \cos(\beta - \alpha)}{\cos(\phi + \beta - \alpha) \sin \phi} \\ &= \frac{200 \text{ MPa} \times 0.5 \text{ mm} \times 5 \text{ mm} \cos(47 - 15)}{\cos(40.2^\circ + 24.5^\circ - 15^\circ) \sin 40.2^\circ} = 1181 \text{ N} \end{aligned}$$

- From equation 7.23:

$$L = \frac{d_c}{\sin \phi} = \frac{0.5}{\sin 40.2^\circ} = 0.77 \text{ mm}$$

From equation 7.22:

$$F_s = \tau_s w L = 200 \times 5 \times 0.77 = 774 \text{ N}$$

Using equations 7.19, calculate

$$F_s = F_c \cos \phi - F_t \sin \phi$$

$$774 = 1181 \cos 40.2^\circ - F_t \sin 40.2^\circ$$

$$F_t = 198 \text{ N}$$

Again, use equations 7.19 to calculate F and N :

$$F = F_c \sin \alpha + F_t \cos \alpha = 1181 \sin 15^\circ + 198 \cos 15^\circ = 497 \text{ N}$$

$$N = F_c \cos \alpha - F_t \sin \alpha = 1181 \cos 15^\circ - 198 \sin 15^\circ = 1090 \text{ N}$$

From equation 4.1, $\mu = F/N = 497/1090 = 0.46$.

Note from the geometry of Fig. 7.24 that $\mu = \tan \beta = \tan 24.5^\circ = 0.46$.

The friction coefficient between the tool and chip is quite high. This is a result of the significant welding/adhesion that can occur between the chip and tool face, which is a major cause of tool wear, discussed in the next section.

7.2.6 Tool wear and tool materials

As indicated in the foregoing example, the friction coefficient between the tool and chip can be quite high. This friction causes a significant temperature increase, as shown in Fig. 7.26 for orthogonal cutting of mild steel. Temperature influences the cutting action in several important ways, including:

1. altering the properties of the machined surface;
2. causing dimensional changes to the workpiece and chip, thereby decreasing dimensional accuracy;
3. adversely affecting the strength, hardness and wear resistance of the cutting tool.

The decrease in hardness and wear resistance of the tool with increasing temperature is the major factor that controls useful tool life. The strength and thermal conductivity of the workpiece, tool material, cutting speed and depth of cut all influence the

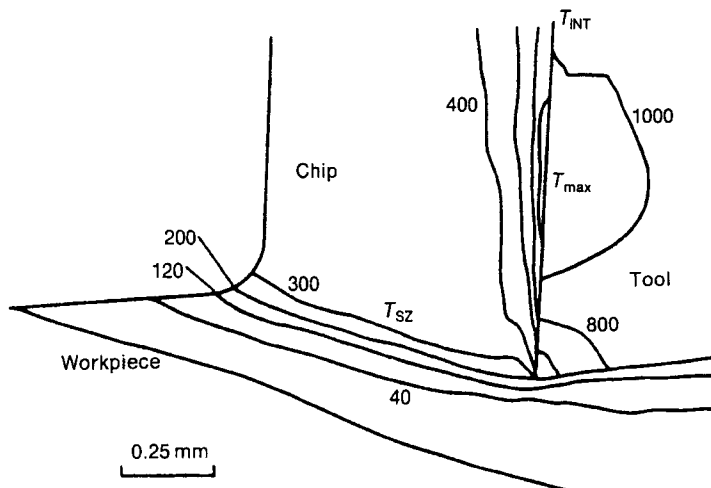


Fig. 7.26 Temperatures ($^{\circ}\text{C}$) during orthogonal machining. Tool rake angle = 5° , cutting depth = 0.25 mm, cutting speed = 244 m/min with a carbide tool cutting AISI 1016 steel; T_{INT} = temperature of tool-workpiece interface; T_{SZ} is the temperature of the shear zone. (Reprinted with permission from *ASM Metals Handbook, Ninth Edition*, Vol. 16, Machining (1989), ASM International, Materials Park, OH 44073-0002, p. 670, Fig. 12.)

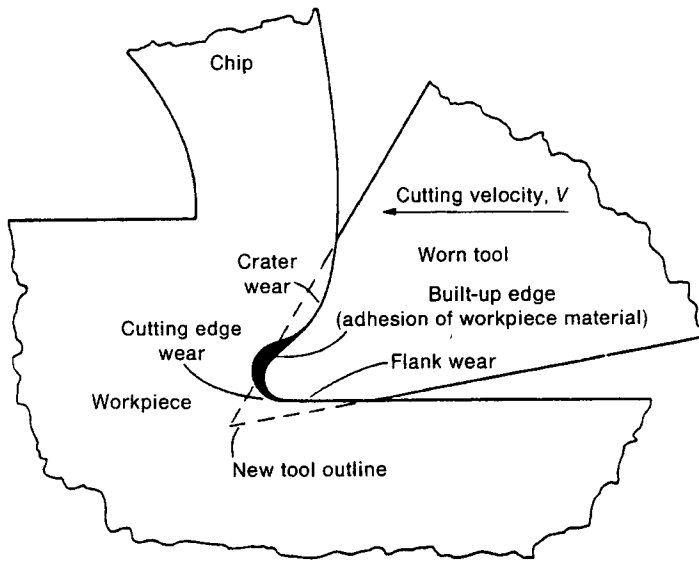


Fig. 7.27 Diagram of tool wear during orthogonal cutting. (Reprinted with permission from *ASM Metals Handbook, Ninth Edition*, Vol. 16, Machining (1989), ASM International, Materials Park, OH 44073-0002, p. 37, Fig. 2.)

maximum temperature during machining, which is dependent on the cutting parameters according to the relation

$$T_M \propto v^a f^b d_c^c \quad (7.27)$$

where: T_M is the mean cutting temperature
 v is the cutting speed
 f is the feed
 d_c is the cutting depth
 a, b, c are constants, with $a > b > c$.

Decreased wear resistance of the cutting tool at temperature results in degradation of the tool profile, as schematically illustrated in Fig. 7.27. It is clear that the cutting geometry is severely altered as the tool profile changes. Crater wear causes a change to the shear angle, while flank wear causes excessive contact between the newly created workpiece surface and the tool, degrading the quality of the machined surface. Both these types of wear increase the cutting power required and effectively decrease the cross-section of the tool, potentially leading to sudden fracture. Under some cutting conditions, workpiece material can adhere to the tool, causing the *built-up edge* shown in Figs. 7.27 and 7.28. This condition occurs more frequently at low cutting speeds and leads to cutting by the built-up edge rather than by the cutting tool per se.

It should be apparent from the foregoing that materials suitable for use as cutting tools must have good resistance to softening at the temperatures encountered during machining. The softening characteristics of several major classes of tool materials are illustrated in Fig. 7.29. Carbon steels soften well below the temperatures shown in Fig. 7.26 and are, therefore, unsuitable for metal cutting.

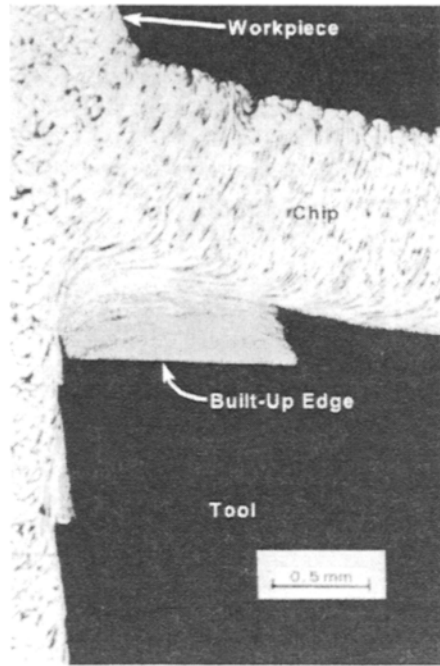


Fig. 7.28 Built-up edge on tool machining Al–Cu at 38 m/min. (Reproduced from E.M. Trent, *Metal Cutting* (1997), with the permission of Butterworth-Heinemann, Oxford.)

Of all the tool materials available, high speed steels (HSS) are most widely used. These steels contain approximately 0.68 wt% C, 3.4 wt% Cr, 1.8 wt% Mo, 0.8 wt% V and 6.5–12 wt% W. Although each of these alloy additions is added for specific purposes, it is the W and Mo that are responsible for the retention of hardness at temperature. These additions react with iron and carbon to form complex carbides with high hardness and good temperature stability. These carbide particles are surrounded by a tough matrix that provides good fracture resistance. HSS tools are relatively inexpensive and retain their hardness to at least 550°C.

Cast cobalt tools retain high hardness levels to higher temperatures than HSS tools. Cast cobalt tools are complex alloys of about 45 wt% Co, 30 wt% Cr, 20 wt% W, 3 wt% C, with further additions of Ta, Nb, Mn, Fe and Ni. These tools have less tendency to form built-up edges than HSS tools and are particularly useful for machining sand castings that may contain residual moulding sand on the surface.

Several different *carbide* tools are available, but the most widely used are the WC–Co tools. These tools are made by embedding high volume fractions of tungsten carbide (WC) in a cobalt matrix, as shown in the micrograph of Fig. 7.30. WC particles are stable to more than 2500°C, and the tool material retains useful hardness levels to temperatures of around 1200°C. In addition, WC–Co tools have high stiffness and good thermal conductivity. However, their fracture resistance is lower than HSS tools. WC–Co tools are susceptible to rapid crater formation when machining steel, which can be overcome by substituting TiC and TaC particles for some of the WC. Unfortunately, the addition of TiC and TaC reduces the fracture and thermal shock resistance of the tool. Most often carbide tools take the form of inserts

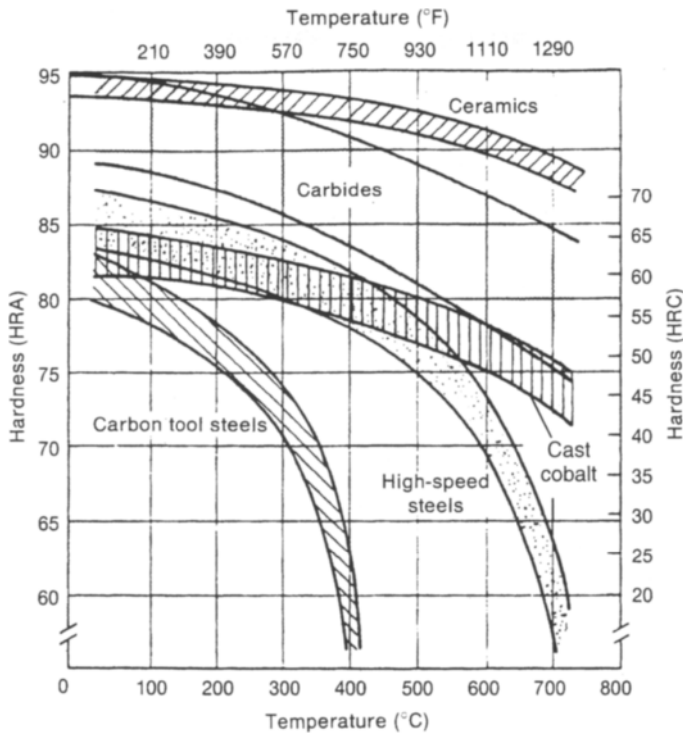


Fig. 7.29 Hardness of tool materials as a function of temperature; HRA = Rockwell A hardness, HRC = Rockwell C hardness. (Reprinted with permission from *ASM Metals Handbook, Ninth Edition*, Vol. 16, Machining (1989), ASM International, Materials Park, OH 44073-0002, p. 69, Fig. 1.)

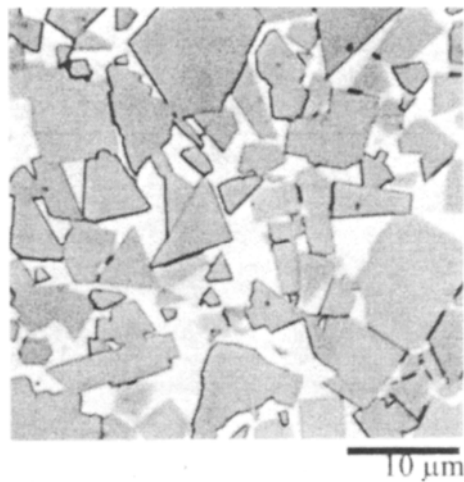


Fig. 7.30 Microstructure of an 85%WC–15%Co tool. (Reprinted with permission from *ASM Metals Handbook, Ninth Edition*, Vol. 16, Machining (1989), ASM International, Materials Park, OH 44073-0002, p. 73, Fig. 3d.)

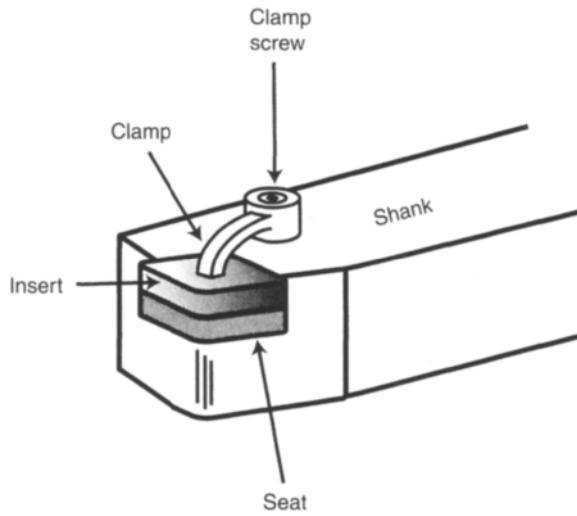


Fig. 7.31 WC–Co insert clamped to a single-point tool.

that are clamped or brazed onto a tougher base, such as that illustrated in Fig. 7.31 for a single-point tool. To combine the fracture resistance of straight WC–Co tools with the resistance to crater formation of TaC/TiC-containing tools, *coated carbides* have been developed. These tools consist of a base of WC (with or without additions of other carbides) with a 5–10 μm coating consisting of one or more layers of TiN, TiO₂, Al₂O₃ or other refractories, as illustrated in Fig. 7.32.

It is evident from Fig. 7.29 that ceramic materials retain the highest hardness levels at high temperatures. Unfortunately, most ceramics have poor fracture resistance and

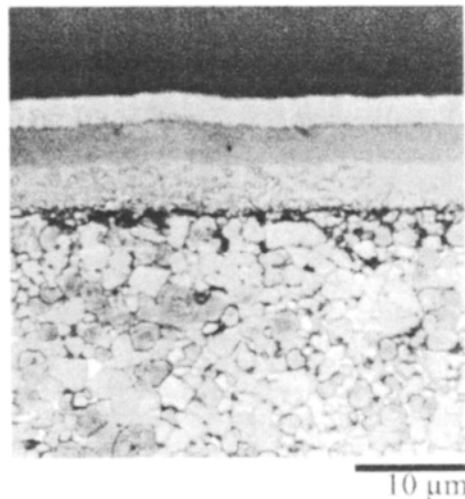


Fig. 7.32 A carbide tool coated with 10 μm of TiC, TiCN and TiN (top layer). (Reprinted with permission from *ASM Metals Handbook, Ninth Edition*, Vol. 16, Machining (1989), ASM International, Materials Park, OH 44073-0002, p. 80, Fig. 17a.)

thermal shock characteristics and are, therefore, most suitable for uninterrupted cutting at high speeds. Ceramic tools are most often used as inserts. They are made from Al_2O_3 (alumina), silicon nitride or SiAlON (a combination of alumina and silicon nitride). Of these, silicon nitride tools have the best fracture resistance, temperature capability and load carrying capacity.

In addition to the foregoing comments regarding tool materials and wear, it is useful to be able to estimate *tool life*. Tool life is defined as the cutting time for which the tool can be used effectively. This may be the time to cause tool breakage, but more often it is the time to a level of tool wear that necessitates replacement or resharpener. It has already been emphasized that the major factor causing wear is the temperature increase of the tool. According to equation 7.27, the cutting speed has the largest influence on the tool temperature. On this basis, the *Taylor tool life* equation has the form

$$vt^n = C \quad (7.28)$$

where: v is the cutting speed
 t is the tool life
 C, n are constants.

As the exponent, n , in the Taylor tool life equation is generally considerably less than one, small changes in cutting speed cause large changes in tool life. As seen in Fig. 7.33, increasing the cutting speed from 20 to 25 m/min decreases the tool life by about an order of magnitude in this particular case, exemplifying the major influence of cutting speed on tool life. Approximate values for C and n are listed in Table 7.3.

Equation 7.28 takes into account the influence of cutting speed only, but the data in Table 7.3 implies that feed and depth of cut also influence tool life. The Taylor tool life equation can be extended, to include the effect of these cutting parameters, which leads to the *generalized tool life equation*,

$$vt^n f^m d_c^p = C' \quad (7.29)$$

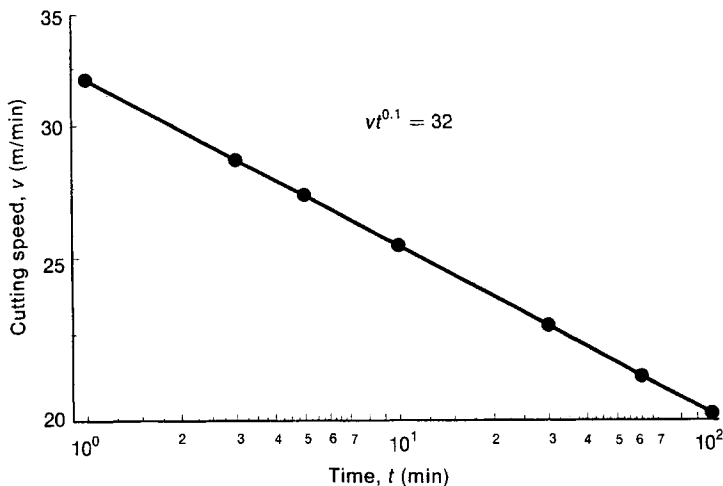


Fig. 7.33 Typical Taylor relationship between cutting speed and tool life.

Table 7.3 Approximate values for constants of Taylor tool life equation

Workpiece	Tool material	Feed (mm/rev)	Depth of cut (mm)	C for v (m/min)	n
Brass	high carbon steel	0.3	2.5	95	0.1
Bronze	high carbon steel	0.3	2.5	75	0.11
Gray Cast Iron	HSS	0.6	1.25	55	0.1
AISI 1035 Steel	HSS	0.3	1.25	40	0.11
AISI 1045 Steel	HSS	0.3	2.5	60	0.11
AISI 4350 Steel	HSS	0.3	2.5	25	0.11
AISI 1060 Steel	carbide	0.6	3.2	215	0.17
	carbide	0.6	6.3	180	0.17
	carbide	1.0	1.6	165	0.16
	carbide	1.5	1.6	130	0.16

where m , p and C' are material constants, and other variables are as defined previously.

The values of m and p must be determined for each cutting condition, but typically $0.6 < m < 0.75$ and $0.15 < p < 0.3$. Note that, based on these exponents, the feed rate has a greater influence on tool life than the depth of cut.

Example 7.4 Estimate of cutting speed

The generalized tool life equation for a turning operation is $vt^{0.1}f^{0.7}d_c^{0.3} = C'$. For the same turning conditions it is known that $vt^{0.1} = 40$ when the feed rate is 0.25 mm/rev and the cutting depth is 4 mm. Determine the cutting speed that should be used if a 30 min tool life is required when the feed rate is halved and the cutting depth is increased to 5 mm.

Solution From the information provided, calculate C' as

$$vt^{0.1}f^{0.7}d_c^{0.3} = C' = 40 \times 0.25^{0.7} \times 4^{0.3}$$

$$C' = 23$$

Then calculate the cutting speed for the required feed rate of 0.125 mm and the cutting depth of 5 mm:

$$v \times 30^{0.1} \times 0.125^{0.7} \times 5^{0.3} = 23$$

$$v = 43.3 \text{ m/min}$$

7.2.7 Cutting fluids

During machining operations the tool–workpiece friction coefficient and the interface temperatures can be quite high (see Example 7.3 and Fig. 7.26). This contributes greatly to tool wear. The purpose of applying a *cutting fluid* is to both reduce the friction and lower the temperature, as well as control the built-up edge, flush away chips and protect the workpiece and tool from corrosion. In this manner, cutting fluids are both lubricants and coolants and when used properly can increase productivity by allowing higher cutting speeds, feed rates and cutting depths.

Cutting fluids can be classified as either solutions or emulsions. Solutions are based on fluids such as mineral oil, petroleum solvents, synthetic fluids or water, and are formulated with various additives that are soluble in the base. Emulsions consist of two phases, one of which is water and the other a discontinuous phase of particles of oil, petroleum or synthetic fluids. As the heat capacity of water is much higher than that of oil, emulsions generally have better cooling capability, but poorer lubricating characteristics.

Modern cutting fluids are complex chemical mixtures specifically designed for machining applications. Many accepted lubricants, useful in other applications, have little or no effect on the cutting action. Two important chemical characteristics of a cutting fluid are a small molecular size to allow rapid diffusion and penetration to the tool-workpiece interface, and a reactive ingredient that reacts with the work material to form a low shear strength compound that can act as a boundary lubricant. Most cutting fluids are formulated with additive packages that may consist of so-called *extreme pressure (EP)* additives. They are particularly useful when the cutting forces are high or high feed rates are used. EP additives provide a more stable, tougher lubricant at the chip-tool interface, which will act to minimize the built-up edge. Most EP additives are organic molecules containing sulphur and chlorine which react at the high temperatures in the cutting zone to form metallic sulphides and chlorides.

Also added may be *detergents* to reduce deposition of solids on the workpiece. Detergents are usually long-chain alcohols and sulphonic acids. *Antimisting* additives, consisting of small quantities of acrylates or polybutanes, are added to encourage the formation of larger particle sizes, thereby reducing airborne contamination by the cutting fluid, which can cause health and safety problems in many large machine shops. *Antifoaming* additives are incorporated to prevent the formation of foam when the fluid is agitated. These additives reduce the free energy of the fluid surface. They consist of polyglycols or high-molecular-weight amides. *Odour masks* of pine oil or cedar oil are often added to mask the disagreeable odor caused by cutting fluids at high temperatures. *Corrosion inhibitors* are necessary, particularly for water-based fluids, to prevent the corrosion of machine tools and associated equipment. Many chemicals, including sulphonates and borates, are used for this purpose. *Antimicrobial agents* are necessary because microbial growth occurs in water-based cutting fluids, or if water is inadvertently introduced to the fluid. Many bacteria, moulds and yeasts can double in population every 15–30 min and compete with one another for nourishment. These microbes, which do not need air, grow at the bottom of oil sumps and attack the sulphur compounds in the EP additives. Several *biocides* are available to combat this attack and can be formulated as part of the cutting fluid or added intermittently.

Cutting fluids are most often applied by flooding the tool and workpiece area. The volume of cutting fluid required is quite high, usually several litres per minute. Sometimes cutting fluids are applied in the form of a mist, which can improve both the cooling and lubricating effectiveness of the cutting fluid. However, care must be taken to guard against build-up of mist in workplace air.

Although most cutting fluids have a low level of toxicity, prolonged exposure of the skin to such fluids can cause a number of minor ailments, including contact dermatitis, acne, pigmentary changes, and benign or malignant tumours. Therefore,

appropriate precautions must be taken, consisting of applying protective creams to the hands before work, frequent washing of the sink facilities with a mild soap, use of protective clothing and careful attention to general cleanliness in the workplace.

7.2.8 Numerically controlled machining

Numerically controlled (NC) machining extends the machining operations described to include a controller and a numerical data entry device. However, for NC machining the tool-workpiece processes remain the same as that described previously, only the method of controlling the tool motion is automated. As such, NC machining does not represent a metal forming process, but rather an automated method of controlling a metal forming process. As automated techniques are widely utilized in industry for machining operations, this section gives a brief overview of some aspects of NC machining.

Numerical control began with the use of sheet metal cards with arrays of punched holes that were used to control weaving machines in the 1800s. However, the modern principles of NC machining were introduced during the 1950s, for the control of milling machines. In most early systems, numerical data required for part production was stored on paper tapes (with appropriate punched holes), which were fed into a tape reader. Most NC systems now make use of a computer (*computer numerical control*, CNC) for each machine centre, providing better flexibility and lower capital investment. Often each CNC machine is part of a local area network, allowing complete integration into the manufacturing system. Numerical control was introduced and developed by the machining industry and this industry still contains the largest concentration of NC machines.

In a CNC system a stored program contains the numerical data required to produce the desired shape. This data includes geometrical information, the cutting speed, feed rate and other machining parameters. Thus, in CNC machining many of the skilled machinist tasks are automated. However, the programmer must have knowledge about cutting tools, cutting fluids, machinability data, fixture design etc. In many cases the advantage of NC machining is not lowering labour costs. Rather, set-up times are decreased and, therefore, actual production time is increased. Further time savings are realized because inspection time is decreased. It has been estimated that during conventional operator controlled machining up to 70% of the production time is spent on dimensional measurements. NC machining can produce higher quality parts with accurate dimensional control, even while producing geometries that are extremely difficult to make by conventional machining. These advantages have made NC and CNC machining very popular, to the point where the sale of conventional milling machines has almost completely stopped.

Several programming techniques are used to control the motion of the tool. *Straight line* or *linear control* moves the cutting tool parallel to one of the major axes of the machine tool at a suitable rate. This is the normal mode of operation for conventional machining. During *continuous path* or *contouring control*, the tool moves in two or more machine axes simultaneously. In this manner curved surfaces can be produced. Typically, contoured control reduces machining time, but requires greater programming time.

The use of NC and CNC techniques allows the introduction of sophisticated automation into many metal forming operations. This has contributed to many new manufacturing management strategies, such as flexible manufacturing systems (FMS), computer integrated manufacturing (CIM) and computer aided design/computer aided manufacturing (CAD/CAM), to name a few. A direct extension of CNC machining is the use of *adaptive* control in which suitable sensors monitor the machining operation, in terms of temperature, cutting forces or other appropriate parameters, and automatically adjust or adapt the machining conditions, such as feed rate, to optimize the productivity of the operation.

7.3 Nontraditional machining processes

The widely used conventional machining processes are not capable of producing some geometries, or machining several of the very hard high-strength temperature-resistant metals. Moreover, an inherent byproduct of conventional machining processes are chips or *swarf*, which are quite difficult to recycle and therefore of low value. As machining usually involves relatively expensive workpiece materials, the cost effectiveness of transforming part of the workpiece into low value swarf is a major drawback. These disadvantages of traditional machining operations have led to the development of several nontraditional processes that use completely different methods of achieving desired shapes.

7.3.1 Abrasive waterjet machining

Abrasive waterjet machining uses the erosion action of a high velocity water stream, containing abrasive particulate for cutting and drilling applications. Even without abrasive particulates, a waterjet can be used for machining nonmetallic materials. Typical abrasives used include garnet, olivine sand and sometimes silica sand. These abrasives are mixed with a waterjet at a pressure of between 200 MPa and 400 MPa, as shown schematically in Fig. 7.34. The stream is focused and impinges on the workpiece surface at velocities of up to 915 m/s.

Many metals have been cut using abrasive waterjets, including aluminium, steel, tungsten carbide and titanium. It has been used successfully to cut honeycomb titanium panels in the aerospace industry, without causing burrs or heat damage that may otherwise cause microstructural changes and alter mechanical properties. Inconel superalloys for high temperature gas turbine applications have also been machined using abrasive waterjet cutting. The major disadvantages are high capital cost and high noise levels during operation.

7.3.2 Electrochemical machining

During electrochemical machining the workpiece material is removed by making it the anode of an electrolytic cell, causing dissolution of the workpiece. As shown in

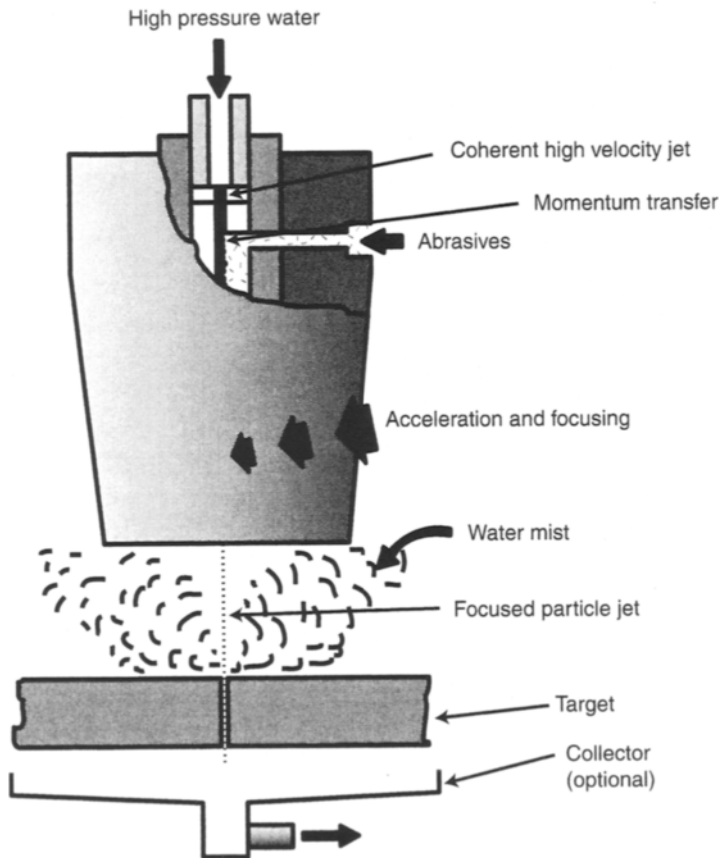


Fig. 7.34 Abrasive waterjet machining.

Fig. 7.35, an electrolyte is pumped through a gap between the tool and workpiece. By appropriately shaping the tool, complex surfaces can be produced. Typical operating parameter ranges are listed in Table 7.4 and the process can achieve metal removal rates of around $2 \text{ cm}^3/\text{min}$ for many common metals.

Electrochemical machining can be applied to most metals but, due to the high equipment costs, is usually used primarily for highly specialized applications involving complex shapes, such as turbine airfoils, valuable parts or noncircular holes in hard steels.

7.3.3 Electrical discharge machining

During electrical discharge machining (EDM) a shaped electrode of graphite or copper is placed a small distance away from the workpiece, and an electrical potential applied between the electrode and workpiece which is immersed in a dielectric, typically of light oil. The general arrangement of the EDM process is illustrated in

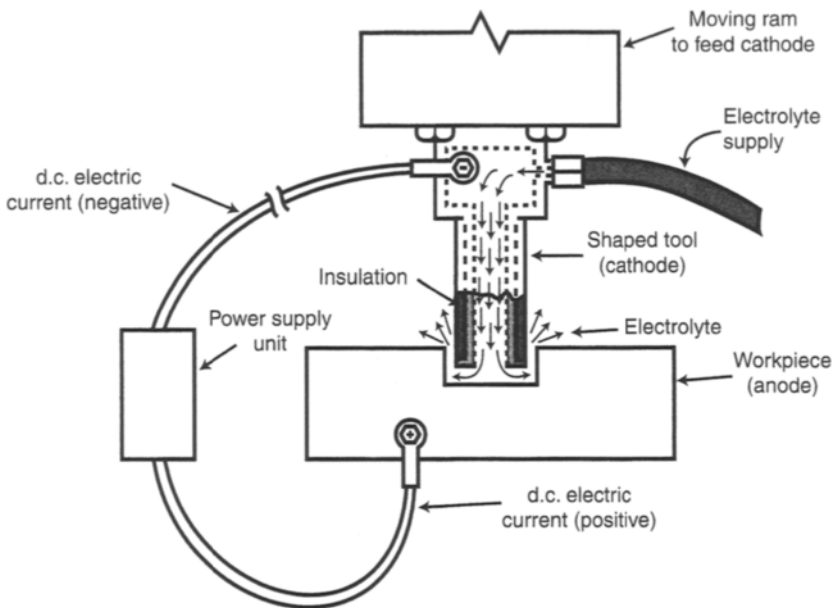


Fig. 7.35 Electrochemical machining. (Reprinted with permission from *ASM Materials Engineering Dictionary*, edited by J.R. Davis (1992), ASM International, Materials Park, OH 44073-0002, p. 137, Fig. 150.)

Fig. 7.36. A potential of between 40 and 400 V (d.c.) and current of up to 400 A is applied in pulses of between 180 and 300 kHz. As the pulse potential rises the temperature of the dielectric between the electrode and workpiece increases, causing a small volume of dielectric to vaporize, ionize and form a spark. The high temperature spark melts and vaporizes a small portion of the workpiece. Between each pulse fresh dielectric flows into the electrode–workpiece gap, flushing the metal removed from the workpiece. This whole process occurs in several microseconds. The advance of the electrode into the workpiece is controlled by continuously monitoring the potential across the dielectric fluid.

EDM is capable of machining hardened materials without distortion or breakage, and has found application in the aerospace, automotive and tool and die industries. Nozzles for automotive fuel injection systems require several holes of about 0.2 mm diameter, which are often fabricated by EDM.

Table 7.4 Electrochemical machining parameters

Process parameter	Range
Current	50–40 000 A
Current density	8–230 A/cm ²
Voltage	4–30 V (d.c.)
Tool–workpiece gap	0.025–0.7 mm
Electrolytes	organic salts, strong acids, NaOH solutions
Electrolyte velocity	15–60 m/s
Electrolyte pressure	70 kPa–2.7 MPa
Electrolyte temperature	25–65°C
Feed rate	0.5–19 mm/min

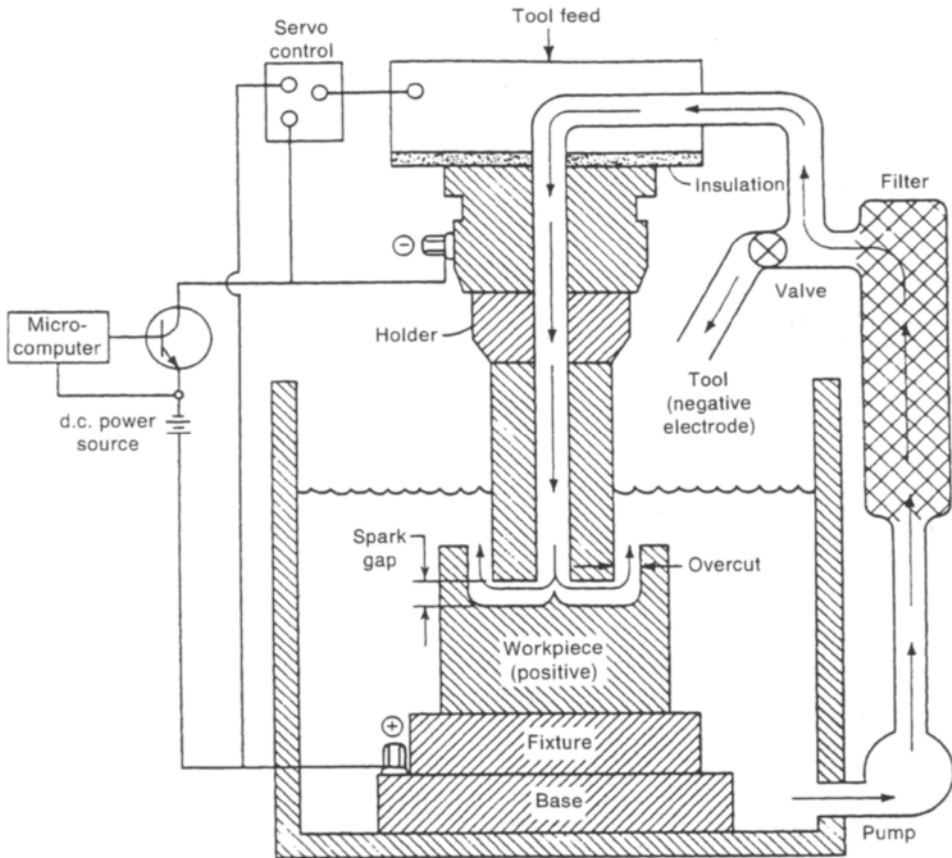


Fig. 7.36 Arrangement of equipment for electrical discharge machining. (Reprinted with permission from *ASM Metals Handbook, Ninth Edition*, Vol. 16, Machining (1989), ASM International, Materials Park, OH 44073-0002, p. 557, Fig. 1.)

7.3.4 Electron beam machining

This machining method involves emitting electrons from a filament and accelerating the electrons to high velocity (about 60% of the speed of light), by passing them through an electrical potential of between 100 and 150 kV. Magnetic coils are used to focus and position the beam of electrons to a high power density of at least 10^6 W/mm^2 . When the electron beam strikes the workpiece its kinetic energy is converted into heat. The high power densities are sufficient to instantly melt and vaporize any material, regardless of melting point or thermal properties. This allows holes to be drilled at penetration rates that far exceed rates achievable by any other process. The major disadvantage of electron beam machining is that the whole process must be carried out in a good vacuum (maximum pressure 1 Pa) and this contributes to relatively high equipment costs.

Electron beam drilling is used predominantly in applications, requiring many holes in thin sections (up to about 10 mm in diameter). Holes can be produced with depth to

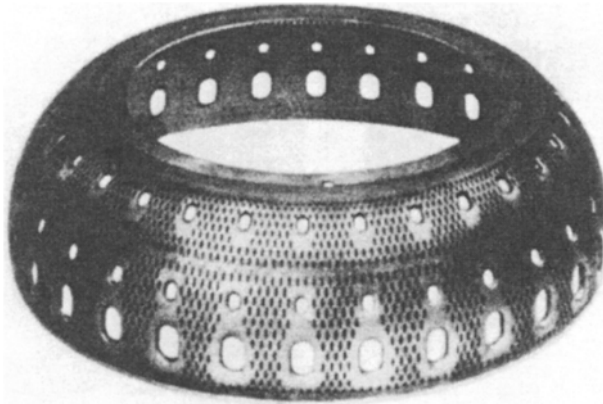


Fig. 7.37 Housing for a jet engine combustor with electron beam drilled cooling holes. (Reprinted with permission from *ASM Metals Handbook, Ninth Edition*, Vol. 16, Machining (1989), ASM International, Materials Park, OH 44073-0002, p. 571, Fig. 8.)

diameter ratios of up to 15:1 and as small as 0.1 mm in diameter. An application that exemplifies the advantages of electron beam drilling is the jet engine combustor shown in Fig. 7.37. This combustor was fabricated from a Cr–Ni–Co–Mo–W steel of 1.1 mm thickness and 3800 holes of 0.9 mm diameter were required. Using electron beam drilling these holes can be produced in about 1 h.

7.3.5 Laser beam machining

Lasers can be used to cut, drill, weld, mark, heat treat surfaces or apply clad layers. As a result of this flexibility the laser processing of materials is a rapidly growing field. Lasers operate by using light to raise atoms to a higher energy level which, when they decay to their base energy level, emit a photon. When this photon contacts another atom in the raised energy state, the second atom reverts to its base energy level and also emits a photon. The two photons produced are identical in wavelength, phase, direction and energy. This sequence is referred to as *stimulated emission*. Although all materials can undergo stimulated emission, there are several conditions that must be satisfied to achieve a workable laser. These conditions are related to the power of the light source and a feedback mechanism to ensure the continued stimulated emission of photons. In fact, most of the photons produced are used to amplify the process through further stimulated emission, with a small portion of the photons allowed to escape as laser light. This sequence of events leads to the name, laser – *light amplification by stimulated emission of radiation*. A major advantage of laser light is a high energy content. A 100 W light bulb at 1 m distance provides a power density of 0.0008 W/cm^2 , whereas a 100 W laser at 1 m with a focused 1 cm diameter beam provides more than 100 000 times this power density. When focused, the laser power density can be increased to $800\,000 \text{ W/m}^2$, enough for heating, melting, welding and cladding applications. For cutting and drilling a focused laser of between

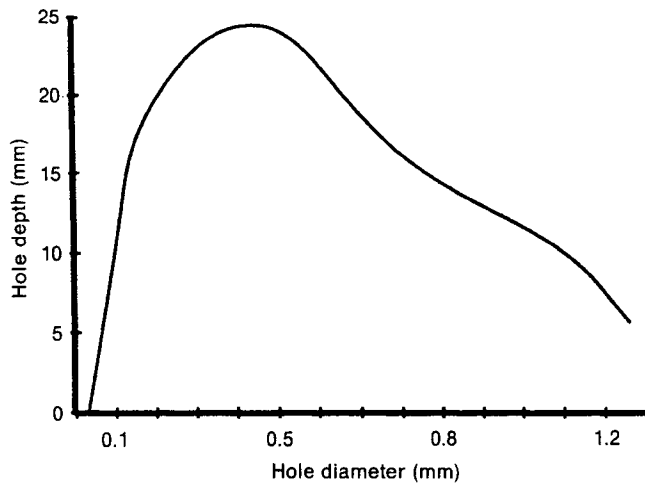


Fig. 7.38 Relationship between hole depth and diameter for laser drilling.

1.5×10^6 and $1.5 \times 10^8 \text{ W/cm}^2$ is required. At these power levels material is removed by sublimation. Laser machining has the advantages of a low heat input rate, it is easily adapted to automatic controls and rapid processing speeds are possible. The disadvantages are a high capital cost, some hole taper, and highly reflective metals can be difficult to machine.

Most metal processing utilizes neodymium–glass (Nd:glass), carbon dioxide (CO_2) or neodymium-doped yttrium aluminium garnet (Nd:YAG) lasers. CO_2 lasers cut faster, but Nd:YAG lasers provide a pulse energy that permits drilling and cutting at angles and thicknesses not possible with CO_2 lasers. Lasers can drill through thicknesses of 25 mm and are typically used for hole diameters between 0.25 and 1 mm. However, not all hole diameters can be produced in all thicknesses, as shown in Fig. 7.38. CO_2 lasers provide faster cutting rates, about 3 m/min to cut 4 mm thick carbon steel. During cutting a gas jet, coaxial with the laser beam, is used to remove molten metal from the cut.

7.4 Comparison of methods

For many applications there is an obvious advantage to the use of one or another particular machining process. This selection may be based on cost, material removal rate or equipment availability. Nevertheless, it is instructive to compare the relative attributes of nontraditional processes versus conventional metal cutting, as illustrated in Fig. 7.39. It is clear that the combination of metal removal rate, power required and capital cost of the conventional machining processes is very favourable, and this fact explains the continued widespread use of these processes. Also, in comparison to many nontraditional techniques, conventional methods can achieve similar surface finish and tolerances. The nontraditional techniques are most widely used for producing geometries not possible by conventional methods, or for applications that can benefit from associated high productivity rates.

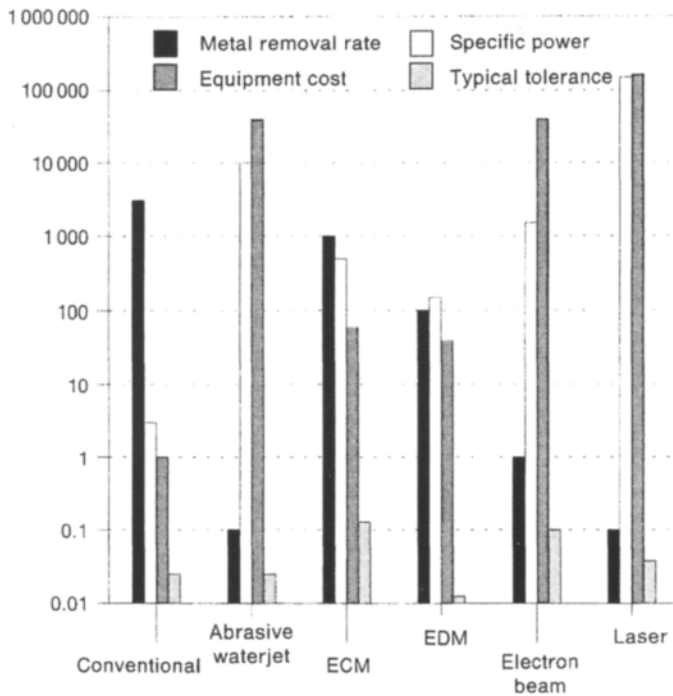


Fig. 7.39 Comparison of machining methods. Units: metal removal rate, mm/s³; equipment cost, conventional = 1; specific power GJ/m³ and typical tolerance, ±mm.

7.5 Problems

- 7.1 Shape castings for a machine part are made from cast iron. The casting has the general shape of a cylinder with an end 250 mm in diameter, which must be faced to ensure dimensional accuracy. The facing operation is performed on a lathe with a 1 kW motor and rotational speed of 100 rpm. The feed is 0.3 mm per revolution and the tool cutting edge angle is 70°. If this cutting operation has an efficiency of 0.7, what is the maximum cutting depth possible?
(Answer: depth of cut = 1.1 mm)
- 7.2 A shaper machines a 2 mm layer of material from the surface of a low carbon steel workpiece. The workpiece is 150 mm wide and 200 mm long. The shaper operates at 50 strokes per minute, with a stroke of 250 mm. The angle of the tool cutting edge is 30° and the feed is 0.25 mm per stroke. Calculate the metal removal rate, power required and estimate the time to remove the 2 mm layer.
(Answer: MRR = 417 mm³/s, power = 2.4 kW, time is 12 min)
- 7.3 A twist drill with a major cutting angle of 60° is used to make a hole in aluminium. If the feed is 0.25 mm per revolution and the maximum power is 1 kW, what is the maximum hole diameter that can be made if the drill speed is 600 rpm? If the drill speed is reduced to 300 rpm, what is the maximum hole diameter?

(Answers: at 600 rpm, maximum hole diameter is 17.8 mm; at 300 rpm, maximum hole diameter is 25.2 mm)

- 7.4 Two 150 mm rods of type 302 stainless steel are 12.5 mm diameter and are to be reduced in diameter to 12 mm. One rod is turned to the new diameter on a lathe in one pass with a rotational speed of 600 rpm, feed of 1 mm with a cutting angle of 60° . The other rod is pulled in uniaxial tension. Compare the energy required for machining to the ideal work of deformation for pulling in uniaxial tension. Comment on the difference. (The limit of homogeneous deformation for 302 occurs at a true strain of about 0.3.)

(Answer: machining energy = 3171 J, energy for uniaxial tension is 713 J)

- 7.5 A plate of copper is to have a slot cut in it of 25 mm width and depth 4 mm. The slot can be machined by grinding or milling. The workpiece is delivered to the grinding wheel or milling tool at 1 mm/s. The grinding wheel and milling tool widths are both 25 mm. The milling tool has 16 teeth, rotates at 40 rpm and has a diameter of 100 mm. Compare the power required for both operations.

(Answer: power for grinding is 823 W, power for milling is 760 W)

- 7.6 An orthogonal machining operation is performed on a mild steel part 5 mm wide. The tool cutting depth is 0.25 mm, thickness of the chip is 0.35 mm and the tool rake angle is 10° . From a tool post dynamometer the cutting force is measured as 1900 N. Determine the shear angle, the friction coefficient between the chip and tool face, and estimate the shear strength of the workpiece material. (Answer: shear angle is 38.5° , friction coefficient is 0.42, workpiece shear strength is about 605 MPa)

- 7.7 (a) An orthogonal machining operation has a tool rake angle of 7° , a cutting depth of 1 mm and the chip thickness is 1.5 mm. Assuming that Merchant's analysis is correct, what is the tool-chip friction coefficient?
 (b) If the tool rake angle is increased to 17° , and assuming that the coefficient of friction is not influenced by the change in tool rake angle, calculate the chip thickness for the new rake angle.

(Answers: (a) $\mu = 0.48$, (b) $d'_c = 1.4$ mm)

- 7.8 A machining operation is found to follow the Taylor tool life equation with $C = 400$ and $n = 0.5$. For this operation calculate the percentage increase in tool life if the cutting speed is reduced by 50%.

(Answer: 300%)

- 7.9 A metal machining operation requires 40 min to complete and during this time one tungsten carbide tool is worn out. To meet increased production requirements, the cutting time can be cut in half by either (a) doubling the speed, or (b) doubling the feed rate. What will be the tool life for these two options? Comment on the advisability of making the change to reduce the production time. Assume the generalized tool life equation for this cutting operation is

$$vt^{0.25}f^{0.75}d^{0.80} = C'$$

(Answers: (a) time is 2.5 min, (b) time is 5 min)

- 7.10 The tooling illustrated in Fig. C4.4 contains a small diameter hole down the centre of the punch used for redrawing and ironing beverage cans. The hole serves to deliver pressurized air to aid removal of the formed can from the punch. The hole is quite small in diameter ($\approx 0.5\text{--}1\text{ mm}$) and at least 20 cm long. Consider the advantages and disadvantages of machining this hole using the various techniques presented in this chapter and decide on the most suitable technique for producing this hole.

Joining processes

8.1 Introduction

All of the previous chapters have focused on processes that primarily change the shape of individual components. *Joining* processes differ in that at least two components are joined together, thereby allowing more complicated or larger structures to be fabricated. A wide range of joining techniques are used in various manufacturing operations, including myriad different mechanical fasteners, adhesives, welding, brazing and soldering. Figure 8.1 classifies some of the major processes associated with each type of joining operation. Several joining operations are more akin to assembly than to metal processing. The major metal processing techniques include *welding*, *brazing* and *soldering*. A characteristic of these techniques is that the interatomic bonding within the base material, or at least on the surface, is altered, potentially changing the properties of the base material. The control of the base material properties during joining requires special attention to process parameters and has important ramifications in terms of serviceability. In light of this situation, and in keeping with the metal processing emphasis of this book, this chapter deals with welding, brazing and soldering.

8.2 Welding

As shown in Fig. 8.1, there are a number of welding processes available for joining. These techniques are applied to structures varying in size from pipelines of several thousand kilometres in length, supertankers and off-shore oil platforms, to intermediate sized structures such as automobiles and railway rolling stock. In addition, many welding techniques are used to produce manufactured assemblies that may not appear to involve welding at all. Welding also has important applications for the repair of structural assemblies. Welding processes are conveniently divided into two classes: *fusion welding* and *solid state welding*. During fusion welding a portion of the base materials to be joined is melted and mixed, often with the addition of a *filler metal*, forming a solid joint after subsequent solidification. As the name implies, during solid state welding the base material is not melted. Joining occurs by a process other than solidification, and very often involves diffusional processes.

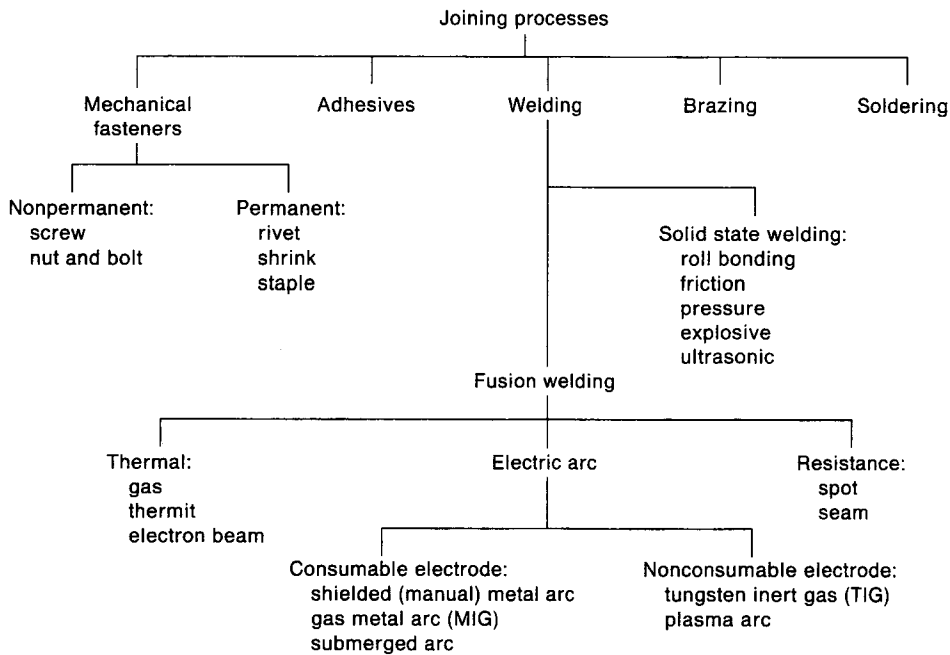


Fig. 8.1 Classification of joining processes.

Although almost all engineering metals can be joined by welding, for many, welding is not recommended due to poor *weldability*. Similar to the problem of quantifying machinability, discussed in the previous chapter, weldability is a poorly defined term. For many engineering metals, even though they may be welded, the properties following welding are so poor as to render the workpiece of no engineering usefulness. Poor properties can be caused by microstructural changes or cracking caused by the welding process. These problems are dealt with later in this chapter.

8.2.1 Fusion welding

Referring to Fig. 8.1, the fusion welding processes are classified in terms of the source of heat used to cause localized melting: *electric arc welding*, *thermal welding* and *resistance welding*. In terms of the absolute number of welds made, fusion welding is the most common welding technique. The following begins by describing each of these welding processes.

Electric arc welding

All of the electric arc welding processes rely on the formation of an arc between an electrode and the base material to provide heat. An electric arc forms when there is an electrical discharge between two metal objects that are not in contact with one another – in the case of arc welding the two objects are the electrode and base metal workpiece. The arc ionizes the gas between the electrode and base metal, thus creating a *plasma*, with temperatures exceeding 10 000°C, which causes local

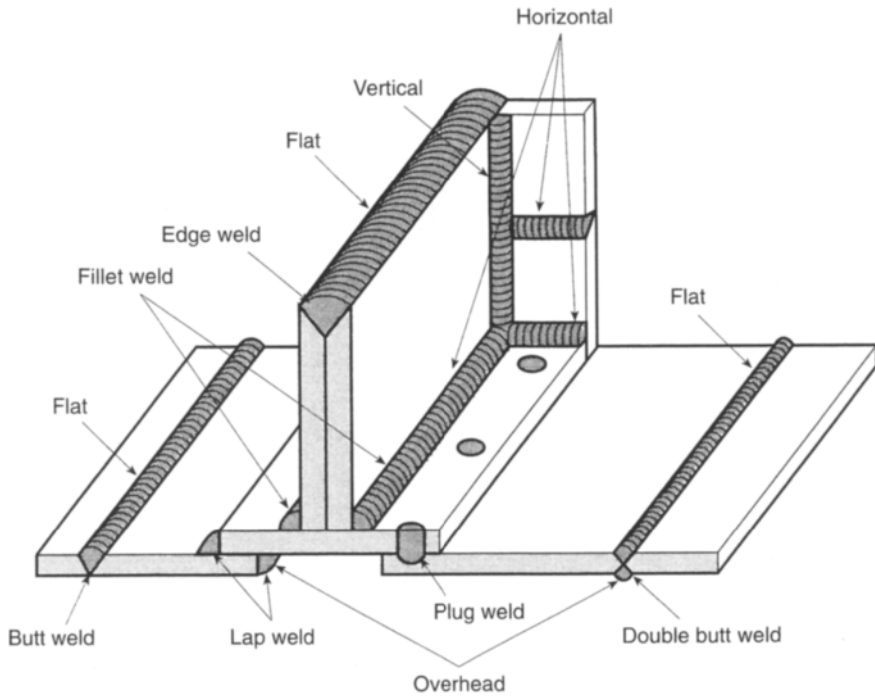


Fig. 8.2 Typical geometries of welds produced by electric arc welding processes.

melting of base metal. Depending on the technique, the electrode may or may not be consumed, i.e. the electrode may form into metal droplets that are added to the weld zone. During fusion welding the high temperatures associated with the melted weld pool can cause rapid oxidation. The oxides that form can be entrapped within the weld metal, severely degrading the mechanical properties and corrosion resistance of the joint. Therefore, in all electric arc processes provision must be made to protect the weld zone from the surrounding atmosphere. This protection most often takes the form of a gaseous shield.

The electric arc processes are used to weld a variety of geometries, such as those illustrated in Fig. 8.2. The weld microstructure resulting from electric arc welding is illustrated in Fig. 8.3. Several important features of arc welding are apparent in Fig. 8.3. First, the edges of the two plates to be welded are usually prepared prior to welding by machining a shape such as a V on each edge of the constituent plates. This forms a repository for the weld metal and helps ensure alignment. Second, the weld of Fig. 8.3 requires access to both sides of the joint with six or seven weld passes applied to each side. The microstructure resulting from each of these passes is delineated in the figure. The weld structure consists of two important zones. A *fusion zone* exists in the centre of each pass in which a molten weld pool has solidified. The fusion zone consists of a columnar grain structure, the result of directional cooling during solidification (see Section 2.3.1). A *heat affected zone* (HAZ) occurs along the edge of the fusion zone. The HAZ consists of base metal that has undergone some form of microstructural modification during welding, but

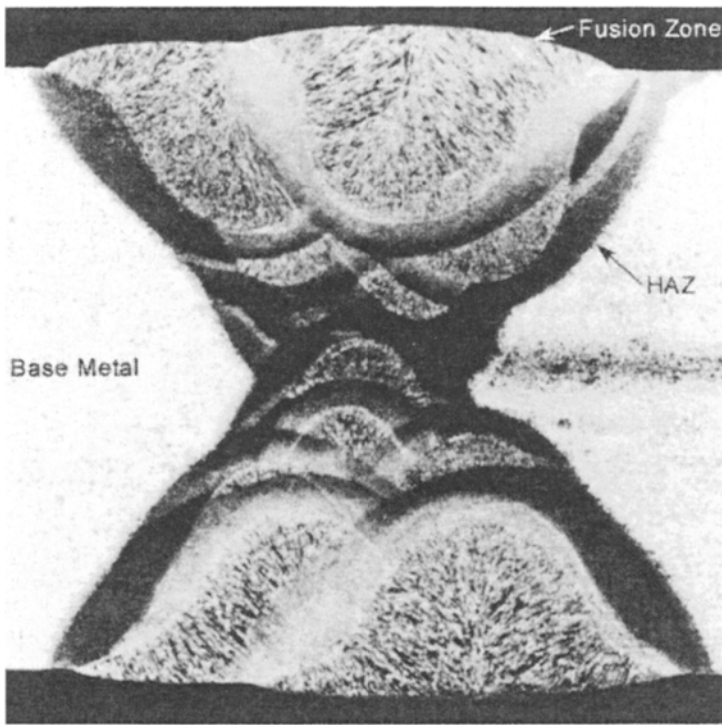


Fig. 8.3 Cross-section of multipass electric arc weld to join two mild steel plates.

no melting has occurred. The importance of these two zones is discussed later in this chapter.

The ability to produce a sound weld requires not only good equipment, appropriate preparation of the base metal, but also a skilled operator. For example, the ability to produce a sound overhead weld is not straightforward. It is unlikely that many engineers or engineering students could produce a sound weld by any technique, let alone an overhead weld, without specific training!

It must be stressed that, like many of the metal processing procedures presented in this book, there are several safety hazards associated with all welding processes. These range from eye damage, to the problem of dealing with pressurized fuels. Therefore, no welding procedure should be undertaken prior to adequate training, which must include health and safety procedures.

Shielded (manual) metal arc welding The shielded or manual metal arc (SMA) process, shown in Fig. 8.4, is widely used for the fabrication of pressure vessels, pipework and pipeline joints, as well as for the repair and maintenance of industrial machinery. An arc is established between the electrode and the base metal at the joint line. The arc melts a portion of the base metal and the electrode to form a weld pool. The molten metal is protected from the surrounding atmosphere by decomposition of the electrode coating which forms a gaseous CO_2 cloud. The electrode coating also contains *fluxes* that remove impurities from the molten metal. The flux aids the formation of a *slag* layer that serves to further protect the cooling weld metal from atmospheric

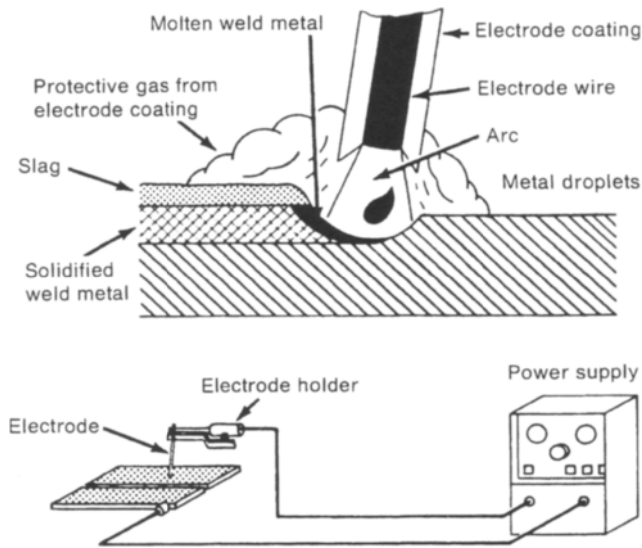


Fig. 8.4 Shielded or manual arc welding. (Reproduced with permission of Nickel Development Institute publication 9002; *Welding of Stainless Steel and Other Joining Methods*.)

contamination. The slag layer is usually removed once the joint area has cooled. The operator moves the electrode along the joint length at a steady rate and, to maintain a constant arc length, moves the electrode holder closer to the weld pool as the electrode is consumed. Electrodes are typically 460 mm in length and are consumed to a final length of about 50 mm. At this point the process is interrupted and the electrode replaced.

The electrode coating tends to absorb moisture which, if present during welding, can lead to hydrogen diffusion into the molten pool and gas porosity, similar to the formation of the gas porosity encountered during casting (Section 2.6.2). Therefore, electrodes must be stored and handled carefully. Usually electrodes are not removed from their protective packaging until immediately before use. Some electrodes require heating to drive off all moisture. Failure to handle electrodes properly, or poor cleanliness around the joint, has led to the failure of many welded joints.

During SMA welding the power supply can deliver either a.c. or d.c. The potential difference between the electrode and the base metal causes ions within the arc plasma to accelerate and strike the electrode or base metal. The kinetic energy of the ions is converted into heat for the welding process. The electrode can be negatively charged, which is referred to as *straight polarity*, or positively charged, referred to as *reverse polarity*. If an a.c. potential is supplied the polarity fluctuates. As negative ions (electrons) are accelerated to higher velocities, they cause greater heating than the positive ions. Therefore, the penetration of the joint region is greater with straight polarity (base metal positively charged), causing deeper welds. Reverse polarity causes faster consumption of the electrode, thereby increasing the amount of the metal deposited into the joint as filler. This may be advantageous if a joint with a large gap is to be welded. Alternating current is sometimes utilized for welding aluminium

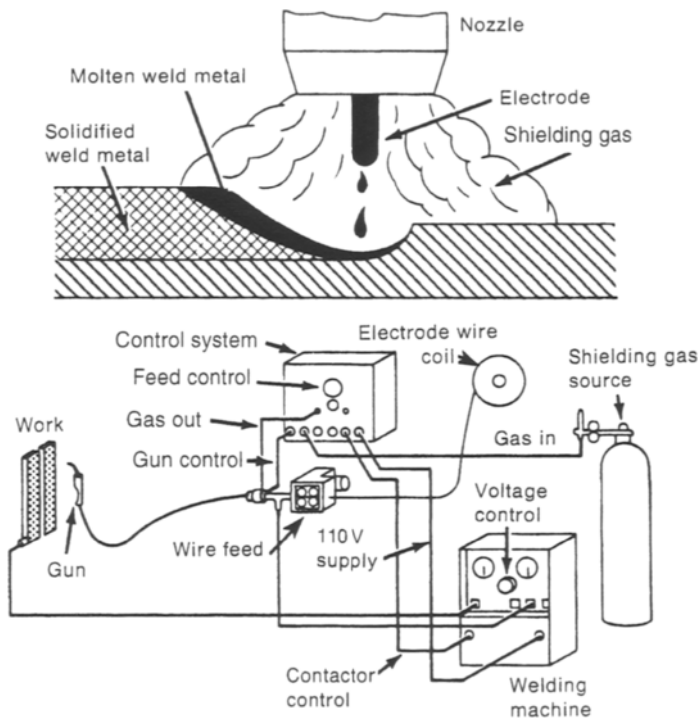


Fig. 8.5 Equipment arrangement for inert gas arc welding. (Reproduced with permission of Nickel Development Institute publication 9002; *Welding of Stainless Steel and Other Joining Methods*.)

or magnesium, which provides enhanced removal of oxides from the molten metal. If the electrode is consumed it becomes part of the joint and must be an alloy compatible with the base metal. Electrodes are classified according to composition, polarity and type of coating.

Metal inert gas arc welding The metal inert gas arc welding (MIG) process, shown in Fig. 8.5, differs from the SMA process in several important respects. The electrode for MIG welding takes the form of an uncoated wire, usually the same alloy as the base metal, which is fed to the joint area from a coil. The molten pool is protected from the atmosphere by a shielding gas, delivered to the welding gun under pressure. The shielding gas is typically argon for ferrous alloys, and an argon/helium mixture for aluminium and copper alloys. The advantages of MIG welding, compared with the SMA process, include: the unrestricted length of the electrode, making the welding of long joints more practical; faster deposition speeds; a more stable arc, which requires less operator skill to control; and improved shielding of the weld pool, leading to welds with lower levels of gas porosity. The major disadvantage is the increased cost of the welding equipment.

Reverse polarity (positive electrode) is used for most MIG welds. This arrangement provides a more stable arc than the straight polarity arrangement, and faster welding speeds are possible. The latter results from electrons striking the consumable electrode (welding wire) which is more quickly melted and deposited into the joint area.

Additionally, as MIG welding involves the transfer of metal droplets from the electrode to the base metal, unlike SMA welding, relatively deeper penetration is obtained with reverse polarity. If straight polarity is used, the large positive ions travelling toward the electrode tend to support the metal droplets, which results in shallow weld penetration. Conversely, the metal droplets are subjected to a considerable downward force by the large positive ions when reverse polarity is used, which results in greater depth penetration.

Tungsten inert gas arc welding In contrast to MIG welding, tungsten inert gas (TIG) arc welding involves the use of a nonconsumable electrode made of tungsten or a tungsten alloy (often W-2 wt% ThO₂). Similar to MIG arc welding, TIG utilizes an inert gas, usually argon, to protect the weld pool from atmospheric contamination. As illustrated in Fig. 8.6, TIG arc welding is sometimes applied without the use of a filler metal, relying on the local melting of the base metal only to provide fusion. This characteristic allows easier joining of dissimilar metals and makes TIG welding more suitable for welding stainless steel, aluminium, and other nonferrous metals. As no filler metal is added, TIG welding requires the base metal to be cleaned well prior to welding for a sound defect-free joint to be produced. If filler metal is required, it may be added manually by the operator in the form of consumable rods, or semi-automatically from coils of wire. Straight polarity is most often used for TIG welding

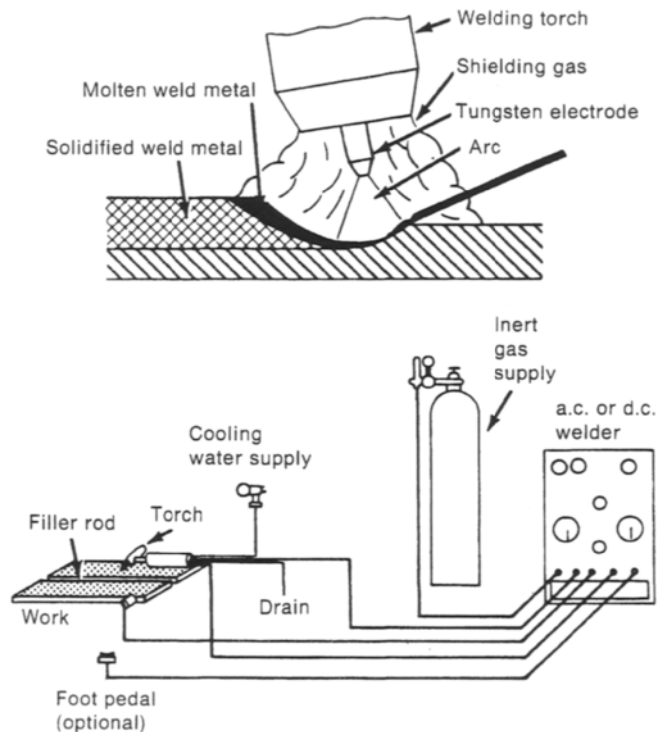


Fig. 8.6 Diagram and equipment arrangement for tungsten inert gas welding. (Reproduced with permission of Nickel Development Institute publication 9002; *Welding of Stainless Steel and Other Joining Methods*.)

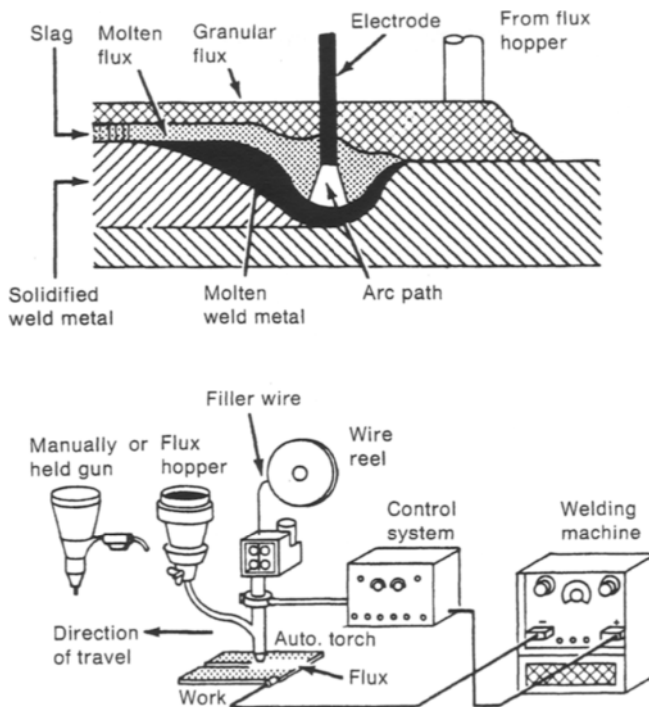


Fig. 8.7 Diagram and equipment arrangement for submerged arc welding. (Reproduced with permission of Nickel Development Institute publication 9002; *Welding of Stainless Steel and Other Joining Methods*.)

because, as with shielded or manual arc welding, this provides the deepest weld penetration into the base metal.

Submerged arc welding The submerged arc welding process utilizes an electrode of consumable wire to produce an arc that is submerged below a flux layer, as shown in Fig. 8.7. Granular flux is applied to the joint area immediately prior to welding. A portion of the flux is melted which acts chemically to lower the oxygen, nitrogen and sulphur contents of the weld pool. The unmelted flux protects the weld from the surrounding environment and eliminates fumes and arc flash, reducing the health risk associated with the process.

Important differences between submerged arc welding and other electric arc welding processes are a substantially higher heat input rate and a lower solidification and cooling rate. The former advantage makes this welding process more suitable for welding thick sections (most commonly greater than 6 mm), whereas the latter advantage offers improved control of the fusion zone and HAZ microstructure. Submerged arc welding has the disadvantage of increased equipment costs and the joint must be positioned horizontally to sustain the granular flux. Submerged arc welding is most often applied to thick sections of pipe, bridges, pressure vessels, shipbuilding or other heavy structural applications. The use of a d.c. electrode potential is most common in North America, whereas elsewhere an a.c. potential is regularly used. Direct currents greater than 1000 A can cause arc stability problems.

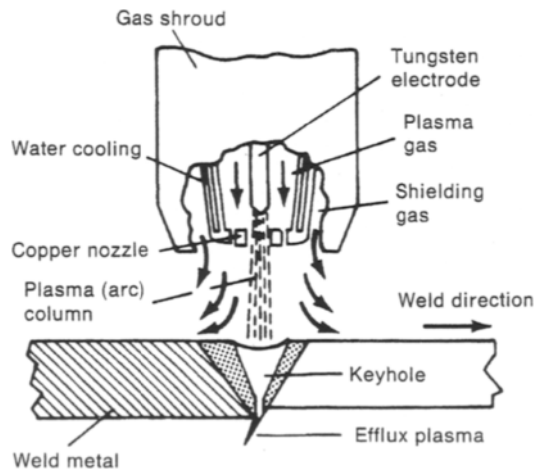


Fig. 8.8 Plasma arc welding process. (Reprinted with permission from *ASM Metals Handbook, Ninth Edition*, Vol. 6, Welding Brazing and Soldering (1993), ASM International, Materials Park, OH 44073-0002, p. 195, Fig. 1.)

Plasma arc welding Like the TIG and MIG processes, the plasma arc welding (PAW) process utilizes an inert gas for shielding the molten weld metal, and like TIG a non-consumable tungsten electrode is used. As seen in Fig. 8.8, the plasma arc is forced through a relatively small copper nozzle, providing a higher energy density within the plasma. The higher energy density permits the welding of greater thicknesses in a single pass with minimal joint preparation.

Although there are several modes of operation for PAW, the mode that highlights the benefits of this method is the *keyhole* method illustrated in Fig. 8.8. In this method the arc fully penetrates the workpiece, forming a hole concentric with the arc. The molten metal flows around this hole and resolidifies behind the arc as it moves along the joint line. Welding currents are typically about 300 A, but can be as high as 500 A. Polarity during plasma arc welding can be d.c. straight polarity or a.c. Similar to shielded or manual arc welding, the reverse polarity phase of the a.c. potential can provide improved removal of the surface oxide from the base metal. This is particularly important when welding aluminium, which has a tenacious surface oxide layer. The major disadvantage of PAW is its higher capital cost, even compared with TIG welding. Also, the constriction of the arc through the copper nozzle reduces the tolerance of the process to joint gaps or misalignment.

The PAW process is widely used to weld stainless steel circumferential pipe joints. This process could be performed using TIG welding, but would require greater joint preparation, a backing ring around the pipe internal diameter, and probably necessitate the use of filler wire. The PAW process permits the welding of square butt joints in one pass on pipe thicknesses up to 7 mm. Thicker pipe sections can be performed in two passes, with filler metal addition during the second pass.

Some of the attributes of the electric arc welding processes presented are summarized in Table 8.1.

Table 8.1 Summary of electric arc welding processes

Process	Shielding	Typical polarity	Current range (A)	Heat input (kJ/s)	Typical applications
Shielded manual metal arc	flux and gas generated by flux	straight, reverse or a.c.	25–350	0.5–11	pressure vessels, ships, repair, pipe
MIG	inert gas	reverse	60–500	1–25	medium gauge fabrication, automobile body repair
TIG	inert gas	straight	10–300	0.2–8	Al, Ni, Cu, stainless steel, sheet metal
Submerged arc	granular flux	a.c. or d.c.	350–2000	9–80	thick plate, pressure vessels, bridges, ships, pipe, structural work
PAW	inert gas	straight or a.c.	115–240		thick plate, stainless steel

Thermal welding

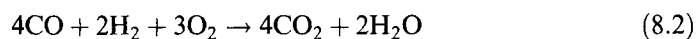
In some sense, all of the electric arc processes described in the previous section could be considered thermal processes, as all rely on heating to provide fusion. However, it is useful to delineate between the processes that generate heat via electric techniques and those generating heat by other methods. In this latter category there are many welding processes, but of particular interest are gas welding, thermit welding and the electron beam process.

Gas welding Gas welding involves mixing a combustible gas (most often acetylene, C_2H_2) and oxygen in a nozzle which is ignited to generate heat. The flame produced is directed onto the joint area to provide rapid melting of the base metal. Acetylene and oxygen are stored in high pressure cylinders and, therefore, the major advantage of the whole process is portability, without the requirement for an electrical supply. Most ferrous and nonferrous metals can be gas welded, usually with the addition of an appropriate filler metal during welding.

A key part of the gas welding system is the mixing nozzle or *torch* shown in Fig. 8.9. The torch contains provision for independently adjusting the acetylene and oxygen flow rates, and a mixing chamber. Initially, the mixed gas is ignited manually as it exits the welding tip and the oxygen and acetylene flows are adjusted to maintain a stable flame. The flame produced has two distinct zones (Fig. 8.10). The *luminous zone* has a dark blue colour and temperatures within this zone reach 3500°C . The reaction occurring in this zone corresponds to



The oxygen in this reaction is supplied from the pressure cylinder. The second zone, the *outer envelope*, achieves temperatures of 2100°C and the combustion corresponds to



The oxygen burned in this zone is supplied from the surrounding atmosphere.

Equation 8.1 assumes that the combustion of acetylene and oxygen occurs at a ratio of about 1 to 1, implying that all acetylene and oxygen are consumed during combustion. This is referred to as a *neutral flame* and is usually desirable for welding steels.

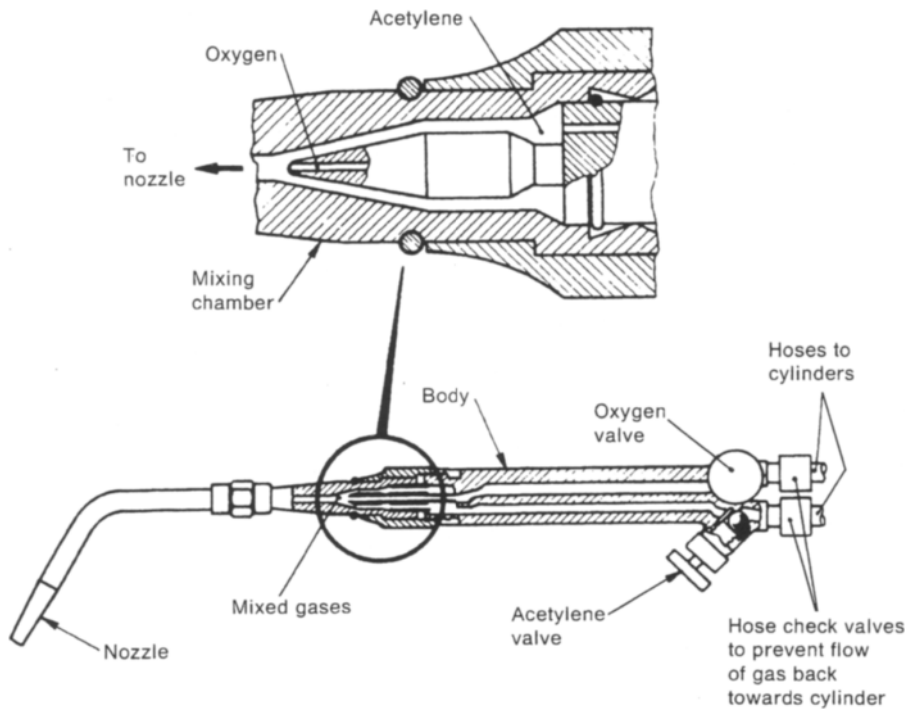


Fig. 8.9 Torch for gas welding with oxygen and acetylene.

If a sufficient excess of acetylene is present, termed a *carburizing flame*, this will produce free carbon during combustion which, at the high base metal temperatures that exist during welding, can diffuse into the base metal and may deleteriously affect the weld properties. For example, it can cause poor corrosion resistance in stainless steels. Nevertheless, slightly carburizing flames are often used for welding steels. Conversely, if excess oxygen is present during the welding of steel, oxides may form in the weld metal, degrading the joint. Strongly *oxidizing flames* are sometimes used for welding copper and some copper alloys, but are rarely suitable for welding ferrous metals. For these metals a sufficiently high oxygen level causes the formation of a protective oxide slag on top of the weld pool, shielding the molten metal from the surrounding atmosphere. An experienced welder can determine the ratio of acetylene and oxygen from the colour, relative size, and shape of the luminous cone and outer envelope of the flame.

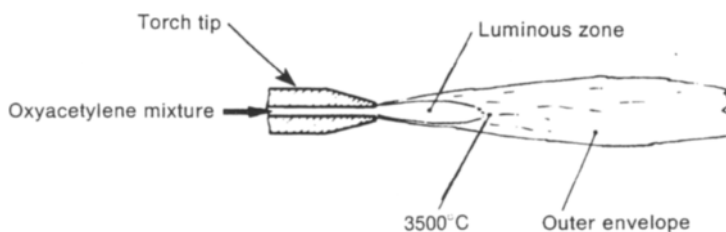
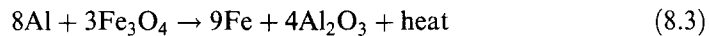


Fig. 8.10 Oxyacetylene flame for gas welding.

Although most of the weld geometries shown in Fig. 8.2 can be made using gas welding, the success of the weld depends in large measure on the skill of the operator and the preparation of the joint. The base metal to be welded must be clean and well fitted, often necessitating clamping the workpieces in jigs to maintain the joint geometry and dimensions during welding.

Thermit welding The heat for thermit welding is generated by the exothermic reaction between finely divided powders of a metal oxide (most commonly iron oxide for welding steels) and aluminium. As aluminium has a higher affinity for oxygen than iron (recall from Section 2.2.1 that aluminium is used as a deoxidizing agent prior to the casting of steel ingots), the exothermic reaction produces alumina and metallic iron according to the reaction



A 1 kg mixture of the reactants will produce about 760 kJ of heat and reach a temperature of over 3000°C. As shown in Fig. 8.11, the powdered reactants, or the *thermit*, are placed in a crucible above the metals to be joined and ignited by applying a magnesium fuse to a mixture of oxidizing agents (peroxides, chlorates etc.). Once the oxidizing agents achieve a temperature of more than 1200°C, the reaction of equation 8.3 will occur spontaneously, producing the products in a molten state. As the alumina is less dense than iron, it will float to the top of the crucible and form a slag that effectively protects the underlying molten iron from the atmosphere. The bottom of the crucible is tapped and the molten iron allowed to flow into a temporary mould surrounding the metal to be joined. The superheated iron causes the surface of the base metal to melt. In essence, the iron from the crucible not only provides the heat for welding, but also acts as a filler metal. After complete solidification and cooling, the temporary mould is removed and it is usually necessary to grind the welded joint to the desired shape.

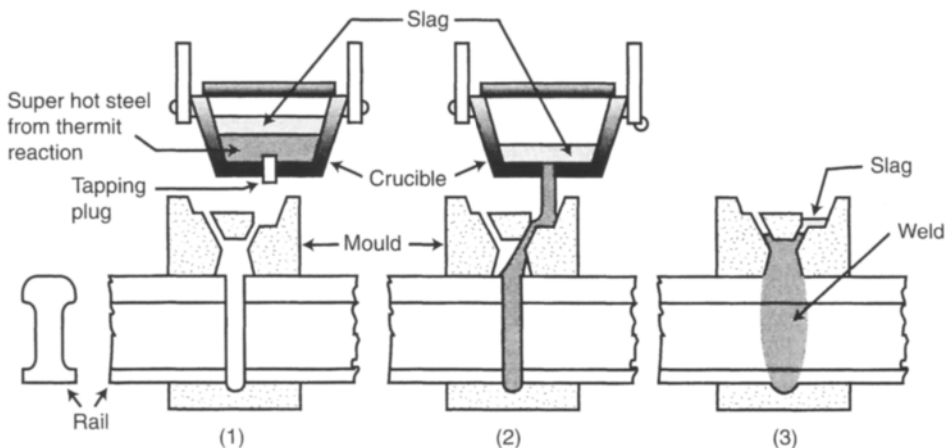


Fig. 8.11 Sequence of thermit welding of railway track. (1) Steel from thermit reaction ready to pour, (2) pouring of steel into temporary mould, and (3) cooling of welded joint prior to removal of temporary mould and grinding.

Thermit welding is used for welding large sections that often cannot be well fitted. It has been used since the 1920s to repair railway rails and recent developments of the process include thermit specifically designed to provide the hardness required for high strength rails. Thermit welding can be used to weld rails with a gap of as much as 75 mm, often allowing rail defects to be repaired without installing a new length of rail. An analogous copper oxide and aluminium reaction can be used for thermit welding of copper.

A hazard related to thermit welding is the presence of moisture within the thermit, crucible, mould or on the base metals. As highlighted in Example 2.1, liquid metals contacting moisture that is trapped within a cavity causes rapid superheating and the associated volume expansion can eject liquid metal from the crucible or mould. Therefore, all tools must be clean and dried by prolonged preheating prior to use.

Electron beam welding The source of heat for electron beam welding is a strongly focused beam of electrons that have been accelerated to about 60% of the speed of light. This is the same process as described for electron beam machining in Section 7.3.4. The high power density of the electron beam causes instant melting and vaporization of the base metals. The high kinetic energy of the electrons causes deep penetration into the base metal, allowing plates up to 75 mm thick to be welded in one pass. By any other method this would require multiple passes. Moreover, as the electron beam can be focused to a much smaller area than the heat supplied by gas or arc welding, a narrower weld is possible, thereby reducing distortion and shrinkage. The narrow beam also means that joints must be well fitted, usually with square rather than the angled edges shown in Fig. 8.3.

Like electron beam machining, electron beam welding must be undertaken in a vacuum. This substantially increases the cost of the process, but also eliminates any atmospheric interactions that may otherwise occur. Electron beam welding is particularly suitable for welding reactive metals, such as titanium or zirconium, which readily react with oxygen and nitrogen. Given these attributes, electron beam welding is capable of producing some very high quality welds in many different metals.

Resistance welding Resistance welding makes use of a material's resistance to an electrical current to provide heat for fusion. The parts to be joined are held together under force and electrodes apply a short electrical pulse (60 ms to 2 s) at low voltage (<10 V), but high current (several thousand amps). The electrical pulse causes melting at the contact between the two parts. When the electrical pulse ceases, the parts remain clamped while the metal parts solidify together and cool. The two major types of resistance welding are *spot welding* (Fig. 8.12) and *seam welding* (Fig. 8.13). For both these processes the electrodes also provide the clamping force to maintain contact between the surfaces to be joined. During spot welding the electrode and workpieces are stationary relative to one another, whereas for seam welding circular electrodes produce a continuous weld along the workpieces.

Resistance welding is ideally suited to the repetitive joining of sheet metal parts up to about 3 mm thickness. Spot welding operations have been highly automated for mass assembly of automobile body components. Seam welding offers the advantage of producing a gas- and liquid-tight seal at relatively high welding speeds (approximately 6 m/min). These attributes make the process suitable for joining sheet metal

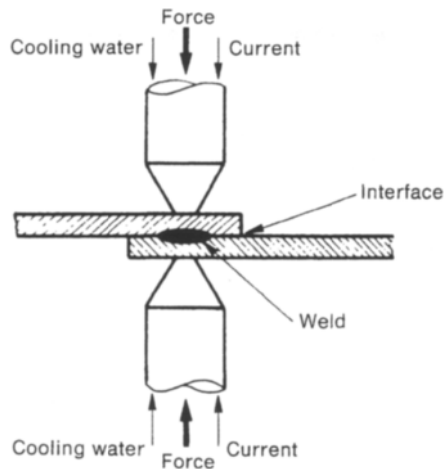


Fig. 8.12 Resistance spot welding.

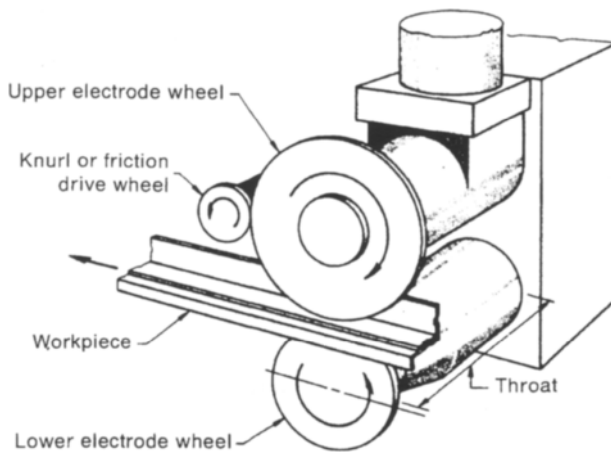


Fig. 8.13 Equipment arrangement for seam welding. (Reprinted with permission from *ASM Metals Handbook, Desk Edition*, edited by H.E. Boyer and T.L. Gall (1985), ASM International, Materials Park, OH 44073-0002 (formerly American Society for Metals, Metals Park, OH 44073), p. 30.48, Fig. 6.)

parts for automobile gas tanks, catalytic converters, mufflers, heat exchangers, water tanks and other similar applications.

Residual stress and distortion during fusion welding

During all fusion welding processes localized melting of the base metals occurs. This process not only introduces high thermal gradients in the base metal, but the molten weld pool undergoes solidification shrinkage during cooling. Shrinkage is restrained by the relative rigidity of the surrounding base material that remains solid throughout the welding process. This restraint gives rise to the formation of residual stresses in the welded region. For the simple geometry of two plates butt welded along one edge, the residual stress distribution is that shown in Fig. 8.14. As within the volume of

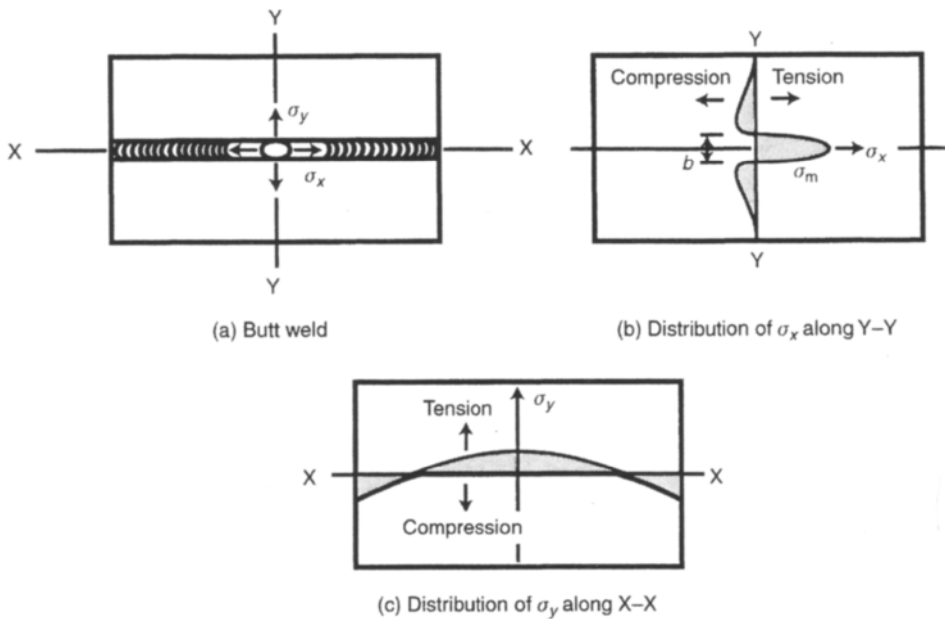


Fig. 8.14 Distribution of residual stresses in a butt joint.

the workpiece forces arising from residual stresses must sum to zero, both tensile and compressive residual stresses are formed. The magnitude of the residual stresses resulting from shrinkage loading can be high, typically approaching the yield strength, σ_m , of Fig. 8.14. Therefore, stresses equivalent to the yield strength exist in many welds, even without any external loading. Residual stresses that would otherwise exceed the yield point are relieved by local plastic deformation, which can lead to distortion of the weld and/or base metal. If the weld or base metal have insufficient plastic capacity to accommodate the distortion, then cracking may occur.

As discussed above, thermal stresses formed during welding cause workpiece distortion. Given the almost infinite number of joint geometries and welding conditions, calculation of the expected distortion is difficult. Numerous numerical computer routines, based on an analysis of the heat transfer and formation of residual stresses during welding, are available to estimate the final geometry of welded parts. The two most common weld geometries are the butt and fillet welds, and the distortion resulting from welding these geometries are shown in Fig. 8.15. Knowing that such distortion will occur, it may be possible to preset the base metal prior to welding to compensate for the deformation that can occur, as shown in Fig. 8.16.

For large structures, presetting may be impossible or impractical. Nevertheless, it is still important to know the magnitude of the welding distortion that will occur so that required component dimensions are respected. For the butt weld geometry of Fig. 8.15 the longitudinal distortion Δl is typically about 1 mm per metre of weld length. For steel, the force F associated with this distortion has been estimated empirically to be

$$F \approx 0.04EA_w \quad (8.4)$$

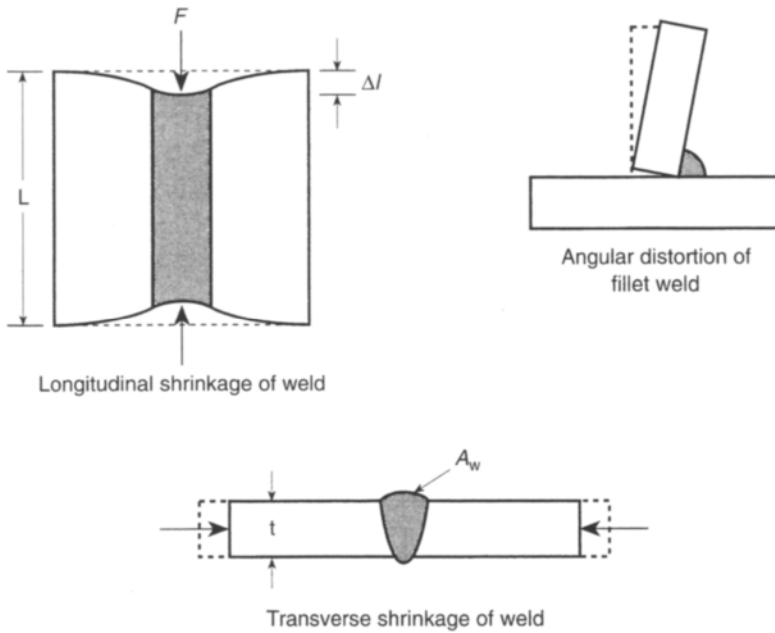


Fig. 8.15 Distortion common to butt and fillet welds. Butt welding results in longitudinal shrinkage, Δl , and angular distortion, δ .

where: E is the elastic modulus

A_w is the weld cross-sectional area (Fig. 8.15).

As shown in Fig. 8.15, rarely is a weld centred along the neutral axis of a workpiece. Therefore, the force causing longitudinal shrinkage also causes a bending moment, giving rise to bowing as illustrated in Fig. 8.17. Bending caused by weld shrinkage can be demonstrated by positioning a longitudinal weld at a location other than the neutral axis of a structural section. The maximum deflection, δ , can be calculated

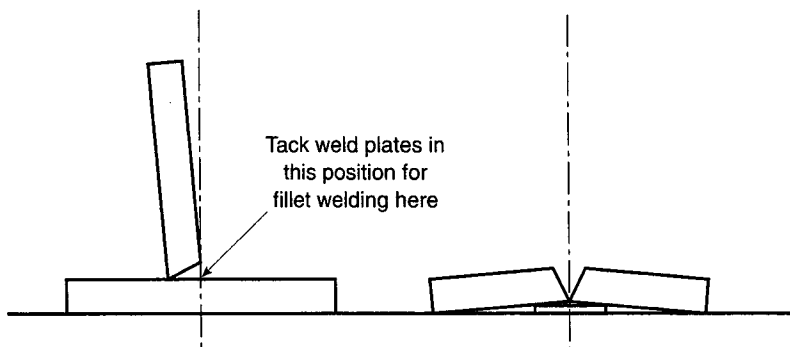


Fig. 8.16 Preset geometry to account for the distortion of a fillet weld (left) and butt weld (right).

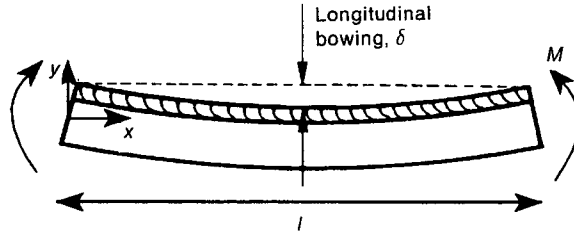


Fig. 8.17 Illustration of longitudinal bowing of a butt weld.

using the Euler bending formula

$$\frac{d^2y}{dx^2} = \frac{M}{EI} \quad (8.5)$$

where: M is the applied moment

I is the second moment of area about the centroid

E is the elastic modulus.

For a beam in pure bending, integrating equation 8.5 twice gives

$$y(x) = \frac{M}{EI} \times \frac{x^2}{2} + C_1x + C_2 \quad (8.6)$$

where C_1 and C_2 are the integration constants.

The integration constants are evaluated from the boundary conditions. One boundary condition is that the slope of the distorted welded plates is zero at the midlength of the weld. The other boundary condition is that at the ends of the welded plates the deflection is zero. These boundary conditions are expressed mathematically as

$$\left. \frac{dy}{dx} \right|_{y(l/2)} = 0; \quad y(0) = 0 \quad (8.7)$$

where l is the length of the weld (Fig. 8.17).

Substituting these boundary conditions into equation 8.6 yields

$$y(x) = \frac{Mx^2 - Mlx}{2EI} \quad (8.8)$$

The bending moment M can be calculated from the applied force as

$$M = F\bar{y} \quad (8.9)$$

where: M is the bending moment (Fig. 8.17)

F is the applied force (Fig. 8.15)

\bar{y} is the distance from the neutral axis to the centroid of the weld.

Combining equation 8.9 with equation 8.8 and evaluating for the maximum longitudinal bowing, δ , gives

$$\delta = y\left(\frac{l}{2}\right) = \frac{F\bar{y}l^2}{8EI} \quad (8.10)$$

Using the empirical expression of equation 8.4 yields

$$\delta = 0.005 \frac{\bar{y} l^2 A_w}{\hat{I}} \quad (8.11)$$

Although equation 8.11 is strictly only correct for butt welds, such as shown in Fig. 8.15, it gives a relatively accurate estimate (within 10%) for the longitudinal bowing of a wide range of fillet weld geometries.

Example 8.1 Distortion of a fillet welded T section

An inverted T section is fabricated by welding two steel plates, as shown in Fig. E8.1. Given the dimensions of the section shown, estimate the longitudinal bowing resulting from the weld, if the length of the welded section is 1 m.

Solution First determine the location of the neutral axis of the fabricated beam, by locating the vertical position of the centre of gravity. This is calculated to be 37.25 mm above the base, as shown in Fig. E8.1. Next determine the moment of inertia for the fabricated beam about the neutral axis (NA), using the *parallel axis theorem*:

$$\hat{I} = \frac{bh^3}{12} + Ay^2$$

where: b is the base of a rectangular section

h is the height of a rectangular section

y is the distance from the centroid of the rectangular section to the NA

A is the area of the rectangular section.

Applying this to the two rectangular sections of the fabricated beam provides a total moment of inertia of $\hat{I} = 3.5 \times 10^6 \text{ mm}^4$. To use equation 8.11, the required weld area

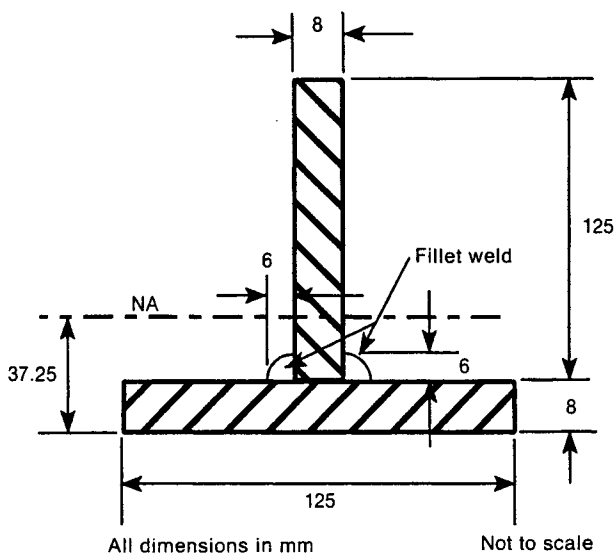


Fig. E8.1 Example 8.1.

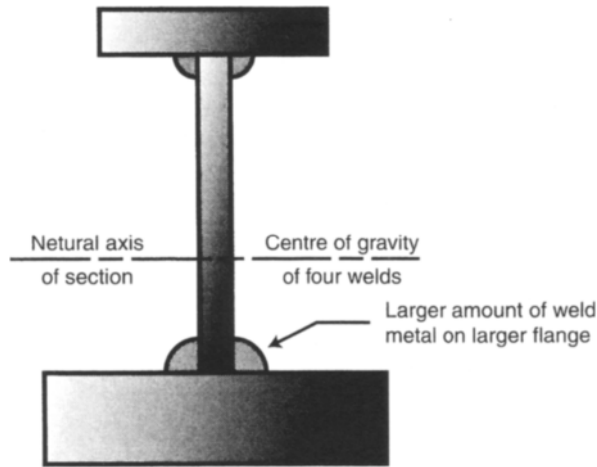


Fig. 8.18 Welding of an unsymmetrical fabricated beam.

A_w is estimated by approximating the weld beads as triangles, each with an area = $bh/2 = 18 \text{ mm}^2$. The distance from the neutral axis to the centroid of the weld is $\bar{y} = 27.25 \text{ mm}$. Using equation 8.11,

$$\delta = 0.005 \frac{\bar{y}^2 A_w}{\hat{I}} = 0.005 \frac{27.25 \text{ mm} \times 1000^2 \text{ mm}^2 \times 36 \text{ mm}^2}{3.5 \times 10^6 \text{ mm}^4} = 1.4 \text{ mm}$$

Despite equation 8.11 being strictly only valid for butt welded plates, the longitudinal bowing of 1.4 mm is within 15% of the actual bowing. Note that the area of the weld was not included in the calculation of the NA location or \hat{I} . The calculation is an estimate only; thus, the exclusion of the weld area does not represent a problem. For the current geometry the weld line is below the NA, and the beam will bow upwards.

If multiple welds are applied to a cross-section the distortion due to welding can be minimized by using the distortion caused by one weld to offset the distortion caused by the other weld. Often it is advantageous to apply the welds closer to the neutral axis first and then allow a second weld further from the neutral axis (with a greater moment arm, \bar{y} , in equation 8.11) to pull the beam straighter. Another example is the welding of unsymmetrical beams, as shown in Fig. 8.18. By making the weld closest to the neutral axis larger (larger A_w in equation 8.11), the distortion can be balanced, despite the different moment arms to the neutral axis.

8.2.2 Solid state welding

As the name implies, during solid state welding the temperature of the base material remains below the melting temperature but, unlike *brazing* and *soldering*, additions of filler metal are not used. Solid state welding relies on the fact that interatomic bonding between two metals will occur spontaneously if two clean and oxide-free metal

surfaces are brought into close contact. Accomplishing this condition is complicated by the tenacious oxide layer formed on the surface of many common metals, but can be achieved when the surface oxide is broken by relative movement between the two surfaces. Numerous solid state welding techniques use this principle to join similar or dissimilar metals.

Pressure welding

Although pressure welding can take several forms, all rely on severe deformation to break up the surface oxide. The basic set-up for *cold pressure welding* is illustrated in Fig. 8.19, which is not dissimilar to the spot welding of Fig. 8.12. Essentially, indentors apply local deformation to the metal to be joined. As the two clean sheets are compressed together and deformed under the pressure of the indenter, the metal flow causes the formation of new unoxidized surfaces that bond together. The process can be used to join sheets of thicknesses between 0.1 and 15 mm. An advantage of cold welding is that a wide range of dissimilar metals can be joined. Using variations of the tooling arrangement, shown in Fig. 8.19 allows butt welds and multilayer tubes to be formed by cold pressure welding.

Forge welding is similar to cold pressure welding, except that the parts to be joined are heated to the welding temperature and then sufficient mechanical deformation is applied to achieve bonding. The process usually involves applying sufficient pressure to firmly seat the faying surfaces against one another, heating the joint to the welding temperature (about 0.85 of the absolute melting temperature) and then rapidly applying additional pressure to bond the contacting surfaces. A wide variety of

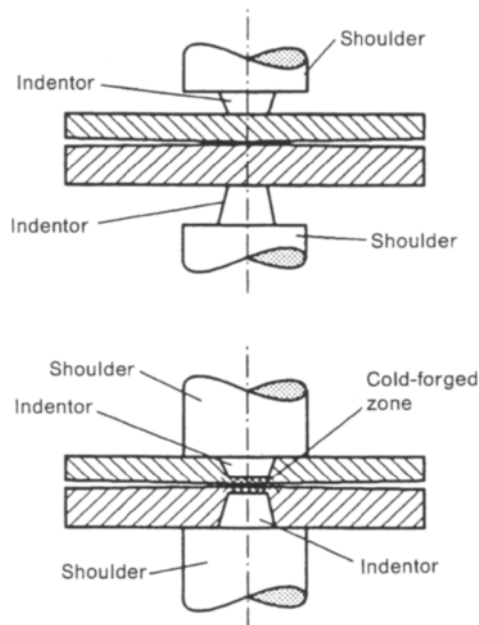


Fig. 8.19 Cold pressure welding. (Reprinted with permission from *ASM Metals Handbook, Ninth Edition*, Vol. 6, Welding Brazing and Soldering (1993), ASM International, Materials Park, OH 44073-0002, p. 302, Fig. 8.)

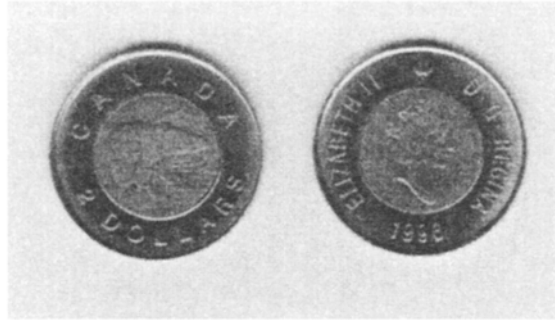


Fig. 8.20 Canadian two-dollar coin with forge welded inner and outer sections. Actual size, but not legal tender!

joint geometries can be joined. This process has recently been used to bond the inner and outer sections of the Canadian two-dollar coin, shown in Fig. 8.20.

Friction welding

During friction welding the energy required for joining is produced by frictional heating of a rotating part as it is pressed against a stationary part, using equipment of the type illustrated in Fig. 8.21. This process is most widely used for joining rods or tubes. To generate rapid frictional heating the rotational speed is high during the initial stage of joining. Once the mating surfaces have been heated to a plasticized state, rotation is stopped, but the welding force joining the surfaces is increased to complete the weld. The localized deformation of the mating surfaces causes the creation of a new surface area which, as it is not exposed to the atmosphere, provides a clean surface for bonding. The whole process can be completed quickly, typically requiring less than 10 s for thin walled tubes of about 10 mm diameter. This rapid heating contributes to the narrow HAZ characteristic of friction welding. Common examples of friction welding are the copper–aluminium joints that form part of the refrigeration tubing of many household refrigerators.

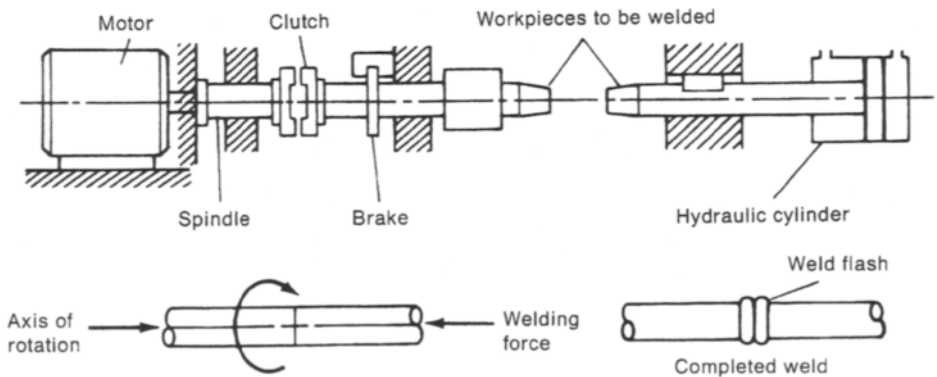


Fig. 8.21 Friction welding: top diagram shows general equipment arrangement, bottom diagram shows the relative movement and geometry of joint.

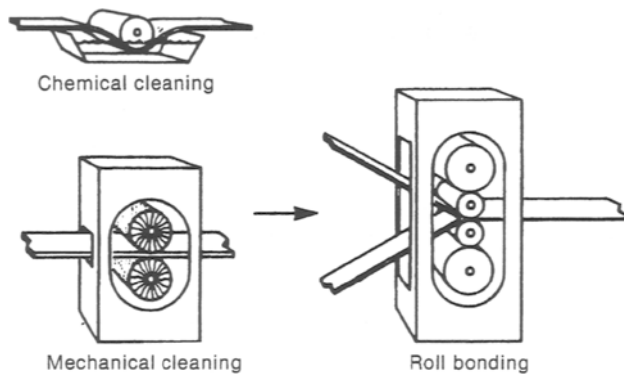


Fig. 8.22 Roll bonding process. Steel brushes can be used for mechanical cleaning.

Roll bonding

Roll bonding differs from other solid state welding processes because it is often used to join much larger workpieces. The process consists of simultaneously applying a large reduction to two sheets by passing them through a rolling mill, as shown schematically in Fig. 8.22. As the thickness is reduced, the length increases, creating new unoxidized surfaces that can bond together. Usually the surfaces are chemically or mechanically cleaned and heated prior to entering the rolling mill, to enhance bonding across the contacting surfaces.

Variations of this process can be used to bond *clad* sheet products. This involves locally welding a plate of one alloy (about 6 cm thick) onto the surface of an ingot (about 60 cm thick) of another alloy prior to hot breakdown rolling, to produce one side clad sheet with a clad thickness of about 10% of the total. This process is used to produce sheets of high strength aluminium alloys clad with a layer of high purity aluminium for improved corrosion resistance, which are widely used for aircraft structures. Other applications include bonding of dissimilar metals. For example, clad layers of 1.2 mm thickness of 75 wt% Cu–25 wt% Ni are roll bonded to a copper base of 5.1 mm. This two-sided clad assembly is rolled in two passes to a thickness of 1.36 mm and used for making 25¢ coins by the US Mint.

Several automotive products are also roll bonded. Stainless steel is roll bonded to carbon steel for use as bright trim. The stainless steel provides an appealing surface, whereas the base of low carbon steel reduces cost. Several bearing alloys (typically Al–Pb, Al–Sn or Al–Si–Cd alloys) are roll bonded to a steel backing for the manufacture of crankshaft and camshaft journal bearings. In this application the steel backing provides good fatigue strength, while the bearing alloy gives a wear-resistant malleable bearing surface.

An innovative use of roll bonding is the manufacture of heat exchanger panels in which a coolant flows in passages formed between the two roll bonded sheets. These passages, such as shown in Fig. 8.23, are formed by printing a graphite pattern of the desired passage configuration on the mating surface of one of the sheets. The two sheets are then roll bonded, except in the areas where bonding is prevented with a graphite pattern, by applying a large reduction (typically about 80%) in one pass. The sheets are annealed to aid diffusion across the bond interface. They are placed between two platens and the passageways are inflated using high pressure air (about

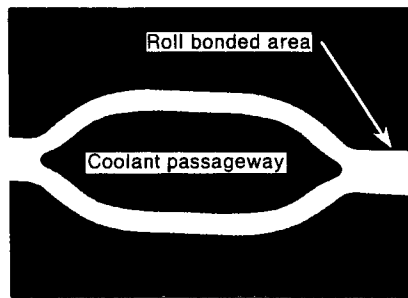


Fig. 8.23 Cross-section of a roll bonded panel with integral cooling passages.

20 MPa pressure). The inflated panel can be trimmed, formed and painted as required for the application. This can be done in a continuous fashion, such that the surface cleaning, printing of the graphite pattern, heating, and roll bonding steps are applied continuously to sheet unwound from two coils and rewound, after bonding, as one coil. This process is widely used to produce evaporator panels for household refrigerators and solar panels, and it has even been used for water and oil coolers for racing cars.

Ultrasonic welding

High frequency vibration between two abutting metal surfaces causes localized elastic and plastic deformation of the surface regions and a temperature increase of as much as 0.5 of the absolute melting temperature. The localized deformation tends to break up the surface oxide, allowing metal to metal contact to occur. Diffusion bonding between the two metal surfaces is enhanced by the increased local temperature. If a clamping force is applied between the abutting surfaces, joining times of under a second can be achieved. Usually, a high frequency power generator is used to boost the normal a.c. frequency (typically 50 or 60 Hz) to 15–75 kHz. This electrical frequency is converted to a vibratory response, using a piezoelectric transducer and appropriate acoustical coupling members to transmit acoustical power to the workpieces. Several equipment arrangements are in use. Two of the more common are shown in Fig. 8.24.

A wide variety of dissimilar metals can be ultrasonically welded and the process is particularly well suited to small parts. Ultrasonic welding is used for many electrical connections, including the attachment of leads to transformer coils, and joining miniaturized components to semi-conductor materials or printed circuit boards. Ultrasonic welding is useful to hermetically seal a wide range of metal packages for the protection of contents that cannot be exposed to heating, associated with other joining processes or from ambient conditions. These packaging applications include food preservation, protection of living tissue cultures, explosives and propellants.

8.2.3 Weld microstructure and properties

During most welding processes, but especially during fusion welding, a very intense, moving heat source is applied to a workpiece. As many metal products are thermally processed during fabrication to achieve specific properties, it is evident that the

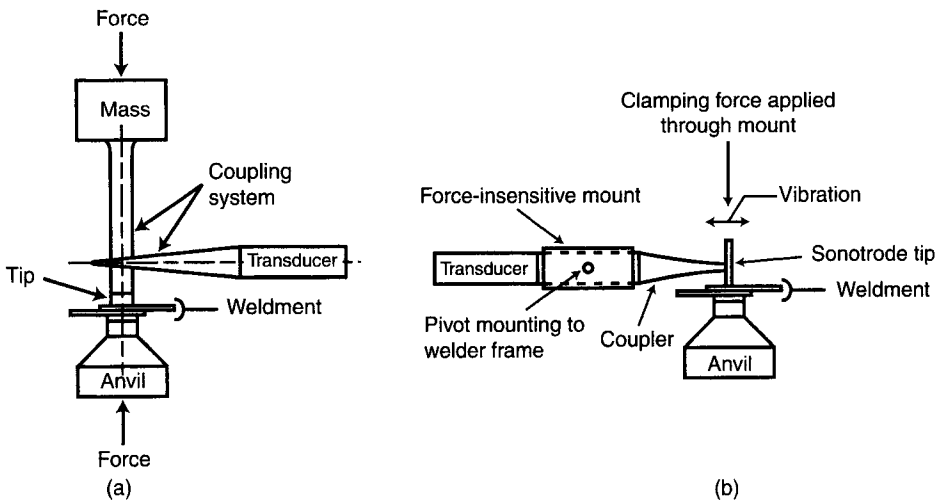


Fig. 8.24 General arrangement for ultrasonic welding: (a) wedge reed ultrasonic spot welder, (b) lateral drive ultrasonic spot welder.

application of heat during welding inevitably alters the microstructure and mechanical properties of the weld zone. Some of the microstructural changes are evident in Fig. 8.3, where it is clear that the fusion and heat-affected zones (HAZ) have markedly different microstructures and, therefore, different mechanical properties. Given the number of different weld geometries and weld metals that are possible, it is well beyond the scope of this text to describe the properties of all possibilities. Rather, the major factors influencing the structure and properties of fusion welded ferrous metals are summarized.

Figure 8.25 is a schematic cross-section of a butt weld, showing the HAZ and fusion zone. The weld is formed by a moving heat source travelling perpendicular to the plane of the page. The properties and structure of each point near the weld are determined by the thermal history associated with that point. The temperature profile of each point identified in Fig. 8.25 is shown schematically in Fig. 8.26. Point 1 is directly below the heat source and rapidly heats to the fusion temperature ($\approx 1540^{\circ}\text{C}$; see Fig. 2.32). Once the heat source moves along the weld this location cools rapidly due to thermal conduction of heat into the adjoining metal. On cooling through 1540°C the cooling rate slows, corresponding to the removal of the latent heat of fusion. Points further away from the heat source cool more gradually than point 1. In the HAZ, points 2, 3 and 4 reach temperatures above 723°C (the minimum austenitization temperature

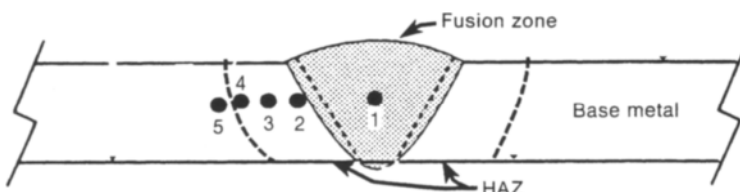


Fig. 8.25 Butt weld, showing fusion zone and HAZ. See text for explanation of numbered points.

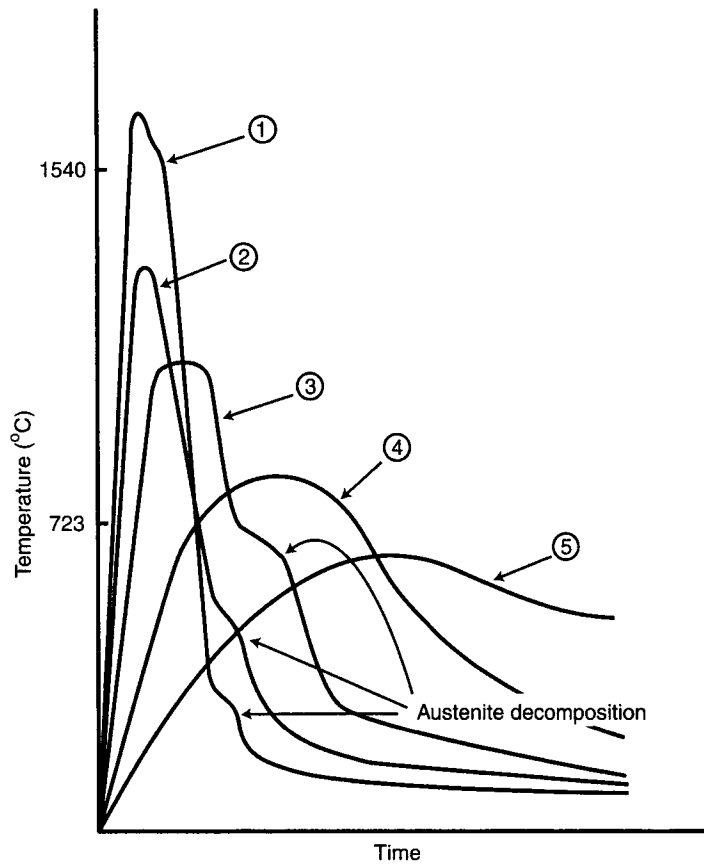


Fig. 8.26 Temperature profile during welding for each point of Fig. 8.25.

for steel), but do not melt. Point 4, at the edge of the HAZ, achieves a temperature just above 723°C , whereas the temperature at point 5, just outside the HAZ, does not exceed 723°C and therefore does not austenitize.

During cooling of the fusion zone and the HAZ, the austenite (γ) phase becomes unstable below 723°C , decomposing to martensite or a mixture of ferrite (α) and cementite (Fe_3C), depending on the cooling rate. The faster cooling of points 1, 2 and 3 may cause these regions to partially transform to martensite. During this transformation the cooling rate is reduced, as shown in Fig. 8.26, corresponding to the latent heat of the $\gamma \rightarrow$ martensite transformation. The much lower cooling rate at point 4 causes the austenite to transform to ferrite and cementite. The latent heat of this transformation is not noticeable in Fig. 8.26 because the transformation occurs over an extended period of time. Importantly, the thermal cycle occurring during welding can result in the formation of considerable martensite in both the fusion and heat-affected zones.

Martensite is a hard and strong phase. Therefore, the welded region can be stronger than the original base metal. However, this is not necessarily desirable. Martensite is also brittle and has minimal plastic capacity. Consequently, the residual stresses and distortion associated with the welding process can cause cracking where martensitic

material has formed. Such hairline cracks in the martensitic region can lead to premature failure of the welded structure.

Although martensite can form in either the fusion zone or the HAZ, the latter is generally considered to be the more sensitive zone because the chemistry is fixed to the base composition. Filler materials are almost always used in fusion welding, which permits control of the fusion zone chemistry to decrease the formation and hardness of martensite. Essentially low carbon filler materials are used as electrodes, which results in low hardness structures in this region.

The tendency for martensite formation in the HAZ can, in principle, be determined with the help of *continuous cooling transformation (CCT)* diagrams that have been specifically developed for welding applications. Figure 8.27 shows such a CCT diagram

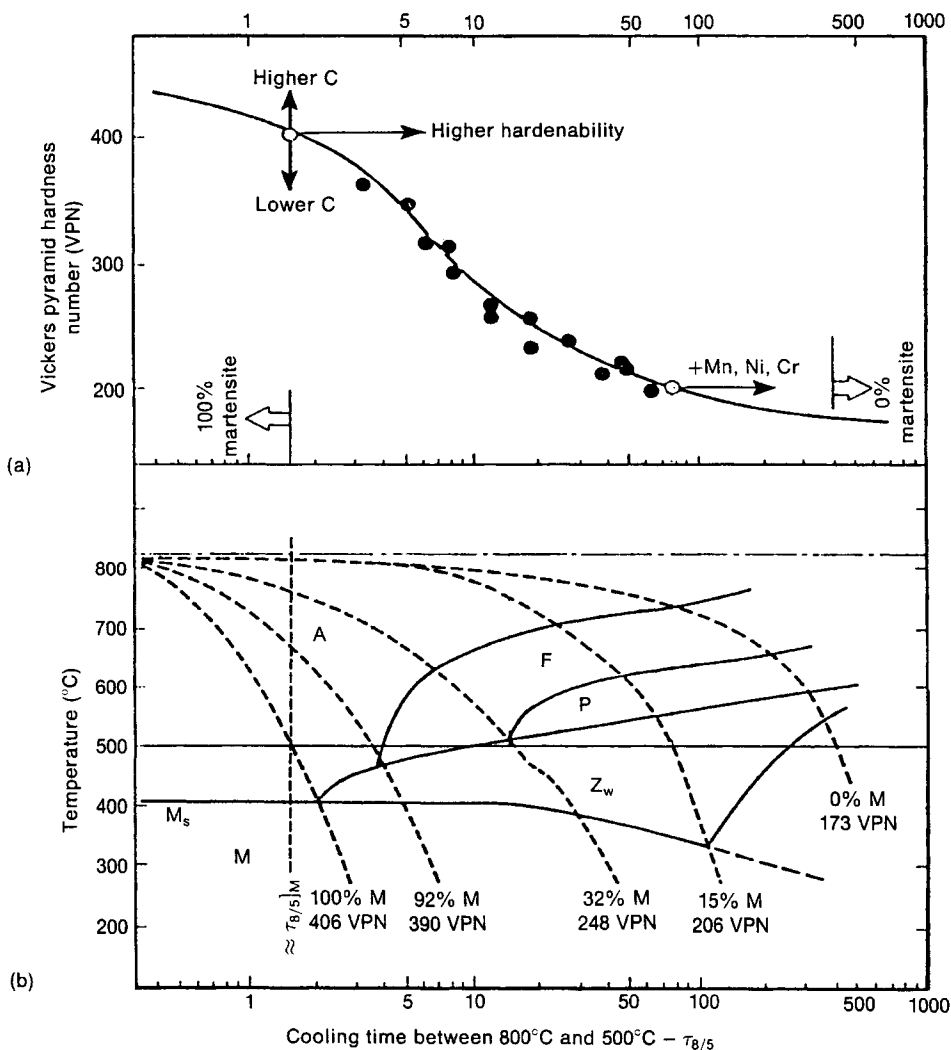


Fig. 8.27 (a) Characteristic hardness curve and (b) welding continuous cooling transformation diagram for a low alloy steel with 0.15 wt% C, 0.37 wt% Si and 1.42 wt% Mn. (Reprinted with permission of Nippon Steel.)

for a typical low alloy steel. Conventional CCT diagrams map the time and temperature at which the austenite will decompose into martensite, bainite or ferrite/pearlite during continuous cooling at a constant rate. A welding CCT diagram differs in that the cooling time, $\tau_{8/5}$, for a weld to cool from 800°C to 500°C is used as the time parameter. The $\tau_{8/5}$ value has become a standard measure of the weld cooling rate in the industry. The other fundamental difference between a welding CCT and a conventional heat treating CCT diagram is the austenitizing temperature. The most sensitive region of the HAZ is the boundary area adjacent to the fusion zone, where the maximum temperature is nearly equal to the melting point of the material. In conventional heat treatment the austenitization heat treatment temperature is much lower. The high temperatures during welding greatly increase the hardenability of a steel, and thereby increase the chances of encountering hardened martensite and bainite structures. Figure 8.27 indicates that for this particular low alloy steel, a cooling time from above the eutectoid temperature of anything less than 1.5 s will result in a fully martensitic structure. Cooling times between 1.5 and 3.5 s result in a mixture of martensite and bainite, whereas longer cooling times cause a mixture of martensite, bainite, ferrite and pearlite structures. A hardness curve ranging from a fully martensitic structure, with a hardness of about 400 VP, to a structure containing no martensite, with a hardness of about 200 VP, is also shown in Fig. 8.27. Such a curve represents a fundamental welding characteristic of a material and is referred to as the *characteristic hardness curve* (CHC). CCT and CHC diagrams are available for most of the commonly welded steel grades.

To use the welding CCT diagram and the accompanying CHC to predict the tendency for martensite formation during welding requires an estimation of the cooling time $\tau_{8/5}$. Cooling times can be estimated by solving the time-dependent equation for heat transfer from a moving point source. Using the coordinate system of Fig. 8.28, this equation is

$$\frac{\partial^2 T}{\partial \xi^2} + \frac{\partial^2 T}{\partial y^2} + \frac{\partial^2 T}{\partial z^2} = -2kv \frac{\partial T}{\partial \xi} \quad (8.12)$$

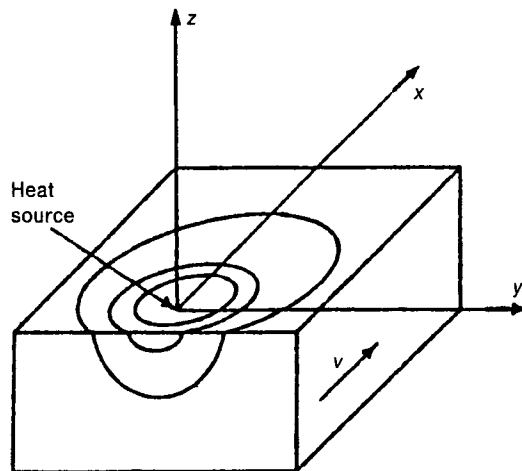


Fig. 8.28 Coordinate system for equation 8.12.

where: T is the metal temperature
 k is the thermal conductivity
 v is the welding speed
 ξ is the distance of the point source along the x -axis ($\xi = x - vt$).

The cooling rate in all three directions away from the welding heat source can be obtained from equation 8.12. However, from the previous discussion and Fig. 8.26 it is clear that the weld centreline (or the x axis of Fig. 8.28) will experience the fastest cooling rate and is, therefore, the most likely location for martensite to form. Yet it has been determined that the cooling times in adjacent positions, and in particular in the HAZ near the fusion zone boundary, are almost the same as the centreline cooling time. Therefore, it has become customary to refer to a single cooling time for a weld, namely the $\tau_{8/5}$.

As mentioned above, cooling times can be derived from the heat flow equation 8.12 when appropriate boundary conditions are applied. However, this is beyond the scope of this book and, therefore, the result is simply stated as follows:

$$\tau_{8/5} = \frac{Q}{2\pi k} \left[\frac{1}{(500^\circ\text{C} - T_o)} - \frac{1}{(800^\circ\text{C} - T_o)} \right] \quad (8.13)$$

where: $\tau_{8/5}$ is the centreline cooling time
 k is the thermal conductivity
 T_o is the base metal ambient temperature
 Q is the net heat input per unit length to the weld.

Equation 8.13 is the relationship that applies to welding thick sections, typically involving more than six passes. For thin plates, where the heat transfer can be considered two dimensional (independent of the thickness or z axis), the corresponding equation is

$$\tau_{8/5} = \frac{(Q/h)^2}{4\pi k \rho C} \left[\left(\frac{1}{500^\circ\text{C} - T_o} \right)^2 - \left(\frac{1}{800^\circ\text{C} - T_o} \right)^2 \right] \quad (8.14)$$

where: h is the base metal thickness
 ρ is the base metal density
 C is the specific heat of the base metal.

For the common metals, the thermal conductivity k , specific heat C , and density ρ , are given in Table 8.2.

For a particular welding geometry, a *relative plate thickness* parameter can be used to decide whether the equation for thick or thin base metal should be used. The relative plate thickness parameter is

$$\lambda = h \sqrt{\frac{\rho C (550^\circ\text{C} - T_o)}{Q}} \quad (8.15)$$

where λ is the relative plate thickness parameter.

If $\lambda > 0.75$ it is said to be a thick plate weld, if $\lambda < 0.75$ it is a thin plate weld. For many steel grades the temperature for the most rapid transformation of austenite

Table 8.2 Physical properties of common metals

Metal	Thermal conductivity, k (W/cm · °C)	Density, ρ (g/cm ³)	Specific heat, C (kJ/kg · °C)
Aluminium (+99% pure)	2.37	2.7	0.9
Al casting alloys	1.2–2.1	2.6–2.8	
Al wrought alloys	1.2–1.8	2.6–3.0	
Copper (+99% pure)	4.01	8.93	0.39
Iron	0.81	7.87	0.44
Low alloy steel	0.32–0.66	7.8–8.0	0.50
Martensitic stainless steel	0.25	7.6–7.7	
Austenitic stainless steel	0.15	7.8–8.0	0.50
Nickel (99.9%)	0.92	8.9	0.44
Titanium alloys	0.024–0.24	4.4–4.8	0.52

is approximately 550°C, giving rise to the 550°C constant in equation 8.16. For the electric welding processes, the net heat input to the weld can be calculated according to

$$Q = \eta \frac{VI}{v} \quad (8.16)$$

where: v is the welding speed (mm/s)

V is the welding voltage

I is the welding current

η is the weld heat transfer efficiency (Table 8.3).

Example 8.2 Welding speed calculation

Two 12 mm thick low alloy steel plates are submerged arc welded together with the following conditions: 25 V, 300 A and an efficiency of 0.9. Test weld beads are deposited at speeds of 6, 7, 8, 9 and 10 mm/s and the hardness is measured on each of the weld cross-sections. The hardness measurements indicate that at welding speeds of 8 mm/s and faster, the structure is fully martensitic in the HAZ next to the fusion zone. If the ambient temperature is initially at 25°C, estimate the cooling time that results in a fully martensitic region in the HAZ.

Solution For the 8 mm/s weld speed the heat input according to equation 8.16 and an η of 0.9 from Table 8.3 is

$$Q = \eta \frac{VI}{v} = 0.9 \frac{25 \times 300}{8} = 844 \text{ J/mm}$$

Table 8.3 Heat transfer efficiency for arc welding processes

Welding process	η
Shielded (manual) metal arc	0.7–0.85
Tungsten inert gas (TIG)	0.22–0.48
Metal inert gas (MIG)	0.66–0.75
Submerged arc	0.90–0.99

The relative plate thickness is calculated from equation 8.15; from Table 8.2, $\rho = 0.0078 \text{ g/mm}^3$ and $C = 0.5 \text{ kJ/kg} \cdot \text{K}$. Therefore,

$$\begin{aligned}\lambda &= h \sqrt{\frac{\rho C (550^\circ\text{C} - T_p)}{Q}} \\ &= 12 \text{ mm} \sqrt{\frac{0.0078 \text{ g/mm}^3 \times 0.50 \text{ J/g} \cdot ^\circ\text{C} (550^\circ\text{C} - 25^\circ\text{C})}{844 \text{ J/mm}}} = 0.59\end{aligned}$$

As $\lambda = 0.59$, thin plate conditions apply. The cooling time is calculated using equation 8.14 and, from Table 8.2, estimate $k = 0.04 \text{ W/mm} \cdot \text{K}$. Then,

$$\begin{aligned}\tau_{8/5} &= \frac{(Q/h)^2}{2\pi k \rho C} \left[\frac{1}{(500 - T_0)^2} - \frac{1}{(800 - T_0)^2} \right] \\ &= \frac{(844 \text{ J/mm/12 mm})^2}{4\pi (0.04 \text{ J/s mm} \cdot ^\circ\text{C}) 0.0078 \text{ g/mm}^3 \times 0.50 \text{ J/g} \cdot ^\circ\text{C}} \left[\frac{1}{480^2} - \frac{1}{780^2} \right] = 6.7 \text{ s}\end{aligned}$$

The maximum cooling time for the formation of a fully martensitic region in the HAZ for this butt weld is about 6.7 s and corresponds to a welding speed of 8 mm/s.

Several researchers have modelled the CHC to permit the calculation of HAZ hardness from the chemical composition of a steel workpiece and the welding parameters. Essentially these formulations are curve fit empirical relationships, but nevertheless have proved useful for determining welding specifications to avoid the possibility of hardened HAZ regions that might lead to failure. One such procedure makes use of the following series of equations. First, the cooling time corresponding to a microstructure of 100% martensite, $\tau_{8/5}]_M$, is determined as

$$\log \tau_{8/5}]_M = 2.5C_{eq} - 1.27 \quad (8.17)$$

where C_{eq} is the equivalent carbon concentration of the steel, calculated from the weight percentage of each alloying element in the steel

$$C_{eq} = C + \frac{\text{Mn}}{3} + \frac{\text{Cu}}{4} + \frac{\text{Ni}}{8} + \frac{\text{Cr}}{10} + \frac{\text{Mo}}{3} + 5B \quad (8.18)$$

If $\tau_{8/5}]_M$ from equation 8.17 is more than $\tau_{8/5}$ calculated from equations 8.13 or 8.14 for thick or thin welds, respectively, then the HAZ hardness is estimated as

$$\text{VPN}_M = 812C + 293 \quad (8.19)$$

where: VPN_M is the Vickers pyramid hardness number of the martensitic HAZ
 C is the carbon content of the steel in weight percent.

If $\tau_{8/5}]_M$ from equation 8.17 is less than $\tau_{8/5}$ calculated from equations 8.13 or 8.14, then the HAZ will decompose to a mixture of martensite, bainite, ferrite and pearlite, with a Vickers pyramid hardness number, VPN_{HAZ} , of

$$\text{VPN}_{HAZ} = \text{VPN}_0 + (\text{VPN}_M - \text{VPN}_0) \exp \left[-0.2 \left(\frac{\tau_{8/5}}{\tau_{8/5}]_M} - 1 \right) \right] \quad (8.20)$$

where VPN_0 is the Vickers pyramid hardness number of the martensitic free base metal. This can be estimated as

$$VPN_0 = 164 \left(C + \frac{Si}{2} + \frac{Cr}{7} + \frac{Mo}{2} + V + Nb + 7B \right) + 153 \quad (8.21)$$

An often-used rough guide is that to avoid cracking the HAZ hardness should not exceed 350 VPN. If there is a danger of stress corrosion cracking during service, for example with welds exposed to sour gas environments, then the HAZ hardness should not exceed 250 VPN. Other HAZ hardness levels may be specified, based on judgement and experience.

Example 8.2 illustrates that the welding speed – and therefore, to a large extent, productivity – is determined by the $\tau_{8/5}$ cooling time. In Example 8.2 the maximum welding speed of 8 mm/s is governed by the requirement to avoid excessive martensite in the heat affected zone. The welding speed can be increased if the temperature T_0 in equations 8.13 and 8.14 is increased. Furthermore, as the temperature difference terms involving T_0 are raised to the second power in equation 8.14, they can have a substantial influence on the cooling time. Examination of equations 8.13 to 8.16 indicate that if the temperature difference is decreased, then the welding speed can be increased for the same $\tau_{8/5}$ cooling time, thereby improving productivity without increasing the susceptibility to the formation of a martensitic weld structure. Decreasing the temperature difference can be achieved by *preheating* the base metal to be welded. As the name implies, preheating involves heating the base metal to an elevated temperature prior to welding. In this manner, the base metal does not conduct heat away from the weld zone as effectively, thereby increasing the cooling time, or alternatively it allows an increase in welding speed. In light of these benefits, many weld procedures require some degree of preheating, which also serves to ensure that the weld is relatively free of moisture, the hydrogen from which can have a devastating effect on the susceptibility to cracking.

Example 8.3 Effect of preheat on welding speed

For the welding conditions of Example 8.2, calculate the welding speed possible if the base metal is preheated to 100°C and fully martensitic regions in the HAZ are to be avoided.

Solution From the previous example it is known that the $\tau_{8/5}$ time required to avoid fully martensitic regions in the HAZ is 6.7 s.

Using this information the new heat input, Q , possible can be estimated. Using equation 8.14, with $T_0 = 100^\circ\text{C}$,

$$\tau_{8/5} = \frac{(Q/h)^2}{4\pi k\rho C} \left[\frac{1}{(500 - T_0)^2} - \frac{1}{(800 - T_0)^2} \right]$$

$$\left(\frac{Q}{12} \right)^2 = \frac{6.7 \times 4\pi \times 0.04 \times 0.0078 \times 0.50}{4.2 \times 10^{-6}} = 3126$$

$$Q = 12\sqrt{3126} = 670 \text{ J/mm}$$

Before proceeding, check that this situation still obeys the thin plate assumption using equation 8.15:

$$\begin{aligned}\lambda &= h \sqrt{\frac{\rho C (T_c - T_p)}{Q}} \\ &= 12 \text{ mm} \sqrt{\frac{0.0078 \text{ g/mm}^3 \times 0.50 \text{ J/g} \cdot \text{K} (550^\circ\text{C} - 100^\circ\text{C})}{670 \text{ J/mm}}} = 0.61\end{aligned}$$

As $\lambda = 0.61 < 0.75$, the thin plate assumption is still valid.

Therefore, using $Q = 670 \text{ J/mm}$, use equation 8.16 to estimate the new welding speed possible:

$$v = \eta \frac{VI}{Q} = 0.9 \frac{25 \text{ V} \times 300 \text{ A}}{670 \text{ J/mm}} = 10.1 \text{ mm/s}$$

The example illustrates that even a modest preheat temperature increases the possible welding speed by about 20%, while still preventing excessive martensite formation. Many welding practices call for preheat temperatures of as low as 50°C . The significance of this preheat on the weld structure should not be underestimated or ignored. Several failures of structures at weld sites have been traced to insufficient application of preheat.

For small structures, preheating can be accomplished by placing the base metal in a furnace set to the appropriate temperature and welding immediately upon removing the workpiece from the furnace. For moderate or large structures that are welded with multiple passes the base metal will be preheated by the prior welds. If such a technique is used the cooling time during the initial pass must still be long enough to avoid localized martensite formation. Alternatively, the steel to be welded can be selected on the basis of its tendency for martensitic formation. Examination of equations 8.17 and 8.18 indicates that $\tau_{8/5} \text{M}$ increases with the addition of alloying elements. As such, the tendency for martensitic formation is minimized by welding plain carbon steels. This factor contributes to the good weldability of these steels. However, for low alloy steels, that often contain additions of more than 1.5 wt% Mn, and possibly Ni, Cr, or Mo as well, the tendency for martensite formation is much greater, even at markedly slower cooling rates. Consequently, particular attention should be given to the specification of the welding parameters for low alloy steels, which may require low welding speeds and/or preheating to avoid martensite formation in the HAZ. In addition, low alloy steel welds are often *stress relieved* to reduce the residual stress in the joint region. Similar arguments can be put forward regarding the filler metal. However, if a filler metal other than the base metal is used, due consideration must be given to other weld properties, such as corrosion resistance.

8.3 Brazing

Brazing achieves joining by the use of a filler metal which is distributed between the surfaces to be mated. The filler metal melts at a temperature above 427°C (800°F), but below the solidus temperature of the base metal. Unlike many welding processes,

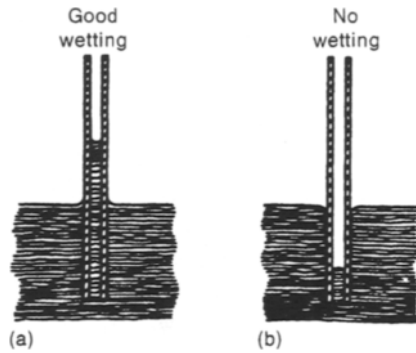


Fig. 8.29 Principle of wetting and capillary action: (a) good wetting, (b) poor wetting. (Reprinted with permission from *ASM Metals Handbook, Ninth Edition*, Vol. 6, *Welding Brazing and Soldering* (1993), ASM International, Materials Park, OH 44073-0002, p. 114, Fig. 1.)

during brazing the base metal does not melt. The filler metal must *wet* the surface of the base metal, so that the filler metal will penetrate between the joint surfaces by *capillary* action. Wetting refers to the tendency for a liquid to spread over a solid surface. Figure 8.29 illustrates the principles of wetting and capillary action. The wetting and capillary action is enhanced when the cohesive force of the liquid is less than the adhesive force between the liquid and solid. As implied by Fig. 8.29, the mating surfaces must be in close proximity for the capillary action to occur, but not clamped with excessive pressure. Based on these physical principles the major brazing steps are:

1. secure the surfaces to be brazed in close proximity;
2. heat the joint area to above the melting temperature of the filler metal (at least 427°C);
3. deliver the filler metal to joint area, or the filler metal can be already placed between surfaces to be brazed;
4. maintain the temperature sufficiently long that the filler metal can flow between the joint surfaces by capillary action and dissolve a small amount of base metal;
5. cool the joint area to solidify the filler metal.

The strength of a brazed joint depends on: the atomic bonding between the filler and base metals; dissolution of a small amount of the base metal into the liquid filler metal which aids wetting and enhances diffusion bonding; and intergranular penetration of the filler metal into the base metal. A diffusion layer in a brazed joint is illustrated in Fig. 8.30.

Compared to welding, brazing has several advantages: almost any metal, including dissimilar metals, can be joined; joining of thin walled parts is possible; less heat and power are required; there are fewer problems with the heat-affected zone in the base metal; and the capillary action means that inaccessible joints can be brazed. However, brazing cannot take the place of welding in all circumstances because brazed joints are usually not as strong as properly welded joints – the strength of a brazed joint is usually less than the strength of the base metals, and elevated temperatures may cause weakening of brazed joints.

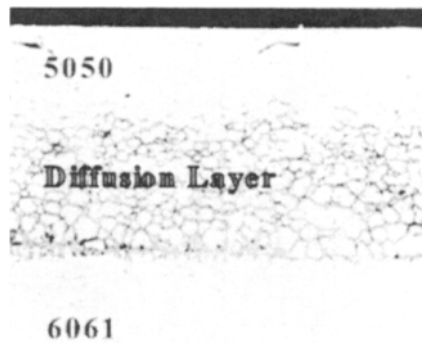


Fig. 8.30 Brazed joint between aluminium alloy 5050 (Al–1.5wt% Mg) top, and aluminium alloy 6061 (Al–1 wt% Mg–0.5 wt% Si) bottom. Filler metal is Al–10 wt% Si–4 wt% Cu.

The advantages of brazing have led to the widespread use of several brazing techniques, some of which are described in the following sections.

8.3.1 Torch brazing

The essence of torch brazing is illustrated in Fig. 8.31. The filler metal is heated by a torch concurrently with heating the base metal. The torch burns acetylene, propane or other gases, with air or oxygen, which can be hand held or often separately mounted for mechanized brazing operations. To prevent excessive oxidation of the joint surfaces the flame is usually adjusted to be slightly reducing. Manual torch brazing is relatively simple and can be mastered quickly by the mechanically adept.

8.3.2 Furnace brazing

For relatively high production quantities it is often more efficient to heat the entire assembly to be brazed in a furnace. For furnace brazing the parts to be brazed

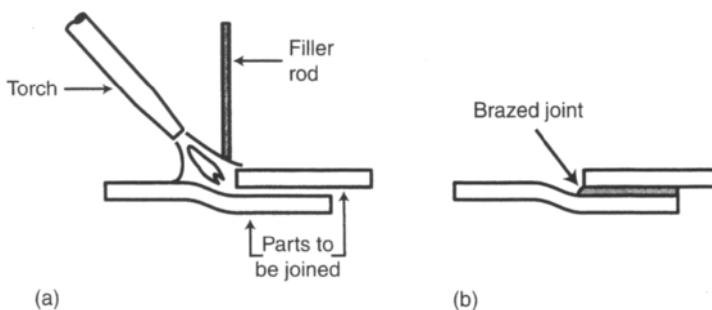


Fig. 8.31 Torch brazing: (a) the process, (b) the final joint.

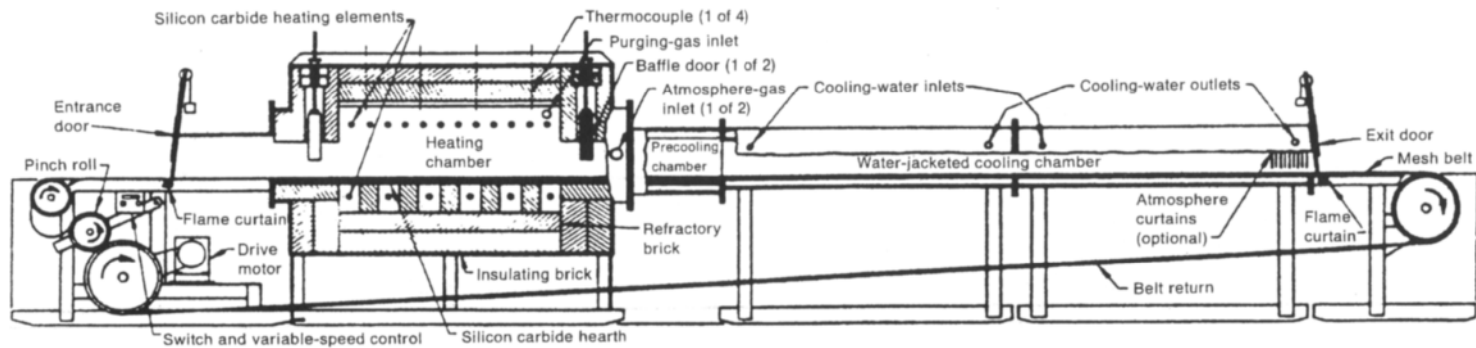


Fig. 8.32 Diagram of a continuous furnace suitable for furnace brazing. (Reprinted with permission from *ASM Metals Handbook, Desk Edition*, edited by H.E. Boyer and T.L. Gall (1985), ASM International, Materials Park, OH 44073-0002 (formerly American Society for Metals, Metals Park, OH 44073), p. 30.62, Fig. 2.)

must be jigged or clamped together in the desired geometry, with the filler metal already in place. The furnace may be of a batch type that is capable of brazing multiple components at once, or a continuous furnace can be used for high production rates. Figure 8.32 shows a typical continuous furnace that consists of an endless belt on which parts are placed as they travel through the heating and cooling zones of the furnace. When brazing many metals, close control of the temperature is required. For example, brazing aluminium alloys requires temperature uniformity of $\pm 3^{\circ}\text{C}$, necessitating a well designed and instrumented furnace.

8.3.3 Dip brazing

In dip brazing the parts to be joined are dipped into a heated bath of either molten salt or molten brazing filler metal. A major advantage of this technique is fast heating times, which reduce the cycle time for the brazing process. For parts to braze together they usually must be clamped or jigged to maintain the desired geometry during immersion in the molten bath.

A major advantage of dip brazing and furnace brazing, compared to torch brazing, is that the whole component is heated uniformly, thereby reducing distortion. Also, a large number of joint surfaces can be brazed simultaneously. However, both furnace and dip brazing require a higher capital investment and to an extent they are less flexible. For example, if the alloys to be brazed are changed in a dip brazing operation, this may require replacement of the molten medium used for heating. This could involve considerable time and expenditure. Nevertheless, both furnace and dip brazing are used for mass-producing brazed products.

8.4 Soldering

Soldering is very similar to brazing, but is associated with lower temperatures. The filler metals used for soldering melt at temperatures below 427°C . During soldering the molten filler metal reacts with a small amount of the base metal, so that upon cooling, the solid filler and base metals are atomically bonded together. The low temperatures inherent to soldering mean that dimensional stability is improved compared to welding or brazing, and this permits soldering of structures that are much smaller than those that are typically brazed or welded. The risk of damaging components in close proximity to the joint area is also reduced. This is particularly important during the soldering of electronic devices. Some of the common soldering alloys are listed in Table 8.4. The major soldering techniques are analogous to the brazing processes.

8.5 Problems

- 8.1 Explain why reverse polarity results in the deepest penetration for MIG welding, but straight polarity causes the deepest penetration during TIG or shielded (manual) metal arc welding.

Table 8.4 Properties of selected soldering alloys

Solder alloy ^a	Liquidus ^b (°C)	Solidus ^b (°C)	Comments and applications
Tin–lead alloys			
63Sn–37Pb	183	183	circuit boards, gas and vacuum assemblies
10Sn–90Pb	268	302	microelectronics, radiators, auto body repair
Tin–antimony			
95Sn–5Sb	233	240	potable water conduit, food handling equipment
Tin–zinc–(aluminium)			
91Sn–9Zn	199	199	for joining Al base metals (avoid galvanic corrosion)
95Zn–5Al	382	382	
Bismuth solders			
58Bi–42Sn	138	138	sealing electronics – expands on solidification
45Bi–23Pb–8Sn–5Cd–19In	47	47	low temperature electronic assemblies
Precious metal solders			
80Au–20Sn	280	280	attaching integrated circuits to packages, hermetic sealing, good oxidation resistance
88Au–12Ge	356	356	
97Au–3Si	363	363	

^a Compositions by weight percent.

^b Solders with the same liquidus and solidus are eutectic compositions.

- 8.2 According to Table 8.3, the submerged arc welding process has a higher heat transfer efficiency than other electric arc welding processes. What characteristic of submerged arc welding accounts for this high efficiency?
- 8.3 The Goldschmidt process can be used to produce commercially pure chromium from chromium sesquioxide (Cr_2O_3). This process is similar to thermit welding, in that Cr_2O_3 is mixed with aluminium powder and ignited by a piece of burning magnesium ribbon. Write down the chemical reaction for this process.
- 8.4 The I-beam in Fig. P8.4 is to have a stiffening plate welded continuously along one flange to provide extra stiffness. The flange will be proud of the I-beam flange on one side to allow fixturing to other structural components. If the distortion of the I-beam is to be minimized, which weld should be performed first? Justify your answer. Should the welds be of different sizes? Explain your answer.

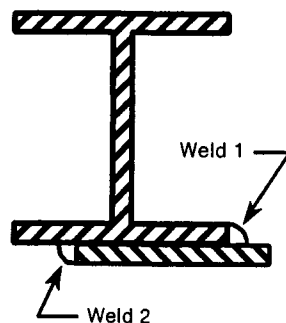


Fig. P8.4 Problem 8.4.

- 8.5 Beams can be fabricated by welding together a variety of structural shapes. To prevent distortion, each of the structural shapes is firmly clamped into position during welding. If the fabricated beam is used for a structural application, what

stress level should be assumed to exist in the fabricated beam, even in the absence of external loading?

- 8.6 A 3 m long steel T-beam (Fig. P8.6) has the same cross-section as shown in Example 8.1. It is welded in the same way as the beam of Example 8.1. It is proposed to remove the distortion due to welding by applying a straightening force after welding, as shown. Ignoring springback effects, estimate the straightening force.

(Answer: ≈ 2.7 kN)

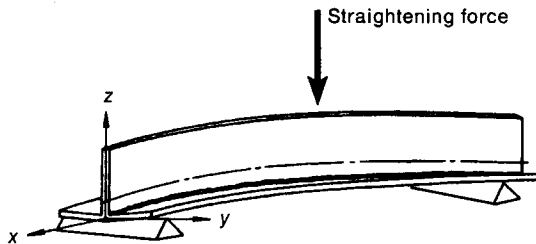


Fig. P8.6 Problem 8.6.

- 8.7 Equation 8.11 provides an estimate of the longitudinal shrinkage of steel caused by welding. Would you expect the longitudinal shrinkage associated with the welding of aluminium to be larger or smaller than that for steel? Explain your answer. (Hint: consider the physical properties listed in Table 8.2.)
- 8.8 5 mm thick plates of the low alloy steel in Fig. 8.27 are butt welded using the shielded (manual) metal arc process at 100 A and 25 V. If the heat affected zones are to contain no regions that are fully martensitic and the base metal is not preheated, what is the maximum welding speed possible? (Answer: 11.3 mm/s)
- 8.9 For the steel of Fig. 8.27 what HAZ hardness would you expect for the welding conditions of Example 8.2? Does the HAZ hardness change as a result of changing to the welding conditions of Example 8.3? Explain your answer. (Answer: $\text{VPN}_{\text{HAZ}} \approx 333$ VPN)
- 8.10 Usually a brazed joint is not as strong as the base metal, but is stronger than the filler metal. Explain the reason for this.

Case study 5:

Processing to produce automobile radiators

The majority of automobiles currently manufactured are equipped with aluminium radiators, similar to that shown in Fig. C5.1. The aluminium radiator was first introduced in the 1970s, displacing those previously made of copper and brass. For many decades copper and brass were the materials of choice for radiators, primarily because of good thermal conductivity, formability, solderability and corrosion resistance. Two major factors have led to the now dominant position of aluminium radiators. First, the initial cost of the materials is lower, and second, a weight reduction of about 50% is possible. The second factor leads to increased fuel economy, but also, because the radiator is usually located forward of the front axle line, decreasing weight at this location serves to improve vehicle dynamics. Given the volumes of metal involved, the aluminium radiator has been the focus of intensive processing design, to ensure that it can be manufactured to provide the service properties required and that it is cost effective.

From Fig. C5.1, it is apparent that the unit consists of two tanks (upper and lower, or often located on either side of the unit), with the body made up of a series of fins and tubes. The fin-tube arrangement is shown in greater detail in Fig. C5.2. The engine coolant mixture of water and glycol antifreeze flows through the tubes, while cooling air passes over the fins on the outside of the tubes. Efficient heat transfer from the cooling liquid, through the tubes to the fins, requires good contact between the fins and tubes. Many radiators made of copper-brass and some aluminium radiators are mechanically clamped together to maintain contact between the fin and tube. This method offers lower assembly costs, but lower heat transfer efficiency compared to joining the fins and tubes. Therefore, the challenge has been to design a process capable of joining the thousands of fin-tube contact points in a practical manner. This is achieved by using a version of furnace brazing.

The fins and tubes are fabricated from aluminium alloy 3003 (or a variant of 3003). The composition and solidus temperature of 3003 are listed in Table C5.1. The brazing metal is an Al-Si alloy (a 4XXX series alloy; see Table C5.1) with a solidus

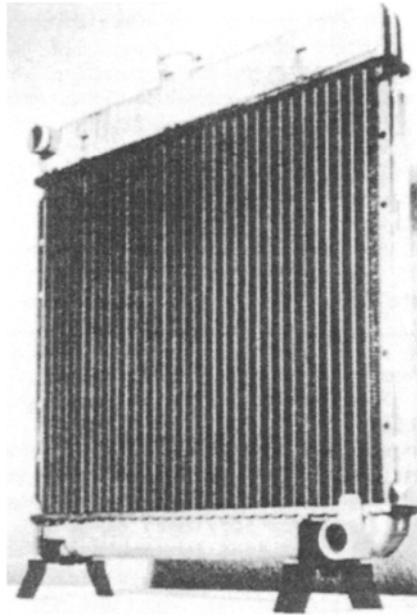


Fig. C5.1 Typical aluminium automotive radiator. (Reproduced from *Aluminium Technology* '86, with permission of The Institute of Materials.)

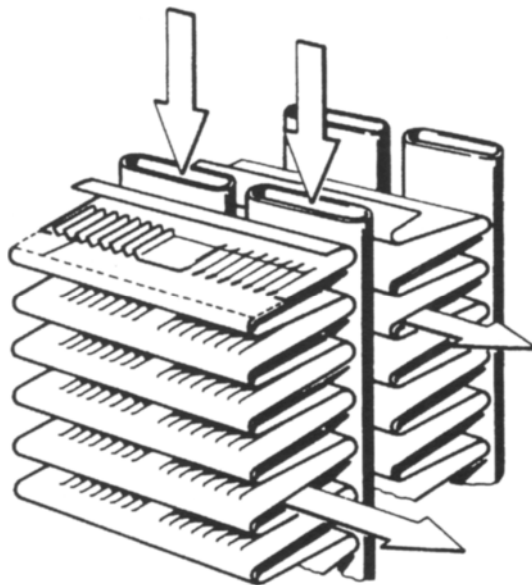


Fig. C5.2 Fin-tube arrangement for automotive radiator. (Reproduced from *Aluminium Technology* '86, with permission of The Institute of Materials.)

Table C5.1 Composition and solidus temperature of radiator aluminium alloys

Alloy	Composition (weight percent)							Solidus temperature (°C)
	Si	Fe	Cu	Mn	Mg	Zn	Bi	
3003	0.6	0.7	0.05–0.20	1.0–1.5	–	0.10	–	640
4004	9.0–10.5	0.8	0.25	0.10	1.0–2.0	0.20	–	554
4104	9.0–10.5	0.8	0.25	0.10	1.0–2.0	0.20	0.02–0.20	
4343	6.8–8.2	0.8	0.25	0.10	–	0.20	–	577
4047	11.0–13.0	0.8	0.30	0.15	0.10	0.20	–	577
7072	0.7 Si + Fe		0.1	0.1	0.1	0.8–1.3	–	641

temperature below 600°C. Therefore, if the fin or tube has a surface layer of an Al–Si brazing alloy, then heating the fin–tube assembly to a temperature above the solidus of the Al–Si brazing alloy, but lower than the solidus of 3003, will result in brazing of all fin–tube contact points. The major processing steps to achieve this desired result are outlined below.

The first joining process is to form the clad layer of Al–Si alloy on the 3003 base. Although there are several methods of accomplishing this, a common technique is to take DC ingots of alloy 3003 and locally weld the desired proportional thickness of the clad layer to the ingot face. For example, on a DC ingot of 3003 of 50 cm thickness is placed a plate of Al–Si alloy of 5 cm thickness, to give an eventual 10% clad thickness. This ingot plate combination is heated to hot rolling temperatures and rolled on a reversing breakdown mill, similar to that of Fig. C3.1. The heat and pressure applied during breakdown roll bond the ingot and plate together. The bonded clad plate is hot and cold rolled to the final thickness required. The cladding is almost always applied to the tubing rather than the fins, as the final thickness of the tubing is greater than that of the fins (about 0.4 mm for tubing and about 0.12 mm for fins). A section through 3003 sheet clad with 4343 is shown in Fig. C5.3, in which the different microstructures of the two alloys are visible, but the bond interface is almost invisible. The clad brazing sheet is formed into tubing by slitting the sheet to the required width, roll forming (Fig. C5.4) and sealing by arc seam welding.

The seam welded tubing and sheet-formed fin stock are assembled by clamping them together into the fin tube arrangement of Fig. C5.2 in preparation for brazing. The assembly can then be heated to a temperature between the solidus of the brazing alloy (Al–Si) and base metal (3003) to achieve bonding. One of the problems associated with brazing is poor bonding caused by the naturally occurring oxide on most metallic surfaces. Aluminium has a tenacious oxide layer that, although very thin, prevents good bonding of the surfaces. To deal with this problem, a *brazing flux* can be applied to the surfaces. Chloride/fluoride-containing fluxes dissolve the aluminium surface oxide. A brazing flux specifically designed for aluminium is potassium fluoroaluminate (K_3AlF_6 – $KAlF_4$), which has a solidus temperature of 570°C. This flux avoids many of the problems associated with other fluxes, because it is noncorrosive to aluminium, and is insoluble in water and so can be easily removed from waste streams, thereby minimizing environmental problems. Radiators can be furnace brazed in an inert atmosphere using this flux (which is designated the trade name NOCOLOK by Alcan Aluminium) and do not require washing for flux removal.

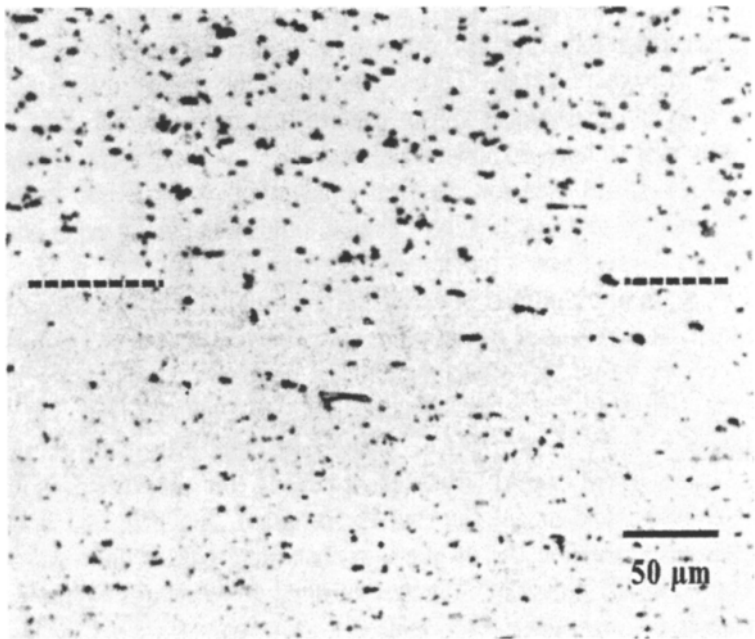


Fig. C5.3 Structure of brazing sheet, with clad layer of 4343 (above) on a base of 3003 (below). Dotted lines indicate bond line. (Reprinted with permission from *ASM Aluminum Properties and Physical Metallurgy*, edited by J. Hatch (1984), ASM International, Materials Park, OH 44073-0002 (formerly American Society of Metals, Metals Park, Ohio, 44073), p. 69, Fig. 15.)

The process of *fluxless* brazing is now also used for the manufacture of radiators. Fluxless brazing makes use of Al–Si brazing alloys that are designed to modify and break up the oxide layer at the brazing temperature. Magnesium and/or bismuth additions to the brazing alloys, such as 4004 or 4104 (see Table C5.1), are effective

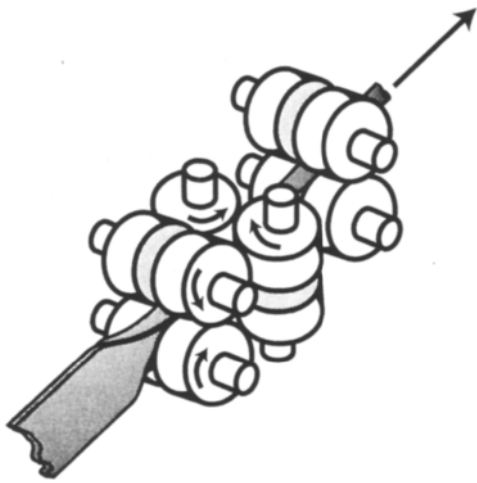


Fig. C5.4 Diagram of roll forming of sheet to make tubing.

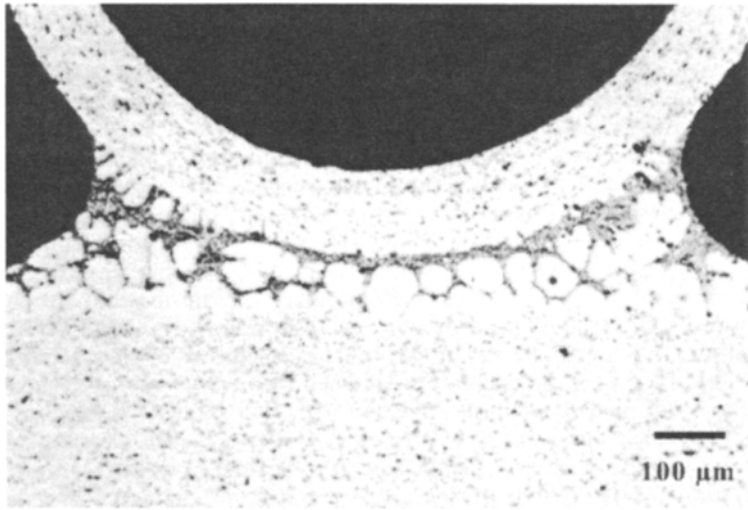


Fig. C5.5 Section of a radiator brazed joint. Fin stock (top) is bars (unclad) 3003 and tube (bottom) is 4343 clad on a 3003 core. (Reprinted with permission from *ASM Aluminum Properties and Physical Metallurgy*, edited by J. Hatch (1984), ASM International, Materials Park, OH 44073-0002 (formerly American Society of Metals, Metals Park, Ohio, 44073), p. 69, Fig. 16.)

in breaking down the surface oxide. Fluxless brazing requires vacuum furnaces with good temperature accuracy, to ensure that the oxide layer is modified and that the brazing processes occur in a controlled manner. The resulting fin–tube join is shown in Fig. C5.5.

Also required for radiator applications is good corrosion resistance, including exposure to salt spray from the use of road deicing salts in many areas. Internal corrosion of tubing is prevented by the use of ‘closed cooling systems’ and appropriate antifreeze solutions. To improve external corrosion, the zinc-containing alloy 7072 (see Table C5.1) is used to clad both sides of the fins. The solidus of 7072 is 641°C and so it does not melt during the brazing process. As 7072 is cathodic to 3003, it provides corrosion protection to the 3003 fins and tubes.

Case study 6: Manufacture of stainless steel automotive exhaust systems

Most drivers have had to replace exhaust system components. The failure of exhaust components is a result of the severe operating environment: external surfaces reach 500°C and are exposed to rain, snow, deicing salts and impact from road debris; and internal surfaces are exposed to slightly oxidizing gases and condensate, with catalytic converter temperatures as high as 900°C. However, primarily due to the introduction of stainless steel for automotive exhaust system components, such failures should occur much less often in the future. To successfully and economically use stainless steel for exhaust system applications requires the intelligent application of many of the principles described in the preceding chapters.

In North America, stainless steel first replaced mild steel for exhaust applications in the early 1960s on V-8 powered vehicles with dual exhaust systems. The lower flow rate of combustion products through each of the exhaust pipes caused longer warm-up times, increasing the volume of corrosive condensate formed, leading to premature muffler perforation, often during the warranty period. Therefore, the more expensive stainless steel was offset by the reduced warranty repairs.

More recently, increased exhaust gas temperatures and government warranty mandates for catalytic converters have provided the driving force for the widespread introduction of stainless steel exhaust systems. The average life of a mild steel exhaust component is about 18 months, for aluminized steel (briefly discussed in Section 9.3.4) it is 30 months, whereas stainless steel systems reliably last 5 years. Because of these factors, in 1990 about 75% of North American exhaust systems were of stainless steel, and by 1994 this figure had increased to 95%. An objective for the year 2000 is <1% failure rate requiring replacement in 10 years. To meet these ever-increasing application requirements has necessitated a concerted effort to develop improved manufacturing and fabrication processes. This case study highlights the major process developments.

Exhaust system components are manufactured from ferritic stainless steels. This class of stainless steels derives its name from its body centred cubic or ferritic crystal

structure and relies on chromium additions of at least 10.5% for corrosion resistance. For many years a problem associated with ferritic stainless steels was poor weldability. During welding, chromium carbides form along grain boundaries, removing chromium from the matrix, leading to rapid intergranular corrosion during service. This phenomenon is usually referred to as *sensitization*.

Improving the weldability necessitates a low carbon and nitrogen content. However, when first introduced into exhaust systems during the early 1960s, most stainless steel was refined in electric arc furnaces similar to that of Fig. 1.5. The thermodynamics of the refining process for Cr-containing steels makes it difficult to produce low carbon and nitrogen contents, while still maintaining the high Cr required for corrosion resistance. Consequently, most ferritic stainless steels of this period contained at least 0.1% carbon, sufficient for sensitization and the associated poor intergranular corrosion resistance after welding. Although austenitic stainless steels with good corrosion resistance, weldability and formability were readily available and suitable for exhaust applications, the Ni and higher Cr content of austenitic stainless steels make them less economical.

A major breakthrough was the introduction in the late 1960s of the argon–oxygen–decarburization (AOD) process for refining stainless steels. The heart of the AOD process is a refining vessel, not dissimilar to a Bessemer converter. However, rather than blowing air through the tuyères of Fig. 1.2, a mixture of oxygen and argon is used. By appropriately altering the oxygen:argon ratio during the refining process, the thermodynamics of the various refining reactions can be controlled to produce a low carbon/nitrogen steel with a high chromium content. The most common ferritic stainless steel used for exhaust system components is type 409, with a typical composition of 0.010 wt% C, 0.25 wt% Mn, 0.40 wt% Si, 11.2 wt% Cr, 0.25 wt% Ni and 0.20 wt% Ti. The economical processing of low carbon stainless steels via the AOD process is a key factor, contributing to the development of weldable ferritic stainless steels suitable for exhaust applications. Once AOD refining achieves the required composition, the steel is continuously cast, using a process similar to that of Fig. 2.3, and rolled to the thickness desired.

Many exhaust system components, such as muffler and catalytic converter shells, have complex shapes necessitating sheet with good formability and deep drawability. Therefore, the rolling process must be designed to produce sheet with the appropriate strain hardening exponent, n , and crystallographic texture. Typically, fully annealed or recrystallized sheet displays the highest n value which, as highlighted in Sections 3.4 and 5.5, is equivalent to the uniform true strain before the onset of necking. Therefore, after rolling, the sheet is annealed to maximize the formability. For type 409 stainless steel the annealed n value is approximately 0.25, with a corresponding yield strength of 240 MPa and ultimate tensile strength of 413 MPa. Formability is also related to the plastic anisotropy parameters introduced in Section 5.7. Improved sheet formability is related to a high mean anisotropy r_m , according to equation 5.16, because thinning due to necking is resisted. However, unlike the strain hardening exponent, the anisotropy is dependent on the prior rolling reduction, as shown in Fig. C6.1, which indicates a large cold reduction prior to annealing should improve formability.

The deep drawability is also dependent on the anisotropy because of the development of a crystallographic texture during rolling. One manifestation of the development of crystallographic texture is the formation of ears during forming, leading to

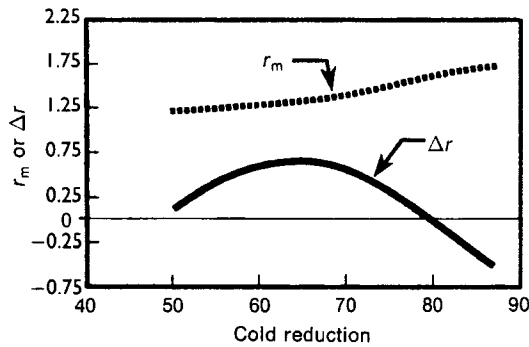


Fig. C6.1 Influence of cold reduction on crystallographic texture of annealed type 409 stainless steel. (Reproduced with permission of ASM International from *Advanced Materials & Processes*, 3/94, p. 18.)

excessive trimming. The tendency for earing can be characterized by calculating the *planar anisotropy*, Δr , according to

$$\Delta r = \frac{r_0 + r_{90} - 2r_{45}}{2}$$

where the r_i terms are defined in Fig. 5.20.

Earing is minimized with a Δr value of zero. As seen from Fig. C6.1, increasing the percentage cold reduction prior to annealing up to about 65% increases the planar anisotropy due to the formation of a crystallographic texture. This texture will lead to the formation of pronounced ears during forming, as exemplified by the four ears of Fig. 5.19(b). However, at higher cold reductions the development of a second texture occurs, leading to the formation of additional ears, each of which is smaller, as exemplified by the eight ears of Fig. 5.19(c). Therefore, appropriate cold rolling prior to annealing can cause the superposition of two crystallographic textures, lowering the Δr value (Fig. C6.1) with $\Delta r \approx 0$ at a cold reduction of 80%. This texture analysis indicates that cold rolling the sheet 80% prior to annealing will minimize the amount of material wastage due to trimming after forming. Although an 80% cold rolling reduction does not maximize the formability, as measured by the r_m of Fig. C6.1, sufficient formability is obtained to allow manufacture of the exhaust system components.

Ferritic stainless steels with low carbon and nitrogen contents can be welded using most of the techniques presented in Chapter 8. Tubes for exhaust pipes are often ultrasonically welded, whereas tube to muffler casings are MIG welded and other seams may be TIG welded or seam welded. During cooling following welding, martensite may form, with the attendant problems outlined in Section 8.2.4. However, as the carbon content of type 409 stainless steel is very low, the martensite formed has relatively low hardness and is not as detrimental to the properties as martensite formed during the welding of plain carbon or low alloy steels. Nevertheless, most ferritic stainless steels have additions of ferrite stabilizers that hinder martensitic transformation. Type 409 contains about 0.2 wt% Ti for ferrite stabilization. The metals Nb and Zr can also be used as ferrite stabilizers for ferritic stainless steels. These stabilizing elements also serve to decrease sensitization, and consequently improve the resistance to intergranular corrosion, as well as improving

high temperature oxidation and creep resistance – all of which are desirable attributes for exhaust system components.

This case study illustrates the application of several of the basic principles presented in the preceding chapters, aimed at the development of an improved product. It is important to note the influence of the various processing steps on the final product properties. It is not insignificant that the introduction of AOD refining was a major factor, providing improved weldability of ferritic stainless steels, which in turn allowed the economical development of improved or new applications for stainless steels. Similar process developments have led to analogous improved or new products made from other materials. This highlights two important factors. First, operations near the beginning of the processing sequence can have a marked influence on final product properties and service performance. Second, knowledge of materials processing principles leads to an understanding of the final product properties, which can then be improved and new products developed.

Surface modification for wear resistance

9.1 Introduction

Previous chapters introduced various processes aimed at changing the shape of a workpiece. Once these processes have been applied and the final desired geometry is obtained, it is often necessary to alter the properties of the workpiece, without changing the geometry, to develop the service performance required. One of the techniques widely used to achieve this objective is the application of *heat treatments* to modify the microstructure and consequently properties. Virtually all alloys are affected by heat treatment to some degree. Most heat treatments change the properties of the workpiece throughout. However, it is sometimes desirable to only modify the surface of the workpiece, to improve wear resistance. Often an advantage of only modifying the surface is that a tough, fracture-resistant microstructure can be retained in the bulk of the workpiece, while a hard wear resistant surface is obtained. Consequently, it is not uncommon to apply a heat treatment that will provide sufficient strength and toughness throughout the part and then apply a surface modification process to impart wear resistance.

Wear is damage involving progressive loss of material due to relative motion between a surface and a contacting substance. There are four *tribological* systems (*tribology* is the science of friction and wear): smooth solids sliding on smooth solids; hard, sharp substances sliding on softer surfaces; surface fatigue caused by repeated stressing; and relative motion between fluids, possibly with suspended solids, and a solid surface. The variety of techniques to reduce the wear rate caused by these tribological systems can be briefly summarized as:

1. separate the contacting surfaces with a lubricant film;
2. choose material combinations that are resistant to sliding interaction;
3. harden the wearing surface;
4. improve the resistance to fracture of a wearing surface;
5. improve the corrosion resistance of an eroding surface;
6. improve the fatigue resistance of a wearing surface.

The benefits of lubricating films were introduced in Sections 4.2.1 and 7.2.7. Material selection criteria are outside the scope of this book, so the following sections will concentrate on techniques that focus on points three to six.

9.2 Types of wear

Before considering the techniques to reduce wear, it is first necessary to understand the nature and types of wear that can occur. Although it is difficult to deal with the hundreds of surface problems encountered, the major types of wear are classified into four groups, as shown in Fig. 9.1. Often, several wear mechanisms act in conjunction.

Abrasion is the result of hard particles forced against a solid surface with relative motion. The types of abrasion listed in Fig. 9.1 are illustrated in Fig. 9.2. During *low stress abrasion* damaging hard particles are not deformed, as is the case for *high stress abrasion*. Examples of low stress abrasion are particles sliding on chutes, plowing soil, or the grinding operations of Fig. 7.19. *Gouging abrasion* often occurs concurrently with low and high stress abrasion as a result of a compressive loading striking the wearing surface. *Polishing wear* is the unintentional removal of material caused by rubbing, without visible scratching. Polishing is closely associated with low stress abrasion and both mechanisms can occur concurrently. The iron oxide particles

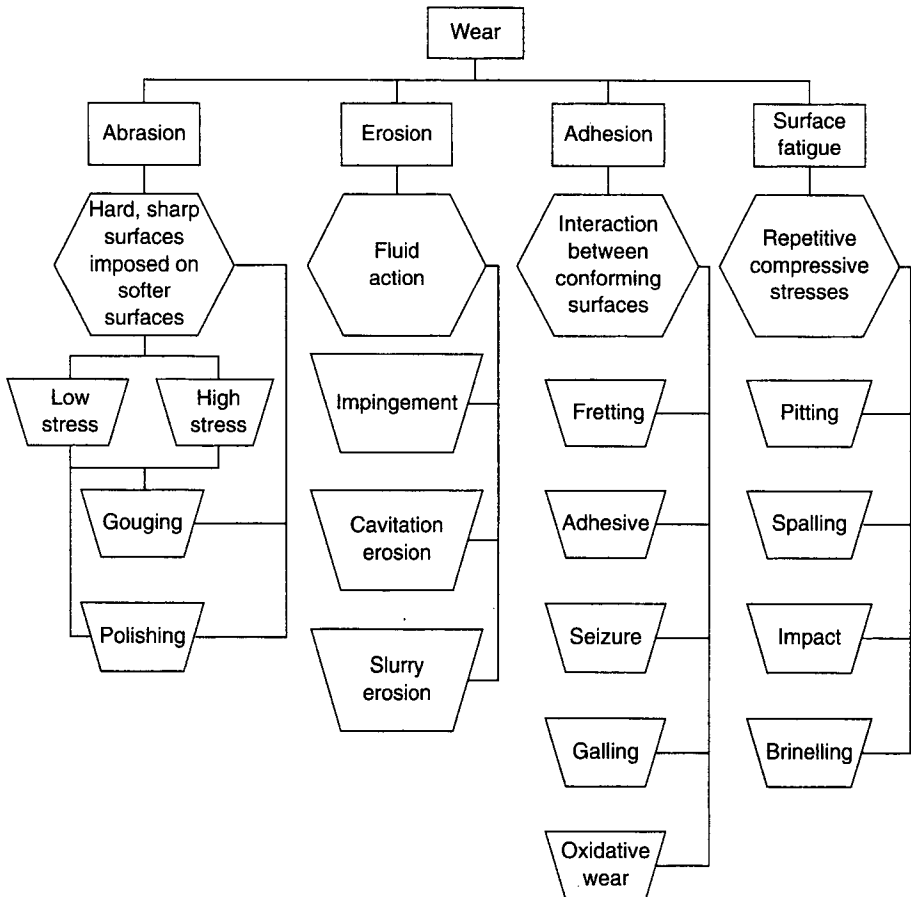


Fig. 9.1 Flow chart relating various types of wear.

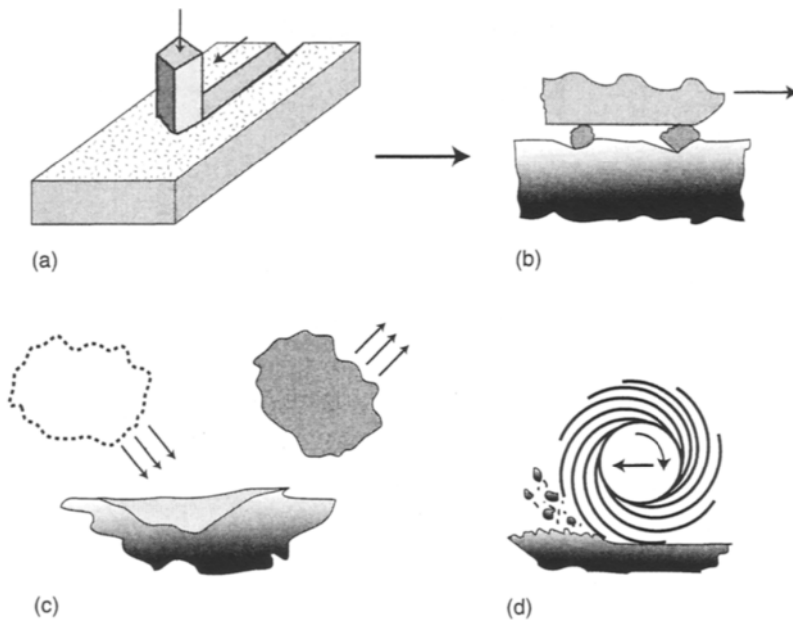


Fig. 9.2 Types of abrasion: (a) low stress abrasion, (b) high stress abrasion, (c) gouging, (d) polishing wear.

contained within magnetic disks and tapes for recording data are usually less than $3\text{ }\mu\text{m}$ in size and cause polishing wear of all surfaces on which they impinge.

Erosion is the gradual loss of material from a solid surface due to relative motion or mechanical interaction between a fluid containing particulate and a solid. The various forms of erosion listed in Fig. 9.1 are illustrated in Fig. 9.3. *Impingement erosion* results from a continuous succession of impacts between solid or liquid particles and a solid surface. Usually this term connotes that the impacting particles are smaller than the solid surface. The impacts cause local plastic deformation of the surface, with each particle causing a small crater and material removal. The rate of impingement wear is proportional to the kinetic energy of the impinging particles and inversely proportional to the hardness of the surface. Many impingement erosion problems exist, such as the ingestion of dirt or sand by aircraft engines, fans operating in dirty environments or high velocity liquid-gas flows in piping. *Cavitation erosion* is caused by the formation and collapse of bubbles within a liquid near a solid surface. Cavitation results from a decrease in local static pressure, as opposed to boiling which is caused by an increasing temperature. Cavitation erosion may occur on ship propellers, pumps and piping systems, as well as other applications. *Slurry erosion* is linked to impingement erosion by fluids. A *slurry* is a mixture of solid particles in a liquid of a consistency that allows the mixture to be pumped like a liquid. Relative motion of a slurry against a solid surface can cause erosion and can occur in mineral flotation pumps, oil well equipment, cement handling equipment etc.

Adhesion wear is the progressive loss of material from a solid surface which is initiated by some form of local bonding between two solid surfaces. If the adhesion wear occurs due to small amplitude oscillatory motion between the two surfaces this is termed *fretting* (Fig. 9.4(a)), with the relative motion between the two surfaces

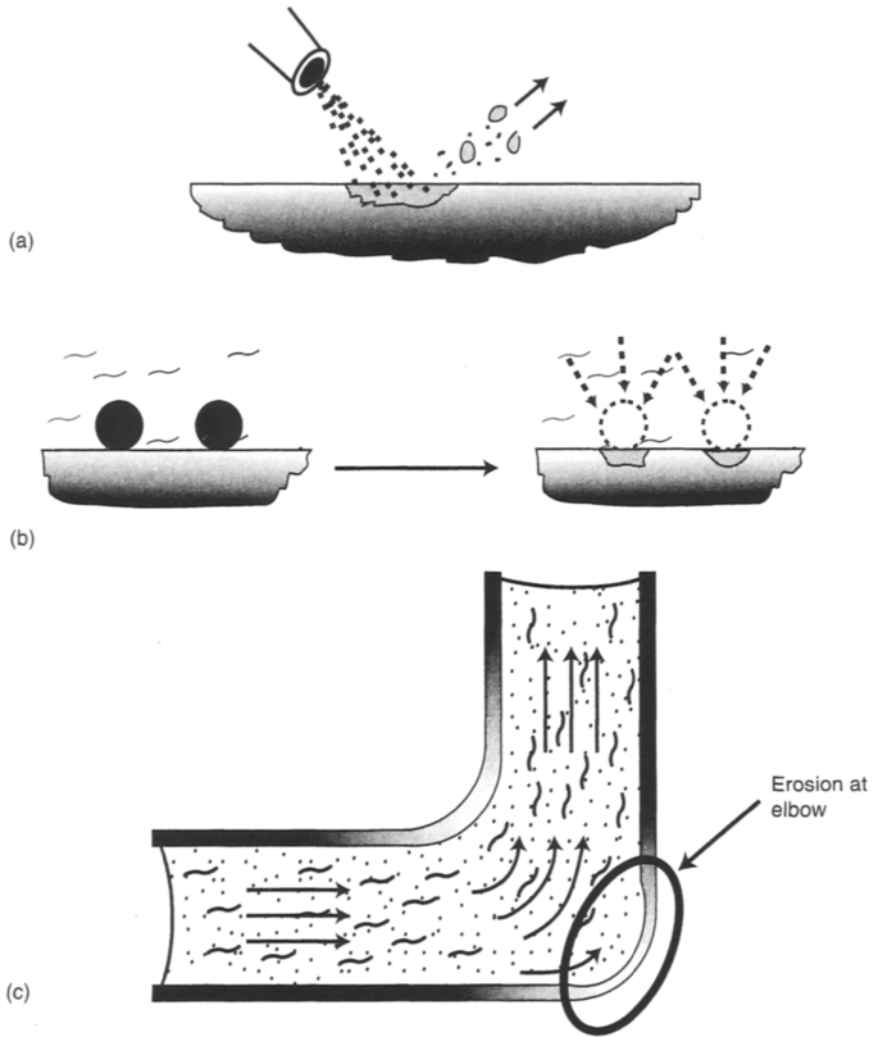


Fig. 9.3 Illustration of erosion mechanisms: (a) impingement erosion, (b) cavitation erosion, (c) slurry erosion.

usually unintentional. Fretting can occur in gears fixed to shafts using a set screw, loose fitting bearings or blade-disc fittings in gas turbines. *Adhesive wear* (Fig. 9.4(b)) is characterized by the local bonding of two solid surfaces causing transfer of material from one surface to the other. The local bonding may often be limited to asperities on the surfaces which, if carrying a load, can be subjected to tremendous pressures. Adhesive wear can occur in a wide range of applications, including O-rings, gears, cams, slides, pistons, bushings and other mechanical devices. *Seizure* causes relative motion between two solid surfaces to stop as a result of a high friction coefficient or gross surface welding (Fig. 9.4(c)). Most often seizure is the result of a loss of clearance between sliding surfaces, possibly due to a loss of lubricant or the build up of wear debris. *Galling* is a less well defined term, often used in conjunction

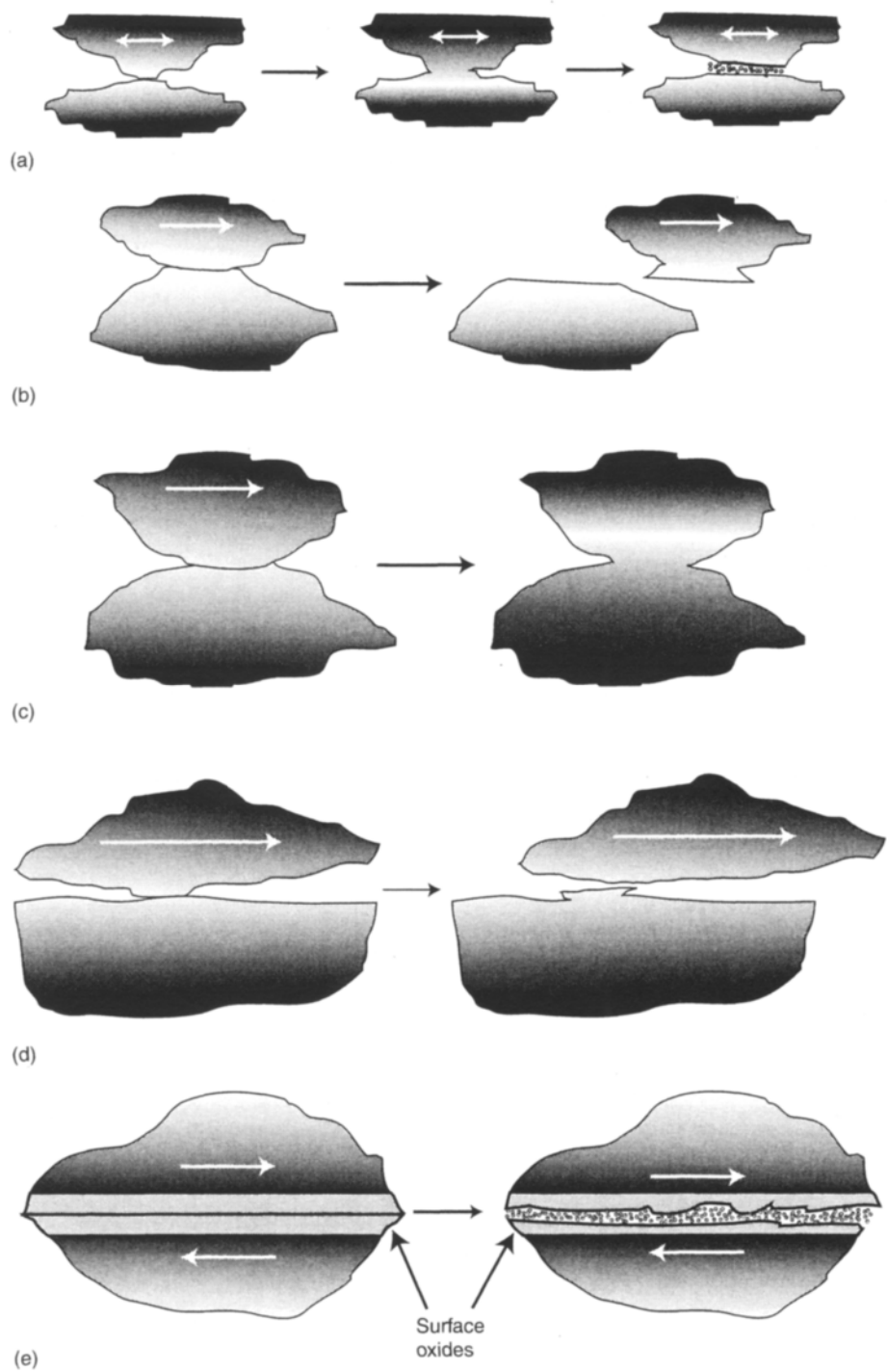


Fig. 9.4 Illustration of adhesion wear: (a) fretting wear, (b) adhesive wear, (c) seizure, (d) galling, (e) oxidative wear.

with *scuffing* or *scoring*. Galling is characterized by severe scuffing between surfaces causing gross surface damage or failure associated with plastic deformation of the area of contact (Fig. 9.4(d)). The plastic deformation causes excrescence from one or both of the solid surfaces, that eventually leads to failure. Galling can occur in sliding members or valves. The beverage can ironing process in Case study 4 is prone to galling and/or scoring if the tooling, lubrication, or sheet metallurgy is not well controlled. During *oxidative wear* the sliding solid surfaces react with the local environment to form surface oxides that separate from the surfaces. Oxidative wear usually has a low wear rate. Typically, surface asperities fracture from the

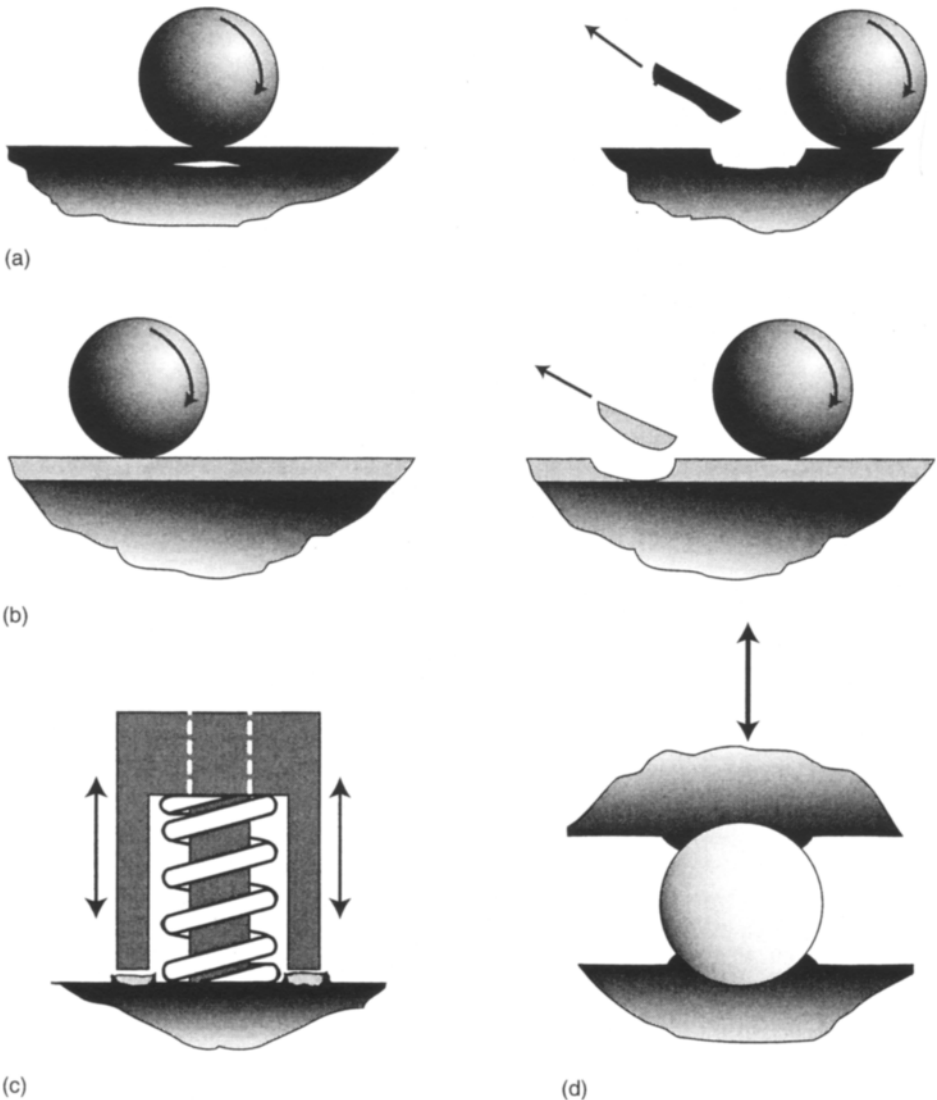


Fig. 9.5 Illustration of surface fatigue mechanisms: (a) pitting, (b) spalling, (c) impacting, (d) brinelling.

surface and then oxidize, but remain in the contact area and serve as a solid lubricant that decreases the wear rate. This form of wear eventually causes loss of dimensional tolerances. Oxidative wear is common to hinges or dry sliding systems, especially in furnaces or ovens.

The repeated rolling or sliding of surfaces can cause wear by *surface fatigue*. A common example of surface fatigue is the wear of bearing races in which a wear track develops from repeated contact with rollers or ball bearings. This type of wear can result in *pitting*, often following subsurface cracking, as shown in Fig. 9.5(a). Pitting can occur in various types of bearings, cams or gear teeth. Separation of flakes from a surface is referred to as *spalling* (Fig. 9.5(b)). Spalling is usually more severe than pitting and is most often associated with bearings and gear teeth. Thin, hard wear coatings on a soft substrate are particularly prone to spalling. *Impact wear* (Fig. 9.5(c)) is caused by the repetitive impacting of surfaces. The impacting causes plastic deformation of one or both of the surfaces. Common instances of impact wear are rivetting tools, machine stops etc. Repeated indentation of a surface by a solid body that causes local impacts or static overload causes *brinelling* (Fig. 9.5(d)). Brinelling results in surface damage characterized by local plastic denting or deformation, often due to the overloading of bearing surfaces.

9.3 Diffusional processes

Diffusional surface modification processes rely on *diffusion* of new atoms into the workpiece to alter the mechanical properties of the surface region. Diffusion is the spontaneous movement of atoms to new sites within the metallic crystal structure. When controlled appropriately, diffusion can create a net flux of atomic movement. Although new atoms move into the workpiece, there is no intentional build-up or increase in the workpiece dimensions.

9.3.1 Carburizing

The most common of the diffusional surface modification processes is the *carburizing* of low carbon steels. The objective of carburizing is to obtain a hard wear-resistant surface with a tough interior. Low carbon steels are tougher than medium or high carbon steels, but low carbon steels cannot be *quench hardened* sufficiently to provide good wear resistance. Quench hardening of steels involves heating the steel into the austenite region (see the Fe–C phase diagram, Fig. 2.32) and cooling sufficiently quickly that martensite forms. As shown in Fig. 9.6, the hardness of martensite increases with increasing carbon content, to a maximum hardness at about 0.5 wt% carbon. To improve wear resistance, additional carbon is diffused into the surface of a steel component during carburizing by exposing it to a carbonaceous atmosphere. The purpose of carburizing is to increase the surface carbon content such that the surface region, or *case*, achieves maximum hardness during subsequent *quench hardening*. Therefore, during carburizing the surface carbon content should be increased to about 0.5 wt%.

Table 9.1 Summary of diffusional surface modification processes

Process	Temperature (°C)	Case depth (mm)	Surface hardness (Rockwell C)	Base metal ^a	Comments
<i>Carburizing</i>					
Pack	815–1090	0.125–1.5	50–63*	lc, lca	low equipment cost, poor control
Gas	815–980	0.075–1.5	50–63*	lc, lca	accurate case depth, gas safety
Liquid	815–980	0.05–1.5	50–65*	lc, lca	faster, salt disposal problems
<i>Nitriding</i>					
Gas	480–590	0.125–0.75	50–70	as, nits, stainless steel	hard case, no quench, slower
<i>Carbonitriding</i>					
Gas	760–870	0.075–0.75	50–65*	lc, lca,	less distortion than carburizing
Liquid	760–870	0.0025–0.125	50–65*	stainless steel, lc	thin case, salt disposal problems
Aluminizing	870–980	0.025–1	<20	lc	oxidation free surface
Siliconizing	1010	0.025–1	30–50	lc	atmosphere control critical
Chromizing	980–1090	0.025–0.05	<30	lc, hc	corrosion–wear resistance

^a lc = low carbon steels, hc = high carbon steels, lca = low carbon alloy steels, nits = nitriding steels, as = alloy steels, ss = stainless steels, * = requires quench.

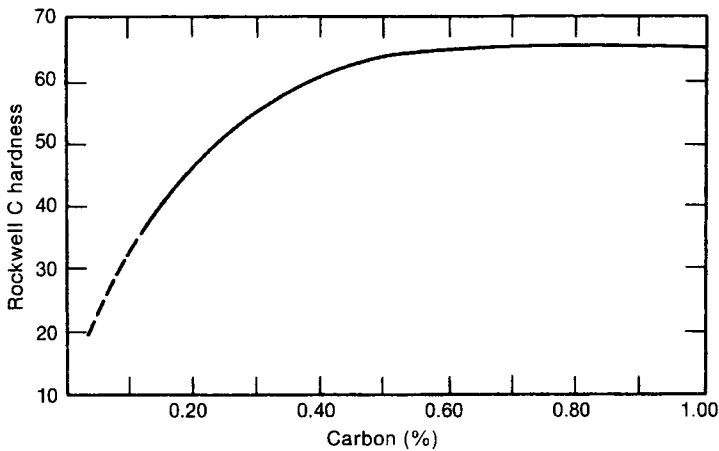


Fig. 9.6 Hardness of martensite as a function of carbon content.

Pack carburizing

Pack carburizing is probably the simplest of the carburizing processes. Pack carburizing involves placing parts to be hardened in a container filled with a suitable carburizing medium (the *pack*), typically charcoal from hardwood. The pack is put in a furnace and heated into the austenite region of the phase diagram (Fig. 2.32) for a sufficient time to allow the diffusion of carbon into the component surface. Little if any carbon diffusion occurs between the charcoal and component directly. Rather, the charcoal forms carbon dioxide which, in the presence of excess carbon within the pack, converts to carbon monoxide according to



At the carburizing temperature this reaction always proceeds to the right. The carbon monoxide then reacts with the steel component, causing absorption of carbon into the component so that equation 9.1 proceeds to the left. The container surrounding the pack must prevent excessive oxygen from entering the pack to prevent the charcoal from burning. The part can be quenched upon removal from the pack, or cooled and then reheated into the austenite region and then quenched. The latter option is necessary if removal of a hot part from the pack is difficult.

Pack carburizing can be done in almost any furnace, the equipment requirements are minimal and relatively deep cases can be achieved. Although pack carburizing requires little operator skill, it is labour intensive and relatively slow. The slowness of the process is caused by poor heat transfer efficiency, because the carburizing medium surrounding the component acts as an insulator, necessitating long heating periods. Some of the characteristics of pack carburizing are summarized in Table 9.1.

Gas carburizing

In *gas carburizing* the component is heated into the austenite region of the Fe–C phase diagram in the presence of a carbon containing gas. Typically, the gas atmosphere is methane, CH_4 . Natural gas is approximately 85% methane. Free carbon is

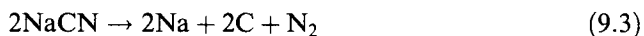
available to diffuse into the component by the reaction



Note that in this equation both the reactants and products contain flammable gases. As the operation is carried out at high temperature, the potential for a furnace explosion exists. Consequently, atmosphere-tight furnaces capable of maintaining pressures just above atmospheric pressure, to prevent infiltration of air, with close control of furnace temperature and atmosphere, are necessary. Gas carburizing provides improved control over the case depth and hardness compared to pack carburizing and, although the labour content is low, more highly skilled personnel are required to maintain the necessary furnace controls.

Liquid carburizing

Liquid carburizing involves placing the workpiece in a molten salt that contains carbon-bearing compounds. Usually the molten salt is contained within an externally heated metal pot. Most carburizing salts contain sodium cyanide, NaCN, as the active chemical. This salt becomes liquid at 538°C and can be used to temperatures of about 950°C. Carbon for diffusion into the workpiece is available from the reaction



In addition to this reaction, the sodium cyanide can react with the workpiece surface, releasing nitrogen, which also diffuses into the case. Nitrogen is a solid solution strengthener in steel and, therefore, increases the hardness of the case above that possible from the diffusion of carbon alone. Liquid carburizing is well suited to low volume production and produces a hard case in a relatively shorter time than other techniques. The shorter time required is associated with the good heat transfer characteristics of the salt bath and lack of scale formation on the surface. However, a major disadvantage of this technique is the use of cyanide salts, which are highly poisonous and may also form poisonous gases when heated. This causes health and disposal problems.

Diffusional flow during carburizing

The case depth is controlled by the diffusion of carbon atoms through the surface layers of the workpiece. Carbon from the surrounding atmosphere or pack quickly saturates the surface layer after the start of the case hardening process. The carbon saturation concentration at the surface is the maximum carbon content that can be absorbed in the austenite phase, determined from the Fe–C phase diagram (Fig. 2.32). This surface layer remains saturated at the same carbon concentration throughout the case hardening treatment, while carbon diffuses inward to form the case. Typical carbon concentration profiles, as a function of depth from the surface, are shown in Fig. 9.7. At any time (e.g. $t_1 > 0$) the carbon concentration decreases from the saturation level (c_s) to the initial carbon concentration in the steel workpiece, usually between 0.1 and 0.45 wt% carbon. At a later time (e.g. $t_2 > t_1$) the concentration profile is similar, except that it is shifted to higher carbon contents at each depth, reflecting the greater amount of carbon diffused into the case.

Figure 9.7 illustrates that the carbon concentration is a function of the depth from the surface (x) and the elapsed time (t). The dependence on depth can be determined

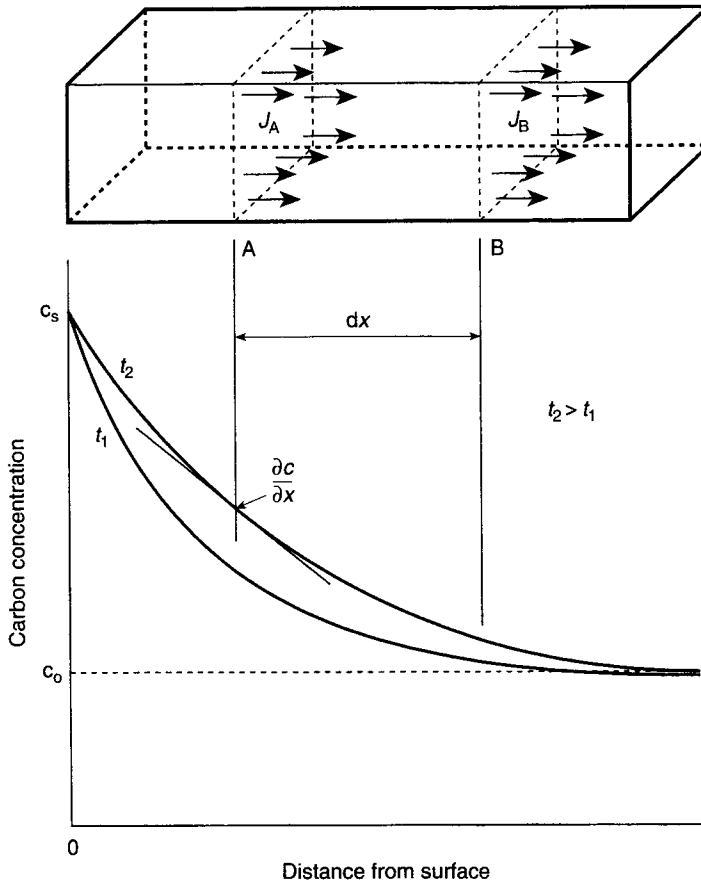


Fig. 9.7 Diffusional flow during carburizing.

from the flux of atoms diffusing across each plane within the workpiece. For example, the instantaneous flux of atoms diffusing across plane A in Fig. 9.7 is expressed as

$$J_A = \frac{1}{A} \times \frac{\partial N_C}{\partial t} \quad (9.4)$$

where: J_A is the flux of atoms across plane A of Fig. 9.7

A is the area of plane A in Fig. 9.7

N_C is the number of carbon atoms crossing plane A.

It is apparent that the flux of carbon atoms crossing the plane is proportional to the concentration gradient in Fig. 9.7. Expressed mathematically this is *Fick's first law*:

$$J = -D \times \frac{\partial c}{\partial x} \quad (9.5)$$

where: c is the carbon concentration

x is the depth from surface

D is the *diffusion constant*.

The negative sign is necessary because the concentration gradient is negative in the direction of flow, i.e. carbon atoms diffuse from a region of high concentration to low concentration.

Fick's first law describes the instantaneous flow of diffusing atoms in the case layer. *Fick's second law* describes the time dependency of the diffusing flow. To develop Fick's second law, consider an element of length dx , bounded by planes A and B (Fig. 9.7). The carbon flux across plane A can be described by Fick's first law as

$$J_A = -D \times \frac{\partial c}{\partial x} \quad (9.6)$$

and the diffusing flux across plane B is

$$J_B = J_A + \frac{\partial J_A}{\partial x} dx \quad (9.7)$$

The accumulation of carbon atoms between the two reference planes is obtained by subtracting equation 9.7 from 9.6, to obtain

$$\begin{aligned} dm &= -\frac{\partial J_A}{\partial x} dx \\ &= -\frac{\partial}{\partial x} \left(-D \frac{\partial c}{\partial x} \right) dx \end{aligned} \quad (9.8)$$

where dm is the number of carbon atoms per unit area per unit time accumulating between planes A and B.

The rate of accumulation, dm , divided by the distance between the two reference planes, dx , represents the change of concentration with time in this region, or

$$\frac{dm}{dx} = \frac{\partial c}{\partial t} \quad (9.9)$$

Substituting equation 9.9 into 9.8 gives the usual form of Fick's second law of diffusion:

$$\frac{\partial c}{\partial t} = \frac{\partial}{\partial x} \left(D \frac{\partial c}{\partial x} \right) \quad (9.10)$$

If the diffusion constant is assumed to be independent of x , which is equivalent to assuming that it is independent of concentration, then equation 9.10 can be simplified to

$$\frac{\partial c}{\partial t} = D \frac{\partial^2 c}{\partial x^2} \quad (9.11)$$

The mathematical form of Fick's first and second laws (equations 9.5 and 9.11) are exactly the same as the equations for conductive heat flow during shape casting (equations 2.1 and 2.2). Also, the carbon concentration gradients of Fig. 9.7 are analogous to the temperature gradients of Fig. 2.22. Both of these physical situations represent the phenomenon of *mass transport in solids* and, therefore, the solution to both physical problems is similar. As such, the equation representing the carbon concentration in the carburized surface region has the same form as equation 2.7, i.e.

$$c(x, t) = c_S + (c_0 - c_S) \operatorname{erf} \left(\frac{x}{2\sqrt{Dt}} \right) \quad (9.12)$$

where: $c(x, t)$ is the carbon concentration at depth x
 c_s is the carbon concentration at the surface
 c_o is the base steel carbon content
 erf is the Gaussian error function (Table 2.2)
 x is the depth from the surface
 D is the diffusion constant
 t is the time.

The diffusion constant D is the material constant that describes the kinetic rate of diffusion. This constant depends on temperature because, as the temperature increases, the energy with which atoms vibrate about their equilibrium positions within the crystal lattice increases. Occasionally an atomic vibration is of a sufficient energy to allow an atom to move to a new lattice position. In steels, during carburizing, carbon atoms diffuse from one interstitial position to an adjacent interstitial site within the iron matrix. As the temperature, and thus the energy, increases, the number of times atoms can jump to a new position increases and, hence, the diffusion rate increases.

The ease with which carbon atoms can move to new interstitial sites is determined by an energy barrier working against such movement. Energy is required to break the existing atomic bonds of the migrating atom and force other atoms to distort slightly from their low energy lattice sites to allow passage of the carbon atom. The energy barrier for the diffusion of relatively small carbon atoms in iron is quite low, at about 142 kJ/mol of diffusing atoms. For the diffusion of the larger iron atoms within the iron matrix, or self-diffusion, the energy barrier is much higher, at about 289 kJ/mol of diffusing atoms.

The energy barrier, or *activation energy*, presents an obstacle to diffusion. However, as the temperature is increased, the atomic vibrations increase in frequency and amplitude. Thus, temperature increases the base energy level of the material, making the energy barrier easier to overcome. Consequently, diffusion is a *thermally activated* process. The relationship between these variables obeys the familiar Arrhenius relationship:

$$D = D_o \exp \left(\frac{-Q}{RT} \right) \quad (9.13)$$

where: D_o is the *frequency factor*
 Q is the *activation energy*
 T is the *absolute temperature (K)*
 R is the *universal gas constant (8.314 J/mol · K)*.

The frequency factor and activation energy are constants for each physical diffusion couple. Table 9.2 lists these constants for diffusional systems often encountered in the surface hardening of steels.

Example 9.1 Carbon profile after carburizing

A piece of SAE1010 steel (0.10% carbon) is carburized at 900°C for 10 h. Calculate and graph the carbon concentration in the case after the 10 h carburizing operation.

Solution

$$t = 10 \text{ h} = 3.6 \times 10^4 \text{ s}, C_o = 0.1\% \text{ carbon}, T = 900^\circ\text{C} = 1173 \text{ K}$$

Table 9.2 Frequency factors and activation energies for diffusional systems

Diffusing atom	Host atom	Frequency factor, D_0 (cm ² /s)	Activation energy, Q (kJ/mol)
Carbon	iron (bcc)	0.0079	76
Carbon	iron (fcc)	0.21	142
Nitrogen	iron (bcc)	0.014	74
Iron (bcc)	iron (bcc)	0.01	289

From Table 9.2, for carbon diffusing in austenite (fcc iron), $Q = 142$ kJ/mol, $D_0 = 0.21$ cm²/s, $R = 8.314$ J/mol. Using the Fe–C phase diagram (Fig. 2.32) at 900°C the maximum solubility of carbon in iron (austenite) is about 1.3%, so $C_s = 1.3\%$.

Using equation 9.13, calculate the diffusion constant:

$$\begin{aligned}
 D &= D_0 \exp\left(-\frac{Q}{RT}\right) \\
 &= 0.21 \text{ cm}^2/\text{s} \times \exp\left(-\frac{142\,000 \text{ J/mol}}{8.314 \text{ J/mol} \cdot \text{K} \times 1173 \text{ K}}\right) = 1.0 \times 10^{-7} \text{ cm}^2/\text{s}
 \end{aligned}$$

Use equation 9.12 to calculate carbon concentration for various depths:

$$\begin{aligned}
 c(x) &= c_s + (c_0 - c_s) \operatorname{erf}\left(\frac{x}{2\sqrt{Dt}}\right) \\
 &= 1.3 - 1.2 \operatorname{erf}\left(\frac{x}{2\sqrt{1 \times 10^{-7} \text{ cm}^2/\text{s} \times 3.6 \times 10^4 \text{ s}}}\right) \\
 &= 1.3 - 1.2 \operatorname{erf}(8.3x)
 \end{aligned}$$

Using Table 2.2 the following can be calculated:

x	$c(x)$
0	1.3
0.01	1.18
0.05	0.76
0.1	0.38
0.2	0.124
0.3	0.1

Plotting these data yields the profile shown in Fig. E9.1.

Carburized case depth

The plot of Example 9.1 clearly indicates that the carbon concentration varies as a function of depth. However, to characterize the carburized layer, a *case depth* is defined as the depth corresponding to a carbon concentration that is the average of the initial and saturation carbon concentrations. Thus the carbon concentration at the case depth is

$$c(x_p) = \frac{c_s + c_0}{2} \quad (9.14)$$

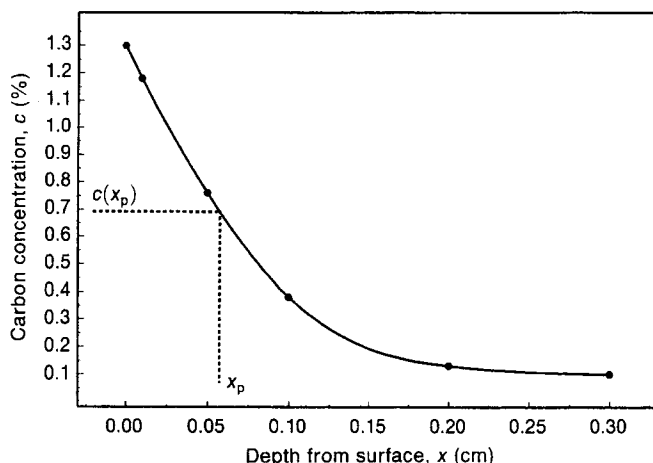


Fig. E9.1 Example 9.1.

where: c_s is the carbon surface saturation concentration
 c_o is the initial carbon content of the steel
 $c(x_p)$ is the carbon concentration at the case depth.

The carbon concentration, $c(x_p)$, is shown on the carbon concentration profile of Example 9.1, and the corresponding case depth, x_p , is identified. By substituting equation 9.14 into the equation for the carbon concentration (equation 9.12), and realizing from Table 2.2 that $\text{erf}(0.5) \approx 0.5$, the case depth is approximated as

$$x_p = \sqrt{Dt} \quad (9.15)$$

The square root form of the distance is often referred to as the *Einstein equation* and is common to many mass transport phenomena. Equation 9.15 is a useful approximation because it provides an easy method of determining the case depth for a particular furnace temperature, which in turn determines the value of the diffusion constant from equation 9.13.

Example 9.2 Case depth

- For the conditions of Example 9.1, calculate the case depth.
- If the conditions of Example 9.1 are repeated but the carburizing temperature is increased to 1000°C, what carburizing time would result in the same case depth?

Solution

- From Example 9.1, $D = 1 \times 10^{-7} \text{ cm}^2/\text{s}$, and $t = 3.6 \times 10^4 \text{ s}$.
Using equation 9.15,

$$x_p = \sqrt{Dt} = \sqrt{1 \times 10^{-7} \text{ cm}^2/\text{s} \times 3.6 \times 10^4 \text{ s}} = 0.06 \text{ cm}$$

The case depth of 0.06 cm is in agreement with the carbon concentration profile of Example 9.1.

- To achieve the same case penetration depth the product Dt must remain constant:

$$Dt = 1 \times 10^{-7} \text{ cm}^2/\text{s} \times 3.6 \times 10^4 \text{ s} = 3.6 \times 10^{-3} \text{ cm}^2$$

From equation 9.13, at 1000°C the diffusion constant is

$$D = D_0 \exp \left(-\frac{Q}{RT} \right)$$

$$= 0.21 \exp \left(-\frac{142\,000 \text{ J/mol}}{8.314 \text{ J/mol} \cdot \text{K} \times 1273 \text{ K}} \right) = 3.1 \times 10^{-7} \text{ cm}^2/\text{s}$$

so, the carburizing time is

$$t = \frac{3.6 \times 10^{-3} \text{ cm}^2}{3.1 \times 10^{-7} \text{ cm}^2/\text{s}} = 1.16 \times 10^4 \text{ s} \approx 3.2 \text{ h}$$

Note: A relatively small change in the carburizing temperature (about 10%) causes a large change in the carburizing time (decreased by a factor of about 3). This is characteristic of thermally activated processes.

The equations presented in this section provide the fundamental basis for carburizing and other diffusional processes. As exemplified by some of the problems at the end of the chapter, these equations can be used to predict the influence of changes to the carburizing conditions. Nevertheless, it is common to determine the case depth using a variety of other methods. One technique involves carburizing a small notched steel pin concurrently with the workpiece. The pin is removed from the furnace without disturbing the workpiece and quenched. Upon fracturing the pin at the notch, the case depth can be readily determined using a loupe and appropriate scale. Alternatively, the microhardness can be measured on a polished section through the case depth, or one of a variety of spot compositional analysis techniques can be used to determine the carbon concentration.

9.3.2 Nitriding

Nitriding is a case hardening process involving the diffusion of nitrogen into the surface region of steels. Nitriding can result in surface hardness up to 70 Rockwell C (about 700 VPN), higher than the hardness obtainable by carburizing (Fig. 9.6). Nitrogen diffusion into the surface region of the steel results in the formation of a layered structure, consisting of a surface layer of Fe_4N about 0.1 mm thick, Fe_3N at depths of about 1–5 mm and nitrogen in solid solution at greater depths. The Fe_4N layer is very brittle and spalls easily in service. Therefore, this outer layer may have to be removed prior to use. As seen in Fig. 9.8, the hardness decreases rapidly from the part surface. Unlike carburizing, nitriding does not depend on the martensitic transformation during quench hardening to achieve the surface hardening. Therefore, quenching following nitriding is not required, reducing the tendency for warping or cracking due to thermal shock.

Several nitriding processes exist, the most widely used being *gas nitriding*, in which the workpiece is heated in an ammonia (NH_3)-containing atmosphere. At the nitriding temperature of 430–590°C, the ammonia in contact with the steel breaks down into atomic nitrogen and hydrogen. The former is available to diffuse into the workpiece, whereas the latter becomes part of the furnace atmosphere. Often, multistep heating cycles are used to minimize formation of the brittle Fe_4N surface layer.

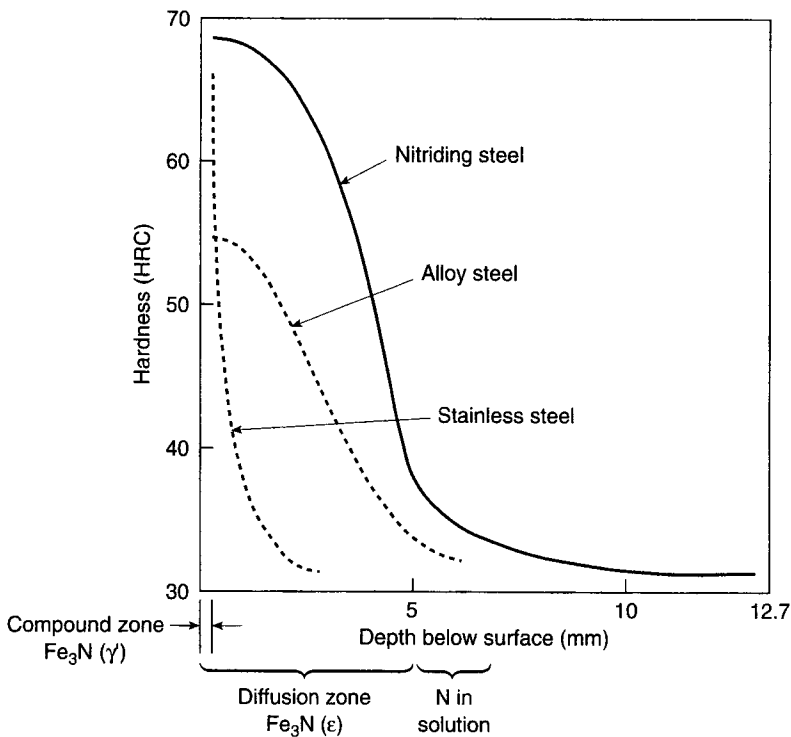


Fig. 9.8 Nitrogen profile in nitrided ferrous metals.

A disadvantage of nitriding is the considerably longer time required, compared to carburizing. The major reason for the longer time, which can be as much as 100 h, is the lower temperature. Again, nitriding relies on diffusion which is a thermally activated process. However, increasing the temperature causes poor case properties and unsuitable decomposition of the ammonia.

Adding aluminium, chromium, vanadium, titanium, tungsten, molybdenum and manganese to steels greatly increases the response to nitriding, because these elements readily form hard nitrides. A series of *Nitralloy* steel grades, specifically designed for nitriding, contain about 1 wt% Al, 0.5 wt% Mn, 1.5 wt% Cr and 0.3 wt% Mo. As illustrated in Fig. 9.8, these nitriding steels develop the hardest and deepest nitride cases.

9.3.3 Carbonitriding

Carbonitriding refers to processes that create a hardened case by diffusing both carbon and nitrogen into the steel. During *gas carbonitriding* the furnace atmosphere contains both ammonia and natural gas and the temperature is typically between 650°C and 885°C. At the lower temperature most of the hardening will be due to nitrogen diffusion, whereas temperatures close to 885°C will cause primarily carbon diffusion. Nitrogen increases the solubility of carbon in the austenite phase and

decreases the temperature at which austenite remains stable. Therefore, parts can be carbonitrided at lower temperatures than carburizing and the increased solubility of carbon makes less severe quenching rates possible. This minimizes the distortion that may be associated with rapid quench rates. Since carbonitriding involves carbon diffusion, in addition to nitrogen diffusion, the cycle time is reduced.

Liquid carbonitriding (often referred to as cyaniding) involves immersing the workpiece in a molten salt bath of sodium cyanide (NaCN), sodium carbonate (Na_2CO_3) and sodium chloride. At carbonitriding temperatures of 760°C – 870°C the NaCN oxidizes to form sodium cyanate (NaCNO), which further dissociates to liberate carbon and nitrogen that can diffuse into the metal. The diffusion of nitrogen into the case imparts high hardness, whereas carbon diffusion makes surface hardening by quenching possible. Typically, components for liquid carbonitriding are small and will be heated using an oxyacetylene torch to red heat prior to immersion in the salt bath. Immersion times are short, in the range of 15 min to 1 h, and this produces a shallow case of high hardness. The lack of stringent process controls often yields variable case depth and hardness, but the process can be applied by maintenance personnel without the need for extensive equipment. Given the toxicity of cyanide, due care must be taken to ensure the molten bath is well vented.

9.3.4 Aluminizing, siliconizing and chromizing

Steels are *aluminized* by coating the surface with a thin layer of aluminium. Aluminizing is somewhat analogous to the zinc *galvanizing* of steels. Both aluminized and galvanized steels have improved atmospheric corrosion resistance, because both zinc and aluminium are anodic to steel. Therefore, even scratches through the aluminized or galvanized layer do not cause corrosion of the underlying steel. Aluminizing is more effective than galvanizing for elevated temperature applications, and for this reason many furnace combustion chambers and automotive exhaust components are aluminized, although the latter application is slowly being displaced by ferritic stainless steels.

The aluminium can be applied either by hot-dipping, spraying or *pack cementation*. Hot-dipped or sprayed aluminium coatings are usually diffused into the base steel by heat treatment at temperatures greater than 870°C . Although aluminium melts at 660°C , an aluminium layer on steel when exposed to $>870^\circ\text{C}$ will not melt, but diffuses into the base steel. Cementation refers to the introduction of one atomic species into another by diffusion. Aluminizing by pack cementation involves packing the steel workpiece in a box or retort with a mixture of aluminium, aluminium oxide powder and a salt, usually aluminium chloride. On heating the salt reacts with the aluminium to release an aluminium-rich gas, providing aluminium for diffusion into the steel workpiece. The aluminium case can be between $25\text{ }\mu\text{m}$ and 1 mm, and it is the formation of the natural Al_2O_3 surface layer that provides good corrosion resistance.

In a manner similar to aluminizing, steels can be siliconized or chromized. Siliconized steels have a surface silicon content of about 13% and exhibit good wear and corrosion resistance in several oxidizing acids. Chromized steels can have a chromium content of as high as 30%. Chromium contents above 12% provide excellent atmospheric corrosion resistance, as exemplified by stainless steels. Siliconizing requires

heating to about 1010°C and exposing the surface to SiCl_4 gas, which decomposes allowing silicon diffusion to form a case of about 1 mm thickness. Chromizing is a cementation process, using chromium powder and a gas, such as ammonium iodide, that at the chromizing temperature of about 1000°C will react with the chromium powder to form nascent chromium that can diffuse into the steel workpiece.

Table 9.1 highlights some of the relevant characteristics of the various diffusional surface modification processes presented in this section.

9.4 Flame and induction hardening

Carburizing processes increase the surface carbon content of low carbon steels, so that localized quench hardening is possible. However, if the steel already contains 0.5 wt% carbon or more, then quench hardening will produce the maximum hardness without the requirement for diffusion of additional carbon into the surface (Fig. 9.6). For many applications the hardening need only be applied to the surface to provide good wear resistance, while maintaining a tough and ductile interior. One widely used technique to achieve this objective is to rapidly heat the component surface to an austenitic temperature followed by quenching. If the heating is sufficiently rapid that heat is not conducted into the interior of the component, only the locally heated surface will transform to the hard, wear resistant martensite structure during quenching. *Flame and induction hardening* are two processes widely used to achieve surface hardening of steels. If the steel contains 0.5 wt% or more carbon then maximum hardness is obtained.

9.4.1 Flame hardening

Flame hardening employs impingement of a high temperature flame directly on the workpiece, followed by a water quench, as shown by the simple arrangement of Fig. 9.9. Using an oxyacetylene flame the surface can be heated to the austenite structure in a few seconds. These short heating times ensure that excessive oxidation

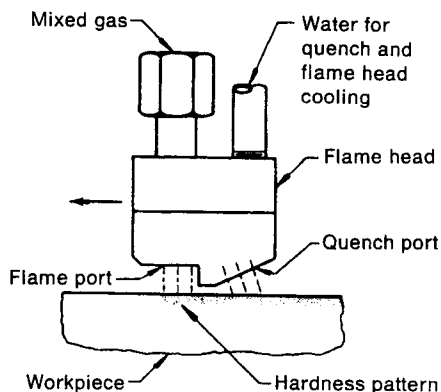


Fig. 9.9 Equipment arrangement for flame hardening.

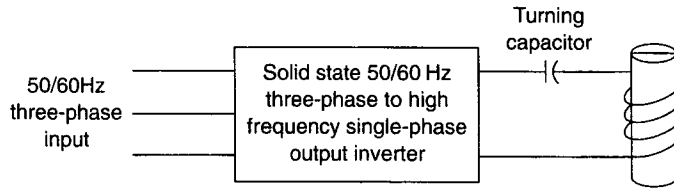


Fig. 9.10 Basic control circuit for induction heating.

of the surface does not occur. A variety of shapes for the flame head can be used to obtain uniform heating of complex surfaces such as gears, cams or shafts. Flame hardening can produce hardened layers of up to 4 mm, but the process requires careful control of the flame combustion (temperature), the stand-off distance of the flame head from the workpiece surface, and the traversing speed.

9.4.2 Induction hardening

Induction hardening relies on the fact that when a conducting material is placed within a magnetic field, an electrical current is induced in the conductor and this induced current causes heating. Using this principle a workpiece can be *induction heated* by making it the secondary of an alternating current transformer (Fig. 9.10). The magnetic lines of flux created by the alternating current in the primary coil cut the workpiece, as shown in Fig. 9.11. Of importance is that the induced alternating magnetic flux causes *eddy currents* to flow within the workpiece. As seen in Fig. 9.11, the eddy currents flow in a direction opposite to the inducing alternating current and, therefore, the magnetic field created by the eddy currents opposes the induction magnetic field. This reduction is greatest at the centre of the workpiece, because all the eddy currents in all the elemental paths (Fig. 9.11) are effective in producing the opposing magnetic field at the centre. Consequently, the magnetic flux is greatest at

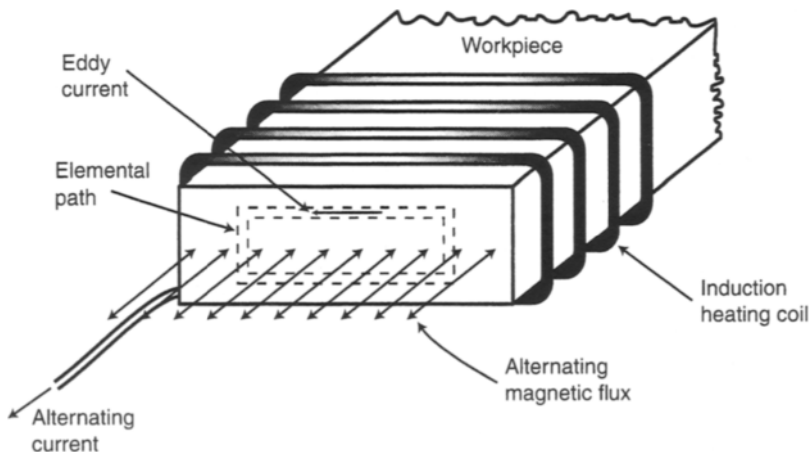


Fig. 9.11 Eddy currents induced in workpiece as a result of alternating current in induction coil.

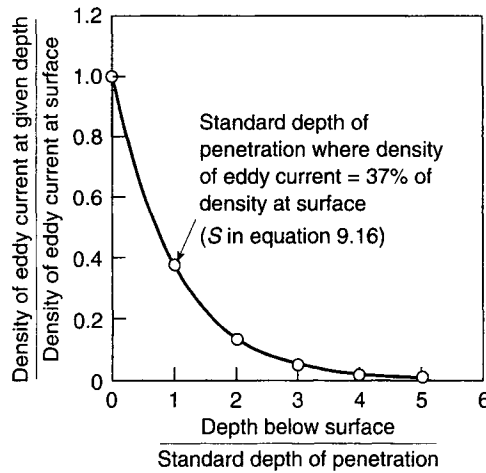


Fig. 9.12 Eddy current density as a function of depth below surface of workpiece. (Reprinted with permission from *ASM Metals Handbook, Desk Edition*, edited by H.E. Boyer and T.L. Gall (1985), ASM International, Materials Park, OH 44073-0002 (formerly American Society for Metals, Metals Park, OH 44073), p. 33.15, Fig. 7.)

the surface and lowest at the centre. This phenomenon, referred to as the *skin effect*, results in greater induced currents, and consequently greater preferential heating, near the surface of the workpiece. The rate at which the eddy current density falls is shown in Fig. 9.12 and is controlled by the equation

$$S = 5092.2 \sqrt{\frac{\rho}{\mu f}} \quad (9.16)$$

where: S is the standard depth of penetration (cm)

ρ is the workpiece resistivity ($\Omega \text{ cm}$)

μ is the relative magnetic permeability

f is the inducing current frequency.

As the resistivity and permeability of carbon steels vary comparatively little, the greatest influence on the depth of heating is caused by the frequency of the inducing alternating current. The significance of these magnetic properties for surface hardening is that metals can be induction heated, with the depth of heating controlled by the inducing current frequency.

A simple arrangement for induction hardening a steel workpiece is shown in Fig. 9.13. The inducing alternating current is applied for between 1 s and 10 s to heat the surface of the workpiece to the austenite structure (at least 723°C). The workpiece is then dropped into the quench tank to transform the austenitic surface to the hard wear-resistant martensitic structure. Alternatively, the inducing current can be shut off as soon as the austenite temperature is reached and water sprays incorporated into the induction coil activated to quench the workpiece.

Typically, the inducing coils are fabricated from copper tubing that is water cooled to prevent overheating. For most commercial steel induction hardening, a frequency

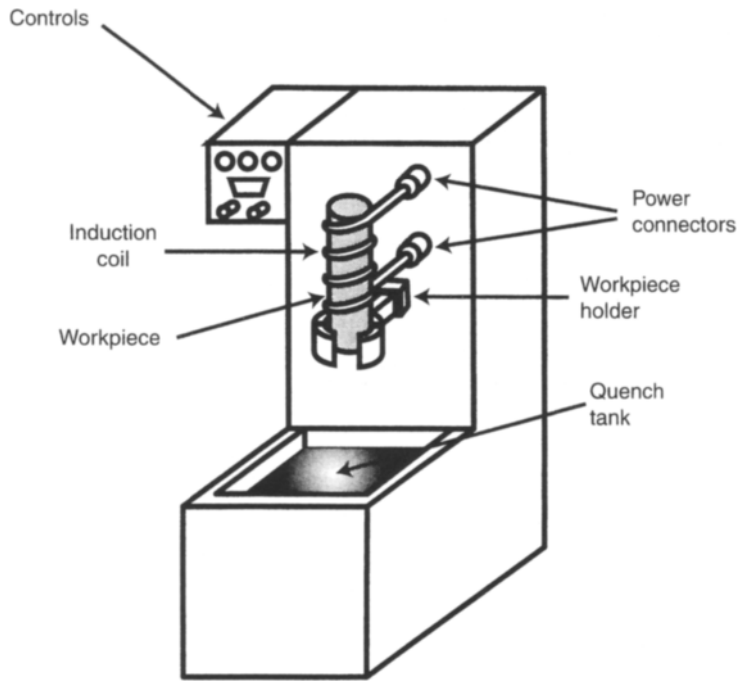


Fig. 9.13 Simple arrangement for induction hardening a steel workpiece by heating and quenching.

of between 100 and 500 kHz is used, giving a surface hardened thickness of between about 0.5 and 0.25 mm, respectively. The generation of these high frequencies is accomplished by a d.c. power supply that converts the a.c. input to d.c., which is then converted to high frequency a.c. by a transistor inverter circuit. Through a feedback control system the output frequency of the inverter is continuously adjusted to match the resonant frequency of the tuning capacitor and induction coil, and corrected for temperature induced changes in the magnetic properties of the workpiece. The capital cost associated with this equipment is the major disadvantage to induction hardening. However, the advantages of a very fast processing time and the fact that the core of the workpiece is not heated, thus retaining its microstructure and properties, makes induction hardening the method of choice for many high volume products. Several automotive and machine parts are induction hardened. An example is shown in Fig. 9.14.

9.5 Plating processes

Plating refers to the application of metallic coatings to substrates by electrochemical or electroless processes. During electrochemical plating or electroplating the workpiece to be plated is made the cathode of an electrolytic cell. On the application of a potential, the anode dissolves into the electrolyte and redeposits on the cathode. This process is shown schematically in Fig. 9.15. When controlled properly an even layer of anode metal adheres evenly to the workpiece. The plating process is governed by Faraday's

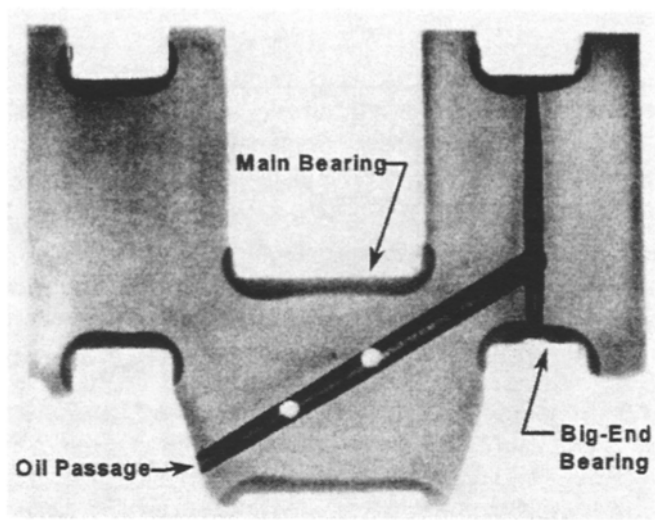


Fig. 9.14 Section through an automotive crankshaft with both main and big-end journal bearing surfaces induction hardened. Note that the interior of the crankshaft is not hardened so that toughness is maintained. (Reprinted with the permission of ASM International, Materials Engineering Institute.)

laws, which are: (1) the mass of the substance liberated during electrolysis is proportional to the quantity of electricity passed through the cell; and (2) the mass of the liberated material is proportional to the atomic weight to valence ratio. These two laws are summarized in the equation

$$W = \eta \frac{wIt}{vF} \tag{9.17}$$

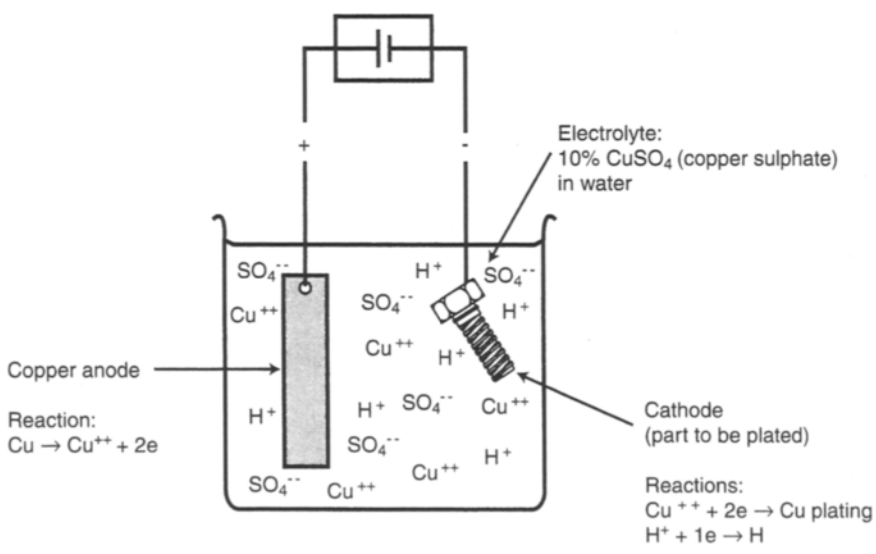


Fig. 9.15 Diagram of electrolytic cell for electroplating.

where: I is the current

t is the plating time

η is the cathode efficiency (typically about 0.9)

W is the mass of the deposited metal

w is the atomic weight of the plating element

v is the normal valence of the plating element

F is one Faraday (96 500 A s/mol).

An important ramification of this equation is that, even at the same applied current, different metals may have different deposition rates. The cathode efficiency reflects that fraction of the electrical energy used for deposition, rather than liberation of hydrogen at the cathode, or redundant chemical reactions. The efficiency can vary between 0.15 and 0.99, depending on the element being deposited. Due to the cathode efficiency, and other limitations, the rate at which electroplated surfaces can be deposited is rarely in excess of 0.1 mm/h.

Many metals can be deposited by electroplating, with copper, nickel, cadmium, zinc, tin and chromium being the most used. These plating metals can provide improved appearance, corrosion resistance or wear resistance. The *hard chromium plating* process shown in Fig. 9.16 is particularly effective for improving wear and corrosion resistance at the same time. This process involves electrodeposition from a solution of chromic acid and a catalyst (usually sulphate). Unlike many other electroplating processes, the anodes used for hard chromium plating are insoluble lead or lead–tin plates, so that all the deposited chromium originates from the electrolyte. Chromium coatings up to 0.5 mm thick can be applied, usually at electrolyte temperatures of 50–70°C, with plating times of between 2 h and 45 h typical. Hard chromium plating is used for rebuilding mismachined or worn components, as well as for valve stems, piston rings, and other surfaces subjected to movements at high applied loads. A chromium plating of up to 250 μm is applied to automotive piston rings, providing an increased in-service life of about five times that of uncoated

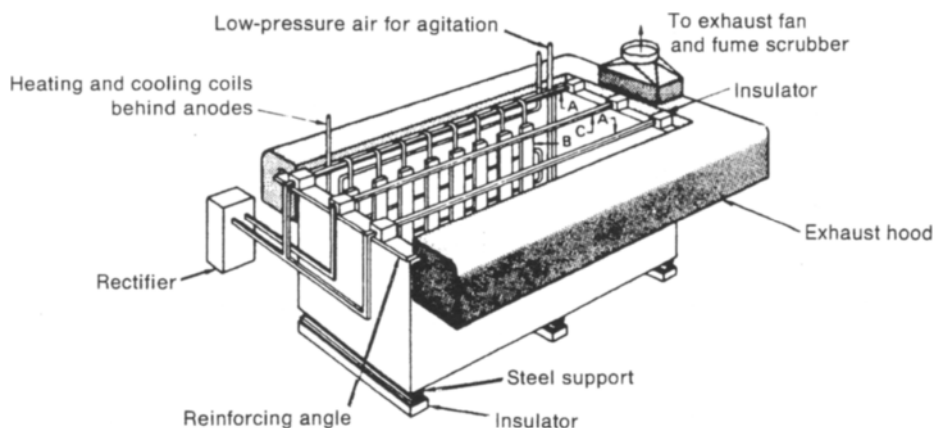


Fig. 9.16 Electroplating bath for hard chromium plating. Components for hard plating are hung from the cathode bar (C). The anodes (B) are hung from the anode bar (A). (Reprinted with permission from *ASM Metals Handbook, Desk Edition*, edited by H.E. Boyer and T.L. Gall (1985), ASM International, Materials Park, OH 44073-0002 (formerly American Society for Metals, Metals Park, OH 44073), p. 29.16, Fig. 1.)

rings. An advantage of hard chromium platings for sliding surfaces is an inherent low coefficient of friction.

Example 9.3 Electroplating

A steel slider with a diameter of 1 cm and length 20 cm is to be hard chromium plated. Estimate the plating time required to deposit a 0.1 mm thick coating over the entire surface of the slider if a current density of 0.3 A/cm^2 is applied. (The atomic weight of chromium is 52 g/mol, it has a normal valence of 3 and a density of 7.19 g/cm^3 . A typical efficiency for a chromium plating bath is 0.2.)

Solution The area of the cylindrical slider to be plated is $2\pi(0.5 \times 20 + 0.5^2) = 64.37 \text{ cm}^2$.

Therefore, the total current will be $I = 64.37 \text{ cm}^2 \times 0.3 \text{ A/cm}^2 = 19.32 \text{ A}$.

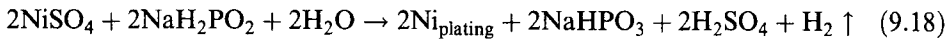
The volume of the deposited chromium required is $64.37 \text{ cm}^2 \times 0.01 \text{ cm} = 0.65 \text{ cm}^3$ and the weight of this coating will be $0.65 \text{ cm}^3 \times 7.19 \text{ g/cm}^3 = 4.67 \text{ g}$.

Using Faraday's equation 9.17 to calculate the time,

$$t = \frac{WvF}{\eta w I} = \frac{4.67 \text{ g} \times 3 \times 96\,500 \text{ A s/mol}}{0.2 \times 52 \text{ g/mol} \times 19.32 \text{ A}} \approx 1.87 \text{ h}$$

The chromium plating process described will require about 1.9 h.

Electroless plating relies only on chemical reactions to drive the plating process; no electrical potential is applied. Typically, an aqueous solution containing a salt of the plating metal, reducing agents and other chemicals to control the pH and reaction kinetics is used, and the workpiece surface itself acts as a catalyst. The electroless process can be used to plate nickel, copper, silver and gold. The main reaction occurring during electroless nickel plating using nickel sulphate and a sodium hypophosphite reducing agent is



The advantage of the process is that no d.c. power supply is needed, complex surface geometries are more easily plated uniformly, and the plated substrate need not be capable of conducting electricity. The last attribute allows the metal plating of plastic parts. The disadvantage of the process is that it is slow – about $10 \mu\text{m}$ of thickness coated per hour; however, this does give rise to accurate control of the coating thicknesses. Electroless nickel coatings have hardnesses of about 43 Rc and are corrosion resistant, but can be brittle and have poor welding characteristics.

9.6 Thin film coatings

Thin film coatings are not applied to the extent as those surface techniques previously discussed, primarily because of the cost of the equipment required. However, the use of these types of coatings is increasing as the techniques are developed more fully, and as greater engineering capability of various components is demanded.

Thin films are usually used because of specific surface properties, such as TiN or TiC coatings applied to carbide tools (Fig. 7.32). Many processes are used for the

application of thin films, but most can be classified as either *physical vapour deposition* (PVD) or *chemical vapour deposition* (CVD). PVD forms a coating on a substrate by physically depositing, from a vapour, atoms, molecules, or ions of the coating species. Typically, the vapour is created by evaporating or sputtering the coating material which subsequently condenses on the substrate. A CVD coating forms by a chemical reaction between the substrate and a vapour.

9.6.1 Physical vapour deposition

The PVD technique involves evaporation of the coating material in a vacuum chamber by resistance or electron beam heating, followed by condensation of the vapour on the substrate to be coated. Figure 9.17 illustrates heating of the coating material by electrical resistance, but the highest evaporation rate and deposition rate (up to $25\text{ }\mu\text{m/min}$) can be achieved by electron beam heating. Evaporative PVD is used to apply oxidation- and erosion-resistant coatings on gas turbine blades and vanes.

Sputtering is the ejection of atoms from a target caused by momentum transfer from bombarding energetic particles, usually argon ions. The equipment arrangement for sputter PVD coating is illustrated in Fig. 9.18. The vacuum chamber is evacuated and backfilled to between 0.1 and 10 Pa of argon pressure. By applying an electrical

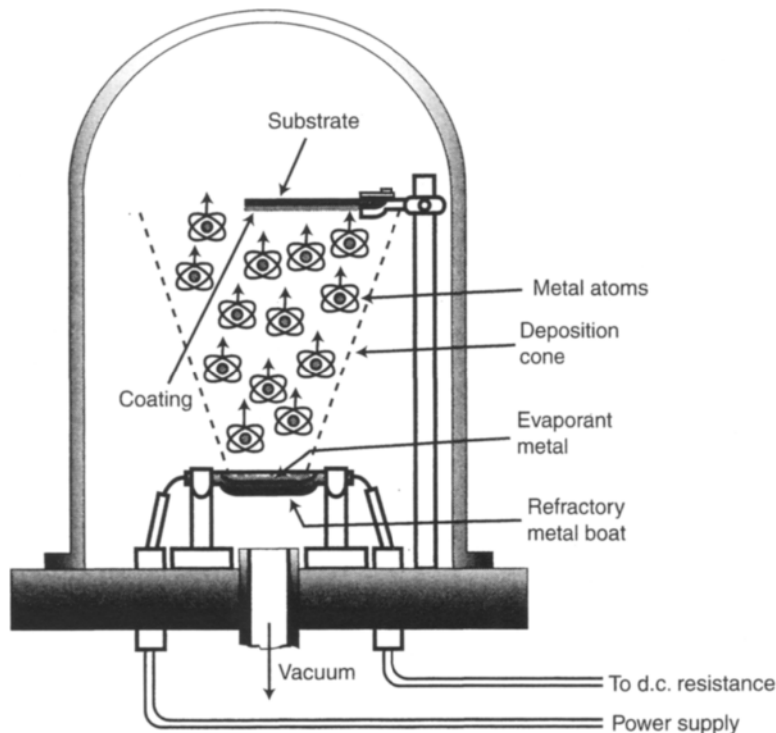


Fig. 9.17 General arrangement of the process of physical vapour deposition by electrical resistance heating.

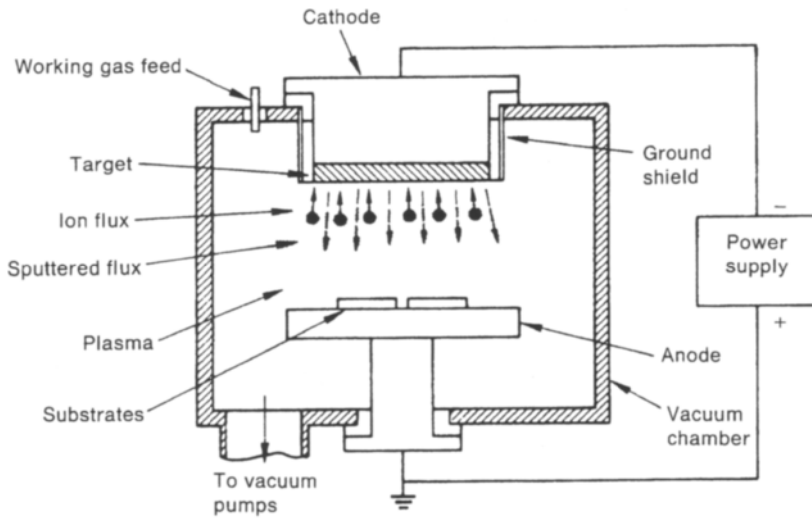


Fig. 9.18 Sputter PVD coating apparatus.

bias to the chamber, the argon becomes ionized (creating the *plasma*) and bombards the target which is made of the material that will form the coating. This bombardment causes atoms in the target to be ejected, forming a vapour, which condenses on the substrate as the coating. The rate at which the coating is deposited depends on the process parameters and the substrate geometry. Recently, several sputtering geometries that use magnetic fields to confine the plasma, referred to as *magnetrons*, have become available, which greatly increases the deposition rate.

9.6.2 Chemical vapour deposition

Chemical vapour deposition (CVD) differs from PVD in that it involves chemical decomposition of a gaseous atmosphere and reaction of one of the products of decomposition with the substrate surface. The reaction between the atmosphere and the substrate causes nucleation and growth of a coating. Often the substrate is heated and the kinetics of the chemical reactions are increased by ultraviolet light or plasma energy sources.

CVD processes exist for many coating–substrate combinations. One of the earliest CVD processes is the *Mond process* for the deposition of Ni coatings from nickel carbonyl, according to



This reaction is used to deposit nickel onto nickel pellets and is one of the final steps in the extraction of nickel from *pentlandite* ore (NiFe_2S_3), which is refined at the major nickel deposits at Sudbury, Ontario. CVD coating is also used to produce surface layers on coated carbide tools, such as those shown in Fig. 7.32, according to the

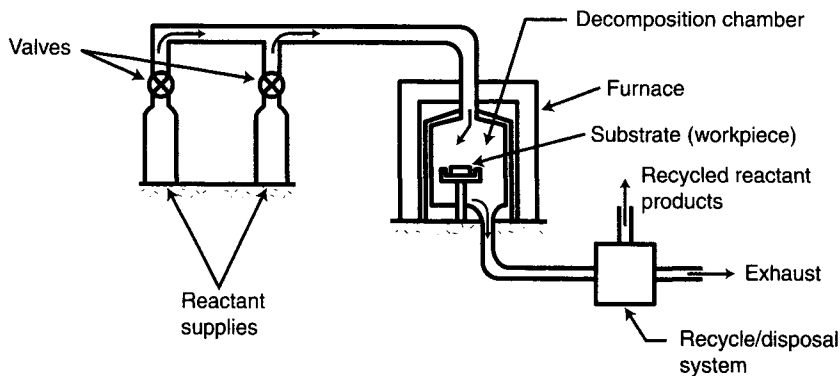
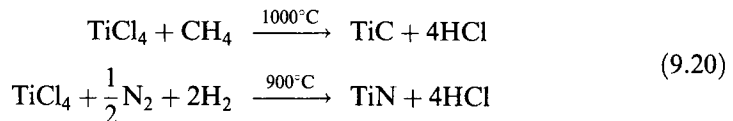
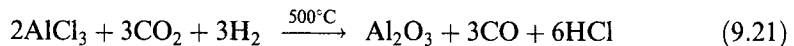


Fig. 9.19 Equipment arrangement for chemical vapour deposition.

reactions



The outer TiN layer (see Fig. 7.32) can also be applied using PVD techniques. Other industrial CVD processes include



for the application of alumina onto carbide tools for machining, and



for refractory coating of gas turbine blades and vanes.

A simple equipment arrangement for CVD coating is shown in Fig. 9.19. Although a basically simple process, an important step is the recycle/disposal system. Several of the CVD processes produce strong acids, which cannot be released to the environment; for example, hydrofluoric acid (HF; equation 9.22) destroys biological substances, such as flesh, plants etc.

9.7 Problems

- 9.1 The diffusion constant for carbon in iron at 900°C is $D = 1.0 \times 10^{-7} \text{ cm}^2/\text{s}$ and at 1000°C it is $D = 3.5 \times 10^{-7} \text{ cm}^2/\text{s}$. If it takes 10 min to carburize a part at 1000°C , how long will it take to carburize the same part to the same depth at 900°C ? (Assume the same surface carbon concentration in both cases.)
(Answer: ≈ 35 min)
- 9.2 Two surface hardening processes for steel are carburizing and induction hardening. Explain the fundamental difference in the hardening mechanism of these two processes.

- 9.3 Your company case hardens steel parts to achieve a carbon concentration required by the customer (solid line in Fig. P9.3). The case hardening operation is performed at 970°C for 2.75 h. The customer is experiencing excessive wear of the part surfaces and has requested that you produce the new carbon profile shown by the dashed line. To meet production requirements the carburizing time cannot be changed. Calculate the temperature required to achieve the new carbon profile.

(Answer: about 1037°C)

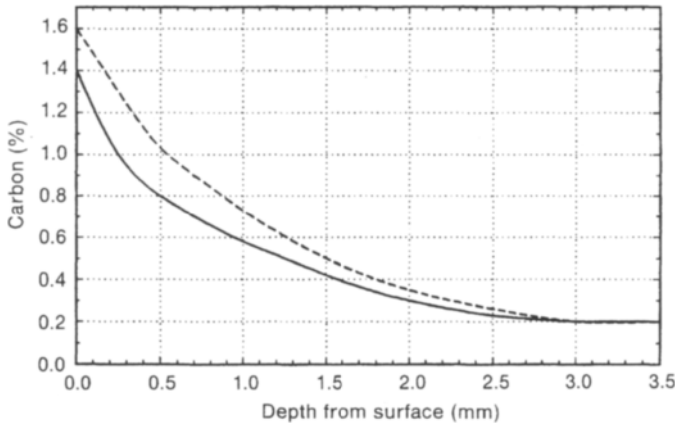


Fig. P9.3 Problem 9.3.

- 9.4 (a) The company you work for operates a gas carburizing facility. Describe concisely the method, advantages and disadvantages of gas carburizing.
- (b) Your company has two customers: Heather's Handy Parts (HHP) and Freddy's Hard Faced Gears (FHFG). The depth profile of carbon required for each of these customers is illustrated in Fig. P9.4. For HHP the carburizing temperature is 900°C and for FHFG the carburizing temperature is

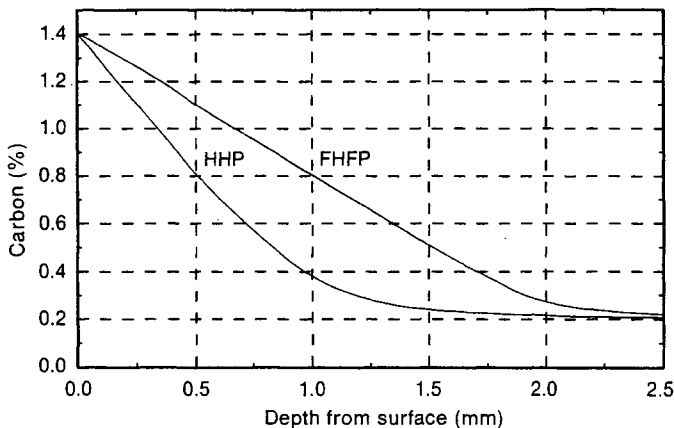


Fig. P9.4 Problem 9.4.

1100°C. To efficiently utilize the gas carburizing equipment, the production manager needs to know the time required to attain each of the customers' case hardened profiles. Calculate these times.

(Answers: for HHP almost 7 h; for FHFG almost 3.5 h)

- 9.5 Your factory surface hardens gears for the automotive industry. Currently you carburize SAE 1020 steel (0.2 wt% carbon) at 1000°C for 8 h. To save on furnace power, your heat treatment supervisor suggests reducing the carburizing temperature to 900°C. However, for the gears to have sufficient hardness, the carbon concentration at the 1000°C case depth must be maintained. Calculate the carburizing time necessary at 900°C. (Assume that $\text{erf}(Z) \approx Z$ for $0.3 < Z < 0.7$.)
(Answer: about 39.5 h)
- 9.6 Cementation is a general term referring to the introduction of one or more elements into the outer portion of a metal object by means of diffusion at elevated temperature. Identify the surface modification processes of this chapter that involve cementation.
- 9.7 You own a factory that is in the business of gas carburizing low carbon steels. A representative from an induction hardening equipment supplier visits your facility in an effort to persuade you to switch from gas carburizing to induction hardening. Should you bother to listen to the sales representative? Explain.
- 9.8 If the frequency of an induction hardening power supply is doubled, what is the expected change in the case hardened depth?
(Answer: penetration depth at doubled frequency is reduced by $\sqrt{1/2}$)
- 9.9 The largest use of silver is to plate stainless steel flatware and tableware. (This usage is strictly decorative, since the ferritic and austenitic stainless steels used for flatware will not corrode even after decades of kitchen use.) Calculate the time required to plate a typical sized table knife that has a surface area of 50 cm² which is plated with silver to a thickness of 25 μm. The silver is deposited from a potassium silver cyanide (KAg(CN)₂) bath at a current density of 0.02 A/cm². Electroplating of silver has a high cathode efficiency; assume it is equal to 1. (Silver has an atomic weight of 107.9 g/mol, a valence of 1, and a density of 10.5 g/cm³.)
(Answer: about 19.5 min)

Appendix A:

Useful constants

Absolute zero temperature = 0 K = -273.2°C

Acceleration due to gravity at surface of earth = $9.806\,65\,\text{m/s}^2$

Avogadro constant = $6.022 \times 10^{23}\,\text{mol}^{-1}$

Electron charge = $1.602 \times 10^{-19}\,\text{C}$

Electron rest mass = $9.11 \times 10^{-31}\,\text{kg}$

Electron volt (eV) = $0.16 \times 10^{-18}\,\text{J}$

Faraday = $9.648 \times 10^4\,\text{C/mol}$

Universal gas constant = $8.314\,\text{J/mol}\cdot\text{K}$

Appendix B:

Useful conversion factors

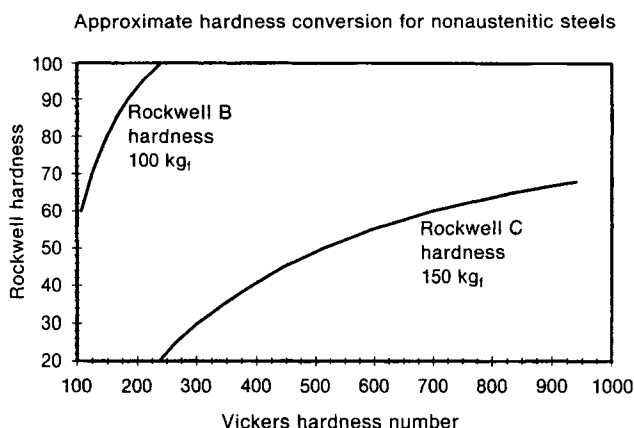
Acceleration	$1 \text{ m/s}^2 = 3.281 \text{ ft/s}^2$
Angles	$1 \text{ rad} = 57.296^\circ$
Area	$1 \text{ mm}^2 = 1.55 \times 10^{-3} \text{ in}^2$ $1 \text{ m}^2 = 10.76 \text{ ft}^2$
Density	$1 \text{ kg/m}^3 = 3.613 \times 10^{-5} \text{ lb}_m/\text{in}^3$ (subscript m = mass) $1 \text{ kg/m}^3 = 6.242 \times 10^{-2} \text{ lb}_m/\text{ft}^3$ $1 \text{ g/cm}^3 = 62.4 \text{ lb}_m/\text{ft}^3$
Electric current	$1 \text{ ampere (A)} = 1 \text{ C/s}$
Energy, work	$1 \text{ J} = 1 \text{ N m} = 1 \text{ W} \cdot \text{s}$ $1 \text{ J} = 9.479 \times 10^{-4} \text{ Btu}$ $1 \text{ J} = 0.7376 \text{ ft lb}_f$ (subscript f = force) $1 \text{ J} = 0.239 \text{ calories}$ $1 \text{ J} = 6.24 \times 10^{18} \text{ eV}$ $1 \text{ kW h} = 3412 \text{ Btu} = 3.6 \times 10^6 \text{ J}$ $1 \text{ Btu} = 252 \text{ calories}$
Force	$1 \text{ N} = 0.2248 \text{ lb}_f$ $1 \text{ kg}_f = 9.807 \text{ N}$
Fracture toughness	$\text{MPa m}^{1/2} = 0.9099 \text{ ksi in}^{1/2}$
Length	$1 \text{ mm} = 0.03937 \text{ in}$ $1 \text{ m} = 3.2808 \text{ ft}$ $1 \text{ micrometer (micron, } \mu\text{m)} = 1 \times 10^{-6} \text{ m}$
Mass	$1 \text{ kg} = 2.2046 \text{ lb}$ $1 \text{ g} = 0.03527 \text{ oz}$ $1 \text{ tonne} = 1000 \text{ kg}$ $1 \text{ ton (US)} = 2000 \text{ lb} = 907.185 \text{ kg}$ $1 \text{ ton (UK)} = 2240 \text{ lb} = 1016.05 \text{ kg}$ $1 \text{ tonne} = 1.1023 \text{ ton (US)}$
Modulus of elasticity	$1 \text{ GPa} = 1.4503 \times 10^5 \text{ lb}_f/\text{in}^2$
Moment of force (torque)	$1 \text{ N m} = 0.7375 \text{ ft lb}_f$
Moment of inertia	$1 \text{ mm}^4 = 2.4 \times 10^{-6} \text{ in}^4$
Power	$1 \text{ W} = 1 \text{ N m/s}$ $1 \text{ kW} = 1.341 \text{ horsepower (hp)}$ $1 \text{ W} = 3.413 \text{ Btu/h}$

Power	$1 \text{ W} = 0.7376 \text{ ft lb}_f/\text{s}$
Specific heat	$1 \text{ J/kg K} = 2.39 \times 10^{-4} \text{ Btu/lb}_m \cdot ^\circ\text{F}$
Stress (pressure)	$1 \text{ MPa} = 145 \text{ lb}_f/\text{in}^2$
	$1 \text{ ksi} = 1000 \text{ lb}_f/\text{in}^2$
Temperature	$\Delta^\circ\text{C} = \Delta\text{K}$
	$\Delta^\circ\text{C} = \text{K} - 273.15$
	$\Delta^\circ\text{C} = 1.8\Delta^\circ\text{F}$
	$^\circ\text{C} = 0.5555(^\circ\text{F} - 32)$
Thermal conductivity	$1 \text{ W/m} \cdot \text{K} = 0.578 \text{ Btu/ft} \cdot \text{h} \cdot ^\circ\text{F}$
Velocity, linear	$1 \text{ mm/s} = 0.03937 \text{ in/s}$
	$1 \text{ m/s} = 3.281 \text{ ft/s}$
Velocity, angular	$1 \text{ rad/s} = 9.55 \text{ rev/min}$
Volume	$1 \text{ mm}^3 = 6.101 \times 10^{-5} \text{ in}^3$
	$1 \text{ m}^3 = 35.31 \text{ ft}^3 = 1.3078 \text{ yd}^3$
	$1 \text{ gal (UK)} = 1.20095 \text{ gal (US)}$
	$1 \text{ L} = 0.21997 \text{ gal (UK)}$
	$1 \text{ m}^3 = 219.969 \text{ gal (UK)}$

Appendix C:

Hardness conversion

In this book reference is made to both the Vickers Pyramid Hardness Number (commonly abbreviated VHN or HV) and the Rockwell hardness. These are two of several widely used hardness measurements for metallic materials. Several Rockwell scales are in use, each appropriate for a particular hardness range. Most often in this book, reference was made to the Rockwell C scale (often abbreviated R_c or HRC). The graph below illustrates the relationship between the Vickers and Rockwell hardness scales for nonaustenitic steels only. The graph is approximate only. For greater information regarding the conversion between other commonly used hardness scales and for metals other than nonaustenitic steels, reference should be made to ASTM specification E140.



Index

- abrasion 58, 280
- abrasive 202
 - waterjet machining 191, 223–4
- acetylene 241–2, 265
- acrylates 221
- activation energy 183, 291–2
- adaptive control 223
- adhesion 214, 280–1
- adhesive 232–3, 264, 280, 282–3
- alcohols 221
- alligating 130–1, 138
- alumina 12, 70, 203, 219, 243, 306
- aluminium 3, 4, 55, 66, 137, 295
 - 319.2, 62
 - AA-1100 79, 90, 120, 135, 136, 163, 208
 - AA-2017 79
 - AA-3003 270–4
 - AA-3004 69, 79, 170–2
 - AA-4004 272
 - AA-4047 272
 - AA-4104 272
 - AA-4343 272–4
 - AA-5050 265
 - AA-5052 163
 - AA-5182 69
 - AA-6061 265
 - AA-7072 272
 - AA-7075 79, 208
 - A356.2 62
 - C355.2 62
 - G6290 62
- alloys 206
- brazing 267
- cans 67–71
- casting alloys 60–2
- chloride 296
- continuous casting 22–3
- deep drawing 159
- degassing 54
- density 260
- die casting 30
- grain refinement 35
- hydrogen solubility 52–3
- ingot 18, 20–1, 41, 138
- killed steel 19, 152
- limiting draw ratio 160
- lubrication 102
- machining 212, 223, 229
- powder 181, 268
- primary processing 12–15
- radiators 270–4
- shape casting 27, 72
- shrinkage 36
- smelter 38
- sow 38–40, 69
- specific heat 260
- thermal conductivity 260
- welding 237, 238, 240, 243, 252, 269
- aluminizing 286, 296
- amalgams, dental 174
- amides 221
- ammonia 178, 294–5
- ammonium iodide 297
- anisotropic sheet 158–62
- anisotropy 106
 - mean 159, 276
 - planar 276
 - plastic 159–64, 276
- anneal 52, 68, 97, 140, 155, 162, 171, 178, 253, 276–7
- anode 223, 225, 300
- antifoaming additive 221

- antifreeze 270, 274
- antimicrobial agents 221
- antimisting additive 221
- antimony 268
- apparent density 180–1
- arc 177
- argon 54, 70, 176–7, 185, 237–8, 304–5
- argon–oxygen–decarburization 276, 278
- Arrhenius relationship 291
- aspiration 55–6
- atomic diffusion 183
- atomic weight 301–3, 308
- atomization 174, 175–7
 - centrifugal 177–8
 - gas 176–7, 188
 - water 175–7, 188
- attrition mill 179
- austenite 58–9, 256–9, 285–8, 292, 295–6, 297, 299
- austenitization 255–6
- automobile
 - body 142, 143, 162, 241, 244
 - camshaft 253
 - connecting rod 174, 253
 - crankshaft 174, 253, 301
 - exhaust 275–8, 296
 - fuel injection 225
 - gas tanks 245
 - radiators 270–4
 - piston rings 302–3
- Avogadro constant 309

- back-up rolls 122–3, 125–7, 140
- bacteria 221
- bainite 258, 261
- ball mill 179–80
- barrelling 104, 109
- basal plane 161
- basic oxygen furnace 9, 12, 16
- bauxite 4, 12, 70
- Bayer Process 12–14, 16, 70
- bend radius 147–8
- bending 146, 148–50, 155, 162
- bending jacks 125, 141
- Bernoulli's equation 56–7
- Bessemer 1, 21
 - converter 7–8, 9, 12, 16, 276
- beverage cans 21, 23, 67–71, 142, 152, 158, 166, 230, 284
- billet 115, 119, 120, 135
- biocides 221

- bismuth 208, 268, 273
- blankholder 152–4
- blast furnaces 4–7, 12, 59
- blisters 52
- blowholes 19
- body centred cubic 161, 275
- bodymaker 166–70
- borates 221
- boring 193–6
- boron nitride 97
- brass 220, 270
- brazing 218, 232–3, 250, 263–7, 269
 - dip 267
 - fluxless 273
 - furnace 265–7, 270
 - sheet 272–3
 - torch 265, 267
- brinelling 280, 284–5
- bronze 30, 131, 220
- buckling 115
- built-up edge 215–16, 220–1
- burr 144–5, 223

- cadmium 253, 268, 302
- calciners 14
- calcium carbonate 5
- camshaft 253
- can body stock 138–41, 166–72
- canmaking 166
- capacitor 300
- capillary 264
- car body 142, 143, 162, 241, 244
- carbide 214, 216–17, 220, 303
- carbon 7, 8, 9, 12, 14–15, 57–60, 66, 216, 242, 257, 276–7, 296, 306
 - dioxide 8, 15, 19, 27, 185, 228, 235, 287
 - electrodes 10, 12
 - equivalent concentration 261
 - interstitial in steel 143
 - monoxide 5, 8, 9, 12, 15, 185, 287
 - oxidize 178
 - steel 9, 206–8, 215, 253, 285, 299
- carbonaceous 184, 285
- carbonitriding 286, 295–6
- carburizing 285–95, 306
 - flame 242
 - gas 286, 287–8, 307
 - liquid 286, 288
 - pack 286, 287
- case 285, 288, 295–6, 307
- case depth 286, 288, 292–3

- cast iron 5, 27, 36, 57–61, 66, 72, 206, 229
 - ductile 60–1
 - gray 58–9, 220
 - malleable 60
 - nodular 60–1
 - white 57–60
- cast cobalt tool 216–17
- casting 18–75, 107, 190
 - continuous 12, 16, 21–3, 24, 35, 47–9, 63, 71, 76, 122, 171, 179, 276
 - die 27–8, 30, 62
 - direct chill 20–1, 35, 70
 - electromagnetic 21, 70, 140
 - gravity 27, 30
 - Hazelett 23
 - ingot 16, 18–21, 23, 24, 63, 76, 115, 122, 170–1
 - investment 29–30, 187
 - lost-wax 29–30
 - permanent mould 27–30
 - sand 25–7, 30, 36–8, 55–6, 61–2, 73, 216
 - shape 16, 23–30, 57–61, 63, 229, 290
- catalytic converters 245, 275, 276
- cathode 225, 300, 302, 308
- cathodic 274
- caustic soda 12
- cavitation 280–1, 282
- cementation 296–7, 308
- cemented carbide 173
- cementite 58–60, 256
- centrifugal atomization 177–8
- ceramic 217–18
- characteristic hardness curve 258, 261
- charcoal 287
- checkers 8
- chemical vapour deposition 304–6
- chill crystals 31–5
- chip 190–1, 209–11, 221, 223
 - thickness 209–10, 213, 230
 - undeformed thickness 194, 196, 198, 201, 203–7
- chlorine 54, 70, 221
- chromic acid 302
- chromium 179, 216, 227, 263, 268, 276, 295, 297, 302
- chromium carbides 276
- chromium sesquioxide 268
- chromizing 286, 296–7
- chuck 192–3
- Chvorinov's rule 46–7
- clad 253, 272
- coal 5
- coated carbides 218, 305
- cobalt 216, 227
- coils 123, 140, 142, 238, 254
 - induction 299
 - magnetic 226
 - transformer 254, 298
- coke 5–6, 178
- cold isostatic pressing 182
- Coldstream process 179–80
- collapsible tube 115
- columnar grains 32–5, 39, 234
- combustion 140
- comminution 179
- compaction
 - cold 174, 181–3, 185, 187, 188
 - hot 174, 181, 185
- computer 140, 162, 188, 222, 246
 - aided design 223
 - aided manufacturing 223
 - integrated manufacturing 223
- concrete 5
- connecting rod 173–4
- constituent particles 170–1
- continuous casting 12, 16, 21–3, 24, 35, 47–9, 63, 71, 76, 122, 171, 179, 276
- continuous cooling transformation diagram 257–8
- continuous path control 222
- contouring control 222
- cope 25–6, 61
- copper 4, 21–3, 33–4, 174, 179, 204, 224, 230, 240
 - cutting energy 206
 - density 181, 184, 260
 - hydrogen solubility 53
 - limiting draw ratio 160
 - machining 208, 212
 - plating 302–3
 - radiator 270
 - roll bonding 253
 - shrinkage 36
 - specific heat 260
 - thermal conductivity 260
 - thermal expansion 36
 - tubing 299
 - welding 242, 252
- copper sulphate 179
- core 25–6, 62, 74
- coring 34, 49, 66

- corrosion 220, 234, 242, 253, 262–3, 270, 274, 276–7, 279, 296, 302–3
- corrosion inhibitors 221
- Cosworth process 27, 61, 72–5
- counterboring 200
- countersinking 200
- crankshaft 174, 253, 301
- creep 278
- crucible 243–4
- cryolite 15
- copper 166, 167
- cupping 143, 166–8
- cutting 144–6, 195
 - depth 191, 195, 201, 204–5, 207, 209–10, 213–15, 219–20, 229, 230
 - edge 191–2, 194, 196, 198–9, 201–6, 213, 229
 - efficiency 204–7
 - feed 191–2, 207
 - fluid 190, 220–2
 - laser 227–8
 - mechanics 209
 - specific energy 203–7
 - speed 191, 192, 194, 207, 214, 215, 219, 220, 222
 - thread 194
 - tool 190, 215, 222
- cyanide 296
- cyaniding 296

- dead metal zone 115–16
- deep drawability 276
- deep drawing 68, 152–5, 157–9, 162, 164–7
- deformation
 - bulk 16, 24, 76, 99–137, 147
 - cold 95
 - elastic 77–8, 81–2, 86, 254
 - homogeneous 78, 86–8, 98, 108
 - hot 91–4, 97, 98, 111, 187
 - ideal work of 89–90, 96, 108, 136, 230
 - inhomogeneous 93, 129, 130–1, 138
 - local 251–2, 254
 - mechanical 251
 - plane strain 111
 - plane stress 111
 - plastic 58, 77–8, 80–2, 86, 91, 97, 99, 143–5, 158–60, 170, 182, 190, 246, 254, 281, 284
 - pressure 119
 - resistance 119
 - shear 211
 - sheet 16, 76
 - work 88–91, 121, 211
- degas 22, 54–5, 68, 70
- degree of densification 181
- dendrite 32–4, 41, 49–50, 63, 107
- dendritic 173, 179
- density 4, 42–5, 47, 183, 187–9, 260, 308, 310
 - apparent 180–1, 187
 - energy 240
 - full 181, 187
 - green 182, 185
 - powder 180
 - power 226, 227
 - tap 180–1
- detergent 221
- dewaxing 184
- die
 - blocker 103–4
 - casting 27–8, 30, 62
 - clearance 144–5
 - closed 103–4, 112–13
 - extrusion 115, 117
 - finishing 103–4
 - geometry factor 148–9
 - holder 117
 - impression 104
 - open 103–4, 112, 113
 - wiping 149, 163
- dielectric 224–5
- diffuse 177, 242, 288, 290, 294, 296
- diffusion 92, 187, 221, 230, 253, 285–97
 - activation energy 193, 291–2
 - atomic 42, 183
 - bonding 254, 264
 - constant 183, 289–94, 306
 - flow 288–91
 - flux 289–90
 - frequency factor 183, 291–2
 - grain boundary 96, 183
 - hydrogen 236
 - layer 264–5
 - surface 183
 - volume 183
- direct reduction 7
- dislocation 58, 78, 92, 143, 172
- draft 61–2, 105
- drag 25–6, 61
- drawing 99–100, 102, 117, 121–2, 128, 133, 155–6, 162
 - deep 68, 152–5, 157–9, 162, 164–7
 - re- 154–8, 166–8, 172, 230

- drill bit 197–9
- drill press 195, 198, 205
- drilling 190, 196–9, 206, 223, 227, 229
- dry scrubber 15
- ductile tears 83
- ductility 80, 82, 171
- dynamic recovery 92, 96, 127
- dynamic recrystallization 92, 96, 127
- earing 159, 171, 277
- ears 159, 170–1, 276
- eddy current 298–9
- Einstein equation 293
- elastic limit 3
- elastic modulus 77, 148, 149, 248, 310
- elastic-plastic method 135
- electric arc furnace 9, 16, 22, 276
- electric arc welding 233–40
- electrical discharge machining 191, 224–6
- electrochemical 300
- electrochemical machining 191, 223–5
- electrode 10, 12, 224–5, 233–40, 244, 257
- electrode coating 235–6
- electrodeposition 302
- electroless 300, 303
- electrolysis 174, 179, 301
- electrolyte 179, 225, 300, 302
- electrolytic cell 179, 223, 300
- electromagnetic
 - casting 21, 70, 140
 - pumping 72–3
- electron 226, 236, 237
 - beam drilling 226–7
 - beam heating 304
 - beam machining 191, 226–7, 244
 - beam welding 233, 241, 244
 - charge 309
 - rest mass 309
 - volt 309
- electroplating 300, 302–3, 308
- elongation 79, 80, 96, 98, 171
- emulsion 169, 221
- engineering strain 77, 80–2, 85, 87, 97, 136
- engineering stress 76–8, 80–1, 87–8, 96, 97
- equivalent carbon concentration 261
- erode 279
- erosion 223, 280–1
 - cavitation 280–1, 282
 - impingement 280–1, 282
 - resistant 304
 - slurry 280–1, 282
- Euler bending formula 248
- eutectic 50, 57–9, 61, 65
- eutectoid 58–9, 258
- exothermic 187, 243
- explosion 39, 140, 187, 288
- explosive welding 233
- extreme pressure additive 221
- extrusion 82, 99–100, 115–21, 128, 133, 134
 - backward 115–16
 - cold 117–20, 135
 - forward 115–17
 - hot 120–1
 - impact 115–16, 120, 164, 165
 - lubrication 102
 - multiplying factor 118
 - pressure 117–18
 - ratio 118
- face centred cubic 161–2
- facing 193–4, 204, 206, 229
- Faraday's laws 300–3
- fatigue
 - failure 177
 - strength 253
 - surface 279, 280, 284–5
- fatty oils 102
- feed rods 193
- feed screws 193
- ferric oxide 178
- ferrite 59–60, 208, 256, 258, 261
- ferromanganese 19
- ferrosilicon 19
- Fick's first law 289–90
- Fick's second law 290
- filler metal 232, 236, 238, 240–1, 243, 250, 263–7
- finite element method 134–5
- fire extinguishers 120–1
- flame carburizing 242
- flame hardening 297–8
- flank 192, 198, 199, 202
- flash gutters 103–4
- flask 25–6
- flat rolling 111, 146
- flatness 141, 166
- flexible manufacturing 223
- flow stress 107, 110, 113, 121
- fluid mechanics 18
 - incompressible 133
 - inviscid 133
- fluorides 15, 54, 272

- flute 198–9
- flux 9, 12, 54, 70, 235, 239, 272, 289–90, 298
- fool's gold 5
- forging 34, 82, 99–100, 102, 103–15, 128, 133, 134, 211
 - closed die 103–4, 112–13
 - cylinders 107–11
 - impression 103–4, 112–13
 - open die 103–4, 112, 114, 135
 - rectangular parts 111–12, 129
- formability 34, 69, 91, 95, 142–4, 151, 158, 162, 171, 270, 276–7
- forming limit 151
- forming limit diagram 152, 171
- fossil fuel 8, 52, 69, 72, 140, 185
- four-high mill 122–3, 125, 129, 136, 138–41
- Fourier 42
- frequency factor 183, 291–2
- fretting 280–1, 282–3
- friction 91, 97, 100–3, 109, 115, 123, 127, 128–9, 132, 135, 136, 157, 170, 279
 - angle 211–12
 - chip-tool 210–11
 - coefficient of 100–2, 109–11, 119, 122, 129, 135, 136, 137, 213–14, 220, 230, 282
 - multiplying factor 109–10
 - pressure 119
 - resistance 119
 - slipping 101
 - sticking 101, 109, 119, 129
 - welding 233, 252
- furnace 72, 173, 263, 287
 - basic oxygen 9, 12, 16
 - batch 140
 - blast 4–7, 12, 59
 - brazing 265–7, 270
 - continuous 266
 - electric 72–3, 185
 - electric arc 9, 16, 22, 276
 - elements 174
 - explosion 288
 - holding 69, 73
 - reheat 22
 - reverberatory 69
 - vacuum 274
- fusion welding 232, 254
- fusion zone 234–5, 239, 255–60
- galling 280, 282–4
- galvanizing 296
- gangue 5, 178
- garnet 223
- gas
 - atomization 176–7, 188
 - carbonitriding 295
 - carburizing 282, 287–8, 307
 - constant, universal 183
 - de- 22, 54–5, 68, 70
 - metal arc welding 233
 - natural 287, 295
 - nitriding 294
 - porosity 52–5, 63, 66, 177, 236, 237
 - turbine 174, 186–7, 223, 282, 304, 306
 - welding 233, 241–4
- Gaussian error function 42–3, 290–1
- generalized tool life equation 219–20
- glass 102–3
- glycol 270
- gold 5, 174, 210, 303
- Goldschmidt process 268
- grain
 - boundary 31, 96, 276
 - boundary diffusion 183
 - boundary sliding 96
 - columnar 32–5, 39, 234
 - equiaxed 34–5, 127
 - growth 127
 - rearrangement 96
 - refine 34–5, 68, 70
 - size 27, 40, 95–6
 - structure 106, 140
- graphite 18, 58–60, 72, 102–3, 111, 186, 224, 253–4
- gravity casting 27, 30
- green density 182, 185
- green strength 181
- grinding 190, 196, 202–3, 205–6, 230, 243, 280
- haematite 5
- Hall–Héroult 1, 12, 14–16, 70
- hard chromium plating 302–3
- hardenability 257–8
- hardness 91, 92, 95, 171, 173, 214, 216–17, 257, 260–1, 269, 281, 285, 296
- Hazelett casting 22
- headstock 192–4
- health and safety
 - acne 221
 - antimisting additive 221
 - carbonitriding 296

- carburizing 287–8
- casting 22, 39–40, 47
- degassing 54
- dermatitis 221
- explosion 39, 140, 187, 288
- eye damage 235
- metallic dust 187
- tumours 221
- welding safety 235, 244
- hearth 6, 69
 - open 8, 16
- heat
 - affected zone 234–5, 239, 252, 255–64, 269
 - capacity 42–3, 221
 - conduction 183
 - conductive flow 290
 - exchangers 245, 253–4
 - flux 41, 43–4, 64
 - latent 31–2, 44–5, 47, 64, 69, 255, 256
 - dimensionless 47
 - sink 42
 - specific 45, 47, 259–60, 311
 - transfer 18, 20, 33, 38, 40–9, 246, 258–9, 270, 287–8
 - treatment 3, 15–16, 52, 63, 174, 208, 227, 258, 279, 296, 308
- helium 237
- hexagonal close packed 161, 164
- high speed steels 216–17, 220
- Höganäs process 178
- Hollomon equation 85, 87–90, 97, 98, 107, 113
- homogenization 68, 71, 170
- Hooke's law 77, 86
- hot cracking 62
- hot isostatic pressing 185–7, 189
- hot line 138–40
- hydrocarbons 185
- hydrofluoric acid 306
- hydrogen 19, 52–4, 66, 70, 72, 178, 185, 236, 262, 294, 302
- ice 36
- ideal deformation work 89–90, 96, 108, 136, 230
- incandescent light bulbs 173
- inclusions 55, 69–70, 72, 171, 177
- Inconel 208, 223
- indenter 251
- induction coil 299–300
- induction hardening 297–300, 306, 308
- induction heating 298–300
- industrial revolution 1, 7
- ingate 25, 57
- ingot 16, 23, 38, 63, 76, 99, 103, 115, 122, 129, 171, 253, 272
 - aluminium 20–1, 41, 69–70, 138
 - capped 19–20
 - killed 19
 - rimmed 19–20
 - semikilled 19
 - steel 18–20
- injection moulding 187–8
- interdendritic 34, 49
- internal energy 133
- interstitial 143–4, 291
- investment casting 29–30, 187
- inviscid 133
- ions 236, 238, 304
- iron 9, 170, 216, 243, 291
 - density 260
 - hydrogen solubility 53
 - powder 174, 178
 - specific heat 260
 - thermal conductivity 260
- iron ore 4, 5, 8
- iron oxide 9, 243, 280
- iron powder 177–8, 181
- iron pyrite 5
- ironing 68, 70, 157–8, 166–72, 230, 284
- isostatic pressing 174, 189
 - cold 182
 - hot 185–7, 189
- joining 16, 76, 232–74
- Kelly, William 1
- keyhole method 240
- kinetic energy 281
- ladle 5–6, 15, 21, 25, 30, 38, 54, 69, 72
- laser
 - carbon dioxide 228
 - cutting 227–8
 - machining 191, 227–8
 - neodymium doped yttrium aluminium garnet 228
 - neodymium-glass 228
- latent heat 31–2, 44–5, 47, 64, 69, 255, 256
- lathe 192–3, 204–6, 229, 230
- launder 20, 55, 69–70

- lead 22–3, 179, 208, 212, 253, 268, 302
- lime 8, 9, 12
- limestone 5, 8, 178
- limit analysis 133
- limiting draw ratio 155–6, 160
- linear control 222
- liquid carbonitriding 296
- liquid carburizing 286, 288
- liquidus 33
- lost-wax 29–30
- lower bound 133
- lubricant 101–3, 119, 125, 127, 131, 135, 136, 137, 140–1, 166–7, 170, 174, 181, 184, 198, 208, 220–1, 279, 282, 285
- lubrication 101–3, 129, 136, 157, 169, 181, 221, 284
- Lüders lines 143–4
- luminous zone 241–2

- machinability 60, 91, 207–9, 222, 233
- machining 16, 20, 30, 76, 91, 107, 173, 188, 190–231
 - boring 193–6
 - comparison of methods 228–9
 - electrical discharge 191, 224–6
 - electrochemical 191, 223–5
 - electron beam 191, 226–7, 244
 - laser 191, 227–8
 - mechanical 191–223
 - Merchant's analysis 210–12, 230
 - metal removal rate 191, 194–6, 198, 203–7, 228–9
 - multiple point 196–203
 - nontraditional 223–9
 - orthogonal 209, 213, 214, 230
 - power 203–7, 228
 - single point 191–6
 - time 191
 - waterjet 191, 223–4, 229
- machinist 222
- macroporosity 37, 39, 46, 49, 52, 65
- magnesium 4, 35, 60, 66, 170, 237, 243, 268, 273
- magnetic 298, 305
- magnetic permeability 299
- magnetite 5, 178
- magnetrons 305
- malleable 253
- manganese 7, 9, 12, 70, 170, 179, 216, 257, 263, 295
- martensite 208, 256–9, 262–3, 277, 285, 297
- martensitic 257–8, 260–2, 269, 294, 299
- mass transport 183, 290, 293
- mean anisotropy 159
- mechanical fasteners 232–3
- mechanical machining 191–23
- Merchant's analysis 210–12, 230
- metal inert gas arc welding 237–8, 241, 260, 267, 277
- metal injection moulding 187–8
- metal removal rate 191, 194–6, 198, 203–7, 228–9
- metal powder 173, 174
- metallic dust 187
- methane 287
- microelectronics 268
- microporosity 49–52, 57, 66
- microsegregation 34, 49, 57
- mill
 - attrition 179
 - ball mill 179–80
 - breakdown 122, 124, 138–9, 272
 - cold 136
 - end 202
 - face 202
 - four-high 122–3, 125, 129, 136, 138–41
 - hot 71
 - mini- 12, 22
 - peripheral 202
 - planetary 126
 - reversing 122, 127
 - rolling 23, 122–32, 136, 253
 - scale 178
 - Sendzimir 125–7, 129
 - stiffness 129
 - tandem 123, 125, 127, 138–40
 - tumbler ball mill 179–80
 - two-high 122–4, 136
 - vibratory ball 179
- milling 190, 196, 199–202, 205–7, 222, 230
- mineral oil 102, 110, 131, 136, 137, 221
- mini-mill 12, 22
- Mohr's circle 171
- molybdenum 174, 179, 180, 216, 227, 263, 295
- molybdenum disulfide 103
- moment of inertia 249, 311
- Mond process 305
- monel 34
- mould 18, 20–8, 31–3, 36, 41, 43, 47, 63, 64, 70–1, 72–3, 182, 243
- multiple point tool 191, 196

- mushy zone 33, 49–51
 near net shaping 173, 186
 necking 78, 80, 82–3, 91, 93, 95, 96, 98, 122, 143, 151–2, 157, 160, 164, 171–2, 276
 neodymium doped yttrium aluminium garnet laser 228
 neodymium–glass laser 228
 neutral axis 147–8, 247, 249–50
 neutral flame 241
 neutral point 128
 nickel 4, 33–4, 53, 179, 186, 216, 227, 253, 260, 263, 276, 302–3, 305
 nickel carbonyl 305
 nickel sulphate 303
 niobium 35, 216, 277
 nitralloy 295
 nitriding 286, 294–5
 nitrogen 8–9, 12, 16, 54, 70, 72, 143, 185, 189, 239, 244, 276–7, 288, 294–6
 NOCOLOK 272
 numerically controlled 190–1, 222–3
 octahedral planes 161–2
 olivine sand 223
 Olsen cupping test 143, 162
 open hearth 8–9
 orange peel 143
 outer envelope 241–2
 oxidation 185, 187, 234, 265, 268, 278, 297, 304
 oxidative wear 280, 283–5
 oxidizing flame 242
 oxyacetylene 296, 297
 pack carburizing 286, 287
 parallel axis theorem 249
 parting line 63
 passivate 188
 pasteurization 170
 pattern 25–6, 36, 61
 pearlite 58–9, 208, 258, 261
 pentlandite ore 305
 permanent mould casting 27–30
 petroleum solvents 221
 phase diagram 51
 Al–Si 65
 Cu–Ni 34
 Fe–C 58
 phosphorus 7, 9, 12, 59
 photon 227
 piezoelectric 254
 pig iron 4, 7, 8, 12, 16, 17, 18
 pipelines 235
 pitting 280, 284–5
 planar anisotropy 277
 plane strain 111, 129
 plane stress 111
 planetary mill 126
 planing 190, 195–7, 205–6
 plasma 233, 305
 plasma arc welding 233, 240
 plastic anisotropy 159–64, 276
 plastic injection moulding 187
 plastics 4, 91, 187, 303
 plate 122, 138, 253
 plate shear 138–9
 platen 107–11, 135, 253
 plating 300–3, 308
 polybutanes 221
 polyglycols 221
 polymers 4
 porosity 173
 casting 19, 28, 63, 73
 gas 52–5, 63, 66, 177, 236, 237
 macro 37, 39, 46, 49, 52, 65
 micro 49–52, 57, 66
 residual 184
 solidification 63
 potassium fluoraluminate 272
 potassium silver cyanide 308
 potential function 133
 potline 15, 69
 pots 15, 38
 pouring basin 25, 55
 powder 268
 density 180
 metallurgy 173–89
 production 175–80
 power 133, 136, 137, 165
 acoustical 254
 cutting 215
 extrusion 119–21
 forging 108
 machining 191, 203–7, 228
 rolling 126, 128–32
 precipitators 13–14
 preheating 262–3, 269
 press brake 146–7
 pressure vessels 235, 239
 pressure welding 250–1

- pressworking 162
- printed circuit boards 254
- prismatic plane 161
- propane 265
- propellers 281
- pulverization 174, 175, 179–80
- punch pressure 119–20
- punch-stretch test 151
- pyramidal planes 161
- Pyron process 178
- pyrophoric 187
- Pythagoras's theorem 129

- quench 287, 296, 299
- quench hardened 285, 294, 297

- radiator 268, 270–4
- rails 8, 244
- reaming 199–200
- recrystallization 34, 92, 99, 107, 113, 115, 127
- recrystallize 140, 276
- recycle 12, 69, 223
- red mud 13–14
- redrawing 154–8, 166–8, 172, 230
- reducing flame 265
- reduction in area 80, 96, 148
- reduction, of metal oxides 177–9
- redundant work 90–1, 109
- refrigerators 252, 254
- regenerators 8
- residual stress 62, 245–9, 256
- resistance welding 233, 244–5
- resistivity 299
- reverse polarity 236–8, 241, 267
- rigid-viscoplastic method 135
- ring compression test 114
- riser 25–7, 36, 37–8, 46, 51, 57, 59, 63, 64–5
- rivet 233, 285
- Rockwell 286, 287, 294, 312
- roll bonding 233, 253–4, 272
- rolling 82, 99–100, 102, 117, 122–34, 163
 - breakdown 253
 - can stock 138–41
 - cold 123, 125, 127, 129, 131, 136, 138–44, 152, 158, 171, 272, 277
 - flat 111, 128–9, 142, 146
 - forces 128–32
 - hot 127, 129, 138–41, 170–1, 272
 - mill 23, 122–32, 136, 253
 - power 128–32
 - separating force 132, 136
 - torque 130, 132
- rotating electrode process 177–8
- runners 25, 57

- salt 267, 274, 275, 288, 296, 303
- sand
 - casting 25–7, 30, 36–8, 55–6, 61–2, 73, 216
 - olivine 223
 - silica 223
 - zircon 73–4
- scalp 20, 68, 71
- scoring 170, 284
- scuffing 284
- segregation 20, 173
 - micro- 34, 49, 57
- seizure 280, 282–3
- semi-conductor 254
- Sendzimir mill 125–7, 129
- sensitization 276–7
- shape analysis 162
- shape casting 16, 23–30, 57–61, 63, 229, 290
- shape sensor roll 141
- shaping 190, 195–7, 205–6, 229
- shear
 - angle 209, 212, 215, 230
 - plane 209–12
 - spinning 150
 - strength 119, 145, 211, 230
 - stress 101, 171
- shearing 144–6, 162, 170
- sheet forming 142–72
- sheet metal 82, 99, 136, 142, 144–7, 244
- shielded (manual) metal arc welding 233, 235–7, 240, 260, 267, 269
- shipbuilding 239
- shrinkage 244
 - centreline 63
 - liquid 36
 - solid 36
 - solidification 25, 36–41, 53, 59, 62, 186, 245
 - volume 36
- SiAlON 219
- siderite 5
- Sievert's law 53
- silica 73, 223
- silicon 7, 9, 15, 19, 27, 61, 71, 170, 253, 257, 268, 297
- silicon carbide 203

- silicon nitride 219
- siliconizing 286, 296–7
- silver 5, 174, 268, 303, 308
- single point tool 191–6
- sinter 173–4, 187–8
- sintering 181, 183–5, 187
- skin effect 299
- skip incline 5–6
- slag 5–6, 7, 8, 9, 12, 19, 21, 54, 70, 171, 235–6, 243
- slip-line analysis 133–5
- slip systems 143, 159–62
- slipping friction 101
- slitter 138–9
- slitting 68, 146, 272
- slug 115–16, 120, 165
- smelter 38, 68–9
- soap 102, 222
- sodium
 - aluminate 13–14
 - carbonate 296
 - chloride 296
 - cyanate 296
 - cyanide 288, 296
 - hypophosphite 303
- solderability 270
- soldering 232, 250, 267
- solid solution 170
- solid state welding 232, 250–4
- solidification 18–75, 107, 171, 176, 239
 - directional 234
 - expansion 268
 - mechanism 30–5
 - pipe 37–8
 - porosity 63
 - shrinkage 25, 36–41, 53, 59, 62, 186, 245
 - time 43–4
- solidus 33, 263, 270, 272, 274
- solute atmosphere 143–4
- sow 38–40, 69
- spalling 280, 284–5
- specific cutting energy 203–7
- specific energy 88
- specific heat 45, 47, 259–60, 311
- spinning 150
- split ends 130
- spray can 115
- springback 147–9, 269
- sprue 25–7, 55–7, 63
- sputtering 304–5
- stainless steel 186, 213,
 - austenitic 207–8, 260, 276, 308
 - exhaust systems 275–9
 - ferritic 275–8, 296, 308
 - lubrication 102
 - martensitic 260
 - nitriding 295
 - roll bonding 253
 - sensitization 276–7
 - type 302 79, 86, 91, 110–11, 230
 - type 304 208
 - type 409 276
 - type 410 79, 86, 189
 - welding 238, 240, 242
- stamping 162
- steadite 59
- steel 3, 18, 102, 212, 223
 - AISI 1008 79, 163
 - AISI 1015 79
 - AISI 1016 214
 - AISI 1020 207, 208
 - AISI 1035 220
 - AISI 1040 208
 - AISI 1045 79
 - AISI 1060 220
 - AISI 1112 207, 208
 - AISI 3140 208
 - AISI 4140 208
 - AISI 4350 220
 - AISI 8620 79
- alloy 206
- aluminium killed 152
- aluminized 275
- carbon 9, 206–8, 215, 253, 285, 299
- continuous casting 21–2
- converters 7–12, 16
- degassing 54
- deoxidized 19
- ductile 155
- embrittle 8
- grain refinement 35
- high carbon 220
- high speed 216–17, 220
- ingot casting 18–20
- integrated mills 12
- limiting draw ratio 160
- low alloy 9, 257–8, 260, 263, 269, 277
- low carbon 76–8, 143, 162, 208, 229, 285, 297, 308
- low interstitial 144
- lubrication 102

- steel *cont.*
 - mild 23, 230, 275
 - mini-mill 12, 22
 - nitralloy 295
 - nitriding 295
 - plain carbon 12, 263, 277
 - SAE1010 291
 - scrap 7, 12
 - shrinkage 36
 - tool 135, 162, 180
- steelmaking 4–12, 178, 185, 189
- sticking friction 101, 109, 119, 129
- stimulated emission 227
- straight line control 222
- straight polarity 236–7, 240–1, 267
- strain
 - elastic 78
 - engineering 77, 80–2, 84–5, 97, 136
 - hardening 78, 91, 96, 99, 108, 117, 123, 127, 133, 137, 155, 157, 172, 182
 - hardening exponent 79, 85–6, 91, 95, 96, 107, 143, 151, 162, 164, 208, 276
 - incremental 81–2
 - inhomogeneous 83
 - major 152
 - minor 152
 - plane 111, 129
 - plastic 78
 - rate 92–3, 95, 96, 97, 98, 107–9, 113, 115, 120, 130, 133–5
 - rate sensitivity exponent 79, 94, 108, 151
 - rate strength constant 79, 93, 108
 - true 80–9, 93, 96, 97, 99, 107–8, 135, 136, 147–8, 163, 276
- strand 21, 76
- stream function 133
- strength constant 79, 85, 96, 107, 164
- stress
 - 0.2% offset yield 78
 - corrosion cracking 262
 - drawing 121
 - elastic 86
 - engineering 76–8, 80–1, 87–8, 96, 97
 - flow 107, 110, 113, 121
 - mean true flow 89, 96, 117, 129, 130–1
 - plane 111
 - relieving 63, 263
 - residual 62, 245–9, 256, 263
 - shear 101, 171
 - thermal 62, 246
 - true 80–2, 86–9, 93, 96, 98, 99, 113, 120
 - yield 78, 135, 148, 154
- stretch forming 150–2, 162
- stretcher strain marks 143
- strip 123, 128–9, 136, 142, 144
- sublimation 228
- submerged arc welding 233, 239, 241, 260, 268
- sulphate 302
- sulphonates 221
- sulphonic acids 221
- sulphur 5, 7, 9, 12, 178, 221, 239
- sulphur dioxide 15
- superalloys 174, 208, 223
- superplasticity 95–6, 97, 98
- surface
 - diffusion 183
 - energy 31, 183–4
 - machined 191, 193, 197, 200
 - tension 183
 - transient 191, 193, 197, 200
 - work 191, 193, 197
- swarf 223
- tailstock 150, 193
- talc 25
- tandem mill 123, 125, 127, 138–40
- tantalum 216
- tap density 180–1
- Taylor tool life equation 219–20, 230
- temper 171–2
- temper roll 143
- texture 140, 159–62, 171, 276–7
- thermal
 - conduction 255
 - conductivity 41, 42, 45, 47, 74, 214, 216, 259–60, 270, 311
 - diffusivity 42, 183
 - distortion 185
 - expansion 123
 - expansion coefficient 36, 74
 - gradients 245
 - shock 294
 - shock resistance 216
 - shrinkage 105
 - stress 62, 246
 - undercooling 33–4
 - welding 233, 241–5
- thermally activated 183, 187, 291, 294–5
- thermit welding 233, 241, 243–4, 268
- thermoplastic 187
- thin film 303–6

- tin 212, 253, 268, 302
- titanium 13, 35, 161, 186, 223, 277, 295
 - density 4, 260
 - diboride 35, 70
 - limiting draw ratio 160
 - powder 177
 - specific heat 260
 - thermal conductivity 260
 - welding 244
- tool
 - age 1
 - carbide 214, 303, 305–6
 - face 191–2
 - feed 193
 - generalized life equation 219–20
 - life 207–8, 214, 219–20
 - materials 214–19
 - multiple point 191
 - post 192–3, 211, 230
 - rake angle 209, 212, 214, 230
 - single-point 191–6
 - Taylor life equation 219–20, 230
 - wear 191, 213–20
- top gas 5
- torch 241–2, 265, 267, 296
- toxicity 221
- transformer 254, 298
- transistor inverter 300
- transport, mass 183, 290, 293
- Tresca 101, 119
- tribological 279
- tribology 279
- true strain 80–9, 93, 96, 97, 99, 107–8, 135, 136, 147–8, 163, 276
- true stress 80–2, 86–9, 93, 96, 98, 99, 113, 120
- tumbler ball mill 179–80
- tundish 21–4, 175–6
- tungsten 173, 177–9, 180, 216, 223, 227, 238, 240, 295
- tungsten carbide 180, 216, 223, 230
- tungsten inert gas arc welding 233, 238–9, 260, 267, 277
- turbine
 - airfoils 224
 - blades 30
 - discs 174
 - gas 174, 186–7, 223, 282, 304, 306
- turning 190–6, 220, 230
- tuyères 7, 276
- two-high mill 122–4, 136
- ultimate tensile strength 62, 78, 79, 98, 141, 148, 164, 276
- ultrasonic welding 233, 254–5, 277
- ultraviolet 305
- undeformed chip thickness 194, 196, 198, 201, 203–7
- undercool 31–2, 33–4
 - constitutional 33–4
 - thermal 33–4
- universal gas constant 183, 291, 309
- upper bound 114, 130, 133
- upsetting 107–11
 - cold 107–8, 110–11
 - hot 108–9
- valence 301–3, 308
- vanadium 35, 216
- vibratory ball mill 179
- Vickers pyramid hardness 257, 261–2, 312
- viscoelastic 4
- viscosity 102
- visioplasticity 134
- volume
 - constancy 83, 85, 94, 110, 133
 - diffusion 183
 - expansion 244
- water atomization 175–7, 188
- water glass 27
- waterjet machining 191, 223–4
- WC–Co 216–18
- wear 101–2, 253, 279–308
 - adhesion 280–1
 - adhesive 280, 282–3
 - impact 280, 284–5
 - oxidative 280, 283–5
 - polishing 280
 - tool 191, 213–20
- weldability 233, 276–7
- welding 214, 232–63, 264, 282, 303
 - butt 234, 240, 245–7, 249–50, 255, 269
 - cold 182, 183
 - cooling time 258–63
 - current 260
 - distortion 245–50
 - electric arc 233
 - electron beam 233, 241, 244
 - explosive 233
 - fillet 234, 246–7, 249
 - forge 249–50
 - friction 233, 252

- welding *cont.*
 - fusion 232–50, 254, 256
 - gas 233, 241–4
 - gas metal arc 233
 - heat affected zone 234–5, 239, 252, 256–64, 269
 - heat transfer efficiency 260, 268
 - laser 227
 - metal inert gas arc 237–8, 241, 260, 277
 - microstructure 254–63
 - plasma arc 233, 240–1
 - preheating 262–3, 269
 - pressure 250–2
 - properties 254–63
 - resistance 233, 244–5
 - roll bonding 233, 253–4
 - seam 233, 244–5, 272
 - shielded (manual) metal arc 233, 235–7, 240, 260, 267, 269
 - solid state 232, 250–4
 - speed 259–62, 269
 - spot 233, 244–5, 250
 - submerged arc 233, 239, 241, 260, 268
 - thermal 233, 241–5
 - thermit 233, 241, 243–4, 268
 - torch 241–2
 - tungsten inert gas arc 233, 238–9, 241, 260, 277
 - ultrasonic 233, 254–5, 277
 - voltage 260
- wet 264
- wire 121, 237–9
- work 310
 - deformation 88–91, 121, 211
 - hardening 91–2, 97, 172
 - ideal deformation 89–90, 96, 108, 136, 230
 - redundant 90–1, 109
 - rolls 122–3, 125–7, 129, 136, 140–1
 - surface 191, 193, 197
- X-ray gauge 138–9
- yeasts 221
- yield strength 3, 62, 79, 97, 121–2, 141, 149, 159, 171–2, 213, 246, 276
- yield stress 78, 135, 148, 154
- Young's modulus 77, 86
- zinc 4, 5, 22–3, 30, 160–1, 164, 165, 268, 274, 296, 302
- zircon 73–4
- zirconium 244, 277